L'éléphant de mer austral, bio-échantillonneur de la distribution des ressources marines

Yves Le Bras

UNIVERSITÉ DE LA ROCHELLE

ÉCOLE DOCTORALE GAY LUSSAC

LABORATOIRE : Centre d'Études Biologiques de Chizé

THÈSE présentée par :

Yves LE BRAS

soutenue le : **29 mars 2017**

pour obtenir le grade de : **Docteur de l'université de La Rochelle**

Discipline : **Biologie de l'environnement, des populations, écologie**

L'éléphant de mer austral, bio-échantillonneur de la distribution des ressources marines

---

JURY :

Francesco d'Ovidio	Université Paris VI (UMR 7159)	Rapporteur
Jean-Marc Fromentin	Université Montpellier II (UMR 212)	Rapporteur
Cécile Vincent	Université de La Rochelle (UMR 7372)	Examinateur
Hélène De Pontual	IFREMER – Centre de Bretagne	Examinateur
Christophe Guinet	Université de La Rochelle (UMR 7372)	Directeur de thèse

Table des matières

Remerciements

Je souhaite remercier :

La région Poitou-Charente, le Département des Deux-Sèvres et les contribuables pour avoir financé cette thèse.

L'IPEV, les TAAF et la réserve naturelle des TAAF pour leur support aux recherches scientifiques et pour m'avoir accordé l'opportunité de découvrir Kerguelen.

Xavier Bonnet en tant que directeur du laboratoire, Henri Weimerskirsh en tant que chef de l'équipe "Prédateurs marins" et Paco Bustamante en tant que directeur de l'école doctorale pour avoir guidé le navire à bon port et pour m'avoir accueilli dans leur équipe.

Christophe Guinet, mon directeur de thèse, pour avoir partagé ses connaissances et son savoir-faire, pour son encadrement bienveillant, toujours constructif et encourageant, pour m'avoir donné cette chance et fait confiance dès le départ, pour m'avoir communiqué sa passion pour la science et les éléphants de mers, pour m'avoir permis de partir à leur découverte et pour m'avoir toujours encouragé et soutenu aux moments opportuns.

Ceux qui ont participé de plus loin à l'encadrement scientifique de la thèse à travers leurs relectures et leurs précieux conseils, en particulier les membres du jury et les chercheurs du laboratoire. Merci à : Fransceco d'Ovidio, Cécile vincent, Hé-

lène de Pontual, Jean-Marc Fromentin, Yves Cherel, Vincent Ridoux, Charly Bost, Yan Ropert-Coudert, Christophe Barbraud, Mathieu Authier, David Nérini, Christophe Laplanche, Pascal Monestiez, Patrick Duncan, Cédric Cotté, Jerome Spitz, Akiko Kato, David Pinaud, Vincent Bretagnolle, Sylvie Houtte, Frédéric Bailleul, Olivier Duriez et Simon Benhamou. Merci également aux relecteurs anonymes.

Ceux qui ont contribué à cette thèse, avant même son commencement, grâce à leur travaux, à leurs conseils et à leurs connaissances : Patrick Lehodey, Anna Conchon, Anne-Cécile Dragon, Jade Vacquié-Garcia, Thomas Jaud, Morgane Viviant, Kevin Le Rest, Pierrick Devoucoux.

Le personnel du laboratoire. Arnaud Phillipe pour avoir veillé sur le matériel informatique si précieux à l'équipe éléphant de mer. Les équipes des secrétariats qui m'ont guidé et aidé sur le plan administratif où j'ai quelques déficiences : Isabelle Irsch, Jennifer de la Corte-Gomez, Delphine Bonnet, Annie Telias, Martine Lacalle et Dominique Besson.

Tous les stagiaires passés au sein de l'équipe "éléphant de mer" pour l'énorme travail collectif accompli, avec une mention spéciale pour Guillaume Bessigneul et Alexandre Génin qui m'ont précédé et dont les travaux ont été particulièrement utiles aux miens, ainsi qu'à Charles Rhodes, Louise Day et Julie Mestre avec qui j'ai eu grand plaisir à travailler.

Tous les autres stagiaires et travailleurs de passage à Chizé et que j'ai eu le plaisir de rencontrer : fêtards, naturalistes, joueurs de go ou de fléchettes, guitaristes, amateurs de musique, de gastronomie, de jardinage etc.

Aux collègues du laboratoire avec qui j'ai pu faire une partie du chemin et qui chacun ont contribué à faire du CEBC un endroit où règne la bonne humeur, le sérieux et la passion : Cécile Bon, Sabrina Tartu, Aurélie Goutte, Loriane Mendez, Gaëtane Le Provost, Mathilde Huon, Charlotte Lambert, Paul Deroulers, Rui Catarino et Camille Coux (liste nécessairement non exhaustive).

Les collaborateurs, équipiers de terrain et rencontres fortuites avec qui j'ai partagé des expériences professionnelles et personnelles enrichissantes : Samantha Patrick, Alice Della Penna, Timothée Poupard, Karine Heerah, Pedro Monroy, Karine Delord, Fabrice Lebouard, Elie Gaget, Antoine Protin, Ayala Loisel, Sara Labrousse, Pierrick Blanchard et Marine Desprez.

Mes collègues proches et amis, pour tous les évènements quotidiens qui ont rendu ces années si agréables et les feront perdurer dans ma mémoire : Samantha Cox (and Tom), Andréas Dupoué, Gaëtan Richard, Pierre Blévin, Laurie Thiers, Alizée

Meillère, Héloise Guillot, Julien Collet Anaïs Janc, mes fantastiques camarades de bureau, Joffrey Jouma'a, Baptiste Picard et Nathan Pacoureau, mes délicieux colocataires de longue date, Alice Carravieri, Rémi Fay et Florian Orgeret sans oublier les plus éphémères, Sophie de Grissac, Aurélien Prudor, Paul Tixier et Sophie Dupont.

Mes amis qui à un moment ou à un autre ont traversé le pays pour s'aventurer dans le marais Poitevin.

Mes frères et sœurs, parents et grands-parents, pour leurs encouragements constants et parfois mêlés d'incompréhension.

Anna, pour m'avoir toujours soutenu et supporté dans les moments difficiles et surtout pour ta patience et ton courage face à la distance qui nous a tenu séparés tant d'années.

Avant-Propos

Cette thèse, effectuée sous la direction de Christophe Guinet, a débuté en novembre 2013 grâce aux financements de la région Poitou-Charente et du département des Deux-Sèvres. Elle fait suite aux thèses de Frédéric Bailleul (2006), Matthieu Authier (2011), Anne-Cécile Dragon (2011) et plus particulièrement de Jade Vacquié-Garcia (2014), dont les travaux se sont intéressés aux interactions prédateur-proies.

Au cours des dernières années, l'équipe "éléphant de mer" du laboratoire (CEBC-CNRS, UMR 7372, Université de La Rochelle) s'est notamment tournée vers l'étude des proies à travers celle de leur prédateur. Un premier projet, dans lequel s'inscrivent les travaux de Jade Vacquié-Garcia, s'est mis en place en 2010 (ANR TOPP-PATCHES, Frédéric Bailleul) et s'est achevé en 2013. Il s'agissait d'évaluer la distribution des proies par la caractérisation des habitats d'alimentation des éléphants de mer. Dans la continuité, le projet MyctO3D-MAP (Yves Cherel, ANR 2012–2015) dans lequel s'insère les travaux de cette thèse, s'intéresse à utilisation conjointe de données fournies par les prédateurs (les éléphants de mer, mais pas seulement), l'écho-intégration et la modélisation afin de caractériser la distribution et les habitats tri-dimensionnel des myctophidés.

Au cours de ces trois années, j'ai pu participer à des études dans le cadre d'autres projets. Au sujet du comportement de plongée et de la dépense énergétique des éléphants de mer, j'ai collaboré avec mon collègue Joffrey Jouma'a. Dorian Cazau et Julien Bonnel de l'ENSTA Bretagne m'ont également impliqué dans leurs projets ayant trait à la météorologie. Voici, ma contribution personnelle aux différentes études présentées dans cette thèse :

- Concernant les travaux présentés dans le corps du manuscrit (articles 1, 2 et 3 ; voir page xvi) : j'ai, à l'exception du calcul de la vitesse de nage (sous-section 2.3.3), traité l'ensemble les données, conçu et réalisé les analyses statistiques et rédigé les études dans leur ensemble.
- Dans l'article 5 (voir page xvi), j'ai participé à l'écriture de l'article (élaboration de sa structure, relectures), ainsi qu'à la conception des analyses statistiques.
- Pour l'article 6 (voir page xvi), j'ai aidé aux traitement des données (à la reconstruction 3D des plongées), ainsi qu'à la conception des analyses statistiques.
- Dans les articles 4 et 7 et 8 (voir page xvi), ma contribution se limite au traitement d'une partie des données et à une assistance pour réaliser cette tâche sur pour la partie restante.

Publications, conférences et formations

Publication	Statut	Partie
1. Le Bras Y., Jouma'a J., Picard B., Guinet C. (2016). How elephant seals (Mirounga leonina) adjust their fine scale horizontal movement and diving behaviour in relation to prey encounter rate. *Plos One*.	Publié	Chapitre 3
2. Le Bras Y., Jouma'a J., Guinet C. (2016). Three-dimensional space use during the bottom phase of southern elephant seal dives. *Movement Ecology*.	Publié	Chapitre 4
3. Le Bras Y., Jouma'a J., Guinet C. (2016). In situ measurements of marine resources distribution from instrumented elephant seals. *Progress in Oceanography*.	En prép.	Chapitre 5
4. Guinet C., Vacquié-Garcia J., Picard B., Bessigneul G., Le Bras Y., Dragon A.-C., Viviant M., Arnould J. P. Y., Bailleul F. (2014). "Southern elephant seal foraging success in relation to temperature and light conditions : insight into prey distribution". *Marine Ecology Progress Series*. 499. 285-301	Publié	Annexe E
5. Jouma'a J., Le Bras Y., Richard G., Vacquié-Garcia J., El Ksabi N., Picard B., Guinet C. (2016). Adjustment of diving behaviour with prey encounters and body condition in a deep diving predator : the Southern Elephant Seal. *Functional Ecology*. 30(4). 636-648	Publié	Annexe F
6. Jouma'a J., Le Bras Y., Picard B., Guinet C. (2016). Three-dimensional assessment of hunting strategies in a deep diving predator. *Marine Ecology Progress Series*.	En révision	Annexe G
7. Cazau D., Bonnel J., Jouma'a J., Le Bras Y., Guinet C. (2017). Measuring the marine soundscape of the Indian Ocean with Southern Elephant Seals used as acoustic gliders of opportunity. *Journal of Atmospheric and Oceanic Technology*	Publié	Annexe H
8. Jouma'a J., Le Bras Y., Picard B., Guinet C. (2016). Spatio-Temporal Variations in Field Metabolic Rate of Post-Moulting Southern Elephant Seals	En prép.	Annexe I

Titre		
Influence of the diving behaviour of souther elephant seal on the distance travelled at surface, with respect to oceanic currents and fishing success. Bio-Logging Symposium 5	Poster	Sep. 2014
Le comportement de plongées des éléphants de mer en trois dimensions. 4^{ième} Journées Éléphants de Mer du CEBC–CNRS	Présentation	Oct. 2014
Gestion de bases de données et langage SQL. CEBC–CNRS.	Formation	Déc. 2014
Southern elephant seal, living samplers of the marine resources distribution. Université de La Rochelle	Poster & Présentation	Mai 2015
Distribution verticale des proies de l'éléphant de mer en relation avec les conditions océanographiques. Université La Rochelle.	Présentation	Mai 2015
Initiation aux Systèmes d'Information Géographique. CEBC–CNRS	Formation	Juil. 2015
L'éléphant de mer austral, bio-échantillonneur des conditions océanographiques et de la distribution des ressources marines. 31^{ième} Festival du film ornithologique international, Ménigoute	Présentation	Oct. 2015
L'éléphant de mer austral, bio-échantillonneur des conditions océanographiques et de la distribution des ressources marines. 7^{ième} congrès Ecolo'Tech, Université Montpellier	Présentation	Nov. 2015
Ajustement du comportement de plongée en relation avec la densité en proies chez l'éléphant de mer austral. Université Paris 6	Présentation	Déc. 2015
Recherche documentaire spécialisée. Université de La Rochelle.	Formation	Déc. 2015
Molécules, physiologie et comportement. Université de La Rochelle.	Formation	Jan. 2016
Chimie et changement climatique. Maison de la chimie, Paris.	Formation	Fév. 2016
Estimation des concentrations en phytoplancton et de la densité des organismes bioluminescents à partir de mesure de lumière collectées par des éléphants de mer. 5^{ième} Journées Éléphants de Mer du CEBC–CNRS	Présentation	Avr. 2016
Statistiques pour l'écologie avec R. CEBC–CNRS.	Formation	Juil. 2016

CHAPITRE

1

Introduction

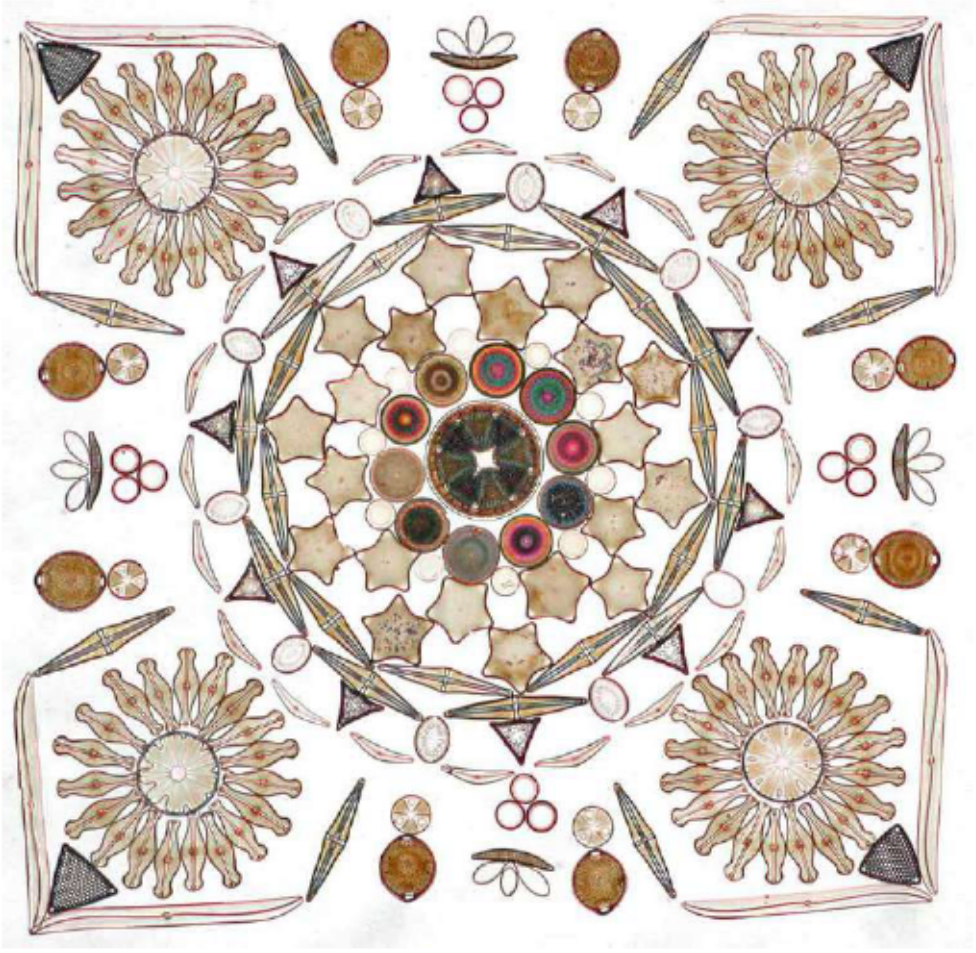

Exemple moderne d'arrangement géométrique de diatomées vu au microscope optique, un art en vogue à l'époque victorienne. Crédit : Klaus Kemp

1.1 Hétérogénéité du milieu pélagique

1.1.1 Notion de paysage océanographique

Le paysage peut être défini simplement comme une zone géographique caractérisée par l'existence d'une hétérogénéité spatiale (Turner, 1989). Bien que le milieu pélagique puisse sembler homogène, les paramètres océanographiques varient dans l'espace et constituent ainsi ce que l'on appelle le **paysage océanographique**. Avec les travaux pionniers de Clarke et al. (1970) et du Coastal Zone Color Scanner (Hovis et al., 1980) en matière de télédétection, apparaissent les premières images du paysage océanographique visibles depuis la surface des océans (figure 1.1). En effet, ces photographies mettent en évidence l'hétérogénéité spatiale de la production primaire. La notion de paysage est intrinsèquement liée à celle **d'échelle** car la mesure de l'hétérogénéité est fonction de l'échelle spatiale ou temporelle à laquelle elle est effectuée (Turner, 1989). Ainsi, on peut observer sur la figure 1.1 l'existence de disparités à large échelle, par exemple la côte ouest de la Floride est nettement plus riche que la partie centrale du golfe, mais également à de plus fines échelles, comme en témoignent les formes dessinées par les nuances de bleu au centre du golfe. Ces motifs tortueux, qui ne sont pas sans rappeler ceux créés par le mélange du café et du lait à la surface d'une tasse, suggèrent une forte implication des processus physiques dans la formation de ce paysage.

1.1.2 Caractéristiques physiques du milieu pélagique

Non seulement l'océan représente 71% de la surface de notre planète mais, sur la majorité de cette surface, le plancher océanique se situe à plus de 4000 mètres de profondeur. Le milieu océanique est un donc un **milieu tri-dimensionnel** qui occupe la majorité du volume de la biosphère. La figure 1.1 présente une image bi-dimensionnelle du paysage océanographique mais la stratification de l'eau de mer en raison de sa densité conduit à des variations des paramètres océanographiques selon la dimension verticale. L'augmentation de la profondeur se traduit par une augmentation linéaire (mais importante) de la pression (Pascal, 1663) et une diminution exponentielle de l'intensité lumineuse (Bouguer, 1729) mais également par d'éventuels changements de température, salinité, pH, concentration en oxygène et minéraux dissous etc... Or, ces paramètres physico-chimiques peuvent influer sur les processus biologiques et, par conséquent, sur la distribution des organismes marins pélagiques (du grec

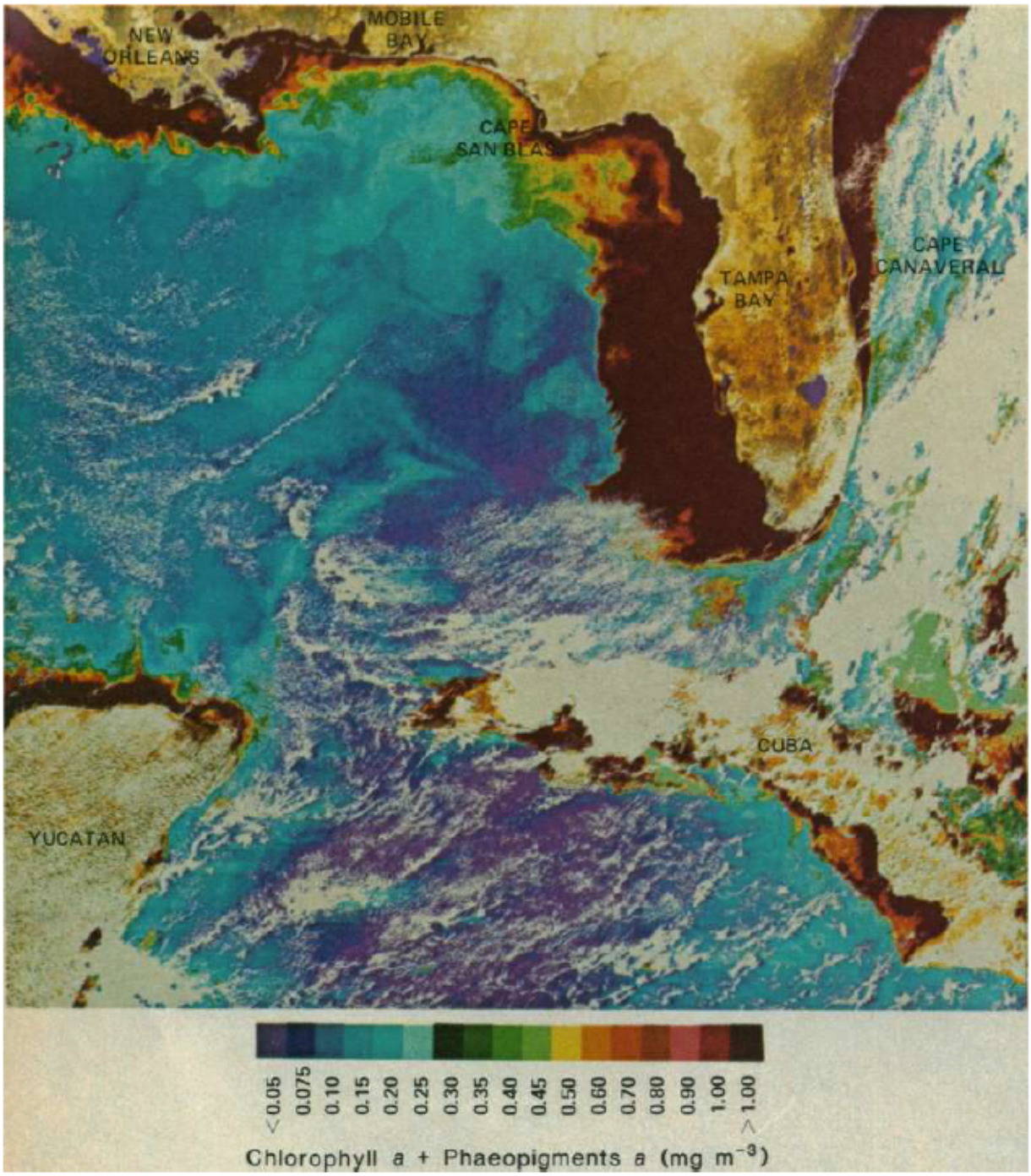

Figure 1.1: Première carte de la production primaire à l'échelle d'un bassin océanique obtenue par télédétection – *Photographie du Golfe du Mexique par le satellite Nimbus-7 le 2 novembre 1978 (fausses couleurs) mettant en évidence l'hétérogénéité spatiale de la production primaire. Figure tirée de* Hovis et al. *(1980).*

πέλαγος, pélagos, que l'on peut traduire par "haute mer"), c'est à dire ceux qui vivent au sein de la colonne d'eau dans le milieu océanique. Le paysage océanographique offre donc au monde vivant une mosaïque tridimensionnelle de masses d'eaux aux caractéristiques écologiques variées.

Comparé au milieu terrestre, une caractéristique fondamentale du milieu marin est sa nature fluide. Dans un tel milieu, les frontières du paysage océanographique sont constamment en mouvement sous l'effet des courants. Il s'agit donc d'un milieu fortement **dynamique** où les processus physiques agissent à des échelles spatiales et temporelles très variées (figure 1.2). Dans le milieu dynamique qu'est le milieu océanique, les caractéristiques physico-chimiques et biologiques de l'environnement évoluent bien plus rapidement qu'au sein du milieu terrestre, jusqu'à des vitesses comparables à celles des mouvements d'animaux. C'est le cas de la méso-échelle et de la sub-méso-échelle (1 à 100 km, de quelques jours à quelques mois, figure 1.2). Les structures à cette échelle sont ubiquitaires dans les océans (Chelton et al., 2007) et assurent un rôle de première importance dans la circulation de surface et le transport de la chaleur. On peut considérer que les changements d'échelle spatiale concordent avec les changements d'échelle temporelle (voir la figure 1.2 où le "relief" s'organise selon la diagonale). Ainsi, les interactions entre processus physiques et biologiques aux différentes échelles sont à l'origine d'une distribution des ressources marines organisée en structures emboitées de plus en plus grandes et stables dans le temps. Pour décrire conceptuellement la distribution des ressources marines dans cet environnement, on utilise l'image de **mosaïque de parcelles emboitées** ("hierachical patch system") dans laquelle les contrastes en termes de densité des ressources marines et la stochasticité augmentent vers les plus fines échelles (Kotliar and Wiens, 1990; Fauchald, 1999).

1.1.3 Notion de niche écologique : le cas du phytoplancton

Les organismes vivants sont adaptés à des conditions environnementales plus ou moins aptes à leur permettre de réaliser leur cycle biologique (Darwin, 1859). Les espèces constituant le phytoplancton ne sont donc pas à même de se distribuer librement dans tout le volume offert par le milieu pélagique mais occupent plutôt des **niches écologiques**.

Par exemple, la quantité de lumière solaire reçue par la surface des océans décroît rapidement avec la profondeur. Or celle ci est nécessaire à la photosynthèse, c'est à dire au développement de la production primaire. La distribution du phytoplancton

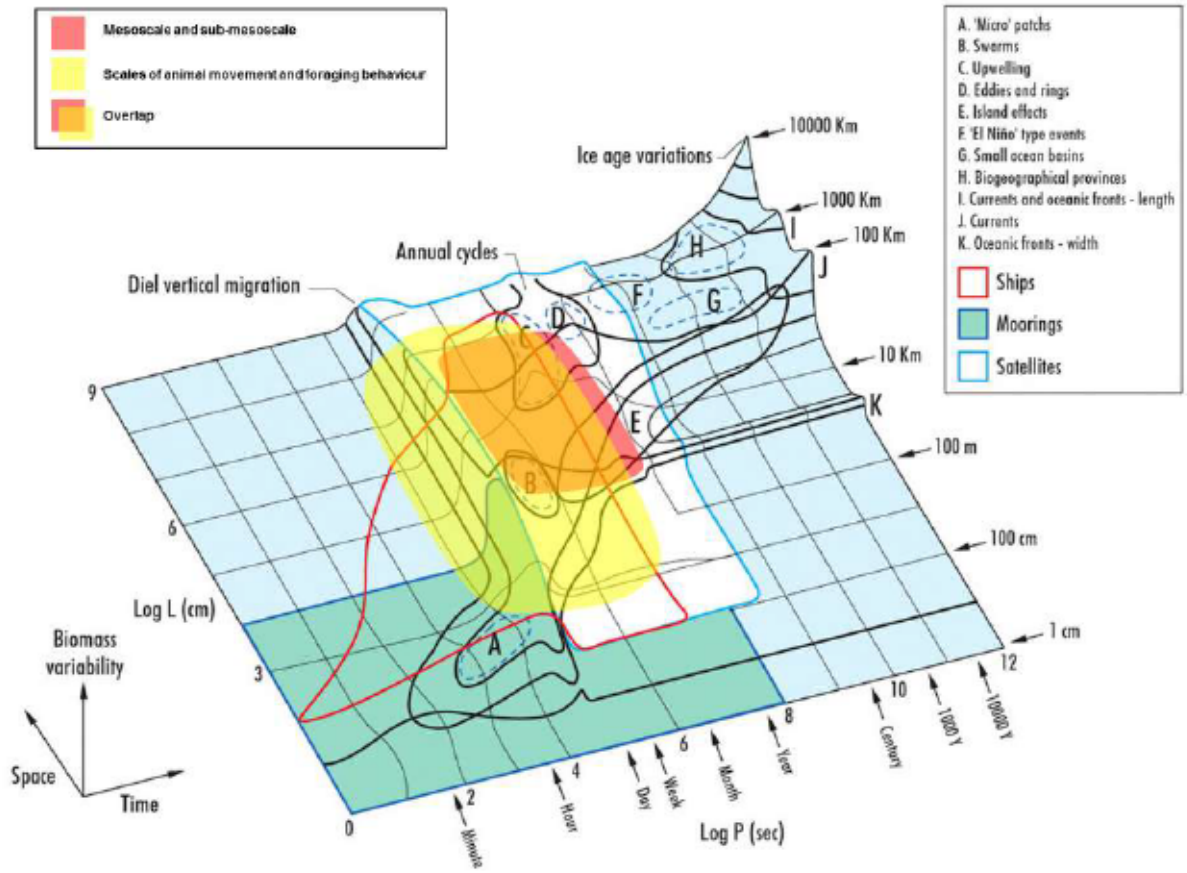

Figure 1.2: Diagramme de Stommel : échelles spatio-temporelles et variabilité de la biomasse en milieu pélagique – *Figure tirée de Kaiser (2011) à laquelle ont été ajoutées des figurés présentant la méso-échelle & sub-méso-échelle (aire en rouge transparent) ainsi que les échelles caractéristiques du mouvement animal (aire en jaune transparent). Le chevauchement de ces deux domaines (aire en orange transparent) est notable. Nous avons évoqué dans le texte l'importance de la méso-échelle et de la sub-méso-échelle dans l'organisation de la distribution du plancton. On peut constater la remarquable superposition de ces échelles avec celles couvertes par l'imagerie satellitaire (aire blanche cernée de bleu). Les premières versions de ce diagramme sont consacrées à la planification expérimentale en océanographie Stommel (1963), mais l'usage de cette représentation s'est largement étendu à l'écologie (Haury et al., 1978) afin de montrer les interactions entre processus physiques et écologiques en milieu dynamique (voir Vance and Doel (2010) pour une revue de l'histoire de cet usage).*

est donc limitée à la superficie des océans suffisamment riche en lumière pour soutenir son développement, la couche photique. Les concentrations en minéraux tels que nitrates, phosphates, silice ou fer constituent d'autres facteurs pouvant limiter la croissance du phytoplancton dans le milieu pélagique (Thomalla et al., 2011; Gandhi et al., 2012). Ces facteurs limitants expliquent pourquoi, à l'échelle globale, la productivité

primaire est plus importante dans les hautes latitudes et les régions de remontée d'eau profonde ("upwelling"). Il s'agit là d'exemples de **contraintes abiotiques** reconnues pour avoir une forte influence sur la distribution de ces organismes.

Au sein du domaine océanique, on divise classiquement les organismes en deux catégories selon leurs capacités natatoires. On distingue **plancton** du grec ancien *πλαγκτός* (*plagktos*) qui signifie "errant" ou "divaguant", et **necton**, du grec ancien *νηκτός* (*nêktós*) qui signifie "nageant". Comme son nom l'indique, les mouvements du phytoplancton sont fortement influencés par les courants. La méso-échelle et la sub-méso-échelle ont été identifiées comme des échelles clés dans la distribution du phytoplancton (Abraham, 1998; Volker et al., 2002; Lévy, 2003; Martin, 2003; d'Ovidio et al., 2010; Lévy et al., 2012; Lévy et al., 2012). En effet, à ces échelles, les transports vertical et horizontal des masses d'eau conduisent à l'injection d'éléments nutritifs en surface et à l'agrégation du plancton. L'hétérogénéité spatiale de la production primaire peut alors être aussi importante qu'à l'échelle d'un bassin océanique.

Outre l'environnement physique, les relations inter-spécifiques participent également à la formation d'une niche écologique. Ces interactions contribuent à expliquer la distribution et l'abondance des différentes espèces. Par exemple, la compétition entre espèces occupant la même fonction (une même "niche fonctionnelle") dans un écosystème conduit à l'exclusion des espèces les moins compétitives (Gause, 1934; Hardin, 1960). De légères différences dans l'environnement physique peuvent donc *théoriquement* mener à la dominance d'une ou quelques espèces (Hutchinson, 1961; Roy and Chattopadhyay, 2007). La prédation est un autre exemple de contrainte biotique. Le phytoplancton est consommé par les consommateurs primaires tels que le zooplancton. Dans le milieu pélagique, la pression de prédation exercée sur la production primaire (le "broutage") est particulièrement importante (Wiegert and Owen, 1971). Aussi, il est reconnu que le zooplancton joue un rôle primordial dans la distribution du phytoplancton (Abraham, 1998; Thomalla et al., 2011).

La distribution du phytoplancton est observable sur de vastes zones, à des échelles spatio-temporelles pertinentes et est fortement tributaire des processus physiques. L'étude des interactions entre les processus physiques et la production primaire a ainsi pu aboutir à une bonne compréhension de la distribution du phytoplancton. Les organismes autotrophes chimiosynthétiques ont une abondance bien inférieure à celle du phytoplancton. D'autre part, les macro-algues sont généralement limitées aux zones côtières. Ainsi, le phytoplancton assure la majorité de la production primaire

des océans (écosystèmes côtiers et océaniques réunis), à plus forte raison, du milieu océanique et constitue la principale source d'énergie de la chaine alimentaire. **Dès lors, il y a un intérêt à comprendre comment l'hétérogénéité spatio-temporelle de la distribution de la production primaire se propage aux autres organismes des écosystèmes pélagiques.**

1.2 De la physique des océans à la distribution des organismes marins

1.2.1 Réseaux trophiques pélagiques

Les facteurs limitant le développement et/ou la reproduction peuvent varier selon les espèces, le lieu et dans le temps. Cependant, l'acquisition d'énergie est un enjeu majeur pour le déroulement du cycle de vie, notamment pour les prédateurs supérieurs (Pimm et al., 1991). Pour comprendre comment et avec quelles conséquences l'hétérogénéité spatiale de la production primaire se propage au sein des écosystèmes, il faut s'intéresser au processus de circulation de l'énergie.

Dans le vocabulaire courant, cette circulation est désignée par l'expression de "chaine alimentaire". En réalité la chaine alimentaire est largement ramifiée, en témoigne la figure 1.3 qui présente de façon simplifiée le cas de l'écosystème antarctique. Nous préfèrerons donc parler de **réseau trophique** afin d'illustrer la complexité de la circulation de l'énergie au sein des écosystèmes. Les réseaux trophiques font intervenir de nombreux intermédiaires et et de nombreuses relations entre ces intermédiaires (les relations trophiques) et constituent des systèmes complexes. Le transfert d'énergie d'un niveau trophique au niveau supérieur s'accompagne d'un **décalage temporel** dû au temps nécessaire à l'assimilation d'énergie par le métabolisme du prédateur et d'une **perte d'énergie**. La vitesse de ce transfert croît géométriquement avec la température (Arrhenius, 1889) ($\times 2$ tous les 10°C environ) tandis que son rendement moyen est estimé à 10% (Lindeman, 1942).

Dans le milieu marin, le niveau trophique des organismes dépend dans une large mesure de leur taille (Lundvall et al., 1999; Brose et al., 2006; Barnes et al., 2008; Jennings, 2010). En conséquence, les organismes appartenant à des espèces massives ont des niveaux trophiques élevés mais variables en fonction du stade de développement (Pimm and Rice, 1987; Rice, 1995). Aussi, le cannibalisme est un phénomène largement observé dans les réseaux trophiques marins (Claessen et al., 2000) et deux

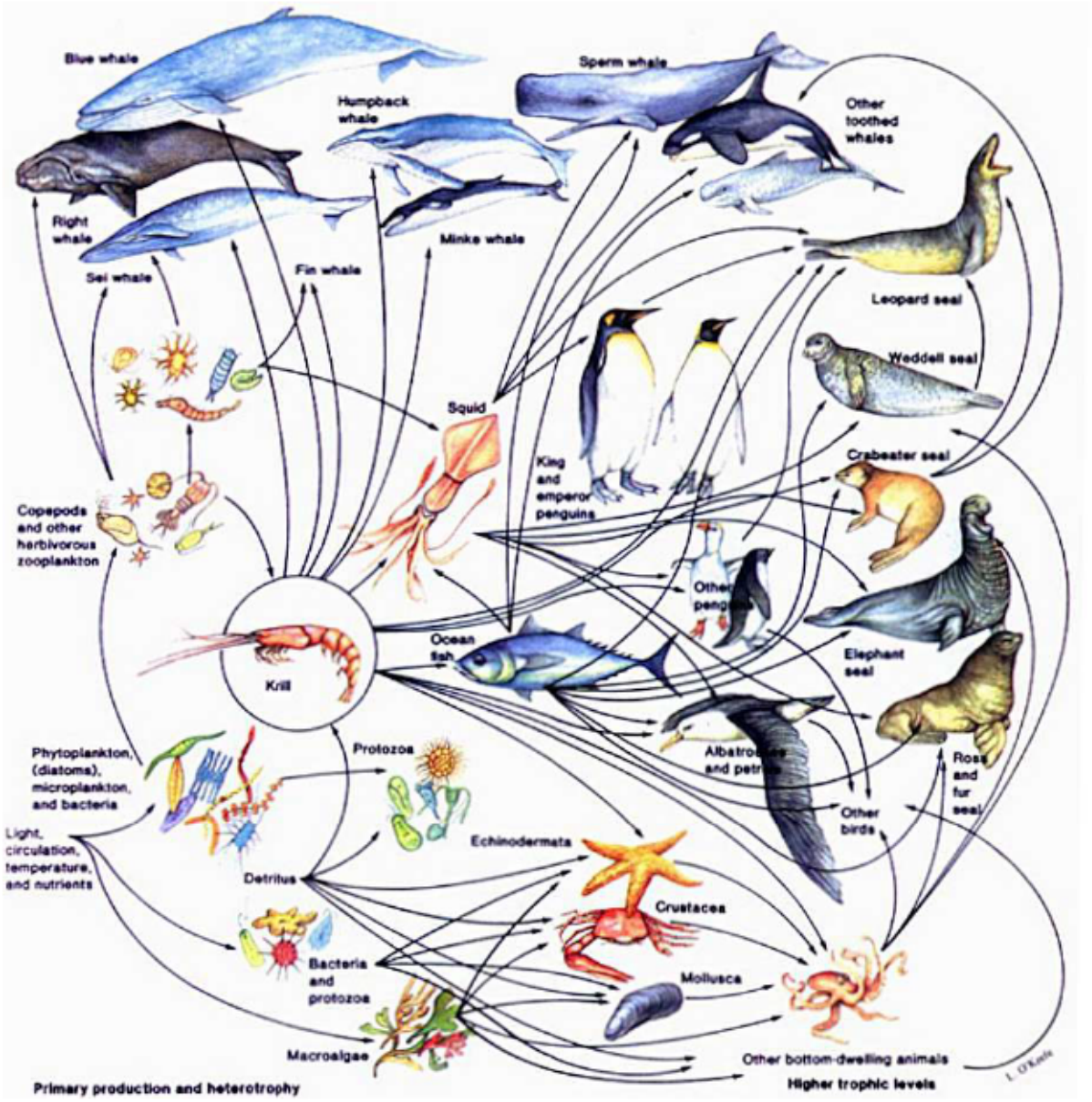

Figure 1.3: Schéma simplifié du réseau trophique antarctique – *La diversité des niveaux trophiques intermédiaires y est largement sous-représentée, en particulier celle du micronecton (représenté par un céphalopode et un thon – ce dernier étant plutôt à considérer comme un prédateur supérieur). Cette figure insiste sur l'importance du krill (Euphausia superba) dans l'écosystème antarctique, une vision à relativiser compte tenu de la mise en évidence d'un second chemin trophique majeur (Flores et al., 2008, 2011; David et al., 2016) impliquant le micronecton, et notamment les myctophidés. Crédit : L. O'Keefe.*

espèces peuvent être mutuellement proies et prédateurs l'une de l'autre en fonction de leur stade de développement (Stokes, 1992). La masse des organismes marins s'étend, du phytoplancton aux grands requins, sur plus de 20 ordres de grandeur (Barnes et al., 2010). En conséquence, comparés au milieu terrestre, les réseaux trophiques marins forment, pour reprendre l'image du vocabulaire courant, des chaines alimentaires plus longues (Hairston, 1993) et cela malgré une productivité globale plus faible (Hairston, 1993) : en moyenne 4–4.67 niveaux trophiques (Pauly and Christensen, 1995; Jake Vander Zanden and Fetzer, 2007).

De nombreux travaux se sont intéressés aux mécanismes de régulation des réseaux trophiques pour comprendre quels rôles jouent la structure d'un réseau et les différents groupes d'organismes dans la productivité, la stabilité et la résilience d'un écosystème. Les réseaux trophiques marins sont classés en trois catégories en fonction du niveau trophique des organismes dont l'abondance exerce le plus d'influence sur celle des autres niveaux : régulation par le bas (**"Bottom-Up"**) ou par le haut (**"Top-Down"**) et régulation taille de guêpe (**"Wasp-Waist"**) (Cury et al., 2003). Le premier type de contrôle, "Bottom-Up", correspond aux situations où les nutriments et/ou la production primaire sont les facteurs limitant l'abondance des niveaux trophiques supérieurs. Il s'agirait du cas de figure le plus courant (Micheli, 1999). Le contrôle "Top-Down" correspond à la situation inverse où quelques espèces de niveaux trophiques élevés exercent un fort effet sur l'abondance des niveaux trophiques inférieurs. Ce contrôle se transmet alors "en cascade" des intermédiaires à leurs proies ce qui conduit à l'alternance de fortes et de faibles biomasses le long d'une **cascade trophique**. Enfin, les niveaux trophiques intermédiaires peuvent exercer à la fois un contrôle "Top-Down" sur les niveaux trophiques inférieurs et un contrôle "Bottom-Up" sur les niveaux trophiques supérieurs, cette situation concernant surtout les zones de remontée d'eaux profondes ("Upwelling") (Cury et al., 2003).

Les connaissances acquises sur la distribution du phytoplancton, couplées au contrôle de type "Bottom-Up" prédominant, encourage à essayer d'inférer la distribution spatiale des organismes de niveaux trophiques intermédiaires et supérieurs à partir de celle de la production primaire. Rappelons que les espèces sont soumises à des niveaux de contraintes différents vis à vis de leur environnement. Par exemple, les ectothermes, comme la plupart des poissons, seront plus sensibles à la température ambiante que les endothermes tels que les mammifères marins et certains poissons (thons, espadons ou requins) mais ces derniers ont en revanche une demande éner-

gétique plus élevée. En moyenne, plus grande est la taille d'un organisme, outre un niveau trophique généralement plus élevé, meilleures seront ses capacités natatoires. Par conséquent, l'importance relative du comportement par rapport à l'environnement se trouve renforcée. L'augmentation de la taille s'accompagne aussi d'une complexification des trajectoires d'histoire de vie (deYoung et al., 2004) : les capacités de mémorisation et l'espérance de vie augmentant de pair. Le comportement a donc, non seulement un rôle plus important, mais il est également plus complexe. Enfin, le décalage temporel nécessaire à l'assimilation de l'énergie depuis la production primaire jusqu'à l'organisme d'intérêt croit également. L'ensemble de ces facteurs combinés rend plus difficile qu'espérée la tâche de prédire la distribution des organismes selon une approche "Bottom-Up". Néanmoins, comme pour le plancton, l'association entre necton et les structures méso-échelles et/ou sub-méso-échelles a été souvent constatée : chez les poissons (Bakun, 2006; Sabarros et al., 2009; Godø et al., 2012), les céphalopodes (Waluda et al., 2001), les mammifères et oiseaux marins (Nel et al., 2001; Bailleul et al., 2010b; Cotté et al., 2011, 2015) ou encore les tortues (Polovina et al., 2006). Les mécanismes impliqués dans ce phénomène restent cependant encore mal connus.

1.2.2 Hétérogénéité des connaissances sur milieu pélagique

Si dans l'ensemble les écosystèmes pélagiques sont mieux connus que les écosystèmes côtiers de la zone intertidale (Mann et al., 2005), il existe de fortes disparités dans l'état des connaissances pour les différents niveaux trophiques constituant les écosystèmes pélagiques (deYoung et al., 2004; Tyler et al., 2011). En effet, production primaire et prédateurs supérieurs bénéficient de la collecte d'un plus grand volume de données et de davantage d'études que les niveaux trophiques intermédiaires (figure 1.4).

Production primaire et consommateurs primaires

De précieuses données concernant l'abondance et la distribution du phytoplancton peuvent être récoltées dans les zones non couvertes de nuages, par des techniques d'imageries (Clarke et al., 1970). Il s'agit d'estimer un *indice* d'abondance de la production primaire (la concentration en chlorophylle *a* dans les premiers mètres sous la surface) mais dont l'erreur d'observation est relativement faible (environ 5% (Bailey and Werdell, 2006)). Depuis le premier capteur mesurant la couleur de l'eau, le CZCS (Nimbus-7, opérationnel en 1978, USA), les techniques de télédétection sont en pro-

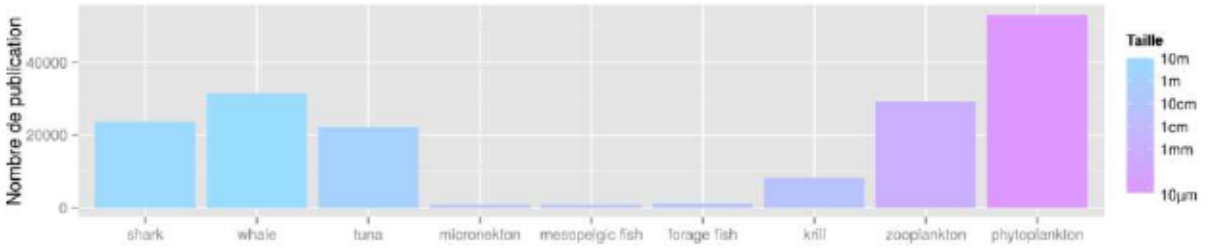

Figure 1.4: Nombre de publications en fonction de la taille des organismes – *Nombre de résultats disponibles sur sciencedirect.com par mot clé, rangé en fonction de la taille des organismes qui fournit une indication du niveau trophique. Les niveaux trophiques intermédiaires apparaissent défavorisés. Figure tirée de Conchon (2016).*

grès constants. Ce capteur avait une résolution spatiale de 825 m, 6 bandes spectrales et une largeur de bande d'observation ("swath") de 1566 km. Les capteurs de dernière génération tels que le OLCI (Sentinel-3, 2013, Europe) ou le SGLI (GCOM-C, 2014, Japon) ont des résolutions de 250–300 m, 19-21 bandes spectrales et des largeurs de bande d'observation 1270–1400 km. Avec l'augmentation du nombre de bandes spectrales il est aussi possible de dériver des informations sur le type phytoplanctonique (Alvain et al., 2008). L'imagerie satellite permet d'échantillonner des données sur la quasi-totalité de la surface de la planète (90% (McClain, 2009)) et cela plusieurs fois par jour ("seulement" 14 fois car les observations photographiques en lumière visible imposent des orbites héliosynchrones). Les observations concernant le phytoplancton, bien que limitées à la superficie des océans, sont donc abondantes tant dans l'espace que dans le temps. Les organismes planctoniques, possédant des capacités de déplacement actif plus réduites, sont fortement soumis aux contraintes abiotiques. Ainsi les techniques de simulation numérique ont pu aboutir à une compréhension détaillée des mécanismes qui régissent leur distribution (Abraham, 1998; Volker et al., 2002; Lévy, 2003; Martin, 2003; d'Ovidio et al., 2010; Lévy et al., 2012; Lévy et al., 2012). Enfin, la production primaire, constituant la base du réseau trophique, est souvent une ressource limitante de la productivité de l'écosystème (Micheli, 1999; Frederiksen et al., 2006). Ces facteurs lui valent un large intérêt de la part de la communauté scientifique. En conséquence, zooplancton et surtout phytoplancton figurent parmi les ressources les plus étudiées et les mieux connues (figure 1.4).

Prédateurs supérieurs

Dans le milieu marin, les prédateurs supérieurs ont généralement un plus fort intérêt économique (Pauly et al., 1998; Christensen et al., 2003; Reynolds et al., 2005; Shephard et al., 2012) et/ou patrimonial (Tyler et al., 2011) que les taxons de taille et niveau trophique inférieurs ce qui facilite et motive la recherche et l'acquisition de données les concernant. Étant donné leur position au "sommet" du réseau trophique, ils intègrent l'effet des perturbations sur l'ensemble du réseau et sont souvent considérés comme régulateurs des écosystèmes (Cury et al., 2003; Sala, 2006; Heithaus et al., 2008; Estes et al., 2011). Ces caractéristiques en font des modèles d'études prisés en écotoxicologie (phénomène de bio-accumulation) et, plus généralement, pour la **bio-indication** des changements affectant les écosystèmes (Sergio et al., 2008).

Par exemple, dans le cas de la Directive Cadre Stratégie sur le Milieu Marin (DCSMM) des prédateurs supérieurs sont utilisés comme indicateurs biologiques pour juger de l'état des écosystèmes du fait de leur niveau trophique élevé. L'approche heuristique employée dans la DCSMM pour mesurer l'état général des réseaux trophiques marins consiste à évaluer la prospérité démographique (productivité et biomasse, indicateurs 4.1.1 et 4.2.1) de ces animaux (Rombouts et al., 2013). Cependant, il convient de rappeler qu'en matière de bio-indication il existe un compromis entre la fiabilité d'un indicateur et l'état préalable des connaissances sur l'écologie et sur l'histoire de l'écosystème étudié. En effet, ces connaissances doivent permettre de pouvoir identifier avec certitude les causes des variations mesurées de l'indicateur. Dans cet exemple, la pollution, la dégradation de l'habitat du prédateur, la mortalité par pêche ou par prédation ou les potentiels changements de régime alimentaire sont autant de facteurs externes qui peuvent affecter les indicateurs de la DCSMM et, par conséquent, doivent être documentés. Aux enjeux économiques (qui concernent les espèces exploitées) et aux enjeux de conservation (qui concernent les espèces "charismatiques"), peuvent s'ajouter des enjeux de recherches sur les prédateurs supérieurs qui concernent la gestion de nombreuses autres espèces (gestion écosystémique).

En raison de leur grande taille, il devient possible d'équiper les prédateurs supérieurs d'enregistreurs électroniques capables de collecter des informations précises sur leur environnement et leur activité. Le développement technologique dans les secteurs de l'industrie informatique et de la téléphonie mobile à largement profité à la création et à l'amélioration de tels d'enregistreurs (Ropert-Coudert and Wilson, 2005). Ces améliorations concernent la diminution de la taille et du prix de tels appareils

mais également l'amélioration de leurs performances : variété, précision et fréquence d'échantillonnage des capteurs, nombre de capteur embarqués, capacité de stockage de données et autonomie de la batterie. Selon la méthode de récupération des données (i) relayées en temps réel par des antennes ou satellites (ii) par récupération physique de la carte mémoire de l'appareil, on parle respectivement de **télémétrie** ou de **bio-logging**. Le choix de la méthode dépend de la résolution spatio-temporelle des données que l'on souhaite obtenir (bien supérieure dans le cas du bio-logging) et du niveau de difficulté que pose la récupération physique des appareils (généralement très élevé). Ces techniques permettent d'observer l'environnement naturel des animaux et leur comportement au sein de cet environnent dans de nombreux cas où l'observation directe "naturaliste" serait impossible. Cela est particulièrement vrai dans le milieu marin et pour l'observation du comportement de plongée, domaines dans lesquels bio-logging et télémétrie se sont rapidement développés (Boehlert et al., 2001; Ropert-Coudert and Wilson, 2005). Qu'il s'agisse de données de télémétrie ou de bio-logging, un large volume de données collectées par les prédateurs supérieurs est aujourd'hui disponible (exemple dans l'océan Pacifique : figure 1.5).

Niveaux trophiques intermédiaires

Les niveaux trophiques intermédiaires assurent le lien entre les deux extrêmes de la chaine alimentaire dont nous venons de parler. Ce sont des éléments importants du réseau trophique : outre leur éventuel rôle de régulateurs du réseau trophique (Cury et al., 2003), ils sont des consommateurs majeurs de la production primaire (Huntley et al., 1991; Kozlov, 1995). Dans le cadre de cette thèse, nous nous intéresserons au **micronecton** pélagique. On désigne sous ce terme les organismes ("micro" :) de petite taille (entre 1 et 20 cm de long (Kloser et al., 2009; Ménard et al., 2007)) mais ("necton" :) doués d'une capacité à nager à l'encontre des courants (Brodeur and Yamamura, 2005). Cette appellation regroupe des organismes taxonomiquement variés mais principalement de petits poissons qui constituent les proies de nombreux prédateurs (Sabourenkov, 1991). Certains organismes gélatineux et les céphalopodes font également partie du micronecton.

Les organismes micronectoniques peuvent se distribuer selon une large gamme de profondeur (de 0 à 1000 m) et nombre d'entre eux réalisent des **migrations nycthémérales** (Roe, 1974; Watanabe et al., 1999; Pearre, 2003; Watanabe et al., 2006a). En réalisant ces migrations verticales de quelques centaines de mètres rythmées par le

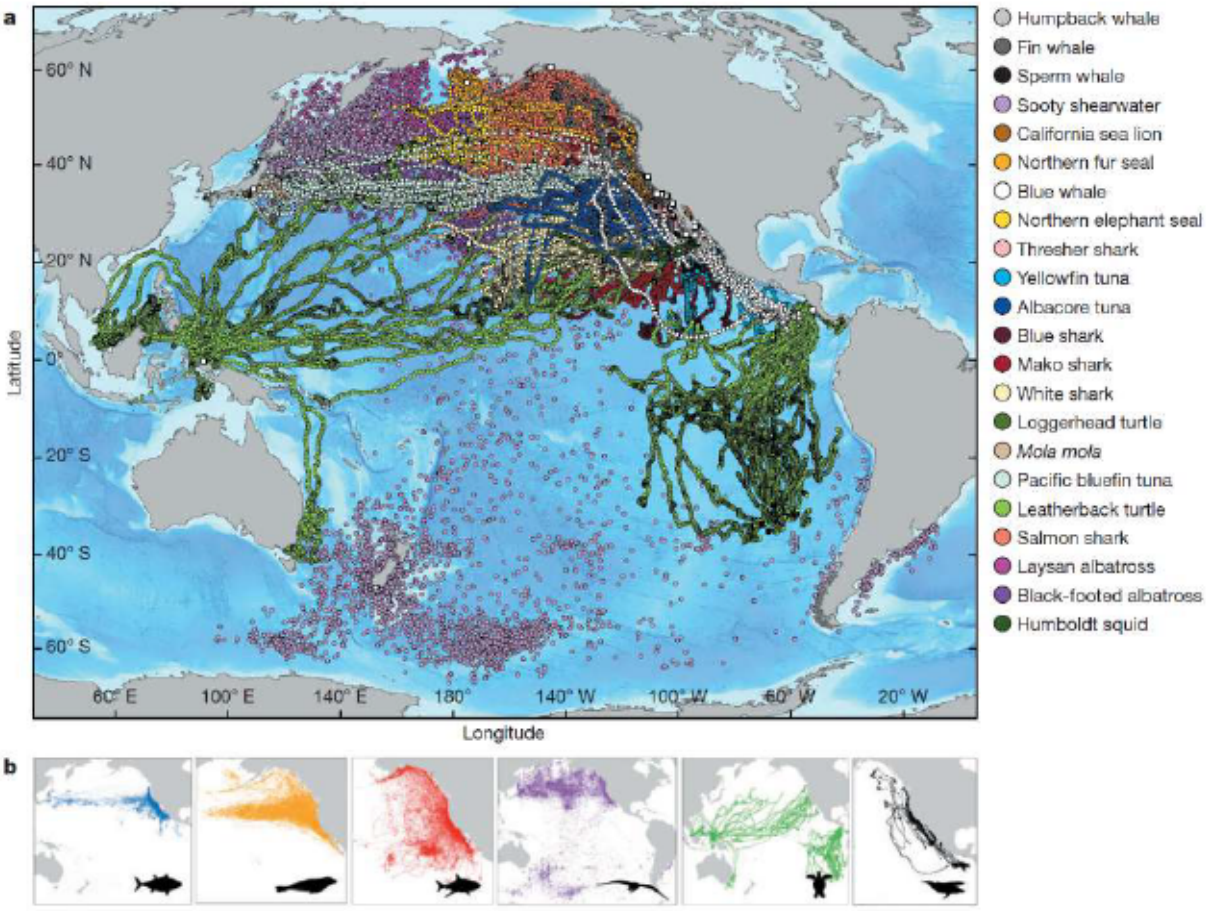

Figure 1.5: Localisations de prédateurs supérieurs collectées dans l'océan pacifique – *Données collectées dans le cadre du programme "Tagging of Pacific Predators" (TOPP). (a) positions moyennes journalières des différentes espèces (◯) et lieux de déploiement (□). (b) positions moyennes journalières pour les principaux groupes d'espèces (thons, pinnipèdes, requins, oiseaux, tortues, cétacés). Une large quantité de données semblables dans le monde entier est disponible sur le portail Movebank. Figure tirée de Block et al. (2011)*

cycle du jour et de la nuit ("diel vertical migration", figure 1.2), le micronecton assure ainsi un rôle écologique essentiel (Longhurst et al., 1990; Pakhomov et al., 1996; Zhang and Dam, 1997; Hays, 2003; Flores et al., 2008; Bianchi et al., 2013) : la **pompe biologique**. Ce rôle consiste à transférer vers les profondeurs de l'océan le carbone inorganique assimilé en surface par photosynthèse.

Cependant, comme en témoigne la figure 1.4, le micronecton est assez mal connu (Handegard et al., 2013) et en particulier les invertébrés (Tyler et al., 2011). Le déficit de connaissances concernant le micronecton s'explique en partie par la difficulté que pose leur échantillonnage. En effet, l'échantillonnage du micronecton est couteux et

souffre de biais (Pakhomov et al., 2010) (voir sous-section 1.3.1). Ces organismes sont généralement inconnus du grand public et ont, sauf dans certains cas d'abondance exceptionnelle (e.g. anchois du Pérou, *Engraulis ringens*), peu d'intérêt économique. Dans l'océan Austral, du fait de l'isolement géographique de cette région, ces phénomènes se trouvent renforcés. **Quels moyens existent-ils pour combler les lacunes dans les connaissances de la distribution et/ou l'écologie de ces niveaux trophiques intermédiaires dans l'océan Austral ?**

1.3 Moyens d'investigation de l'écologie des niveaux trophiques intermédiaires

1.3.1 Moyens conventionnels

Chalutage

Le chalutage est la méthode d'échantillonnage traditionnelle du micronecton pélagique. Un filet de forme évasée est remorqué en pleine eau par un bateau pour collecter les organismes dans son extrémité (le "cul de chalut"). Il est ainsi possible de remonter à la surface des échantillons afin d'identifier taxonomiquement les organismes et déterminer leur biomasse et la distribution de leur taille, autant d'informations d'importance capitale sur l'écologie de base du micronecton. La fiabilité de la caractérisation taxonomique des échantillons est l'avantage majeur de cette méthode. Le chalutage réalise des mesures de nature ponctuelle : le chalut cible une certaine gamme de profondeur dans une zone donnée.

Le premier travers de cette méthode est son coût financier ou logistique important (Ariza et al., 2015). Le micronecton est trop petit pour être capturé avec les chaluts de pêche commerciale et trop mobile pour l'être avec les filets planctoniques (Brodeur and Yamamura, 2005). Il faut donc mobiliser un navire, du matériel de pêche et des opérateurs compétents spécifiquement dédiés à l'échantillonnage du micronecton. Par ailleurs, le chalutage pélagique du micronecton pose de nombreux problèmes d'échantillonnage (Pakhomov et al., 2010). En effet, l'aptitude des différents organismes à éviter le filet crée des biais d'échantillonnage qui posent problème dans l'estimation de leur abondance totale et relative (Pearcy, 1983; Kaartvedt et al., 2012). Les difficultés posées par ce phénomène sont suffisamment importantes pour qu'une "Avoidance Theory" (Barkley, 1964, 1972) se soit développée en réponse. La conta-

mination des échantillons lors de la remontée du chalut introduit aussi du bruit et rend difficile la détermination de la limite profonde de la distribution des différentes espèce. Cependant, il existe des chaluts équipés de dispositif d'ouverture/fermeture des filets programmables ou commandables qui permettent de limiter cette contamination (Pearcy, 1983). La précision que l'on peut attendre de l'échantillonnage par chalutage dépend du morcellement de la distribution ("patchiness") du micronecton (Wiebe, 1971), un facteur pouvant varier selon l'heure du jour, la saison ou le stade de développement des organismes (Pearcy, 1983). Enfin, une dernière limitation de cette méthode concerne l'échelle spatio-temporelle de l'échantillonnage qui est limité aux moyennes et larges échelles. En effet, la manipulation du chalut (remontée/récupération de l'échantillon/mise à l'eau) requiert du temps. De plus, afin d'être certain de collecter un échantillon de taille assez conséquente, le chalut doit demeurer un minimum de temps en profondeur. En pratique il est donc difficile d'échantillonner à des échelles inférieures à 500 m dans l'espace et 30 minutes dans le temps.

Acoustique active

L'acoustique active, permet aussi d'échantillonner le micronecton. Le coût de cette méthode est équivalent au chalutage en terme de matériel ; si elle requiert aussi le recours d'un navire, sa mise en place sur le long terme est plus simple car elle nécessite moins d'opérateurs de terrain. Cette technique se base sur le temps du parcours des ondes *sonores* ("acoustique") *émises* par un appareil embarqué ("active") puis réfléchies au contact de matériaux dont la densité diffère de celle du milieu de propagation. L'acoustique active permet donc de sonder la colonne d'eau à la recherche d'organismes présentant un écart de densité avec l'eau de mer. Par rapport au chalutage, cette technique présente l'avantage de fournir des données *en continu* et donc avec une haute fréquence d'échantillonnage. Contrairement au chalutage, la biomasse est estimée plutôt que mesurée mais cette estimation est généralement considérée comme plus précises qu'avec cette première technique (Catul et al., 2010).

Cependant l'identification taxonomique du micronecton est difficile car seul un indice de réflexion des ondes sonores est disponible pour décrire les organismes. Cependant, cet indice peut être enrichi par d'autres en utilisant plusieurs fréquences d'ondes sonores. Dans ce cas il devient possible de décrire la "couleur acoustique" des sources réfléchissantes (Logerwell and Wilson, 2004). La force de la réflexion et la couleur acoustique peuvent renseigner sur certaines caractéristiques biologiques

des organismes détectés (e.g. classe de taille ou présence de vessie natatoire) ce qui peut permettre leur identification taxonomique assez grossière (généralement au niveau de la famille ou du genre) (Benoit-Bird, 2006). On comprend que cette tache nécessite d'avoir au préalable des informations sur les propriétés réfléchissantes des organismes échantillonnés. En conséquence, afin de tirer le plus grand parti des données acoustiques, il est souhaitable de réaliser en parallèle un échantillonnage par chalut (O'Driscoll et al., 2002).

Enfin, il existe un compromis entre la portée du signal acoustique et sa résolution. Plus la fréquence de l'onde acoustique sera élevée plus petite pourra être la taille des organismes détectés mais plus faible sera la portée des ondes dans la colonne d'eau.

1.3.2 Les prédateurs supérieurs, sentinelles des océans

Bio-acquisition et bio-indication

Nous avons évoqué la notion de bio-acquisition de données grâce à des prédateurs supérieurs instrumentés d'enregistreurs électroniques. À ce jour, ces enregistreurs (aussi appelés "loggers" ou "tags") peuvent être dotés de capteurs très variés (par exemple mesurant profondeur, température, intensité lumineuse, salinité, concentration en oxygène, fluorescence, environnement acoustique, accélération, champ magnétique terrestre, trajectoire de l'animal, vitesse de nage de l'animal, rythme cardiaque de l'animal, etc...) ouvrant la voie à de nombreux questionnements biologiques et/ou océanographiques. Concernant l'échantillonnage du micronecton une avancée importante dans le domaine du bio-logging a été franchie avec la détection des *évènements de tentatives de capture de proies* à partir des données d'accélération (Naito, 2007).

La collection de données *via* les prédateurs supérieurs peut présenter plusieurs avantages par rapport aux moyens conventionnels. D'abord le prix, car le coût associé à l'utilisation d'un navire scientifique est très élevé. Ensuite, la flexibilité des animaux. En effet, ceux-ci sont capables d'évoluer sans difficulté là où des moyens conventionnels seraient inopérants. Ainsi, les éléphants de mer pourront fournir des données dans les zones riches en glace de mer ou les régions de plateaux continentaux (où la bathymétrie est faible) quand cela pose problème aux profileurs ARGO (Roquet et al., 2009, 2014) et jusqu'à 2000 m de profondeurs (McIntyre et al., 2010) quand l'acoustique active est limitée à 300 m. Les prédateurs échantillonnent *conjointement* leur environnement biologique et physique et leur contribution dans ce domaine est

(i) loin d'être négligeable (Boehme et al., 2009; Roquet et al., 2009; Fedak, 2013; Roquet et al., 2014) et (ii) complémentaire des moyens d'échantillonnages traditionnels (figure 1.6). Ainsi, en 2013, plus de 80% des données océanographiques collectées aux latitudes sud inférieures à 60°S l'ont été par des prédateurs supérieurs (Fedak, 2013, voir aussi la figure 1.6).

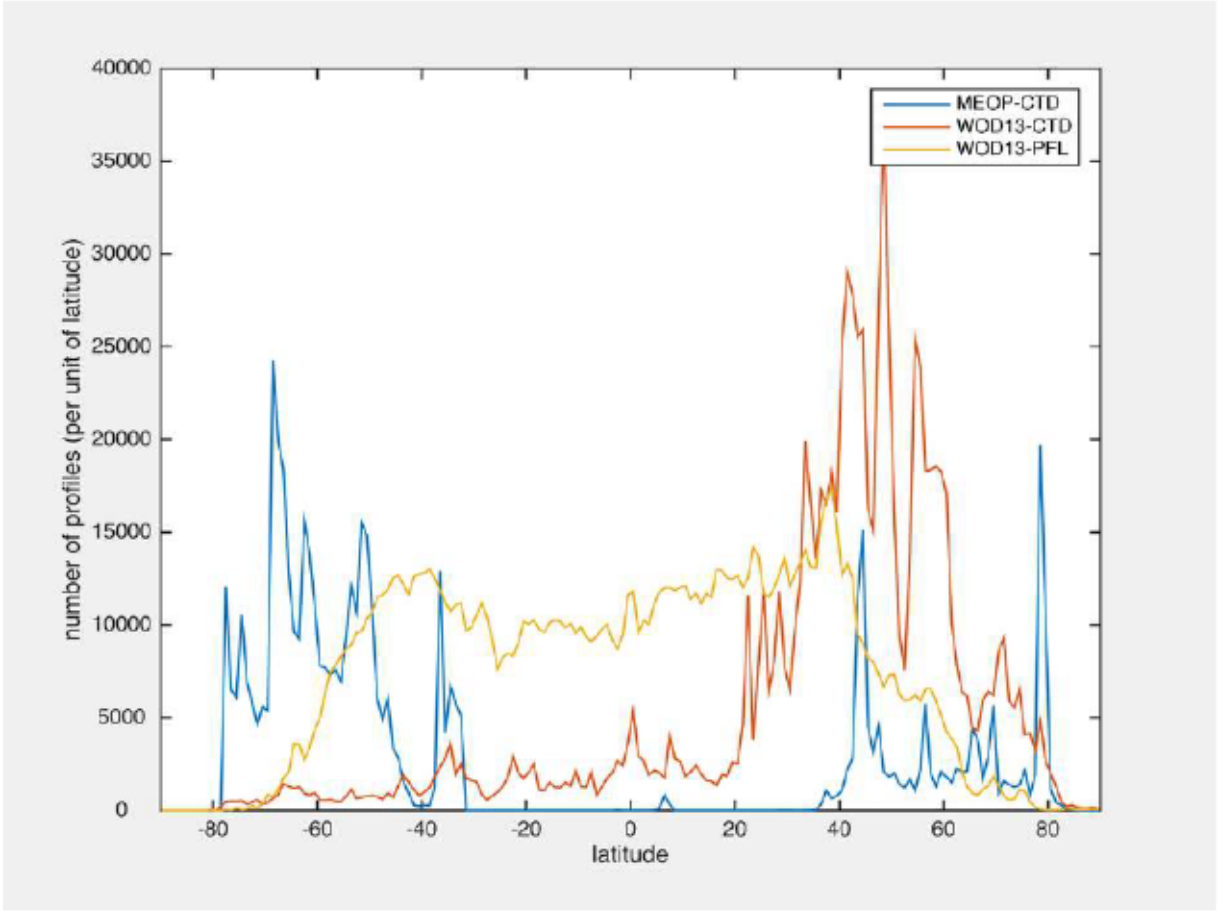

Figure 1.6: Sources des données océanographiques en fonction de la latitude – *MEOP-CTD : données collectées par des mammifères marins (disponibles sur le portail "Marine Mammal Exploring the Oceans Pole to Pole" – MEOP). WOD13-CTD/WOD13-PFL : données d'origine conventionnelle (disponible dans "World Ocean Database" – Levitus et al. (2013, WOD13)) : l'acronyme CTD désigne les données collectées par les navires océanographiques, l'acronyme PFL désigne les données de issues de dispositifs flottants tels que les profileurs ARGO (Gould et al., 2004). Crédit : Fabien Roquet.*

Une caractéristique fondamentale du bio-logging est l'adoption du point de vue de l'animal. L'échantillonnage des données est tributaire de leur comportement. Les données comportent donc des biais d'échantillonnage, mais ceux-ci sont porteurs d'informations sur les lieux, les périodes et les échelles pertinentes pour comprendre leur écologie (Fedak, 2004). Les loggers n'enregistrent pas seulement les paramètres physiques mais aussi, *de façon concomitante*, des informations sur le comportement des animaux lesquelles peuvent servir à étudier leur écologie ou celle de leur proies. Ainsi, la compréhension du comportement de "dérive passive" chez l'éléphant de mer (Crocker et al., 1997; Mitani et al., 2010) a rendu possible le suivi de la condition corporelle des prédateurs durant leurs voyages alimentaires et, par la suite, la révélation de la nature des habitats de pêche favorables à ces prédateurs (Biuw et al., 2007; Bailleul et al., 2007b). Plus généralement, l'usage du comportement à des fins de bio-indication s'appuie sur la **théorie de l'approvisionnement optimal** ("optimal foraging theory").

Théorie de l'approvisionnement optimal

Dans un environnement aux ressources alimentaires limitées et inégalement réparties (Fauchald, 1999; Charnov, 1976), les individus ayant adopté les **stratégies d'approvisionnement**, c'est à dire un ensemble de décisions afin de s'alimenter, les plus efficaces seront favorisés par la sélection naturelle (MacArthur and Pianka, 1966; Pyke, 1984). Les stratégies d'approvisionnement les plus pertinentes dans un environnement donné aboutissent à une amélioration de la **valeur sélective** ("fitness") et sont donc amenées à se propager dans la population.

La théorie de l'approvisionnement optimal (MacArthur and Pianka, 1966; Pyke, 1984) postule que les animaux ont adapté leur comportement de façon à apporter une **solution optimale** au problème de l'approvisionnement. Dans ce contexte, le problème de l'approvisionnement peut être abordé à la manière des sciences économiques. Ainsi, une stratégie optimale d'approvisionnement permettrait de maximiser une devise ("currency"), le taux d'acquisition net d'énergie à long terme (Schoener, 1971; Charnov, 1976). Il convient de rappeler qu'un tel postulat d'optimalité est une hypothèse plutôt qu'une certitude (MacArthur and Pianka, 1966; Pierce and Ollason, 1987), néanmoins, cette approche offre un cadre conceptuel permettant la comparaison quantitative de stratégies d'approvisionnement et la réalisation de prédictions sur le comportement des animaux en fonction de leur environnement. Autrement dit, la

théorie de l'approvisionnement optimal offre un cadre conceptuel pour interpréter le comportement animal.

Application à l'écologie des proies

La gamme des comportements pouvant influencer le succès de l'alimentation est extrêmement variée : choix du type de proie (MacArthur and Pianka, 1966), de la stratégie d'évitement de la compétition et de la prédation (Brown, 1988), de la zone d'alimentation (Stephens and Krebs, 1986), de la tactique de chasse et de déplacement (Houston and Carbone, 1992; Hedenstrom and Alerstam, 1995; Williams et al., 2000). Les travaux développés dans cette thèse se rattachent aux deux derniers aspects qui font intervenir les relations entre les mouvements des prédateurs et la distribution/l'écologie des proies.

La distribution des proies et celle de leurs prédateurs sont nécessairement liées. Les prédateurs sont à la recherche de zones riches en proies tandis que ces dernières ont intérêt à éviter leur prédateurs (Sih, 2005). La corrélation spatiale entre les distributions de ces deux groupes résulte donc d'un équilibre entre leur réponses mutuelles : dans le cas d'un prédateur très mobile par rapport à ses proies, on s'attend à observer une corrélation positive (Sih, 1984). Dans la mesure où ils dépendent pour leur alimentation de zones où les proies peuvent être capturées efficacement, l'observation des prédateurs tels que les oiseaux marins peut être utilisée pour inférer la position de zones riches en organismes de niveaux trophiques intermédiaires (Ainley and DeMaster, 1990). Ainsi l'observation des oiseaux marins est depuis longtemps utilisée par les pêcheurs afin de repérer à grande distance d'éventuels bancs de poissons pélagiques (Bost et al., 2008). Cette même propriété est utilisée par les oiseaux eux-même pour améliorer leur efficacité de recherche alimentaire, phénomène connu sous le nom de "local enhancement" (Fauchald, 2009).

Le développement récent du bio-logging offre la possibilité d'obtenir des informations détaillées sur les mouvements d'une vaste gamme de prédateurs, y compris de prédateurs plongeurs dont l'observation nous serait impossible autrement. La théorie de l'approvisionnement optimal offre des outils conceptuels pour interpréter ces informations. Par exemple, l'analyse du temps passé par secteur des prédateurs via l'identification de périodes de Recherche en Zone Restreinte ("Area-Restricted Search", Kareiva and Odell (1987); Fauchald and Tveraa (2003)), a permis de mettre en évidence que certaines structures méso-échelles (fronts et les tourbillons) sont des habitats de

pêche favorables aux prédateurs supérieurs (Bailleul et al., 2010b; Cotté et al., 2011, 2015).

Dans ces différents exemples, les données de bio-logging collectées par les prédateurs supérieurs sont un moyen de décrire et de comprendre la dynamique spatio-temporelle de la distribution des niveaux trophiques intermédiaires.

1.3.3 Modélisation

Que se soit à des fins d'exploitation ou de conservation des ressources naturelles, il existe un besoin d'outils permettant de prédire la dynamique spatio-temporelle de ces ressources. La prise de conscience de la nécessité d'une approche écosystémique de la gestion des ressources (Larkin, 1996; Davis et al., 1998) impose de s'intéresser à l'ensemble des organismes constituant les écosystèmes, et donc notamment aux niveaux trophiques intermédiaires. Des outils capables de prédire la dynamique spatio-temporelle des organismes permettraient dans une certaine mesure de pallier à la disparité des données et d'anticiper la réponse des écosystèmes face à des changements environnementaux (naturels ou antropogéniques).

De tels outils pourraient certes permettre de prendre dans le futur des décisions de gestion éclairées mais ils présentent dans l'immédiat un deuxième intérêt majeur d'ordre plus théorique. En effet, la conception d'un modèle écosystémique – la formalisation mathématique – impose des simplifications qui se révèlent être l'occasion de faire une synthèse explicite de nombreux travaux de recherche. La modélisation peut ainsi permettre **de résumer et d'organiser** les connaissances. En outre, l'aptitude des prédictions d'un modèle à décrire la réalité des observations permet **d'accréditer** les conceptions sur le fonctionnement d'un écosystème sur lesquelles repose la formalisation du modèle ou de **générer des hypothèses** quant aux processus écologiques encore insuffisamment compris. La modélisation constitue donc un moyen d'investigation, souvent complémentaire de l'échantillonnage, mais il est à noter qu'elle peut aussi être le seul dans le cas d'expériences à grande échelle qui seraient trop couteuses ou impossibles.

Les modèles bio-chimiques et physiques, d'ores et déjà bien développés en océanographie, appellent à être étendus aux réseaux trophiques. Cependant, le couplage des modèles bio-chimiques et physiques avec la dynamique des réseaux trophiques se heurte à des problèmes inhérents à l'écologie des niveaux trophiques intermédiaires et supérieurs que nous avons déjà évoqués (sous-section 1.2.1). En réponse à ce pro-

blème, deYoung et al. (2004) suggèrent d'adopter une approche "rhomboïdale" de la modélisation qui consiste à apporter progressivement de la complexité à la formalisation des processus écologiques en raison de leur proximité/pertinence vis a vis du problème écologique ou des organismes au centre de l'intérêt.
Conformément à ce principe, de nombreux modèles simulant la dynamique spatio-temporelle des réseaux trophiques ont été développés. Certains se concentrent par exemple sur la dynamique du *zooplancton* (modèles "Nutrients – Phytoplankton – Zooplankton – Detritus" ou NPZD) d'autres tel Ecopath[1] (Polovina, 1984; Christensen and Pauly, 1992) sont flexibles quant au groupe d'organismes cible et se concentrent sur la *cohérence du flux de biomasse* dans le réseau trophique. OSMOSE (Object-oriented Simulator of Marine biOdiverSity Exploitation, Shin and Cury (1999, 2001)) est un autre modèle qui s'intéresse aux flux de biomasse dans le réseau trophique adoptant une *conception opportuniste des relations trophiques* (basée sur la taille et la co-occurence spatio-temporelle, contrairement à Ecopath où elles sont plutôt basées sur la taxonomie).
La difficulté commune à tous les modèles écosystémiques est leur **validation** qui nécessite de gros volumes de données (Plagányi and Butterworth, 2004; Shin et al., 2004). Compte tenu des difficultés particulières à l'océan Austral en termes d'échantillonnage (sous-sous-section 1.2.2), les données de bio-logging collectées par les prédateurs supérieurs représentent là encore une opportunité. C'est dans ce contexte que, dans cette thèse, nous nous intéresserons au modèle SEAPODYM (Spatial Ecosystem and Population Dynamics Model) et plus précisément à sa partie dédiée au niveaux trophiques intermédiaires[2].

1.4 Objectifs et structure de la thèse

1.4.1 Problématique et objectifs généraux

Les écosystèmes pélagiques sont le siège d'interactions nombreuses et complexes entre les organismes vivants et les conditions physico-chimiques de cet environnement. Le jeu de ces interactions, fonction des différentes contraintes affectant les espèces (voir "niche écologique", sous-section 1.1.3) aux différentes échelles spatio-temporelles (figure 1.2) aboutit à une distribution des ressources marines organisée

[1] Ecopath a été par la suite enrichi de façon à pouvoir simuler les dynamiques temporelle et spatiale (Ecosim & Ecospace, Pauly et al. (2000); Christensen and Walters (2004)).
[2] le modèle SEAPODYM micronecton dont une description détaillée sera donnée au chapitre 6.

en une mosaïque de parcelles emboitées dynamique. La compréhension de cette distribution et des phénomènes sous-jacents est encore largement incomplète, en particulier concernant les niveaux trophiques intermédiaires (sous-section 1.2.2) et tout particulièrement dans l'océan Austral. En effet, l'acquisition de données sur l'écologie des niveaux trophiques intermédiaires se heurte à des difficultés techniques et logistiques du fait de l'isolement géographique de cette région. Or, dans le même temps, l'essor du bio-logging fait émerger la collecte de données via les prédateurs supérieurs comme un moyen efficace de pallier à ce problème afin de compléter les connaissances de l'hydrographie de cette région (sous-section 1.3.2). Un large volume de données collectées par les prédateurs supérieurs, l'éléphant de mer austral au premier rang (McIntyre, 2014), est ainsi disponible à l'heure actuelle. Mais au-delà de l'utilité de ces données en termes d'océanographie, de nombreuses questions écologiques peuvent être abordées à travers l'analyse des informations sur le comportement des animaux contenues dans ces données (sous-section 1.3.2).

Dans ce travail de thèse nous nous sommes demandés quelles connaissances sur les niveaux trophiques inférieurs, particulièrement sur leur distribution mais plus généralement sur leur écologie, pouvaient apporter les données issues de l'instrumentation d'un prédateur supérieur, l'éléphant de mer austral.

Les travaux développés dans cette thèse s'appuient sur des données collectées par des **éléphants de mer du sud** dont les caractéristiques de l'espèce (section 2.1) en ont fait un modèle d'étude prisé par les chercheurs (sous-section 2.1.5). Plus précisément, nous nous sommes concentrés sur les **femelles** en raison de leur alimentation en milieu pélagique (Bailleul et al., 2010a) et sur leur **voyage post-reproduction** en raison des contraintes techniques qui caractérisent la collecte des données de bio-logging utilisées dans cette thèse. En effet, il s'agit de données de profondeur, température, lumière, accélération (et occasionnellement de champs magnétique et d'environnement acoustique) à **haute fréquence d'échantillonnage**. De telles données sont particulièrement riches en informations sur le comportement des animaux équipés mais limitées à deux mois d'échantillonnage par l'autonomie des appareils. L'intérêt majeur de ces données par rapport à la problématique de cette thèse est la possibilité d'identifier les évènements probables de rencontre entre le prédateur et ses proies. Les travaux développés dans cette thèse peuvent se rattacher à deux objectifs généraux.

1. Mettre en évidence les caractéristiques de l'ajustement comportemental des élé-

phants de mer en réponse aux variations de la densité de proies à fine échelle.

2. Extraire des données collectées par les éléphants de mer des informations sur la distribution spatiale des ressources marines de niveau trophique inférieur, et plus particulièrement sur celle de leur proies.

1.4.2 Structure de la thèse

Le corps du manuscrit s'articule en quatre chapitres dont trois sont l'objet d'articles scientifiques (chapitres 3, 4 et 5). Le dernier chapitre est quant à lui rédigé intégralement en français. Outre ces quatre parties constituant le cœur du travail de la thèse, un "matériels et méthodes" général (chapitre 2) et une discussion générale (chapitre 7) sont proposés afin de remettre les travaux dans une perspective scientifique plus vaste. Les détails techniques ayant trait à chaque chapitre (*informations supplémentaires*) sont inclus en annexes A–E. Enfin, les travaux secondaires effectués en tant que *coauteur* sont fournis en annexes F–J.

Chapitre 2 : Matériels et méthodes général. Dans ce chapitre, nous détaillons les caractéristiques du site d'étude ainsi que de l'écologie de notre modèle d'étude et de ses proies. Nous présentons aussi les différents appareils de collecte de données et les principales méthodes de traitement de données employées. Il est à noter que la mise en œuvre de ces méthodes, principalement au sein de l'équipe de recherche, s'est appuyé sur leur implémentation sous la forme d'une librairie de fonctions documentées ("package" R) ce qui a fait l'objet d'un volume de travail assez conséquent durant la thèse. Des détails concernant ce travail sont disponibles en annexe A.

Chapitre 3 : How elephant seals adjust their fine scale horizontal movement and diving behaviour in relation to prey encounter rate. Dans ce chapitre nous étudions les ajustements du comportement de plongée de l'éléphant de mer face aux variations locales du taux de rencontre de proies. Dans le contexte de la détection des zones de recherche alimentaire intensive ("Area Rectricted Search"), nous quantifions l'effet de ces ajustements sur la distance horizontale parcourue en surface. Nous nous sommes de plus intéressés aux conséquences de ces ajustements sur la proportion du temps de plongée pouvant être consacré à la période de fond (efficacité de plongée). Enfin, compte tenu du lien entre

comportement de plongée et taux de rencontre de proies, nous nous sommes intéressés aux variations du taux de rencontre de proies en fonction des régions de la colonne d'eau exploitées par les éléphants de mer.

1. Le Bras Yves, Jouma'a Joffrey, Picard Baptiste, Guinet Christophe. (2016). How elephant seals (Mirounga leonina) adjust their fine scale horizontal movement and diving behaviour in relation to prey encounter rate. *Plos One*. **Publié**
Informations supplémentaires en annexe B.

Chapitre 4 : Three-dimensional space use during the bottom phase of southern elephant seal dives. En milieu pélagique, la recherche alimentaire peut se traduire par des mouvements dans la dimension verticale mais également sur le plan horizontal. Or ce dernier aspect est encore largement méconnu en raison des difficultés que pose la reconstruction tri-dimensionnelle du mouvement des animaux durant leurs plongées. Dans ce chapitre, il s'agit de décrire et de comprendre les trajectoires tri-dimensionnelles adoptées par les éléphants de mer durant la phase de fond de leurs plongées, phase qui constitue le cœur de l'activité d'alimentation chez ce prédateur. Plus particulièrement, nous nous demandons quelle est l'importance relative des mouvements horizontaux et verticaux et, quelles en sont les implications en termes de perception des proies par le prédateur et de distribution des proies à fine échelle.

2. Le Bras Yves, Jouma'a Joffrey, Guinet Christophe. (2016). Three-dimensional space use during the bottom phase of southern elephant seal dives. *Movement Ecology*. doi: 10.1186/s40462-017-0108-y
Informations supplémentaires en annexe C. Cette étude est complémentée par une autre, inclue en annexe G, portant sur une analyse à plus fine échelle encore des mouvements tri-dimensionnels.

Chapitre 5 : *In situ* measurement of marine resources distribution from instrumented elephant seals. Ici, nous nous concentrons sur l'analyse d'un type de données largement répandu mais peu utilisé, les données d'intensité lumineuse, afin d'étudier la distribution spatiale d'organismes de niveaux trophiques inférieurs à l'éléphant de mer. Deux signaux ont été extraits de ces données. D'une part le coefficient d'atténuation de la lumière en fonction de la profondeur. D'autre part, les évènements d'émission de lumière d'origine biologique. Nous avons constaté l'existence de deux modes dans les profils d'atténuation de la lumière

dans la colonne d'eau. L'un en surface pour lequel il nous a été possible de montrer qu'il était principalement dû à la présence de phytoplancton. L'autre situé bien en deçà de la couche photique, et dont la localisation dans la colonne d'eau répond sensiblement aux variations de l'intensité lumineuse. Afin de préciser la nature des relations trophiques pouvant caractériser ces deux modes d'atténuation, nous nous sommes intéressés aux relations de l'intensité de l'atténuation de lumière dans ces modes d'une part, avec le taux de rencontre de proies des éléphants de mer, et d'autre part, avec l'occurrence d'évènements de bioluminescence en profondeur.

3. Le Bras Yves, Jouma'a Joffrey, Guinet Christophe. In situ measurements of marine resources distribution from instrumented elephant seals. **En préparation** Informations supplémentaires en annexe D.

Chapitre 6 : Peut-on prédire les zones pélagiques favorables aux éléphants de mer depuis l'espace ? Ce chapitre présente les résultats d'analyses exploratoires et interdisciplinaires visant à étudier la dynamique spatio-temporelle du micronecton à méso-échelle. Les variations du taux de rencontre de proies sont comparées aux prédictions de biomasse de micronecton du modèle SEAPODYM, et analysées à la lumière de l'environnement tourbillonnaire des éléphants de mer.

Chapitre 7 : Discussion générale. Ce dernier chapitre est dédié à la synthèse et à la discussion des principaux résultats de la thèse.

Chapitre

2

Matériels et méthodes

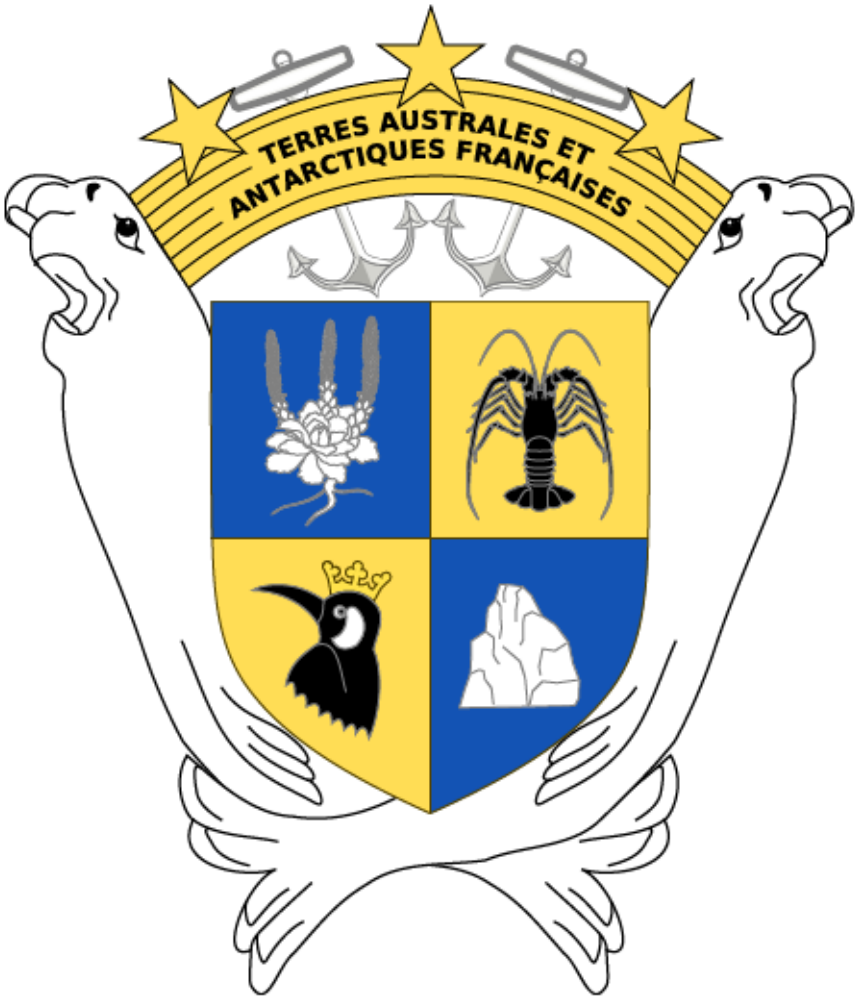

Armoiries des Terres Australes et Antarctiques Francaises.

2.1 Le modèle d'étude : l'éléphant de mer du sud

2.1.1 Généralités

La famille des phocidés comprend 19 espèces (Ferguson and Higdon, 2006) dont deux appartenant au genre *Mirounga* (Gray, 1827), l'éléphant de mer du nord (*Mirounga angustirostris*, Gill, 1866) et l'éléphant de mer du sud (*Mirounga leonina*, Linnaeus, 1758). Comme l'indiquent leurs noms, ces deux espèces occupent respectivement l'hémisphère nord et l'hémisphère sud, avec chacune une large aire de répartition. Cependant, alors que l'éléphant de mer du nord se trouve principalement dans le secteur Nord–Est du Pacifique (du nord de la côte Californienne jusqu'au Golfe de l'Alaska), l'éléphant de mer du sud a quant à lui une distribution circumpolaire (Hindell et al., 2016). L'éléphant de mer du sud est aussi légèrement plus massif que son cousin nord américain. C'est le représentant le plus imposant de la famille des phocidés. À terre, l'éléphant de mer du sud séjourne principalement sur les îles antarctiques et subantarctiques, mais également sur les côtes au Sud du Chili et d'Argentine (Campagna and Lewis, 1992) ainsi que sur le continent antarctique (Bester, 1988; Heimark and Heimark, 1986; Murray, 1981).

L'éléphant de mer du sud est caractérisé par un important dimorphisme sexuel (figure 2.1), l'un des plus important du règne animal (McCann, 1981). En effet, on estime que les mâles peuvent être huit à dix fois plus lourds que les femelles (Hindell et al., 1991a). Le poids moyen des adultes est de 2 tonnes pour une longueur moyenne de 4 mètres chez les mâles et de 500 kilogrammes pour 2,5 mètres de long chez les femelles (Slip et al., 1994).

2.1.2 Populations

Les éléphants de mer du sud ont été chassés de la fin du XIX^{ème} jusqu'à la seconde moitié du XX^{ème} siècle pour l'utilisation de leur graisse. Leurs populations ont donc fortement diminué durant cette période et, malgré l'interdiction de la chasse dans les années 1950, les populations ont continué de décliner jusque dans les années 1980-90 (Guinet et al., 1999; McMahon et al., 2009; Authier et al., 2011). Aujourd'hui l'espèce apparait dans la Liste Rouge de l'UICN avec un statut de conservation correspondant à la catégorie "préoccupation mineure" (Hofmeyr, 2014). McMahon et al. (2005) estiment la population mondiale d'éléphant de mer du sud à 740 000 individus répartis en quatre populations situées : en Géorgie du Sud (400 000 individus), dans

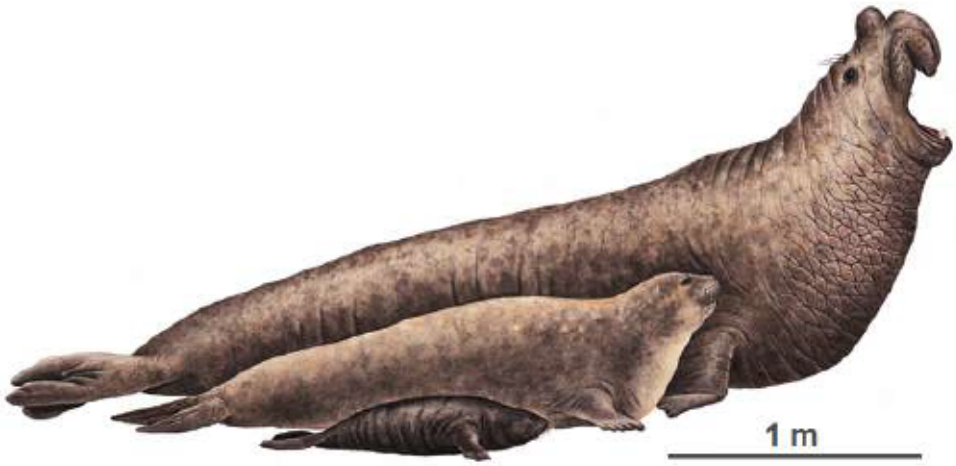

Figure 2.1: L'éléphant de mer du sud, *Mirounga leonina* – *Du premier au dernier plan : juvénile, femelle adulte et mâle adulte. Crédit : P. Folkens.*

l'archipel des Kerguelen (220 000 individus), sur l'île Macquarie (76 000 individus) et au niveau de la péninsule de Valdès en Argentine (42 000 individus). La population de Kerguelen (49°21′0″ S, 70°13′0″ E), dont les individus constituent l'objet d'étude de cette thèse, est le second plus gros site de reproduction de cette espèce, avec un effectif démographique stable depuis une vingtaine d'années (Authier et al., 2011).

2.1.3 Cycle Biologique

Le cycle biologique de l'éléphant de mer du sud comprend deux périodes à terre, chacune d'environ un mois, durant lesquelles les animaux jeûnent : l'une pour la reproduction et l'autre pour le renouvellement du pelage (mue). Entre ces deux séjours à terre ils effectuent deux longs voyages d'alimentation en mer (figure 2.2).

Reproduction

La sexualité des éléphants de mer est polygyne, ce qui signifie que les mâles se reproduisent avec de multiples femelles se regroupant en harem sur leur territoire. Les mâles parvenus à la maturité sexuelle vers 4-6 ans (Carrick et al., 1962) se livrent à des combats pour établir leur domination sur un territoire donné et ainsi, obtenir un accès exclusif aux femelles d'un harem. Seul les mâles assez puissants (les "pachas") parviennent à ce statut, en général à partir de 9 ou 10 ans. Cependant, les mâles dépourvus de harem (les mâles "périphériques") peuvent parfois réussir à se reproduire. Les femelles quant à elles se reproduisent dès leur maturité sexuelle vers 3-4 ans.

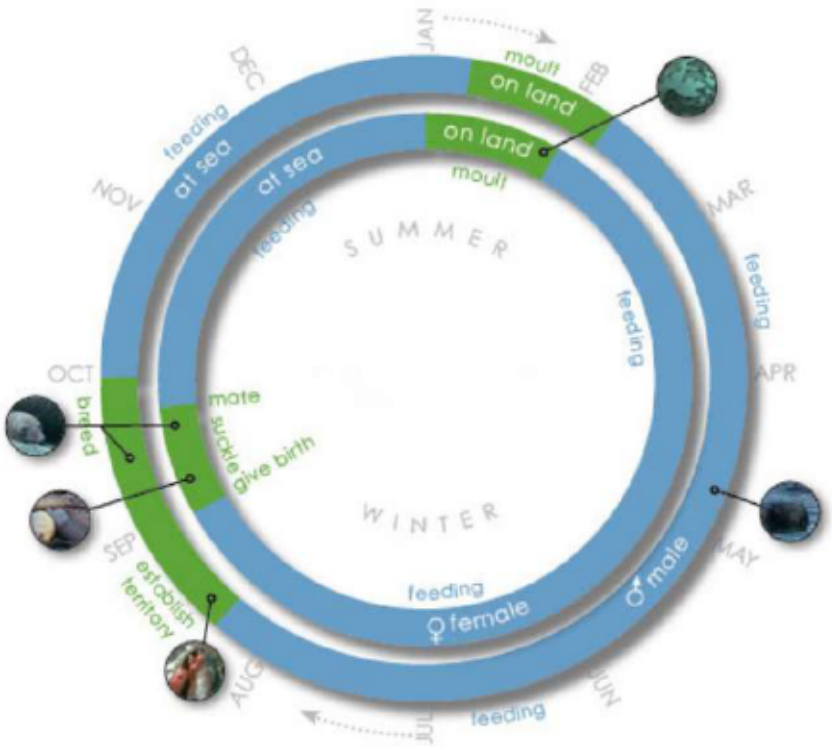

Figure 2.2: Cycle biologique de l'éléphant de mer du sud adulte – *Figure tirée du site SEaOS (2016) consacré à la biologie de l'éléphant de mer.*

Les mâles retournent à terre en août et établissent leur territoire (figure 2.2). Les femelles les y rejoignent en septembre pour mettre bas dans les 2 à 5 jours (figure 2.2) suite à une gestation de neuf mois. Les nouveaux nés éléphants de mer, un par femelle, pèsent en moyenne 35-40 kg (Guinet, 1991). Une fois sevrés, après un peu plus de 20 jours d'allaitement, ils font environ 110-120 kg (Guinet, 1991). Durant la période du sevrage les femelles sont saillies, mais le blastocyte ne s'implante que trois mois plus tard (Gibbney, 1953). Après s'être reproduits, mâles et femelles repartent avec quelques jours de différences (figure 2.2) pour un voyage en mer de trois mois (le **voyage post-reproduction**).

Mue

Les éléphants de mer muent lors d'une seconde période à terre (figure 2.2). Cette période peut avoir lieu entre mi-décembre et fin avril selon l'âge et le sexe des individus. Elle dure environ un mois. Les éléphants de mer renouvellent alors leur peau et leur pelage (Worthy et al., 1992), dont la couleur argentée apparait à mesure que l'ancien

pelage (de couleur marron) se détache en plaques. C'est un processus coûteux en énergie durant lequel les animaux jeûnent et perdent en moyenne 24 % de leur masse (Champagne et al., 2012). Une fois la mue accomplie, les animaux repartent en mer (voyage post-mue) pour sept à huit mois (figure 2.2).

Voyages alimentaires

Les éléphants de mer passent près de dix mois par an en mer pour s'alimenter, ce qui représente en moyenne 85% de leur vie (McIntyre et al., 2010). Ils plongent alors continuellement (Leboeuf et al., 1986), alternant des plongées d'une durée moyenne comprise entre 20 et 30 minutes, avec des périodes de récupération en surface de 2-3 minutes (McConnell et al., 1992). Les plongées ont une profondeur moyenne de 550 m chez les mâles et de 470 m chez les femelles (McIntyre et al., 2010). Il est pourtant assez commun qu'elles atteignent 800 mètres chez les deux sexes. Le record de profondeur a été observé chez un mâle adulte et se situe à une profondeur comprise entre 2133 et 2165 m (McIntyre et al., 2010).
Durant leurs voyages alimentaires, les éléphants de mer du sud parcourent des milliers de kilomètres, explorant ainsi un secteur géographique très vaste (figure 2.3). Ce secteur s'étend de 40°S jusqu'à l'Antarctique et tout autour du continent (figure 2.3). Les habitats de pêche privilégiés par les éléphants de mer de Kerguelen varient en fonction du sexe et de l'âge. Les mâles adultes fréquentent principalement le plateau de Kerguelen et le plateau Antarctique, à la recherche de proies benthiques (Bailleul et al., 2010a). Les juvéniles et femelles adultes vont s'alimenter en milieu pélagique, dans la zone marginale des glaces antarctiques (Bailleul et al., 2007a), mais surtout dans la zone sub-antractique (Bailleul et al., 2010a; Ducatez et al., 2008; Cherel et al., 2008).

2.1.4 Alimentation

Régime alimentaire

Au retour à terre des éléphants de mer, le contenu de leur estomac est en état de digestion avancé et donc fortement enrichi en organismes dotés de pièces non digestes (e.g. bec de céphalopodes) ou capturés peu de temps avant. Les analyses isotopiques indiquent que les femelles éléphants de mer se nourrissent principalement de myctophidés (Cherel et al., 2008; Ducatez et al., 2008) et non de céphalopodes comme on le pensait auparavant (Rodhouse et al., 1992; Slip, 1995). D'autre part ces analyses ont

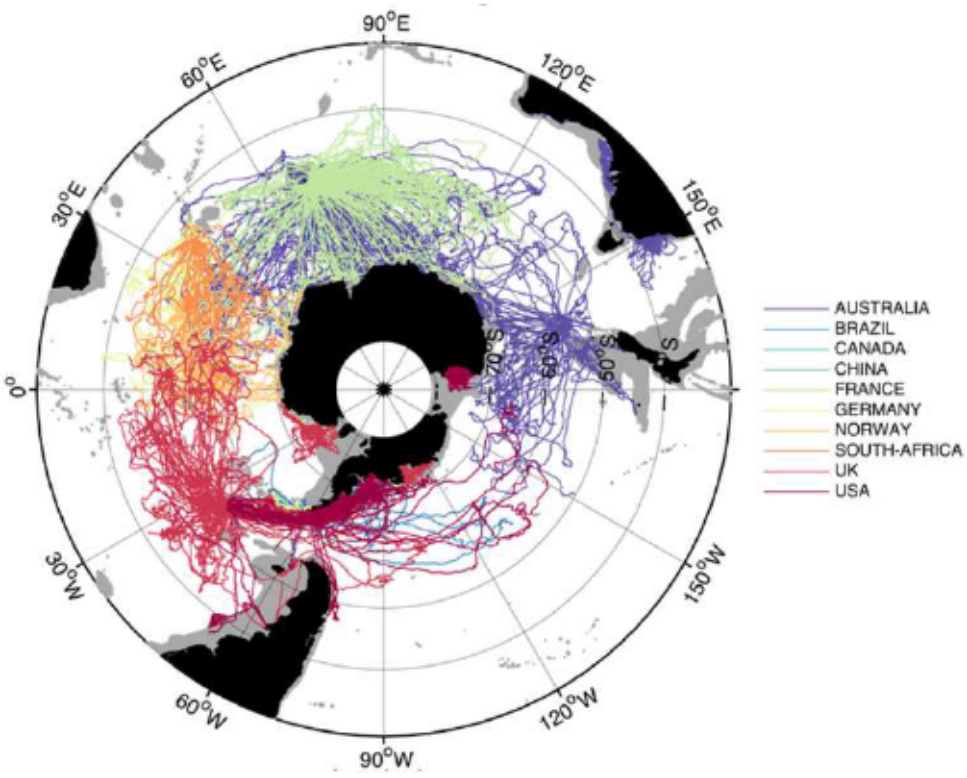

Figure 2.3: Distribution circumpolaire des éléphants de mer du sud – *Trajectoires Argos des éléphants de mers du sud équipés par différents pays. Figure issue du portail MEOP. Crédit : F. Roquet.*

révélé un changement progressif du régime alimentaire des mâles. Les jeunes mâles se nourrissent d'abord comme les femelles mais évoluent vers des proies de plus haut niveau trophique (Chaigne et al., 2013). Leur diète comporterait davantage de céphalopodes que les femelles (*Psychroteuthis glacialis*, *Gonatus antarcticus* et *Kondakovia longimana*, Slip (1995); Daneri et al. (2000); van den Hoff et al. (2003)) ainsi que de la légine australe (*Dissostichus eleginoides*, Slip (1995)).

Dans la suite de cette thèse les travaux porteront exclusivement sur les femelles adultes. Nous feront l'hypothèse que les myctophidés représentent la plus grande partie du régime alimentaire des femelles adultes. Dans ce contexte nous apportons ici les principaux aspects de la biologie des myctophidés.

Les myctophidés

La famille des myctophidés compte 248 espèces (Catul et al., 2010; Fishbase, 2017) dont 40 sont endémiques de l'océan Austral (Pakhomov et al., 1996). A l'exception de l'Arctique, les myctophidés sont présents dans tous les océans (Catul et al., 2010).

Il s'agit d'une ressource de première importance à l'échelle planétaire et notamment dans l'océan Austral (Gjøsaeter and Kawaguchi, 1980), où leur abondance totale a été estimée entre 70 et 200 millions de tonnes (Catul et al., 2010). Pakhomov et al. (1996) reprend une estimation allant jusqu'à 396 millions de tonnes, présentée dans une ancienne étude rédigée en russe (Lubimova et al., 1987). Des résultats récents de Irigoien et al. (2014) suggèrent que la biomasse des poissons mésopélagiques est largement sous-estimée.

Les myctophidés sont des poissons mésopélagiques qui vivent à des profondeurs comprises entre 200 et 1200 m (Fishbase, 2017). Ils sont aussi appelés poissons lanterne en raison de leur bioluminescence (Vacquié-Garcia et al., 2012). En effet, ils ont sur leur face ventrale et leur nageoire caudale de nombreux petits photophores (figure 2.4) qui peuvent émettre une lumière bleue brillante vers le bas ou vers les côtés (Haddock et al., 2010). Les myctophidés sont également connus pour leur adaptation aux faibles concentrations en oxygène (Catul et al., 2010) et leur migrations nycthémérales (Barham, 1966; Roe, 1974; Watanabe et al., 1999; Pearre, 2003; Watanabe et al., 2006a; Catul et al., 2010). Ils sont en général dotés d'une vessie natatoire (Barham, 1966; Fishbase, 2017). Cette structure, plus ou moins remplie de gaz, a pour fonction le contrôle de la flottabilité. Elle rend les poissons facilement détectables par les sonars mais il faut garder à l'esprit qu'elle n'est pas systématiquement présente chez tous les myctophidés. De plus, sa présence/absence et sa composition (gaz/lipide) dépendent du stade de développement (Neighbors and Nafpaktitis, 1982).

Le niveau trophique des myctophidés varie entre 3 et 4.6 (Irigoien et al., 2014) et leur taille entre 2 et 30 cm. Ce sont des organismes de niveaux trophiques intermédiaires qui assurent le lien entre méso-zooplancton (ils se nourrissent de façon opportuniste des espèces les plus communes de copépodes et d'euphausiacés, Pakhomov et al. (1996); Catul et al. (2010)) et prédateurs supérieurs. Du fait de leur forte abondance et de leur migration quotidienne, on estime qu'ils jouent un rôle majeur dans le transfert du carbone depuis la surface vers les profondeurs (Longhurst et al., 1990; Pakhomov et al., 1996; Zhang and Dam, 1997; Hays, 2003; Flores et al., 2008; Bianchi et al., 2013). Les myctophidés sont généralement des poissons gras ayant une haute valeur énergétique (Benoit-Bird, 2004). Ils entrent dans le régime alimentaire de l'éléphant de mer et de nombreux autres prédateurs (Sabourenkov, 1991; Koz, 1995), notamment du manchot à jugulaire *Pygoscelis antarcticus* (Jansen et al., 1998), du manchot royal *Aptenodytes patagonicus* (Kooyman et al., 1992), du gorfou macaroni *Eudyptes chryso-*

lophus (Deagle et al., 2007) et de l'otarie à fourrure antarctique *Arctocephalus gazella* (Casaux et al., 1998).

Les otolithes des myctophidés *Gymnoscopelus nicholsi*, *Electrona antarctica* (figure 2.4) et *Electrona calsbergi* ont été retrouvées dans l'estomac des éléphants de mer du sud (Slip, 1995; Daneri and Carlini, 2002). Ce sont des poissons de petite taille (respectivement 7-14, 2-9 et 13-18 cm, Pakhomov et al. (1996)) qui figurent parmi les espèces dominantes de l'ichtyofaune de l'océan Austral (Pakhomov et al., 1994; Pusch et al., 2004; Loots et al., 2007; Collins et al., 2008; Flores et al., 2008; Gauthier et al., 2014). Ces trois espèces vivent entre 300 et 500 m de profondeur le jour et remontent sous la surface, entre 0 et 100 m, la nuit (Koubbi et al., 2014). Leur distribution est cirumpolaire, bornée au nord par le front subantarctique (figure 2.5). Dans le secteur indien de l'océan Austral, *E. antarctica* est beaucoup plus abondante au sud du front polaire qu'au nord (jusqu'au continent antarctique) et inversement pour *E. calsbergi* et *G. nicholsi* (Koubbi et al., 2014).

Figure 2.4: *Electrona antarctica* – *À gauche un dessin de l'espèce tiré de Günther (1887), crédit : R. Mintern. À droite une photographie montrant sa bioluminescence tirée de Haddock et al. (2010), crédit S. Haddock.*

2.1.5 Intérêt en tant que modèle d'étude

Les caractéristiques de l'éléphant de mer du sud en font un modèle d'étude très prisé dans le domaine du bio-logging (McIntyre, 2014) :

- Abondant, peu farouche et séjournant de longues périodes à terre[1], il est facile pour les chercheurs d'en trouver et de les équiper/déséquiper d'enregistreurs électroniques (aussi appelés balises).

[1]Notamment dans des environnements peu hostiles à l'homme, tels que la Péninsule Courbet à Kerguelen.

- En raison de sa grande taille il peut supporter la pose d'appareils qui seraient trop encombrants pour d'autres espèces. Ces derniers ont alors longue autonomie et collectent des données variées et précises.
- De plus, les appareils seront probablement récupérables, car les individus arrivés à l'âge adulte ont un taux de survie élevé. Ils sont aussi assez fidèles au site où ils ont été équipés. Il est donc possible de collecter des données avec une haute fréquence d'échantillonnage et d'utiliser ces coûteuses balises à plusieurs reprises.
- Lors de ses longs voyages alimentaires, l'espèce explore des habitats variés (pélagiques/benthiques, entre 60°S et 40°S, tout autour du continent Antarctique), ce qui permet aux chercheurs de collecter des données sur une vaste zone géographique.
- Les éléphants de mer plongent profondément et échantillonnent ainsi une fraction importante de la colonne d'eau.
- Dans la mesure où ces animaux respirent à la surface, il est également possible de les localiser par satellite et de collecter des données en temps quasi-réel.
- Pour se reposer ou pour digérer, les éléphants de mer (du nord et du sud) réalisent des plongées de dérive (Crocker et al., 1997) qui permettent de suivre l'évolution de leur condition corporelle (Biuw et al., 2003).
- Sa taille et son abondance font de cette espèce une grande consommatrice de ressources dans l'océan Austral (Guinet et al., 1996; Hindell et al., 2003).
- Enfin, cela étant plus subjectif, sa vie dans l'environnement extrêmement dynamique du milieu pélagique de l'océan Austral et son écologie alimentaire sont des sujets passionnants et encore largement inexplorés.

2.2 Le site d'étude : le secteur indien de l'océan Austral

2.2.1 L'océan Austral

L'océan Austral se situe à la confluence des océans Atlantique, Indien et Pacifique. L'identité physique de l'océan Austral se caractérise par la présence d'un fort courant,

le courant circumpolaire antarctique, qui circule d'Ouest en Est tout autour du continent Antarctique. Il s'agit du courant le plus puissant du monde. L'océan Autral se caractérise alors par une structure annulaire, avec de faibles gradients longitudinaux et de forts gradients latitudinaux.
Différents fronts ont été définis afin de délimiter les principales masses d'eau qui composent l'océan Austral et qui forment de vastes régions aux caractéristiques écologiques différentes (figure 2.5). Les tracés des différents fronts dépendent de la bathymétrie. En raison de la nature dynamique du milieu, ces tracés peuvent varier dans le temps, mais globalement ils s'organisent en anneaux concentriques autour du continent Antarctique. Les principaux fronts sont les fronts sub-tropical, sub-antarctique, polaire et antarctique (Orsi et al., 1995; Belkin and Gordon, 1996). Le front sub-tropical correspond à la frontière nord du courant circumpolaire antarctique (Orsi et al., 1995) et peut être considéré comme la limite de l'océan Austral par rapport aux océans Atlantique, Indien et Pacifique. La limite sud de ce courant est donnée par la position du front antarctique (Southern ACC front, figure 2.5). Dans la zone du courant circumpolaire on distingue les régions sub-antarctique et antarctique respectivement situées au nord et au sud du front polaire. Enfin, le front sub-antarctique, défini par l'isotherme de surface 8°C (Orsi et al., 1995), sépare la région sub-antarctique en deux zones : la zone subantarctique *stricto sensu* au nord et la zone polaire au sud.

2.2.2 Kerguelen et le secteur indien de l'océan Austral

Notre site d'étude est le secteur indien de l'océan Austral et plus précisément la région des îles Kerguelen faisant l'objet de programmes de recherche interdisciplinaires depuis 2005 (KEOPS-1 (2005), KEOPS-2 (2010) et MyctO-3D-MAP (2011)).
Les îles Kerguelen sont bordées par un plateau qui fait obstacle au courant circumpolaire antarctique (figure 2.6). La rencontre de ce courant provenant de la plaine abyssale avec le relief plateau est à l'origine d'une dynamique complexe de circulation de l'eau dans ce secteur (Park et al., 2008; Roquet et al., 2009). Celle-ci se traduit par la remontée du front polaire et la stimulation de la formation de tourbillons (Kostianoy et al., 2004; Sokolov and Rintoul, 2007; Park et al., 2014) (figure 2.6).
L'océan Austral se caractérise par des eaux HNLC[2], riches en nutriment mais pauvres en chlorophylle (Pitchford and Brindley, 1999). Cependant, la région de Kerguelen est connue pour abriter, durant l'été austral (octobre–décembre), un bloom phytoplank-

[2]High Nutrients Low Chlorophyll.

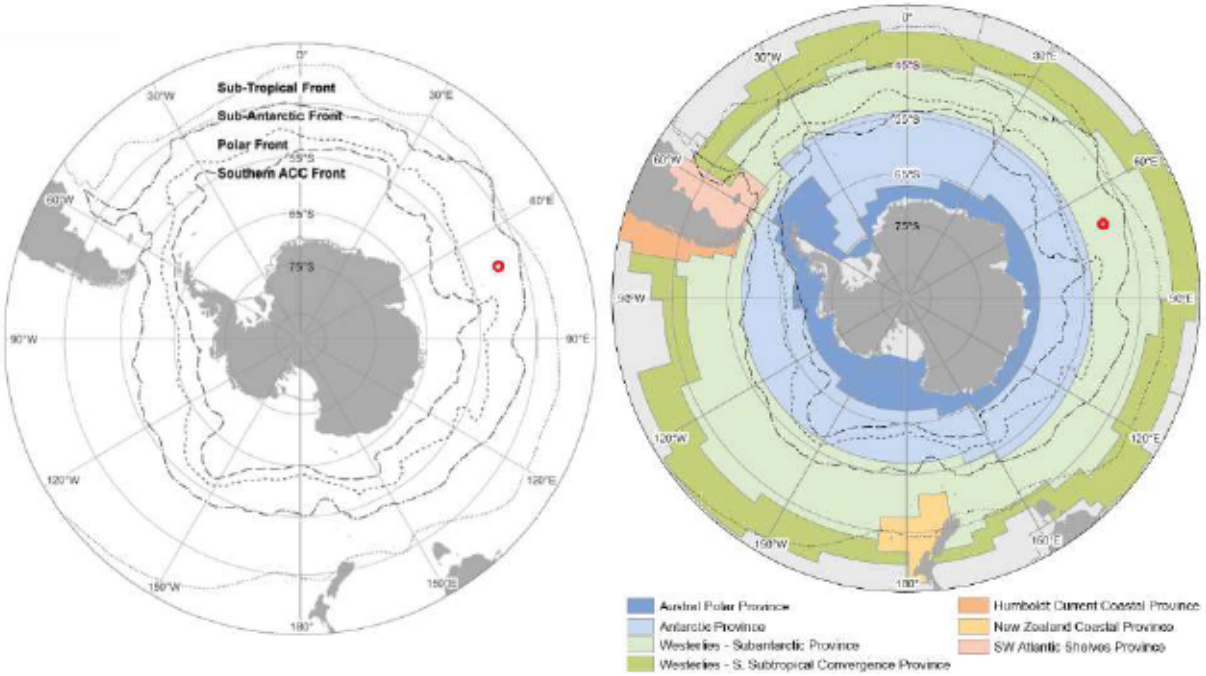

Figure 2.5: Carte de l'océan Austral – *À gauche, le tracé des principaux fronts océanographiques. À droite, les principales provinces biogéochimiques Longhurst (2007). Les cercles rouges marquent la position des îles Kerguelen. Figures tirées de Koubbi et al. (2014).*

tonique important (Mongin et al., 2008; Moore and Abbott, 2000), probablement dû à un apport en fer provenant des îles Kerguelen (Sullivan et al., 1993; Blain et al., 2001, 2007; d'Ovidio et al., 2015). La production primaire est transportée vers l'Est par les courants formant ainsi un secteur particulièrement riche biologiquement, où de nombreux prédateurs (Bost et al., 2009)), et notamment des femelles éléphant de mer (Cotté et al., 2015), viennent s'alimenter.

2.3 Instrumentation des animaux et principaux traitements des données

2.3.1 Description des appareils embarqués

Nous présentons ici les différents types balises dont les données ont été utilisées dans cette thèse. Entre l'année des premiers jeux de données (2010) et celle des derniers, certains modèles ont subi des évolutions. La configuration des balises peut aussi changer selon les années. Nous ne donnons pas ici ces détails, ils seront mentionnés au

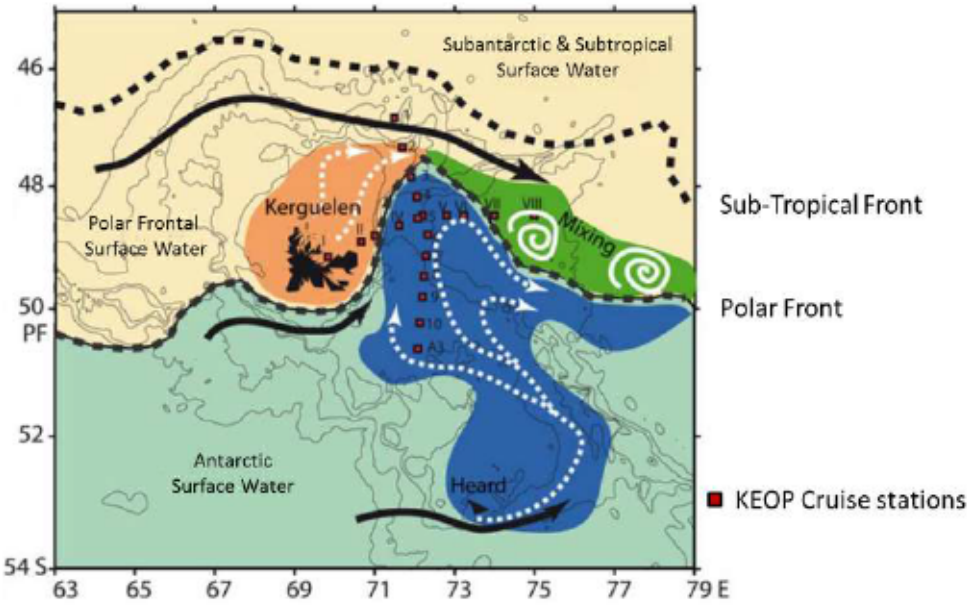

Figure 2.6: Dynamique des courants autour de Kerguelen – *Les flèches noires représentent les grandes lignes du trajet emprunté par le courant circumpolaire antarctique. Les zones colorées en bleu (au Sud-Est de Kerguelen) et saumon (autour de Kerguelen) schématisent deux masses d'eau dont le mélange aboutit à la zone colorée en vert (caractérisée par une forte turbulence méso-échelle). Les flèches blanches pointillées montrent les grandes lignes de courant à l'intérieur des zones colorées. Figure tirée de Park et al. (2014). Crédit : Y.-H. Park.*

moment opportun dans les différents chapitres de la thèse.

SPOT Les balises SPOT (Wildlife Computers™, 119 g) sont les appareils les plus simples que nous utilisons. Elles sont dotées d'une longue autonomie et permettent de localiser les animaux via le système Argos. Ce système offre chaque jour entre 10 et 30 localisations transmises en temps quasi-réel, avec une précision comprise entre 500 m et 10 km (Costa et al., 2010). Nous n'utilisons jamais les SPOT seuls, mais combinés à d'autres balises. Les SPOT nous permettent alors de connaître le moment où les éléphants de mer retournent à terre et de les localiser afin de pouvoir récupérer les différents appareils ayant été posés.

CTD-SRDL Les balises CTD-SRDL (Conductivity-Temperature-Depth Satellite Relayed Data Logger, 545 g, figure 2.7) sont fabriquées à l'université de Saint Andrews par l'équipe du Sea Mammal Research Unit. Elles offrent les mêmes possibilités que les balises SPOT en termes d'autonomie et de localisation. De plus, elles sont dotées

de capteurs de pression, de température et de salinité. Certains modèles (CTD/fluo-SRDL, 680 g) sont, de plus, équipés d'un capteur de fluorescence. Durant les plongées, ces variables sont mesurées et enregistrées toutes les deux secondes. L'algorithme "Brokenstick" (Fedak et al., 2001) permet de compresser les données collectées avant que celles-ci soient transmises via le système Argos. On peut alors obtenir en temps quasi-réel des profils de plongée (temps-profondeur), de température (profondeur-température) et de salinité (profondeur-salinité), résumés en six points. Les données échantillonnées avec une résolution de 0.5 Hz peuvent être téléchargées à la condition que l'appareil soit récupéré physiquement.

MK10-X et TDR10-DD Les balises MK10-X (Wildlife Computers™, 58 g, figure 2.8) et TDR10-DD (Wildlife Computers™, 117 g, figure 2.8) ne permettent pas la transmission de données par relai satellite et doivent donc être récupérées physiquement sur les animaux, afin d'être téléchargées. Elles mesurent la profondeur, la température, l'intensité lumineuse avec une fréquence de 1 Hz et l'accélération (selon les axes longitudinal, latéral et vertical de l'appareil) avec une fréquence de 16 Hz. Enfin, les TDR10-DD sont également équipés d'un magnétomètre qui mesure la direction et l'intensité du champ magnétique terrestre selon les mêmes axes et avec la même fréquence que l'accéléromètre.

SPLASH10-F Les balises SPLASH10-F (Wildlife Computers™, 217 g, figure 2.9) enregistrent la profondeur, la température et l'intensité lumineuse à 1 Hz, et collectent des localisations Argos. Les localisations Argos peuvent être transmises en temps quasi-réel et nous aider à retrouver les éléphants de mer à terre. Les autres données (à 1 Hz) doivent être téléchargée de la carte mémoire des balises. Enfin, les SPLASH10-F enregistrent les signaux reçus de la part des satellites du réseau GPS. Ces informations permettent de calculer les positions GPS des animaux une fois la balise récupérée. Ces positions offrent une résolution bien supérieure au système Argos car elles sont à la fois plus fréquentes (une plongée sur deux environ) et plus précises (dans l'océan Austral l'erreur est de quelques dizaines de mètres).

Acousonde Les Acousondes™ (Acoustimetrics – Greeneridge Sciences Inc., 262 g, figure 2.10) mesurent la profondeur et la température à 1 Hz, ainsi que l'accélération et le champs magnétique à 5 Hz et selon les trois axes de la balise. La particularité

Figure 2.7: Balise CTD-SRDL et CTD/fluo-SRDL – *À gauche le modèle classique de CTD-SRDL et à droite le modèle avec fluorimètre. Dimensions du modèle classique :* $10.5 \times 7 \times 4$ *cm. Crédit : SMRU Instrumentation*

Figure 2.8: Balises MK10-X et TDR10-DD – *MK10-X à gauche et TDR10-DD à droite. Ces balises mesurent respectivement* $5.6 \times 3.8 \times 2$ *cm et* $7.4 \times 5.7 \times 3.6$ *cm. Crédit : Wildlife Computers*

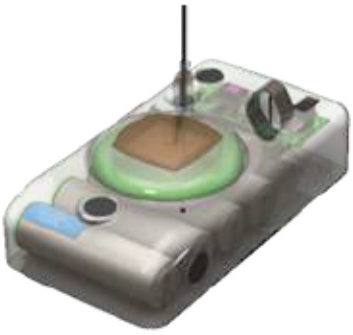

Figure 2.9: Balise SPLASH10-F – *Dimensions :* $10.5 \times 5.6 \times 3$ *cm. Crédit : Wildlife Computers*

Figure 2.10: Balise Acousonde™ modèle 3A – *Longueur : 22.1 cm. Crédit : acoustimetrics*

de cette balise par rapport à un TDR10-DD vient du fait qu'elle comprend un hydrophone. En contrepartie l'autonomie de ces balises est assez faible. Afin enregistrer les données sur une plus longue période, les hydrophones ont été configurés selon l'année de déploiement, pour enregistrer 3 h toutes les 12 ou 24 h et avec une fréquence d'échantillonnage de 6 ou 12 kHz .

2.3.2 Protocole de déploiement

Le déploiement des balises s'effectue sur les îles Kerguelen dans le cadre du programme 109 de l'institut Paul-Émile Victor (IPEV), en particulier dans la partie Est de la Grande Terre : la péninsule Courbet et sa façade Sud où est située la base de Port-aux-Français. J'ai participé au travail de terrain de novembre 2014 à février 2015, pour la récupération des balises posées lors de la période de reproduction précédente et pour la pose des balises lors de la période de mue. Cependant, les données utilisées au cours de cette thèse sont en grande partie issues des campagnes de terrains antérieures à celle que j'ai pu effectuer, les données les plus anciennes ayant été collectées en 2010.

Dans le cas le plus simple, une seule balise de type CTD-SDRL est posée, mais l'équipement d'un individu fait généralement intervenir plusieurs balises : une première qui doit être capable de renseigner en temps quasi-réel sa position, puis d'autres équipées en fonction des données que l'on souhaite collecter. Les balises sont d'abord configurées selon les besoins en matière de fréquence d'échantillonnage et d'autonomie, et de façon à être chacune synchrone avec le Temps Universel Coordonné (UTC). Elles sont alors mises en veille pour que l'enregistrement des données commence lors de leur première immersion dans l'eau de mer. La base des balises est enduite de "pâte marine" (une pâte adhérente et malléable à chaud) qui peut être découpée, ce qui facilite l'opération de récupération quelques mois plus tard.

Pour minimiser les risques d'accident, la pose s'effectue de préférence sur un individu isolé de ses congénères, dans une zone plane à l'écart d'un point d'eau, et présentant une taille moyenne. Si l'on procède à une pose, il est d'ailleurs important de tenir compte du fait que l'animal reviendra à terre avec une masse bien plus importante. Au moment de la pose, deux opérateurs se présentent face à l'animal et glissent une capuche sur la tête de l'éléphant de mer. Cette capuche aveugle l'animal et entrave partiellement sa mâchoire. C'est à ce moment que les deux opérateurs (éventuellement aidés d'autres) appliquent leur poids sur l'avant de l'animal tout en relevant

ses nageoires pectorales, ceci afin de l'immobiliser temporairement. Dans le même temps, une troisième personne réalise une anesthésie au moyen d'une piqure intraveineuse (McMahon et al., 2000) constituée d'un mélange 1 : 1 de tilétamine et de zolazépam. À raison de 0,8 mL pour 100 kg, l'anesthésie dure entre 20 à 40 minutes. Quand l'anesthésie fait effet (après 2-3 minutes), l'animal est libéré de ses entraves et la pose/récupération des appareils peut débuter.

- S'il s'agit d'une pose, la pelage est d'abord nettoyé à l'acétone puis recouvert (i) d'une couche de colle époxy d'approximativement 4 mm dont on prend soin d'assurer la prise avec le poil, puis (ii) d'un filet dans lequel sont enchevêtrés deux colliers colson. La balise est alors positionnée de façon à aligner ses axes longitudinal et latéral avec ceux de l'animal. La pose s'achève quand, une fois la colle légèrement durcie, on resserre fermement les colliers colson autour de la balise. On se place alors en retrait de l'animal pour observer la bonne reprise de ses capacités.

- S'il s'agit d'une récupération, les colliers colson et la pâte marine sont simplement coupés. La colle époxy restante se détachera avec la pelage lorsque celui-ci sera renouvelé.

2.3.3 Principaux traitements des données

Bien que chaque chapitres comporte des spécificités, les méthodes employées se recoupent largement. Le socle méthodologique commun aux différents chapitres est issu du travail collectif des nombreuses personnes ayant participé au projet "éléphant de mer" du laboratoire au fil des années. J'ai contribué à leur développement mais de nombreuses méthodologies sont antérieures à mon arrivée au sein de l'équipe. Durant cette thèse je me suis largement investi dans le projet de regrouper tous ces outils dans un même langage (R : R Core Team (2014)), les documenter, les améliorer et les rendre disponibles au plus grand nombre. Le résultat de ce travail se présente sous la forme d'un *paquet* (ou "R package", l'unité fondamentale de code reproductible et partageable dans ce langage) disponible en ligne (Le Bras, 2017) et dont un descriptif et un manuel sont fournis en annexe A. Quand une méthode donnée est implémentée dans le projet, le nom de la fonction correpondante est indiqué `en caractères de machine à écrire`.

Délimitation des phases de plongée

Les capteurs de pression peuvent se dérégler au cours du temps. La première étape consiste à corriger ce défaut (`correct_depth`), ce qui est assez simple puisque l'on sait que les animaux retournent régulièrement en surface pour respirer. Les plongées sont ensuite définies comme les périodes durant lesquelles les éléphants de mer restent continûment à plus de 15 m de profondeur (`dive_delim`). Les phases de surface sont définies comme les périodes séparant les plongées.
Chaque plongée est ensuite divisée en trois phases : la descente, la phase de fond et la remontée. La descente et la montée, aussi appelées phases de transit, se caractérisent par des vitesses verticales importantes de signe constant (figure 2.11). La phase de fond, ou phase "efficace", correspond à la période d'une plongée durant laquelle les animaux dépensent leur temps dans une zone plus restreinte de la colonne d'eau. Leur vitesse verticale peut alors être importante mais surtout plus variable que durant les phases de transit (figure 2.11). Il existe de nombreuses méthodes pour délimiter les phases de plongées (`bottom_delim`). Celle qui est employée dans la plupart des publications de l'équipe depuis 2013 est basée sur Le Bras (2012) (`bottom_delim_vspd`).
Pour chaque plongée, une régression polynomiale de degré 4 est ajustée sur la relation entre le temps (t) et la vitesse verticale (v_z). Ce modèle s'écrit $v_z \sim N(at^4 + bt^3 + ct^2 + dt + e, \sigma)$. Le quatrième degré autorise la présence de trois points d'inflexion, ce qui permet de s'ajuster correctement à des profils de plongée ayant une forme de "V", de "U" ou de "W". La série temporelle de la vitesse verticale, ainsi simplifiée sous la forme d'un polynôme, est soumise à un seuil de 0.75 $\mathrm{m\,s^{-1}}$ (Le Bras, 2012). La descente prend fin quand la valeur absolue du polynôme passe pour la première fois sous le seuil, tandis que la montée débute quand elle le dépasse pour la dernière fois (figure 2.11). Le seuil utilisé correspond à la valeur pour laquelle les résultats de cette méthode automatique s'approchent le plus de la délimitation visuelle effectuée par des humains[3] (Le Bras, 2012).

Tentatives de capture de proies

L'identification des tentatives de captures consiste à détecter les mouvements brusques de la mâchoire. Ceci est réalisé à partir des données d'accélération, selon la méthode décrite par Vacquié-Garcia et al. (2015) (`prey_catch_attempts`) dérivée de celle de Viviant et al. (2010). La méthode de Viviant et al. (2010) a été développée chez les

[3]Plan d'expérience : 5 observateurs × 40 plongées × 13 éléphants de mer

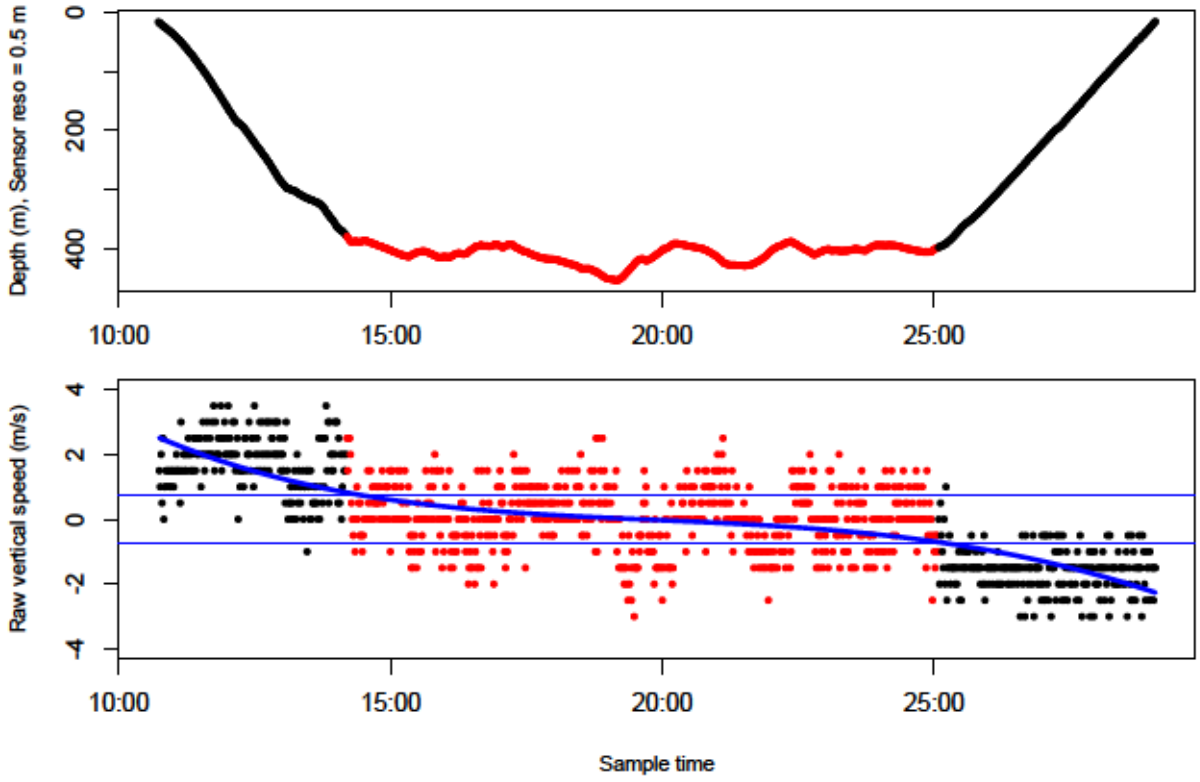

Figure 2.11: Délimitation de la phase de fond – *En haut, le profil de plongée où la phase de fond est en rouge. En bas , la vitesse verticale en fonction du temps. L'aspect discret des observations s'explique par la résolution des données de profondeur : 0.5* m. *La phase de fond est en rouge, le polynôme de degré 4 en bleu (ligne épaisse) et les valeurs seuils de -0.75 et 0.75* $\mathrm{m\,s^{-1}}$ *sont en bleu (lignes fines).*

otaries de Steller (*Eumetopias jubatus*) et utilise deux accéléromètres, l'un sur la tête et l'autre sous la mâchoire. Les résultats de Viviant et al. (2010) montrent qu'un seul accéléromètre est suffisant.

L'accélération correspondant aux mouvements rapides est extraite avec un filtre de Butterworth passe-haut ($f > 2.64$ Hz) appliqué à chacun des trois axes de l'accéléromètre. Pour chaque seconde, on calcule l'écart-type de l'accélération filtrée (Vacquié-Garcia et al., 2015). Un écart-type mobile sur une fenêtre de cinq secondes est ensuite appliqué à chacun des axes (Vacquié-Garcia et al., 2015). Les valeurs obtenues sont enfin classées en deux catégories, les valeurs "hautes" et les valeurs "basses", par l'algorithme des 2-moyennes (c'est à dire l'algorithme des "k-means" avec k = 2). Les observations faites sur chacun des axes sont ramenées à une série uni-dimensionnelle de 0/1. Un 1 est attribué lorsque des valeurs hautes sont observées sur les trois axes

simultanément. On considère alors qu'une tentative de capture est en cours. Une tentative de capture est définie comme une série continue de 1.

Effort de nage

Le calcul de l'effort de nage (`swimming_effort`) consiste à mesurer le nombre et l'amplitude des coups de nageoire caudale. L'accélération latérale présente une densité spectrale de puissance bimodale (figure 2.12), avec un mode dans les fréquences très faibles (correspondant aux mouvement lents), et un autre bien marqué entre 0.5 et 1 Hz. Nous supposons que ce dernier mode est dû aux mouvements de queue de l'animal. En conséquence, l'accélération latérale est traitée avec un filtre de Butterworth passe bande de fréquence $1 > f > 0.44$ Hz. Le signal obtenu est résumé à 1 Hz en calculant pour chaque seconde sa moyenne quadratique ("Root Mean Square").

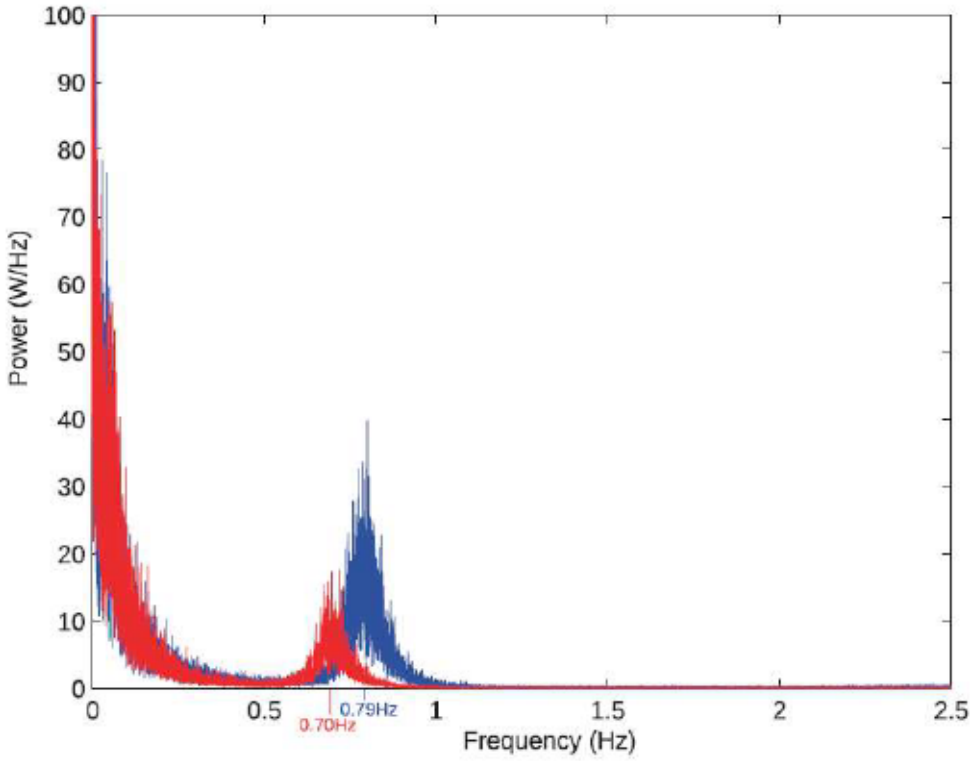

Figure 2.12: Densité spectrale de puissance de l'accélération latérale – *Les deux couleurs montrent les spectres de deux individus distincts. Les repères colorés en abscisse indiquent la valeur des pics de puissance pour le second mode. Figure extraite de Genin et al. (2005). Crédit : A. Génin.*

Orientation du corps des animaux

L'accélération peut enfin nous permettre de calculer l'inclinaison (i) de l'axe longitudinal par rapport à l'horizontale et (ii) de l'axe latéral par rapport à la verticale. Pour ce faire, nous avons besoin de connaître la direction du vecteur $\vec{g}$ de la gravité terrestre par rapport à l'accéléromètre, c'est à dire la direction de la composante gravitationnelle de l'accélération.

Cette composante, aussi connue sous le nom d'accélération statique (`static_acc`), correspond aux mouvements lents des animaux (le mode de faible fréquence sur la figure 2.12). Elle est extraite au moyen d'un filtre de Butterworth passe bas de fréquence $f < 0.2$ Hz, appliqué à chaque axe de l'accéléromètre. Le signal obtenu est normé, c'est à dire que les coordonnées de chaque axe (longitudinal x, latéral y et vertical z) sont divisées par la norme du vecteur ($\sqrt{x^2+y^2+z^2}$), car seul la direction de $\vec{g}$ nous intéresse. Dans l'idéal, la norme de l'accélération statique est constante et égale à 9.81 $\mathrm{m\,s^{-2}}$. Les angles de tangage θ ("pitch") et de roulis ϕ ("roll") sont alors dérivés des formules $\theta = -atan(x/\sqrt{y^2+z^2})$ et $\phi = atan(y/z)$ (Ozyagcilar, 2015).

Ces informations peuvent être complétées par le calcul de l'angle de lacet (aussi connus sous les noms de "heading", "bearing" ou "yaw"), dans le cas où l'on dispose de la direction du champ magnétique terrestre en plus de celle du vecteur $\vec{g}$. Les trois axes du magnétomètre sont filtrés de la même façon que l'accélération. L'angle de lacet est obtenu à partir de ce signal filtré, ainsi que des angles θ et ϕ, par l'application de formules trigonométriques. Par rapport à l'intérêt que nous leur portons, ces formules sont trop complexes pour être présentées ici. Le lecteur intéressé pourra se reporter à l'un des nombreux documents issus de l'industrie des téléphones mobiles expliquant leurs bases mathématiques et fournissant le code pour les mettre en œuvre (e.g Ozyagcilar (2015)).

Vitesse de nage

Bien que les TDR10-DD soient équipés d'une hélice pour mesurer la vitesse de nage des animaux, ces dernières n'ont jamais pu accomplir leur mission (cavité de l'hélice bouchée avant même le départ en mer). L'obtention de cette information n'a été possible que sur les animaux équipés d'Acousonde™. Nous estimons la vitesse de nage à partir des données acoustiques selon la méthode utilisée par Fletcher et al. (1996); Burgess et al. (1998); Goldbogen et al. (2006) et Simon et al. (2009), et implémentée par Alexandre Génin (2013, non publié) sous Matlab (v8.1 ; The MathWorks).

Le principe de cette méthode est d'utiliser les phases de transit, durant lesquelles la vitesse de nage v peut être calculée de façon fiable par la formule $v = v_z/sin(\theta)$, pour modéliser la relation entre vitesse de nage et bruit d'écoulement de l'eau (B) et enfin prédire la vitesse de nage sur l'ensemble des périodes au cours desquelles le son a été enregistré. Dans les 150-200 premiers mètres de la colonne d'eau le corps des éléphants de mer n'est pas compressé au maximum. Par conséquent leur flottabilité est accrue et la vitesse verticale plus faible (cf l'augmentation progressive de la vitesse verticale dans les premières minutes de plongée, figure 2.11). L'objectif étant de prédire la vitesse de nage durant la phase de fond des plongées, la calibration de la relation $v = f(B)$ (figure 2.13) ne s'appuie que sur le calcul de v à des profondeurs supérieures à 200 m. Afin d'obtenir B, l'enregistrement acoustique est filtré à l'aide d'un filtre passe bas de fréquence $f < 110$ Hz, puis moyenné sur les périodes où la vitesse de nage a été calculée.

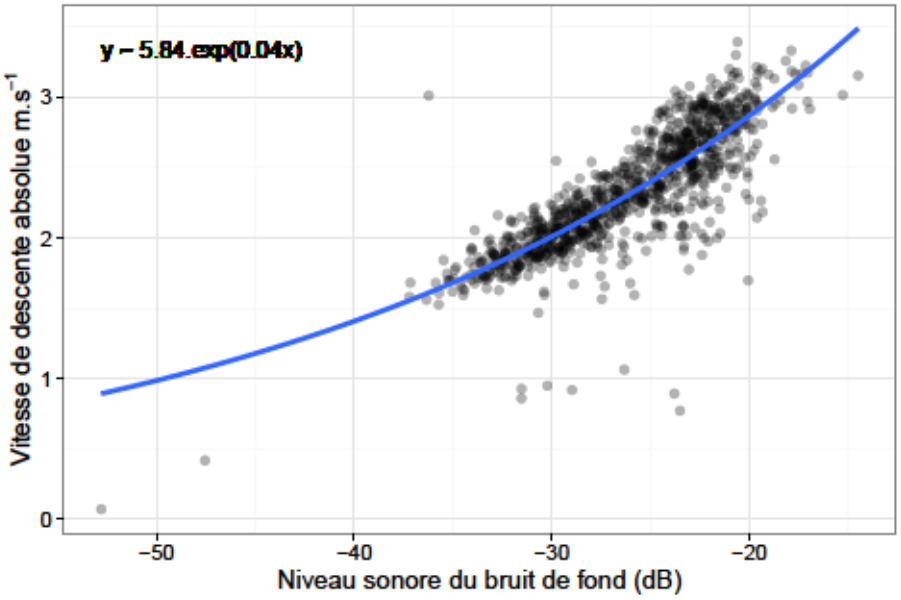

Figure 2.13: Relation entre entre le bruit et la vitesse de nage – *Acousonde A032 – Déploiement 2011. Crédit : J. Jouma'a & A. Génin.*

CHAPITRE

3 How elephant seals adjust their fine scale horizontal movement and diving behaviour in relation to prey encounter rate

La cabane de rivière du nord (49°10′38.40″S, 70°8′16.60″E). Crédit : J. Laborie.

1. Le Bras Yves, Jouma'a Joffrey, Picard Baptiste, Guinet Christophe. (2016). How elephant seals (Mirounga leonina) adjust their fine scale horizontal movement and diving behaviour in relation to prey encounter rate. *Plos One*. doi: 10.1371/journal.pone.0167226

► Les annexes de cet article sont disponibles en annexe B du manuscrit.

3.1 Abstract

Understanding the diving behaviour of diving predators in relation to concomitant prey distribution could have major practical applications in conservation biology by allowing the assessment of how changes in fine scale prey distribution impact foraging efficiency and ultimately population dynamics. The southern elephant seal (Mirounga leonina, hereafter SES), the largest phocid, is a major predator of the southern ocean feeding on myctophids and cephalopods. Because of its large size it can carry bio-loggers with minimal disturbance. Moreover, it has great diving abilities and a wide foraging habitat. Thus, the SES is a well suited model species to study predator diving behaviour and the distribution of ecologically important prey species in the Southern Ocean. In this study, we examined how SESs adjust their diving behaviour and horizontal movements in response to fine scale prey encounter densities using high resolution accelerometers, magnetometers, pressure sensors and GPS loggers. When high prey encounter rates were encountered, animals responded by (1) diving and returning to the surface with steeper angles, reducing the duration of transit dive phases (thus improving dive efficiency), and (2) exhibiting more horizontally and vertically sinuous bottom phases. In these cases, the distance travelled horizontally at the surface was reduced. This behaviour is likely increase the contribution from water currents to the seals' displacement, as they try to remain within favourable prey patches. The prey encounter rate at the bottom of dives decreased with increasing diving depth, suggesting a combined effect of decreased accessibility and prey density with increasing depth. Prey encounter rate also decreased when the bottom phases of dives were spread across larger vertical extents of the water column. This result suggests that the vertical aggregation of prey can regulate prey density, and as a consequence impact the foraging success of SESs. To our knowledge, this is one of only a handful of studies showing how the vertical distributions and structure of prey fields influence the prey encounter rates of a diving predator.

3.2 Introduction

Foraging behaviour and more specifically, foraging success, is critical to the growth, reproduction and survival of animals and is therefore subject to natural selection (Stephens and Krebs, 1986). As a result, foraging behaviour is expected to be optimized so that net energy gains are maximized for a given level of time and energy spent

foraging (MacArthur and Pianka, 1966; Charnov, 1976; McNamara, 1982). While foraging at sea, diving predators are central place foragers from the ocean's surface, where they need to come back to breathe between dives required to reach their prey at depth (Kooyman, 1989; Guinet et al., 2014). Under such constraints, the efficient diving behaviour of a predator is presumably the key to the optimization of their energy balance.

As the movements of free-ranging animals reflect how they interact with their physical and biological environment, spatial patterns in their trajectories provide a basis from which to understand foraging behaviour as well as gain insights on prey distribution and accessibility (Guinet et al., 2014; Bost et al., 2015). Recent technological advances in miniaturised electronic devices have enabled the detection of foraging events and the description of diving behaviour over very fine scales. Indeed, tri-axial jaw-mounted (Viviant et al., 2010; Naito et al., 2010; Watanabe and Takahashi, 2013) or head-mounted (Gallon et al., 2013; Foo et al., 2016) accelerometers has been successfully used to detect Prey Encounter Events (PEE hereafter) in several diving species of pinniped. Pitch angle, derived from three-dimensional acceleration data, provides spatial information on the vertical movements which cannot be obtained from time-depth dive profiles. As such, pitch angle can be helpful in addition to dive profiles for interpreting the diving behaviour of diving predators (Mitani et al., 2010; Sala et al., 2011). Three-dimensional magnetometry allows the computation of heading angle which, similarly to pitch angle according to vertical movement, complements time-depth data with information on horizontal movements. In this study, the spatial information obtained from pressure, accelerometer and magnetometer data are used to quantitatively assess how changes in vertical and horizontal diving behaviours relate to prey encounter rate.

Without acceleration data, accurate feeding indices are often difficult to obtain. A large number of studies use changes in surface GPS track patterns (Robinson et al., 2007; Kirkman et al., 2016; Hindell et al., 2016; Lascelles et al., 2016) or diving behaviour (Dragon et al., 2012b; Hanuise et al., 2010; McIntyre et al., 2011b, 2013) as foraging indices. In various predator species, resource acquisition has been linked to a type of behaviour called area-restricted search (ARS) (Kareiva and Odell, 1987). In a patchy environment, such as the open ocean, an animal will intensify its foraging in response to an increase in prey density (Hindell et al., 2016). Therefore, ARS is characterized by a decrease in displacement speed and an increase in track sinuosity in areas of

putative prey aggregation (Kareiva and Odell, 1987; Parker and Stuart, 1976).

Similarly, according to the vertical dimension, diving seabirds, marine mammals and leatherback turtles are expected to adjust their diving behaviour according to the quality and depth of the targeted prey patch (Thompson and Fedak, 2001; Sparling et al., 2007; Doniol-Valcroze et al., 2011). A number of species, such as penguins and pinnipeds, perform behavioural adjustments in relation to prey density, such that they modulate the duration of the bottom phase of a dive (Jouma'a et al., 2015; Cornick and Horning, 2003; Tremblay and Cherel, 2000). The bottom phase of a dive has been validated as the time when most feeding occurs in several species including Antarctic fur seals (*Arctocephalus gazella*) (Hooker et al., 2002; Viviant et al., 2014), northern elephant seals (*Mirounga angustirostris*) (Naito et al., 2013), grey seals (*Halichoerus grypus*) (Austin et al., 2006), Magellanic penguins (*Spheniscus magellanicus*) (Wilson et al., 2002), Weddell seals (*Leptonychotes weddellii*) (Davis et al., 2003) and leatherback turtles (*Dermochelys coriacea*) (Fossette et al., 2008). King penguins and macaroni penguins perform behavioural adjustments during the descent and ascent phases of their dives in relation to prey encounter rates during the previous dive (Sato et al., 2004; Hanuise et al., 2013), as predicted by Thompson and Fedak (2001). Similarly, elephant seals increase their dive angles on putative foraging dives (Robinson et al., 2007; Hassrick et al., 2007). These adjustments take place mainly through changes in body angle, rather than through a change in swimming speed (Hanuise et al., 2013; Ropert-Coudert et al., 2001; Miller et al., 2012). However, there is a lack of studies investigating quantitatively the mechanisms explaining how changes in diving behaviour (such as pitch angle adjustments during descent and ascent phases or pitch and heading variability during bottom phase) in response to prey encounter rate may impact the horizontal speed of the animal track at surface. Indeed, in most studies relating dive behaviour to horizontal speed measured from surface locations, no acceleration data were available and analyses were conducted on pressure-only dive metrics.

Living in the Southern Ocean, female Southern Elephants Seals (SES hereafter) with their large size and their great diving abilities are well suited for studying foraging behaviour, as using bio-logging tools causes minimal disturbance. SES spend 10 months a year at sea, covering thousands of kilometres during foraging trips and 90% of which is spend diving (Hindell et al., 1991a). An average dive lasts between 20 and 30 minutes, at a depth ranging generally between 300–500 m, punctuated by surface periods of 2–3 minutes (McConnell et al., 1992). As for many diving predators, SES

forage mostly at the bottom of their dives (Guinet et al., 2014; Foo et al., 2016; Schreer et al., 2001).
Female SES feed mainly on myctophids and cephalopods (Cherel et al., 2008), both ecologically important groups of species within the Southern Ocean (Kock, 1987; Rodhouse and White, 1995; Pakhomov et al., 1996; Collins and Rodhouse, 2006). Because of its overall abundance and individual body mass, the SES is a major consumer of Southern Ocean marine resources (Guinet et al., 1996; Hindell et al., 2003). As such, understanding better the foraging behaviour of data rich species such as SES (McIntyre, 2014) could provide valuable insight toward the biology and distribution of these important groups of species which are otherwise difficult to sample (Pakhomov et al., 2010). Prey abundance and density within the water column are likely to be key factors in the foraging success of these predators. As such, understanding the diving behaviour of SES in response to prey density could help to predict how changes in prey distribution may impact predator populations.
In this study, we examine (1) how diving behavior relates to prey encounter rates during the bottom phase of a dive, (2) the repercussions of these relationships on the travel transit rate of SESs and (3) their diving efficiency.

1. To achieve (1), we used two metrics of diving behaviour describing (i) the vertical location of foraging activity through the water column (such as the depth of the bottom phase and its vertical extent through the water column) and (ii) fine-scale indicators of active foraging search (such as directional changes in pitch and heading angles). Then, we addressed a series of two sub-objectives. First, quantitatively measure the behavioural response of SES to changes in a proxy of prey density (prey encounter rate). Second, assess how this proxy relates to the vertical foraging location in the water column for a given level of active foraging search as it could help to predict how prey distribution may impact SES population in the future.

2. Horizontal speed, measured using GPS locations at the surface, with the track sinuosity, is one of the main metrics used in state-space models to infer intensive foraging behaviour. Therefore objective (2) of the study is to understand, using fine scale information, how the vertical and horizontal diving behaviours related to prey encounter rate mechanistically translate into a change of horizontal speed.

3. Our final objective (3) is to better understand the response of SES to the prey encounter rate in terms of foraging strategy, by investigating how adjustments in diving behaviour, and particularly diving angle, benefit diving efficiency, as indicated by the proportion of a dive's total duration dedicated to the bottom phase.

3.3 Materials and Methods

3.3.1 Ethic statement

All fieldwork involving SES was approved and authorized by the ethics committee of the French Polar Institute (Institut Paul Emile Victor—IPEV) in May 2008. This Institute does not provide any permit number or approval ID, however animals were handled and cared for in total accordance with the guidelines and recommendations of this committee (dirpol@ipev.fr).

3.3.2 Animal handling and electronic devices

During the breeding seasons (October and November) of 2010 through to 2014, a total of 9 female SESs of the Kerguelen Islands (49°21′0″ S, 70°13′0″ E) were equipped with (1) a Daily Diary tag (TDR10-DD, Wildlife Computers™, USA) and (2) a location collector device. The location detector device was either a Conductivity-Temperature-Depth satellite-relay data logger (CTD-SRDL, Sea Mammal Research Unit—University of St Andrew), a Time-Temperature-Depth Fastloc GPS data logger (SPLASH10-F, Wildlife Computers™, USA) or a Smart Position or Temperature Transmitting tag (SPOT, Wildlife Computers™, USA). Animals were captured with a canvas head-bag and anesthetized using a 1 :1 combination of Tiletamine and Zolazepam (Zoletil 100) injected intravenously (McMahon et al., 2000). A TDR10-DD was then glued on each seal's back and the location collector devices to the head using quick-setting Araldite (Araldite AW 2101). One individual was equipped with an additional accelerometer on its head. Details about the length and weight of each individual, logger-type deployment details are provided in the Table A in appendix B.1.
The TDR10-DD logs depth (range = 0 to 2000 m, resolution = 0.5 m, accuracy = 1% of reading value, sampling frequency = 1Hz), temperature (range = -40°C to +60°C resolution = 0.05°C, accuracy = 0.1°C, sampling frequency = 1 Hz), and light (range = 5×10^{-10} W cm^{-2} to 5×10^{-2} W cm^{-2} (8 decades), resolution = 20 units per decade,

sampling frequency = 1 Hz) as well as tri-axial acceleration (range = –2 g to +2 g, resolution = 0.05 m s^{-2} sampling frequency = 16 Hz), tri-axial magnetometry (direction and strength of local magnetic field vector, range = -100 nT to +100 nT, resolution = 0.2 nT, sampling frequency = 16 Hz), and velocity (as the relative speed of the logger in surrounding water). The velocity sensor did not function correctly because of a build-up of dirt shortly after deployments which obstructed the propeller. Acceleration and magnetometry were measured along the same axes of the logger which were : (1) longitudinal (positive forward), (2) lateral (positive rightward) and (3) vertical (positive downward). TDR10-DD's were positioned so that the logger's X and Y axes approximately match longitudinal and lateral midlines of the SES.

The SPLASH10-F was the other type of data logger used in this study. They provided GPS locations 60% of the times the SES were back at surface to breathe. SPLASH10-F also measures depth, temperature and light (as described for the TDR10-DD) but these data were only used to synchronize with datasets from other loggers when it was necessary (when comparing head and back mounted accelerometers on a same individual, Figure A in B.2 Appendix). The CTD-SRDL and SPOT tags provided Argos locations (along with salinity and temperature in the case of CTD-SRDLs) that were used to locate the seals and retrieve the tags when they were back on land (but oceanographic data were not in this study).

3.3.3 Acceleration and magnetometry data processing

All data processing was performed using R version 3.1.1 (R Core Team, 2014). The majority of acceleration and magnetometry data analyses used in this study were done using the R package `rbl` (unless otherwise stated), available online at (Le Bras, 2017).

Prey Encounter Events

The detection of Prey Encounter Events (PEE) was performed following Guinet et al. (2014) and Vacquié-Garcia et al. (2015). Dynamic accelerations, resulting from rapid head movements, were extracted from the longitudinal, lateral and vertical axes of the logger using an order 3 high-pass digital Butterworth filter with a normalized cut-off frequency of 2.64 Hz (performed with the `signal` package, Signal developers (2013)). For each axis, a one-second fixed window was used to calculate the standard deviation. Signals were then processed using a moving standard deviation across a

window of five seconds. Finally, a two-mean clustering was performed for each signal to distinguish "high state" from "low state". A PEE occurred when the three axes were simultaneously in "high state" (see Vacquié-Garcia et al. (2015) for graphical illustration of the method). A continuous succession of "high state" was considered as a single PEE. One individual had both head-mounted and back-mounted accelerometers, so we used these data to check that these two acceleration data resulted in similar results (Pearson's product moment correlation coefficient = 93%, see Figure B in B.2 Appendix).

Body posture angles

Pitch and roll describe the body posture of a SES with respect to the direction of the earth gravity vector whilst heading angle is in reference to the earth magnetic vector. Static acceleration is caused by the position of the gravity center of an animal compared with the gravity vector, which is always vertically orientated and can be used to infer pitch and roll angles. Static acceleration was obtained with an order 3 low-pass digital Butterworth filter with a normalized cut-off frequency of 0.20 Hz applied to the three axes as described in Richard et al. (2014). The filtered output was then scaled to a unitary norm (function `static_acceleration` from the `rbl` package) so that pitch and roll angles could be computed directly from trigonometry formulas. Pitch and Roll angles were then calculated from this static acceleration, expressed in the North-East-Down (NED) frame of reference, using the pitch and roll functions from the `animalTrack` package (Farrell and Fuiman, 2013). The low-pass filter used to obtain static acceleration was applied to the magnetic data as well. Heading angle was then calculated (using the `tilt_compensate` function from the `animalTrack` package) from the pitch and roll angles alongside the filtered magnetic data expressed in the NED frame of reference.

Swimming effort

The frequency spectrum of the lateral acceleration displayed a clear bimodality (see Génin et al. (2015)). The high-frequency peak corresponds to the dynamic acceleration due to tail movements (Sato et al., 2003; Watanabe et al., 2006b) which was extracted using an order 3 band-pass (from 0.44 Hz to 1.02 Hz) digital Butterworth filter (Richard et al., 2014; Sato et al., 2003; Watanabe et al., 2006b; Aoki et al., 2011). To measure the frequency and magnitude of these tail movements, the absolute value of the resulting signal is then averaged to 1 Hz. We called the latter "swimming effort"

and used it as a proxy of the cost of locomotion. This method is implemented in the `swimming_effort` function of the `rbl` package.

3.3.4 Dive analyses

Dives

We defined dives as periods where animals were continuously deeper than 15 m under the surface. Because there is drift in the pressure readings of the tags over time, a zero offset correction of the depth time sequence was applied prior to the delimitation of dives (function `offset_correction` from the `rbl` package). SESs occasionally perform subsurface incursions, which results in a short number of atypical short and shallow dives. Moreover, unpredictable gaps in the time-depth sequence (due to a malfunction of the depth sensor) can sometimes cause different dives to be merged as a single very long one. According to the quantiles of all dive durations, dives lasting less than 8.33 min (500 s, Q1% = 511 s) or more than 32.50 min (1950 s, Q99% = 1947 s) were excluded in order to get rid of these irregular cases.

Dives phases

Each dive was divided into three phases : descent, bottom and ascent phases following Halsey et al. (2007). This method defines the bottom of a dive as the period between the first and the last wiggle or step being deeper than a given depth threshold which is expressed as a percentage of the maximum depth in the dive. Steps and wiggles are time-depth patterns observed in the bottom of dives. Steps are defined as periods where the vertical velocity slows down but stays above 0 $m\,s^{-1}$ while wiggles as periods where depth increases and then decreases, drawing a concave shape in the dive profile (Halsey et al., 2007). The upper limits of vertical velocity threshold applied to identify the steps in the time-depth dive profiles was kept to its value for king penguins (0.35 $m\,s^{-1}$, Halsey et al. (2007)) as it is close from observed values of non-swimming SES (see histogram of drift rates in Bailleul et al. (2007b)). In our datasets the large majority of PEE occurred deeper than 75% of the maximum dive depth (77.24% of all PEE) so this ledge threshold value from Halsey et al. (2007) was kept. This method is implemented in the `bottom_delim` function of the `rbl` package. We choose this method to delimitate bottom phases of dives instead of the method we previously used in Jouma'a et al. (2015) to make sure that bottom phase limits could not fall within a step or a wiggle which would introduce mistakes when counting

them. Indeed, by definition, the method developed by Halsey et al. (2007) defines the limits of the bottom at the start and the end of such events.

3.3.5 Dive statistics

A proxy of prey encounter density, PEE rate, was calculated as the total PEE of a bottom phase divided by its total duration in minutes. Our estimate of prey density is thus dependent on SES behavior. The diving behaviours to be used as explanatory variables were divided into two categories : variables related to the area of the water column targeted during the bottom phase and variables related to SES foraging activity, as described below.

Water column area targeted by elephant seals

The median depth at the bottom of dives is a standard variable to describe diving behaviour. During the bottom phase, a SES's focus is expected to be on foraging whilst descent and ascent phases are primarily used for transit to this foraging ground. The median depth of the bottom phase reflects the vertical location of the resources on which the predator decided to forage on. As such, the bottom phase depth is positively related to the amount of time and energy that a SES spends to access their prey at depth. As the objectives of SESs are different in transit and in bottom phase, we focused on the bottom and selected the PEE rate at bottom as an index of the prey encounter density which is independent from the duration of the transit phases. In this study the bottom median depth is used to test whether or not the prey encounter density varies according to depth.

To describe in more detail the vertical location of the bottom phase, "bottom vertical extent" was defined as the depth range between the 10% and 90% depth quantile. Using the quantiles rather than extremes of depth yields a more robust measure of the vertical extent of the water column layer targeted by SES, excluding extreme values from unrealistic bottom phase delineation or atypical diving behaviour (where SES perform a high amplitude wiggle thus exploring a wide depth range but only for very short time).

Foraging activity

The number of wiggles has been used as a proxy of the foraging success for various diving predators (e.g. Northern Elephant Seals and King penguins, Hanuise et al.

(2010); Robinson et al. (2010)) and are also encountered in the bottom of SES dives. While wiggles are correlated to the number of PEE, the steps rather resemble a gliding pattern (slow ascending or descending vertical speed) and it is not clear yet if this diving pattern is associated with foraging or not. Percentage of the bottom duration during which SES were performing steps and wiggles were included in the analyses as they stand for two distinct diving behaviors describing the foraging activity during the bottom phase.

The mean descent and ascent pitch angle (circular mean, `CircStats` package Lund and Agostinelli (2012)), as well as the average descent and ascent swimming effort were computed to account for the transit time adjustments made by the SES in response to the foraging success and to the targeted bottom depth. In a way to assess the amount of directional changes performed by SESs during the bottom phase of their dives, the circular variance of the pitch and heading angles were calculated. The circular variance of the pitch and heading angles provide comparable indices of the sinuosity according to of the vertical (pitch angle) and horizontal (heading angle) dimensions. While pitch variance could be considered redundant with the percentage of time doing wiggles at bottom, it is actually complementary. Indeed for a given quantity of wiggles the greater the pitch variance the steeper they are. Another advantage of this measure over the wiggles is that it is a simple summary statistic of a quantitative variable and does not depend on an algorithm to detect specific events. Hence, it varies continuously, which results in a subtle description of the diving behaviour, and has no detection error issue.

Because our focus is on dives associated with foraging, drift dives, during which SES are resting and/or digesting (Crocker et al., 1997), were removed from the dataset prior to the statistical analysis.

3.3.6 Statistical analysis

We implemented five models (numbered 1a, 1b, 2, 3 and 4) relating to the objectives articulated in the introduction (numbered 1, 2 and 3).

The first objective is to describe the relationships between the PEE rate at the bottom (the response variable) and the diving behaviours during daytime (model 1a) and night-time (model 1b). This allows testing whenever the PEE rate varies according to depth independently of the effect of daily vertical migrations of the SES prey. Namely, the diving behaviours used as explanatory variables in these models are : the median

depth at the bottom of dives, the bottom phase vertical extent, the proportion of bottom time spent doing wiggles or steps during the bottom phase, the mean pitch angle in the descent and ascent phases and the variances of pitch and heading angles. We used the number of PEE at the bottom as the response variable of a count model (log link) but actually modelled PEE rate as response by providing the log-transformed bottom duration as an offset variable (the effect of an offset variable is not estimated but forced to one). Poisson family GLMs indicated over-dispersion. We used the Negative Binomial family GLM (`MASS` package, Venables and Ripley (2007)) to address over-dispersion. The inter-individual differences in PEE rate were modelled by specifying the SES identities as fixed effects intercepts.

The second objective is to examine how the horizontal speed at surface during dives — measured from the distance and duration between SES locations taken as they surface before and after dives – relates to the diving behaviours (model 2). To have a reliable estimate of this surface horizontal speed, we used only dives where observed GPS locations preceding and following the dive (39% of dives). This subset introduces a bias toward the selection of dives with longer recovery time that we could not account for (surface periods lasting 127 s for located surfaces but 120 s otherwise, see Table A and Figure B in B.3 Appendix for details). We used a Linear Mixed Model (LMM, `nlme` package, Pinheiro et al. (2015)) with the horizontal speed at surface as the response variable, and the same diving behaviours used in models 1a and 1b as explanatory variables and an individual as a random intercept.

The third objective is to investigate the effects of diving behaviours on dive efficiency (model 3). Diving efficiency is defined as the bottom phase duration divided by the full dive duration. The proportions typically display more variability around their mean so we used a variable dispersion beta regression model (`betareg` package, Cribari-Neto and Zeileis (2010)) to handle the heteroskedastic nature of this response variable. The diving behaviours used as explanatory variables are the same as in previous models (models 1a, 1b and 2) and the SES identities were specified as fixed effects intercepts.

The last model implemented in this study (model 4) is related to the third objective and aims at clarifying how the transit between surface and the bottom phase location may be regulated by diving behaviour adjustment. As for model 2, we implemented a LMM. In this model, the response variable is the duration of the phase, and the explanatory variables are the type of phase (ascent or descent), the maximum depth

reached during the phase and the average swimming effort during the phase. A random intercepts of SES individual was included. A single model was used for both types of transit phase (ascent or descent). We tested for interactions between the type of phase and other explanatory variables to enable the estimation of distinct relationships during ascent and descent phases.

The model selection procedure was performed in two stages. The first stage consisted in a stepwise AIC starting from the full model with all explanatory variables and dropping variables step by step until the AIC reached a minimum. In order to allow potentially non-linear relationships in the five models that we implemented, linear combinations of the powers of covariates (polynomials) were tested. These polynomials allow fitting a relationship of any shape but the more complex is the shape the more parameters it requires and the stronger it is penalized by AIC. Thus, the second stage of the model selection procedure was to test for non-linear relationships by computing the AIC with polynomials of the previously selected explanatory variables of increasing degree until the model AIC reached a new minimum. During the model selection, models were fitted with Maximum-Likelihood algorithm. Final models were re-fitted with Restricted Maximum Likelihood algorithm. For each of the five models the final set of explanatory variables selected is displayed on the corresponding figure. The specification of correlation structures (such as AR, ARMA or ARIMA) induces very large computation time and is not implemented for all types of model that we used. We addressed the temporal autocorrelation issue by selecting one dive every ten. The existence of an autocorrelation structure in the models' residuals was assessed by plotting their auto-covariance function for each individual (performed with the `acf` function). Colinearity issues between covariates was checked prior to model selection using Variance Inflation Factor ($VIF < 5$, `usdm` package, Naimi (2015)).

Various pseudo-R^2 were used to assess the amount of variation explained by the top models. For LMMs (models 2 and 4) we used an equivalent of the Ordinary Least-Squares (OLS) R^2 which has been developed by Nakagawa and Schielzeth ((Nakagawa and Schielzeth, 2013), implemented in the `MuMIn` R package, Barton (2016)). It has a "marginal" (R^2_m) and a "conditional" (R^2_c) component which can be interpreted as the variance explained by fixed effects only (R^2_m) and by the entire model (R^2_c). For GLMs (models 1a and 1b) we calculated the percentage of the null model deviance explained (D^2, Table 3.1) by the top models as a substitute to OLS R^2 (Guisan and

Zimmermann, 2000). Moreover, for these models, we calculated the null model deviance explained (hereafter abbreviated NDE) by each explanatory variable. Finally, to evaluate goodness-of-fit of the beta regression (model 3) and to compare it to the other models, we calculated a pseudo R^2 metric defined as the squared Pearson's correlation coefficient between observed values (transformed with the link function) and fitted values of linear predictor. This pseudo R^2 metric (noted Pearson^2 in Table 3.1) ranges from 0 to 1 and provides an indication of correlation between predicted values and actual values (where the closer to 1 the better).

Table 3.1: Goodness-of-fit of the top models as indicated by pseudo-R^2 – *See the "Statistical analysis" section for details about these metrics.*

Model		D^2	Nakagawa et al. R^2	Pearson^2
1a	(Neg. Bin. GLM)	58%		56%
1b	(Neg. Bin. GLM)	63%		60%
2	(LMM)		$R^2_m = 41\%$, $R^2_c = 48\%$	47%
3	(Beta regression)			87%
4	(LMM)		$R^2_m = 93\%$, $R^2_c = 94\%$	85%

3.4 Results

3.4.1 Overall diving behaviour

A total of 20189 dives were recorded from the 9 post-breeding female SESs. Of these 8.4% were classified as drift dives. Mean dive duration was 18.38 min (1103 s) $\pm SD =$ 5.13 min (308 s) and mean bottom duration was 7.95 min (477 s) $\pm SD = 4.12$ min (247 s). The overall average of mean depth at bottom was 409 m $\pm SD = 192$ m with a maximum of 1307 m. PEEs were detected in 91.1% of non-drift dives. 10.48% of PEE occurred in descents, 78.03% in bottom phases and 11.49% in ascent. Additional descriptive statistics of diving behaviours are available in the Table C in B.1 Appendix.

3.4.2 Relationships between prey encounter rate and diving behaviours

The models 1a and 1b selected by the model selection process included ascent pitch diving angle, angular variances of pitch and heading during bottom phase, the median depth and vertical extent of bottom phase and, for model 1a only, the percentage

of bottom time spent doing wiggle. The PEE rate at the bottom during day and night is positively related to ascent pitch diving angle (3% NDE for daytime and 11% NDE at night) and to the angular variances of pitch (5% NDE for daytime and 20% NDE at night) and heading (31% NDE for daytime and 6% NDE at night) angles at bottom (Figs 3.1 & 3.2). Negative relationships were found between PEE rate and the bottom median depth (10% NDE for daytime and 15% NDE at night) and to the bottom vertical extent (3% NDE for daytime and 1% NDE at night) (Figs 3.1–3.3). PEE rate at bottom responded to bottom time doing wiggles during day only (1% NDE).

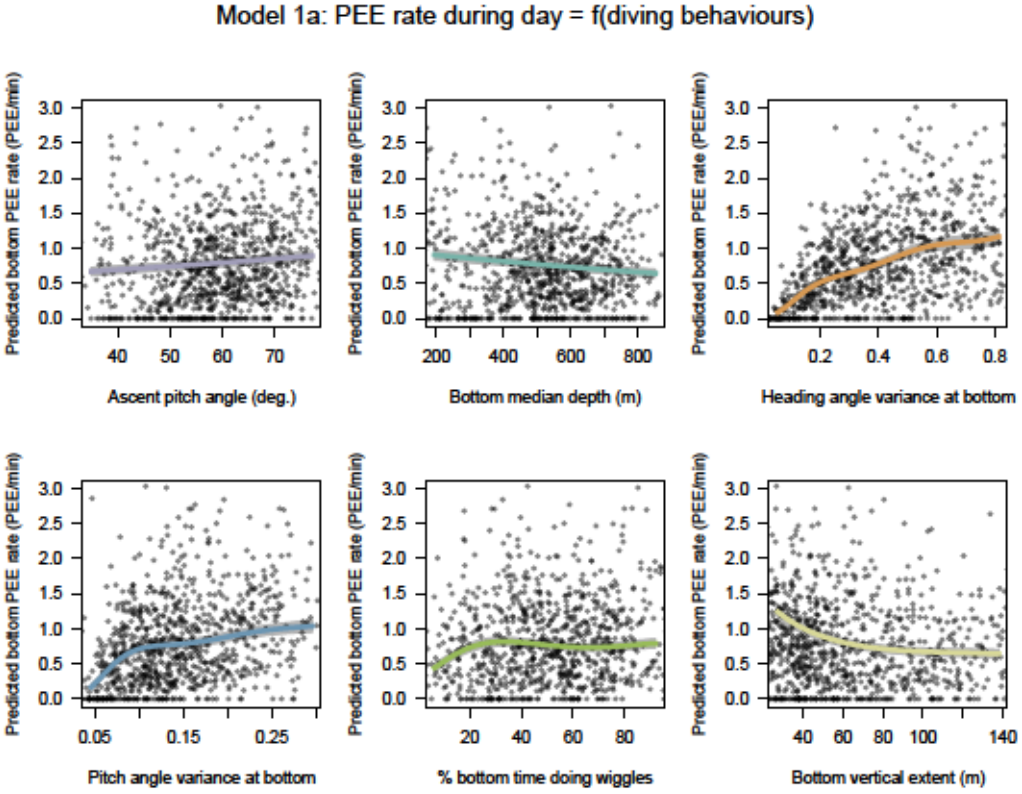

Figure 3.1: Estimated effects of covariates selected in model 1a – *Expected response predicted with a covariate varying from the 5% to the 95% quantile of its observed values with other covariates at their mean. The x axes have been scaled to range from -2 to 2 normalized so that regression slopes are comparable but are annotated with raw units so that units are comprehensible. The grey shades around the regression lines indicate the standard error of the mean prediction estimates.*

According to the regression slopes, the strongest effects on prey encounter rate during the day are heading and pitch angle variances at the bottom (particularly for low values), the bottom vertical extent (again for low values) and the bottom median depth (Fig 3.1). Below 20% of bottom phase duration, the time at bottom spent doing

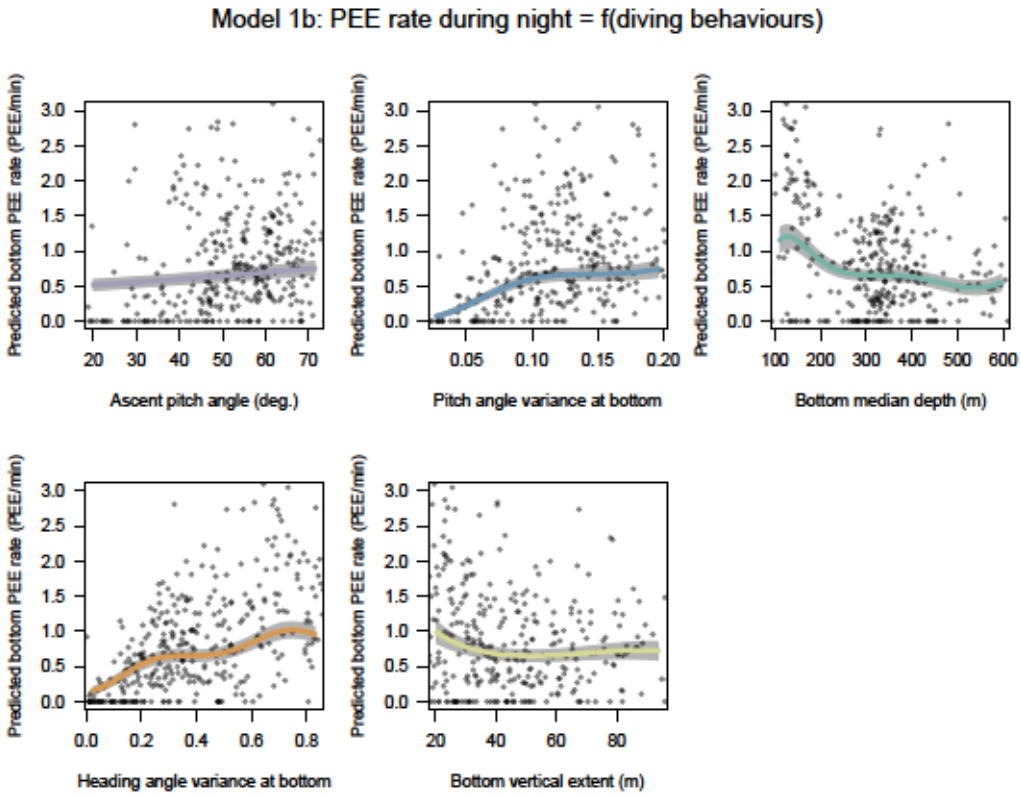

Figure 3.2: Estimated effects of covariates selected in model 1b – *The predictions for each covariate varying from the 5% to the 95% quantile of observed values with other covariates at their mean. The x axes have been scaled to range from -2 to 2 normalized so that regression slopes are comparable but are annotated with raw units so that units are comprehensible. The grey shades around the regression lines indicate the standard error of the mean prediction estimates.*

wiggles has a large and positive effect on the PEE rate at bottom, but beyond this point the effect is weak (Fig 3.1). Similarly, the negative effect of the vertical extent of the bottom phase decreases from 60 m toward higher values (Fig 3.1).

Regression slopes for the night model (model 1b, Fig 3.2) display similar patterns to those of the day model. As in model 1a, the negative effect of the bottom vertical extent on the PEE rate at bottom decreases from low to high values going from a strong negative below 20 m, to an approximately flat relationship beyond this threshold (Fig 3.2). The regression line estimated for the bottom median depth differs from model 1a by displaying a non-linear shape and a steeper negative slope overall (Fig 3.2).

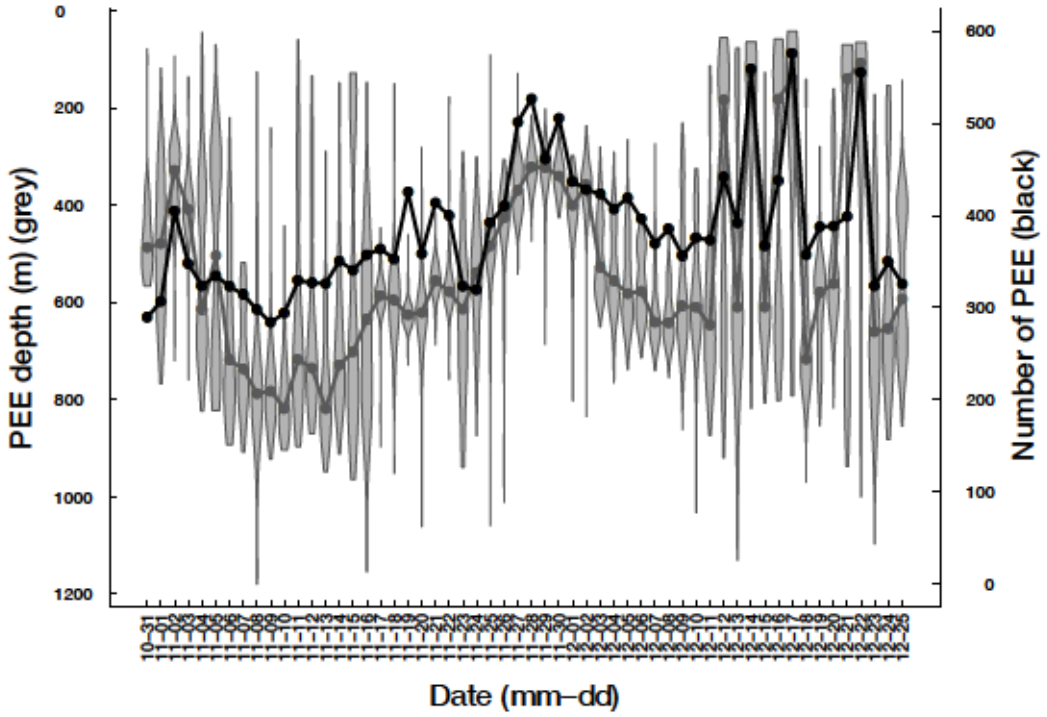

Figure 3.3: Time series of the vertical distribution of PEE in the bottom of dives and of the PEE rate (individual 2011–28) – *The black lines stand for the PEE rate (number of bottom PEE per day, daytime only), the grey violins for the vertical distribution of daytime bottom PEE (with median depth of daily PEE indicated by the grey dots).*

3.4.3 Relationships between horizontal speed at surface and diving behaviours

The model 2 with average pitch diving angle in descent and ascent phases, angular variance of pitch and heading, and percentage of time spent doing steps was selected by the model selection process. Descent and ascent diving angles and variances of heading angle at bottom have a linear negative effect on the horizontal speed measured at surface with GPS locations (Fig 3.4). We found a negatively orientated non-linear effect of the pitch angle variance at bottom on the surface speed (Fig 3.4). Finally, the amount of time doing steps in the bottom has a low positive effect in the range of low values (< 25%, Fig 3.4) but a negative effect beyond 25% (Fig 3.4). The strongest slopes are observable for ascent pitch angle and heading variance at bottom (Fig 3.4).

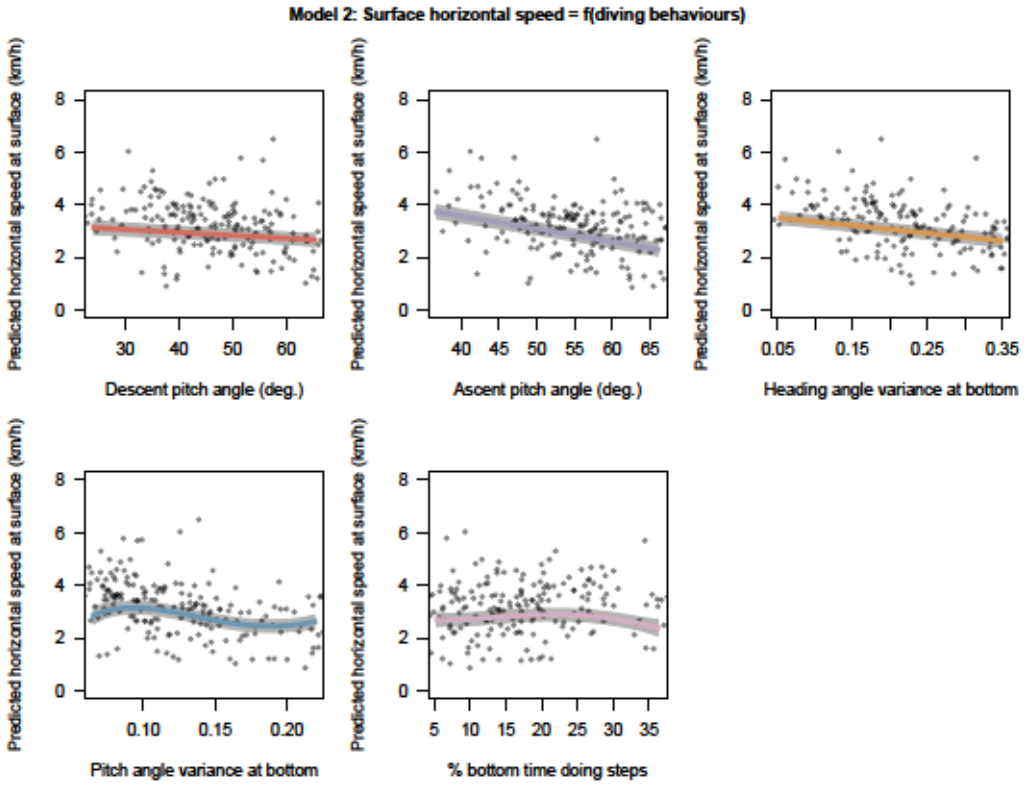

Figure 3.4: Estimated effects of covariates selected in model 2 – *The predictions for each covariate varying from the 5% to the 95% quantile of observed values with other covariates at their mean. The x axes have been scaled to range from -2 to 2 normalized so that regression slopes are comparable but are annotated with raw units so that units are comprehensible. The grey shades around the regression lines indicate the standard error of the mean prediction estimates.*

3.4.4 Relationships between diving efficiency and diving behaviours

The model 3 with average pitch diving angle in descent and ascent phases, angular variance of pitch and heading, percentage of time spent doing wiggles and median depth in bottom phase was selected by the model selection process. The diving efficiency (proportion of dive time spent in the bottom phase) is positively related to descent and ascent pitch angle, and negatively related to the bottom median depth and the variance of heading angle at the bottom (Fig 3.5). In comparison to these diving behaviours, the bottom time spent doing wiggles, the bottom vertical extent and the variance of pitch angle at the bottom have weak effects (Fig 3.5).

The model 4 with average pitch diving angle, average swimming effort and maximum depth of the phases was selected by the model selection process. Descent and ascent

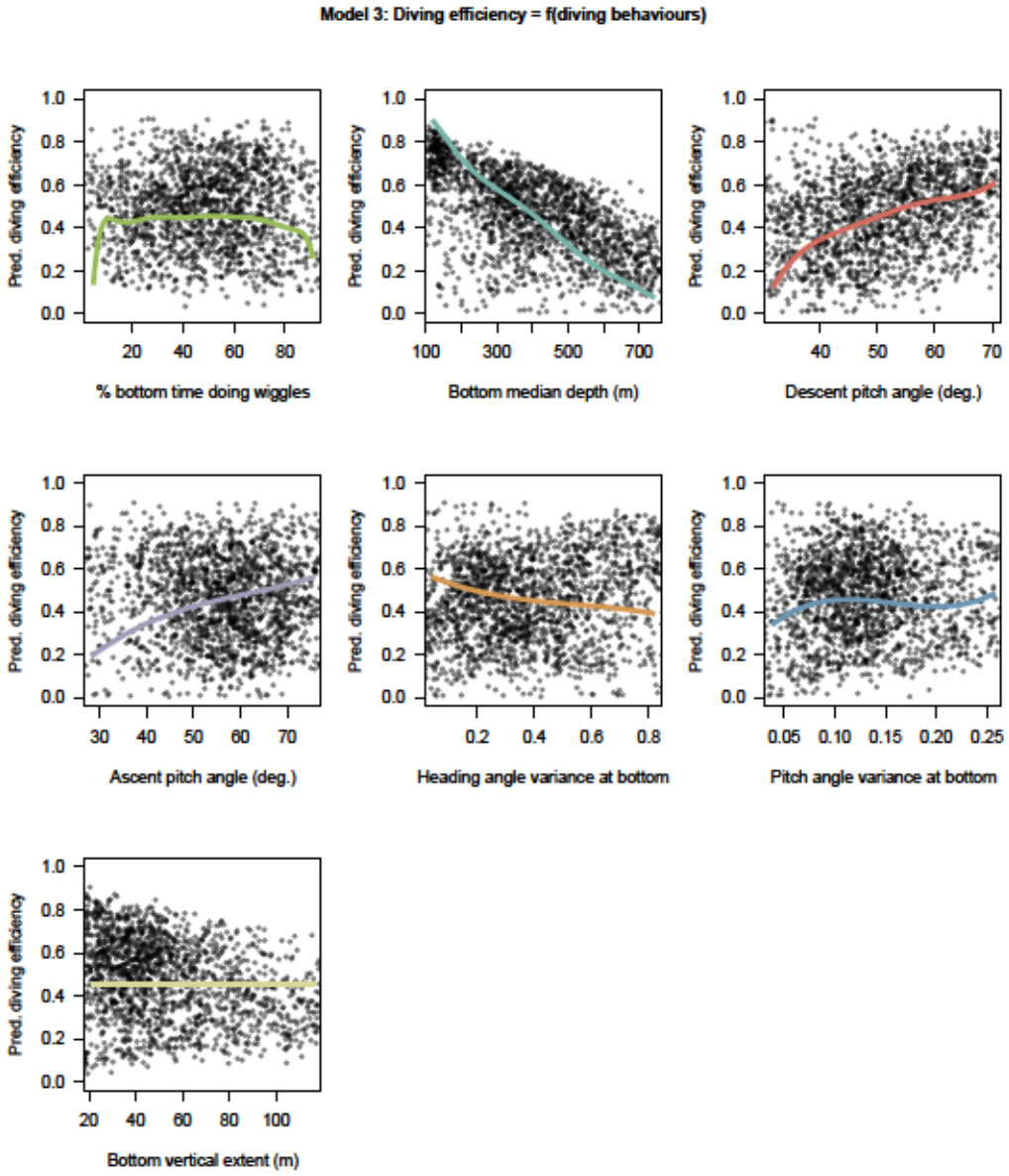

Figure 3.5: Estimated effects of covariates selected in model 3 – *The predictions for each covariate varying from the 5% to the 95% quantile of observed values with other covariates at their mean. The x axes have been scaled to range from -2 to 2 normalized so that regression slopes are comparable but are annotated with raw units so that units are comprehensible.*

durations are both negatively related to the steepness of pitch angles and positively related to the depth (Fig 3.6). The swimming effort is another significant driver of the ascent duration but not of the descent duration (Fig 3.6). While increasing the ascent vertical speed implies greater swimming effort per unit of time it is associa-

ted to smaller duration and consequently to a smaller amount of swimming effort cumulated over the complete ascent phase (Fig C & Table E in B.4 Appendix).

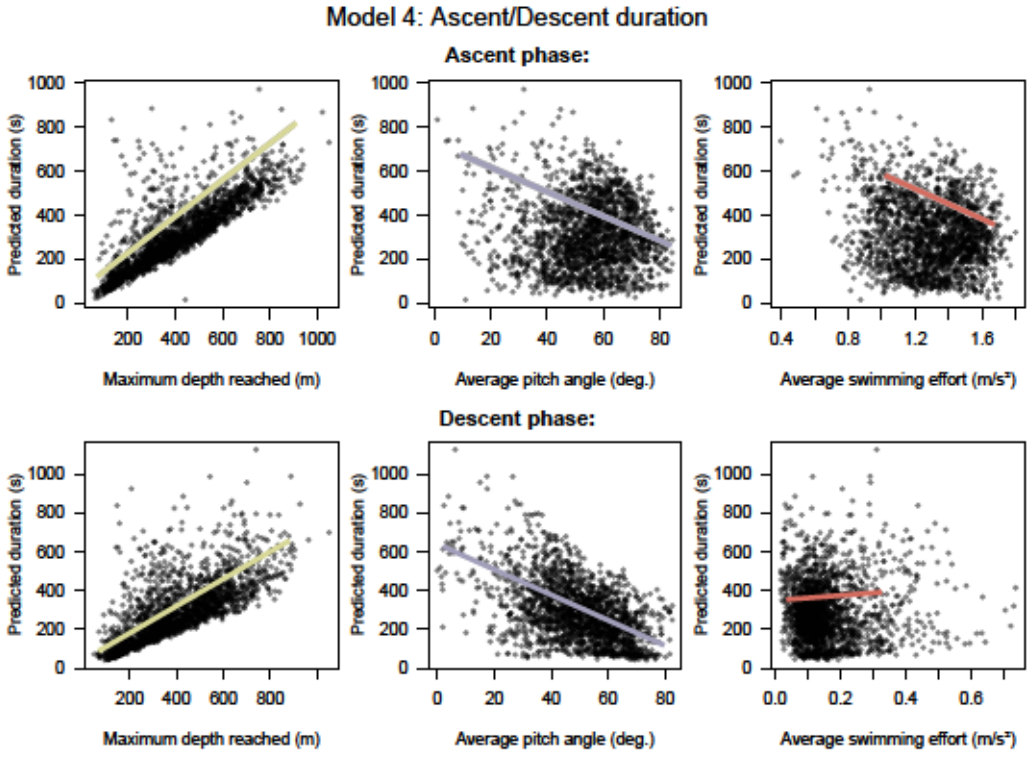

Figure 3.6: Estimated effects of covariates selected in model 4 – *The predictions for each covariate varying from the 1% to the 99% quantile of observed values with other covariates at their mean. The x axes have been scaled to range from -3 to 3 normalized so that regression slopes are comparable but are annotated with raw units so that units are comprehensible. The grey shades around the regression lines indicate the standard error of the mean prediction estimates.*

3.4.5 Models results

The datasets contained 950 complete observations for model 1a (30.64 observations per parameter) and 364 for model 1b (12.55 observations per parameter), 212 for model 2 (17.67 observations per parameter) and 1,823 for model 3 (41.43 observations per parameter). The pseudo-R^2 used to assess the response variation explained by the top models (Nakagawa and Schielzeth's R^2 for LMMs, D^2 for GLMs) or their goodness-of-fit (Pearson^2 for beta regression) are provided in Table 3.1.

3.5 Discussion

These results reveal that the prey encounter rate of SESs is driven by two main factors : (1) the depth (i.e. the vertical accessibility) of a prey patch from the surface, where the closer to the surface the better, and (2) the bottom vertical extent, where lower values were associated with higher PEE rate. This suggests that the prey catch rate of female SESs increased when well defined, narrow layers of high density prey were encountered. As such, the fine scale density within the water column, possibly rather than the overall prey density over the whole water column visited by the SES, appears to be one of the main drivers of SES prey catch rate. When high prey encounter rate is met, elephant seals adjust their diving behaviour by increasing both their descent and ascent angle (Figs 3.1 and 3.2), likely to minimize their transit time (Figs 3.5 and 3.6), and increase both their horizontal and vertical sinuosity during the bottom phase of their dive zigzagging within the prey patch layer (Figs 3.1 and 3.2). The negative relationship between the horizontal transit rate and putative feeding activity has been observed for numerous marine predators (SES (Dragon et al., 2012b) see also Figure A in B.3 Appendix, northern elephant seals (*Mirounga angustirostris*) (Kuhn et al., 2009), wandering albatross (*Diomedea exulan*), antarctic fur seals (*Arctocephalus gazella*) (Iwata et al., 2015)). A number of these variables that impacted on the PEE rate at bottom (models 1a and 1b) affected oppositely the horizontal speed measured at surface with GPS location (model 2). Namely, these variables were the diving angle in ascent phase and the variances pitch and heading angle during bottom phases (Figs 3.1, 3.2, 3.4). As a consequence, the horizontal speed measured at surface decreases when encountering more prey.

3.5.1 Behavioural adjustments to prey encounter rate

To reduce transit time and increase diving efficiency, SESs increase their vertical transit speed with steeper pitch angles mainly but also, in ascent, by increasing their swimming effort (Fig 3.6). We found that swimming effort had a greater importance on vertical speed in the ascent phase compared to the descent phase of the dives (Fig 3.6). This lower contribution of the swimming effort to the vertical speed during the descent is likely to be related to the negative buoyancy of post-breeding SES females, which tend to glide down to the bottom of their dive (Richard et al., 2014; Aoki et al., 2011). Indeed, the SES leaving Kerguelen after breeding are in poor condition and the

post-breeding foraging trips do not last long enough to fully restore their lipid provisions. During the ascent phase, negatively buoyant female SES both increase their ascent angle and their swimming effort, with both factors having an equivalent contribution to explain the increased vertical transit speed (Fig 3.6). However, the overall swimming effort in response to an increased vertical speed is negative, with a greater swimming effort per unit of time being compensated by shorter transit duration (Figure C in B.4 Appendix).

Steeper pitch angles in descent and ascent phases were found to slow down significantly the horizontal component of SES movement (model 2, Fig 3.4) and to increase the proportion of time the SES spent in bottom phase during their dives (model 3, Fig 3.5). Adjustments in diving angles lead to a trade-off between the amount of time the animal can spend to forage at depth and the horizontal speed. In an environment with a high prey density, steep diving angles allow individuals to spend longer time at depth in contact with prey and to remain in the same area for their next dives. However, in low prey density area, flat diving angles speed up horizontal transit rate and shorten search time to find a new prey patch. The positive relationship between the steepness of ascent angle and the PEE rate at bottom (model 1, Figs 3.1, 3.2) could be interpreted according to the optimal foraging theory as a behavioural adjustment to maximize the time spent in high prey density environment. This relationship was weak in model 1a, suggesting that the deeper dives performed during daytime leave less room for such adjustments. As the diving angle in descent could be a way to regulate the horizontal speed it is likely to respond not only to the prey patch quality but also to the migration stage of the SES (Miller et al., 2012). Oblique descent angles have also been suggested to relate to prey location where it could help the SES to combat the camouflage of squids in the downward light (Hassrick et al., 2007).

Diving depth had the strongest impact on the diving efficiency, which can be explained by the greater transit duration to reach those greater depths which reduces the amount of time SES could allocate to foraging at the bottom (model 3). The energetic cost of transit to the bottoms of dives is also related to the body buoyancy. Swimming energy expenditure is the lowest at neutral buoyancy allowing the seals to increase their diving efficiency (Richard et al., 2014). Seals also tend to adjust their diving efficiency according to the foraging success of the current and the previous dives (Jouma'a et al., 2015).

The prey encounter rate was positively related to the circular variances of both pitch

and heading angles (Figs 3.1, 3.2) which are indicative of the vertical and horizontal sinuosity of the bottom. These diving behaviours also impacted strongly on the horizontal speed at surface, thus increasing the residence time of SES in a given area. This is consistent with observations of Area Restricted Search behaviour in other diving seabirds and pinnipeds or, at larger spatial and temporal scales, with SES (Dragon et al., 2012b; Bailleul et al., 2007b, 2008; Dragon et al., 2010) alongside side optimal foraging theory which predicts longer residence in high prey density grounds. The heading angle variances at the bottom was detrimental to diving efficiency (model 3, Fig 3.5), suggesting that increased horizontal sinuosity is associated with prey chasing or handling and to a greater energy expenditure.

The bottom time spent performing wiggles was related to PEE rate at the bottom in day conditions. Its effect displayed a plateau at intermediate-high values (> 30% Fig 3.1). Wiggles were also found to impact on diving efficiency toward extreme values (Fig 3.5). Pitch and heading angular variances during the bottom phase of the dive had greater and more consistent effect over the complete range of observed values and appear to be a more reliable indicator of PEE rate. The bottom time spent doing steps related solely to horizontal speed at the surface and displayed contrasting effects (Fig 3.4), suggesting that this behaviour is employed for multiple purposes. From our perspective, steps may represent short drifting periods or gliding periods allowing horizontal travel at low expense or to locate prey during the bottom phase of the dive.

Della Penna et al. (2015) showed that when foraging dynamic oceanographic mesoscale structures, such as eddies, the horizontal displacements of SES encountering a high PEE rate could be as passive as those of lagrangian drifters. Thus, the SES would keep in contact with the foraging resources by reducing their horizontal displacements. As currents are supposed to contribute significantly to the horizontal movements of SES when they forage intensively (Della Penna et al., 2015), the varying current strength encountered by the animal along its trajectory is a source of noise when trying to compute the actual horizontal speed of SES from satellite locations. Despite this methodological limitation, our results highlight that foraging intensive behaviours—increasing of descent and ascent diving angles, but also of horizontal and vertical sinuosity during the bottom phase of their dive—have a negative effect on the horizontal component of their movement. As a consequence they remain within the prey patch, but become more sensitive to current transportation (Della Penna et al., 2015; Gaspar et al., 2006) and are passively transported with the prey patch

by the current. Under such a situation, with a high current velocity the ARS/non ARS behaviour detected from the surface track could result primarily from the current velocity field rather than from the active horizontal movements from the animals. As such, inference of foraging state of the animal using state space models could be erroneous.

3.5.2 Area of the water column targeted by SES

SESs were more successful when foraging closer to the surface (model 1a and 1b). Either in day (Figs 3.1, 3.3) or in night conditions (Fig 3.2), the greater the bottom depth the lower PEE per unit of time they were, showing that this observation cannot be explained by diel vertical migrations of SES prey. This negative relationship between the bottom depth and the prey encounter rate at the bottom could indicate a decrease in prey density, a change in prey type/size or a decrease of the ability of SES to catch prey items with increasing depth. Other studies have led to similar results. For example, Vacquié-Garcia et al. (2012) observed that the occurrence of bioluminescent events detected from light sensors carried by foraging elephant seals was negatively related to their diving depth. Williams and Koslow (1997) sampled micronekton between the surface and a depth of 900 m with a mid-water trawl and found a decreasing micronekton biomass with depth at night and, in autumn, during daytime as well.

Predators should match their foraging effort to prey distribution. Seventy seven percent of all PEE took place in the bottom phase of a dive. W ith regards to the accessibility and abundance of resources, the bottom phase is valuable enough to motivate the SES to stop the descent phase and focus on the search of prey at depth. Once the bottom depth is reached, the vertical extent of the bottom phase is expected to provide an indication on the vertical distribution of prey. The PEE rate at the bottom was negatively related to the vertical span of the water column explored during the bottom phase (model 1, Figs 3.1, 3.2, 3.3), suggesting that the dispersion of prey along the vertical dimension regulates the prey density encountered at depth by SES. To our knowledge this is the first time that this relationship is highlighted and could be a novel aspect that is worth considering when investigating fine scale prey density underwater.

A range of diving behaviours (e.g. dive depth, descent speed an dive duration) have been associated with mesoscale oceanographic features such as cyclonic eddies, where SES exhibit shallower diving depth compared to anti-cyclonic eddies and other ocea-

nographic domains (Dragon et al., 2010; Dragon, 2011). Water temperature was found to have a direct influence on the diving depth of SES, with SES diving deeper in warmer waters to access their prey (Guinet et al., 2014; Dragon et al., 2010). Furthermore, bottom depth was shown to be strongly negatively related to light intensity at depth which is attenuated by phytoplankton concentration within the euphotic layers (Jaud et al., 2012). Characteristics such as a high chlorophyll concentration and cold water at surface are observed in cold-core eddies (Volker et al., 2002; Kahru et al., 2007), shown to be successful foraging areas where the SES dive depth is close from surface (Dragon, 2011). While underlying determinants leading SES to explore a narrow vertical depth range in their dive bottom phases remain unclear, one could hypothesize that similar bio-physical oceanographic processes could locally constrain prey to aggregate vertically in thinner yet denser prey layers. Future work could try to assess the validity of this hypothesis.

This study could only focus on the vertical dimension of prey distribution because, due to sensor malfunction, we did not have access to the actual swimming velocity when the seal was foraging at the bottom of its dive to allow for a more accurate description of the 3D spatial structure of the prey field. Without that information we could not estimate the volume of water prospected by SES and compare it to the number of PEE in order to get an indication of prey density independent from SES behaviour (in PEE m^{-3} instead of PEE per unit of SES bottom time). Additional studies may use 3D dive reconstructions (Mitani et al., 2010; Iwata et al., 2015; Davis et al., 1999; Johnson and Tyack, 2003; Goldbogen et al., 2015) to determine if the effect of the vertical extent of the bottom on the foraging success would be related to the presence/absence of small scale schooling-prey patches (leading to a small vertical extent of the bottom) or conversely, due to changes at a larger scale in the vertical aggregation of prey layers within the water column. We believe that the findings of this study are likely to be generalized to other air breathing divers foraging on small prey items such as mesopelagic fishes or crustaceans, but differences are likely to be found for diving predators foraging on large prey items. Instead, the latter may abort their dive after catching very large preys to return to the surface to feed as observed in Weddell seals (Leptonychotes weddellii) feeding on Antarctic toothfish (*Dissostichus mawsoni*) (Ainley and Siniff, 2009).

The prey encounter events detected from acceleration data only provide quantitative information about prey. How the prey species and size relate to the diving beha-

viour and the decreasing prey encounter rate that we observed along depth remain unknown. Moreover, bio-logging data are collected by free-ranging diving predators which are unlikely to cover the entire range of habitat available to their prey. This makes it difficult to assess the deeper limit of the prey patch on which the SES feed at the bottom of their dives or to test predictions about their foraging behaviour. The development of video camera (Naito et al., 2013; Davis et al., 1999; Takahashi et al., 2004) and miniaturized sonar loggers (Lawson et al., 2015) may help to overcome these difficulties by providing information about the prey quality and extend our perception range of environment surrounding the SES.

CHAPITRE

4 Three-dimensional space use during the bottom phase of southern elephant seal dives

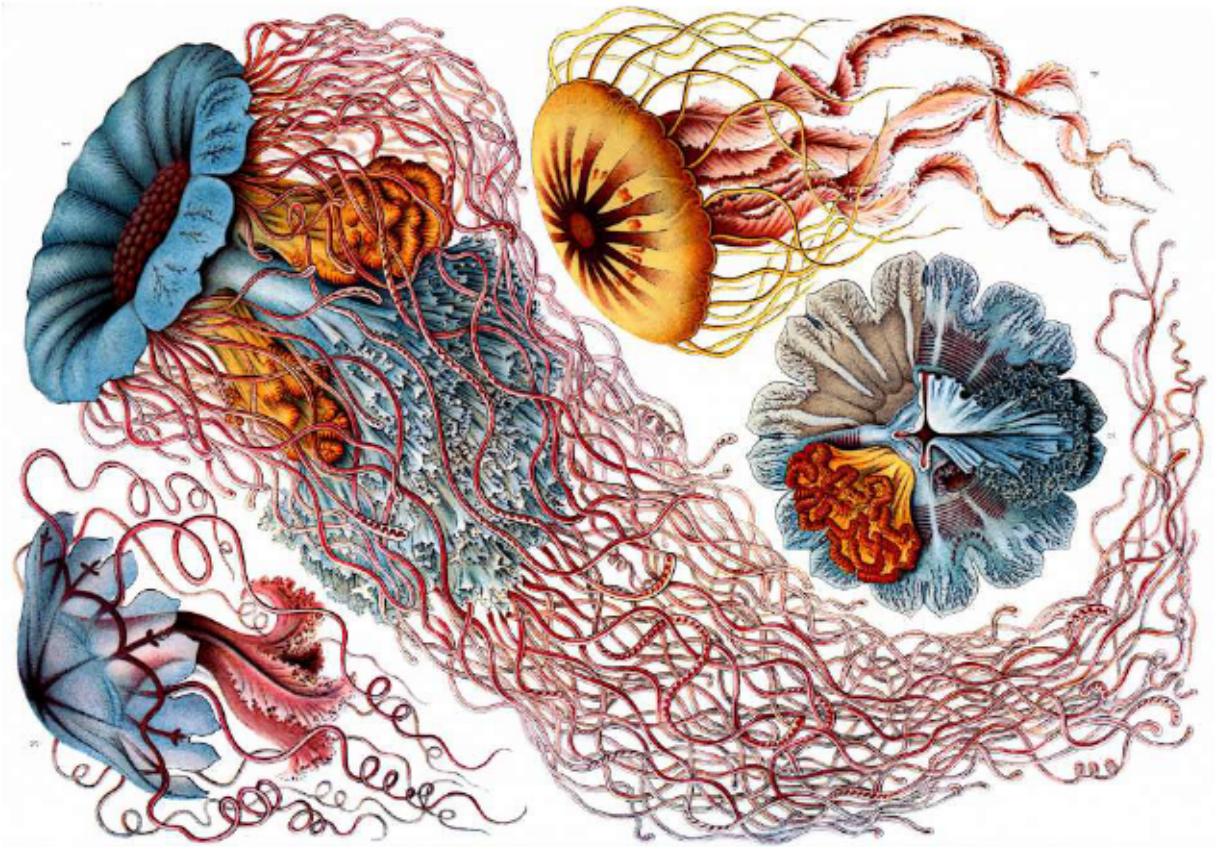

"Discomedusae" – Formes artistiques de la nature de Haeckel (1904, planche 8/100)

2. Le Bras Yves, Jouma'a Joffrey, Guinet Christophe. (2016). Three-dimensional space use during the bottom phase of southern elephant seal dives. *Movement Ecology*. doi: 10.1186/s40462-017-0108-y

► Les annexes de cet article sont disponibles en annexe C du manuscrit.

4.1 Abstract

Background In marine pelagic ecosystems, the spatial distribution of biomass is heterogeneous and dynamic. At large scales, physical processes are the main driving forces of biomass distribution. At fine scales, both biotic and abiotic parameters are likely to be key determinants in the horizontal and vertical distribution of biomass, with direct consequences on the foraging behaviour of diving predators. However, fine scale three-dimensional (3D) spatial interactions between diving predators and their prey are still poorly known.

Results We reconstructed and examined the patterns of southern elephant seals 3D path during the bottom phase of their dives, and related them to estimated prey encounter density. We found that southern elephant seal tracks at bottom are strongly dominated by a single horizontal direction. In high prey density areas, seals travelled shorter distances but their track remained strongly orientated according to a main linear direction. Horizontal, and more importantly, vertical deviations from this main direction, were related negatively to the estimated prey density. We found that prey encounter density decreased with diving depth but tended to be more predictable.

Conclusion Southern elephant seal behaviour during the bottom phase of their dives suggest that the prey are dispersed and distributed into layers in which their density relates to the vertical spread of the layer. The linear trajectories performed by the elephant seals would allow to explore the largest volume of water, maximizing the opportunities of prey encounter, while travelling great horizontal distances.

Key-words : diving behaviour ; three-dimensional path reconstruction ; prey density ; prey distribution ; prey patch

4.2 Background

Distributions of predators and prey are necessarily linked. Optimal foraging theory (MacArthur and Pianka, 1966; Pyke, 1984; Stephens and Krebs, 1986) predicts that a predator should seek out areas with high prey density while prey should avoid high predator density areas (Sih, 2005). The correlation between the spatial distributions of

predator and prey depends on the balance between the responses of one to another (Sih, 1984). In the case of a mobile predator that feeds on a more static prey, the spatial distributions of the predator and of the prey are expected to be positively correlated (Sih, 1984). For instance, diel vertical migrations performed by myctophids (Catul et al., 2010) are related to a similar pattern in the diving depth of elephant seals, *Mirounga angustirostris* (Leboeuf et al., 1988) and *M. lenonina* (Biuw et al., 2010; McIntyre et al., 2011b; Jaud et al., 2012). Consequently, the hypothesis that movements of predators mimic the spatial patterns of their prey is commonly encountered in the bird and marine mammal literature. A typical example is the detection of Area-restricted search behaviour (Kareiva and Odell, 1987; Fauchald and Tveraa, 2003) (ARS) from GPS tracks to infer the location and characteristics of important feeding areas of various marine predators (Robinson et al., 2007; Scheffer et al., 2010; Robinson et al., 2010; Lascelles et al., 2016; Hindell et al., 2016; Kirkman et al., 2016).

Studying the distributions of predators and prey as well as their interactions is particularly challenging in the open ocean, because of the dynamic nature of this environment and the difficulty of observing the animals. In the last few decades, technological advances have driven the emergence of bio-logging as a way to simultaneously monitor the activity of free-ranging marine predators and sample their physical environment. The use of electronic devices embedded on free-ranging animals have provided novel insights into the foraging behaviour and habitat of marine predators at large and intermediate scales. For example, it has been highlighted that large and meso scale oceanographic structures such as fronts, eddies and filaments are of significant importance to the foraging ecology of top predators Bost et al. (2009); Nordstrom et al. (2013); Monte et al. (2012); Cotté et al. (2007); Dragon et al. (2010); Volker et al. (2002); Guinet et al. (2014). At fine scales, both biotic and abiotic parameters are likely to be key determinants in the dynamics of biomass distribution Levin (1992); Hunt et al. (1999), but these processes are still poorly understood. To study fine scale patterns in prey distribution, and their mechanistic relationships with predator behaviours, we used bio-logging data collected by southern elephant seals (SES) and focused our interest on the scale of a dive bottom phase. Indeed, this dive phase represents a fundamental organizational unit of the foraging strategy for many diving predators, including SES, where most of feeding occurs (Hooker et al., 2002; Viviant et al., 2014; Naito et al., 2013; Austin et al., 2006; Wilson et al., 2002; Davis et al., 2003; Fossette et al., 2008).

Southern elephant seals can dive at an average depth of 400 m (up to 2000 m, (McIntyre et al., 2010)) and explore a large extent of the water column. Their foraging strategy can be modified by adjusting both horizontal and vertical movements (Davis et al., 1999; Simpkins et al., 2001; Austin et al., 2006), therefore it is worth examining how the three spatial dimensions are involved in the interactions between diving predators and their prey. However, most studies investigating the space use by marine predators have either analysed animals' behaviour from their GPS track (time + 2D approach), or from time-depth data (time + 1D approach). Some efforts have been made to combine these two approaches – horizontal dimensions at surface and time-depth dive profiles – in order to examine the foraging strategies according to horizontal and vertical dimensions (time + pseudo 3D approach) (Bailleul et al., 2008; Bestley et al., 2015; Ramasco et al., 2015). However, a detailed understanding of how diving predators use their 3D spatial environment and interact with prey requires the actual reconstruction of their 3D path underwater. This is nowadays achievable using bio-logging data from large diving predators that are able to carry sophisticated loggers with minimal disturbance Davis et al. (1999, 2001); Mitani et al. (2010); Matsumura et al. (2011); Goldbogen et al. (2015); Adachi et al. (2016). Such loggers can also provide information regarding the likely occurences of prey encounters Viviant et al. (2010); Gallon et al. (2013); Foo et al. (2016). Three-dimensional path analysis has started to provide new insights into the behaviour of elephant seals (Mitani et al., 2010; Matsumura et al., 2011) and other diving predators (Davis et al., 1999; Mitani et al., 2004; Shiomi et al., 2008; Wilson et al., 2008; Narazaki et al., 2009; Benoit-Bird et al., 2013), but also into the fine scale patterns of their prey distribution (Adachi et al., 2016).

In this study, six datasets with acoustic recording, tri-axial acceleration and magnetometry, sampled at high frequency, allowed us to reconstruct the three-dimensional underwater path of SES using well established dead-reckoning methods Wensveen et al. (2015). According to the optimal foraging theory, the predators should exhibit the greatest residency time in the highest prey density grounds, but the general shape of the animal path can also convey information on the predator-prey interactions. Complementarily to ARS-like approaches that focus on specific part of the trajectories with high residency time, we decided to extract the main trends of the SES path in dives' bottom phases. We described the 3D space use exhibited by SES at the bottom phase of their dives using principal component analysis, and assessed the volume-

tric density of prey encounter events under various prey detection range scenarios. Finally, to explain how the SES space use could relate to its perception range and to the fine-scale patterns in prey distribution, we examined relationships between the estimated prey encounter densities and the three-dimensional diving behaviour in bottom phase trajectories.

4.3 Methods

Deployment of devices and data collection

During the breeding seasons (October and November) of 2011 and 2012, a total of six SES females of the Kerguelen Islands (49°21′0″ S, 70°13′0″ E), were equipped with an acoustic tag (Acousondes^{TM} model 3A, manufactured by Acoustimetrics, Greeneridge Sciences, Inc, USA) and a Time-Temperature-Depth Fastloc GPS data logger (SPLASH10-F^{TM} manufactured by Wildlife Computers, USA) to collect locations while the animals were at sea. The tags were programmed to sample depth, light and temperature at 1 Hz, tri-axial (longitudinal, lateral and vertical axes of the logger) body acceleration, tri-axial earth magnetic field at 5 Hz and sound. Animals were captured with a canvas head-bag and anaesthetized using a 1 :1 combination of Tiletamine and Zolazepam (Zoletil 100) injected intravenously (McMahon et al., 2000). Using quick-setting Araldite (Araldite AW 2101), the tags were glued on the seals (acoustic tags on their back, GPS tags on their head) so that longitudinal axes of the animals and loggers aligned. Details about the length and weight of the equipped animals are provided in Table 4.1 (average lengths of $2.37 \pm SD = 0.12$ m and average weights of $277.67 \pm SD = 47.31$ kg). Passive acoustic recording is power-consuming. To extend the acoustic sampling on longer periods, we programmed the tags to record sound at a frequency of 6 kHz for three hours every 12 hours in 2011 and at a frequency of 12.2 kHz for three hours every 24 hours for the four individuals equipped in 2012.

Table 4.1: Deployment details. All individuals are post-breeding females.

SES name	Length (m)	Weight (kg)	n 3D dives / n dives	Recording duration (day)
2011-16	2.54	255	144 / 822	13
2011-18	2.28	245	238 / 1081	13
2012-01	2.32	230	248 / 1945	24
2012-02	2.35	362	68 / 409	12
2012-04	2.48	282	50 / 289	4
2012-08	2.25	292	244 / 1777	29

Dive analysis

Unless otherwise specified, data processing and analysis described in this section were performed using the R statistical software R Core Team (2014). The custom code used for the archive data processing is available online as a R package called `rbl` Le Bras (2017).

Dives and dive phases

We defined dives as periods where animals were continuously deeper than 15 m under the surface. This conservative threshold avoids considering brief sub-surface excursions as actual dives. Because there is a drift in the pressure readings of the tags over time, a zero offset correction of depth time sequence was applied prior to the delimitation of dives. Each dive was then divided into three phases – descent, bottom and ascent – using the method described in (Jouma'a et al., 2015). The bottom phase is defined as the period of a dive where the vertical speed signal, modelled using a polynomial of degree 4, stays under a threshold of 0.75 $m\,s^{-1}$. Modeling the vertical speed signal using a polynomial fit allows the method to be sensitive to the overall shape of the time-depth trajectory but not to small scale anomalies such as steps performed in the middle of the descent and ascent phases. The fourth degrees provide enough freedom for the model to handle V-shaped and squared (U-shaped) dives. Eventually, the vertical speed threshold was chosen after a blind experiment minimizing the difference between the automatic and the visual delineation of the bottom phases.
Drift dives are specific dives where SES are resting and/or digesting Crocker et al. (1997) and, as a result, not expected to react when encountering prey. Since our focus is on spatial patterns related to predator-prey interactions, we identified and removed these dives from our dataset prior to the statistical analysis.

Prey encounter events

To identify a prey encounter event we implemented the method described in Vacquié-Garcia et al. (2015); Guinet et al. (2014); Jouma'a et al. (2015) (but see Vacquié-Garcia et al. (2015) for details) on the acceleration data collected by the tags. The dynamic acceleration resulting from rapid movements was extracted from the three axes with an order 3 high-pass digital Butterworth filter with a normalized cut-off frequency of 2.4 Hz (performed with `butter` and `filtflit` functions from the `signal` package Signal

developers (2013)). For each axis, a one-second fixed window was used to calculate the standard deviation every second. Signals were then processed using a moving standard deviation with a window size of five seconds. Finally, a two-mean clustering was performed for each signal to distinguish "high state" from "low state". These successive operations are performed using the `prey_catch_attempts` function from the `rbl` package. A prey encounter event (hereafter PEE) is believed to be occurring when the three axes are simultaneously in "high state". A continuous succession of "high state" is considered as a single PEE. A comparison of PEE detection results of this method derived from both the head-mounted and back-mounted accelerometer data is provided in (Le Bras et al., 2016, additional file 2). We counted PEE to obtain an indication of the number of prey encounters in the bottom phases but the corresponding prey types are not known.

Three-dimensional path reconstruction

Three-dimensional reconstruction by dead-reckoning (also called "path integration") is calculated by summing the successive velocity-vectors of the animal (in our case, every second) starting from a known location (in our case, a GPS location collected in the surface period preceding the dive). When the arrival point is known, the reconstructed track can be scaled to match the observed locations at departure and arrival (GPS location collected in the surface period following the dive) and reduce positional uncertainty Wensveen et al. (2015).

Pitch, roll and heading angles describe the body posture of SES with respect to the direction of the earth's gravity vector (pitch and roll angles) and earth's magnetic vector (heading angle). Assuming that the animal always moves in the direction of their longitudinal axis, pitch and heading angles provide all the necessary directional information for 3D path reconstruction. The static acceleration is the gravity based acceleration component. It can be obtained by applying the appropriate low-frequency filter to the acceleration signal. As in Richard et al. (2014), we used an order 3 low-pass digital Butterworth filter with a normalized cut-off frequency of 0.20 Hz applied to the three axes. The direction of the gravity vector according to the accelerometer provides a reference to calculate the pitch and roll angles of the SES (we used the `pitch` and `roll` functions from the `animalTrack` package Farrell and Fuiman (2013)). The low-pass filter was applied to the magnetic data as well. The resulting signal, combined with pitch and roll information allows to calculate the heading angle (performed

using `tilt_compensate` function from the `animalTrack` package).

Aside from body posture angles, 3D path reconstruction requires knowledge of the SES swimming speed. We assessed swimming speed of SES relatively to surrounding water using sound Burgess et al. (1998) recorded by acoustic tag. This task was performed in MATLAB using custom code which is available on request. We estimated the swimming speed (v_{seal}) in descent and ascent phases from pressure changes (v_z) and pitch angle (α) : $v_{seal} = v_z/sin(\alpha)$. Water flow noise level was calculated from the low-frequency noise extracted with a 110 Hz low-pass filter applied to acoustic data. Then we calibrated the relationship between the water flow noise level and the swimming speed estimations and extrapolated it to predict swimming speed over the entire dive periods from noise level.

The 3D path (Figure 4.1) of each animal was calculated by dead-reckoning (`dead_reckoning` function of the `animalTrack` package Farrell and Fuiman (2013) applied to body posture angles, swimming speed and GPS data). The observed GPS location during the surface period preceding the dives is used as the starting point of the reconstructed path. Finally, the reconstructed paths are corrected so that their arrival point matches the observed GPS location collected during the surface period following the dives. This correction applies uniformly over the entire dive, simulating the effect of a current of constant speed and direction that would result in the difference observed between the reconstructed and GPS arrival points. Because the acoustic tags were programmed to record acoustic data only at specific hours of the day, we could not predict the swimming speed at night, and as a consequence, all the 3D dives of our dataset occurred during daytime.

Shape of bottom phase trajectories

To describe how the SES used the 3D space during the bottom of their dives, we extracted the main components of the animals path during the bottom phases. This was achieved by implementing a Singular values Decomposition (calculation of the eigenvalues and eigenvectors) of the variance-covariance matrix of SES locations during dives' bottom phase. The variance-covariance matrix can be seen as a linear application that would transform Gaussian noise (in 3D, this would be a spherical cloud of data points with maximum density at its center) into the observed data. Such a transformation can be decomposed into simpler transformations, rotations whose characteristics are described by the eigenvectors, and scaling described by the square roots of the

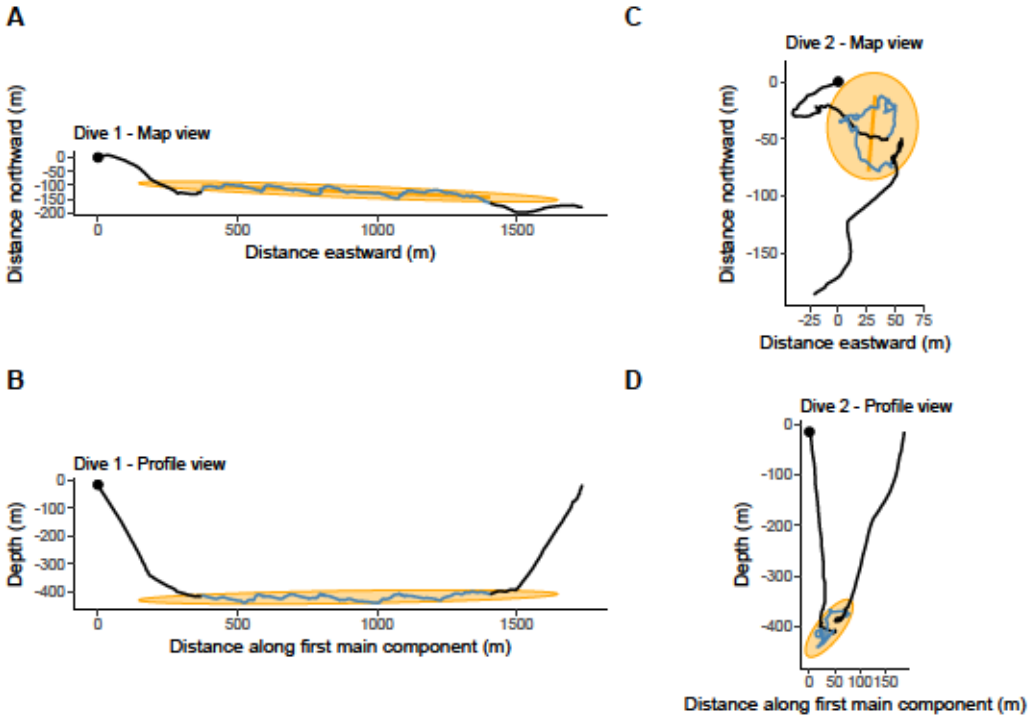

Figure 4.1: Two 3D dives examples – *These dives have about the same depth but show two contrasting situations : on the left (A and B) the first main component explains a very large part of the total dispersion while on the right (C and D), the dispersion explained by the first main component is particularly low. The blue part represents the dive's bottom phase. The black points give location of starting points. The orange ellipses stand for the 2D projections of a 3D ellipsoid whose axis are the three main components. On the "Map views" (A and C) the orange line display the direction of the first main component which is used to construct the best "Profile Views" (B and D). More example, in interactive 3D plots, may be found at* `https://github.com/SESman/SES_3Ddives`.

eigenvalues. In our case study which relates to the extraction of main components of the 3D SES path, eigenvectors provides the direction of the main components and their eigenvalues quantifies how much of the dispersion (also called inertia) of SES locations each of these components can account for. All-equal eigenvalues would indicate that SES did not favour any direction of movement in their trajectories. The sum of the eigenvalues represents the total dispersion of the data. To describe the shape of the SES trajectories, we used the raw SES location data as well as eigenvectors and eigenvalues describing the main linear trends in the SES path. The variables that we calculated are listed and briefly desribed in table 4.2. Additional explanations for the variables that require it is provided in the next paragraphs :

Table 4.2: Variables used to describe the shape of SES trajectories

Variable name	Brief description
Mean depth	Average depth in the bottom phase.
Total dispersion	Sum of the eigenvalues : $\lambda_1 + \lambda_2 + \lambda_3$
First main component dispersion	Defined as $\frac{\lambda_1}{\lambda_1+\lambda_2+\lambda_3}$
Vertical and horizontal extent of first main component	These two variables describe the extent of SES exploration along the path of the first main component. See details in text.
Vertical and horizontal width	These variables quantify the vertical and horizontal spread of the deviations from the first main component path. See details in text.
Swimming speed variability	Standard deviation of SES swimming speed. See details in text.

First main component dispersion The first main component (abbreviated MC1) is the main component with the greatest eigenvalue, that is the primary direction of movement. A perfect balance between the directions of movements is characterised by a value of one third (in which case all eigenvalues are equal). Values larger than one third indicate that some directions of movement dominate in the SES path. The larger is this value the stronger is the dominance but a value of 1 corresponds to a perfectly linear path.

The first main component dispersion was fairly large while the first main component orientation revealed a strong consistency across dives (see results section). Conversely, the second and third main components far less dispersion and their orientation varied importantly from a dive to another. On this basis, we chose to describe the dispersion not explained by the first main component with behaviour metrics based on the horizontal and vertical dimensions rather than according to the second and third main components. Using this frame of reference which is both consistent between dives and meaningful in terms of biological and physical processes allows to simplify the interpretation of the models' results.

Vertical and horizontal extent of first main component We calculated the horizontal and vertical distances separating the ends of the first main component. For robustness, we defined the ends as 10% and 90% quantiles of first main component scores instead of the minimum and maximum values.

Vertical and horizontal width To calculate these variables we defined two orthogonal planes : Plane A, passing through the gravity center of the trajectory and encompassing the first eigenvector and the gravity vector (blue plane on figure 4.2) ; Plane B, passing through the gravity center of the trajectory, encompassing the first eigenvec-

tor and a vector orthogonal to plane A (orange plane on figure 4.2). Horizontal width was defined as the range from the 10% to the 90% quantile of distances between SES locations and plane A Vertical width was defined as the range from the 10% to the 90% quantile of distances between SES locations and plane B

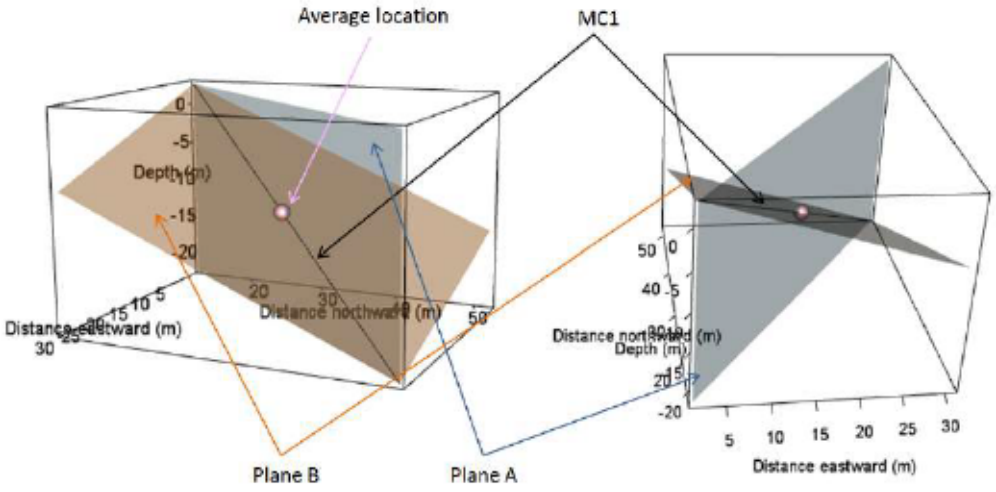

Figure 4.2: Schematic presenting the two reference planes for the calculation of vertical and horizontal width – *The first main component is represented by the thick black line at the center. The blue (respectively orange) plane stands for plane A (respectively plane B). The pink sphere indicates the average location of the animal.*

Swimming speed variability A high swimming speed variability is believed to be related to prey chasing Hassrick et al. (2007), while a low swimming speed variability can indicate a drifting or gliding behaviour Dragon et al. (2012a) which is believed to be related to low foraging effort (Crocker et al. (1997); Aoki et al. (2011)). Besides the shape-description variables, we used the standard deviation of the swimming speed during the bottom phase as a proxy of foraging effort in order to be able to distinguish between these behaviours.

Volume of water prospected by SES at the bottom of their dives

We estimated the volume of water prospected by SES, that is to say the volume of water where SES would have been able to detect a prey during the bottom phase of a dive. To achieve this, we assumed that SES could see in any direction around their current position within a given radius. We considered three "detection-distance" scenarios for the sphere radius : a short distance of 1.5 m to simulate the case where

prey catches would be opportunistic events as well as 9 and 18 m according to the foraging scale highlighted by Adachi et al. (2016) on the northern elephant seals. SES may exhibit an infinite variety of 3D path during their dives' bottom phase, including turning back to visit the same areas several times. Hence, we could not use a generic equation to assess the volume of water they may have prospected. Instead, we used a numerical method called Monte Carlo integration. Details about the implementation and accuracy of this method are provided in additional file 1. Once the prospected water volume was computed, we used it to compute a proxy of the prey encounter density at the bottom of SES dives, defined as the ratio between the number of PEE and the prospected water volume (expressed in µPEE m^{-3} units).

Statistical analysis

We modelled the prey density proxy (µPEE per m^3 of water prospected at bottom) according the descriptors of bottom trajectory previously described (mean depth, total dispersion, first main component dispersion, first main component extent on the horizontal and vertical dimensions, horizontal and vertical widths and standard deviation of the swimming speed) using Generalized Linear Models (GLM). We fitted three models, one for each detection radius.

We started the model selection with Poisson family GLMs, adapted to predict a count variable such as PEE count at bottom. The link function was set to logarithm (the standard link function for these GLMs) and the log-transformed volume of prospected water was included in the model as an offset term. With this implementation, we could model the PEE per unit of water prospected at bottom as response variable while using the appropriate count family distribution to predict the number of PEE at bottom.

These Poisson models indicated over-dispersion ($\theta = \sigma^2/\mu$, $\theta_{1.5m} = 2.93$, $\theta_{9m} = 2.68$, $\theta_{18m} = 2.73$) so we switched to the more flexible Negative Binomial distribution (`MASS` package Venables and Ripley (2007)) which allows for higher variance/mean ratio. We observed a large proportion of zeros in our data (27.44%) incorrectly predicted by the GLMs. We then tested the zero-inflated variants of Poisson and Negative Binomial models (using `zeroinfl` from the `pscl` package Zeileis et al. (2008)). These models led to very significant improvement of Akaïke Information Criterion (AIC) and Vuong's test (p-values were < 0.01 for all models).

The explanatory variables considered for selection in the count part of the zero-

inflated model were identical to the Poisson and Negative Binomial models. The choice of explanatory variable for the zero excess part was restricted to the non shape-description variables, individual identity, mean depth, swimming speed variability and log-transformed bottom duration (the latter was not included in the count part of the model). Seals' identity captures variability due to differences in accelerometer attachment and individuals' foraging behaviour. Swimming speed variability can account for the shift between drifting/gliding and active swimming behaviour in terms of foraging effort. Mean depth provides basic information about the environment which is a likely source of excess zeros. Finally, log-transformed bottom duration has an obvious link to the probability of PEE occurrence. We tested quadratic effects for the swimming speed variability (in both count and zeros excess parts) and the vertical and horizontal extent of the trajectory across the first main component. We tested all the possible combinations of explanatory variables and ranked the best candidates according to AIC. For each radius, we selected the model with the best AIC where all explanatory variables were significant at level $\alpha = 5\%$.

4.4 Results

Shape of SES trajectories at the bottom of their dives

The first main component explained 93.75% $\pm SD = 8.34\%$ of the total dispersion (Figure 4.3, Table 4.3). Moreover, the first main component was almost exclusively oriented in a horizontal direction (Figure 4.4). The left dive on figure 4.1 is an example of a typical dive that exhibiting these characteristics. No bi-modality pattern is noticeable of figure 4.4 but, apart the obvious peak near one, a wide range of values is covered by a few observations. The vertical component of the first main component range between 17% to 76% in a few bottom phases (5%) which correspond to deep diving depths (680 m vs. 481 m, t-test p-value = 1.40×10^{-13}). On average, SES travelled horizontal distances of 429m $\pm CV = 92\%$ in their descent phases, 706m $\pm CV = 77\%$ in bottom phases and 393m $\pm CV = 90\%$ in ascent phases. Because the first main component are horizontally oriented, the first main component dispersion is highly correlated to the length of first main component according to the horizontal plane (first main component horizontal extent). As a result, when checking for multicollinearity before model selection, the first main component horizontal extent was removed.

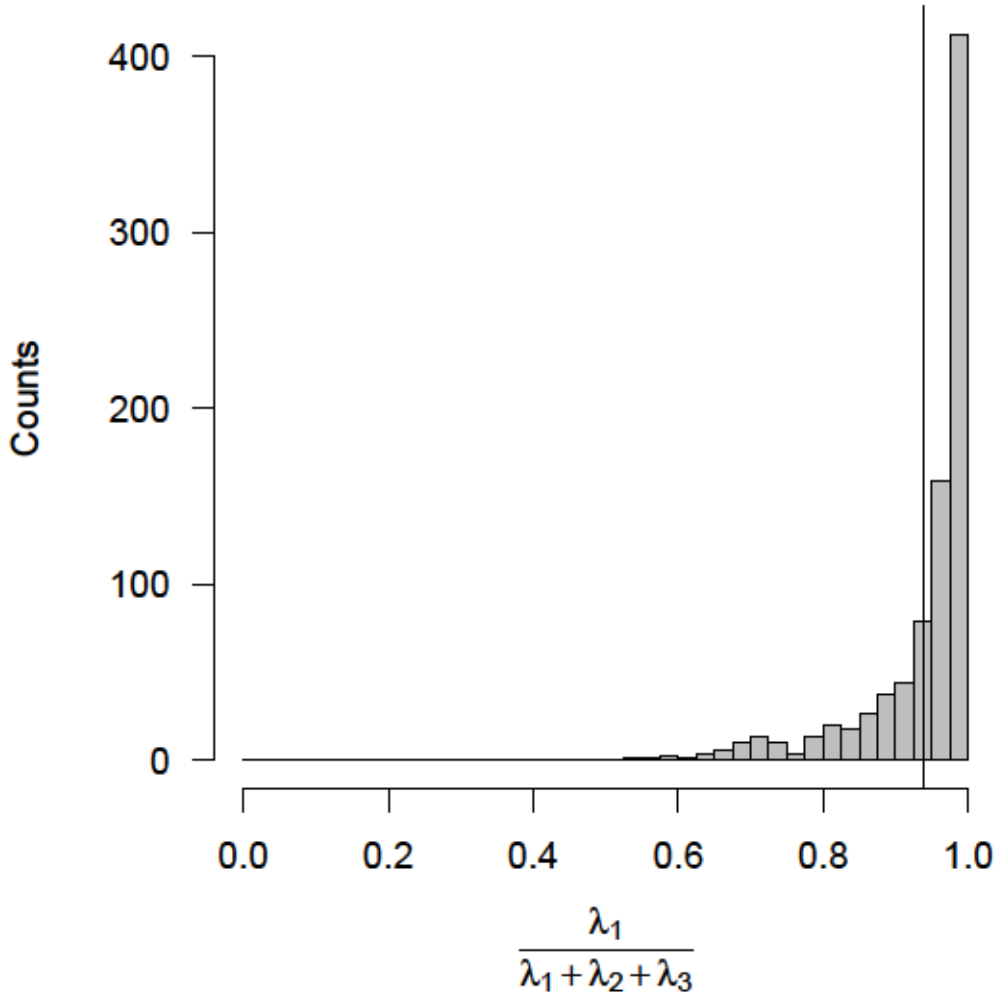

Figure 4.3: Contribution of the first eigenvalue to the total dispersion – *A linear path would be indicated by a 100% contribution. Conversely, a well balanced 3D path would be indicated by equivalent contribution of the three eigenvalues to the total dispersion, that is a 33% contribution of the first eigenvalue. The black vertical line stands for the average, at 93.75% of the total dispersion.*

Prey field density at the bottom of SES dives

The prey encounter density spread in a wide range according to the detection radius (two orders of magnitude, Table 4.4), due to the strong impact of this parameter on the estimates of the water volume prospected by SES. We can adopt the predator's point of view by taking the inverse of the prey density estimates reported in the table 3 : considering prey detection radius of 1.5, 9 and 18 m, SES have to explore average volumes of $1.40 \times 10^3\,m^3$, $5.39 \times 10^4\,m^3$ and $2.08 \times 10^5\,m^3$ respectively to encounter a

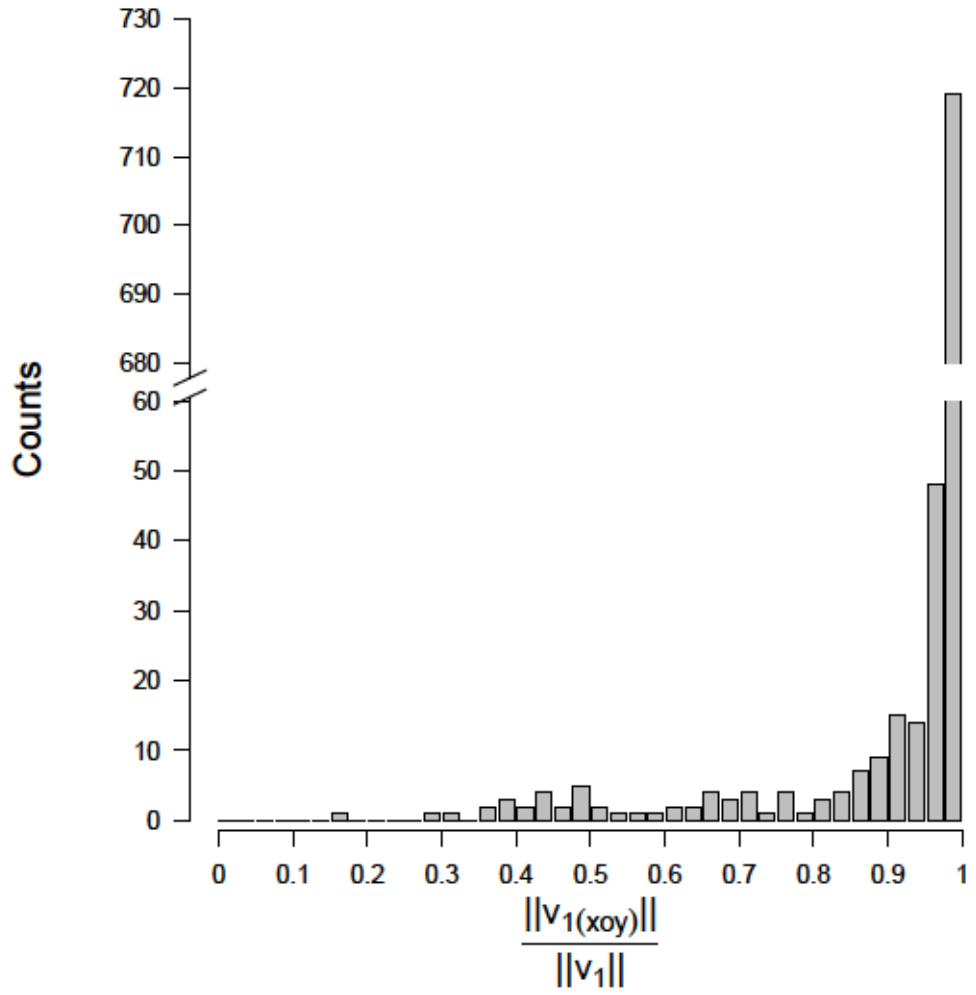

Figure 4.4: Length ratio between the first eigenvector projected on the horizontal plane ($v_{1(xoy)}$) and the first eigenvector in 3D space (v_1) – *A ratio of 0 indicates that the first main component is perfectly vertical while a ratio of 1 indicate that the first main component is perfectly horizontal.*

prey during their dives' bottom phase.

Prey density model

Results were consistent across all models with similar coefficient estimates and standard errors (Table 4.5). In the count part of the model, the strongest effect is observed for total dispersion for which a one SD increase is associated with 38% lower PEE density (Table 4.5). In decreasing order of effect strength, vertical width, mean bottom phase depth and horizontal width have negative effects in all three count models

Table 4.3: Descriptive statistics of the shape parameters of bottom trajectories. $n = 866$ 3D dives. Refer to methods for detailed explanation about what these variables represent and how they were computed.

	Nb prey encounter event at bottom	Bottom duration (s)	Mean bottom depth (m)	Horizontal width (m)
Min	0.00	54.00	53.59	0.35
Max	28.00	1732.00	847.91	139.37
Median	2.00	451.00	435.78	20.39
Mean	3.37	500.39	441.86	23.20
SE mean	0.13	6.67	5.25	0.45
$CI_{95\%}$ mean	0.25	13.10	10.30	0.88
Variance	13.79	38 572.57	23 833.89	175.57
SD	3.71	196.40	154.38	13.25
	MC1 vertical width (m)	MC1 horiz. width (m)	Total dispersion (m^2)	MC1 dispersion (%)
Min	0.04	36.80	562.55	53.30
Max	383.55	1775.42	401 082.90	99.97
Median	26.80	409.09	24 073.35	97.20
Mean	48.68	431.17	32 638.69	93.75
SE mean	2.16	7.25	1110.50	0.28
$CI_{95\%}$ mean	4.23	14.23	2179.59	0.56
Variance	4023.07	45 544.02	1 067 959 847.62	69.62
SD	63.43	213.41	32 679.65	8.34
	Vertical width (m)	Bottom speed SD ($m\,s^{-1}$)	Bottom vertical speed SD ($m\,s^{-1}$)	
Min	2.10	0.11	0.16	
Max	154.18	1.15	2.01	
Median	23.21	0.32	0.79	
Mean	31.45	0.35	0.85	
SE mean	0.80	0.01	0.01	
$CI_{95\%}$ mean	1.57	0.01	0.02	
Variance	556.80	0.03	0.09	
SD	23.60	0.17	0.30	

Table 4.4: Estimated prey encounter event density in dives' bottom phases. $n = 866$

Radius	Mean prey encounter event density $\pm CI_{95\%}$			SD
1.5 m	715.09	±	53.70	760.13
9 m	18.56	±	1.45	20.58
18 m	4.81	±	0.39	5.45

Values expressed in $\mu PEE\,m^{-3}$ unless otherwise specified.

(Table 4.5). However, mean depth of bottom phase has a positive influence on the probability of catching at least one prey item (Table 4.5, Figure 4.5). As expected, swimming speed variability had positive effects in both count and zero-excess parts of the model. Nonetheless we observed a negative quadratic effect for high values ($> 0.90\ m\,s^{-1}$) in the zero-excess part (Table 4.5, Figure 4.5).

Differences between the $r = 18$ m and the two other models ($r = 9$ and 1.5 m) were only observed for the least significant variable (Table 4.5). With $r = 18$ m dispersion explained by first main component was selected whereas models with $r < 18$ m

favoured vertical extent of the first main component. These variables were associated with smaller PEE density for all models (Table 4.5). Partial regression lines for models with $r < 18$ m are provided in the additional file 2C.2.

The dispersion parameter (θ) decreased with the chosen detection radius ($\theta_{1.5m} = 3.38$, $\theta_{9m} = 3.24$, $\theta_{18m} = 3.18$). The final models could explain 17.04%, 19.52% and 20.46% of the deviance of null models for 1.5 m, 9 m and 18 m radius. Goodness of fit as indicated by the pseudo-r^2 (squared correlation coefficient between observed and predicted values of the PEE density) also increased with the detection radius (27.53%, 31.03%, 33.91% for 1.5 m, 9 m and 18 m radius).

4.5 Discussion

4.5.1 Schooling behaviour

The principal component analysis revealed that SES trajectories at the bottom of their dives are strongly dominated by a path in a single direction (Figure 4.3) as it was noted by Davis et al. (2001) on northern elephant seals. This results support the hypothesis that SES prey tend to not aggregate in large discrete schools. Indeed, in such a situation the predator is expected to adopt an overall sinuous and spherical trajectory. A spherical first passage time (SFPT, Bailleul et al. (2010c)) analysis performed on our dataset revealed that "Volume-restricted search" (VRS) could be detected in the bottom of half of the SES dives in which case they accounted for 37.8% of the bottom phase duration but 67.4% of PEE Jouma'a et al. (2017). The typical scale of VRS, $45.3 \pm SD = 28.9$ m, was similar for all individuals and the average prey encounter rate was $1.2 \pm SD = 0.3$ PEE min^{-1} inside VRS and $0.9 \pm SD = 0.4$ PEE min^{-1} outside VRS Jouma'a et al. (2017)). These results indicate that the prey density may vary at finer scales than the one typically investigated in this study (entire bottom phases), but not by a very large amount. Moreover, the VRS were (mechanically) related to a decrease of the SES swimming speed and greater path sinuosity but the SES trajectories remained dominated by a single direction. These patterns of the 3D path of SES at the bottom of their dives suggest that the deep scattering layer consists of dispersed solitary prey or small group of individuals.

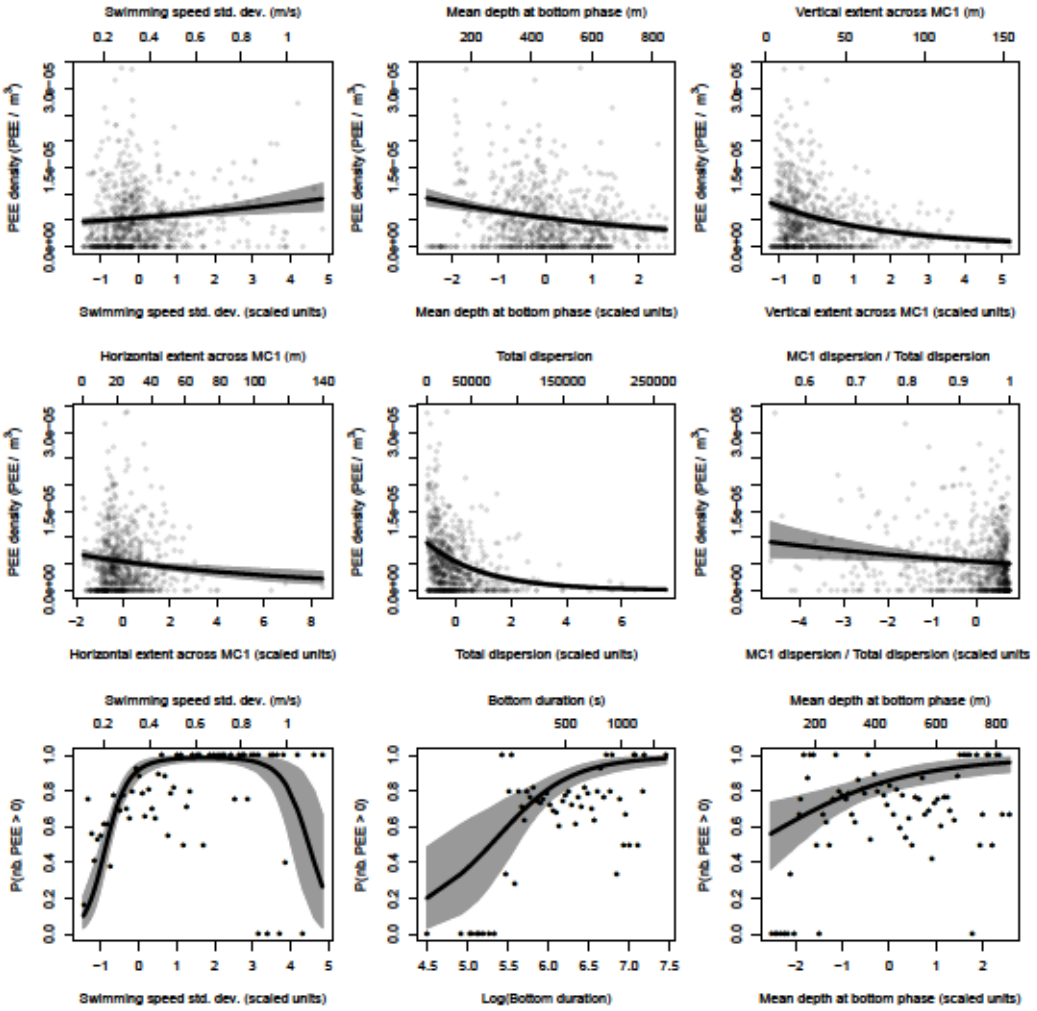

Figure 4.5: Estimated relationships between the PEE density proxy and the descriptive parameters of the bottom phase trajectories – *Results obtained for 18* m *radius. The top six graphics present the estimated effect of the count model and the bottom three graphics the estimated effects of the zero excess model. The thick black curves display the expected means at population level and the grey shades surrounding them stand for the 95% confidence interval of this expected mean. The figures obtained for 1.5 and 9* m *radii are included in the additional file 2.*

4.5.2 PEE density along depth

The dominant direction in the trajectories of SES at dives' bottom was primarily horizontal (Figure 4.4). This indicates that SES target specific layers of the water column during the bottom phase of their dive McIntyre et al. (2013); Blanchet et al. (2015). Shallower layers require less time and energy to be reached by SES it and, therefore, are more accessible and more profitable. Performing dives' bottom phase at grea-

Figure 4.5: Results of the three zero-inflated models – *Please notice that, for historical reasons, the binomial part of zero-inflated models (labelled "Zero-excess") predicts the absence of prey encounter event instead of presence. For better readability, the intercept estimates were not included in this table.*

		Coefficients			Standard Error			p-values			Exponentiated Coef $\pm CI95\%$
		1.5 m	9 m	18 m	1.5 m	9 m	18 m	1.5 m	9 m	18 m	
Count	Swimming speed SD	0.14	0.12	0.10	0.04	0.04	0.04	0.00	0.00	0.01	
	Mean depth	-0.16	-0.19	-0.21	0.04	0.04	0.04	0.00	0.00	0.00	
	Vertical width	-0.21	-0.23	-0.33	0.04	0.04	0.05	0.00	0.00	0.00	
	Horizontal width	-0.10	-0.09	-0.11	0.04	0.04	0.04	0.01	0.02	0.00	
	Total dispersion	-0.46	-0.51	-0.48	0.05	0.05	0.05	0.00	0.00	0.00	
	MC1 dispersion			-0.11			0.04			0.02	
	MC1 vertical extent	-0.08	-0.08		0.04	0.04		0.03	0.04		
Zero-excess	Swimming speed SD	-2.38	-2.38	-2.35	0.44	0.44	0.44	0.00	0.00	0.00	
	Swimming speed SD^2	0.66	0.66	0.65	0.12	0.12	0.12	0.00	0.00	0.00	
	Mean depth	-0.61	-0.64	-0.62	0.22	0.22	0.21	0.00	0.00	0.00	
	log(Bottom duration)	-1.81	-1.95	-2.04	0.60	0.60	0.60	0.00	0.00	0.00	

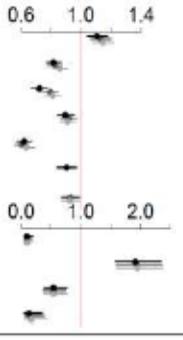

^{2} refers to quadratic term.

ter depth was found to be associated with smaller prey encounter density (Table 4.5). While the SES and their prey perform diel vertical migrations Catul et al. (2010); Biuw et al. (2010); McIntyre et al. (2011b); Jaud et al. (2012), this process cannot explain our result because all the 3D dives in our dataset occurred during daytime. A previous study, based on likelihood of detecting bioluminescence Vacquié-Garcia et al. (2012) highlighted a similar pattern. The impact of the changes in the size or species composition of the mesopelagic community in relation with this decreasing prey encounter density could not be examined with the tools available to us but they could have substantial importance. Assuming that the energy content of a prey item does not vary with depth, the deep dives would imply smaller energy income (because of reduced encounter rates) but larger expenditure (because of the longer transit between surface and bottom). Thus, these dives would be be doubly detrimental to the SES energy balance. However, the probability that no PEE occur decreased with the SES diving depth (Table 4.5), suggesting that a better resource predictability in deep waters might compensate to some extent for this energy shortfall. SES were found to dive deeper north of the Sub-Antarctic Front but yet to maintain their mass gain which suggesting that they could target larger and/or richer prey Guinet et al. (2014). Similarly, SES could expand their diet to other prey types and/or sizes when foraging at depth, allowing steadier prey catch rate and ensuring a baseline level of energy intake.

We distinguished between two sources of vertical exploration in the explanatory variables : depth range covered by SES (1) by moving along the first main component

and (2) by moving orthogonally to this component. An increase in any of these was associated with a decrease of the prey density proxy (Table 4.5). The amount of horizontal exploration orthogonally the main direction of the bottom trajectory was also negatively related to the prey density encountered but to a lesser degree than observed in the vertical dimension (Table 4.5). Not only the SES target specific layers, but the prey density in this layer is primarily determined according to the vertical dimension. This result suggest that local prey density could by driven by vertical constraints that delineate the vertical extent of the deep scattering layer. The nature of these constraints could be biotic (e.g. predation risk, aggregation into reproductive swarms) or abiotic (e.g. habitat preferences regarding temperature, light intensity or oxygen concentration). For instance, harbour seals (*Phoca vitulina*) have been reported to adjust their diving depth to in relation to the mixed layer depth Blanchet et al. (2015). In addition to the effect of oceanographic parameters on the prey abundance, such conditions could impact locally on the foraging success of SES by modulating the prey density Takahashi et al. (2008); McIntyre et al. (2013).

A trade-off between feeding resources richness (primary production taking place in the well-lit sub-surface water) and predation risk (expected to be greater in luminous environment) is responsible for the diel vertical migration pattern phenomenon Iwasa (1982). The light level intensity, decreasing with depth, delineate the upper boundary of many pelagic species distribution and, consequently, relates to the diving depth of SES Jaud et al. (2012). Because diving predators are constrained to return to the surface in order to breathe, they do not benefit from pursuing deeper when an exploitable prey patch is encountered. With bio-logging, data sampling relies on the decisions of free-ranging animals Ropert-Coudert and Wilson (2005). The so collected presence-only data makes it difficult to assess the deeper limit of the prey patch on which the SES forage. Therefore, the relationship between the PEE density and the vertical extent of the SES path underwater conveys more qualitative than quantitative information about the link between thickness of the deep scattering layer and its corresponding density.

4.5.3 Foraging behaviour

The prey density proxy was negatively related to an increase of the overall travel distance in the bottom phase (total dispersion, Table 4.5). In high density patches, the SES would travel shorter overall distances which could be explained by a grea-

ter locomotion cost, more active swimming behaviours related to hunting strategy or prey pursuing could force them to end the bottom phase early. Dominance of the first main component (MC1 dispersion, Table 4.5) which corresponds predominantly to horizontal movements (Figure 4.4) was associated with smaller PEE density (18 m model, Table 4.5). This results indicates that SES trajectories in denser prey environment tend to be slightly less linear. However, this effect was not consistently observed across all models.

On the whole, horizontal exploration mainly takes place moving forward according to the first main component. Based on their observation of the behaviour of *Thunnus maccoyii*, Bestley et al. (2010) suggested that feeding during periods of straight movement could be more common than expected from the optimal foraging theory. At the scale of a complete foraging trip at sea, SES feeds to a large extent during the transit part of their trip but this pattern seems to be observable within the dives' bottom phase where foraging is expected to be the primary objective of the diving predator. Such an extensive-search behaviour is expected when prey are well dispersed in the environment Hill et al. (2002) which seems consistent with the suspected non-schooling behaviour of SES prey that we have previously discussed.

Sensory perception of the surrounding environment has direct consequences on the predator-prey interactions as it mediates animal's ability to locate prey and/or escape predation. The notion of prey dispersion is thus relative to the sensory detection range of the predator. While the scale of this perception in natural conditions is largely unknown for elephant seals, more information about the senses involved are available from functional anatomy and pool experimentations on northern elephant seals. Northern and southern elephant seals forage at great depth and thus, under very dark conditions Mcgovern et al. (2015). Peak sensitivity of their vision, occurring at around $\lambda = 485$ nm, is adapted to a spectrum of low light intensity Lythgoe and Dartnall (1970) and bioluminescence Vacquié-Garcia et al. (2012) such as that emitted by some of their myctophid prey. Additionally, elephant seals possess enhanced visual sensitivity and rapid adaptation to darkness Levenson and Schusterman (1999). Like many other pinnipeds, elephant seals have highly sensitive whiskers Mcgovern et al. (2015), that repeatedly protract before prey captures Naito et al. (2013). However, while it can be assumed that these senses (vision and tactile) are used to locate prey, the extent of their spatial coverage is unclear. Very little information about the auditory capacity of elephant seals is available. It is known that pinnipeds do not echolocate Schusterman

et al. (2000) but, as myctophids can emit sound, elephant seals could use passive audition instead. Finally, a recent study of the 3D underwater path of northern elephant seals Adachi et al. (2016) highlighted volume-restricted search spatial-scales of 8–10 m and 17–19 m, possibly related to prey distribution and/or perception range of the predator. On that basis, we considered a wide range of prey detection distance, 1.5 m, 9 m and 18 m (according to Adachi et al. (2016)), to define the boundaries of water volume within which we hypothesize that SES could detect the presence of prey items. If the spread of prey items largely exceeds the perception range of the predator a straight path is an efficient sampling strategy to scan large volumes of water. In view of the strong linear trend exhibited by the SES in their 3D path, our results bring best supports to a short detection distance scenario.

Besides the hypothesis that behaviour is driven by the prey distribution, active feeding in travel could be due to migratory constraints. Indeed, such a situation could result from the evolution of migratory opportunistic predators that need to meet its energetic requirements while moving rapidly Bestley et al. (2010). Given the very wide range of oceanographic conditions the elephant seal explore Vacquié-Garcia et al. (2015), the opportunistic behaviour may a be relevant point. However, it is unclear if the migratory constraint applies to SES. Indeed, the primary goal of their trip at sea is believed to be foraging but they do so to a greater or lesser extent all along their trip wandering about 43 km day^{-1} in intensive foraging and 75 km day^{-1} otherwise Cotté et al. (2015).

Our estimates of the prey density changed very quickly according to the chosen detection radius ranging in four orders of magnitude from a few µPEE m^{-3} to hundreds µPEE m^{-3}. Sampling micronekton with a large mid-water trawl, Williams and Koslow (1997) found an average micronekton biomass of 2.50×10^{-3} g m^{-3} during the day (250 µPEE m^{-3} considering an average fish weight of 10 g). Furthermore, Gauthier et al. (2014) estimations of micronekton density ranged from 0 to 6000 µPEE m^{-3}. Among the detection radius we tested, the 1.5 m radius yields the closest results ($715 \pm SD = 760$ µPEE m^{-3}, Table 4.4). Our estimation of the prey density rely on the idea that SES do attempt to catch a prey when they detect one. The prey avoidance as well as the probability of multiple simultaneous prey encounters could not be taken into account. These special cases however seem less likely in a short detection distance scenario such as a 1.5 m radius. Despite the correspondence between the amount of PEE detected from head-mounted and back-mounted acceleration data (Le Bras et al.,

2016, Additional file 2), the latter have a tendency to miss some events. As a result we expect our estimations of the prey encounter density to be underestimated. We suggest that the hunting tactics of SES may be opportunistic in the sense that prey item would be detected at short distances and suddenly be captured without substantial chase (Jouma'a et al. (2017)).

4.5.4 Limitations of the study

Each method used to assess the micronekton resources of the pelagic ecosystem have their own weaknesses. Trawl sampling allows identification of size and species but is costly Ariza et al. (2015), requires good weather operating conditions and net avoidance of the different species are still unknown but highly expected Kaartvedt et al. (2012). Bio-logging implies a bias sampling due to different range of habitat available to the predators and prey (a typical example for diving predators is the depth range) and difficulties to distinguish between what is related to animal behaviour and to the environment. For instance, the predator decision to attack a prey can involve many parameters such as the type of prey, its size, its energetic content, its handling time, and abundance. As such, implicit hypothesis are often made to simplify animal behaviours interpretation : animals are assumed to be always efficient to catch their prey ; the potential effect of nearby predators on the behaviour is neglected etc... Eventually, bio-logging studies are also limited by the number of individuals that could be equipped Ropert-Coudert and Wilson (2004) and generally lack the information on prey species . Acoustic surveys depend on presence/absence of a swim bladder as well as on its composition (gas or lipid) which, for some species, is known to change according to the stage of development. Distinguishing between species and estimating biomass is thus difficult with communities of mixed species and/or mixed ages. Spatial resolution of the data also decrease with depth as lower signal frequencies are required. In this context, pairing these approaches – for instance by deploying sonar tags or synchronizing in space and time the trawling survey with predators feeding areas – could greatly assist the scientist to better understand the micronekton ecology.

Because of the small number of individuals for which we could reconstruct 3D path (six), it is still unclear if the diving behaviour we observed extends at the population level. Concerning the negative effect of (i) the mean depth and (ii) the vertical spread of the bottom phases on the estimated prey encounter density, it is to be noted that similar relationships have been highlighted on nine other individuals Le Bras

et al. (2016). The strong dominance of a single direction in the elephant seal path was consistently observed for all our individuals, but this trend has not been previously reported for southern elephant seal. Nonetheless, (Davis et al., 2001) highlighted a similar pattern on a single northern elephant seal (20 dives). Stronger evidence on the prevalence of these behaviours may accumulate as 3D path analysis will develop in the future.

Due to the limited Acousondes^{TM} battery life, we could only sample the first part of the SES foraging trips, where they tend to adopt a faster horizontal transit rate Due to this sampling bias, our results could overstate the dominance of linear horizontal paths at the bottom of dives. We found that higher prey density are associated with shorter bottom phases (Total dispersion, Table 4.5). Furthermore, foraging dives of SES are characterized by steep pitch angle in descent and ascent phases, minimizing horizontal displacement Sala et al. (2011). These factors could explain the correlation between transit rate slowing and SES prey density better than changes of the bottom path sinuosity. Further studies could analyse underwater 3D trajectories in other parts of SES trip to overcome the sampling bias of our study and adjudicate this issue. Area-restricted search are supposedly periods where SES meet high prey densities and are likely to exhibit larger horizontal sinuosity in their bottom phase 3D path. As such, the ARS appear like interesting periods to address this particular issue.

The 3D reconstruction of the SES path underwater by dead-reckoning assumes that the direction of travel of the animal is always parallel to the body orientation. More sophisticated methods such as the one developed by Laplanche et al. (2015) which is free of this assumption, attest that this approximation can have an impact on the reconstructed tracks. However, such methods require large computation times and are not suitable for datasets of several hundreds of dives. Dead-reckoning is also subject to cumulative errors. Therefore, uncertainties about the shape of the SES trajectories at the bottom of their dives increase with the dive depth and the duration of bottom phase. Conversely to other methods (Laplanche et al. (2015); Wensveen et al. (2015)), our method did not estimate position uncertainties. So, we could not account for its effects in the analysis of the 3D trajectories. The last discussion point about the 3D reconstruction method implemented in this study relates to the assessment of SES swimming speed. The water-flow noise to water-flow speed relationship in the descent phase, extrapolated to entire dives to estimate SES swimming speed, presuppose that the flow behaves similarly throughout the dives. This is yet to be verified.

4.5.5 Perspectives

The straightness of the SES underwater path has been reported by Davis et al. (2001) who highlight its consistency from one dive to another. It is not clear how SES orientate themselves and how migratory objectives contribute to this pattern. Examining this pattern in relation to currents Chapman et al. (2011) would be interesting in order to study the navigation skill of SES.

We could only focus on the quantitative aspect of prey field because information about the nature of PEE was not available. Thus, it is unclear if the results mainly concern one type of prey such as a specific myctophid species more abundant in the study area – the eastern edge of the Kerguelen shelf – or partially apply to the different prey types targeted by SES. We could not test for the role of the quality of prey items (size and species) which could imply distinct types of predator-prey spatial interaction due to different detectability, aggregative behaviour or predator-escaping abilities (responsiveness, speed, maneuverability). To address these issues a camera is needed in order to identify the species and size of the prey items Naito et al. (2013); Watanabe and Takahashi (2013); Hooker et al. (2002). However, the high power consumption of these devices and the very dark environment the SES forage in are still technical constraints to their usage. Miniaturized sonar Lawson et al. (2015) could bring the power of high-frequency acoustic signals to identify prey type at new depths. In quantitative terms it is also promising tool : by extending the perception range of bio-logging outside of the very intimate sphere surrounding the animals it could allow to examine thoroughly the fine-scale prey distribution, the range and mechanisms of the prey detection and hunting tactics of SES.

4.6 Conclusion

Analysis of main components of 3D SES paths in their dives' bottom phase allowed us to describe the main trends in SES movements in these key periods of foraging. Such an approach, examining the overall use of space, may be complementary to ARS/VRS analysis that focus on the most sinuous part of the the animal paths, and conveys new information on predator-prey interactions.

The 3D space use of SES at the bottom of their dives suggests that prey do not tend to form large discrete schools but rather adopt a scattered distribution structured in layers. The prey encounter density in these layers decreased with depth but then, SES

tended to exhibit prey encounter events on a more regular basis. However, it is not clear how to interpret this tendency given that qualitative information of the prey (size and species) is missing. We suggest that the prey density decrease with depth but that their distribution tends to standardize yielding higher predictability. The extent of the vertical exploration performed by the SES during their bottom phases related negatively to prey encounter density, seemingly indicating that the thickness of the layers targeted by SES mechanically impacts micronekton density. These results underline the primary importance of the vertical dimension into the spatial organization of the micronekton.

The 3D trajectories in our dataset were essentially linear paths. While the vertical deviations from this path were of the the same order of magnitude of the horizontal ones, they better related to the prey encounter density. Under such circumstances, the widely used time-depth recorders can be considered as an effective simplification of the SES movements at scales of few-hundreds meters. Adaptive mechanisms underlying this behaviour, such as a trade-off between the travel speed and energetic requirements or an unbalanced ratio between SES sensory perception range and prey distribution and avoidance, remain unclear. These observations could be related to a number of combined factors : prey field organized in layers, short prey detection distance, external constraint such as the purpose for SES to move away rapidly from their breeding site.

We believe that this study highlights the importance of knowledge about the three-dimensional predator-prey interactions and gives support to the usage of bio-logging to unravel and monitor fine-scale micronekton distribution, particularly in remote areas such as the deep pelagic ecosystems of the Southern ocean.

CHAPITRE

5 *In situ* measurement of marine resources distribution from instrumented elephant seals

Camaïeu de couleur éléphant de mer. Crédit : J. Laborie.

3. Le Bras Yves, Jouma'a Joffrey, Guinet Christophe. (2016). In situ measurement of marine resources distribution from instrumented elephant seals. **En préparation**

► Les annexes de cet article sont disponibles en annexe D du manuscrit.

5.1 Abstract

Data acquisition in the remote Southern ocean is costly, both regarding hydrographic or biological data. Through bio-logging, diving predators have become the largest source of hydrographic data at high latitudes. With the development of accelerometers the animal platform have also gained interest in order to study the distribution of biological resources but the scope of such data is limited to the predators' prey. Cheap and low power consumption light level sensors are installed on a wide range of data loggers and commonly deployed on diving predators such as the southern elephant seal (SES). However, few studies has focused on such data. These studies highlighted various patterns related to marine resources such as light attenuation due to phytoplankton or deep scattering layer and light emission due to bioluminescent species. We propose a method to extracted these patterns from light level data measured by Wildlife Computers$^{TM\prime}$ loggers attached to SES. We found that light attenuation at surface well relates to *in situ* fluorescence measures and that its distribution appeared to be shaped vertically and horizontally by thermic structures, namely mixed-layer depth and submesoscale features. We observed a consistent increase of light attenuation around light levels of 10^{-10} W cm^{-2}. Then we examined the relationships between these light attenuation patterns and (1) the prey encounter rate of the SES and (2) with the occurrence of bioluminescence. Prey encounter rate of SES related negatively to the deep light attenuation but did not relate to surface light attenuation. Conversely, occurrence of bioluminescence tended to be negatively related to surface light attenuation but not to light attenuation occurring at depth. These results highlight the existence of a spatio-temporal mismatch between primary production richness and SES prey density. Besides phytoplankton, we could not relate directly light-based information to specific species or group of species. The exact cause of deep light attenuation remains unclear but our results suggest that it is possibly related to mid-trophic organisms not targeted by SES such as gelatinous organisms. As a whole our study support the idea that light data has potential to study the distribution of a wide range of marine organisms in the water column but that such a task will require to combine it with other data types and/or to improve the light sensors to extract further information.

Key-words : southern elephant seal ; light attenuation ; phytoplankton ; deep scattering layer

5.2 Introduction

Remote sensing has made a large amount of oceanographic data available to scientists and has been particularly useful in remote areas such as Antarctica. However, remote sensing is limited to the few upper meters of the oceans. A challenge in oceanography is to collect data over a significant extent of the water column exceeding 2000 m in most of the oceans. Dedicated instruments such as Argos floats have been developed to address this issue and provide high-quality hydrographic data up to 2000 m but animal-borne oceanographic instruments represents a cost-efficient alternative approach (Roquet et al., 2009).

The southern elephant seal (hereafter, SES) are diving marine predators with a circumpolar distribution and great diving abilities. Performing long foraging trips in the southern ocean, they dive continuously reaching an average depth of 400 m (up to 2000 m) in dives lasting 20–25 min on average (McIntyre et al., 2010). Their large size allow them to carry logger with minimal disturbance (McMahon et al., 2008; Guinet et al., 2014) which can be deployed and retrieved by scientists when the SES come back on land for breeding and moulting. These characteristics have made the SES a species commonly used to collect oceanographic data (Fedak, 2013; McIntyre, 2014).

The technological advances in computer and mobile phone industries has improved sampling frequency, variety and accuracy of sensors that can be deployed on marine predators (Ropert-Coudert and Wilson, 2005). Recent electronic devices can sample diverse physical parameters such as temperature, salinity (Fedak, 2004) or oxygen concentration (Bailleul et al., 2015). SES provide the largest quantity of data south of 60° South (Fedak, 2013) and in shelf/sea-ice areas Argos floats cannot operate (Roquet et al., 2014). Being able to retrieve the loggers when animal come back on land allows to download high-resolution data thus enabling studies at mesoscale submesoscale (Roquet et al., 2009).

Beside access to remote areas, another interesting aspect of this approach is that sampling is made at the relevant time, location and scale to study biologic processes taking place in open ocean (Fedak, 2004). Thus, in addition to physical parameters, biologging could can also help to sample biological marine resources. However, achieving such a task with simple sensors raises special problems. Detection of prey encounter events using acceleration data (Viviant et al., 2010; Naito et al., 2010; Watanabe and Takahashi, 2013; Gallon et al., 2013) and measurement of chlorophyll concentration with fluorescence have been major advances (Naito, 2007; Guinet et al., 2013). A number

of loggers used on marine predators include miniaturized, low-cost and low power consumption light level sensor. These sensors were originally aimed at delineating daytime and night periods along the animal trip and can provide coarse estimates of their location (Hill and Braun, 2001). Ocean color has been long-used in remote sensing to obtain information on the quantity (Clarke et al., 1970) and quality (Alvain et al., 2008) of phytoplankton at surface. Similarly, it appeared that light data from bio-logging could be valuable to calculate chlorophyll concentration proxies at surface (O'Toole and Lea, 2014; Teo et al., 2009; Bayle et al., 2015). Light is a more widely available data than fluorescence which is commonly used to as a proxy of chlorophyll a concentration in water column. Having access to both fluorescence (from SMRU CTD-Fluo tags) and light data (from Wildlife Computers^{TM} tags) we propose to assess the validity of a phytoplankton proxy based on light which could offer fine-scale and *in situ* measures about the abundance of primary production in the water column. A new level of complexity arise with mid-trophic level resources such as squids, myctophids and many gelatinous organisms inhabiting the deep scattering layer that are more difficult to sample. Organisms such as myctophids can enter in the diet of SES (Cherel et al., 2008) and other top predators (Kooyman et al., 1992; Jansen et al., 1998; Casaux et al., 1998). They represent a large amount of the overall biomass (Pakhomov et al., 1994), including ecologically important species such as the abundant *Electrona antarctica*. However, since they are difficult to sample, they are still poorly known organisms (Pakhomov et al., 2010). Camera (Naito et al., 2013) and miniaturized acoustic sonar (Lawson et al., 2015) deployed on elephant seals have started to provide new ways to study the micronekton but at present they still represent a niche source of data. The work of Teo et al. (2009) on light data collected by data loggers highlighted the occurrence of light attenuation at around 400 m presumably associated to the deep scattering layer. Furthermore, Vacquié-Garcia et al. (2012) revealed the detection of biological light emission (i.e. bioluminescence) produced by marine organisms through data-loggers equipped with light sensors. On this basis, it seems that light data could provide useful information on the ecology of mid-trophic level organisms inhabiting the meso and bathy pelagic southern ocean. Yet, this abundant source of data remains underutilized for that purpose. In this study, we propose to extract these patterns – light attenuation in the water column and bioluminescence emission – from bio-logging light data and to further investigate about them :

1. by comparing light attenuation with fluorescence in the upper 180 m(which is

the deeper bound of fluorescence profiles) of the water column.

2. by examining relationships between light attenuation and the prey encounter rate of SES.

3. by examining relationships between light attenuation and the occurrence of bioluminescence.

5.3 Material and methods

5.3.1 Animal handling

During the breeding seasons (October and November) of 2011 through to 2015, a total of 14 female SES of the Kerguelen Islands (49°21′0″ S, 70°13′0″ E) were equipped with an accelerometer (TDR10–DD or TDR10–X, Wildlife Computers™, USA, see deployment details in table 5.1) and (2) a location collector device. The location detector device was either a Conductivity-Temperature-Depth satellite-relay data logger (CTD-SRDL, Sea Mammal Research Unit - University of St Andrew), a Time-Temperature-Depth Fastloc GPS data logger (SPLASH10-F, Wildlife Computers™, USA) or a Smart Position or Temperature Transmitting tag (SPOT, Wildlife Computers™, USA). Among the 14 individuals, half were equipped with fluorometers embedded on CTD-SRDL (Table 5.1). Animals were captured with a canvas head-bag and anaesthetized using a 1 :1 combination of Tiletamine and Zolazepam (Zoletil 100) injected intravenously (McMahon et al., 2000). The tags were then glued on the seal's head or back (Table 5.1) using quick-setting Araldite (Araldite AW 2101).
All fieldwork involving SES was approved and authorized by the ethics committee of the French Polar Institute (Institut Paul Emile Victor – IPEV) in May 2008. This Institute does not provide any permit number or approval ID, however animals were handled and cared for in total accordance with the guidelines and recommendations of this committee (dirpol@ipev.fr).

5.3.2 Light data processing

Light sensors

The light sensors of the Wildlife Computers™ loggers were originally designed to locate the equipped animals from sunset and sunrise time (Hill and Braun, 2001). The sensor measures range from 5×10^{-12} to 5×10^{-2} W cm^{-2}with a resolution of 20 units

Table 5.1: Deployment details. Individual and loggers information

Seal name	TDR10	Fluorometer	Weight (kg)	Length (m)
2011-21	–X		245	2.25
2011-26	–X		255	2.32
2011-28	–X*		249	2.40
2012-14	–X	✓	258	2.29
2012-15	–X	✓	275	2.35
2012-16	–X	✓	425	2.65
2013-11	–DD*	✓	277	2.40
2013-12	–DD*	✓	279	2.30
2013-13	–X	✓	264	2.40
2014-22	–X		244	2.37
2014-23	–X		235	2.15
2014-34	–X	✓	236	2.31
2015-27	–X		223	2.59
2015-28	–X		283	2.43

* indicate that this logger was mounted on seal's back.

per order of magnitude for TDR10-X (Wildlife Computers, 2016b), from 5×10^{-10} to 5×10^{-2} W cm^{-2}(with the same resolution) for TDR10-DD (Wildlife Computers, 2016a). The light intensity readings from the sensors can be converted to international system units (W cm^{-2}) using the following equation, provided by the manufacturer : $L_{sensor} = 250 + 20 \times log_{10}(E)$ where L_{sensor} is the light intensity in sensor units and E the blue light intensity in W cm^{-2}.

Beside sunset and sunrise, it appeared that these data could be further promoted. Indeed, the light attenuation coefficient can be calculated from these data (Jaud et al., 2012; Teo et al., 2009; Bayle et al., 2015) and relates well to the SES diving depth (Jaud et al., 2012) and to remote-sensed chlorophyll a concentration estimates O'Toole and Lea (2014). In addition, Vacquié-Garcia et al. (2012) highlighted the detection of biological light emission (bioluminescent event, hereafter BLE) in the dark environment visited by SES.

Following this latter observation, laboratory experiments were performed to test the sensitivity of these sensors to the light intensity and to different wavelengths (Vacquié-Garcia, 2014, Chapter VI). The sensor is sensitive to a range of wavelength with a peak of sensitivity for blue light (maximum at 465-470 nm). Submitted to a steady light intensity, the sensor readings stayed in a range of $\pm$ 2 sensor units. Thus, a difference between two measured light intensities was considered reliable as soon as it exceeded

2 sensor units which translates in the W cm^{-2}scale by a ratio $E_{high}/E_{low} \geqslant 1.26$. We noted that sensors have a fast response to increasing light intensity but a slow response to decreasing light intensity (hereafter called "sensor-delay"). This behaviour is responsible for the recognisable shape of bioluminescent event in the time-light signal (Figure 5.1) but raises some specific issues regarding the calculation of light attenuation coefficient and the detection of BLE. Indeed, sensor readings may not reflect the actual light intensity immediately after a BLE (Figure 5.1) or when the light intensity in the environment changes more rapidly than the sensor delayed response. The latter case could be encountered under the effect of light attenuation in the water column if SES perform their dives' descent phase with high vertical velocity. To account for these limitations we examined the response of light sensors to decreasing light intensity. In order to predicts the minimal light intensity measurable at $t+1$ given the observed light intensity at t, we implemented a model describing the delayed response of sensors to light intensity (see details in D.1).

The light signal results from the mixed effects of multiple processes : light attenuation with depth, animal body posture, bioluminescence emission and sensor limitations (Figure 5.1). To extract accurately the BLE and light attenuation coefficients from these data, we used our sensor-delay model to distinguish two mutually exclusive categories of observations in the time-light profiles : (1) observations where the measured light intensity is close from the expected value of our sensor-delay model and therefore, likely to be driven by the sensor limitations; (2) other cases : increasing light intensity or significant difference between observed decrease and predicted maximal decrease. Category (1) observations occur at depth, where light intensity is very low and appears to be independent from depth variations and changes in the SES posture (Figure 5.1, red points). Category (2) observations occur in brighter and shallower environments, where light intensity varies in a wide range of values according to light irradiance at surface and changes in depth and seals' posture (Figure 5.1, black points). Relying on the transition points between these categories, we defined two domains. Domain A approximately corresponds to the dives' bottom phase. It starts and finishes at the first and last observations of the Time–Light profile classified in category (1) (Figure 5.1). Domain B is defined as the fraction of the ascent phase located outside the domain A (Figure 5.1).

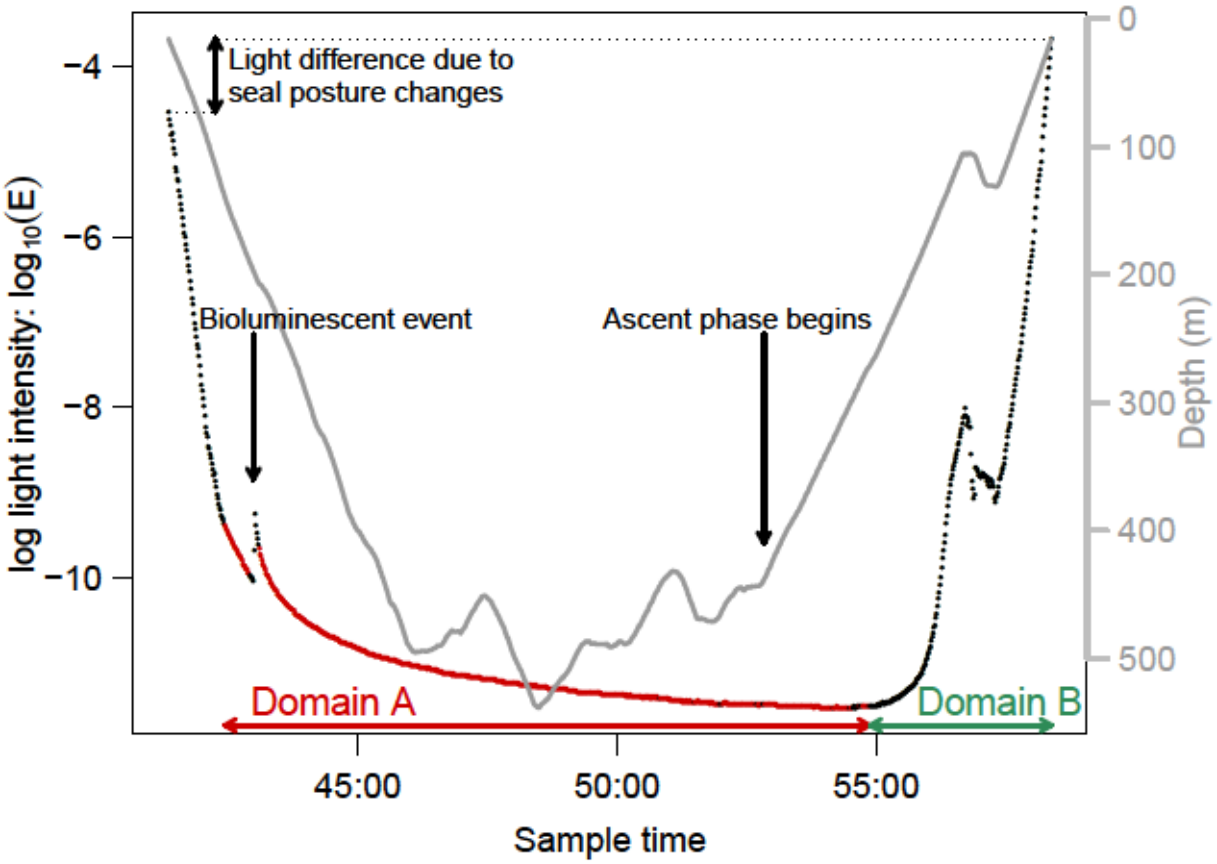

Figure 5.1: Example of time-light and time-depth profiles during a daytime dive – *Light sensor readings classified as belonging to category (1) – respectively (2) – are coloured in red – respectively black on the time-light profile. The red horizontal segment indicate the section of dive dedicated to BLE detection (Domain A). The green horizontal segment indicate the section of dive dedicated to the calculation of light attenuation coefficients (Domain B).*

Bioluminescent events

To distinguish biological light emission from other possible sources of light intensity variation, we restricted BLE detection to domain A, where it is independent from variations of seals' depth and posture but rather due to sensor's delayed response (Figure 5.1). Therefore, an increasing trend in the signal can unambiguously be associated to BLE despite their very weak energy level (Figure 5.1). We use the BLE detection method developed by Vacquié-Garcia et al. (2012), adapted to the sampling frequency of in our data (1 Hz instead of 0.5 Hz). Detailed explanation about this method are provided by Vacquié-Garcia et al. (2012). The R source code of our implementation is available in D.2 and online as part of a R package (Le Bras, 2017).

Light attenuation

For each dive, chronologically-ordered data were transformed into vertical profiles. We divided the water column into 5 m layers which offered a good trade-off between the spatial resolution of the resulting profiles and the temporal resolution of original data. Indeed, with these setting, the profiles contained no missing value due to SES performing descent and ascent phases at high vertical speed with 5 m bins. Depth–Light profiles were computed on the data belonging to domain B (Figure 5.1). Depth–Fluorescence profiles were calculated at the same resolution but are limited to 180 m because CTD-SRDL tags were programmed to measure fluorescence between 180 m depth and surface.

Beer Lambert law describes the attenuation of light intensity in fluids. In the ocean, the light attenuation depends on the chemical composition of water and the quality and quantity of suspended material such as plankton and detritus. Attenuation coefficients is commonly defined by equation (5.1).

$$K_d(z) = -\frac{1}{E_d(z)}\frac{dE_d(z)}{dz} \tag{5.1}$$

Where z is the depth at the center of a layer (increasing downward), $K_d(z)$ the diffuse attenuation coefficients at depth z, and $E_d(z)$ the blue light intensity in $\mathrm{W\,cm^{-2}}$at depth z. The influence of light wavelengths on the attenuation coefficient was not taken into account. Given the small space-time scale involved, we considered attenuation coefficient as constant within each layers of Depth–Light profiles and calculated it with the following equation : $K_d(z) \approx log_{10}(E_d(z)/E_d(z+5))/5$. Prior to calculation of light attenuation coefficient, the light intensity signal was smoothed using constrained B-Splines (Ng and Maechler, 2007) with a negative relationship constraint. This constraint allows to avoid inconsistent attenuation coefficient due to some abrupt changes of SES posture in bright environments. The number of knots was selected using Akaike Information Criterion (AIC). The implementation of this method (in R code) is provided in D.2. Light attenuation profiles were computed for daytime only. We defined day as the period when the sun elevation angle is exceeds 7° (threshold justification in D.3).

5.3.3 Prey encounter events

The detection of Prey Encounter Events (PEE) was performed following Guinet et al. (2014) and Vacquié-Garcia et al. (2015). Dynamic accelerations, resulting from rapid movements, were extracted from the longitudinal, lateral and vertical axes of the logger using an order 3 high-pass digital Butterworth filter with a normalized cut-off frequency of 2.64 Hz (performed with the signal package Signal developers (2013)). For each axis, a one-second fixed window was used to calculate the standard deviation. Signals were then processed using a moving standard deviation across a window of five seconds. Finally, a two-mean clustering was performed for each signal to distinguish "high state" from "low state". A PEE is occurring when the three axes are simultaneously in "high state" (see Vacquié-Garcia et al. (2015) for graphical illustration of the method). A continuous succession of "high state" was considered as a single PEE.

5.3.4 Mixed-Layer Depth

We assessed mixed-layer depth using Depth–Temperature profiles. Water temperature between 15 and 20 m was chosen as reference. Mixed-layer depth was then defined as the first depth of profiles for which absolute temperature deviation from this reference exceeded 0.2 °C.

5.3.5 Statistical analysis

We evaluated the relationship between light attenuation and fluorescence measured by CTD-SDRLs-Fluo with linear models. Because fluorescence measurements are submitted to quenching in bright environments, we limited the comparison to data obtained deeper than 30 m (Guinet et al., 2013). We tested how the quality of the relationship, assessed using adjusted r^2, responded to ambient light intensity and whenever or not a single intercept or slope could be used for all individuals. Our dataset was constituted of 240 daytime profiles from seven individuals (Table 5.1) providing a total of 5578 observations (i.e points located in the middle of 5 m layers with non-missing depth, light attenuation coefficient and fluorescence information).

Light attenuation in the water column is known to drive SES diving depth (Jaud et al., 2012) which, in turn, impacts negatively the PEE rate of their dives (Guinet et al., 2014). We tested the effect of light attenuation on the PEE rate of the SES du-

ring their dives apart from its influence of the diving depth. We used Generalized Linear Models (GLMs) of poisson and negative binomial (when over-dispersion was observed) families with the count of PEE that occurred within dives as response and log-transformed dive duration (the exposure variable) as offset. Temporal autocorrelation was handled by selecting one dive every 15.

Occurrence of BLE was also found to decrease with depth (Vacquié-Garcia et al., 2012). We examined if the occurrence of bioluminescence was related to the light attenuation in the water column given the SES diving depth (depth of domain A). This was accomplished with the same tools as the previous model, setting the number of BLE as response and the log-transformed duration of domain A (exposure variable) as offset.

5.4 Results

5.4.1 Fine-scale distribution of phytoplankton

In situ fluorescence could well explain the variations of the attenuation coefficient in the upper 180 m of the water column (Figure 5.2). The relationship was sensitive to the range of ambient light intensity (E_d) considered to fit the model. The highest goodness-of-fit was observed when the light intensity was at least $10^{-8.09} = 8.13 \times 10^{-9}$ W cm^{-2}(with adjusted r^2 of $r^2_{mod.1} = 0.52$, $r^2_{mod.2} = 0.58$, $r^2_{mod.3} = 0.59$) and decreased rapidly when including observations with $E_d < 10^{-8.4}$ W cm^{-2}(Figure 5.2). These results emphasize that light attenuation observed in the upper 180 m of water column is mainly related to phytoplankton concentration. In any ambient light conditions, models 2 and 3 (both with an intercept per individual) provided a better fit than model 1 (with a single intercept), highlighting the need for different intercepts for each individual. This result suggest that light sensors and/or fluorometers are not well inter-calibrated from one individual to another. Differences between the main phytoplankton types encountered by the seals can also be a source of variation. Models 2 and 3 provided similar performances indicating that relative changes of light attenuation coefficients can be interpreted, in terms of relative changes of chlorophyll concentration proxy (fluorescence), in the same manner from individual to another.

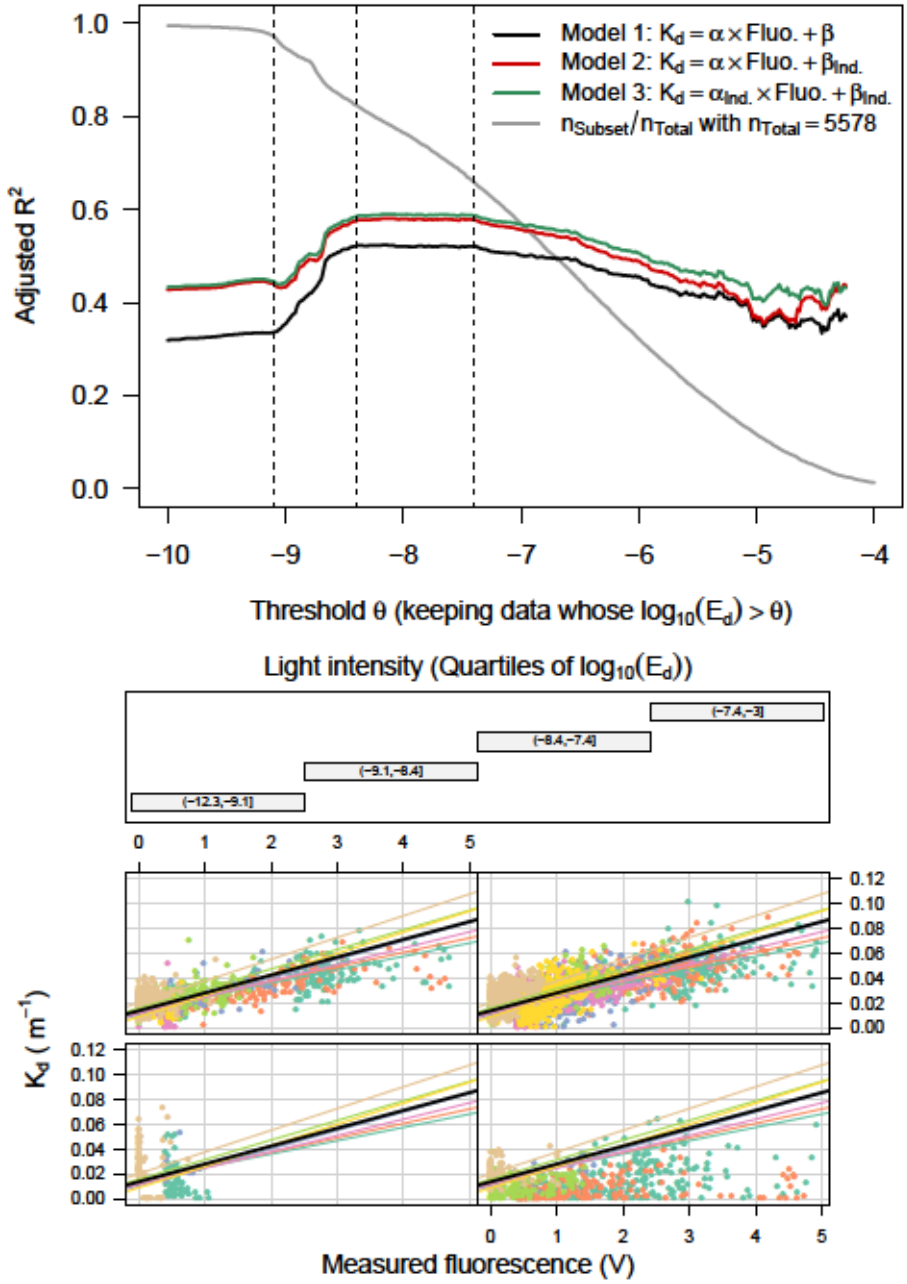

Figure 5.2: Linear relationship between light attenuation coefficient and fluorescence – *Up : Adjusted r^2 of the three models according to the threshold (θ) applied to light intensity (E_d). Down : Relationship in various light intensity conditions, delimited on the upper graphic by vertical dashed lines. Panels of this graphics are read from bottom to top and left to right. Colors stand for the individual identity. Black line stands for the population-level regression line obtained in model 3 for optimal $\theta = -8.09$ ($r^2 = 0.59$).*

5.4.2 Link with oceanographic parameters

The surface attenuation mode is limited by mixed-layer depth (Figure 5.3 A–D, red arrows 3) and more generally by thermic structures (Figure 5.3 and 5.4). Indeed, in area affected by complex water masses mixing (such as Figure 5.3 A&D and 5.4) we observed synchronous horizontal discontinuities between thermic and light attenuation profiles (indicated by red arrows 1). In these areas light attenuation can occasionally pursue deeper than the mixed-layer depth to create a deep chlorophyll maximum (Figure 5.3 A, red arrows 2). A second mode of light attenuation is observable at depth following the convolutions of the 10^{-10} W cm^{-2}isolume (Figure 5.3 A–D, red arrows 4). Based on the very low light level at these depths, this light attenuation is unlikely due to phytoplankton. This second attenuation mode was also observed by Teo et al. (2009) which noted a matching with the location of the deep scattering layer identified using Acoustic Doppler current profiler (ADCP) backscattering signal. Deep attenuation was observed consistently across individuals and along their trip with some rare anomalies such as pointed by red arrow 5 and 6 on Figure 5.3 C&D. However, given the very low light level associated with this attenuation mode it is unclear if it is not caused by changes in sensor response to light intensity. From Time–Light and Time–Depth profiles such as Figure 5.1 we could not detect obvious issues in domain B around 10^{-10} W cm^{-2}.

Hereafter we define (1) "surface attenuation" as the median value between surface and mixed-layer depth and (2) "deep attenuation" as the median value between isolumes $10^{-10.5}$ and $10^{-9.5}$ W cm^{-2}.

5.4.3 Relationship with PEE

The most parsimonious model without light attenuation is model 11 ($AIC_{11} = 5458.41$, Table 5.2) which includes an intercept for individuals and a single linear term for maximum diving depth. This model can be used as reference to test the significance of the effect of light attenuation in the mixed layer and at depth.

Adding to this reference model the surface attenuation among explanatory variables (model 13 and 14, Table 5.2) increases the AIC ($\Delta AIC_{13-11} = 0.99; \Delta AIC_{14-11} = 1.11$). Therefore, the quantity of phytoplankton does not improve the fishing success of SES apart from its effect on their diving depth.

Conversely, adding light attenuation at depth yield lower AIC ($\Delta AIC_{8-11} = -2.20$,

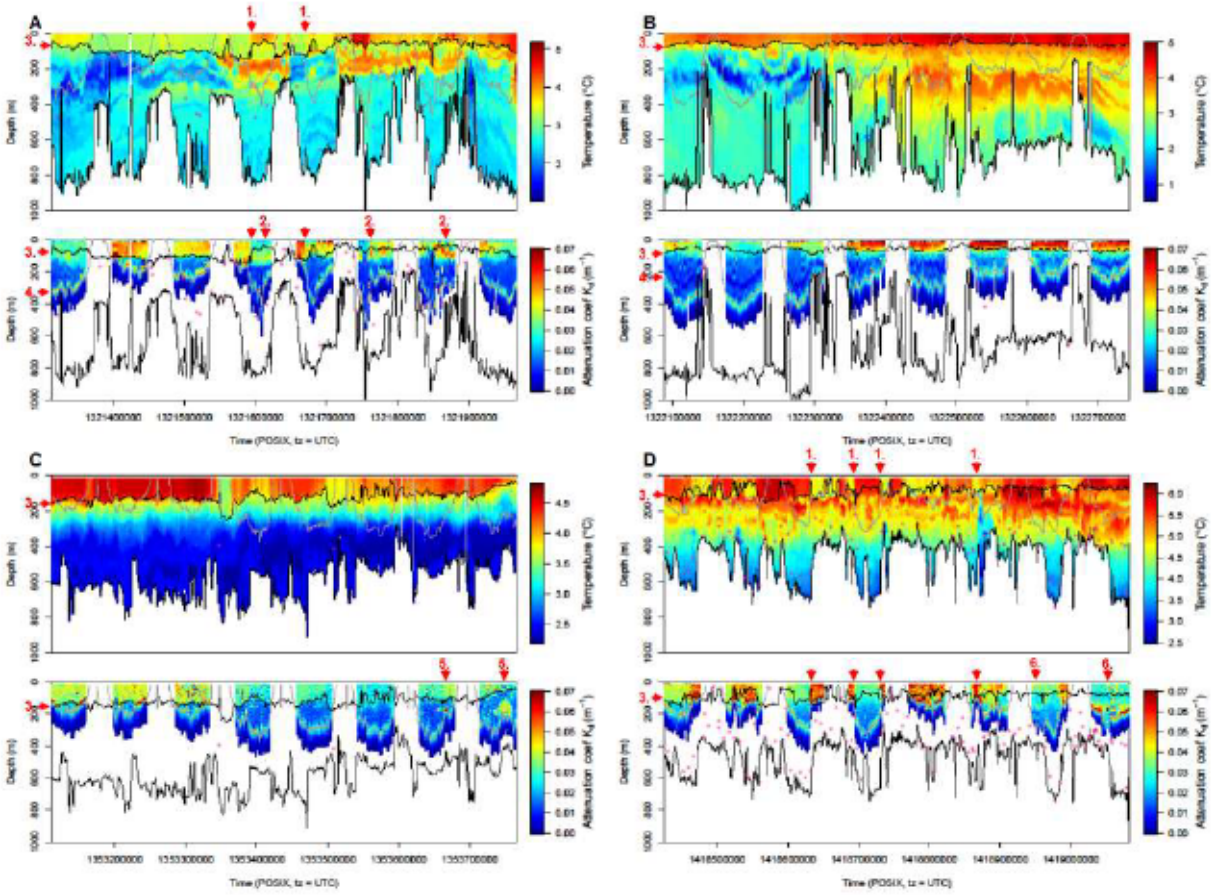

Figure 5.3: Temperature and light attenuation profiles over 8-days samples of 4 individuals – *(A. 2011-21, B. 2011-26, C. 2012-16, D. 2014-23). Interruptions in light attenuation profiles correspond to night periods. The shallowest black line indicates the Mixed-Layer Depth, the deepest one displays the diving depth of the seal. The grey line stands for isolume* 10^{-10} W cm^{-2}*. The pink points display the location of BLE. Red arrows indicate the location of specific various events such as 1. Abrupt changes of light attenuation in horizontal dimensions, 2. Deep Chlorophyll Maximum, 3. Mixed Layer Depth delineating the lower limit of surface light attenuation, 4. Isolume* 10^{-10} W cm^{-2}*driving the vertical distribution of deep attenuation, 5. Unusual deep attenuation structures, 6. Local disappearance of deep attenuation.*

$\Delta AIC_{3-11} = -8.67$, Table 5.2). According to *AIC*, the best model with significant main effects including deep attenuation is model 2. The estimated coefficient of deep attenuation in model 2 is -4.05×10^1 PEEm.

Despite the fact that surface attenuation is penalized by *AIC*, a large *AIC* difference is observable between models 1 and 2 ($\Delta AIC_{1-2} = -5.90$, Table 5.2) while the main effect is not significant in model 1. This result indicates that surface attenuation does convey relevant information to explain the fishing success of SES but the relationships

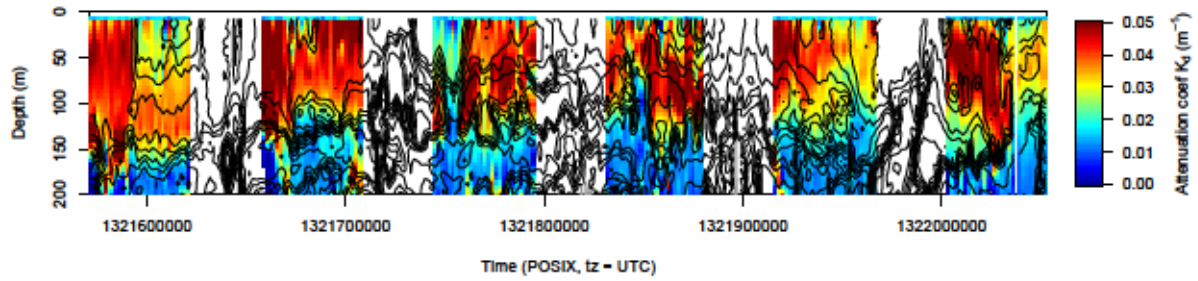

Figure 5.4: Detailed view of the upper 200 m of profiles presented on Figure 5.3 – *A. Interruptions in light attenuation profiles correspond to night periods. Isotherms every 0.2 °C are displayed as black contour lines superimposed on colour-coded light attenuation.*

Table 5.2: Negative binomial GLMs explaining the PEE rate during SES′ dives – $n = 896$ *dives*

Model					df	AIC
#	ID	Max. depth	Att_{surf}	Att_{deep}		
1	✓*	/ID*	/ID	/ID*	33	5443.66
2	✓*	/ID*		/ID*	25	5449.56
3	✓*	✓*		/ID*	18	5449.74
4	✓*	✓*	/ID	/ID*	26	5450.67
5	✓*	/ID*	/ID		25	5452.39
6	✓*	/ID*	✓	✓*	19	5454.97
7	✓*	/ID*		✓*	18	5455.47
8	✓*	✓*		✓*	11	5456.21
9	✓*	✓*	✓	✓*	12	5456.98
10	✓*	/ID*	✓		18	5458.39
11	✓*	✓*			10	5458.41
12	✓*	/ID*			17	5458.52
13	✓*	✓*	✓		11	5459.40
14	✓*	✓*	/ID		18	5459.52
15		✓*			3	5546.56
16	✓*				9	5555.27
Null					2	5584.42

✓and /ID indicate if the explanatory variables were included with (✓) "main" effect only, (/ID) "main" effect and "interactions" according to individual
* indicates that "main" effect is significant at level $\alpha = 5\%$.

Table 5.3: Poisson GLMs explaining the occurrence of BLE during SES′ dives – $n = 896$ *dives*

Model					df	AIC
#	ID	Max. depth	Att_{surf}	Att_{deep}		
1	✓	/ID	✓*		17.00	572.56
2	✓	/ID	✓*	✓	18.00	574.37
3	✓	/ID			16.00	575.80
4	✓	/ID		✓	17.00	577.43
5	✓	/ID	/ID		24.00	580.36
6	✓	/ID		/ID	24.00	586.31
7	✓*	✓*	✓		10.00	589.94
8	✓*	✓*	✓*	✓	11.00	590.82
9	✓	/ID	/ID	/ID	32.00	591.37
10	✓*	✓*			9.00	591.97
11	✓*	✓*		✓	10.00	593.17
12	✓	✓*	/ID		17.00	597.20
13	✓*				8.00	597.40
14	✓	✓*		/ID	17.00	598.68
15	✓	✓*	/ID	/ID	25.00	604.91
Null					1.00	650.84
16		✓			2.00	652.58

✓and /ID indicate if the explanatory variables were included with (✓) "main" effect only, (/ID) "main" effect and "interactions" according to individual
* indicates that "main" effect is significant at level $\alpha = 5\%$.

vary according to individuals and there is no consistent trend applying to all of them. Given the correlation between surface attenuation landscape and submesoscale water masses (Figure 5.3) which are known to impact the foraging success of marine predator (Bost et al., 2009; Nordstrom et al., 2013; Monte et al., 2012; Cotté et al., 2007; Dragon et al., 2010; Volker et al., 2002; Guinet et al., 2014), we interpret these effects as the effect of local oceanographic conditions encountered by the various individuals rather than as causal biotic relationships.

5.4.4 Relationship with bioluminescence

We examined in the same manner the influence of maximum diving depth and light attenuation on the occurrence of BLE. According to AIC, the best model without light attenuation is model 3 ($\Delta AIC_{3-Null} = -75.04$, Table 5.3) and then model 10 ($AIC_{3-10} = -16.17$, $\Delta AIC_{10-Null} = -58.87$, Table 5.3). However, none of the effects implemented in model 3 is significant (Wald-test p-values > 0.98 for all 16 parameters). Conversely, model 10 includes significant intercepts for individuals, reflecting the fact that number of BLE differs according to individuals (Figure 5.3, $\Delta AIC_{13-Null} = -53.44$, Table 5.3), and a significant negative effect of maximum diving depth, consistently with findings of Vacquié-Garcia et al. (2012). On this basis, only the models including a single term for maximum diving depth, namely, models 7 and 8 are considered valid for interpretation.

As indicated by the AIC scores of these two models ($\Delta AIC_{7-8} = -0.88$, Table 5.3), deep attenuation has no effect on the occurrence of BLE in SES's dives. Surface attenuation is significant in model 8 but is estimated as sub-significant in model 7 (Wald-test p-values $= 0.0504$) with a negative coefficient of -1.84×10^{1} BLE m.

5.5 Discussion

5.5.1 Surface attenuation

Comparison of light attenuation and fluorescence in the upper 180 m of the water column suggests that light attenuation derived from low-cost and low-power consumption light sensors could be a useful proxy of phytoplankton abundance (Figure 5.2). This approach offers new possibilities to complement remote-sensed ocean color observations in cloudy areas or to enrich them with measures deeper in the water column. However, the quality of this proxy appears to be sensitive to the ambient light level. For instance, the accuracy suddenly decreases when ambient light dropped under 3.98×10^{-9} W cm^{-2}restricting it potential use to daytime periods ($\theta < -8.4$, Figure 5.2). Similarly, the quality of the relationship between light attenuation coefficient and measured fluorescence decreased progressively when ambient light exceeded 3.98×10^{-8} W cm^{-2}($\theta > -7.4$, Figure 5.2), possibly due to the coarser light sensor resolution at these levels and/or to remaining quenching effect affecting fluorescence. Beer-Lambert law is also subject to quenching at very high concentrations.

Our observations of light attenuation in the mixed-layer, although descriptive, depic-

ted a phytoplankton landscape shaped by submesoscale structures on the horizontal dimensions, as previously highlighted on phytoplankton communities by d'Ovidio et al. (2010), but also according to vertical dimension (Figures 5.3 and 5.4). Animal platforms already constitute the main source of data in high latitudes (Fedak, 2013; Roquet et al., 2014). Light attenuation profiles obtained through animal platforms seems to be an interesting tool to understand the role of vertical water mixing on primary production and shaping of the marine resource distribution of high latitudes.

SES forage at great depth in low light level environments that their prey inhabit. This fact is long known from bio-logging data collected in early 1990s (Hindell et al., 1991b) that provided information about their diving depth and revealed daily migration patterns. More recently, Jaud et al. (2012) demonstrated that phytoplankton concentration, by reducing the penetration of sunlight in the water column, had a strong effect on diving depth, bringing SES closer from surface during daytime in high phytoplankton concentration areas. Phytoplankton-rich water masses are thus profitable to SES foraging success by allowing them to access their prey at lower depth that is to say the amount of time and energy they can spend at the bottom of their dives which is the efficient foraging phase of the dive. However, apart from this indirect effect via vertical accessibility of prey, water masses with higher phytoplankton concentration were not housing higher prey densities as we found no relationship between phytoplankton and concurrent PEE rate of seals (Table 5.2). Furthermore, we observed that surface attenuation had a nearly significant negative effect on the occurrence of BLE at depth (Table 5.3). This constitutes another sign of the time and therefore spatial lag necessary to transform primary production to higher trophic levels biomass. This mismatch between primary production and putative prey density suggests that a "maturation time" or water mass ageing is required before primary production creates favourable foraging areas to SES. Therefore, accounting for the duration of vertical energy transfer appears necessary in order to predict future high foraging success areas of SES and other deep diving predators. Further work could assess the relevancy of models such as SEAPODYM micronekton (Lehodey et al., 2010b) which predicts micronekton potential biomass in time and space by modelling the integration of primary production into mid-trophic levels biomass using remote-sensed chlorophyll concentration, temperature and currents.

5.5.2 Deep attenuation

The calculation of light attenuation from Wildlife Computers$^{TM\prime}$ data loggers revealed a similar pattern than that found by Teo et al. (2009) using Lotek data loggers. Indeed, a light attenuation peak was consistently observed in low light level environment at around 10^{-10} W cm^{-2}, at depths ranging between 300 and 500 m during daytime. While Teo et al. (2009) could highlight that this peak matched the one of ADCP backscatter signal, we had no such an independent source of data to specify the nature or origin of our similar observation. Because Wildlife Computers$^{TM\prime}$ light sensor measurements range from 5×10^{-12} and 5×10^{-2} W cm^{-2}, or from 5×10^{-10} and 5×10^{-2} (section 5.3.2), which is close from the light level condition of the deep attenuation peak, artefactual causes of this signal feature can not be discarded yet. However, we found that this attenuation related negatively to PEE rate encountered by SES which suggests that deep attenuation is not purely artefactual, in other words, only due to light sensors limitations. This negative relationship also suggest that the biomass for which this attenuation might stand for is competing with SES's or myctophids' prey. The light attenuation that we observed at depth does not appear to be related to the presence of mid-trophic organisms such as copepods, which would support SES-favourable trophic chains. Given the location of deep attenuation mode, typically shallower than the SES bottom depth (Figure 5.3), an hypothesis is that vertical energy transfer of primary production from surface to depth would be partially intercepted, for instance, by gelatinous organisms. The nature of these organisms is open to conjecture. However, no relationship was found with the occurrence of BLE (table 5.3). As such, bioluminescent species appear less likely to be responsible for the light attenuation we observed at around 10^{-10} W cm^{-2}.

5.5.3 Methodology

We proposed a new methodology to estimate light attenuation along water column using light data collected by diving predators equipped with Wildlife Computers$^{TM\prime}$ tags. In particular we proposed a method to deal with two issues encountered with such light level data collected by a deep diving predator : (1) the delayed response of the sensor to decreasing light intensity and (2) the limited sensitivity range of these sensors to investigate on light attenuation above 200 m. Regarding the first issue, we proposed a way to overcome this problem by classifying data into two domains

(domains A & B, Figure 5.1) that discriminates periods of the dataset that are suitable to identify BLE (domain A) or to calculate light attenuation coefficient (domain B).
It should be noted that "sensor-delay", while responsible for the pattern called "domain A", is not necessarily a nuisance. Indeed, by reducing the effect of depth changes and SES body posture on measured light level it allows to detect bioluminescence with greater confidence.
The closer from surface the SES were, the more sensitive to posture changes light data seemed to be. For this reason we recommend to smooth the Depth–Light profiles with a negative relationship constraint prior to the calculation of light attenuation coefficient.
Approximating measured light level as being vertical light beams regardless of animal posture is another issue that is worth examining. Such an approximation introduces errors that increases when SES posture moves away from the vertical direction or becomes more variable. We propose to restrict the calculation light attenuation coefficient to dives' ascent phase, where SES pitch angle is steep and steady, in order to reduce this source of error.

5.5.4 Perspectives

The next step might be to adjudicate the issue raised about the causes of light attenuation at depth (so called "deep attenuation"). Active acoustic tags appear as a promising tool on this subject yet many improvements on the light sensors could be achieved. For instance, regarding their sensitivity range. From ten to twelve orders of magnitude seems to be a reasonable objective to target given the current state of technology and the location of deep light attenuation in the water column. Faster response time to light level variations would also facilitate the analysis of such data and alow to include data collected during dives' descent phases.
Remote-sensed ocean color have made a forward step by classifying phytoplankton types according to their absorption spectrum (Alvain et al., 2008) but these datasets are greatly limited by cloud coverage. Combining several light sensors on dataloggers, each with a special wavelength sensitivity, could provide qualitative details on the particules that are responsible of light attenuation within water column. Such data could complement remote-sensed observations vertically as well as in cloudy areas.
As for the influence of SES posture on measured light level, data loggers could be improved by controlling the incidence angle of light beams on the sensor. For example,

by measuring average "all direction confounded" (scalar irradiance) ambient light intensity (Teo et al., 2009), or downward irradiance using a constantly vertical aperture. This latter solution, matching the exact conditions of Beer-Lambert law application, would also allow to detect when SES would roll on their back, such as drifting periods (Mitani et al., 2010).

5.5.5 Conclusion

Our results suggest that light level data collected by low power consumption sensors can allow to turn diving predators such as SES into samplers of a wide range of organisms including ones that do not belong to the predator's diet. We confirmed that light attenuation derived from Wildlife Computers™' sensors can inform on the fine scale abundance and vertical distribution of phytoplankton within the euphotic layer. Moreover, light attenuation at depth could provide data about higher trophic levels, such as zooplankton or gelatinous organisms. Finally, detection of biological light emission can inform about the abundance of many bioluminescent species in very dark environments.

However, due to the weak specificity level of these proxies and because the light intensity signal results from multiple effects – namely, the influence of depth changes, animal body posture and bioluminescence – light-derived information are still difficult to interpret unambiguously. As a consequence, light data remains largely underutilized. With the increasing variety of data types available to the bio-logging community (e.g. video data loggers (Naito et al., 2013) or active acoustic tags (Lawson et al., 2015)), further studies will be able to remove scientific uncertainties regarding the organisms implied in light attenuation and emission of bioluminescence. Consequently, the widely available light data might offer new insights into the ecology of pelagic ecosystems. Finally, we support the idea that appropriate design of light sensors could achieve many improvements regarding these issues without giving up its advantages : low cost and power consumption.

Chapitre

6 Peut-on prédire les zones pélagiques favorables aux éléphants de mer depuis l'espace ?

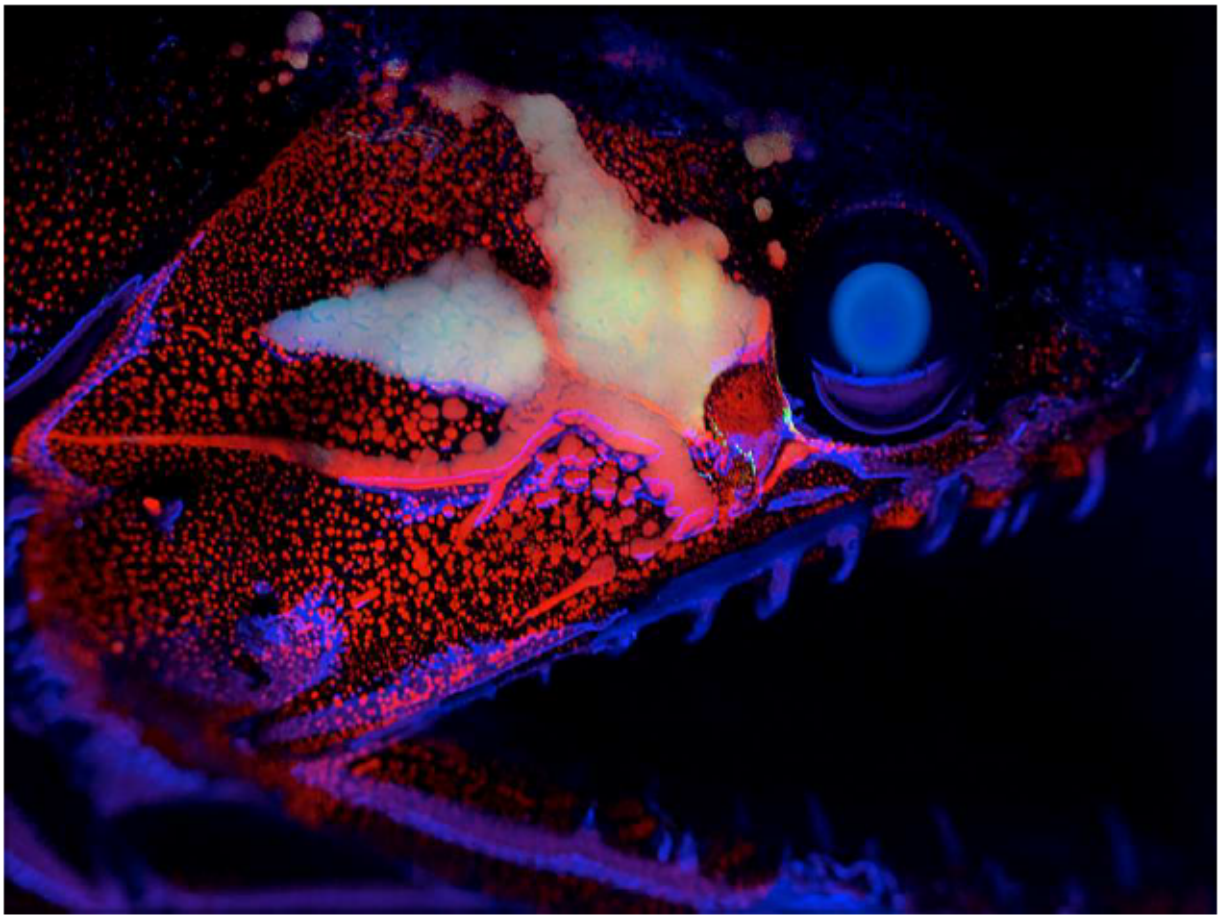

Photographie d'un spécimen de *Trigonolampa miriceps* (FishBase), prise à bord du Marion Dufresne. Crédit : J. Mallefet

6.1 Introduction

Les prédateurs supérieurs sont largement impactés par la disponibilité de leur alimentation. Celle-ci serait la principale contrainte sur la survie de l'éléphant de mer du sud (Guinet et al., 1999; McMahon et al., 2003; Reisinger et al., 2011). À large échelle, la zone interfrontale du secteur indien de l'océan Austral a été identifiée comme une zone productive d'intérêt majeur pour ces prédateurs (Bost et al., 2009; Cotté et al., 2015). À plus fine échelle, la détermination des zones d'intérêt est plus complexe. De nombreux travaux ont reporté les structures méso-échelles, filaments et tourbillons, comme des régions particulièrement productives (Volker et al., 2002; Benitez-Nelson et al., 2007) dans lesquelles les prédateurs supérieurs s'alimentent, et notamment les éléphants de mer (Bailleul et al., 2010b; Dragon et al., 2010; Cotté et al., 2015). Cependant, décrire les interactions trophiques qui se déroulent au sein de ces structures et prédire le succès d'alimentation des prédateurs qui les fréquentent, se révèlent être des problèmes difficiles. Il a été proposé que ces structures agiraient comme des "oasis" de ressources, où le transfert d'énergie vers les niveaux trophiques supérieurs est stimulé (Godø et al., 2012). L'enjeu est donc important de comprendre comment l'assimilation de l'énergie de la production primaire vers les niveaux trophiques supérieurs est affectée par le dynamisme du milieu océanique à méso-échelle.

SEAPODYM (Spatial Ecosystem and Population Dynamics Model) est un modèle visant à simuler ce processus. Il cherche à coupler la bio-chimie et la physique du milieu pélagique avec la dynamique spatio-temporelle de populations de prédateurs supérieurs tels que les thonidés (Lehodey et al., 2008; Senina et al., 2008). À l'origine, ce modèle a été développé pour étudier les populations de thonidés en relation avec leur environnement physique et biologique, et la gestion des pêcheries dans l'océan Pacifique (Lehodey et al., 2010a; Sibert et al., 2012; Lehodey et al., 2013). SEAPODYM modélise l'écosystème au travers d'un réseau trophique très simplifié, selon une succession Phytoplancton (*observé*) > Zooplancton > Micronecton > Prédateurs. Le deuxième étage, SEAPODYM micronecton (Lehodey et al., 2010b), est une composante clé du modèle qui a pour objectif de prédire la dynamique des ressources marines de niveaux trophiques intermédiaires, le micronecton, constitué essentiellement de poissons ayant une taille comprise entre 2 et 20 cm (Lehodey et al., 2010b, Table A-1). De tels organismes constituent justement l'essentiel du régime alimentaire de l'éléphant de mer du sud (sous-section 2.1.4). Celui-ci constitue un bon modèle d'étude pour lequel il existe des indicateurs du succès d'alimentation à fine échelle, les tentatives de

capture de proies (sous-sous-section 2.3.3). Avec les modèles de Loots et al. (2007) et Koubbi et al. (2011), SEAPODYM micronecton constitue l'un des rares modèles ciblant les organismes micronectoniques et couvrant géographiquement l'océan Austral. Cependant les modèles de Loots et al. (2007) et Koubbi et al. (2011) ne modélisent pas les processus trophiques mais s'appuient plutôt sur la corrélation entre l'abondance des myctophidés et les paramètres de l'environnement. À l'inverse, SEAPODYM micronecton procède selon une approche "Bottom-Up", en modélisant le processus d'intégration de la production primaire dans le réseau trophique. Dans ce contexte, il semble intéressant de comparer les prédictions de SEAPODYM micronecton avec les données collectées par des éléphants de mer, afin de juger des performances prédictives du modèle. Dès lors, une première question que l'on souhaite aborder dans ce chapitre peut se formuler ainsi : **la prise en compte du processus d'assimilation de la production primaire et de l'influence des processus d'advection par les courants permet-elle de simuler de façon satisfaisante la dynamique spatio-temporelle des organismes habitant les profondeurs de l'océan austral ?**

Outre l'influence strictement quantitative de la dynamique spatio-temporelle de l'environnement physique sur la distribution des ressources biologiques, on s'intéresse à l'influence de facteurs décrivant la qualité de cette environnement. En effet, toutes les structures ne suscitent pas de manière égale l'intérêt des éléphants de mer qui ont été observés cibler préférentiellement, ou au contraire ignorer, les tourbillons méso-échelle (Bailleul et al., 2010b; Dragon et al., 2010; d'Ovidio et al., 2013; Cotté et al., 2015). Les tourbillons méso-échelle sont dotés d'une capacité de rétention, c'est à dire d'une capacité à transporter une masse d'eau tout en l'isolant du milieu environnant qui lui est fortement brassé. Ces structures forment ainsi des niches écologiques, avec des dynamiques qui leur sont propres, et dont le rôle structurant et sur les communautés phytoplanctoniques a été mis en évidence (Bracco et al., 2000; d'Ovidio et al., 2010). En rapport avec cette notion de niche dynamique, les observations de d'Ovidio et al. (2013) du comportement particulier d'un éléphant de mer dans un tourbillon fortement "rétentif" éveillent l'intérêt au sujet de la capacité de rétention des tourbillons. En complément du paysage micronectonique décrit par SEAPODYM, nous avons donc souhaité **examiner l'influence de la rétention de ces structures méso-échelle sur le taux de tentatives de capture des éléphants de mer.**

Pour résumer et conclure cette introduction, **ce chapitre est un travail d'analyse exploratoire et interdisciplinaire visant à recouper les travaux et/ou pistes de ré-**

flexions issus de différentes équipes de recherche (de CLS[1], du LOCEAN[2] et du CEBC[3]), et visant à comprendre la dynamique des interactions trophiques dans le paysage complexe et dynamique de notre secteur d'étude.

6.2 Matériels et méthodes

6.2.1 Données de télédétection

Description de SEAPODYM micronecton

Modèle conceptuel du micronecton SEAPODYM micronecton est un modèle de type eulérien qui existe en deux résolutions, $\frac{1}{4}° \times 1$sem et $\frac{1}{12}° \times 1$j, correspondant à la méso-échelle. Dans SEAPODYM micronecton, le micronecton évolue entre la surface et 1000 m. La colonne d'eau ainsi définie est divisée en trois couches : épipélagique (notée 1), mésopélagique supérieure (notée 2) et mésopélagique inférieure (notée 3). Dans la mesure où la lumière est le principal facteur régissant le phénomène de migration nycthémérale du micronecton (Catul et al., 2010; Jaud et al., 2012), les limites entre ces couches sont déterminées en fonction de la profondeur euphotique (Z_{eu}). L'estimation de cette profondeur est basée sur les équations de Morel and Berthon (1989), appliquées aux mesures de la concentration en chlorophylle *a* obtenues par imagerie satellitaire (MODIS). Les limites qui définissent les couches ont été établies à partir d'échogrammes (figure 6.1) à $1.5 \times Z_{eu}$ pour la couche épipélagique, $4.5 \times Z_{eu}$ pour la couche mésopélagique supérieure et $min(10.5 \times Z_{eu}, 1000)$ pour la couche mésopélagique inférieure (le modèle se bornant à la simulation des 1000 premiers mètres de la colonne d'eau). Le micronecton est alors divisé en 6 groupes fonctionnels selon leur comportement de migration entre ces couches (figure 6.1). La migration des groupes fonctionnels est par ailleurs contrôlée par l'élévation solaire (nuit : $< -18°$, jour : $> 18°$) qui est fonction des coordonnées spatiales et de la date.

Dynamique spatio-temporelle du micronecton La production (P) d'une nouvelle cohorte d'organismes de niveau trophique TL est fonction de la production primaire disponible PP (dont on dispose d'une estimation issue d'images satellite), et de l'ef-

[1]Collecte Localisation Satellite, CNES Toulouse.
[2]Laboratoire d'Océanographie et du Climat : Expérimentations et Approches Numériques, Université Paris VI
[3]Centre d'Études Biologiques de Chizé, Villiers en Bois

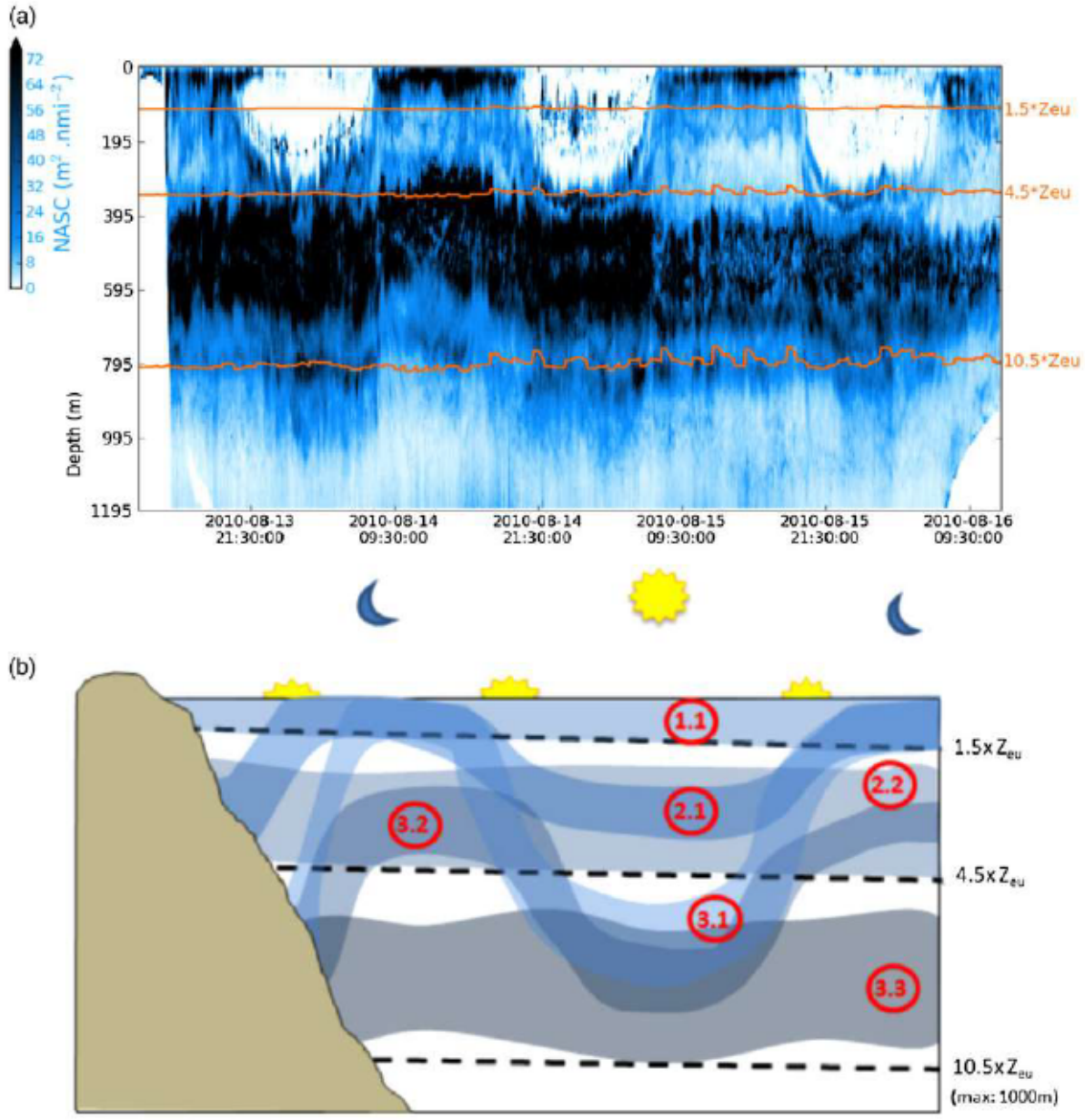

Figure 6.1: Définition des groupes fonctionnels du micronecton – *(a) Echogramme, (b) Schéma conceptuel. Les groupes fonctionnels sont numérotés par les identifiants des couches qu'ils occupent le jour et la nuit (selon la convention jour.nuit) soit : 1.1, 2.1, 2.2, 3.1, 3.2 et 3.3. Figure tirée de Lehodey et al. (2014).*

ficacité du transfert d'énergie E : $P(\tau = 0) = PP.E^{TL-1}$ où τ représente l'âge de la cohorte. La valeur de E à l'échelle globale est choisie (traditionnellement) à 10% (Lindeman, 1942), ce qui correspond à une valeur moyenne au sein du milieu océanique à grande échelle (Iverson, 1990). La production résultant de ce paramètre global est allouée aux différents groupes fonctionnels de micronecton en raison d'une matrice de coefficient de transfert d'énergie (Lehodey et al., 2014, table 1), dont l'estimation est basée sur des données d'acoustique active.

La **dynamique temporelle** de la biomasse B du micronecton est modélisée au moyen de deux termes, l'âge de recrutement τ_r et la mortalité λ : $\frac{dB}{dt} = -\lambda B + P(\tau = \tau_r)$. En se basant sur les travaux de Gillooly et al. (2002), l'âge de recrutement et la mortalité sont considérés comme des fonctions de la température. Nous ne détaillons pas ici cette partie du modèle (voir Lehodey et al. (2010b)). Mentionnons néanmoins qu'à ce stade, SEAPODYM micronecton fait l'hypothèse qu'à tout instant la température instantanée du milieu est proche de la température moyenne rencontrée par les organismes au cours de leur vie[4].

La **dynamique spatiale** du micronecton est modélisée par des équations de diffusion–advection. Le coefficient de diffusion ($\rho = 10000\ \mathrm{m^2\,s^{-1}}$) intègre à la fois la diffusion du micronecton et celle du milieu physique (Lehodey et al., 2010b). La diffusion verticale est considérée comme négligeable. Enfin, la contribution des courants et de la température dans les différents processus est pondérée par le temps de séjour des organismes dans les différentes couches.

Prédictions de SEAPODYM micronecton Pour résumer, SEAPODYM micronecton adopte une vision "Bottom-Up" de la dynamique spatio-temporelle de la distribution du micronecton. Celle-ci est prédite à partir de cartes de la production primaire, dont le transfert d'énergie vers les niveaux trophiques intermédiaires est extrapolé dans le temps et l'espace en fonction des courants et de la température.

Les variables de forçage utilisées en entrée de SEAPODYM micronecton sont donc les suivantes : la production primaire, la température (trois couches) et la vélocité des courants (trois couches). La production primaire est estimée à partir des données SEAWIFS auxquelles sont appliqué l'algorithme Eppley-VGPM (Eppley, 1972; Morel, 1991). Les sorties du modèle SEAPODYM micronecton nous ont été fournies par

[4]hypothèse nécessaire car, en raison de sa nature eulérienne, SEAPODYM ne dispose pas des trajectoires d'histoire vie des organismes.

Patrick Lehodey (CLS–MEMMS, Toulouse) pour deux types de données en entrée :

1. Des données de résolution $\frac{1}{12}° \times 1$j où les variables de forçage de température et de vélocité des courants sont issues d'une version régionale de GLORYS2 (Parent et al., 2012) développée par CLS – MERCATOR Océan et basées sur le modèle de circulation globale NEMO.

2. Des données de résolution $\frac{1}{4}° \times 1$sem où les variables de forçage de température et de vélocité des courants sont issues d'une interpolation des données observées par altimétrie et des dispositifs dérivants : surcouf3D (Mulet et al., 2012, CLS – MERCATOR Océan).

Capacité de rétention des tourbillons

Les tourbillons méso-échelle sont capables, en raison de leur vorticité, d'isoler du milieu environnant une quantité d'eau située en leur centre, et cela pendant plusieurs semaines/mois. Cette propriété, que l'on nomme capacité de rétention, semble leur conférer un rôle écologique particulier. En effet, la capacité de rétention est impliquée dans le phénomène de compétition non-exclusive observé pour le phytoplancton (Hutchinson, 1961; Bracco et al., 2000) via la création de niches écologiques délimitées par les barrières de transport que sont les bordures de tourbillon (d'Ovidio et al., 2010). Plus récemment, l'analyse du cas particulier d'un éléphant de mer à l'Est de Kerguelen suggère que la rétention d'un tourbillon peut influencer le comportement de ces prédateurs (d'Ovidio et al., 2013) : les structures les plus rétentives ayant plus d'attrait sur le prédateur.
La capacité de rétention des tourbillons est mesurée par un paramètre de rétention (PR) dont l'estimation fait intervenir le calcul des trajectoires passées de particules situées à un moment donné au sein d'un tourbillon (identifié par des valeurs négatives du paramètre d'Okubo-Weiss). Intuitivement, le PR s'interprète comme l'âge moyen des eaux piégées au sein d'un tourbillon (d'Ovidio et al., 2013) et donne une indication sur la durée au cours de laquelle le transfert d'énergie a pu s'effectuer, depuis la production primaire vers les niveaux trophiques supérieurs, au sein d'un système quasi-fermé.
À ce titre, le PR peut être vu comme un modèle de la dynamique spatio-temporelle de niches écologiques méso-échelles. Il diffère de SEAPODYM dans la mesure où (i) il se concentre sur les tourbillons, (ii) l'état initial de l'abondance des ressources biologiques est inconnu et (iii) il adhère aux plus près des observations satellitaires et ne

nécessite pas d'hypothèse de construction particulière. Dans ce chapitre nous l'utilisons comme un complément à SEAPODYM, minimaliste mais parcimonieux, permettant de se concentrer sur le rôle des tourbillons méso-échelles dans la formation des habitats d'alimentation des éléphants de mer.

Ces données nous ont été fournies avec une résolution de $\frac{1}{12}° \times 1j$ par Pedro Monroy (IFISC, unité mixte CSIC–UIB, Palma de Mallorca). La rétention des masses d'eau a été calculée conformément à la méthode de d'Ovidio et al. (2013), à partir des données de la vitesse absolue des courants géostrophiques (distribuées par AVISO, SSALTO/-DUACS), issues de la fusion des observations altimétriques de plusieurs satellites (Jason-1 Geodetic Phase, AltiKa, Cryosat-2 et OSTM/Jason-2 ; Niveau de traitement L4p ; Résolution $\frac{1}{4}° \times 1j$).

Tourbillons méso-échelle

Les éléphants de mer et d'autres prédateurs supérieurs tendent à visiter les bordures des tourbillons (Bailleul et al., 2010b; Dragon et al., 2010; Nel et al., 2001). Afin de situer les animaux par rapport à ces bordures, nous avons utilisé la base de données de tourbillons méso-échelles de Faghmous et al. (2015b). L'article fournit la position et la forme de ces structures dans l'ensemble des océans, chaque jour entre début 1994 et fin 2014. Outre leur exhaustivité, l'avantage de ces données est leur nature vectorielle qui facilite le calcul de variables lagrangiennes telles que la position d'un animal par rapport aux bordures du tourbillon le plus proche.

6.2.2 Données de bio-logging

Pour la période de temps couverte par les différentes données citées précédemment (2010-2011), nous disposons, pour six femelles éléphants de mer en voyage post-reproduction (Octobre–Janvier, soit la période du bloom phytoplanctonique), de données à haute fréquence d'échantillonnage pour lesquelles les tentatives de capture de proies ont pu être dénombrées. De plus, ces animaux ont été équipés de GPS fournissant la localisation de façon régulière (une plongée sur deux) et fiable (précision de l'ordre de 20-50 m).

Pour chaque plongée, plusieurs variables ont été extraites : la profondeur euphotique, la durée de la phase de fond, le nombre correspondant de tentatives de capture proie et la profondeur médiane des animaux lors de cette phase. En nous basant sur les coordonnées GPS des animaux et sur l'heure du début des plongées, nous avons

affecté chaque plongée à une période de jour ou de nuit, selon les critères de SEAPODYM (sous-sous-section 6.2.1). Pour les plongées, de nuit la profondeur euphotique a été interpolée à partir des observations réalisées le jour. La profondeur médiane des phases de fond, combinée à la profondeur euphotique, nous a permis d'attribuer à chaque plongée la couche de SEAPODYM micronecton correspondant à la phase de fond. Les biomasses de micronecton prédites par SEAPODYM dans les couches correspondantes ont alors été extraites dans une zone tampon de rayon $\frac{1}{4}°$ autour de la position des éléphants de mer. Ces données à l'échelle de la plongée ont ensuite été agrégées à l'échelle de SEAPODYM micronecton ($\frac{1}{4}° \times$ 1sem), une observation étant définie comme la moyenne[5] correspondant à l'intersection des modalités suivantes : "Pixel de la carte SEAPODYM" $\times$ "Semaine de la carte SEAPODYM" $\times$ "Observation de jour ou de nuit" $\times$ "Identité de l'éléphant de mer".
Les données de rétention n'ont pas été extraites sous les coordonnées des animaux mais sous le centre du tourbillon dont ils étaient le plus proche, avec une zone tampon de rayon $\frac{1}{4}°$. La notion de proximité entre les éléphants de mer et les tourbillons fait ici référence *à la bordure du tourbillon* et non pas à son centre. Pour cette extraction, l'unité d'observation est cette fois définie comme la moyenne correspondant à l'intersection des modalités suivantes : "Pixel de la carte de rétention" $\times$ "Jour de la carte de rétention" $\times$ "Identité de l'éléphant de mer" $\times$ "Identité du tourbillon".

6.2.3 Analyses

SEAPODYM micronecton et taux de rencontre de proies

Les estimations du succès d'alimentation des éléphants de mer fournies par le dénombrement de tentatives de capture des proies ont été comparées aux prédictions concomitantes de la biomasse de micronecton par SEAPODYM micronecton.
Une approche classique en dynamique des populations consiste à considérer que les captures C par unité d'effort E (les CPUE) sont proportionnelles à l'abondance des ressources B : $C = qBE$ où q représente la capturabilité des ressources. La principale difficulté rencontrée dans ce type d'approche concerne la définition de l'unité d'effort (FAO, 1978). Dans notre cas d'étude, nous avons défini l'effort comme le temps passé par les éléphants de mer au fond de leurs plongées. Par ailleurs, les prédictions de SEAPODYM micronecton se présentent sous la forme d'une biomasse potentielle

[5]Pour le nombre de tentative de capture et la durée passé en phase de fond nous avons effectué une somme.

de micronecton exprimée en $g\,m^{-2}$. Cette biomasse est donc en réalité une densité par unité de surface de couche. S'agissant d'un milieu tri-dimensionnel, nous avons estimé la densité moyenne des ressources par unité de volume, en divisant les prédictions par l'épaisseur de la couche concernée. Nous avons donc modélisé une relation linéaire entre le nombre de tentatives de capture par unité de temps au fond des plongées et les prédictions de la densité potentielle du micronecton dans la couche correspondante.

Pour ajuster ce modèle nous avons utilisé des Modèles Linéaires Généralisés (GLM). En effet, le nombre de capture étant une variable de comptage, il est souhaitable de la modéliser comme telle. De plus, il est probable que la variance des observations dépende de leur moyenne. Les GLMs de famille Poisson ou Binomiale Négative sont adaptés à ces cas de figure. La prise en compte du temps passé au fond (l'unité d'effort) est formalisée par la mise en œuvre d'une variable d'exposition, dont l'effet n'est pas estimé mais contraint à 1. La fonction de lien classiquement utilisée dans les GLMs Poissons ou Binomiaux Négatifs est la fonction log. Pour un GLM Poisson on a donc : $log(C) \sim Poisson(\eta)$, avec $\eta = 1 \times log(E) + qB$. Cependant, dans ce dernier modèle, l'effet d'une augmentation linéaire de B sur C/E (les CPUE) est multiplicatif. En effet, $log(C/E)$ augmente alors d'une quantité q, ce qui revient à dire que C/E est multiplié par $exp(q)$. Pour conserver la relation de proportionnalité du modèle initial, nous avons donc log-transformé les prédictions de SEAPODYM. Néanmoins, ce modèle est encore trop simple pour être vraisemblable. Il faudrait probablement prendre en compte les différences individuelles en matière de CPUE moyennes. De plus, la capturabilité des proies n'est pas nécessairement identique pour tous les individus ($i \in \{1;...;6\}$), dans toutes les couches ($l \in \{2;3\}$) et selon si ces dernières sont visitées de jour ou de nuit ($d \in \{Jour; Nuit\}$). Ces deux derniers facteurs pourraient également être associés à des différences dans les CPUE moyennes. Enfin, il peut exister des interactions entres tous ces facteurs.

La formule du modèle complet prenant en compte ces différents effets est donc[6] : $log(C) \sim Poisson(\eta = log(E) + q_{full}.log(B) + \alpha_{full})$ où $full$ désigne l'ensemble des combinaisons possibles des facteurs $\{i; l; d\}$, soit $\{i;\ l;\ d;\ i:l;\ i:d;\ l:d;\ i:l:d\}$.
Le modèle nul s'écrit :

[6]Pour un GLM binomial négatif la formule est la même, excepté qu'un paramètre supplémentaire θ, appelé paramètre de dispersion, est estimé : $log(C) \sim NB(\eta, \theta)$. La loi Binomiale Négative autorise davantage de flexibilité dans la relation moyenne–variance que la loi de Poisson dépourvue de ce paramètre ($\forall B, \mu(B) = \eta(B) = \sigma^2(B)$).

$log(C) \sim Poisson(\eta = log(E) + \mu)$ où μ désigne la moyenne des CPUE pour l'ensemble des individus.
L'ensemble des modèles situés entre ces deux extrêmes a été ajusté sur un même jeu de données ($n = 760$ observations) et l'AIC ("Akaike Information Criterion") de chaque modèle comparé à celui des autres.

Tourbillons méso-échelles et interactions trophiques

Nous souhaitons ici nous concentrer sur l'influence des tourbillons méso-échelles sur les CPUE des éléphants de mer. Plus précisément, nous nous intéressons au rôle que peut jouer leur capacité de rétention.
Il s'agit donc de tester l'effet de la rétention sur les CPUE, effet potentiellement variable selon la nature des interactions de l'éléphant de mer avec ces structures et selon le sens de rotation des tourbillons (cyclonique : sens horaire, anticyclonique : sens trigonométrique). Aucun indice ne nous porte à croire que ces relations sont de nature linéaire. Pour modéliser les interactions potentiellement non-linéaires impliquées dans ce contexte nous avons discrétisé les variables quantitatives :

- Nous avons envisagé quatre localisations possibles pour décrire les interactions des éléphants de mer avec les tourbillons : à l'intérieur, sur la bordure, non-loin, et enfin éloigné du tourbillon. L'identification du type d'interaction s'est appuyé sur les données de Faghmous et al. (2015b) et sur les localisations GPS des animaux. Compte tenu de la résolution des données altimétriques (une trentaine de kilomètres), nous avons considéré les éléphants mer comme *proches* d'un tourbillon si leur distance à la bordure la plus proche est inférieure à 30 km et *éloignés* dans le cas contraire. Si cette distance est inférieure à 15 km les éléphants de mer sont alors considérés en *bordure* de tourbillon. Enfin s'ils sont à l'intérieur de l'ellipse décrivant les limites d'une structure, le statut *à l'intérieur* leur a été attribué.

- Pour la rétention nous avons effectué un choix plus pragmatique que théorique : la variable est divisée en catégories d'effectifs égaux. Cet effectif doit être suffisamment élevé pour permettre d'estimer les effets d'interaction (avec le sens de rotation et le type d'interaction), généralement nombreux avec les variables catégorielles. Nous avons donc choisi une valeur assez élevée de 750 observations, créant ainsi trois catégories : [0.00, 3.79) [3.79, 5.14) et [5.14,10.03] jours[7].

[7]Ces valeurs assez faibles du PR sont dues à la zone tampon utilisée lors de l'extraction afin de

Les familles de modèle utilisées (Poissons/Binomiaux Négatifs) et la méthode de sélection des variables sont identiques à celles utilisées dans la sous-sous-section précédente. Soit $i \in \{1;...;6\}$ l'identité des éléphants de mer, $p \in \{1;2;3;4\}$ la position des animaux par rapport aux tourbillons, $s \in \{1;2\}$ et $r \in \{1;2;3\}$ le sens de rotation et le paramètre de rétention de ces derniers, le modèle complet s'écrit :
$log(C) \sim Poisson(\eta = log(E) + \alpha_{full} + \alpha_i)$ où $full$ désigne l'ensemble des combinaisons possibles pour les facteurs p, s et r soit $\{p;\ s;\ r;\ p:s;\ p:r;\ s:r;\ p:s:r\}$. Le modèle nul s'écrit :
$log(C) \sim Poisson(\eta = log(E) + \mu)$ où μ désigne la moyenne des CPUE pour l'ensemble des individus.
L'ensemble des modèles situés entre ces deux extrêmes a été ajusté sur un même jeu de données ($n = 2314$ observations) et l'AIC de chaque modèle comparé à celui des autres.

Commentaires généraux

Les informations méthodologiques suivantes s'appliquent aux deux projets d'analyses que nous venons de décrire :

- Les tentatives de captures ont été identifiées avec la même méthode que celle utilisée dans les chapitres précédents (voir par exemple 2.3.3).
- Dans la mesure où (i) nous nous intéressons au domaine océanique et où (ii) la simulation SEAPODYM rencontre des problèmes en bordure de masque (valeur anormalement élevée dans la zone Sud-Ouest de la figure 6.5), les observations situées plus au sud de 55° S ont été écartées.
- Pour les deux sessions d'analyses, les plongées de dérives ont été retirées des données. En effet, ces plongées n'ont pas vocation à la capture de proies (Crocker et al., 1997; Mitani et al., 2010). Par conséquent, l'effort de recherche n'est pas comparable à celui déployé dans les autres plongées. Les plongées de dérive ont été définies d'après le comportement observé par Biuw et al. (2003) et Mitani et al. (2010), qui comporte une période où l'animal est sur le dos (angle de roulis supérieur à 90 °), avec une vitesse verticale comprise entre -40 et 60 cm s^{-1} pour une durée d'au moins 100 s.

minimiser les erreurs causées par les écarts entre la position des tourbillons selon Faghmous et al. (2015b) et selon les cartes de rétention. Dans les données brutes, le PR prend communément des valeurs supérieures à 100 jours.

- Pour éviter de recourir à des outils d'analyse sophistiqués dans le cadre de ces travaux préliminaires, deux seuils ont été appliqués, nous permettant de limiter l'abondance de zéros ($C > 0$ proie) et minimiser les problèmes d'hétérogénéité de la variance ($E > 10$ minute). Le premier seuil nous permet de ne pas avoir à recourir à des modèles "zéros-enflés" tandis que le second garantit un minimum de représentativité à chaque observation (10 min correspond approximativement à la durée moyenne d'une phase de fond).

6.3 Résultats

6.3.1 Cohérence spatiale des données

Avant toute analyse quantitative, nous avons souhaité évaluer de façon générale l'adéquation entre les différents types de données utilisées. Pour ce faire, nous les avons inspectées visuellement. Des travaux antérieurs, basés sur les mêmes individus que les présentes analyses, ont mis en évidence l'existence d'un comportement de nage passif associé (i) à des taux de rencontre de proies plus élevés que la moyenne et (ii) à des fronts de transport (Della Penna et al., 2015). Un exemple d'une telle situation est présenté sur la figure 6.2 – (a). On retrouve l'éléphant de mer dans la même situation, sur la bordure d'un tourbillon cyclonique, en utilisant la base de données de Faghmous et al. (2015b), où les tourbillons sont identifiés à partir d'observations altimétriques (figure 6.2 – (b)). En revanche sur la figure 6.2 – (c), il apparait que les données de forçage de SEAPODYM $\frac{1}{12}° \times 1$j ne sont pas en phase avec les observations. Ce problème ne semble pas être présent sur la figure 6.2 – (d) basée sur les données de forçage de SEAPODYM $\frac{1}{4}° \times 1$sem. Pour la suite des analyses, nous écartons donc l'utilisation des prédictions de SEAPODYM $\frac{1}{12}° \times 1$j au profit de celles de résolution $\frac{1}{4}° \times 1$sem.

6.3.2 Relation entre prédiction de SEAPODYM micronecton et taux de tentative de capture de proies

Les résultats de la sélection de modèle sont présentés dans la table 6.1. Les sept meilleurs candidats retenus par la sélection de modèle estiment que les prédictions de SEAPODYM micronecton ont un effet significatif sur les CPUE. Les poids d'Akaike sont assez équilibrés entre les candidats, il n'y a donc pas d'indice solide en faveur d'un modèle particulier. Pour tous les modèles, l'ordonnée à l'origine du modèle

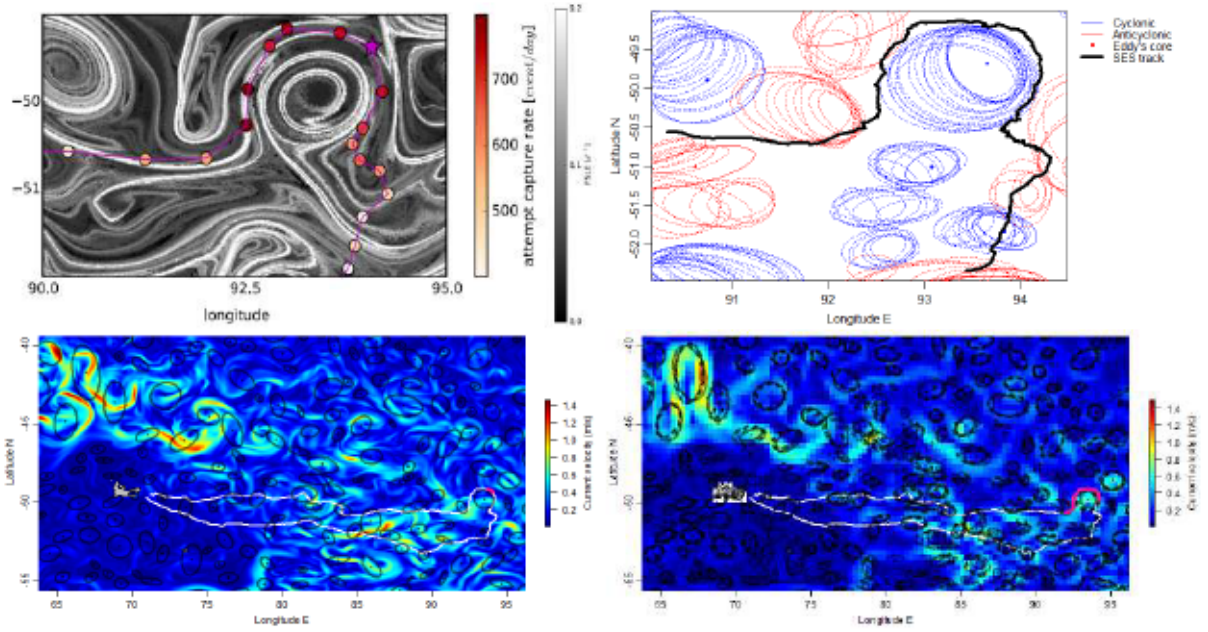

Figure 6.2: De l'importance du forçage physique – ***L'altimétrie révèle l'association éléphant de mer/tourbillon méso-échelle :*** *(a) Figure tirée de Della Penna et al. (2015) mettant en évidence le lien entre un tourbillon à cœur froid et le taux de tentatives de capture d'un individu. Ligne violette : trajectoire de l'animal. Fond de carte : fronts de transport (FSLE) correspondant au jour où la position de l'animal est marquée d'une étoile. (b) la même région, la position des tourbillons et de leur bordure ayant été extraite de la base de donnée de Faghmous et al. (2015b). Les lignes en pointillés représentent les bordures des tourbillons jour après jour, et les lignes pleines les bordures pour la dernière date uniquement.* ***Vitesse des courants extraite du forçage physique de SEAPODYM micronecton en relation avec les tourbillons méso-échelle de la figure (b).*** *(c) Courants issus de GLORYS2, utilisés pour le forçage de SEAPODYM $\frac{1}{12}° \times 1$j. (d) Courants issus de surcouf3D, utilisés pour le forçage de SEAPODYM $\frac{1}{4}° \times 1$sem.*

Table 6.1: Résultat de la sélection de modèle pour la relation entre CPUE et Biomasse SEAPODYM micronecton – *Il s'agit de GLM de famille binomiale négative, les GLM Poissons testés ayant indiqués de la sur-dispersion. Sont inclus uniquement les modèles de $\Delta AIC < 4$. $log(\mathcal{L})$ désigne la log vraissemblance, ΔAIC l'écart de l'AIC des candidats par rapport à celui classé premier, w_{AIC} est le poids d'Akaike, enfin η est le prédicteur linéaire.*

	n param.	$log(\mathcal{L})$	AIC	ΔAIC	w_{AIC}	η
1	36	-3077.26	6226.53	0.00	0.25	$log(E) + q_{l;\ i;\ l:i}.log(B) + \alpha_{full}$
2	42	-3071.60	6227.20	0.67	0.18	$log(E) + q_{l;\ i;\ d;\ l:i;\ i:d}.log(B) + \alpha_{full}$
3	37	-3076.86	6227.73	1.20	0.13	$log(E) + q_{l;\ i;\ d}.log(B) + \alpha_{full}$
4	38	-3076.41	6228.82	2.29	0.08	$log(E) + q_{l;\ i;\ d;\ l:i;\ l:d}.log(B) + \alpha_{full}$
5	26	-3088.42	6228.85	2.32	0.08	$log(E) + q_{l}.log(B) + \alpha_{full}$
6	43	-3071.50	6229.00	2.47	0.07	$log(E) + q_{l;\ i;\ d;\ l:i;\ l:d;\ i:d}.log(B) + \alpha_{full}$
7	37	-3077.51	6229.02	2.49	0.07	$log(E) + q_{l;\ i;\ d;\ l:i;\ d:i}.log(B) + \alpha_{full}$

complet (α_{full}) a été retenue, ce qui indique des différences notables entre les CPUE moyennes, selon les combinaisons des trois facteurs i (l'identité de l'animal), l (la couche visitée) et d (le jour ou la nuit). En revanche, les formules diffèrent quant à la capturabilité. Un large éventail d'interactions avec les différents facteurs est représenté, mais le modèle 5 où la capturabilité ne dépend que de la couche visitée lors de la phase de fond constitue le socle commun pour tous les candidats. C'est aussi le modèle le plus parcimonieux, avec dix paramètres de moins que n'importe quel autre modèle candidat, et le seul pour lequel la capturabilité ne dépend pas de l'identité des animaux. Ces caractéristiques en font le meilleur candidat dans l'optique de réaliser des prédictions à partir des données de densité de micronecton de SEAPODYM. La figure 6.3 présente la droite de régression entre les CPUE et la densité du micronecton estimé par le GLM 5 (pente de la droite $q = -0.48$, $p_{Z-test} = 2.45 \times 10^{-6}$; $q_{l=2} = -0.81, q_{l=3} = -0.14$, $p_{Z-test} = 9.63 \times 10^{-4}$ et paramètre de dispersion $\theta = 4.19$), *comme pour tous les autres modèles c'est un effet négatif*. Nous reviendrons dans la discussion sur ce résultat surprenant. La déviance expliquée (Guisan and Zimmermann, 2000, voir sous-section 3.3.6) par ce modèle est de 38.01%. Si l'on retire le terme $q_l.log(B)$ du modèle, sa déviance expliquée chute à 36.46% ce qui représente 4.09% de la valeur précédente et 1.55% de la déviance du modèle nul. Le pouvoir explicatif des prédictions de densité du micronecton est donc faible.

6.3.3 Rôle des structures méso-échelles et de leur capacité de rétention

Relation entre la rétention et la biomasse de micronecton

Sur les figures 6.4 et 6.5, nous pouvons observer une corrélation négative assez nette entre la biomasse de micronecton et la rétention. Les tourbillons constituent en général des minima locaux de biomasse prédite, les maxima se situant plutôt dans le milieu environnant (figure 6.5).

Relation entre la rétention et taux de tentatives de capture de proies

Les résultats de la sélection de modèle concernant les analyses des relations entre taux de tentatives de capture de proies et paysage tourbillonnaire sont présentés dans la table 6.2. Notre interprétation de ces résultats se concentre sur les deux premiers modèles candidats. En effet, le candidat 4 présente un poids d'Akaike trois fois inférieur

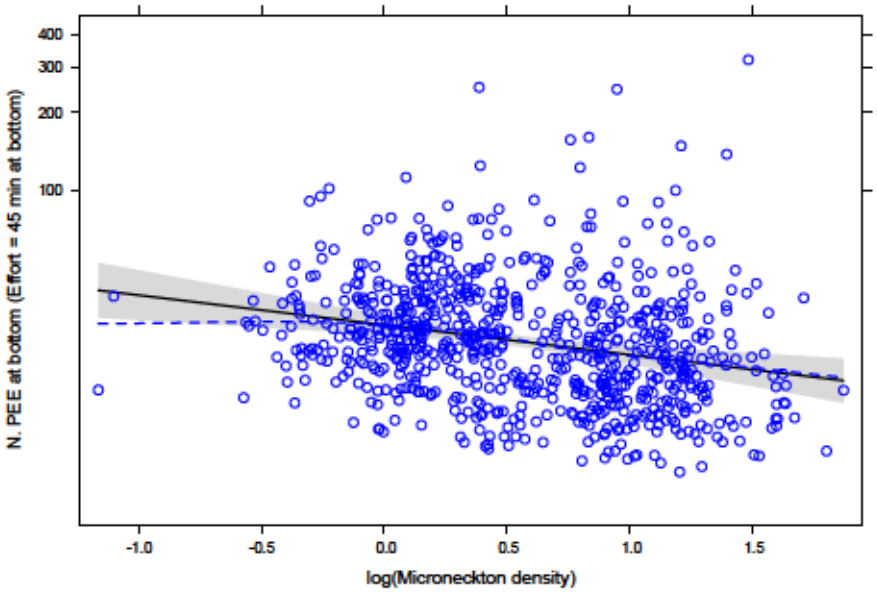

Figure 6.3: Effet estimé de la densité du micronecton sur les CPUE des éléphants de mer – *La ligne noire représente la droite de régression cernée en gris de son intervalle de confiance à 95%. Les points bleus sont les résidus partiels.*

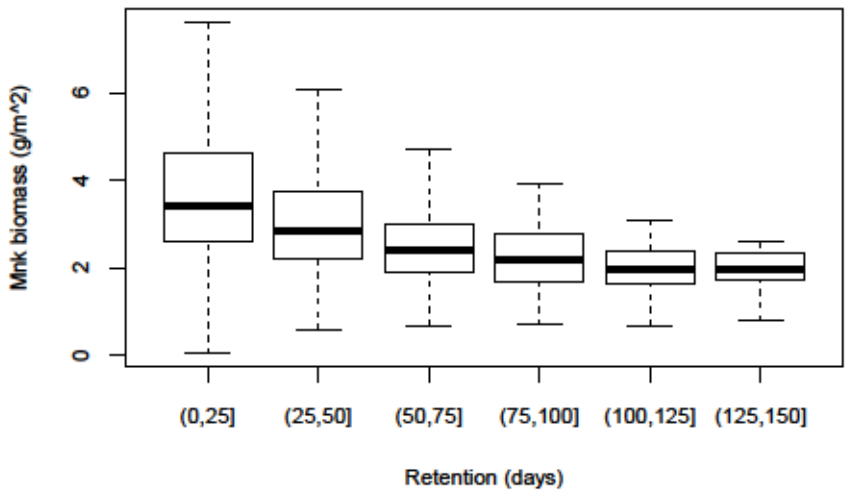

Figure 6.4: Relation entre rétention et prédictions de SEAPODYM micronecton, diagramme en boîte – *Diagramme en boîte montrant la relation entre les valeurs des cartes de rétention et celles de biomasses de micronecton mesopélagique correspondant au graphique du haut sur la figure 6.5.*

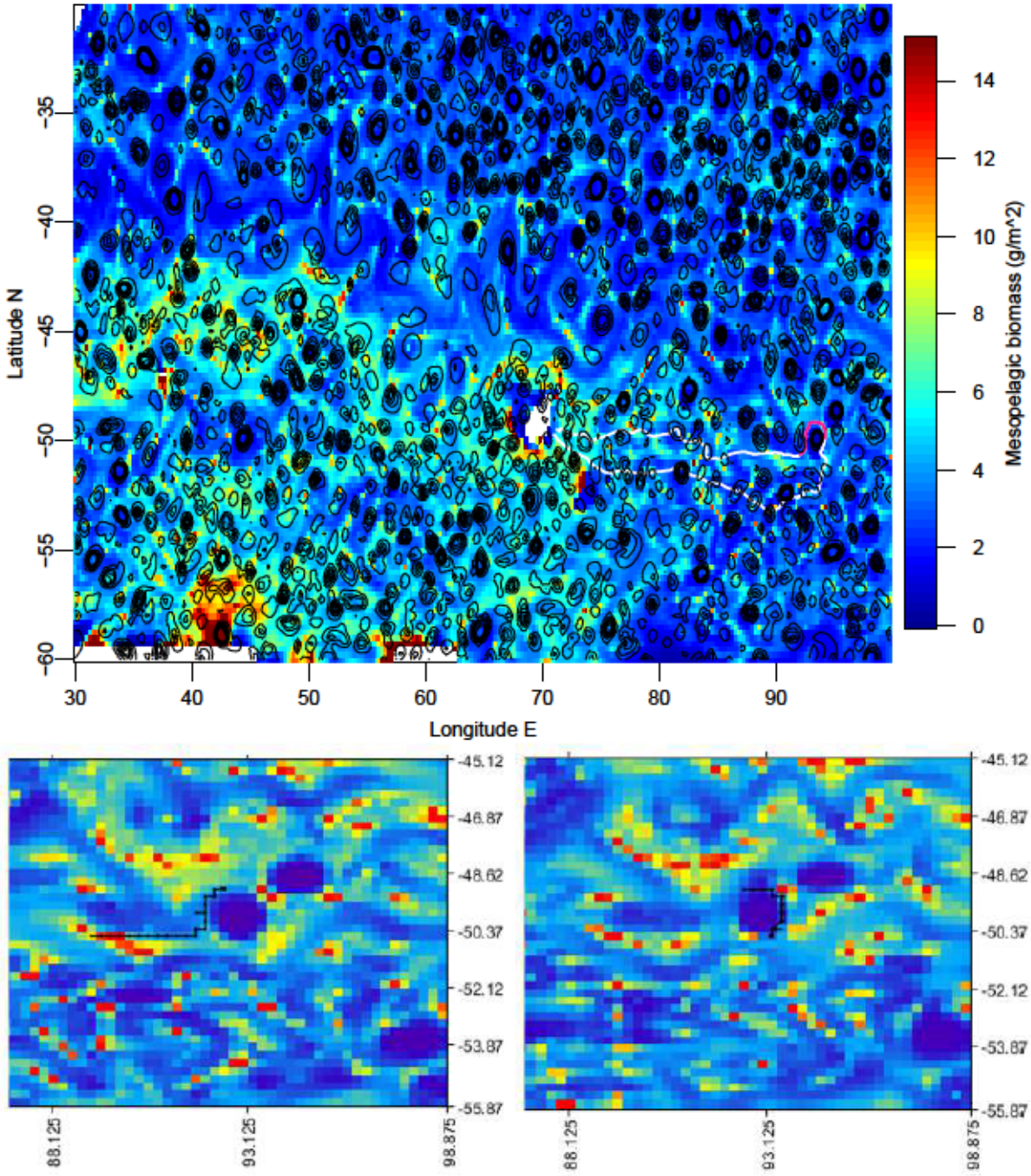

Figure 6.5: Relation entre rétention et prédictions de SEAPODYM micronecton – *En haut, le fond de carte montre la distribution du micronecton prédite par SEAPODYM (somme des couches mésopélagiques) entre le 27 Nov. et le 3 Dec. 2011. Les lignes de contour noir superposées représentent la rétention (la première ligne de niveau pour une rétention de 2.5 j, puis une ligne par incrément de 7.5 j jusqu'à 50 j). La trajectoire de l'éléphant de mer présentée sur la figure 6.2 est en blanc, la position correspondante au fond de carte en rose. Les données de rétention ont été moyennées jusqu'à la résolution temporelle et spatiale de la carte SEAPODYM micronecton. En bas, le gros plan sur les prédictions de SEAPODYM micronecton dans la région du tourbillon présenté sur la figure 6.2.*

au candidat 2 et plus de quatre fois inférieur au candidat 1. Le modèle 3 quant à lui est jugé trop complexe, avec huit paramètres de plus que le condidat 2 pour un AIC inférieur.

Table 6.2: Résultat de la sélection de modèle pour la relation entre CPUE et caractéristiques des tourbillons – *Il s'agit de GLM de famille binomiale négative, les GLM Poissons testés ayant indiqués de la sur-dispersion. Sont inclus uniquement les modèles de $\Delta AIC < 4$. $log(\mathcal{L})$ désigne la log vraissemblance, ΔAIC l'écart de l'AIC des candidats par rapport à celui classé premier, w_{AIC} est le poids d'Akaike, enfin η est le prédicteur linéaire.*

	n param.	$log(\mathcal{L})$	AIC	ΔAIC	w_{AIC}	η
1	22	-8560.91	17165.83	0.00	0.37	$log(E) + \alpha_{r;\ s;\ p;\ s:p;\ r:p} + \alpha_i$
2	16	-8567.22	17166.45	0.62	0.27	$log(E) + \alpha_{r;\ s;\ p;\ s:p} + \alpha_i$
3	24	-8559.38	17166.75	0.93	0.23	$log(E) + \alpha_{p;\ s;\ r;\ p:s;\ p:r;\ s:r} + \alpha_i$
4	18	-8566.29	17168.58	2.76	0.09	$log(E) + \alpha_{r;\ s;\ p;\ s:p;\ r:s} + \alpha_i$

Les modèles 1 et 2 ont en commun l'effet de la rétention (r) et du sens de rotation des tourbillons (s), ainsi que l'effet de la position des éléphants de mer par rapport aux tourbillons (p), ce dernier effet étant jugé différent selon le sens de rotation des structures ($s : p$). Dans le modèle 1, légèrement meilleur que le second ($w_{AIC1}/w_{AIC2} = 1.37$), l'effet de la rétention sur les CPUE dépend de la position des animaux ($r : p$). Nous commençons l'interprétation de ces résultats par le modèle 2 qui est le plus simple.

Le candidat 2 explique 18.41 % de la déviance du modèle nul. Le modèle estime que les hautes capacités de rétention ont un effet négatif sur les CPUE ($exp(\alpha_{r=3}) = 0.91$[8], $p_{Z-test} < 0.01$, figure 6.6) mais ne détecte pas de différence significative entre les structures de capacité moyenne ou faible. Globalement, les tourbillons cycloniques (rotation de sens horaire, cœur froid) sont associés à des CPUE plus hautes ($exp(\alpha_{s=2}) = 1.24$, $p_{Z-test} < 10^{-4}$, figure 6.6). Enfin, la situation des éléphants de mer par rapport aux tourbillons joue aussi un rôle, mais celui-ci varie selon le sens de rotation des tourbillons. La situation de bordure, considérée en dehors de toute interaction, est associée aux taux de tentatives de capture les plus élevés. La prise en compte du sens de rotation du tourbillon nuance cette vision :

- Pour les tourbillons anticycloniques, les animaux ont réalisé des CPUE plus

[8]Ces coefficients exponentiés ont un effet multiplicatif. Ils sont à comparer à la première modalité du facteur qui sert de référence. Dans le cas présent $exp(\alpha_{r=1}) = exp(0) = 1$ pour les structures de faible rétention (comprise entre 0 et 3.8 jours).

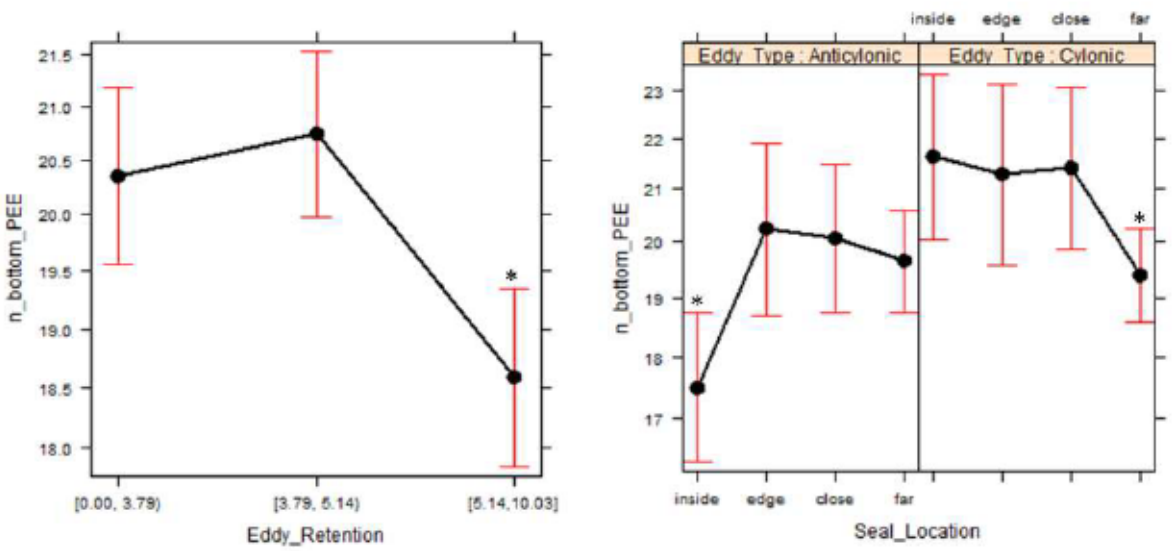

Figure 6.6: Effets estimés par le modèle 2 – *Exposition = 32 minutes. Les étoiles désignent les effets significatifs. L'effet individu n'est pas présenté.*

faibles à l'intérieur des tourbillons qu'ailleurs ($exp(\alpha_{p=2|s=1}) = 1.16$, 1.15 et 1.12 pour les modalités 3 et 4 de la position des animaux, $p_{Z-test} < 0.01$, figure 6.6), mais pas de différence significative n'est constatée entre les autres situations. La bordure a donc un effet positif au même titre qu'une situation où l'animal est éloigné du tourbillon.

- Pour les tourbillons cycloniques c'est précisément l'inverse, seuls les animaux situés au loin de ces structures ont des CPUE significativement différentes ($exp(\alpha_{p=4|s=2}) = 0.80$, $p_{Z-test} < 0.001$, figure 6.6). La bordure a donc un effet positif au même titre qu'une situation où l'animal n'est pas éloigné du tourbillon.

Le modèle 1 explique 18.84% de la déviance du modèle nul. Les effets que nous venons de décrire pour le modèle 2 sont encore valables (figure 6.7). La particularité de ce modèle réside dans l'interaction entre la capacité de rétention et la position des éléphants de mer. Cet interaction nous intéresse particulièrement. En effet, nous souhaiterions savoir si la situation où l'éléphant de mer rencontre de nombreuse proies alors qu'il fréquente la bordure d'un tourbillon de forte rétention (figure 6.2) se généralise à l'ensemble du jeu de données. Cependant, l'ajout de cette interaction se limite à l'estimation d'un effet positif de l'éloignement des animaux par rapport aux tourbillons à forte capacité de rétention ($exp(\alpha_{p=4|r=3}) = 1.18$, $p_{Z-test} < 0.05$, figure 6.7). Il est en effet assez logique que l'effet négatif des fortes capacités de rétention,

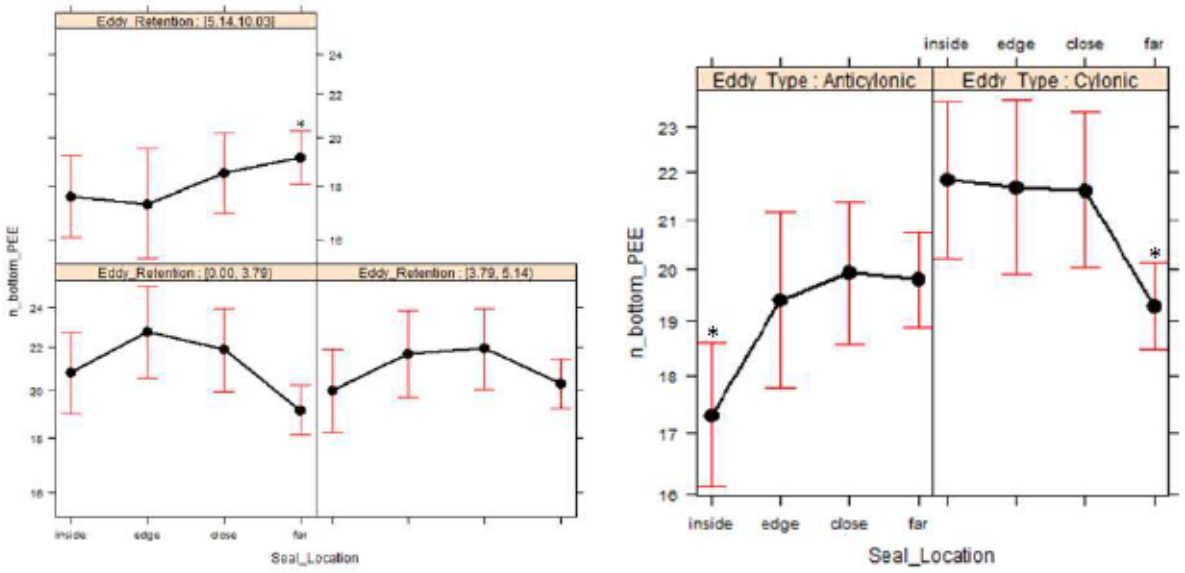

Figure 6.7: Effets estimés par le modèle 1 – *Exposition = 32 minutes. Les étoiles désignent les effets significatifs. L'effet individu n'est pas présenté.*

observé dans le modèle 2, ne concerne pas les animaux éloignés de ces structures. D'autre part, il semble que dans le cas de tourbillons à faible capacité de rétention, la situation tende à s'inverser (figure 6.7 : Rétention = [0, 3.79) × Position éloignée, effet non significatif). Aucun effet de la situation de bordure en interaction avec la capacité de rétention ne s'observe. Néanmoins, sur l'ensemble des graphiques présentés sur les figures 6.6 et 6.7, les erreurs-types associées à la position "bordure" sont légèrement, mais systématiquement, plus importantes que celles associées aux autres positions. Cette observation laisse présager l'existence de CPUE plus variables en bordure de tourbillon, un contraste qu'aucune des variables du modèle 1 ne parvient à expliquer.

6.4 Discussion

6.4.1 Cohérence spatiale des données

Forçage du modèle SEAPODYM

Le premier résultat que nous souhaitons souligner concerne la comparaison du forçage physique de SEAPODYM micronecton avec les données d'altimétrie de Faghmous et al. (2015a). Cette comparaison (figure 6.2) met en évidence la nécessité, dans ce secteur, d'intégrer une physique plus proche de la réalité celle produite actuellement par le modèle opérationnel GLORYS2 au $\frac{1}{12}°$. À ce jour, les prédictions de SEAPODYM (Lehodey et al., 2010b) basées sur le produit surcouf3D (Mulet et al., 2012) ($\frac{1}{4}°$sem) semblent plus à même de reproduire la structure du paysage méso-échelle traversé par les animaux (figures 6.2, 6.5).

Organisation de la biomasse micronectonique à méso-échelle

Les prédictions issues de SEAPODYM–surcouf3D révèlent une distribution du micronecton fortement structurée par les tourbillons méso-échelles. Dans ce paysage, les tourbillons correspondent globalement à des minima locaux de biomasse (figure 6.5). Plus les capacités de rétention de ces structures sont élevées, plus SEAPODYM les prédit comme des zones pauvres en ressources (figure 6.4). Dans SEAPODYM, la biomasse de micronecton est directement liée à la production primaire. Cette relation s'expliquerait par le fait qu'en cette période de bloom phytoplanctonique (Moore and Abbott, 2000), les tourbillons ayant une haute capacité de rétention ont (i) emprisonné l'eau avant le bloom, ou bien (ii) retenu captives des masses d'eau où la production primaire s'est épuisée. Cette hypothèse est cohérente avec l'observation de taux de capture plus faibles à proximité des tourbillons ayant les plus fortes capacités de rétention (figures 6.6 et 6.7). L'examen des images satellites (figure 6.8) pour la même période révèle une couverture nuageuse trop importante pour valider ou invalider cette hypothèse. Néanmoins, la zone correspondant au tourbillon cyclonique visité par l'éléphant de mer est partiellement visible (figure 6.9). On y constate effectivement que le cœur de ce tourbillon à forte capacité de rétention est dépourvu de chlorophylle en surface.

Sur ces dernières images du satellite TERRA, la position du tourbillon ne semble pas conforme à l'altimétrie (figure 6.9), ni aux données collectées *in situ* par les éléphants

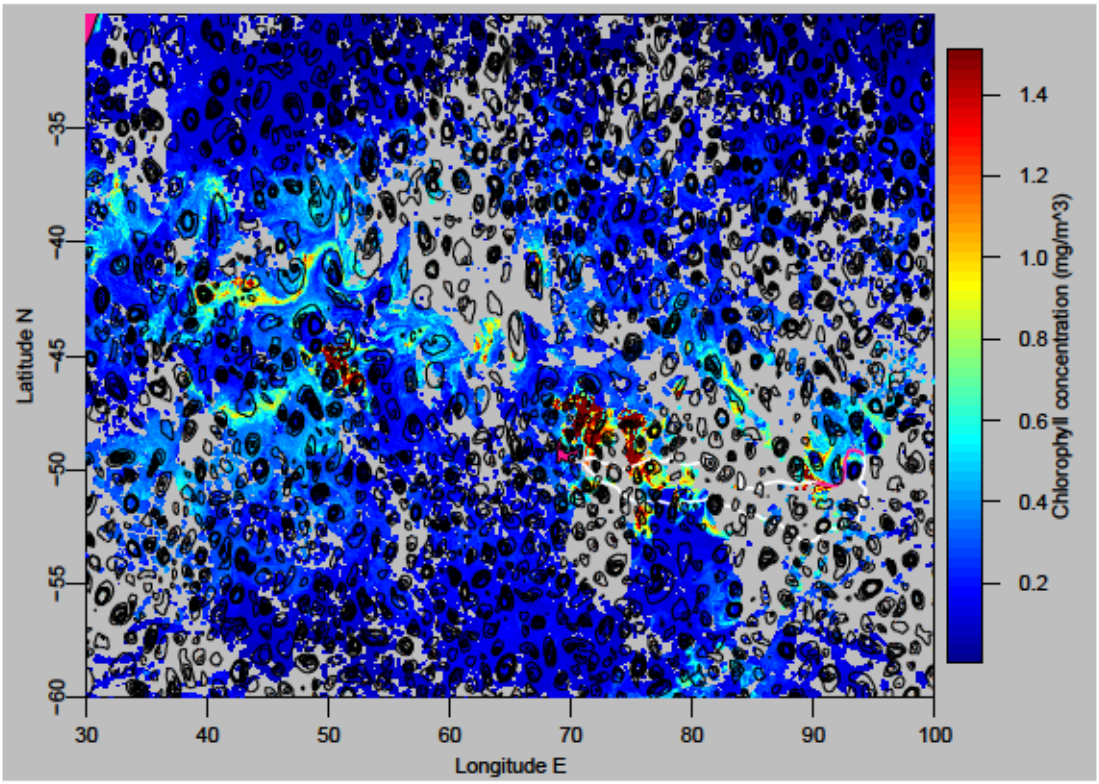

Figure 6.8: Production primaire TERRA/MODIS du 25/11/2011 au 02/12/2011 – *Zone correspondant à la figure ??, données de rétention moyennées sur les huit jours.*

de mer. En effet, on y voit l'éléphant de mer traverser une zone froide et très riche en chlorophylle, avant de remonter vers le nord, jusqu'à sortir de la zone de bordure productive. Or, les profils verticaux de température et d'atténuation de la lumière mesurés *in situ* par les balises au passage de l'animal (figure 6.10) dressent un portait assez différent des conditions océanographiques rencontrées : durant la période correspondant à la portion de trajectoire en rose, la couche de mélange est continûment chaude et caractérisée par une forte atténuation de la lumière. Même s'il n'est pas exclu que l'atténuation de lumière soit due à un maximum de chlorophylle profond ou à la présence d'autres organismes (zooplancton), les conditions océanographiques semblent radicalement différentes selon le point de vue adopté. On peut donc légitimement s'interroger sur la capacité des images de surface à décrire l'environnement réellement exploré par ces prédateurs plongeant à plusieurs centaines de mètres.

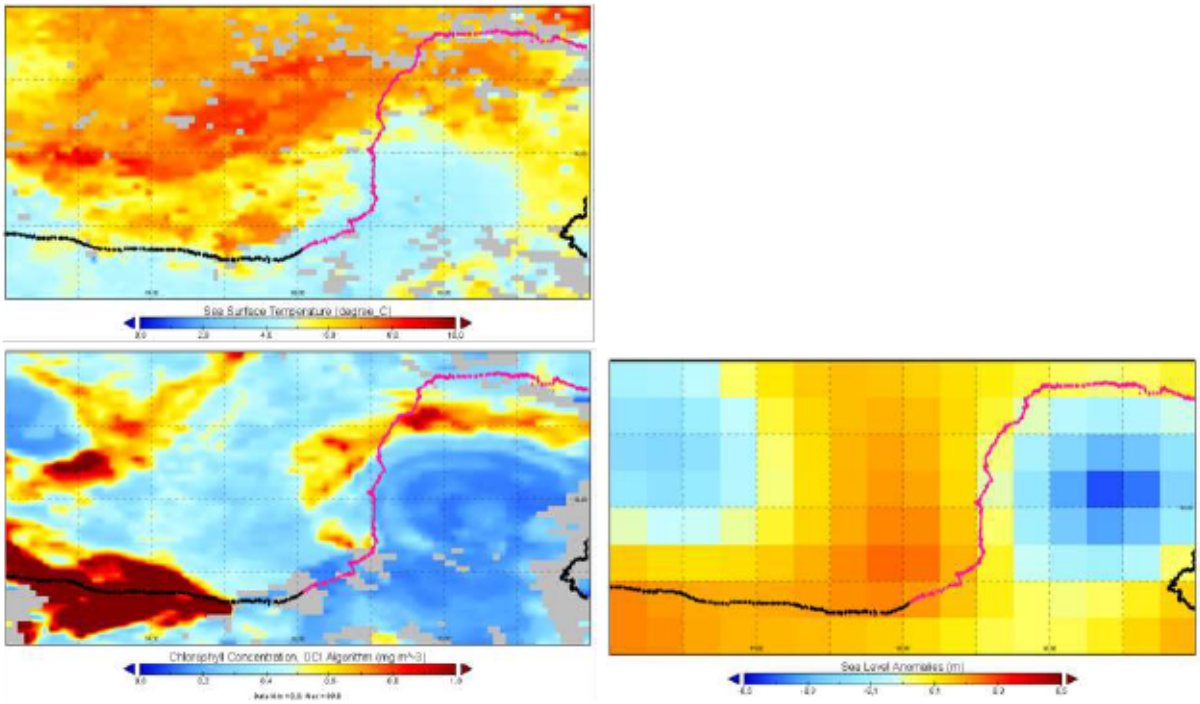

Figure 6.9: Cartes de la température de surface et de concentration rencontrées par l'individu 2011-28 – *À gauche, les cartes de la température de surface et de production primaire (mois de novembre) (Terra/MODIS, 4 km mensuel). À droite ont été ajoutées les anomalies de hauteur d'eau (OSTM/Jason-2, quart de degré quotidien) afin de rappeler la position du tourbillon selon l'altimétrie. La portion de trajectoire en rose correspond à la période présentée sur la figure 6.5.*

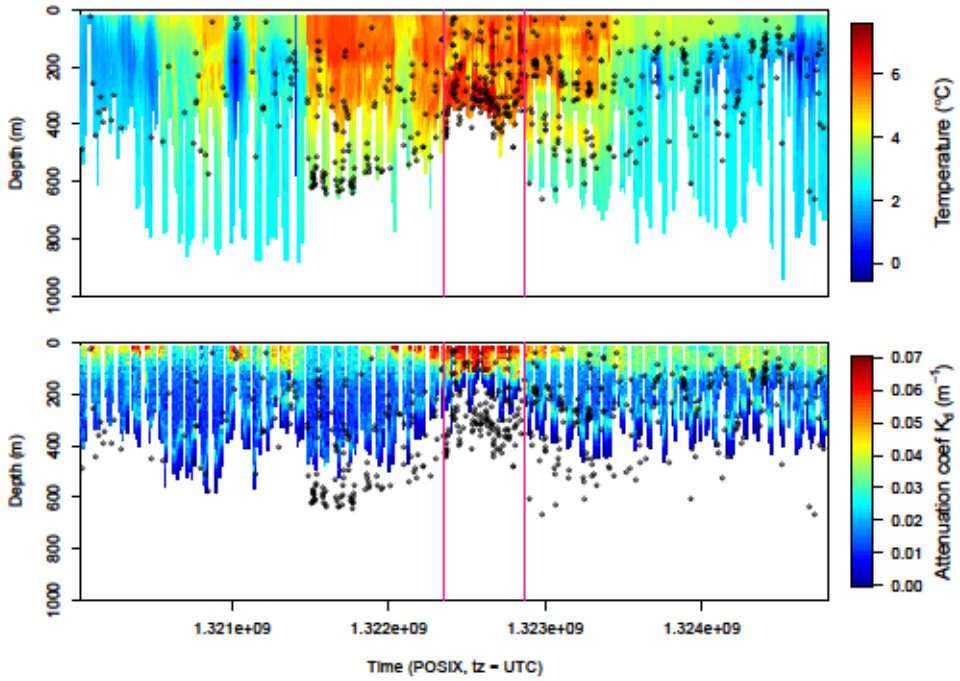

Figure 6.10: Profils verticaux des données de température et d'atténuation du lumière collectées par l'individu 2011-28 – *Les points noirs sont les évènements de bioluminescence (voir chapitre 5). Les dates qui correspondent au début et à la fin de la période présentée sur la figure 6.5 sont représentées par des barres verticales rose. L'évolution du nombre et de la distribution verticale des tentatives de capture de proies est présentée sur la figure 3.3.*

6.4.2 Variations du taux de capture dans le paysage tourbillonnaire

Outre l'effet négatif de la proximité des tourbillons très rétentifs sur le taux de capture de proies (figure 6.7 et 6.6), nous avons constaté que les structures cycloniques sont associées à de plus fort taux de rencontre de proies que les structures anticycloniques (figure 6.7 et 6.6). Ce résultat est conforme aux observations antérieures de Dragon et al. (2010) ou de Bailleul et al. (2010b).

D'autre part, la densité de proies rencontrée localement par les éléphants de mer varie selon leur position par rapport aux tourbillons et selon le sens de rotation de ces derniers. Ainsi, pour les tourbillons anticycloniques, les CPUE sont plus faibles à l'intérieur des tourbillons anticycloniques. En revanche, pour les tourbillons cycloniques, les CPUE les plus faibles sont observés au loin de ces structures, suggérant ainsi que les environs des tourbillons cycloniques constituent des zones plus denses en proies. Quelque soit le sens de rotation des tourbillons, les situations de bordure ou de relative proximité vis à vis des tourbillons sont favorables (figure 6.7 et 6.6).

Les images à fine résolution du satellite TERRA (figure 6.9) révèlent une bordure remarquablement productive (la zone est détectable même à large échelle : figure 6.8). L'origine de cette productivité peut être sujet à discussion. En période de bloom, et pour un tourbillon de cet "âge" (plusieurs semaines), il est possible que cette structure ait concentré les ressources par advection (Chelton et al., 2011), tout comme elle a transporté l'éléphant de mer durant plus d'une semaine (Della Penna et al., 2015).

En conclusion, il semble important de rappeler que nous avons étudié les variations du nombre de tentatives de proie par unité de temps lors des phases de fond des plongées. Cette variable nous a servi d'*indicateur* de la densité locale des proies, mais ne reflète pas l'intérêt d'une zone pour un prédateur plongeur tel que l'éléphant de mer. En effet, l'accessibilité verticale des ressources n'est pas prise en compte. Ainsi, afin de juger de l'intérêt des tourbillons pour ces animaux, il serait également intéressant d'étudier l'influence du paysage tourbillonnaire sur la profondeur de plongée en parallèle de l'influence sur le taux de captures.

6.4.3 SEAPODYM en tant que modèle prédictif

Une relation faible

À la lumière des résultats obtenus, il semble que pour prédire la densité des proies des éléphants de mer, une approche du type "Bottom-Up" telle qu'employée par SEAPO-

DYM n'est pas efficace en comparaison avec d'autres méthodes basées sur le comportement de plongée (e.g. Vacquié-Garcia et al. (2015); Labrousse et al. (2015)). En effet, Vacquié-Garcia et al. (2015) ont pu montrer que les informations issues des trajectoires des animaux (vitesse de déplacement et angle de virage) permettent d'expliquer 19% des variations du nombre de captures quotidien. Ce chiffre passe à 75% si l'on dispose en plus des profils de plongée.

Une relation négative

Nous avons observé une relation négative, faible mais significative, entre le taux de tentatives de capture au fond des plongées et la densité prédite de micronecton. Il était attendu une relation de direction opposée. Nous nous sommes donc interrogés quant à la structure du modèle et plus précisément sur la notion de *densité* du micronecton. Dans les résultats présentés ici, la densité du micronecton est rapportée à un volume de couche ($g\,m^{-3}$ de couche). Les analyses ont été également faites en considérant (i) les estimations de SEAPODYM brutes (c'est à dire en $g\,m^{-2}$ de couche), et (ii) la somme des estimations des trois couches (c'est à dire $g\,m^{-2}$ de 0 à $min(1000, 10.5z_{eu})$ m de profondeur[9]). Le cas (i) revient à supposer qu'à partir du moment où un éléphant de mer visite une couche alors l'intégralité du micronecton est accessible, tandis que le cas (ii) revient à négliger totalement la dimension verticale, dont la modélisation constitue un atout de SEAPODYM. Toutefois, ces différents changements de définition concernant la densité du micronecton ont tous abouti à une relation négative avec le taux de capture. Finalement, nous avons fait le choix de présenter le résultat des modèles où la biomasse est ramenée au volume de couche, car cette définition semble plus cohérente avec les conclusions des précédents chapitres (3 et 4), à savoir que l'étalement vertical des ressources est relié négativement à leur densité.

Hypothèses

Un certains nombre d'indices, accumulés au cours de l'analyse détaillée de la trajectoire d'un éléphant de mer, convergent vers l'idée que les bordures de tourbillon jouent un rôle structurant :

- L'animal est effectivement passé en bordure d'un tourbillon : adéquation entre les fronts de transport et la trajectoire de l'animal (Della Penna et al., 2015)

[9] D'après la définition de la limite inférieure de la couche mesopélagique profonde.

(figure 6.2).

- L'environnement qu'il a traversé est biologiquement riche : profil d'atténuation et occurrence d'évènements de bioluminescence (figure 6.10).

- L'intérieur de ce tourbillon est pauvre : résultat des modèles pour les fortes rétentions (figure 6.6) et observations satellitaires (figure 6.9).

- Les bordures de ce tourbillon sont riches en chlorophylle : observations satellitaires (figure 6.9)

D'autre part, la relation négative entre prédictions de SEAPODYM et taux de capture de proies suggère l'existence de biais systématiques liés à un processus manquant ou incorrectement modélisé. L'échelle caractéristique des bordures de tourbillon (sub-méso-échelle) est plus fine que la résolution actuelle du modèle ($\frac{1}{4}°$). De plus, la comparaison des cartes de biomasse SEAPODYM et des cartes de rétention (dont la grille est au $\frac{1}{12}°$) révèle la formation d'auréoles pauvres en micronecton autour des cœurs rétentifs des tourbillons (figure 6.5). Pour expliquer un tel résultat négatif, les propositions peuvent être variées (définition des couches, paramétrisation de la dynamique temporelle du micronecton, etc). Toutefois il semble qu'un problème de résolution des données, couplé aux phénomènes de bordure observés, constitue une hypothèse convaincante.

6.4.4 Limites et perspectives

Préciser le rôle des tourbillons dans le façonnement de la distribution du micronecton

Le volume de données utilisé dans les présents travaux (six individus) est assez faible en vue de l'objectif de décrire précisément les relations entre le paysage méso-échelle et les variations du taux de captures des animaux. Ainsi, les analyses réalisées avec tous les individus confondus semblent avoir souffert d'un certain manque de puissance statistique, et ce malgré la discrétisation assez grossière des données de rétention en trois classes. Le volume de données pourrait être doublé en incluant les déploiements d'accéléromètres de 2014 et 2015, même s'il manque encore la mise en place du produit surcouf3D pour ces années. Pour compenser le manque de données,

nous nous sommes penchés sur l'analyse détaillée d'un cas particulier. Le recoupement des informations, issues de modèles, d'images de télédétection et de mesure *in situ* sur une portion de trajectoire, semble indiquer que les bordures de tourbillon pourraient jouer un rôle structurant sur la distribution des proies de l'éléphant de mer.

Dans ce contexte, il semble intéressant de vérifier si, comme nous l'avons supposé, les tourbillons hautement rétentifs durant l'été austral retiennent globalement des eaux pauvres en chlorophylle, et si leur bordure est quant à elle plus riche que le milieu environnant. La question des mécanismes impliqués dans la formation de bordures biologiquement riches en niveaux trophiques intermédiaires (Godø et al., 2012), stimulation (McGillicuddy et al., 1998; Benitez-Nelson et al., 2007; Klein and Lapeyre, 2009) ou agrégation (Chelton et al., 2011), est encore l'objet de débats. Ceux-ci sont susceptibles de varier selon la nature des facteurs limitant la production primaire (Lévy et al., 2012), qui eux mêmes évoluent au cours des saisons.

Cotté et al. (2015) ont montré la flexibilité du comportement dont font preuve les femelles éléphants de mer à l'échelle annuelle. En effet, en comparant les voyages post-mue et post-reproduction, il apparaît que leur fréquentation des structures méso-échelles est modulée par la productivité moyenne dans l'environnement. Les résultats soulignent que la probabilité d'observer un comportement de recherche intensive (Area-Restricted Search, Kareiva and Odell (1987)) au sein des tourbillons est plus faible en post-reproduction. Par ailleurs, la théorie de l'approvisionnement optimal prédit qu'une parcelle continue à être exploitée tant que le taux d'acquisition des ressources est supérieur à celui attendu dans l'environnement moyen (Charnov, 1976). La mise en relation des variations du taux de captures (à l'intérieur ou sur la bordure des tourbillons ainsi que dans les eaux libres) avec la productivité moyenne des eaux libres pourrait nous renseigner sur la densité des proies dans ces différents contextes. Ce sujet à l'interface entre les questionnements sur la distribution des ressources et la stratégie d'approvisionnement des éléphants de mer pourrait être passionnant à approfondir.

Chemins trophiques et niches dynamiques

La notion de niche dynamique évoque l'idée d'un habitat mobile et instable, mais fait également écho à la notion de niche écologique traditionnelle, qui implique l'interaction des organismes vivants avec leur environnement physique. Nous avons observé

des taux de tentatives de captures variables selon le type cyclonique/anticyclonique des tourbillons fréquentés par les éléphants de mer. Ce constat rappelle la nécessité, à terme, de modéliser la dynamique spatiale des organismes de façon plus complexe, en dépassant les simples processus de diffusion-advection et faire intervenir des processus écologiques. Dans le cadre du développement de SEAPODYM micronecton, la question est actuellement à l'étude. Une option serait de complexifier davantage la représentation du modèle trophique, pour l'instant une "chaîne" trophique, en y incorporant une bifurcation aboutissant à deux groupes fonctionnels bien distincts. En effet, à partir des types phytoplanctoniques dominants (Alvain et al., 2008), il serait question de distinguer une voie diatomées > zooplancton > poisson, et une voie haptophytes > zooplancton > gélatineux.

Chapitre

7

Discussion

Une discussion musclée entre deux mâles, le *skua* semble hésiter à se joindre au débat. Crédit : L. Kernaleguen

7.1 Synthèse des principaux résultats

7.1.1 Analyse du comportement de plongée à fine échelle

Le paysage océanographique peut être vu comme un emboitement de niches écologiques tri-dimensionnelles (Kotliar and Wiens, 1990; Fauchald, 1999) évoluant de plus en plus dynamiquement vers les fines échelles (sous-section 1.1.2). À large échelle, la distribution des proies est liée à la formation d'habitats globalement favorables[1] que l'on estime être prévisibles par les prédateurs en raison de leur stabilité (Fauchald et al., 2000). À fine échelle les processus sont plus stochastiques et les processus biotiques, tels que l'évitement des prédateurs, modèlent la distribution des proies (Fauchald et al., 2000). Dans le secteur étudié, les informations sur le micronecton en général, et sur sa distribution à fine échelle en particulier, sont peu abondantes (sous-section 1.2.2). Celles-ci sont généralement obtenues par des navires océanographiques (sous-section 1.3.1). Dans le cadre de cette thèse, nous avons mis en oeuvre l'utilisation de données collectées par des éléphants de mer avec une haute fréquence d'échantillonnage comme moyen d'investigation complémentaire.
Afin de mieux comprendre les interactions entre prédateurs et proies ainsi que la distribution à fine échelle de ces dernières, nous avons étudié les relations entre le comportement de plongée des prédateurs et des indicateurs de la densité des proies à l'échelle de la plongée (chapitres 3 et 4). Ces relations permettent de comprendre comment les prédateurs modifient leur comportement en fonction de la densité et de l'accessibilité des ressources alimentaires. Il s'agit d'un pré-requis indispensable pour définir ce en quoi consistent les stratégies d'approvisionnement des prédateurs, interpréter leurs coûts et bénéfices[2] (Thums et al., 2011), et obtenir indirectement des informations sur les proies des éléphants de mer.

La première étude (chapitre 3) s'appuie principalement sur l'analyse du comportement de plongée des éléphants de mer en deux dimensions (le temps et la profondeur) ce qui correspond au cas de figure le plus courant en matière de données de bio-logging. Cependant, décrire en deux dimensions un comportement en réalité quadri-dimensionnel constitue une approximation et soulève des problèmes quant à l'interprétation du comportement (Davis et al., 2003). Pour cette raison, nous avons

[1] Les travaux présentés dans l'annexe E s'inscrivent dans ce cadre.

[2] Voir par exemple l'étude des modalités déterminant l'allocation du temps passé dans la phase de de fond des plongées présentée en annexe F.

mis à profit les informations disponibles sur la variabilité de l'orientation du corps de ces animaux afin d'obtenir une indication du niveau de sinuosité des trajectoires selon les dimensions horizontales. Les résultats de ces premiers travaux peuvent se résumer en trois principaux points.

1. Dans un premier temps, nous avons modélisé les relations entre taux de rencontre de proies et comportements de plongée. Il est apparu que les animaux qui rencontraient davantage de proies par unité de temps réalisaient (i) des phases de descente et de remontée avec des angles **plus proches de la verticale**, (ii) et adoptaient des directions plus variées lors de leur phase de fond. Nous avons interprété cette augmentation de la variabilité des directions empruntées lors de la phase de fond des plongées comme un **accroissement de la sinuosité de leur trajectoire**. Cette hypothèse concernant l'interprétation de cet indicateur semble raisonnable compte tenu (i) que ce type de comportement est généralement considéré comme représentatif de l'activité de chasse et (ii) de sa relation avec le taux de rencontre de proies.

2. Dans un second temps, nous nous sommes intéressés aux potentielles répercussions de ces ajustements comportementaux d'une part, sur la vitesse des animaux en surface[3] et d'autre part, sur l'efficacité de plongée. Nous avons alors constaté que ces ajustements comportementaux impliquaient une **diminution de la vitesse horizontale des éléphants de mer en surface**. D'une part, l'ajustement des angles de plongée lors du transit entre la surface et le fond des plongées modifie le rapport entre les composantes horizontales et verticales du déplacement en faveur des dernières. D'autre part, l'accroissement de la sinuosité horizontale de la trajectoire au fond se traduit logiquement par un raccourcissement de la distance horizontale séparant les points de départ et d'arrivée de cette phase. Les effets de ces ajustements comportementaux sur la distance horizontale permettent d'expliquer la diminution de la vitesse horizontale avec le succès d'alimentation des prédateurs ; relation empiriquement utilisée pour identifier les zones de recherche alimentaire intensive chez de nombreux prédateurs (Kareiva and Odell, 1987; Fauchald and Tveraa, 2003; Bailleul et al., 2007b;

[3]Ne pas confondre avec le cumul des distances horizontales instantanées parcourues lors de la plongée selon la trajectoire des animaux. Ici et dans la suite du texte "vitesse horizontale" ou "distance horizontale" feront référence à des calculs basés sur la distance horizontale séparant les localisations GPS collectées juste avant et après la plongée (la résultante globale à l'échelle de la plongée).

Weimerskirch et al., 2007; Dragon et al., 2012a).

De plus, l'accentuation des angles de plongée se traduit par une **augmentation de l'efficacité de plongée**[4]. Cette amélioration est imputable à un **gain dans la vitesse du transit vertical** qui s'accompagne d'un **moindre coût de locomotion**. L'ajustement des angles de descente et de montée est donc au cœur d'un **compromis** entre vitesses de transit vertical (entre la surface et le fond de la plongée) et horizontal (écart entre les points de départ et d'arrivée de la plongée). L'existence d'un tel compromis souligne la difficulté d'interprétation du comportement dans l'espace car, par exemple, une réduction de la vitesse horizontale dans un secteur donné peut être liée à un changement dans la distribution verticale des proies sans que la densité des proies "par unité de surface" ne change. Malgré les bénéfices engendrés par l'accentuation des angles de plongée (moindre dépense énergétique durant le transit, extension de la fraction efficace du temps de plongée), l'utilisation systématique de cette stratégie n'est pas attendue dans le cadre d'une stratégie d'approvisionnement optimale car alors, le temps nécessaire à la découverte de nouveaux secteurs riches en proies (selon les dimensions horizontales) augmente.

Si les ajustements comportementaux en réponse aux taux de capture de proies correspondent globalement à une baisse de la vitesse horizontale en surface, la réciproque n'est pas forcément vraie. En effet, ces mêmes comportements se traduisent mécaniquement par une augmentation de la **contribution des courants océaniques aux déplacements horizontaux** des éléphants de mer. Ces observations à fine échelle sont cohérentes avec celles à méso-échelle où les éléphants de mer adoptent un comportement quasi-planctonique au sein de zones à fort taux de tentatives de capture (Della Penna et al., 2015). L'utilisation de la vitesse horizontale afin d'identifier les zones à fort succès d'alimentation ("Area Restricted Search" – ARS, Kareiva and Odell (1987); Benhamou and Bovet (1989)) ne peut donc ignorer l'influence des courants.

3. Enfin dans un troisième temps, nous nous sommes demandés, compte tenu des relations entre comportement de plongée et taux de rencontre de proies que

[4]Rappelons ici que l'efficacité de plongée est définie comme le rapport de la durée de la phase de fond sur la durée totale de la plongée. La phase de fond est considérée comme la phase "efficace" où l'animal explore la gamme de profondeur ayant le plus d'intérêt alimentaire et concentre son activité de chasse.

nous avons mis en évidence, comment la distribution verticale de la phase de fond de la plongée influait sur notre indicateur de la densité des proies. À ce sujet, nous avons constaté (i) une **diminution du taux de rencontre de proies avec la profondeur** et (ii) un accroissement de ce taux lorsque les phases de fond ciblaient **des parties plus localisées de la colonne d'eau**. Ces résultats sont valables de jour comme de nuit et ne sont donc pas liés aux variations de densité de proies relevant de leurs migrations nycthémérales. La corrélation négative entre le taux de rencontre de proies, indicateur de la densité locale des proies, et la fraction de la colonne d'eau explorée lors de la phase de fond suggère l'intervention de contraintes verticales, biotiques ou abiotiques, qui exercent un contrôle sur la densité locale des proies en agissant sur leur dispersion verticale dans un secteur donné de la colonne d'eau. Bien que les études à ce sujet soient peu nombreuses, il a été suggéré que les myctophidés se stratifient en fonction de leur âge/taille avec les plus gros individus vers le fond (Frost and McCrone, 1978, région sub-arctique du pacifique). Dès lors, une seconde hypothèse qui pourrait expliquer les relations négatives que nous avons observé serait que le taux de capture diminue car les proies capturées seraient plus grosses et nécessiteraient un temps de manipulation plus élevé.

Cependant, en l'absence de données précises sur les mouvements horizontaux des éléphants de mer durant leurs plongées, ces résultats sur la distribution des proies se limitent à la dimension verticale. En réponse à ce problème et compte tenu des limitations de l'approche temps-profondeur évoquées précédemment, nous avons poursuivi ces travaux par une nouvelle étude (chapitre 4) basée cette fois sur l'analyse des trajectoires tri-dimensionnelles, reconstituées par navigation à l'estime ("dead-reckoning"). Chez les prédateurs capables de plonger à plusieurs centaines de mètres, tels que les manchots royaux ou les éléphants de mer, la recherche des proies s'étend largement sur la dimension verticale. Leur stratégie d'approvisionnement se met en place dans les trois dimensions spatiales puisqu'elle peut être modifiée en agissant sur les mouvements verticaux et horizontaux (Davis et al., 1999; Simpkins et al., 2001; Austin et al., 2006). Nous avons donc souhaité décrire l'utilisation, encore méconnue, que les éléphants de mer font de l'espace à l'échelle d'une phase de plongée : la phase de fond. Pour cela, nous nous sommes appuyés sur l'analyse des composantes principales des trajectoires décrites par les animaux lors de ces phases. Le premier résultat de ce travail est le constat qu'à cette échelle la première des trois composantes prin-

cipales couvre à elle seule 94% de la dispersion spatiale[5] au fond des plongées. Ces trajectoires sont essentiellement linéaires et donc **très fortement anisotropiques**. Le second résultat est le constat que ces axes de déplacement privilégiés ne sont pas orientés uniformément dans toutes les directions mais, au contraire, s'inscrivent **dans le plan horizontal** dans une très vaste majorité des cas. En corollaire, il apparait que les déplacements horizontaux des animaux au fond des plongées sont de nature unidimensionnelle et que, **dans le cas de l'éléphant de mer, on puisse affirmer que la représentation temps-profondeur du comportement de plongée est une bonne approximation du comportement tri-dimensionnel**. En termes de stratégie d'approvisionnement, ces caractéristiques de forme de trajectoire sont performantes afin de maximiser le volume d'eau échantillonné : une telle stratégie se révèlerait intéressante au sein d'un champs de proies diffus où la distance entre les micro-parcelles de proies excède la portée de leur détection par le prédateur. Ces résultats semblent indiquer que les éléphants de mer ne s'alimentent donc pas de proies ayant un comportement grégaire les conduisant à former de larges bancs bien délimités dans l'espace. Celles-ci seraient **plutôt dispersées au sein de couches spécifiquement ciblées par les prédateurs**.

Nous avons ensuite estimé la densité spatiale des rencontres de proies. Cette étape a requis la formulation d'hypothèses sur les modalités de perception des proies par les éléphants de mer dont la plus forte concerne la distance de détection des proies. En nous basant (i) sur un scénario de faible distance de détection et (ii) sur les échelles pour lesquelles Adachi et al. (2016) ont observé la plus forte variabilité dans le "temps passé par volume" chez *Mirounga angustirostris* (espèce cousine de notre modèle d'étude), nous avons envisagé des distances de détection de 1.5, 9 et 18 m. Parmi ces différents scénarios, la **distance de 1.5 m fournie les estimations de densité de proies les plus proches de celles des méthodes de chalutage**.

Enfin, les différentes estimations de la densité spatiale des rencontres de proies ont été mises en relation avec les caractéristiques de forme des trajectoires. Nous avons là encore constaté une **diminution de la densité estimée des proies avec la profondeur** des plongées et **une relation négative entre l'exploration de plus vaste étendues verticales lors des phases de fond et la densité estimée des rencontres de proies,**

[5]La *dispersion spatiale* fait référence à la notion *d'inertie*, une grandeur homogène à la variance et utilisée en analyse de composantes principales. Dans notre cas, il s'agit d'une mesure de la dispersion des positions occupées par les éléphants de mer lors de leurs phases de fond autour des positions moyennes.

confortant ainsi les résultats obtenus dans le chapitre 3 (portant sur des individus différents). Néanmoins, dans ces nouveaux travaux, l'approfondissement des plongées était également accompagné d'une diminution du risque de ne capturer aucune proie, ce que nous avons interprété comme un **accroissement de l'homogénéité de la distribution des proies**. Pour les éléphants de mer, le fait de plonger plus profondément serait un désavantage énergétique (augmentation du coût du transit par unité de temps efficace, densité de proies globalement plus faible en profondeur) mais un investissement plus fiable à court terme (gain de prédictibilité des ressources due à leur homogénéisation spatiale).

La profondeur de l'habitat des myctophidés soulève des problèmes techniques dans la caractérisation de leur distribution à fine échelle par des moyens conventionnels d'échantillonnage (sous-section 1.3.1). La résolution des données de bio-logging ne se dégrade pas avec la profondeur. Ainsi, leur utilisation dans les travaux que nous venons de présenter[6] nous a permis de contourner certains de ces problèmes techniques.

7.1.2 Bio-aquisition de données sur la distribution des ressources marines

Les résultats présentés jusqu'ici dépendent de la pertinence de l'interprétation qui est faite du comportement des animaux. Dans la suite, nous nous sommes employés à nous extraire autant que possible de cette dépendance, en d'autres termes, à passer de la bio-indication à la bio-acquisition[7] de données sur la distribution des ressources marine.

À cet égard, les données d'intensité lumineuses collectées par les éléphants de mer présentent un potentiel intéressant. En effet, Teo et al. (2009) apportent la preuve de l'idée que de telles données renseignent sur l'abondance du phytoplancton, et Vacquié-Garcia et al. (2012) démontrent la possibilité de détecter des organismes bioluminescents, organismes dont le micronecton est largement constitué. La collecte de ces données par une grande variété d'enregistreurs est le fait d'un processus historique[8] plus que d'une véritable demande de la part de la communauté scientifique.

[6] Voir en annexe G une analyse des trajectoires 3D à encore plus fine échelle.

[7] L'annexe H présente un exemple de bio-acquisition en météorologie à partir des données qui ont servi de support aux analyses du chapitre 4.

[8] Le déploiement des capteurs de lumière a émergé dans les débuts du bio-logging afin d'estimer

Quoi qu'il en soit, ces données sont assez largement disponibles mais peu exploitées. Des données temps-profondeur-lumière, nous avons pu extraire (chapitre 5) les valeurs du coefficient d'atténuation de la lumière en fonction de la profondeur et localiser les évènements d'émission de bioluminescence. Cette tâche a été l'occasion (i) d'adapter la méthode de calcul des profils profondeur-atténuation de Teo et al. (2009) à des capteurs véritablement embarqués sur des animaux et (ii) d'accroitre l'étendue du domaine de détection des évènements de bioluminescence par la prise en compte du délai de réaction des capteurs. À l'instar de Teo et al. (2009), nous avons constaté dans la colonne d'eau l'existence de deux zones (ou *modes*) d'atténuation de la lumière vraisemblablement d'origine biologique : dans la couche de mélange où l'atténuation était fortement corrélée aux mesures de fluorescence ; en dehors de la couche photique, à des profondeurs variant de 150 à 400 m selon la pénétration verticale de la lumière mais non fréquentées par les éléphants de mer lors des phases de fond des plongées.

Afin de préciser la nature des organismes responsables de ce second mode d'atténuation, nous avons mis en relation l'intensité de l'atténuation dans les deux modes avec les taux de rencontre de proies et d'organismes bioluminescents. L'amplitude de l'atténuation lumineuse dans le mode profond est apparu anti-corrélée à l'occurrence des rencontres entre les éléphants de mer et leurs proies. Au sein d'un réseaux trophique sous contrôle "Bottom-up", ce résultat suggère que l'atténuation lumineuse observée en profondeur est **liée à l'abondance de ressources en compétition alimentaire avec les proies de l'éléphant de mer**, par exemple des organismes gélatineux. L'atténuation lumineuse en surface améliore l'accessibilité verticale des proies (Jaud et al., 2012) et par conséquent le nombre de capture par unité de temps en plongée. En revanche, **nous n'avons pas pu établir de lien direct entre l'intensité de l'atténuation lumineuse en surface et le taux de rencontre de proies au fond des plongées**, indiquant que les densités locales de proie ne sont pas plus importantes mais seulement plus accessibles. Ce découplage entre production primaire et taux de capture chez un prédateur supérieur était attendu compte tenu de l'échelle temporelle des mesures (quelques minutes) en relation avec le décalage spatio-temporel entre production primaire et production des ressources alimentaires des éléphants de mer. L'observation

la position des animaux. Légers et économes en énergie, ces capteurs ont continué à être intégrés par défaut sur les enregistreurs. Les premières traces de leur utilisation concernent l'éléphant de mer du nord (Delong et al., 1992; Hill, 1994) mais, du fait de leur faible encombrement, cet usage s'est rapidement étendu aux oiseaux.

d'un tel découplage n'est pas un cas isolé. Par exemple Irigoien et al. (2014) montrent la corrélation entre production primaire mesurée par télédétection et biomasse de poissons mésopélagiques à l'échelle globale, mais cette relation n'est pas observée plus localement (centaines de kilomètres × dizaines de jour) par Saijo et al. (2016). En revanche, Saijo et al. (2016) trouvent une corrélation positive entre biomasse des poissons et zones fréquentées par les éléphants de mer du nord.

Il nous semble qu'un aspect important de cette étude est la mise en évidence du potentiel des données de lumière : peu coûteuse à échantillonner et d'ores et déjà abondantes, elles peuvent être un moyen d'estimer à assez fine échelle l'abondance d'organismes marins de niveaux trophiques variés, et cela simultanément à la présence d'un prédateur supérieur. Concernant le phytoplancton, elles pourraient **compléter selon la dimension verticale les données de télédétection**. Concernant les niveaux trophiques intermédiaires, l'interprétation de ces données pose encore problème mais l'élargissement de leur utilisation à plus grande échelle (avec d'autres éléphants de mer en voyage post-reproduction ou en voyage post-mue[9] et avec d'autres modèles et secteurs d'étude) pourrait lever certains mystères et contribuer au projet d'écorégionalisation de l'océan Austral. De plus, les capteurs de lumière semblent être restés sensiblement les mêmes depuis les débuts du bio-logging. Compte tenu des progrès technologiques réalisés dans ce domaine, les capteurs de lumières peuvent très certainement être améliorés pour ce type d'application, par exemple en termes de précision, de résolution, de gamme de sensibilité, d'angle de réception, de spécificité spectrale et de diversité des bandes spectrales.

7.1.3 Modélisation des réseaux trophiques et hétérogénéité des ressources

Jusqu'ici nos analyses se sont concentrées à l'échelle d'une plongée ou d'une phase de plongée, l'adoption de cette échelle étant propice à étudier les mécanismes comportementaux résultant directement des interactions prédateur-proies. Le processus de transmission de l'énergie depuis la production primaire jusqu'aux niveaux trophiques intermédiaires se produit à des échelles spatio-temporelles plus grandes, de l'ordre de dizaines de jours et de centaines de kilomètres. Comme nous l'avons mentionné précédemment (sous-section 7.1.2), il nous a été impossible de mettre en rela-

[9] Car ces données peuvent être échantillonnées sans problème sur de longues durées.

tion l'abondance de la production primaire avec le succès de pêche des éléphants de mer. Nous avons évoqué l'importance de l'échelle sur la distribution des ressources et sur sa prévisibilité pour les prédateurs (sous-section 1.1.2). Cependant, l'augmentation de la prévisibilité de la distribution des proies avec l'échelle (Wiens, 1989) coïncide avec la diminution (i) de la densité moyenne des proies (Fauchald, 2009) et (ii) des capacités de perception (Turner, 1989; Kotliar and Wiens, 1990) et de déplacement des prédateurs. Compte tenu de l'antagonisme de ces processus et de l'importance des méso-échelles et sub-méso-échelles sur la production primaire (sous-section1.1.2), ces échelles constituent un cadre pertinent pour analyser l'hétérogénéité de la disponibilité des ressources marines pour les prédateurs. Pour mieux comprendre le processus de formation des habitats de pêche favorables aux éléphants de mer nous avons eu recours aux données de télédétection dont l'échelle d'échantillonnage permet d'apprécier le paysage méso-échelle dans lequel évoluent ces prédateurs (figure 1.2). Outre le changement d'échelle opéré dans ce chapitre 6, ces nouveaux travaux saisissent l'opportunité de s'intéresser davantage à l'hétérogénéité de la distribution du micronecton selon les dimensions horizontales alors que jusqu'ici elle a principalement été étudiée selon la dimension verticale (observation valable dans le cadre de cette thèse mais peut-être aussi à l'échelle de la littérature sur l'approvisionnement des prédateurs plongeurs).

Dans un premier temps, les analyses ont mis en évidence que la physique issue du modèle opérationnel GLORYS2 au $12^{\text{ième}}$ de degré n'offre pas une précision spatiale suffisante pour décrire fidèlement la dynamique de l'environnement des animaux. Nous avons observé une relation faible entre la biomasse de micronecton prédite et le taux de capture local des éléphants de mer. De plus, cette relation est négative, ce qui suggère l'existence de biais systématiques dans les prédictions du modèle.

Nous nous sommes particulièrement intéressés aux liens entre les tourbillons et la distribution des ressources. Il est apparu que la fréquence des rencontres de proies des éléphants de mer varie en fonction du contexte méso-échelle. En particulier (et à l'inverse de ce que nous attendions), les taux de tentatives de capture locaux étaient plus importants à proximité des tourbillons moyennement ou faiblement âgés. La comparaison des biomasses de micronecton prédites par SEAPODYM avec l'âge des masses d'eau retenues captives dans les tourbillons va dans le même sens. En effet, au cours de la période étudiée (été austral), le cœur des tourbillons est prédite d'autant plus pauvre en ressources que la capacité de rétention des structures est élevée.

Les images satellites de la production primaire semblent confirmer cette tendance, mais la couverture spatiale est largement incomplète dans cette région. Ces dernières observations sont à vérifier avec davantage de données.

L'analyse détaillée d'une portion de la trajectoire d'un animal ayant rencontré de nombreuses proies à proximité d'un tourbillon cyclonique (Della Penna et al., 2015), suggère qu'il en est autrement au niveau des bordures d'une telle structure. En effet, dans la zone de bordure visitée par l'animal, les mesures *in situ* des balises montrent une forte atténuation de la lumière dans la couche de mélange et la présence de nombreux évènements de bioluminescence en profondeur. Les images satellites de la production primaire révèlent également que le tourbillon est entouré au Nord-Ouest d'une auréole riche en chlorophylle. Il est à noter qu'il en réalité difficile de dire s'il s'agit bien de la zone de bordure car la position du tourbillon sur ces images ne correspond pas à celle révélée par l'altimétrie. Quoi qu'il en soit, les cartes de la distribution du micronecton prédite par SEAPODYM (au quart de degré) ne reproduisent pas l'existence d'une zone biologiquement riche autour de ce tourbillon. Nous proposons l'hypothèse que la résolution du modèle est insuffisante pour simuler fidèlement la dynamique des régions de bordure de tourbillon, et que ceci pourrait être à l'origine de la relation négative observée entre biomasse prédite et taux local des rencontres de proies.

D'autre part, le recoupement des différentes sources de données met en évidence certains décalages inattendus. Par exemple, la position du tourbillon varie selon comment celle-ci est observée, sur la carte de la production primaire en surface ou sur la carte des anomalies de hauteur d'eau. Les concentrations de chlorophylle et les températures mesurées en surface ne semble pas non plus correspondre aux conditions mesurées dans la colonne d'eau et *in situ* par les balises posées sur l'animal.

Pour résumer, les travaux de ce chapitre suggèrent l'existence de deux compromis qui compliquent la mise en relation de la dynamique spatio-temporelle du micronecton modélisée aux (sub)méso-échelles avec les variations du taux de rencontre de proies des prédateurs. D'une part, **un compromis entre la résolution des données de télédétection et leur fidélité aux conditions physique réelles**, les plus fines résolutions étant pour l'heure trop imprécises. D'autre part, **un compromis entre la résolution des données et la qualité de la représentation de l'environnement biologique modélisé**, les plus basses résolution conduisant à une description trop grossière de la distribution des ressources. Enfin, nos observations soulignent les incertitudes

associées à l'extrapolation des données collectées à la surface des océans jusqu'aux profondeurs exploitées par un prédateur plongeur tel que l'éléphant de mer.

7.2 Limites

7.2.1 De l'utilisation d'indicateurs

En écologie, les variables d'intérêt sont souvent non observables ou non mesurables. De ce fait des indicateurs sont utilisés en remplacement. La principale qualité d'un indicateur est sa corrélation avec la variable d'intérêt. Nous nous sommes largement appuyé sur l'usage d'indicateurs dans les différents travaux présentés dans cette thèse. Il semble donc important de nommer leurs faiblesses.

Évènements de tentative de capture

Quantifier le succès d'alimentation de prédateurs plongeurs dans leur environnement naturel est un enjeu majeur si l'on s'intéresse à leur stratégie d'approvisionnement ou à la distribution de leurs ressources alimentaires. Les capteurs de température oesophagienne ou stomacale, les capteurs à effet Hall, les accéléromètres et les enregistreurs vidéo ont apporté des avancées majeures dans l'estimation du succès d'alimentation en fournissant des mesures moins dépendantes du comportement des animaux (Naito, 2007). Cependant, chacun de ces dispositifs a des limites. Les capteurs de température oesophagienne sont rapidement régurgités (Naito, 2007). La température stomacale est soumise à une certaine inertie ce qui rend impossible la détection de capture de proies rapprochées dans le temps, ces capteurs peuvent également être évacués et être difficiles à récupérer (Naito, 2007). Les caméras sont couteuses, difficiles à déployer et n'ont que peu d'autonomie (Biuw et al., 2003; Thums et al., 2011) (limitations de mémoire et de batterie). De plus leur utilisation à des profondeurs importante nécessite un éclairage (donc encore moins d'autonomie et une possible violation de la neutralité du dispositif sur le phénomène mesuré). Enfin, les capteurs à effet Hall sont assez difficiles à poser (Liebsch et al., 2007; Ropert-Coudert et al., 2004) et semblent relativement invasifs pour les animaux.

Finalement, les accéléromètres sont les dispositifs les plus utilisés. Ils permettent de dénombrer les évènements de tentative de capture, une quantité au cœur de chacun des chapitres de cette thèse. Bien qu'ils ne fournissent qu'un indicateur du taux de capture, ils peuvent enregistrer sur de longues durées, sont robustes, peu invasifs

et dotés d'une haute fréquence d'échantillonnage. De plus, ils fournissent d'autres informations utiles : sur la dépense énergétique (Halsey et al., 2009; Hindle et al., 2010; Gleiss et al., 2011) ou sur l'orientation des animaux (Nowacek et al., 2001; Watanabe et al., 2006b; Sala et al., 2011).

Comme son nom semble l'indiquer, la première limite de cet indicateur concerne la possible surestimation du nombre de proies ingérées puisqu'il s'agit bien de *tentatives*. Ce biais dépend des erreurs de type I et II de la méthode[10] utilisée pour détecter les évènements ainsi que de la sensibilité des axes de l'accéléromètre et de la fréquence d'échantillonnage. Dans la mesure où ces caractéristiques ne varient pas au cours du voyage des animaux, il semble légitime de faire l'hypothèse que le biais de l'indicateur est constant pour un déploiement donné. Il est par conséquent raisonnable d'utiliser l'indicateur afin de juger des variations du taux de capture au cours du voyage d'un éléphant de mer. En revanche, les calculs de valeurs absolues à partir de l'indicateur, ce que nous avons fait lors de la comparaison de la densité des rencontres de proies avec les mesures réalisées par chalutage, doivent être interprétés avec précaution.

La seconde faiblesse de cet indicateur est l'**absence d'information qualitative** sur les captures potentielles. Ce dernier point fut particulièrement contraignant quant à l'étendue des questionnements que nous avons pu aborder et à la portée de nos résultats. En effet, nous savons que les éléphants de mer s'alimentent de céphalopodes et de diverses espèces de myctophidés (sous-section 2.1.4). Cependant, il nous a été impossible de prendre en compte la taxonomie des proies ou leur taille dans nos analyses et leur interprétation. Les incertitudes quant à la qualité des proies peuvent être à l'origine de facteurs confondants. En effet, selon leur taxonomie ou leur taille, les proies sont susceptibles de présenter différentes sensibilités aux conditions environnementales et différentes interactions avec l'éléphant de mer.

Les caméras sont à l'heure actuelle le seul moyen de surmonter ces faiblesses mais nous ne disposons pas de telles données pour réaliser nos analyses ou valider notre indicateur. Des résultats indépendants tels que les travaux de Foo et al. (2016) ou l'existence d'une signature acoustique corrélée aux évènements de tentative de capture[11] (G. Labadie, communication personnelle) rassurent quant à la première faiblesse évoquée. À plus large échelle (7-15 jours), il est possible d'utiliser les fluctuations de flottabilité des animaux pour identifier les secteurs où les animaux restaurent

[10] Selon Foo et al. (2016) la détection des évènements présente plus de faux négatifs que de faux positifs et serait donc plutôt conservative.

[11] Les captures sont réalisées par aspiration des proies (Kienle and Berta, 2015).

ou dégradent leurs réserves lipidiques (Biuw et al., 2003, 2007; Bailleul et al., 2007b). Ces variations prennent en compte la taille et la densité énergétique des proies mais aussi les dépenses effectuées pour les acquérir. Il s'agit donc d'une mesure objective du gain net d'énergie et par conséquent du succès d'alimentation. Nous avons pu établir l'existence d'une corrélation positive entre les variations de taux de capture et celles de la flottabilité des femelles éléphants de mer (Richard et al., 2016) ce qui suggère que les tentatives de capture constituent un bon indicateur de la prise alimentaire chez cette espèce.

Autres indicateurs

D'autres indicateurs sont utilisés, nous discutons de manière plus succincte leurs faiblesses en raison de leur utilisation plus ponctuelle et donc moins critique dans le cadre général de la thèse.

Effort de nage (chapitre 3) Les indicateurs de la dépense énergétique dérivés de l'accélération (somme de l'accélération dynamique (ODBA), norme vectorielle de l'accélération dynamique (VeDBA) ou effort de nage)ont, tous, deux faiblesses en commun. Premièrement, l'approximation due à la méthode de filtrage du signal d'accélération destinée à extraire la composante d'intérêt. Deuxièmement, leur recouvrement très partiel de la dépense énergétique globale qui constitue un problème dans le cadre de leur utilisation générale dans la théorie de l'approvisionnement optimal. En effet, seul le coût de la locomotion est pris en compte tandis que les dépenses liées au métabolisme de base, à la digestion des proies et aux besoins de la thermorégulation dans des eaux froides sont ignorées. Néanmoins, l'interprétation que nous avons faite de l'effort de nage en tant qu'indicateur s'est bornée au coût de locomotion. À ce titre, nos résultats ne sont sensibles qu'à la première des limites mentionnées et en réponse à laquelle nous avons basé notre indicateur sur des méthodes préalablement développées (Sato et al., 2003; Watanabe et al., 2006b; Aoki et al., 2011; Richard et al., 2014; Génin et al., 2015).

Vitesse de nage estimée (chapitre 4) La vitesse de nage des animaux par rapport à l'eau environnante a été estimée à partir de sa relation avec l'intensité du niveau de bruit. Le plan d'expérience sur lequel se fonde la calibration de cette relation est biaisé puisqu'il ne comprend que des phases de montée ou de descente tandis que la relation est extrapolée aux phases de fond des plongées. En raison du caractère plus

régulier du comportement de nage des animaux lors des phases de transit, on peut estimer que l'écoulement de l'eau sur les hydrophones est moins turbulent durant ces périodes. Il est donc possible que la vitesse de nage estimée pour reconstruire les trajectoires des éléphants de mer au fond des plongées soit surestimée, un écoulement plus turbulent produisant probablement plus de bruit pour une vitesse donnée (P. Miller, communication personnelle). En conséquence, les composantes principales des trajectoires de fond serait exagérées d'un facteur donné, exagération qui se transmet à l'analyse de l'anisotropie des trajectoires au fond des plongées. Compte tenu de la très forte anisotropie que nous avons pu observer, ce biais nous parait probable mais trop faible en amplitude pour changer qualitativement l'interprétation des résultats.

Atténuation lumineuse et fluorescence (chapitre 5) L'intensité d'une lumière de longueur d'onde donnée décroit exponentiellement en fonction de la longueur de son trajet dans un milieu (Bouguer, 1729). Cette décroissance est également fonction de la concentration en particules dissoutes ou en suspension (Beer, 1852), ce qui nous a permis d'utiliser l'atténuation de l'intensité lumineuse dans la colonne d'eau comme indicateur de l'abondance de matière d'origine organique en suspension, par exemple la quantité de phytoplancton. La fluorescence est un autre indicateur largement répandu à cet usage et utilisé dans le chapitre 5. Il convient de mentionner les principales faiblesses de ces indicateurs. La fluorescence est soumise à un effet "quenching" en cas de forte luminosité (dans les couches de surface en milieu de journée ensoleillée) et conduit alors à sous-estimer la concentration en chlorophylle (Guinet et al., 2013). Le quenching est dû à la photo-inhibition du phytoplancton, une protection physiologique déployée lorsqu'il est soumis à un excès de lumière. Le comportement non linéaire d'un indicateur n'empêche pas son emploi mais le complique, car des corrections doivent être apportées. Ainsi, l'effet quenching a été pris en compte dans le chapitre 5. Par ailleurs, l'atténuation de lumière telle que calculée dans le chapitre 5 est également soumise à des biais. En effet, la relation entre atténuation de lumière et concentration de matière absorbante dépend de nombreux paramètres dont les principaux sont : longueur d'onde de la lumière, absorbance de l'eau de mer pure, concentration et nature des espèces dissoutes et taille et nature des éléments en suspension. L'influence de ces paramètres n'a pas pu être prise en compte, néanmoins nous avons observé une relation franche avec la fluorescence (figure 5.2). L'atténuation de la lumière dans les couches de surface pourrait servir à quantifier l'effet quenching

car la lumière demeure atténuée par le phytoplancton même quand celui-ci est photo-inhibé. L'utilisation de l'atténuation à des fins de bio-acquisition nécessitera la mise en place d'expériences de calibration en vue d'améliorer la précision et l'interprétabilité des mesures. L'amélioration des capteurs de lumière (précision, résolution, gamme de sensibilité, angle de réception de la lumière et spécificité spectrale) devrait aider à mieux respecter la mise en application de la loi de Beer-Lambert, améliorant ainsi la fiabilité de cet indicateur.

7.2.2 De l'adoption du point de vue du prédateur

L'une des limites que nous avons rencontrée dans la mise en ouvre de l'étude du micronecton via les données de bio-logging est l'adoption du point de vue du prédateur. Les données collectées au gré des décisions du porteur des instruments comportent des biais d'échantillonnage, certes porteurs d'informations sur l'écologie des prédateurs et de leurs proies, mais néanmoins contraignants.

Les résultats obtenus dans les chapitres 3 et 4 s'appuient sur l'analyse du comportement de plongée des éléphants de mer. Dès lors, la pertinence des résultats dépend de celle de l'interprétation du comportement des animaux, comportement qui par ailleurs est imparfaitement observé (sous-section 7.1.1). Ainsi, par exemple, nous avons résumé les plongées en trois phases afin de délimiter "transit" (descente et montée) et "recherche alimentaire" (phase de fond), le comportement étant considéré homogène au sein de chaque phase. Il s'agit d'une simplification du comportement de plongée qui peut être remise en question. En effet, la complexité du comportements durant la phase de fond est probablement plus grande : puisque nous avons observé l'existence de zones "de recherche intensive" (ARS) au sein de cette phase (annexe G) elle pourrait comprendre de multiples périodes de transit et de chasse. Dans leur méthode d'analyse des plongées Heerah et al. (2014) distinguent en moyenne sept phases par plongée chez l'éléphant de mer austral. L'approche classique en trois phases semble toutefois pertinente dans la mesure où (i) les périodes de chasse sont dominantes au sein de la phase de fond (Heerah et al., 2014) et (ii) l'écart entre les taux de capture à l'intérieur et à l'extérieur des ARS sont du même ordre de grandeur (annexe G).

Implicitement, nous avons réalisé deux autres hypothèses. Premièrement, nous n'avons pas envisagé d'influence de potentiels prédateurs de l'éléphant de mer sur le comportement de ce dernier, malgré leur existence connue (Guinet et al., 1992; McMahon

et al., 2003; Hoff and Morrice, 2008). Deuxièmement, il s'agit là d'un postulat quasi-universel dans le domaine du bio-logging, que les enregistreurs ne produisent pas de modification du comportement, ni chez les prédateurs (dont l'hydrodynamisme est mécaniquement affectée) ni chez les proies (certains appareils émettent de faibles lumières rouges). Si ces hypothèses simplifient considérablement le travail d'interprétation du comportement, elles sont des approximations de la réalité et doivent donc être fondées. Ainsi des études ont évalué leur crédibilité : l'alimentation serait la principale contrainte sur la survie des éléphants de mer (Guinet et al., 1999; McMahon et al., 2003; Reisinger et al., 2011), l'impact des enregistreurs sur le gain de masse suite à un voyage alimentaire semble négligeable (McMahon et al., 2008) et la lumière rouge n'aurait que très peu d'effet sur le comportement des poissons des profondeurs (Widder et al., 2005).

Plonger plus profondément dans la colonne d'eau a un coût énergétique pour les animaux et il est attendu que ceux-ci ne le fassent qu'en échange d'un gain alimentaire quantitatif ou qualitatif. Ce biais d'échantillonnage de la colonne d'eau n'est pas sans conséquence. L'un des résultats de ce travail de thèse qui nous semble intéressant est l'anticorrélation entre densité des tentatives de capture de proies (par unité de temps ou de volume) et étalement vertical de la phase de fond. Nous aurions souhaité caractériser plus en détail les couches de la colonne d'eau préférentiellement explorées par les éléphants de mer. Cependant, les animaux ne permettent probablement pas l'identification de la limite inférieure de la distribution de leurs proies. En effet, une fois la limite supérieure d'une couche riche en proies identifiée, les animaux n'ont pas nécessairement intérêt à sonder celle-ci jusqu'à sa limite inférieure.

Dans l'alinéa précédent, ou pour interpréter la signification biologique de l'anisotropie des trajectoires, nous avons du recourir à la théorie de l'approvisionnement optimal. Or, rappelons que l'optimalité du comportement des prédateurs est une hypothèse (sous-section 1.3.2). À ce propos, la discussion entre Pierce and Ollason (1987) et Stearns and Schmid-Hempel (1987) apporte des précisions quant au véritable sens qu'il faut apporter au mot "optimal". Dans le cadre de la théorie, cette notion ne désigne pas "le meilleur parmi l'ensemble des possibles" (sens commun) mais "le meilleur compte tenu de certaines conditions" (sens technique de la théorie), sans quoi il est paradoxal d'affirmer que l'évolution (qui ne dispose que d'une réserve limitée de variabilité génétique) puisse optimiser le comportement (Stearns and Schmid-Hempel, 1987). Dans chacun des théorèmes de la théorie de l'approvisionne-

ment optimal, des formules mathématiques et des contraintes décrivent les processus biologiques et leur environnement, ce qui constitue autant de conditions d'application des prédictions de la théorie. La mise en œuvre de ces prédictions peut donc s'avérer délicate. En raison de l'adoption du point de vue du prédateur dans nos différents travaux, il était difficile de nous affranchir du cadre d'interprétation offert par la théorie de l'approvisionnement optimal. À cet égard, notons cependant que l'un des atouts de cette thèse est l'utilisation d'un indicateur du taux de capture mesuré directement par l'enregistreur en lieu et place d'indicateurs basés sur l'interprétation du comportement[12].

Fondamentalement, c'est bien la diversité qui permet de faire l'hypothèse d'optimalité (locale) du comportement. Il est donc naturel d'observer une certaine stochasticité du comportement d'un individu à l'autre. Or, c'est l'une des faiblesses du bio-logging, si l'on dispose de centaines de plongées pour caractériser le comportement des individus, l'effectif de ces derniers est généralement faible (entre 6 et 14 individus selon les chapitres). L'échantillonnage de la variabilité individuelle est ainsi limité, si bien que la généralisation des résultats à l'échelle d'une population – voir d'une espèce – est délicate.

7.3 Perspectives et portée générale des travaux

7.3.1 L'hétérogénéité des ressources et leur perception par les prédateurs

Les ajustements comportementaux observés en réponse à une augmentation du taux de rencontre de proies permettent de réduire la durée du transit vertical (prolongeant ainsi le temps passé en profondeur au contact de la ressource) et conduisent dans le même temps à une diminution de la vitesse horizontale. Il est connu que d'autres prédateurs accentuent leurs angles de plongée en fonction de la densité des ressources (Ropert-Coudert et al., 2001; Hanuise et al., 2013, : manchots royaux et Adélie). Ce compromis entre vitesse des transits verticaux et horizontaux soulève des questions quant au comportement optimal que les prédateurs plongeurs devraient adopter dans un champ de proies hétérogène selon trois dimensions. Quand faut-il privilégier l'une à l'autre ? L'éléphant de mer plonge continuellement (Leboeuf et al., 1986) mais ajuste

[12]Par exemple l'indicateur du "bottom time" dont sont pointées les limites en annexe F.

localement le rapport entre les composantes horizontales et verticales de son déplacement (chapitre 3). D'autres prédateurs plongeurs tels les manchots royaux (*Aptenodytes patagonicus*) ou les otaries de Californie (*Zalophus californianus*) réalisent un découpage plus net entre ces deux activités en séparant des séquences de plongées ("bouts") par des périodes de déplacement rapide en surface (Ponganis, 2015). L'opposition entre ces deux stratégies a été étudiée en termes de physiologie (Ponganis, 2015) et de coûts de la locomotion. Ces coûts seraient plus élevés pour se déplacer à l'interface air-eau. Les éléphants de mer dotés d'aptitudes à l'apnée hors-norme parviennent à se déplacer en effectuant de longues plongées. Il semble intéressant de se demander, dans l'hypothèse d'un comportement optimal, ce que pourrait impliquer le choix d'une stratégie plutôt que l'autre vis à vis de l'évitement des prédateurs mais également en rapport avec l'hétérogénéité des ressources alimentaires dans l'espace.

D'autre part, se pose la question de la façon dont les prédateurs perçoivent et réagissent à l'hétérogénéité des ressources. En effet, nous avons considéré la densité de proies comme le déterminant principal du comportement des éléphants de mer et avons effectivement observé des changements du comportement de plongée en réponse à un indicateur de la densité des ressources. De façon générale, on estime que les prédateurs répondent directement à la densité des proies à fine échelle mais, la prédictibilité augmentant avec l'échelle (Wiens, 1989), que ceux-ci adoptent alors des stratégies basées sur leur mémoire (Weimerskirch, 2007) et des indices environnementaux (Hunt and Schneider, 1987; Hunt et al., 1999). De telles stratégies échelle-dépendantes ont été mises en évidence chez les procellariiformes (Fritz et al., 2003; Weimerskirch et al., 2007; Pinaud and Weimerskirch, 2007). Ainsi les traces olfactives de Dyméthyle Sulfite (DMS) (Nevitt et al., 1995; Nevitt, 2000; Nevitt and Bonadonna, 2005; Savoca and Nevitt, 2014) ou la présence de congénères (Fauchald, 2009) sont autant d'indices environnementaux aidant les procellariiformes à identifier des secteurs assez vastes et abritant potentiellement des parcelles riches en proies. La stratégie de recherche alimentaire à large échelle s'appuierait sur l'obtention d'information : une "infotaxis" (Vergassola et al., 2007) plutôt qu'une "preytaxis" (Kareiva and Odell, 1987). Ainsi, selon l'échelle observée, les paramètres environnementaux pourraient contribuer à expliquer le comportement des animaux. Chez l'éléphant de mer, les différents sens que l'on estime être impliqués dans la recherche alimentaire sont : la vue (Levenson and Schusterman, 1999; Mcgovern et al., 2015), la sensibilité des vibrisses aux vibrations de l'eau (Dehnhardt, 2001; Mcgovern et al., 2015; Naito et al., 2013) et

l'ouïe (Kastak and Schusterman, 1999). Mais la portée de ces moyens de perception est probablement faible, si bien que les modalités de la perception qu'ont les éléphants de mer de leur environnement à méso-échelle sont mal connues. De nombreux paramètres océanographiques (température, salinité, lumière, etc...) pourraient être des indices environnementaux utilisables. La question du rôle des indices environnementaux et de leur perception dans la stratégie de recherche alimentaire des prédateurs est un problème complexe et fascinant. Ce problème semble important afin de tirer le meilleur parti de l'étude du comportement des prédateurs et de mieux comprendre les interactions prédateur-proies. Une première étape pourrait consister à mettre à profit la haute fréquence d'échantillonnage des données de bio-logging afin de décrire la résolution spatio-temporelle de la perception des éléphants de mer, par exemple au moyen d'une analyse fractale des mouvements (With, 1994; Fritz et al., 2003). Il serait alors intéressant de tester si les conditions océanographiques, indépendamment de la densité locale des proies, peuvent expliquer les variations du comportement des éléphants de mer à différentes échelles.

7.3.2 Méthodes et outils du bio-logging

Le bio-logging est un domaine en pleine expansion (Ropert-Coudert and Wilson, 2005; McIntyre, 2014; Hussey et al., 2015). Afin d'aider au partage et à l'amélioration des méthodes au cours du temps, entre équipes de recherche et entre modèles d'étude, des efforts ont été déployés au cours de cette thèse. Ils se manifestent dans les informations supplémentaires et dans l'initiation du projet `rbl` où est partagé le code des méthodes que nous avons développées ou utilisées : algorithme "Broken-stick" et le calcul du "Time-At-Depth" Fedak et al. (2001), algorithme "Dive Zone Index" Photopoulou et al. (2015), détection des évènements de bioluminescence Vacquié-Garcia et al. (2012), des ondulations ("wiggles") Halsey et al. (2007), des phases de plongées Le Bras (2012), des tentatives de capture Vacquié-Garcia et al. (2015), de l'effort de nage Richard et al. (2014) etc... Ce projet se poursuit par l'extension des différents outils développés dans le cadre de l'analyse des plongées proposé par Heerah et al. (2014, 2015) (voir sous-section 7.2.2). Parmi les travaux encore en cours qui n'ont pas pu être présentés dans cette thèse, se trouve le développement de méthodes permettant de mieux estimer les variations de condition corporelle de prédateurs plongeurs variés, une mesure du succès d'alimentation particulièrement utile pour enquêter sur les habitats de pêche favorables aux prédateurs (Biuw et al., 2007; Bailleul et al., 2007b)

Jusqu'à présent les découvertes et les possibilités de questionnement se sont démultipliées au rythme des avancées techniques (Ropert-Coudert and Wilson, 2005). Certaines limites rencontrées au cours de cette thèse sont en passe d'être dépassées par le développement de nouveaux outils. Le développement d'accéléromètres capables d'enregistrer sur de plus longues durées permettront de suivre les éléphants de mer durant leur voyage post-mue, ouvrant la voie à de nombreuses études à fine échelle de l'océan Austral entre les mois de mars et septembre. Les prochaines années marqueront peut-être l'avènement de caméras (Davis et al., 2003; Naito et al., 2013) et de sonar (Lawson et al., 2015) miniaturisés performants. Ces outils semblent être très prometteurs pour étudier la distribution des proies de l'éléphant de mer et des autres organismes de niveau trophique intermédiaire. Les avancées technologiques peuvent lever certains verrous mais il est réducteur d'affirmer que ces derniers limitent le progrès scientifique. Il est d'ailleurs amusant de constater comment de nouvelles méthodes et applications insoupçonnées sont continuellement découvertes. Par exemple, le détournement des accéléromètres embarqués sur les éléphants de mer pour mesurer la hauteur des vagues et des magnétomètres pour estimer la direction du vent (Cazau et al., en préparation), des capteurs de lumière pour la détection des organismes bioluminescents (Vacquié-Garcia et al., 2012), des GPS posés sur les oiseaux pour mesurer la vitesse des vents (Treep et al., 2016) etc... Dans tous les cas, il sera passionnant d'observer les évolutions du bio-logging et de ses applications mêlant océanographie physique et écologie alimentaire.

7.3.3 Bio-indication et conservation

La notion de bio-indication est assez ancienne, elle est par exemple proposée par Nylander (1866) à travers l'utilisation des lichens comme outil de mesure de la pollution de l'air. Dans les années 1990 émerge l'idée d'utiliser les prédateurs supérieurs (Croxall et al., 1992; Furness, 1993; Furness and Camphuysen, 1997) notamment pour suivre l'état des stocks de poisson. La mise en œuvre d'un tel procédé requiert la possession de données sur le long terme et, préférentiellement, la combinaison de plusieurs mesures ou d'indices provenant de différentes espèces. Cependant, dans l'océan Austral où l'acquisition des données conventionnelles est coûteuse et où l'activité de nombreux prédateurs supérieurs (oiseaux et prédateurs plongeurs) est surveillée, cette approche est attrayante. Cette thèse ne s'inscrit pas directement dans ce cadre mais plutôt indirectement et/ou à plus petite échelle :

1. Indirectement, nous avons contribué à l'amélioration de la compréhension du comportement des prédateurs. Nous l'avons évoqué dans la sous-section 7.2.2, l'interprétation du comportement animal est un enjeu important et difficile, tant et si bien que le plein potentiel des données collectées depuis une décennie ne semble se libérer qu'actuellement (Carter et al., 2016). Les données temps-profondeur sont de loin les plus courantes et constituent les fondations de l'analyse du comportement de plongée. Nous avons montré que l'approximation des mouvements tri-dimensionnels au fond des plongées par des données classiques temps-profondeur est appropriée. De plus, l'identification des "zones de recherche alimentaire intensive" (ARS) à partir des données de trajectoires GPS ou Argos, bien que de moins en moins utilisée (au profit d'indicateurs tels que les tentatives de capture), reste un outil incontournable dans les études à grande échelle et/ou multi-espèces (Hindell et al., 2016; Kirkman et al., 2016; Lascelles et al., 2016). Nous avons vu comment les ajustements comportementaux dans les zones riches en proies conduisent, mécaniquement, à une contribution plus forte de l'advection sur la trajectoire mesurée par GPS. Ces résultats semblent utiles à l'interprétation des nombreuses études passées se basant sur ce type de données et pourraient aussi aider à l'amélioration des méthodes dans des études futures.

2. À fine échelle, nous avons pu décrire certains aspects de la distribution des proies de l'éléphant de mer, en premier lieu, au sujet de l'importance de la dimension verticale sur la distribution des proies. Les résultats de nos analyses du comportement des éléphants de mer au fond de leurs plongées suggèrent en effet que leur densité décroit avec la profondeur et que ces dernières se répartissent au sein de couches (dont l'étendue verticale contrôle en partie la densité) où les proies seraient dispersées plutôt que regroupées en larges bancs compacts.

Bio-acquisition et bio-indication semblent être des approches particulièrement pertinentes dans le milieu océanique. En raison de sa nature très dynamique, une gestion efficace de ces écosystèmes ne peut simplement imiter celle du milieu terrestre où des frontières entre zones protégées ou non-protégées sont érigées pour des décennies. À l'heure actuelle de nombreuses données sont collectées en temps presque réel par les prédateurs supérieurs et les satellites. Il est possible d'imaginer une gestion plus dy-

namique des écosystèmes pélagiques qui profiterait de ces données afin de diminuer les interactions négatives entre l'homme et la faune marine. Les données de télémétrie peuvent renseigner instantanément sur les points chauds ("hotspots") où s'alimentent les prédateurs. D'autre part, les données de télédétection peuvent permettre de prédire avec une large couverture spatiale les lieux où les mesures de gestion seraient les plus efficaces. Une telle gestion ne peut se passer d'une compréhension fine des interactions entre les différents niveaux trophiques et l'environnement physique. Ainsi, nous avons constaté des variations du taux de tentatives de capture au fonds des plongées en relation avec les tourbillons méso-échelles. Nos résultats suggèrent qu'au cours de l'été austral les bordures de ces structures ont un rôle structurant sur la distribution des proies de l'éléphant de mer. D'autre part, des différences notables ont été observées en fonction du type du tourbillon, les tourbillons cycloniques constituant des zones plus riches en proies. Ces observations montrent la pertinence de la notion de niche dynamique pour comprendre les stratégies alimentaires des prédateurs supérieurs voyageant dans le milieu océanique. Par ailleurs, nos résultats ont aussi souligné les faiblesses et les difficultés actuellement rencontrées lors de la mise en œuvre de modèles prédisant la densité des proies de prédateurs plongeurs tels que l'éléphant de mer.

7.3.4 Rôle des paramètres océanographiques

Quand il s'agit d'anticiper certains processus écologiques reposant sur l'interprétation d'une mesure biologique, il est impératif de prendre en compte l'ensemble des facteurs pouvant influencer la mesure. Le débat entre McIntyre et al. (2011a, 2012) et Boersch-Supan et al. (2012) en offre un exemple. McIntyre et al. (2011a) remarquent que les éléphants de mer plongent plus profondément dans les eaux chaudes et suggèrent que le réchauffement de l'eau induirait une migration des proies vers les profondeurs[13]. Boersch-Supan et al. (2012) font alors la critique que ces conclusions sont basées sur une corrélation entre profondeur de plongée et température sans observation concernant les proies. Dans ces conditions, il est impossible de déterminer si le phénomène détecté au travers des variations de la prodondeur de plongée des éléphants de mer est lié (i) à une migration des proies en fonction de la température McIntyre et al. (2011a) ou bien (ii) à l'observation de deux champs de proies distincts et associés à des températures différentes (Boersch-Supan et al., 2012) (annexe E). Or,

[13]Ce qui aurait pour probable conséquence une baisse du succès alimentaire des éléphants de mer

les connaissances manquent sur les conditions abiotiques qui caractérisent l'habitat des myctophidés et sur l'effet des paramètres physiques sur leur distribution (Gjøsaeter and Kawaguchi, 1980; Catul et al., 2010).
Nous aurions souhaité développer davantage le travail de caractérisation des niches écologiques des myctophidés tel qu'initié par Guinet et al. (2014, annexe E) et Vacquié-Garcia et al. (2015). Cependant, relier zones d'alimentation des prédateurs, conditions océanographiques et composition en proie est un défi (Kloser et al., 2009; Young et al., 2015), particulièrement ardu si l'on ne dispose que de données de présence (sous-section 7.2.2) et pas d'indications sur la qualité des proies (sous-sous-section 7.2.1). Pour dépasser ces limitations il serait certainement fécond de combiner les différentes approches. L'échantillonnage conventionnel en relation avec bio-logging (Saijo et al., 2016) permet d'évaluer ce qui est disponible (densité et composition) dans l'environnement et de le comparer à ce qui est exploité par les prédateurs. La combinaison de différents indicateurs (tentatives de captures, effort de nage et variations de condition corporelle des animaux) peut aussi renseigner sur la qualité des proies (Richard et al., 2016). Les travaux de Richard et al. (2016) ont montré qu'en dépit de taux de capture bien inférieurs au nord du front sub-antarctique, les femelles éléphants de mer améliorent tout aussi vite leur condition corporelle. Ces résultats suggèrent l'existence de champs de proie différents de part et d'autre du front sub-antarctique, avec au Nord des proies plus grosses et/ou de plus fortes densités énergétiques. Cette approche, tentant de caractériser les différents habitats écologiques du milieu pélagique, reste encore à faire à méso-échelle. En lien avec de tels travaux, la télédétection de la taxonomie des types phytoplanctoniques dominants (Alvain et al., 2008) ouvre des perspectives prometteuses.

Bibliographie

Abraham, E. R. (1998). The generation of plankton patchiness by turbulent stirring. *Nature*, 391(6667) :577–580. doi:10.1038/35361. 6, 11

Adachi, T., Costa, D. P., Robinson, P. W., Peterson, S. H., Yamamichi, M., Naito, Y., and Takahashi, A. (2016). Searching for prey in a three-dimensional environment : hierarchical movements enhance foraging success in northern elephant seals. *Functional Ecology*. doi:10.1111/1365-2435.12686. 78, 86, 96, 154

Ainley, D. G. and Siniff, D. B. (2009). The importance of Antarctic toothfish as prey of Weddell seals in the Ross Sea. *Antarctic Science*, 21(04) :317–327. doi:10.1017/S0954102009001953. 73

Ainley, D. and DeMaster, D. (1990). The upper trophic levels in polar marine ecosystems. In *Polar Oceanography : Chemistry, Biology, and Geology*. Elsevier. ISBN 372. 20

Alvain, S., Moulin, C., Dandonneau, Y., and Loisel, H. (2008). Seasonal distribution and succession of dominant phytoplankton groups in the global ocean : A satellite view. *Global Biogeochemical Cycles*, 22(3) :GB3001. doi:10.1029/2007GB003154. 11, 104, 119, 148, 172

Aoki, K., Watanabe, Y. Y., Crocker, D. E., Robinson, P. W., Biuw, M., Costa, D. P., Miyazaki, N., Fedak, M. A., and Miller, P. J. O. (2011). Northern elephant seals adjust gliding and stroking patterns with changes in buoyancy : validation of at-sea metrics of body density. *The Journal of Experimental Biology*, 214(17) :2973–2987. doi:10.1242/jeb.055137. 56, 69, 85, 162

Ariza, A., Garijo, J. C., Landeira, J. M., Bordes, F., and Hernández-León, S. (2015). Migrant biomass and respiratory carbon flux by zooplankton and micronekton in the subtropical northeast Atlantic Ocean (Canary Islands). *Progress in Oceanography*, 134 :330–342. doi:10.1016/j.pocean.2015.03.003. 15, 97

Arrhenius, S. (1889). *Über die Reaktionsgeschwindigkeit bei der Inversion von Rohrzucker durch Säuren*, volume 4 of *Z. Physik. Chem.* Wilhelm Engelmann. 7

Austin, D., Bowen, W. D., McMillan, J. I., and Iverson, S. J. (2006). Linking movement, diving and habitat to foraging success in a large marine predator. *Ecology*, 87(12) :3095–3108. doi:10.1890/0012-9658(2006)87[3095 :lmdaht]2.0.co ;2. 52, 77, 78, 153

Authier, M., Delord, K., and Guinet, C. (2011). Population trends of female Elephant Seals breeding on the Courbet Peninsula, îles Kerguelen. *Polar Biology*, 34(3) :319–328. doi:10.1007/s00300-010-0881-1. 28, 29

Bailey, S. W. and Werdell, P. J. (2006). A multi-sensor approach for the on-orbit validation of ocean color satellite data products. *Remote Sensing of Environment*, 102(1–2) :12–23. doi:10.1016/j.rse.2006.01.015. 10

Bailleul, F., Charrassin, J.-B., Ezraty, R., Girard-Ardhuin, F., McMahon, C. R., Field, I. C., and Guinet, C. (2007)a. Southern elephant seals from Kerguelen Islands confronted by Antarctic Sea ice. Changes in movements and in diving behaviour. *Deep Sea Research Part II : Topical Studies in Oceanography*, 54(3–4) :343–355. doi:10.1016/j.dsr2.2006.11.005. 31

Bailleul, F., Charrassin, J.-B., Monestiez, P., Roquet, F., Biuw, M., and Guinet, C. (2007)b. Successful foraging zones of southern elephant seals from the Kerguelen Islands in relation to oceanographic conditions. *Philosophical Transactions of the Royal Society B : Biological Sciences*, 362(1487) :2169–2181. doi:10.1098/rstb.2007.2109. 19, 57, 71, 151, 162, 168

Bailleul, F., Pinaud, D., Hindell, M., Charrassin, J.-B., and Guinet, C. (2008). Assessment of scale-dependent foraging behaviour in southern elephant seals incorporating the vertical dimension : a development of the First Passage Time method. *Journal of Animal Ecology*, 77 (5) :948–957. doi:10.1111/j.1365-2656.2008.01407.x. 71, 78

Bailleul, F., Authier, M., Ducatez, S., Roquet, F., Charrassin, J.-B., Cherel, Y., and Guinet, C. (2010)a. Looking at the unseen : combining animal bio-logging and stable isotopes to reveal a shift in the ecological niche of a deep diving predator. *Ecography*, 33(4) :709–719. doi:10.1111/j.1600-0587.2009.06034.x. 23, 31

Bailleul, F., Cotté, C., and Guinet, C. (2010)b. Mesoscale eddies as foraging area of a deep-diving predator, the southern elephant seal. *Marine Ecology Progress Series*, 408 :251–264. doi:10.3354/meps08560. 10, 21, 122, 123, 128, 144

Bailleul, F., Lesage, V., and Hammill, M. O. (2010)c. Spherical First Passage Time : A tool to investigate area-restricted search in three-dimensional movements. *Ecological Modelling*, 221 (13–14) :1665–1673. doi:10.1016/j.ecolmodel.2010.04.001. 91

Bailleul, F., Vacquié-Garcia, J., and Guinet, C. (2015). Dissolved Oxygen Sensor in Animal-Borne Instruments : An Innovation for Monitoring the Health of Oceans and Investigating the Functioning of Marine Ecosystems. *PLoS ONE*, 10(7) :e0132681. doi:10.1371/journal.pone.0132681. 103

Bakun, A. (2006). Fronts and eddies as key structures in the habitat of marine fish larvae. *Scientia Marina*, 70(SUPPL. 2) :105–122. ISSN 0214-8358, url : `http://scimar.icm.csic.es/scimar/index.php/secId/6/IdArt/194/`. 10

Barham, E. G. (1966). Deep Scattering Layer Migration and Composition : Observations from a Diving Saucer. *Science*, 151(3716) :1399–1403. doi:10.1126/science.151.3716.1399. 33

Barkley, R. A. (1964). The Theoretical Effectiveness of Towed-Net Samplers as Related to Sampler Size and to Swimming Speed of Organisms. *ICES Journal of Marine Science*, 29(2) : 146–157. doi:10.1093/icesjms/29.2.146. 15

Barkley, R. A. (1972). Selectivity of towed-net samplers. *Fish. Bull*, 70(3) :799–820, url : https://swfsc.noaa.gov/publications/CR/1972/7204.PDF. 15

Barnes, C., Bethea, D. M., Brodeur, R. D., Spitz, J., Ridoux, V., Pusineri, C., Chase, B. C., Hunsicker, M. E., Juanes, F., Kellermann, A., Lancaster, J., Ménard, F., Bard, F.-X., Munk, P., Pinnegar, J. K., Scharf, F. S., Rountree, R. A., Stergiou, K. I., Sassa, C., Sabates, A., and Jennings, S. (2008). Predator and Prey Body Sizes in Marine Food Webs. *Ecology*, 89(3) : 881–881. doi:10.1890/07-1551.1. 7

Barnes, C., Maxwell, D., Reuman, D. C., and Jennings, S. (2010). Global patterns in predator–prey size relationships reveal size dependency of trophic transfer efficiency. *Ecology*, 91 (1) :222–232. doi:10.1890/08-2061.1. 9

Barton, K. (2016). *MuMIn : Multi-Model Inference*. url : http://CRAN.R-project.org/package=MuMIn. 01139 R package version 1.15.6. 61

Bayle, S., Monestiez, P., Guinet, C., and Nerini, D. (2015). Moving toward finer scales in oceanography : Predictive linear functional model of Chlorophyll a profile from light data. *Progress in Oceanography*, 134 :221–231. doi:10.1016/j.pocean.2015.02.001. 104, 106

Beer, A. (1852). Bestimmung der Absorption des rothen Lichts in farbigen Flüssigkeiten. In *Annalen der Physik*, volume 86, pages 78–88. Joh. Ambr. Barth, Leipzig, url : http://gallica.bnf.fr/ark:/12148/bpt6k151715. 163

Belkin, I. M. and Gordon, A. L. (1996). Southern Ocean fronts from the Greenwich meridian to Tasmania. *Journal of Geophysical Research : Oceans*, 101(C2) :3675–3696. doi:10.1029/95JC02750. 36

Benhamou, S. and Bovet, P. (1989). How animals use their environment : a new look at kinesis. *Animal Behaviour*, 38(3) :375–383. doi:10.1016/S0003-3472(89)80030-2. 152

Benitez-Nelson, C. R., Bidigare, R. R., Dickey, T. D., Landry, M. R., Leonard, C. L., Brown, S. L., Nencioli, F., Rii, Y. M., Maiti, K., Becker, J. W., Bibby, T. S., Black, W., Cai, W.-J., Carlson, C. A., Chen, F., Kuwahara, V. S., Mahaffey, C., McAndrew, P. M., Quay, P. D., Rappé, M. S., Selph, K. E., Simmons, M. P., and Yang, E. J. (2007). Mesoscale Eddies Drive Increased Silica Export in the Subtropical Pacific Ocean. *Science*, 316(5827) :1017–1021. doi:10.1126/science.1136221. 122, 147

Benoit-Bird, K. (2006). Effects of scattering layer composition, animal size, and numerical density on the frequency dependence of volume backscatter. *The Journal of the Acoustical Society of America*, 120(5) :3001–3001. doi:10.1121/1.4786994. 17

Benoit-Bird, K. J., Battaile, B. C., Nordstrom, C. A., and Trites, A. W. (2013). Foraging behavior of northern fur seals closely matches the hierarchical patch scales of prey. *Marine Ecology Progress Series*, 479 :283–302. doi:10.3354/meps10209. 78

Benoit-Bird, K. (2004). Prey caloric value and predator energy needs : foraging predictions for wild spinner dolphins. *Marine Biology*, 145(3). doi:10.1007/s00227-004-1339-1. 33

Bester, M. N. (1988). Marking and monitoring studies of the Kerguelen stock of southern elephant seals Mirounga leonina and their bearing on biological research in the Vestfold Hills. *Hydrobiologia*, 165(1) :269–277. doi:10.1007/BF00025596. 28

Bestley, S., Patterson, T. A., Hindell, M. A., and Gunn, J. S. (2010). Predicting feeding success in a migratory predator : integrating telemetry, environment, and modeling techniques. *Ecology*, 91(8) :2373–2384. doi:10.1890/08-2019.1. 95, 96

Bestley, S., Jonsen, I. D., Hindell, M. A., Harcourt, R. G., and Gales, N. J. (2015). Taking animal tracking to new depths : synthesizing horizontal–vertical movement relationships for four marine predators. *Ecology*, 96(2) :417–427. doi:10.1890/14-0469.1. 78

Bianchi, D., Stock, C., Galbraith, E. D., and Sarmiento, J. L. (2013). Diel vertical migration : Ecological controls and impacts on the biological pump in a one-dimensional ocean model. *Global Biogeochemical Cycles*, 27(2) :478–491. doi:10.1002/gbc.20031. 14, 33

Biuw, M., Boehme, L., Guinet, C., Hindell, M., Costa, D., Charrassin, J.-B., Roquet, F., Bailleul, F., Meredith, M., Thorpe, S., Tremblay, Y., McDonald, B., Park, Y.-H., Rintoul, S. R., Bindoff, N., Goebel, M., Crocker, D., Lovell, P., Nicholson, J., Monks, F., and Fedak, M. A. (2007). Variations in behavior and condition of a Southern Ocean top predator in relation to in situ oceanographic conditions. *Proceedings of the National Academy of Sciences*, 104(34) :13705–13710. doi:10.1073/pnas.0701121104. 19, 162, 168

Biuw, M., McConnell, B., Bradshaw, C. J. A., Burton, H., and Fedak, M. (2003). Blubber and buoyancy : monitoring the body condition of free-ranging seals using simple dive characteristics. *Journal of Experimental Biology*, 206(19) :3405–3423. doi:10.1242/jeb.00583. 35, 132, 160, 162

Biuw, M., Nøst, O. A., Stien, A., Zhou, Q., Lydersen, C., and Kovacs, K. M. (2010). Effects of Hydrographic Variability on the Spatial, Seasonal and Diel Diving Patterns of Southern Elephant Seals in the Eastern Weddell Sea. *PLOS ONE*, 5(11) :e13816. doi:10.1371/journal.pone.0013816. 77, 93

Blain, S., Tréguer, P., Belviso, S., Bucciarelli, E., Denis, M., Desabre, S., Fiala, M., Martin Jézéquel, V., Le Fèvre, J., Mayzaud, P., Marty, J.-C., and Razouls, S. (2001). A biogeochemical study of the island mass effect in the context of the iron hypothesis : Kerguelen Islands, Southern Ocean. *Deep Sea Research Part I : Oceanographic Research Papers*, 48(1) :163–187. doi:10.1016/S0967-0637(00)00047-9. 37

Blain, S., Quéguiner, B., Armand, L., Belviso, S., Bombled, B., Bopp, L., Bowie, A., Brunet, C., Brussaard, C., Carlotti, F., Christaki, U., Corbière, A., Durand, I., Ebersbach, F., Fuda, J.-L., Garcia, N., Gerringa, L., Griffiths, B., Guigue, C., Guillerm, C., Jacquet, S., Jeandel, C., Laan, P., Lefèvre, D., Lo Monaco, C., Malits, A., Mosseri, J., Obernosterer, I., Park, Y.-H., Picheral, M., Pondaven, P., Remenyi, T., Sandroni, V., Sarthou, G., Savoye, N., Scouarnec, L., Souhaut, M., Thuiller, D., Timmermans, K., Trull, T., Uitz, J., van Beek, P., Veldhuis, M., Vincent, D., Viollier, E., Vong, L., and Wagener, T. (2007). Effect of natural iron fertilization on carbon sequestration in the Southern Ocean. *Nature*, 446(7139) :1070–1074. doi:10.1038/nature05700. 37

Blanchet, M.-A., Lydersen, C., Ims, R. A., and Kovacs, K. M. (2015). Seasonal, Oceanographic and Atmospheric Drivers of Diving Behaviour in a Temperate Seal Species Living in the High Arctic. *PLOS ONE*, 10(7) :e0132686. doi:10.1371/journal.pone.0132686. 92, 94

Block, B. A., Jonsen, I. D., Jorgensen, S. J., Winship, A. J., Shaffer, S. A., Bograd, S. J., Hazen, E. L., Foley, D. G., Breed, G. A., Harrison, A.-L., Ganong, J. E., Swithenbank, A., Castleton, M., Dewar, H., Mate, B. R., Shillinger, G. L., Schaefer, K. M., Benson, S. R., Weise, M. J., Henry, R. W., and Costa, D. P. (2011). Tracking apex marine predator movements in a dynamic ocean. *Nature*, 475(7354) :86–90. doi:10.1038/nature10082. 14

Boehlert, G. W., Costa, D. P., Crocker, D. E., Green, P., O'Brien, T., Levitus, S., and Le Boeuf, B. J. (2001). Autonomous Pinniped Environmental Samplers : Using Instrumented Animals as Oceanographic Data Collectors. *Journal of Atmospheric and Oceanic Technology*, 18(11) : 1882–1893. doi:10.1175/1520-0426(2001)018<1882 :APESUI>2.0.CO ;2. 13

Boehme, L., Kovacs, K., Lydersen, C., Nøst, O., Biuw, M., Charrassin, J.-B., Roquet, F., Guinet, C., Meredith, M., Nicholls, K., Thorpe, S., Costa, D., Block, B., Hammill, M., Stenson, G., Muelbert, M., Bester, M., Plötz, J., Bornemann, H., Hindell, M., Rintoul, S., Lovell, P., and Fedak, M. (2009). Biologging in the global ocean observing system. In Hall, J., Harrison, D., and Stammer, D., editors, *Proceedings of Ocean Obs 09 : Sustained ocean observations and information for society*, number WPP-306, Vol. 2 in ESA Publication, Venice, Italy. European Space Agency, url : http://nora.nerc.ac.uk/14472/. 18

Boersch-Supan, P., Boehme, L., Read, J., Rogers, A., and Brierley, A. (2012). Elephant seal foraging dives track prey distribution, not temperature : Comment on McIntyre et al. (2011). *Marine Ecology Progress Series*, 461 :293–298. doi:10.3354/meps09890. 171

Bost, C. A., Jaeger, A., Huin, W., Koubbi, P., Halsey, L. G., Hanuise, N., and Handrich, Y. (2008). Monitoring Prey Availability via Data Loggers Deployed on Seabirds : Advances and Present Limitations. *Fisheries Bethesda*, pages 121–137, url : http://www.terrapub.co.jp/onlineproceedings/fs/wfc2008/index.html. 00015. 20

Bost, C. A., Cotté, C., Bailleul, F., Cherel, Y., Charrassin, J. B., Guinet, C., Ainley, D. G., and Weimerskirch, H. (2009). The importance of oceanographic fronts to marine birds and mammals of the southern oceans. *Journal of Marine Systems*, 78(3) :363–376. doi:10.1016/j.jmarsys.2008.11.022. 37, 77, 115, 122

Bost, C. A., Cotté, C., Terray, P., Barbraud, C., Bon, C., Delord, K., Gimenez, O., Handrich, Y., Naito, Y., Guinet, C., and Weimerskirch, H. (2015). Large-scale climatic anomalies affect marine predator foraging behaviour and demography. *Nature Communications*, 6 :8220. doi:10.1038/ncomms9220. 51

Bouguer, P. (1729). *Essai d'optique sur la gradation de la lumière*. C. Jombert, Paris, url : http://gallica.bnf.fr/ark:/12148/bpt6k10405749. 2, 163

Bracco, A., Provenzale, A., and Scheuring, I. (2000). Mesoscale vortices and the paradox of the plankton. *Proceedings of the Royal Society of London B : Biological Sciences*, 267(1454) : 1795–1800. doi:10.1098/rspb.2000.1212. 123, 127

Brodeur, R. and Yamamura, O. (2005). Micronekton of the north pacific. Technical Report 30, PICES Scientific Report, url : http://meetings.pices.int/publications/scientific-reports. 13, 15

Brose, U., Jonsson, T., Berlow, E. L., Warren, P., Banasek-Richter, C., Bersier, L.-F., Blanchard, J. L., Brey, T., Carpenter, S. R., Blandenier, M.-F. C., Cushing, L., Dawah, H. A., Dell, T.,

Edwards, F., Harper-Smith, S., Jacob, U., Ledger, M. E., Martinez, N. D., Memmott, J., Mintenbeck, K., Pinnegar, J. K., Rall, B. C., Rayner, T. S., Reuman, D. C., Ruess, L., Ulrich, W., Williams, R. J., Woodward, G., and Cohen, J. E. (2006). Consumer–Resource Body-Size Relationships in Natural Food Webs. *Ecology*, 87(10) :2411–2417. doi:10.1890/0012-9658(2006)87[2411 :CBRINF]2.0.CO ;2. 7

Brown, J. S. (1988). Patch use as an indicator of habitat preference, predation risk, and competition. *Behavioral Ecology and Sociobiology*, 22(1) :37–47. doi:10.1007/BF00395696. 20

Burgess, W. C., Tyack, P. L., Le Boeuf, B. J., and Costa, D. P. (1998). A programmable acoustic recording tag and first results from free-ranging northern elephant seals. *Deep Sea Research Part II : Topical Studies in Oceanography*, 45(7) :1327–1351. doi:10.1016/S0967-0645(98)00032-0. 46, 82

Campagna, C. and Lewis, M. (1992). Growth and Distribution of a Southern Elephant Seal Colony. *Marine Mammal Science*, 8(4) :387–396. doi:10.1111/j.1748-7692.1992.tb00053.x. 28

Carrick, R., Csordas, S. E., and Ingham, S. E. (1962). Studies on the southern elephant seal, mirounga leonina (l.). IV. breeding and development. *CSIRO Wildlife Research*, 7(2) :161. doi:10.1071/cwr9620161. 29

Carter, M. I. D., Bennett, K. A., Embling, C. B., Hosegood, P. J., and Russell, D. J. F. (2016). Navigating uncertain waters : a critical review of inferring foraging behaviour from location and dive data in pinnipeds. *Movement Ecology*, 4(1). doi:10.1186/s40462-016-0090-9. 170

Casaux, R., Baroni, A., and Carlini, A. (1998). The diet of the Antarctic fur seal Arctocephalus gazella at Harmony Point, Nelson Island, South Shetland Islands. *Polar Biology*, 20(6) : 424–428. doi:10.1007/s003000050324. 34, 104

Catul, V., Gauns, M., and Karuppasamy, P. K. (2010). A review on mesopelagic fishes belonging to family Myctophidae. *Reviews in Fish Biology and Fisheries*, 21(3) :339–354. doi:10.1007/s11160-010-9176-4. 16, 32, 33, 77, 93, 124, 172

Chaigne, A., Authier, M., Richard, P., Cherel, Y., and Guinet, C. (2013). Shift in foraging grounds and diet broadening during ontogeny in southern elephant seals from Kerguelen Islands. *Marine Biology*, 160(4) :977–986. doi:10.1007/s00227-012-2149-5. 32

Champagne, C. D., Crocker, D. E., Fowler, M. A., and Houser, D. S. (2012). Fasting Physiology of the Pinnipeds : The Challenges of Fasting While Maintaining High Energy Expenditure and Nutrient Delivery for Lactation. In McCue, M. D., editor, *Comparative Physiology of Fasting, Starvation, and Food Limitation*, pages 309–336. Springer Berlin Heidelberg. ISBN 978-3-642-29055-8 978-3-642-29056-5. doi:10.1007/978-3-642-29056-5_19. 31

Chapman, J. W., Klaassen, R. H. G., Drake, V. A., Fossette, S., Hays, G. C., Metcalfe, J. D., Reynolds, A. M., Reynolds, D. R., and Alerstam, T. (2011). Animal Orientation Strategies for Movement in Flows. *Current Biology*, 21(20) :R861–R870. doi:10.1016/j.cub.2011.08.014. 00065. 99

Charnov, E. L. (1976). Optimal foraging, the marginal value theorem. *Theoretical Population Biology*, 9(2) :129–136. doi:10.1016/0040-5809(76)90040-X. 19, 51, 147

Chelton, D. B., Gaube, P., Schlax, M. G., Early, J. J., and Samelson, R. M. (2011). The influence of nonlinear mesoscale eddies on near-surface oceanic chlorophyll. *Science*, 334(6054) :328–332. doi:10.1126/science.1208897. 144, 147

Chelton, D. B., Schlax, M. G., Samelson, R. M., and de Szoeke, R. A. (2007). Global observations of large oceanic eddies. *Geophysical Research Letters*, 34(15) :L15606. doi:10.1029/2007GL030812. 4

Cherel, Y., Ducatez, S., Fontaine, C., Richard, P., and Guinet, C. (2008). Stable isotopes reveal the trophic position and mesopelagic fish diet of female southern elephant seals breeding on the Kerguelen Islands. *Marine Ecology Progress Series*, 370 :239–247. doi:10.3354/meps07673. 31, 53, 104

Christensen, V. and Pauly, D. (1992). ECOPATH II — a software for balancing steady-state ecosystem models and calculating network characteristics. *Ecological Modelling*, 61(3–4) : 169–185. doi:10.1016/0304-3800(92)90016-8. 22

Christensen, V. and Walters, C. J. (2004). Ecopath with Ecosim : methods, capabilities and limitations. *Ecological Modelling*, 172(2–4) :109–139. doi:10.1016/j.ecolmodel.2003.09.003. 22

Christensen, V., Guénette, S., Heymans, J. J., Walters, C. J., Watson, R., Zeller, D., and Pauly, D. (2003). Hundred-year decline of North Atlantic predatory fishes. *Fish and Fisheries*, 4(1) : 1–24. doi:10.1046/j.1467-2979.2003.00103.x. 12

Claessen, D., de Roos, A. M., and Persson, L. (2000). Dwarfs and Giants : Cannibalism and Competition in Size-Structured Populations. *The American Naturalist*, 155(2) :219–237. doi:10.1086/303315. 7

Clarke, G. L., Ewing, G. C., and Lorenzen, C. J. (1970). Spectra of Backscattered Light from the Sea Obtained from Aircraft as a Measure of Chlorophyll Concentration. *Science*, 167(3921) : 1119–1121. doi:10.1126/science.167.3921.1119. 2, 10, 104

Collins, M. A. and Rodhouse, P. G. K. (2006). Southern Ocean Cephalopods. In Alan J. Southward , and Lee A. Fuiman, C. M. Y., editor, *Advances in Marine Biology*, volume 50, pages 191–265. Academic Press, url : `http://www.sciencedirect.com/science/article/pii/S0065288105500038`. 53

Collins, M. A., Xavier, J. C., Johnston, N. M., North, A. W., Enderlein, P., Tarling, G. A., Waluda, C. M., Hawker, E. J., and Cunningham, N. J. (2008). Patterns in the distribution of myctophid fish in the northern Scotia Sea ecosystem. *Polar Biology*, 31(7) :837–851. doi:10.1007/s00300-008-0423-2. 34

Conchon, A. (2016). *Modélisation du zooplancton et du micronecton marin*. PhD thesis, l'Université de La Rochelle, CLS. 11

Cornick, L. A. and Horning, M. (2003). A test of hypotheses based on optimal foraging considerations for a diving mammal using a novel experimental approach. *Canadian Journal of Zoology*, 81(11) :1799–1807. doi:10.1139/z03-179. 52

Costa, D. P., Robinson, P. W., Arnould, J. P. Y., Harrison, A.-L., Simmons, S. E., Hassrick, J. L., Hoskins, A. J., Kirkman, S. P., Oosthuizen, H., Villegas-Amtmann, S., and Crocker, D. E. (2010). Accuracy of ARGOS locations of pinnipeds at-sea estimated using fastloc GPS. *PLoS ONE*, 5(1) :e8677. doi:10.1371/journal.pone.0008677. 38

Cotté, C., Park, Y.-H., Guinet, C., and Bost, C.-A. (2007). Movements of foraging king penguins through marine mesoscale eddies. *Proceedings of the Royal Society B : Biological Sciences*, 274 (1624) :2385–2391. doi:10.1098/rspb.2007.0775. 77, 115

Cotté, C., d'Ovidio, F., Chaigneau, A., Lévy, M., Taupier-Letage, I., Mate, B., and Guinet, C. (2011). Scale-dependent interactions of Mediterranean whales with marine dynamics. *Limnology and Oceanography*, 56(1) :219–232. doi:10.4319/lo.2011.56.1.0219. 10, 21

Cotté, C., d'Ovidio, F., Dragon, A.-C., Guinet, C., and Lévy, M. (2015). Flexible preference of southern elephant seals for distinct mesoscale features within the Antarctic Circumpolar Current. *Progress in Oceanography*, 131 :46–58. doi:10.1016/j.pocean.2014.11.011. 10, 21, 37, 96, 122, 123, 147

Cribari-Neto, F. and Zeileis, A. (2010). Beta Regression in R. *Journal of Statistical Software*, 34 (2). doi:10.18637/jss.v034.i02. 60

Crocker, D. E., Boeuf, B. J. L., and Costa, D. P. (1997). Drift diving in female northern elephant seals : implications for food processing. *Canadian Journal of Zoology*, 75(1) :27–39. doi:10.1139/z97-004. 19, 35, 59, 80, 85, 132

Croxall, J. P., Callaghan, T., Cervellati, R., and Walton, D. W. H. (1992). Southern Ocean Environmental Changes : Effects on Seabird, Seal and Whale Populations [and Discussion]. *Philosophical Transactions of the Royal Society of London B : Biological Sciences*, 338(1285) :319–328. doi:10.1098/rstb.1992.0152. 169

Cury, P., Shannon, L., and Shin, Y. (2003). The functioning of marine ecosystems : a fisheries perspective. In Sinclair, M. and Valdimarsson, G., editors, *Responsible fisheries in the marine ecosystem*, pages 103–123. CABI, Wallingford. ISBN 978-0-85199-633-2, url : http://www.cabi.org/cabebooks/ebook/20103194519. 9, 12, 13

Daneri, G. and Carlini, A. (2002). Fish prey of southern elephant seals, Mirounga leonina, at King George Island. *Polar Biology*, 25(10) :739–743. doi:10.1007/s00300-002-0408-5. 34

Daneri, G., Carlini, A., and Rodhouse, P. (2000). Cephalopod diet of the southern elephant seal, Mirounga leonina, at King George Island, South Shetland Islands. *Antarctic Science*, 12 (01). doi:10.1017/S0954102000000031. 32

Darwin, C. (1859). *The Origin of Species*. Cambridge University Press, Cambridge. ISBN 978-0-511-69429-5 978-1-108-00548-7, url : http://ebooks.cambridge.org/ref/id/CBO9780511694295. 4

David, C., Schaafsma, F. L., van Franeker, J. A., Lange, B., Brandt, A., and Flores, H. (2016). Community structure of under-ice fauna in relation to winter sea-ice habitat properties from the weddell sea. *Polar Biology*. doi:10.1007/s00300-016-1948-4. 8

Davis, A. J., Jenkinson, L. S., Lawton, J. H., Shorrocks, B., and Wood, S. (1998). Making mistakes when predicting shifts in species range in response to global warming. *Nature*, 391(6669) :783–786. doi:10.1038/35842. 21

Davis, R. W., Fuiman, L. A., Williams, T. M., Collier, S. O., Hagey, W. P., Kanatous, S. B., Kohin, S., and Horning, M. (1999). Hunting Behavior of a Marine Mammal Beneath the Antarctic Fast Ice. *Science*, 283(5404) :993–996. doi:10.1126/science.283.5404.993. 73, 74, 78, 153

Davis, R. W., Fuiman, L. A., Williams, T. M., and Le Boeuf, B. J. (2001). Three-dimensional movements and swimming activity of a northern elephant seal. *Comparative Biochemistry and Physiology Part A : Molecular & Integrative Physiology*, 129(4) :759–770. doi:10.1016/S1095-6433(01)00345-2. 78, 91, 98, 99

Davis, R. W., Fuiman, L. A., Williams, T. M., Horning, M., and Hagey, W. (2003). Classification of Weddell seal dives based on 3 dimensional movements and video-recorded observations. *Marine Ecology Progress Series*, 264 :109–122. doi:10.3354/meps264109. 52, 77, 150, 169

Deagle, B. E., Gales, N. J., Evans, K., Jarman, S. N., Robinson, S., Trebilco, R., and Hindell, M. A. (2007). Studying seabird diet through genetic analysis of faeces : A case study on macaroni penguins (eudyptes chrysolophus). *PLoS ONE*, 2(9) :e831. doi:10.1371/journal.pone.0000831. 34

Dehnhardt, G. (2001). Hydrodynamic trail-following in harbor seals (phoca vitulina). *Science*, 293(5527) :102–104. doi:10.1126/science.1060514. 167

Della Penna, A., De Monte, S., Kestenare, E., Guinet, C., and d'Ovidio, F. (2015). Quasi-planktonic behavior of foraging top marine predators. *Scientific Reports*, 5 :18063. doi:10.1038/srep18063. 71, 133, 134, 144, 145, 152, 159

Delong, R. L., Stewart, B. S., and Hill, R. D. (1992). Documenting Migrations of Northern Elephant Seals Using Day Length. *Marine Mammal Science*, 8(2) :155–159. doi:10.1111/j.1748-7692.1992.tb00375.x. 156

deYoung, B., Heath, M., Werner, F., Chai, F., Megrey, B., and Monfray, P. (2004). Challenges of Modeling Ocean Basin Ecosystems. *Science*, 304(5676) :1463–1466. doi:10.1126/science.1094858. 10, 22

Doniol-Valcroze, T., Lesage, V., Giard, J., and Michaud, R. (2011). Optimal foraging theory predicts diving and feeding strategies of the largest marine predator. *Behavioral Ecology*, page arr038. doi:10.1093/beheco/arr038. 52

d'Ovidio, F., Della Penna, A., Trull, T. W., Nencioli, F., Pujol, M.-I., Rio, M.-H., Park, Y.-H., Cotté, C., Zhou, M., and Blain, S. (2015). The biogeochemical structuring role of horizontal stirring : Lagrangian perspectives on iron delivery downstream of the Kerguelen Plateau. *Biogeosciences*, 12(19) :5567–5581. doi:10.5194/bg-12-5567-2015. 37

d'Ovidio, F., Monte, S. D., Alvain, S., Dandonneau, Y., and Lévy, M. (2010). Fluid dynamical niches of phytoplankton types. *Proceedings of the National Academy of Sciences*, 107(43) : 18366–18370. doi:10.1073/pnas.1004620107. 6, 11, 117, 123, 127

d'Ovidio, F., Monte, S. D., Penna, A. D., Cotté, C., and Guinet, C. (2013). Ecological implications of eddy retention in the open ocean : a Lagrangian approach. *Journal of Physics A : Mathematical and Theoretical*, 46(25) :254023. doi:10.1088/1751-8113/46/25/254023. 123, 127, 128

Dragon, A., Bar-Hen, A., Monestiez, P., and Guinet, C. (2012)a. Comparative analysis of methods for inferring successful foraging areas from Argos and GPS tracking data. *Marine Ecology Progress Series*, 452 :253–267. doi:10.3354/meps09618. 85, 152

Dragon, A.-C. (2011). *Modélisation des stratégies d'approvisionnement des éléphants de mer australs - influence de la variabilité de la production primaire et des conditions océanographiques physiques*. phdthesis, Université Pierre et Marie Curie - Paris VI, url : https://tel.archives-ouvertes.fr/tel-00660213/document. 73

Dragon, A.-C., Monestiez, P., Bar-Hen, A., and Guinet, C. (2010). Linking foraging behaviour to physical oceanographic structures : Southern elephant seals and mesoscale eddies east of Kerguelen Islands. *Progress in Oceanography*, 87(1–4) :61–71. doi:10.1016/j.pocean.2010.09.025. 71, 73, 77, 115, 122, 123, 128, 144

Dragon, A.-C., Bar-Hen, A., Monestiez, P., and Guinet, C. (2012)b. Horizontal and vertical movements as predictors of foraging success in a marine predator. *Marine Ecology Progress Series*, 447 :243–257. doi:10.3354/meps09498. 51, 69, 71

Ducatez, S., Dalloyau, S., Richard, P., Guinet, C., and Cherel, Y. (2008). Stable isotopes document winter trophic ecology and maternal investment of adult female southern elephant seals (Mirounga leonina) breeding at the Kerguelen Islands. *Marine Biology*, 155 :413–420. doi:10.1007/s00227-008-1039-3. 31

Eppley, R. W. (1972). Temperature and phytoplankton growth in the sea. *Fish. Bull*, 10(4) : 1063–1085, url : http://fishbull.noaa.gov/70-4/eppley.pdf. 126

Estes, J. A., Terborgh, J., Brashares, J. S., Power, M. E., Berger, J., Bond, W. J., Carpenter, S. R., Essington, T. E., Holt, R. D., Jackson, J. B. C., Marquis, R. J., Oksanen, L., Oksanen, T., Paine, R. T., Pikitch, E. K., Ripple, W. J., Sandin, S. A., Scheffer, M., Schoener, T. W., Shurin, J. B., Sinclair, A. R. E., Soule, M. E., Virtanen, R., and Wardle, D. A. (2011). Trophic downgrading of planet earth. *Science*, 333(6040) :301–306. doi:10.1126/science.1205106. 12

Faghmous, J. H., Frenger, I., Yao, Y., Warmka, R., Lindell, A., and Kumar, V. (2015)a. A daily global mesoscale ocean eddy dataset from satellite altimetry. *Scientific Data*, 2 :150028. doi:10.1038/sdata.2015.28. 00000. 141

Faghmous, J. H., Frenger, I., Yao, Y., Warmka, R., Lindell, A., and Kumar, V. (2015)b. Global mesoscale ocean eddy features. doi:10.5061/dryad.gp40h/1. 128, 131, 132, 133, 134

FAO. (1978). General aspects of population biology. In *Mammals in the Seas*, volume 1 of *FAO Fisheries Series*, pages 142–154. Food & Agriculture Organisation. ISBN 978-92-5-100511-8, url : https://books.google.fr/books?id=-lqiLtuWSa8C. 129

Farrell, E. and Fuiman, L. (2013). *animalTrack : Animal track reconstruction for high frequency 2-dimensional (2D) or 3-dimensional (3D) movement data.* url : http://CRAN.R-project.org/package=animalTrack. 56, 81, 82

Fauchald, P. (1999). Foraging in a Hierarchical Patch System. *The American Naturalist*, 153(6) : 603–613. doi:10.1086/an.1999.153.issue-6. 4, 19, 150

Fauchald, P. (2009). Spatial interaction between seabirds and prey : review and synthesis. *Marine Ecology Progress Series*, 391 :139–151. doi:10.3354/meps07818. 20, 158, 167

Fauchald, P. and Tveraa, T. (2003). Using First-Passage Time in the analysis of Area-Retricted Search and habitat selection. *Ecology*, 84(2) :282–288. doi:10.1890/0012-9658(2003)084[0282 :UFPTIT]2.0.CO;2. 20, 77, 151

Fauchald, P., Erikstad, K. E., and Skarsfjord, H. (2000). Scale–dependent predator–prey interactions : the hierarchical spatial distribution of seabirds and prey. *Ecology*, 81(3) :773–783. doi:10.1890/0012-9658(2000)081[0773 :SDPPIT]2.0.CO ;2. 150

Fedak, M. A. (2013). The impact of animal platforms on polar ocean observation. *Deep Sea Research Part II : Topical Studies in Oceanography*, 88–89 :7–13. doi:10.1016/j.dsr2.2012.07.007. 18, 103, 117

Fedak, M. A., Lovell, P., and Grant, S. M. (2001). Two Approaches to Compressing and Interpreting Time-Depth Information as as Collected by Time-Depth Recorders and Satellite-Linked Data Recorders. *Marine Mammal Science*, 17(1) :94–110. doi:10.1111/j.1748-7692.2001.tb00982.x. 39, 168, 214

Fedak, M. (2004). Marine animals as platforms for oceanographic sampling : a "win/win" situation for biology and operational oceanography. *Memoirs of National Institute of Polar Research. Special issue*, 58 :133–147. ISSN 03860744, url : http://ci.nii.ac.jp/naid/110000010604/en. 19, 103

Fedak, M., Lovell, P., McConnell, B., and Hunter, C. (2002). Overcoming the Constraints of Long Range Radio Telemetry from Animals : Getting More Useful Data from Smaller Packages. *Integrative and Comparative Biology*, 42(1) :3–10. doi:10.1093/icb/42.1.3. 214

Ferguson, S. H. and Higdon, J. W. (2006). How seals divide up the world : environment, life history, and conservation. *Oecologia*, 150(2) :318–329. doi:10.1007/s00442-006-0489-x. 28

Fishbase. (2017). Myctophidae - Lanternfishes, url : http://www.fishbase.org/summary/FamilySummary.php?ID=167. 32, 33

Fletcher, S., Boeuf, B. J. L., Costa, D. P., Tyack, P. L., and Blackwell, S. B. (1996). Onboard acoustic recording from diving northern elephant seals. *The Journal of the Acoustical Society of America*, 100(4) :2531–2539. doi:10.1121/1.417361. 46

Flores, H., Putte, A. P. V. d., Siegel, V., Pakhomov, E. A., Franeker, J. A. v., Meesters, E. H. W. G., and Volckaert, F. A. M. (2008). Distribution, abundance and ecological relevance of pelagic fishes in the Lazarev Sea, Southern Ocean. *Marine Ecology Progress Series*, 367 : 271–282. doi:10.3354/meps07530. 8, 14, 33, 34

Flores, H., van Franeker, J.-A., Cisewski, B., Leach, H., de Putte, A. P. V., Meesters, E. H., Bathmann, U., and Wolff, W. J. (2011). Macrofauna under sea ice and in the open surface layer of the lazarev sea, southern ocean. *Deep Sea Research Part II : Topical Studies in Oceanography*, 58(19-20) :1948–1961. doi:10.1016/j.dsr2.2011.01.010. 8

Foo, D., Semmens, J. M., Arnould, J. P. Y., Dorville, N., Hoskins, A. J., Abernathy, K., Marshall, G. J., and Hindell, M. A. (2016). Testing optimal foraging theory models on benthic divers. *Animal Behaviour*, 112 :127–138. doi:10.1016/j.anbehav.2015.11.028. 51, 53, 78, 161

Fossette, S., Gaspar, P., Handrich, Y., Maho, Y. L., and Georges, J.-Y. (2008). Dive and beak movement patterns in leatherback turtles Dermochelys coriacea during internesting intervals in French Guiana. *Journal of Animal Ecology*, 77(2) :236–246. doi:10.1111/j.1365-2656.2007.01344.x. 52, 77

Frederiksen, M., Edwards, M., Richardson, A. J., Halliday, N. C., and Wanless, S. (2006). From plankton to top predators : bottom-up control of a marine food web across four trophic levels. *Journal of Animal Ecology*, 75(6) :1259–1268. doi:10.1111/j.1365-2656.2006.01148.x. 11

Fritz, H., Said, S., and Weimerskirch, H. (2003). Scale–dependent hierarchical adjustments of movement patterns in a long–range foraging seabird. *Proceedings of the Royal Society of London B : Biological Sciences*, 270(1520) :1143–1148. doi:10.1098/rspb.2003.2350. 167, 168

Frost, B. W. and McCrone, L. E. (1978). Vertical Distribution, Diel Vertical Migration, and Abundance of Some Mesopelagic Fishes in the Eastern Subarctic Pacific Ocean in Summer. *Fish. Bull.*, 76(4) :21, url : https://ntrl.ntis.gov/NTRL/dashboard/searchResults/titleDetail/ADA095514.xhtml. 153

Furness, R. W. (1993). Birds as monitors of pollutants. In Furness, R. W. and Greenwood, J. J. D., editors, *Birds as Monitors of Environmental Change*, pages 86–143. Springer Netherlands. ISBN 978-94-015-1324-1 978-94-015-1322-7. doi:10.1007/978-94-015-1322-7_3. 169

Furness, R. W. and Camphuysen, K. C. J. . (1997). Seabirds as monitors of the marine environment. *ICES Journal of Marine Science : Journal du Conseil*, 54(4) :726–737. doi:10.1006/jmsc.1997.0243. 169

Gallon, S., Bailleul, F., Charrassin, J. B., Guinet, C., Bost, C. A., Handrich, Y., and Hindell, M. (2013). Identifying foraging events in deep diving southern elephant seals, Mirounga leonina, using acceleration data loggers. *Deep Sea Research Part II : Topical Studies in Oceanography*, 88–89 :14–22. doi:10.1016/j.dsr2.2012.09.002. 51, 78, 103

Gandhi, N., Ramesh, R., Laskar, A. H., Sheshshayee, M. S., Shetye, S., Anilkumar, N., Patil, S. M., and Mohan, R. (2012). Zonal variability in primary production and nitrogen uptake rates in the southwestern Indian Ocean and the Southern Ocean. *Deep Sea Research Part I : Oceanographic Research Papers*, 67 :32–43. doi:10.1016/j.dsr.2012.05.003. 5

Gaspar, P., Georges, J.-Y., Fossette, S., Lenoble, A., Ferraroli, S., and Le Maho, Y. (2006). Marine animal behaviour : neglecting ocean currents can lead us up the wrong track. *Proceedings of the Royal Society B : Biological Sciences*, 273(1602) :2697–2702. doi:10.1098/rspb.2006.3623. 71

Gause, G. F. (1934). *The struggle for existence*. The Williams & Wilkins company,, Baltimore,, url : http://www.biodiversitylibrary.org/bibliography/4489. 6

Gauthier, S., Oeffner, J., and ODriscoll, R. L. (2014). Species composition and acoustic signatures of mesopelagic organisms in a subtropical convergence zone, the New Zealand Chatham Rise. *Marine Ecology Progress Series*, 503 :23–40. doi:10.3354/meps10731. 34, 96

Génin, A., Richard, G., Jouma'a, J., Picard, B., El Ksabi, N., Vacquié Garcia, J., and Guinet, C. (2015). Characterization of postdive recovery using sound recordings and its relationship to dive duration, exertion and foraging effort of southern elephant seals (Mirounga leonina). *Marine Mammal Science*. doi:10.1111/mms.12235. 56, 162

Genin, A., Jaffe, J. S., Reef, R., Richter, C., and Franks, P. J. S. (2005). Swimming Against the Flow : A Mechanism of Zooplankton Aggregation. *Science*, 308(5723) :860–862. doi:10.1126/science.1107834. 45

Gibbney, L. (1953). Delayed Implantation in the Elephant Seal. *Nature*, 172(4378) :590–591. doi:10.1038/172590a0. 30

Gillooly, J. F., Charnov, E. L., West, G. B., Savage, V. M., and Brown, J. H. (2002). Effect of size and temperature on developmental time. *Nature*, 417. doi:10.1038/417070a. 126

Gjøsaeter, J. and Kawaguchi, K. (1980). *A Review Of The World Resources Of Mesopelagic Fish Fao Fisheries Technical Paper No 193*. Food And Agriculture Organization Of The United Nations, url : http://archive.org/details/reviewoftheworld034721mbp. 33, 172

Gleiss, A. C., Wilson, R. P., and Shepard, E. L. C. (2011). Making overall dynamic body acceleration work : on the theory of acceleration as a proxy for energy expenditure. *Methods in Ecology and Evolution*, 2(1) :23–33. doi:10.1111/j.2041-210X.2010.00057.x. 161

Godø, O. R., Samuelsen, A., Macaulay, G. J., Patel, R., Hjøllo, S. S., Horne, J., Kaartvedt, S., and Johannessen, J. A. (2012). Mesoscale Eddies Are Oases for Higher Trophic Marine Life. *PLoS ONE*, 7(1) :e30161. doi:10.1371/journal.pone.0030161. 10, 122, 147

Goldbogen, J. A., Calambokidis, J., Shadwick, R. E., Oleson, E. M., McDonald, M. A., and Hildebrand, J. A. (2006). Kinematics of foraging dives and lunge-feeding in fin whales. *Journal of Experimental Biology*, 209(7) :1231–1244. doi:10.1242/jeb.02135. 46

Goldbogen, J. A., Hazen, E. L., Friedlaender, A. S., Calambokidis, J., DeRuiter, S. L., Stimpert, A. K., and Southall, B. L. (2015). Prey density and distribution drive the three-dimensional foraging strategies of the largest filter feeder. *Functional Ecology*, 29(7) :951–961. doi:10.1111/1365-2435.12395. 73, 78

Gould, J., Roemmich, D., Wijffels, S., Freeland, H., Ignaszewsky, M., Jianping, X., Pouliquen, S., Desaubies, Y., Send, U., Radhakrishnan, K., Takeuchi, K., Kim, K., Danchenkov, M., Sutton, P., King, B., Owens, B., and Riser, S. (2004). Argo profiling floats bring new era of in situ ocean observations. *Eos, Transactions American Geophysical Union*, 85(19) :185–191. doi:10.1029/2004EO190002. 18

Guinet, C., Jouventin, P., and Weimerskirch, H. (1992). Population changes, movements of southern elephant seals on Crozet and Kerguelen Archipelagos in the last decades. *Polar Biology*, 12(3-4) :349–356. doi:10.1007/BF00243106. 164

Guinet, C., Cherel, Y., Ridoux, V., and Jouventin, P. (1996). Consumption of marine resources by seabirds and seals in Crozet and Kerguelen waters : changes in relation to consumer biomass 1962–85. *Antarctic Science*, 8(01) :23–30. doi:10.1017/S0954102096000053. 35, 53

Guinet, C., Xing, X., Walker, E., Monestiez, P., Marchand, S., Picard, B., Jaud, T., Authier, M., Cotté, C., Dragon, A. C., Diamond, E., Antoine, D., Lovell, P., Blain, S., D'Ortenzio, F., and Claustre, H. (2013). Calibration procedures and first dataset of Southern Ocean chlorophyll a profiles collected by elephant seals equipped with a newly developed CTD-fluorescence tags. *Earth System Science Data*, 5(1) :15–29. doi:10.5194/essd-5-15-2013. 103, 110, 163

Guinet, C. (1991). Growth from Birth to Weaning in the Southern Elephant Seal (Mirounga leonina). *Journal of Mammalogy*, 72(3) :617–620. doi:10.2307/1382147. 30

Guinet, C., Jouventin, P., and Weimerskirch, H. (1999). Recent population change of the southern elephant seal at Îles Crozet and Îles Kerguelen : the end of the decrease ? *Antarctic Science*, 11(02). doi:10.1017/S0954102099000255. 28, 122, 165

Guinet, C., Vacquié-Garcia, J., Picard, B., Bessigneul, G., Le Bras, Y., Dragon, A. C., Viviant, M., Arnould, J. P. Y., and Bailleul, F. (2014). Southern elephant seal foraging success in relation to temperature and light conditions : insight into prey distribution. *Marine Ecology Progress Series*, 499 :285–301. doi:10.3354/meps10660. 51, 53, 55, 73, 77, 80, 93, 103, 110, 115, 172

Guisan, A. and Zimmermann, N. E. (2000). Predictive habitat distribution models in ecology. *Ecological Modelling*, 135(2–3) :147–186. doi:10.1016/S0304-3800(00)00354-9. 61, 135

Günther, A. C. L. G. (1887). *Report on the deep-sea fishes collected by H.M.S. Challenger during the years 1873-1876*. London, url : http://archive.org/details/reportondeepseaf00gn. 34

Haddock, S. H., Moline, M. A., and Case, J. F. (2010). Bioluminescence in the sea. *Annual Review of Marine Science*, 2(1) :443–493. doi:10.1146/annurev-marine-120308-081028. 33, 34

Haeckel, E. (1904). *Kunstformen der Natur*. url : http://gallica.bnf.fr/ark:/12148/btv1b525055842. 75

Hairston, N. G. (1993). Cause-Effect Relationships in Energy Flow, Trophic Structure, and Interspecific Interactions. *The American Naturalist*, 142(3) :379–411. ISSN 0003-0147, url : http://www.jstor.org/stable/2462650. 9

Halsey, L. G., Bost, C.-A., and Handrich, Y. (2007). A thorough and quantified method for classifying seabird diving behaviour. *Polar Biology*, 30(8) :991–1004. doi:10.1007/s00300-007-0257-3. 57, 58, 168, 214

Halsey, L. G., Green, J. A., Wilson, R. P., and Frappell, P. B. (2009). Accelerometry to Estimate Energy Expenditure during Activity : Best Practice with Data Loggers. *Physiological and Biochemical Zoology : Ecological and Evolutionary Approaches*, 82(4) :396–404. doi:10.1086/589815. 161

Handegard, N. O., Buisson, L. d., Brehmer, P., Chalmers, S. J., De Robertis, A., Huse, G., Kloser, R., Macaulay, G., Maury, O., Ressler, P. H., Stenseth, N. C., and Godø, O. R. (2013). Towards an acoustic-based coupled observation and modelling system for monitoring and predicting ecosystem dynamics of the open ocean. *Fish and Fisheries*, 14(4) :605–615. doi:10.1111/j.1467-2979.2012.00480.x. 14

Hanuise, N., Bost, C.-A., and Handrich, Y. (2013). Optimization of transit strategies while diving in foraging king penguins. *Journal of Zoology*, 290(3) :181–191. doi:10.1111/jzo.12026. 52, 166

Hanuise, N., Bost, C.-A., Huin, W., Auber, A., Halsey, L. G., and Handrich, Y. (2010). Measuring foraging activity in a deep-diving bird : comparing wiggles, oesophageal temperatures and beak-opening angles as proxies of feeding. *The Journal of Experimental Biology*, 213(22) : 3874–3880. doi:10.1242/jeb.044057. 51, 58

Hardin, G. (1960). The Competitive Exclusion Principle. *Science*, 131(3409) :1292–1297. doi:10.1126/science.131.3409.1292. 6

Hassrick, J. L., Crocker, D. E., Zeno, R. L., Blackwell, S. B., Costa, D. P., and Le Boeuf, B. J. (2007). Swimming speed and foraging strategies of northern elephant seals. *Deep Sea Research Part II : Topical Studies in Oceanography*, 54(3–4) :369–383. doi:10.1016/j.dsr2.2006.12.001. 52, 70, 85

Haury, L. R., McGowan, J. A., and Wiebe, P. H. (1978). Patterns and Processes in the Time-Space Scales of Plankton Distributions. In Steele, J. H., editor, *Spatial Pattern in Plankton Communities*, number 3 in NATO Conference Series, pages 277–327. Springer US. ISBN 978-1-4899-2197-0 978-1-4899-2195-6. doi:10.1007/978-1-4899-2195-6_12. 5

Hays, G. C. (2003). A review of the adaptive significance and ecosystem consequences of zooplankton diel vertical migrations. *Hydrobiologia*, 503(1-3) :163–170. doi:10.1023/B :HYDR.0000008476.23617.b0. 14, 33

Hedenstrom, A. and Alerstam, T. (1995). Optimal Flight Speed of Birds. *Philosophical Transactions of the Royal Society of London B : Biological Sciences*, 348(1326) :471–487. doi:10.1098/rstb.1995.0082. 20

Heerah, K., Hindell, M., Guinet, C., and Charrassin, J.-B. (2014). A new method to quantify within dive foraging behaviour in marine predators. *PLOS ONE*, 9(6) :1–15. doi:10.1371/journal.pone.0099329. 164, 168

Heerah, K., Hindell, M., Guinet, C., and Charrassin, J.-B. (2015). From high-resolution to low-resolution dive datasets : a new index to quantify the foraging effort of marine predators. *Animal Biotelemetry*, 3(1) :42. doi:10.1186/s40317-015-0074-3. 168

Heimark, R. J. and Heimark, G. M. (1986). Southern elephant seal pupping at Palmer Station, Antarctica. *Journal of mammalogy*, 67(1) :189–190. ISSN 0022-2372, url : `http://cat.inist.fr/?aModele=afficheN&cpsidt=7941187`. 28

Heithaus, M. R., Frid, A., Wirsing, A. J., and Worm, B. (2008). Predicting ecological consequences of marine top predator declines. *Trends in Ecology & Evolution*, 23(4) :202–210. doi:10.1016/j.tree.2008.01.003. 12

Hill, R. D. (1994). Theory of Geolocation by Light Levels. In Le Boeuf, B. J. and Laws, editors, *Elephant Seals : Population Ecology, Behavior, and Physiology*, pages 227–236. University of California Press, 1 edition. ISBN 978-0-520-08364-6, url : `https://books.google.fr/books?id=S1tTslFJkSQC&pg=PA227`. 156

Hill, R. D. and Braun, M. J. (2001). Geolocation by Light Level. In Sibert, J. R. and Nielsen, J. L., editors, *Electronic Tagging and Tracking in Marine Fisheries*, number 1 in Reviews : Methods and Technologies in Fish Biology and Fisheries, pages 315–330. Springer Netherlands. ISBN 978-90-481-5871-3 978-94-017-1402-0. doi:10.1007/978-94-017-1402-0_17. 104, 105

Hill, S., Burrows, M. T., and Hughes, R. N. (2002). Adaptive search in juvenile plaice foraging for aggregated and dispersed prey. *Journal of Fish Biology*, 61(5) :1255–1267. doi:10.1111/j.1095-8649.2002.tb02469.x. 95

Hindell, M., Burton, H., and Slip, D. (1991)a. Foraging areas of southern elephant seals, *Mirounga leonina* , as inferred from water temperature data. *Marine and Freshwater Research*, 42(2) :115. doi:10.1071/MF9910115. 28, 52

Hindell, M., Slip, D., and Burton, H. (1991)b. The Diving Behavior of Adult Male and Female Southern Elephant Seals, Mirounga-Leonina (Pinnipedia, Phocidae). *Australian Journal of Zoology*, 39(5) :595–619. doi:10.1071/ZO9910595. 117

Hindell, M. A., Bradshaw, C. J. A., Sumner, M. D., Michael, K. J., and Burton, H. R. (2003). Dispersal of female southern elephant seals and their prey consumption during the austral summer : relevance to management and oceanographic zones. *Journal of Applied Ecology*, 40 (4) :703–715. doi:10.1046/j.1365-2664.2003.00832.x. 35, 53

Hindell, M. A., McMahon, C. R., Bester, M. N., Boehme, L., Costa, D., Fedak, M. A., Guinet, C., Herraiz-Borreguero, L., Harcourt, R. G., Huckstadt, L., Kovacs, K. M., Lydersen, C., McIntyre, T., Muelbert, M., Patterson, T., Roquet, F., Williams, G., and Charrassin, J.-B. (2016). Circumpolar habitat use in the southern elephant seal : implications for foraging success and population trajectories. *Ecosphere*, 7(5). doi:10.1002/ecs2.1213. 28, 51, 77, 170

Hindle, A. G., Rosen, D. A. S., and Trites, A. W. (2010). Swimming depth and ocean currents affect transit costs in Steller sea lions Eumetopias jubatus. *Aquatic Biology*, 10(2) :139–148. doi:10.3354/ab00279. 161

Hoff, J. V. D. and Morrice, M. G. (2008). Sleeper shark (somniosus antarcticus) and other bite wounds observed on southern elephant seals (mirounga leonina) at macquarie island. *Marine Mammal Science*, 24(1) :239–247. doi:10.1111/j.1748-7692.2007.00181.x. 165

Hofmeyr, G. J. G. (2014). Mirounga leonina. *The IUCN Red List of Threatened Species*. doi:10.2305/IUCN.UK.2015-4.RLTS.T13583A45227247.en. 28

Hooker, S. K., Boyd, I. L., Jessopp, M., Cox, O., Blackwell, J., Boveng, P. L., and Bengtson, J. L. (2002). Monitoring the Prey-Field of Marine Predators : Combining Digital Imaging with Datalogging Tags. *Marine Mammal Science*, 18(3) :680–697. doi:10.1111/j.1748-7692.2002.tb01066.x. 52, 77, 99

Houston, A. I. and Carbone, C. (1992). The optimal allocation of time during the diving cycle. *Behavioral Ecology*, 3(3) :255–265. doi:10.1093/beheco/3.3.255. 20

Hovis, W. A., Clark, D. K., Anderson, F., Austin, R. W., Wilson, W. H., Baker, E. T., Ball, D., Gordon, H. R., Mueller, J. L., El-Sayed, S. Z., Sturm, B., Wrigley, R. C., and Yentsch, C. S. (1980). Nimbus-7 Coastal Zone Color Scanner : System Description and Initial Imagery. *Science*, 210(4465) :60–63. doi:10.1126/science.210.4465.60. 2, 3

Hunt, G. L. and Schneider, D. C. (1987). Scale-dependent processes in the physical and biological environment of marine birds. In Croxall, J. P., editor, *Seabirds : Feeding Ecology and Role in Marine Ecosystems*, pages 7–41. Cambridge University Press. ISBN 978-0-521-30178-7. 167

Hunt, G. L., Mehlum, F., Russell, R. W., Irons, D., Decker, N. D., and Becker, P. H. (1999). Physical processes, prey abundance and the foraging ecology of seabirds. volume 22, pages 2040–2056, Durban. BirdLife South Africa, url : `http://www.nhbs.com/series/89092`. 77, 167

Huntley, M. E., Lopez, M. D., and Karl, D. M. (1991). Top predators in the Southern ocean : a major leak in the biological carbon pump. *Science*, 253(5015) :64–66. doi:10.1126/science.1905841. 13

Hussey, N. E., Kessel, S. T., Aarestrup, K., Cooke, S. J., Cowley, P. D., Fisk, A. T., Harcourt, R. G., Holland, K. N., Iverson, S. J., Kocik, J. F., Flemming, J. E. M., and Whoriskey, F. G. (2015). Aquatic animal telemetry : A panoramic window into the underwater world. *Science*, 348(6240) :1255642. doi:10.1126/science.1255642. 168

Hutchinson, G. E. (1961). The Paradox of the Plankton. *The American Naturalist*, 95(882) : 137–145. doi:10.1086/282171. 6, 127

Irigoien, X., Klevjer, T. A., Røstad, A., Martinez, U., Boyra, G., Acuña, J. L., Bode, A., Echevarria, F., Gonzalez-Gordillo, J. I., Hernandez-Leon, S., Agusti, S., Aksnes, D. L., Duarte, C. M., and Kaartvedt, S. (2014). Large mesopelagic fishes biomass and trophic efficiency in the open ocean. *Nature Communications*, 5 :3271. doi:10.1038/ncomms4271. 33, 157

Iverson, R. L. (1990). Control of marine fish production. *Limnology and Oceanlogy*, 35(7) : 1593–1604. 126

Iwasa, Y. (1982). Vertical Migration of Zooplankton : A Game Between Predator and Prey. *The American Naturalist*, 120(2) :171–180. doi:10.1086/283980. 94

Iwata, T., Sakamoto, K. Q., Edwards, E. W. J., Staniland, I. J., Trathan, P. N., Goto, Y., Sato, K., Naito, Y., and Takahashi, A. (2015). The influence of preceding dive cycles on the foraging decisions of Antarctic fur seals. *Biology Letters*, 11(7) :20150227. doi:10.1098/rsbl.2015.0227. 69, 73

Jake Vander Zanden, M. and Fetzer, W. W. (2007). Global patterns of aquatic food chain length. *Oikos*, 116(8) :1378–1388. doi:10.1111/j.0030-1299.2007.16036.x. 9

Jansen, J. K., Boveng, P. L., and Bengtson, J. L. (1998). Foraging modes of chinstrap penguins : contrasts between day and night. *Marine Ecology Progress Series*, 165 :161–172. doi:10.3354/meps165161. 33, 104

Jaud, T., Dragon, A.-C., Vacquié-Garcia, J., and Guinet, C. (2012). Relationship between Chlorophyll a Concentration, Light Attenuation and Diving Depth of the Southern Elephant Seal Mirounga leonina. *PLoS ONE*, 7(10) :e47444. doi:10.1371/journal.pone.0047444. 73, 77, 93, 94, 106, 110, 117, 124, 156

Jennings, S. (2010). Size-based analyses of aquatic food webs. In Belgrano, A., Scharler, U. M., Dunne, J., and Ulanowicz, R. E., editors, *Aquatic Food Webs : An Ecosystem Approach*. Oxford University Press. ISBN 978-0-19-856483-6, url : `http://www.oxfordscholarship.com/view/10.1093/acprof:oso/9780198564836.001.0001/acprof-9780198564836`. 7

Johnson, M. and Tyack, P. (2003). A digital acoustic recording tag for measuring the response of wild marine mammals to sound. *IEEE Journal of Oceanic Engineering*, 28(1) :3–12. doi:10.1109/JOE.2002.808212. 73

Jouma'a, J., Le Bras, Y., Richard, G., Vacquié-Garcia, J., Picard, B., Ei Ksabi, N., and Guinet, C. (2015). Adjustment of diving behaviour with prey encounters and body condition in a deep diving predator : the Southern Elephant Seal. *Functional Ecology*. doi:10.1111/1365-2435.12514. 52, 57, 70, 80

Jouma'a, J., Le Bras, Y., Picard, B., and Guinet, C. (2017). Three-dimensional assessment of hunting strategies in a deep diving predator, southern elephant seal Mirounga leonina. *Marine Ecology Progress Series*, 573 :255–268. doi:10.3354/meps12191. 91, 97

Kaartvedt, S., Staby, A., and Aksnes, D. (2012). Efficient trawl avoidance by mesopelagic fishes causes large underestimation of their biomass. *Marine Ecology Progress Series*, 456 : 1–6. doi:10.3354/meps09785. 15, 97

Kahru, M., Mitchell, B. G., Gille, S. T., Hewes, C. D., and Holm-Hansen, O. (2007). Eddies enhance biological production in the Weddell-Scotia Confluence of the Southern Ocean. *Geophysical Research Letters*, 34(14) :L14603. doi:10.1029/2007GL030430. 73

Kaiser, M. (2011). *Marine ecology : processes, systems, and impacts*. Oxford University Press, Oxford New York. ISBN 9780199227020. 5

Kareiva, P. and Odell, G. (1987). Swarms of predators exhibits "preytaxis" if individual predators use area-restricted search. *The American Naturalist*, 130(2) :233–270, url : http://www.jstor.org/discover/10.2307/2461857. 20, 51, 52, 77, 147, 151, 152, 167

Kastak, D. and Schusterman, R. J. (1999). In-air and underwater hearing sensitivity of a northern elephant seal (mirounga angustirostris). *Canadian Journal of Zoology*, 77(11) : 1751–1758. doi:10.1139/z99-151. 168

Kienle, S. S. and Berta, A. (2015). The better to eat you with : the comparative feeding morphology of phocid seals (pinnipedia, phocidae). *Journal of Anatomy*, 228(3) :396–413. doi:10.1111/joa.12410. 161

Kirkman, S. P., Yemane, D. G., Lamont, T., Meÿer, M. A., and Pistorius, P. A. (2016). Foraging Behavior of Subantarctic Fur Seals Supports Efficiency of a Marine Reserve's Design. *PLOS ONE*, 11(5) :e0152370. doi:10.1371/journal.pone.0152370. 51, 77, 170

Klein, P. and Lapeyre, G. (2009). The Oceanic Vertical Pump Induced by Mesoscale and Submesoscale Turbulence. *Annual Review of Marine Science*, 1(1) :351–375. doi:10.1146/annurev.marine.010908.163704. 147

Kloser, R. J., Ryan, T. E., Young, J. W., and Lewis, M. E. (2009). Acoustic observations of micronekton fish on the scale of an ocean basin : potential and challenges. *ICES Journal of Marine Science*, 66(6) :998–1006. doi:10.1093/icesjms/fsp077. 13, 172

Kock, K.-H. (1987). Marine consumers : Fish and squid. *Environment International*, 13(1) :37–45. doi:10.1016/0160-4120(87)90042-0. 53

Kooyman, G. L., Cherel, Y., Maho, Y. L., Croxall, J. P., Thorson, P. H., Ridoux, V., and Kooyman, C. A. (1992). Diving Behavior and Energetics During Foraging Cycles in King Penguins. *Ecological Monographs*, 62(1) :143–163. doi:10.2307/2937173. 33, 104

Kooyman, G. L. (1989). *Diverse Divers : Physiology and Behavior*. Springer-Verlag. ISBN 978-3-540-50274-6. 00513. 51

Kostianoy, A., Ginzburg, A., Lebedev, S., Frankignoulle, M., and Delille, B. (2004). Oceanic fronts in the southern indian ocean as inferred from the NOAA SST, TOPEX/poseidon and ERS-2 altimetry data. *Gayana (Concepción)*, 68(2). doi:10.4067/s0717-65382004000300003. 36

Kotliar, N. B. and Wiens, J. A. (1990). Multiple Scales of Patchiness and Patch Structure : A Hierarchical Framework for the Study of Heterogeneity. *Oikos*, 59(2) :253–260. doi:10.2307/3545542. 4, 150, 158

Koubbi, C. d. B. . P., Griffiths , Cedric d'Udekem d'Acoz, A. V. d. P. w. H. B. R., Danis , Susie Grant, J. G. C. H. G. H. B. B. D., and Huettmann, A. P. . Y. R.-C. F., editors. (2014). *Biogeographic Atlas of the Southern Ocean*. Scientific Committee on Antarctic Research, Cambridge, 1st edition edition. ISBN 978-0-948277-28-3, url : http://atlas.biodiversity.aq/. 34, 37

Koubbi, P., Moteki, M., Duhamel, G., Goarant, A., Hulley, P.-A., O'Driscoll, R., Ishimaru, T., Pruvost, P., Tavernier, E., and Hosie, G. (2011). Ecoregionalization of myctophid fish in the Indian sector of the Southern Ocean : Results from generalized dissimilarity models. *Deep Sea Research Part II : Topical Studies in Oceanography*, 58(1–2) :170–180. doi:10.1016/j.dsr2.2010.09.007. 123

Koz, A. (1995). A review of the trophic role of mesopelagic fish of the family myctophidae in the southern ocean ecosystem. *CCAMLR Science*, 2 :71–77, url : http://archive.ccamlr.org/ccamlr_science/Vol-02-1995/05kozlov.PDF. 33

Kozlov, A. (1995). A REVIEW OF THE TROPHIC ROLE OF MESOPELAGIC FISH OF THE FAMILY MYCTOPHIDAE IN THE SOUTHERN OCEAN ECOSYSTEM. *CCAMLR Science*, 2 :71–77, url : https://www.ccamlr.org/en/publications/science_journal/ccamlr-science-volume-2/ccamlr-science-volume-271-77. 13

Kuhn, C. E., Crocker, D. E., Tremblay, Y., and Costa, D. P. (2009). Time to eat : measurements of feeding behaviour in a large marine predator, the northern elephant seal Mirounga angustirostris. *Journal of Animal Ecology*, 78(3) :513–523. doi:10.1111/j.1365-2656.2008.01509.x. 69

Labrousse, S., Vacquié-Garcia, J., Heerah, K., Guinet, C., Sallée, J.-B., Authier, M., Picard, B., Roquet, F., Bailleul, F., Hindell, M., and Charrassin, J.-B. (2015). Winter use of sea ice and ocean water mass habitat by southern elephant seals : The length and breadth of the mystery. *Progress in Oceanography*, 137, Part A :52–68. doi:10.1016/j.pocean.2015.05.023. 145

Laplace, P.-S. (1809). Mémoire sur les approximations des formules qui sont fonctions de très grands nombres et sur leur application aux probabilités. In *Oeuvres complètes de Laplace*, number 12 in Mémoires de l'Académie des Sciences de Paris, pages 301–345. Gauthier-Villars, Paris, académie des sciences edition, url : http://gallica.bnf.fr/ark:/12148/bpt6k77600r. 249

Laplanche, C., Marques, T. A., and Thomas, L. (2015). Tracking marine mammals in 3d using electronic tag data. *Methods in Ecology and Evolution*, pages n/a–n/a. doi:10.1111/2041-210X.12373. 98

Larkin, P. A. (1996). Concepts and issues in marine ecosystem management. *Reviews in Fish Biology and Fisheries*, 6(2) :139–164. doi:10.1007/BF00182341. 21

Lascelles, B. G., Taylor, P. R., Miller, M. G. R., Dias, M. P., Oppel, S., Torres, L., Hedd, A., Le Corre, M., Phillips, R. A., Shaffer, S. A., Weimerskirch, H., and Small, C. (2016). Applying global criteria to tracking data to define important areas for marine conservation. *Diversity and Distributions*, 22(4) :422–431. doi:10.1111/ddi.12411. 51, 77, 170

Lawson, G. L., Hückstädt, L. A., Lavery, A. C., Jaffré, F. M., Wiebe, P. H., Fincke, J. R., Crocker, D. E., and Costa, D. P. (2015). Development of an animal-borne "sonar tag" for quantifying prey availability : test deployments on northern elephant seals. *Animal Biotelemetry*, 3(1) : 22. doi:10.1186/s40317-015-0054-7. 74, 99, 104, 120, 169

Le Bras, Y. (2012). Master 1 report : Développement d'une procdure de traitement des données issues de loggers embarqués sur des éléphants de mer austraux. Master's thesis, École Nationale Supérieure d'Agronomie de Toulouse (INP–ENSAT), France. 43, 168

Le Bras, Y. (2017). rbl : Biologging tools for diving predators in r, url : https://github.com/SESman/rbl. 0.1.28-4605a15. 42, 55, 80, 108

Le Bras, Y., Jouma'a, J., Picard, B., and Guinet, C. (2016). How Elephant Seals (Mirounga leonina) Adjust Their Fine Scale Horizontal Movement and Diving Behaviour in Relation to Prey Encounter Rate. *PLOS ONE*, 11(12) :e0167226. doi:10.1371/journal.pone.0167226. 81, 96, 97

Leboeuf, B. J., Costa, D. P., Huntley, A. C., Kooyman, G. L., and Davis, R. W. (1986). Pattern and depth of dives in Northern elephant seals, Mirounga angustirostris. *Journal of Zoology*, 208(1) :1–7. doi:10.1111/j.1469-7998.1986.tb04705.x. 31, 166

Leboeuf, B., Costa, D., Huntley, A., and Feldkamp, S. (1988). Continuous, Deep Diving in Female Northern Elephant Seals, Mirounga-Angustirostris. *Canadian Journal of Zoology*, 66 (2) :446–458. doi:10.1139/z88-064. 77

Lehodey, P., Senina, I., Sibert, J., Bopp, L., Calmettes, B., Hampton, J., and Murtugudde, R. (2010)a. Preliminary forecasts of Pacific bigeye tuna population trends under the A2 IPCC scenario. *Progress in Oceanography*, 86(1–2) :302–315. doi:10.1016/j.pocean.2010.04.021. 122

Lehodey, P., Senina, I., and Murtugudde, R. (2008). A spatial ecosystem and populations dynamics model (SEAPODYM) – Modeling of tuna and tuna-like populations. *Progress in Oceanography*, 78(4) :304–318. doi:10.1016/j.pocean.2008.06.004. 122

Lehodey, P., Murtugudde, R., and Senina, I. (2010)b. Bridging the gap from ocean models to population dynamics of large marine predators : A model of mid-trophic functional groups. *Progress in Oceanography*, 84(1–2) :69–84. doi:10.1016/j.pocean.2009.09.008. 117, 122, 126, 141

Lehodey, P., Senina, I., Calmettes, B., Hampton, J., and Nicol, S. (2013). Modelling the impact of climate change on Pacific skipjack tuna population and fisheries. *Climatic Change*, 119(1) : 95–109. doi:10.1007/s10584-012-0595-1. 122

Lehodey, P., Conchon, A., Senina, I., Domokos, R., Calmettes, B., Jouanno, J., Hernandez, O., and Kloser, R. (2014). Optimization of a micronekton model with acoustic data. *ICES Journal of Marine Science : Journal du Conseil*, page fsu233. doi:10.1093/icesjms/fsu233. 125, 126

Levenson, D. H. and Schusterman, R. J. (1999). Dark Adaptation and Visual Sensitivity in Shallow and Deep-Diving Pinnipeds1. *Marine Mammal Science*, 15(4) :1303–1313. doi:10.1111/j.1748-7692.1999.tb00892.x. 00048. 95, 167

Levin, S. A. (1992). The Problem of Pattern and Scale in Ecology : The Robert H. MacArthur Award Lecture. *Ecology*, 73(6) :1943–1967. doi:10.2307/1941447. 77

Levitus, S., Antonov, J., Baranova, O., Boyer, T., Coleman, C., Garcia, H., Grodsky, A., Johnson, D., Locarnini, R., Mishonov, A., Reagan, J., Sazama, C., Seidov, D., Smolyar, I., Yarosh, E., and Zweng, M. (2013). The World Ocean Database. *Data Science Journal*, 12(0). doi:10.2481/dsj.WDS-041. 18

Lévy, M., Iovino, D., Resplandy, L., Klein, P., Madec, G., Tréguier, A.-M., Masson, S., and Takahashi, K. (2012). Large-scale impacts of submesoscale dynamics on phytoplankton : Local and remote effects. *Ocean Modelling*, 43-44 :77–93. doi:10.1016/j.ocemod.2011.12.003. 6, 11

Liebsch, N., Wilson, R. P., Bornemann, H., Adelung, D., and Plötz, J. (2007). Mouthing off about fish capture : Jaw movement in pinnipeds reveals the real secrets of ingestion. *Deep Sea Research Part II : Topical Studies in Oceanography*, 54(3–4) :256–269. doi:10.1016/j.dsr2.2006.11.014. 160

Lindeman, R. L. (1942). The Trophic-Dynamic Aspect of Ecology. *Ecology*, 23(4) :399–417. doi:10.2307/1930126. 7, 126

Logerwell, E. A. and Wilson, C. D. (2004). Species discrimination of fish using frequency-dependent acoustic backscatter. *ICES Journal of Marine Science : Journal du Conseil*, 61(6) : 1004–1013. doi:10.1016/j.icesjms.2004.04.004. 16

Longhurst, A. R., Bedo, A. W., Harrison, W. G., Head, E. J. H., and Sameoto, D. D. (1990). Vertical flux of respiratory carbon by oceanic diel migrant biota. *Deep Sea Research Part A. Oceanographic Research Papers*, 37(4) :685–694. doi:10.1016/0198-0149(90)90098-G. 14, 33

Longhurst, A. R. (2007). *Ecological Geography of the Sea*. Academic Press, Burlington, 2 edition. ISBN 978-0-12-455521-1. doi:10.1016/B978-012455521-1/50009-7. 37

Loots, C., Koubbi, P., and Duhamel, G. (2007). Habitat modelling of Electrona antarctica (Myctophidae, Pisces) in Kerguelen by generalized additive models and geographic information systems. *Polar Biology*, 30(8) :951–959. doi:10.1007/s00300-007-0253-7. 34, 123

Lund, U. and Agostinelli, C. (2012). *CircStats : Circular Statistics, from "Topics in circular Statistics" (2001)*. url : `http://CRAN.R-project.org/package=CircStats`. 59

Lundvall, D., Svanbäck, R., Persson, L., and Byström, P. (1999). Size-dependent predation in piscivores : interactions between predator foraging and prey avoidance abilities. *Canadian Journal of Fisheries and Aquatic Sciences*, 56(7) :1285–1292. doi:10.1139/f99-058. 7

Lythgoe, J. N. and Dartnall, H. J. A. (1970). A "Deep Sea Rhodopsin" in a Mammal. *Nature*, 227(5261) :955–956. doi:10.1038/227955a0. 95

Lévy, M. (2003). Mesoscale variability of phytoplankton and of new production : Impact of the large-scale nutrient distribution. *Journal of Geophysical Research : Oceans*, 108(C11) :n/a–n/a. doi:10.1029/2002JC001577. 3358. 6, 11

Lévy, M., Ferrari, R., Franks, P. J. S., Martin, A. P., and Rivière, P. (2012). Bringing physics to life at the submesoscale. *Geophysical Research Letters*, 39(14) :n/a–n/a. doi:10.1029/2012GL052756. L14602. 6, 11, 147

MacArthur, R. H. and Pianka, E. R. (1966). On Optimal Use of a Patchy Environment. *The American Naturalist*, 100(916) :603–609. ISSN 0003-0147, url : `http://www.jstor.org/stable/2459298`. 19, 20, 51, 76

Mann, K., Lazier, J., Mann, K., and Lazier, J. (2005). Marine Ecology Comes of Age. In *Dynamics of Marine Ecosystems*, pages 1–6. Blackwell Publishing Ltd. ISBN 978-1-118-68790-1, url : `http://onlinelibrary.wiley.com/doi/10.1002/9781118687901.ch1/summary`. 10

Martin, A. (2003). Phytoplankton patchiness : the role of lateral stirring and mixing. *Progress in Oceanography*, 57(2) :125 – 174. doi:http ://dx.doi.org/10.1016/S0079-6611(03)00085-5. 6, 11

Matsumura, M., Watanabe, Y. Y., Robinson, P. W., Miller, P. J. O., Costa, D. P., and Miyazaki, N. (2011). Underwater and surface behavior of homing juvenile northern elephant seals. *Journal of Experimental Biology*, 214(4) :629–636. doi:10.1242/jeb.048827. 78

McCann, T. S. (1981). Aggression and sexual activity of male Southern elephant seals, Mirounga leonina. *Journal of Zoology*, 195(3) :295–310. doi:10.1111/j.1469-7998.1981.tb03467.x. 28

McClain, C. R. (2009). A Decade of Satellite Ocean Color Observations. *Annual Review of Marine Science*, 1(1) :19–42. doi:10.1146/annurev.marine.010908.163650. 11

McConnell, B. J., Chambers, C., and Fedak, M. A. (1992). Foraging ecology of southern elephant seals in relation to the bathymetry and productivity of the Southern Ocean. *Antarctic Science*, 4(04) :393–398. doi:10.1017/S0954102092000580. 31, 52

McGillicuddy, D. J., Robinson, A. R., Siegel, D. A., Jannasch, H. W., Johnson, R., Dickey, T. D., McNeil, J., Michaels#, A. F., and Knap, A. H. (1998). Influence of mesoscale eddies on new production in the sargasso sea. *Nature*, 394(6690) :263–266. doi:10.1038/28367. 147

Mcgovern, K. A., Marshall, c. D., and Davis, R. W. (2015). Are Vibrissae Viable Sensory Structures for Prey Capture in Northern Elephant Seals, Mirounga angustirostris? *The Anatomical Record*, 298(4) :750–760. doi:10.1002/ar.23061. 95, 167

McIntyre, T. (2014). Trends in tagging of marine mammals : a review of marine mammal biologging studies. *African Journal of Marine Science*, 36(4) :409–422. doi:10.2989/1814232X.2014.976655. 23, 34, 53, 103, 168

McIntyre, T., Bruyn, P. J. N. d., Ansorge, I. J., Bester, M. N., Bornemann, H., Plötz, J., and Tosh, C. A. (2010). A lifetime at depth : vertical distribution of southern elephant seals in the water column. *Polar Biology*, 33(8) :1037–1048. doi:10.1007/s00300-010-0782-3. 17, 31, 78, 103

McIntyre, T., Stansfield, L. J., Bornemann, H., Plötz, J., and Bester, M. N. (2013). Hydrographic influences on the summer dive behaviour of Weddell seals (Leptonychotes weddellii) in Atka Bay, Antarctica. *Polar Biology*, 36(11) :1693–1700. doi:10.1007/s00300-013-1384-7. 51, 92, 94

McIntyre, T., Ansorge, I. J., Bornemann, H., Pltz, J., Tosh, C. A., and Bester, M. N. (2011)a. Elephant seal dive behaviour is influenced by ocean temperature : implications for climate change impacts on an ocean predator. *Marine Ecology Progress Series*, 441 :257–272. doi:10.3354/meps09383. 171

McIntyre, T., Bornemann, H., Plötz, J., Tosh, C. A., and Bester, M. N. (2011)b. Water column use and forage strategies of female southern elephant seals from Marion Island. *Marine Biology*, 158(9) :2125–2139. doi:10.1007/s00227-011-1719-2. 51, 77, 93

McIntyre, T., Ansorge, I. J., Bornemann, H., Pltz, J., Tosh, C. A., and Bester, M. N. (2012). REPLY COMMENT Elephant seal foraging dives do indeed track prey distribution, but temperature influences the distribution of prey : Reply to Boersch-Supan et al. (2012). *Marine Ecology Progress Series*, 461 :299–303. doi:10.3354/meps09891. 171

McMahon, C. R., Burton, H., Slip, D., McLean, S., and Bester, M. (2000). Field immobilisation of southern elephant seals with intravenous tiletamine and zolazepam. *Veterinary Record*, 146(9) :251–254. doi:10.1136/vr.146.9.251. 42, 54, 79, 105

McMahon, C. R., Burton, H. R., and Bester, M. N. (2003). A demographic comparison of two southern elephant seal populations. *Journal of Animal Ecology*, 72(1) :61–74. doi:10.1046/j.1365-2656.2003.00685.x. 122, 164, 165

McMahon, C. R., Bester, M. N., Burton, H. R., Hindell, M. A., and Bradshaw, C. J. A. (2005). Population status, trends and a re-examination of the hypotheses explaining the recent declines of the southern elephant seal Mirounga leonina. *Mammal Review*, 35(1) :82–100. doi:10.1111/j.1365-2907.2005.00055.x. 28

McMahon, C. R., Field, I. C., Bradshaw, C. J. A., White, G. C., and Hindell, M. A. (2008). Tracking and data—logging devices attached to elephant seals do not affect individual mass gain or survival. *Journal of Experimental Marine Biology and Ecology*, 360(2) :71–77. doi:10.1016/j.jembe.2008.03.012. 103, 165

McMahon, C. R., Bester, M. N., Hindell, M. A., Brook, B. W., and Bradshaw, C. J. A. (2009). Shifting trends : detecting environmentally mediated regulation in long-lived marine vertebrates using time-series data. *Oecologia*, 159(1) :69–82. doi:10.1007/s00442-008-1205-9. 28

McNamara, J. (1982). Optimal patch use in a stochastic environment. *Theoretical Population Biology*, 21(2) :269–288. doi:10.1016/0040-5809(82)90018-1. 51

Ménard, F., Lorrain, A., Potier, M., and Marsac, F. (2007). Isotopic evidence of distinct feeding ecologies and movement patterns in two migratory predators (yellowfin tuna and swordfish) of the western Indian Ocean. *Marine Biology*, 153(2) :141–152. doi:10.1007/s00227-007-0789-7. 13

Micheli, F. (1999). Eutrophication, Fisheries, and Consumer-Resource Dynamics in Marine Pelagic Ecosystems. *Science*, 285(5432) :1396–1398. doi:10.1126/science.285.5432.1396. 9, 11

Miller, P. J. O., Biuw, M., Watanabe, Y. Y., Thompson, D., and Fedak, M. A. (2012). Sink fast and swim harder! Round-trip cost-of-transport for buoyant divers. *The Journal of Experimental Biology*, 215(20) :3622–3630. doi:10.1242/jeb.070128. 52, 70

Mitani, Y., Watanabe, Y., Sato, K., Cameron, M. F., and Naito, Y. (2004). 3d diving behavior of Weddell seals with respect to prey accessibility and abundance. *Marine Ecology Progress Series*, 281 :275–281. doi:10.3354/meps281275. 78

Mitani, Y., Andrews, R. D., Sato, K., Kato, A., Naito, Y., and Costa, D. P. (2010). Three-dimensional resting behaviour of northern elephant seals : drifting like a falling leaf. *Biology Letters*, 6(2) :163–166. doi:10.1098/rsbl.2009.0719. 00039. 19, 51, 73, 78, 120, 132

Mongin, M., Molina, E., and Trull, T. W. (2008). Seasonality and scale of the Kerguelen plateau phytoplankton bloom : A remote sensing and modeling analysis of the influence of natural iron fertilization in the Southern Ocean. *Deep Sea Research Part II : Topical Studies in Oceanography*, 55(5-7) :880–892. doi:10.1016/j.dsr2.2007.12.039. 37

Monte, S. D., Cotté, C., d'Ovidio, F., Lévy, M., Corre, M. L., and Weimerskirch, H. (2012). Frigatebird behaviour at the ocean–atmosphere interface : integrating animal behaviour with multi-satellite data. *Journal of The Royal Society Interface*, 9(77) :3351–3358. doi:10.1098/rsif.2012.0509. 77, 115

Moore, J. K. and Abbott, M. R. (2000). Phytoplankton chlorophyll distributions and primary production in the Southern Ocean. *Journal of Geophysical Research*, 105(C12). doi:10.1029/1999JC000043. 37, 141

Morel, A. and Berthon, J.-F. (1989). Surface pigments, algal biomass profiles, and potential production of the euphotic layer : Relationships reinvestigated in view of remote-sensing applications. *Limnology and Oceanography*, 34(8) :1545–1562. doi:10.4319/lo.1989.34.8.1545. 124

Morel, A. (1991). Light and marine photosynthesis : a spectral model with geochemical and climatological implications. *Progress in Oceanography*, 26(3) :263–306. doi:10.1016/0079-6611(91)90004-6. 126

Mulet, S., Rio, M. H., Mignot, A., Guinehut, S., and Morrow, R. (2012). A new estimate of the global 3d geostrophic ocean circulation based on satellite data and in-situ measurements. *Deep Sea Research Part II : Topical Studies in Oceanography*, 77–80 :70–81. doi:10.1016/j.dsr2.2012.04.012. 127, 141

Murray, D. (1981). The breeding of the Southern Elephant Seal, (mirounga leonina l.), on the Antartic continent. *Polar Record*, 20(127) :370–371. doi:10.1017/S0032247400018854. 28

Naimi, B. (2015). *usdm : Uncertainty Analysis for Species Distribution Models*. url : `http://CRAN.R-project.org/package=usdm`. R package version 1.1-15. 61

Naito, Y. (2007). How can we observe the underwater feeding behavior of endotherms ? *Polar Science*, 1(2–4) :101–111. doi:10.1016/j.polar.2007.10.001. 17, 103, 160

Naito, Y., Bornemann, H., Takahashi, A., McIntyre, T., and Plötz, J. (2010). Fine-scale feeding behavior of Weddell seals revealed by a mandible accelerometer. *Polar Science*, 4(2) :309–316. doi:10.1016/j.polar.2010.05.009. 51, 103

Naito, Y., Costa, D. P., Adachi, T., Robinson, P. W., Fowler, M., and Takahashi, A. (2013). Unravelling the mysteries of a mesopelagic diet : a large apex predator specializes on small prey. *Functional Ecology*, 27(3) :710–717. doi:10.1111/1365-2435.12083. 52, 74, 77, 95, 99, 104, 120, 167, 169

Nakagawa, S. and Schielzeth, H. (2013). A general and simple method for obtaining R2 from generalized linear mixed-effects models. *Methods in Ecology and Evolution*, 4(2) :133–142. doi:10.1111/j.2041-210x.2012.00261.x. 61

Narazaki, T., Sato, K., Abernathy, K. J., Marshall, G. J., and Miyazaki, N. (2009). Sea turtles compensate deflection of heading at the sea surface during directional travel. *Journal of Experimental Biology*, 212(24) :4019–4026. doi:10.1242/jeb.034637. 78

Neighbors, M. A. and Nafpaktitis, B. G. (1982). Lipid compositions, water contents, swimbladder morphologies and buoyancies of nineteen species of midwater fishes (18 myctophids and 1 neoscopelid). *Marine Biology*, 66(3) :207–215. doi:10.1007/bf00397024. 33

Nel, D. C., Lutjeharms, J. R. E., Pakhomov, E. A., Ansorge, I. J., Ryan, P. G., and Klages, N. T. W. (2001). Exploitation of mesoscale oceanographic features by grey-headed albatross Thalassarche chrysostoma in the southern Indian Ocean. *Marine Ecology Progress Series*, 217 : 15–26. doi:10.3354/meps217015. 10, 128

Nevitt, G. A. (2000). Olfactory Foraging by Antarctic Procellariiform Seabirds : Life at High Reynolds Numbers. *Biological Bulletin*, 198(2) :245–253. doi:10.2307/1542527. 167

Nevitt, G. A. and Bonadonna, F. (2005). Sensitivity to dimethyl sulphide suggests a mechanism for olfactory navigation by seabirds. *Biology Letters*, 1(3) :303–305. doi:10.1098/rsbl.2005.0350. 167

Nevitt, G. A., Veit, R. R., and Kareiva, P. (1995). Dimethyl sulphide as a foraging cue for Antarctic Procellariiform seabirds. *Nature*, 376(6542) :680–682. doi:10.1038/376680ao. 167

Ng, P. and Maechler, M. (2007). A fast and efficient implementation of qualitatively constrained quantile smoothing splines. *Statistical Modelling*, 7(4) :315–328. doi:10.1177/1471082X0700700403. 109

Nordstrom, C. A., Battaile, B. C., Cotté, C., and Trites, A. W. (2013). Foraging habitats of lactating northern fur seals are structured by thermocline depths and submesoscale fronts in the eastern Bering Sea. *Deep Sea Research Part II : Topical Studies in Oceanography*, 88–89 : 78–96. doi:10.1016/j.dsr2.2012.07.010. 77, 115

Nowacek, D. P., Johnson, M. P., Tyack, P. L., Shorter, K. A., McLellan, W. A., and D, A. P. (2001). Buoyant balaenids : the ups and downs of buoyancy in right whales. *Proceedings of the Royal Society of London B : Biological Sciences*, 268(1478) :1811–1816. doi:10.1098/rspb.2001.1730. 161

Nylander, M. W. (1866). Les Lichens Du Jardin Du Luxembourg. *Bulletin de la Société Botanique de France*, 13(7) :364–371. doi:10.1080/00378941.1866.10827433. 169

O'Driscoll, R. L., Rose, G. A., and Anderson, J. T. (2002). Counting capelin : a comparison of acoustic density and trawl catchability. *ICES Journal of Marine Science : Journal du Conseil*, 59 (5) :1062–1071. doi:10.1006/jmsc.2002.1262. 17

Orsi, A. H., Whitworth III, T., and Nowlin Jr., W. D. (1995). On the meridional extent and fronts of the Antarctic Circumpolar Current. *Deep Sea Research Part I : Oceanographic Research Papers*, 42(5) :641–673. doi:10.1016/0967-0637(95)00021-W. 36

O'Toole, M. D. and Lea, M.-A. (2014). Estimating Trans-Seasonal Variability in Water Column Biomass for a Highly Migratory, Deep Diving Predator. *Plos One*, 9(11) :e113171. doi:10.1371/journal.pone.0113171. 104, 106

Ozyagcilar, T. (2015). Implementing a Tilt-Compensated eCompass using Accelerometer and Magnetometer Sensors. Application Note AN4248, Freescale Semiconducto, url : `https://cache.freescale.com/files/sensors/doc/app_note/AN4248.pdf`. 46

Pakhomov, E. A., Perissinotto, R., and McQuaid, C. D. (1996). Prey composition and daily rations of myctophid fishes in the Southern Ocean. *Marine Ecology Progress Series*, 134 :1–14. doi:10.3354/meps134001. 14, 32, 33, 34, 53

Pakhomov, E., Perissinotto, R., and Mcquaid, C. (1994). Comparative Structure of the Macrozooplankton Micronekton Communities of the Subtropical and Antarctic Polar Fronts. *Marine Ecology Progress Series*, 111(1-2) :155–169. doi:10.3354/meps111155. 34, 104

Pakhomov, E., Yamamura, O., Advisory Panel on Micronekton Sampling Inter-calibration Experiment, and North Pacific Marine Science Organization. (2010). *Report of the Advisory Panel on Micronekton Sampling Inter-calibration Experiment*. North Pacific Marine Science Organization (PICES), Sidney, B.C. ISBN 1-897176-69-4 978-1-897176-69-6, url : http://www.pices.int/publications/scientific_reports/Report38/Rep38.pdf. 15, 53, 104

Parent, L., Ferry, N., Barnier, B., Garric, G., Bricaud, C., Testut, C.-E., Galloudec, O. L., Lellouche, J.-M., Greiner, E., Drevillon, M., Rémy, E., Molines, J.-M., Guinehut, S., and Cabanes, C. (2012). Global eddy-permitting ocean reanalyses and simulations of the period 1992 to present. 127

Park, Y.-H., Roquet, F., Durand, I., and Fuda, J.-L. (2008). Large-scale circulation over and around the northern kerguelen plateau. *Deep Sea Research Part II : Topical Studies in Oceanography*, 55(5-7) :566–581. doi:10.1016/j.dsr2.2007.12.030. 36

Park, Y.-H., Durand, I., Kestenare, E., Rougier, G., Zhou, M., d'Ovidio, F., Cotté, C., and Lee, J.-H. (2014). Polar front around the kerguelen islands : An up-to-date determination and associated circulation of surface/subsurface waters. *Journal of Geophysical Research : Oceans*, 119(10) :6575–6592. doi:10.1002/2014jc010061. 36, 38

Parker, G. A. and Stuart, R. A. (1976). Animal Behavior as a Strategy Optimizer : Evolution of Resource Assessment Strategies and Optimal Emigration Thresholds. *The American Naturalist*, 110(976) :1055–1076. ISSN 0003-0147, url : http://www.jstor.org/stable/2460030. 52

Pascal, B. (1663). *Traitez de l'équilibre des liqueurs et de la pesanteur de la masse de l'air*. chez Guillaume Desprez, A Paris, url : http://gallica.bnf.fr/ark:/12148/bpt6k577191. 2

Pauly, D. and Christensen, V. (1995). Primary production required to sustain global fisheries. *Nature*, 374(6519) :255–257. doi:10.1038/374255a0. 9

Pauly, D., Christensen, V., Dalsgaard, J., Froese, R., and Torres, F. (1998). Fishing Down Marine Food Webs. *Science*, 279(5352) :860–863. doi:10.1126/science.279.5352.860. 12

Pauly, D., Christensen, V., and Walters, C. (2000). Ecopath, Ecosim, and Ecospace as tools for evaluating ecosystem impact of fisheries. *ICES Journal of Marine Science : Journal du Conseil*, 57(3) :697–706. doi:10.1006/jmsc.2000.0726. 22

Pearcy, W. G. (1983). Quantitative Assessment of the Vertical Distributions of Micronektonic Fishes with Opening/Closing Midwater Trawls. *Biological Oceanography*, 2(2-4) :289–310. doi:10.1080/01965581.1983.10749463. 00015. 15, 16

Pearre, S. (2003). Eat and run ? The hunger/satiation hypothesis in vertical migration : history, evidence and consequences. *Biological Reviews*, 78(1) :1–79. doi:10.1017/S146479310200595X. 13, 33

Photopoulou, T., Lovell, P., Fedak, M. A., Thomas, L., and Matthiopoulos, J. (2015). Efficient abstracting of dive profiles using a broken-stick model. *Methods in Ecology and Evolution*, 6 (3) :278–288. doi:10.1111/2041-210X.12328. 168, 214, 217

Pierce, G. J. and Ollason, J. G. (1987). Eight Reasons Why Optimal Foraging Theory Is a Complete Waste of Time. *Oikos*, 49(1) :111–118. doi:10.2307/3565560. 19, 165

Pimm, S. L. and Rice, J. C. (1987). The dynamics of multispecies, multi-life-stage models of aquatic food webs. *Theoretical Population Biology*, 32(3) :303–325. doi:10.1016/0040-5809(87)90052-9. 7

Pimm, S. L., Lawton, J. H., and Cohen, J. E. (1991). Food web patterns and their consequences. *Nature*, 350(6320) :669–674. doi:10.1038/350669a0. 7

Pinaud, D. and Weimerskirch, H. (2007). At-sea distribution and scale-dependent foraging behaviour of petrels and albatrosses : a comparative study. *Journal of Animal Ecology*, 76(1) : 9–19. doi:10.1111/j.1365-2656.2006.01186.x. 167

Pinheiro, J., Bates, D., DebRoy, S., Sarkar, D., and R Core Team. (2015). *nlme : Linear and Nonlinear Mixed Effects Models*. url : http://CRAN.R-project.org/package=nlme. 60

Pitchford, J. and Brindley, J. (1999). Iron limitation, grazing pressure and oceanic high nutrient-low chlorophyll (HNLC) regions. *Journal of Plankton Research*, 21(3) :525–547. doi:10.1093/plankt/21.3.525. 36

Plagányi, É. E. and Butterworth, D. S. (2004). A critical look at the potential of Ecopath with ecosim to assist in practical fisheries management. *African Journal of Marine Science*, 26(1) : 261–287. doi:10.2989/18142320409504061. 22

Polovina, J. J. (1984). An overview of the ECOPATH model. *ICLARM Fishbyte*, 2(2) :2–7, url : http://137.110.142.7/publications/CR/1984/8472.PDF. 22

Polovina, J., Uchida, I., Balazs, G., Howell, E. A., Parker, D., and Dutton, P. (2006). The Kuroshio Extension Bifurcation Region : A pelagic hotspot for juvenile loggerhead sea turtles. *Deep Sea Research Part II : Topical Studies in Oceanography*, 53(3–4) :326–339. doi:10.1016/j.dsr2.2006.01.006. 10

Ponganis, P. J. (2015). *Diving Physiology of Marine Mammals and Seabirds*. Cambridge University Press. ISBN 9780521765558, url : http://www.cambridge.org/fr/academic/subjects/life-sciences/zoology/diving-physiology-marine-mammals-and-seabirds. 167

Pusch, C., Hulley, P. A., and Kock, K. H. (2004). Community structure and feeding ecology of mesopelagic fishes in the slope waters of King George Island (South Shetland Islands, Antarctica). *Deep Sea Research Part I : Oceanographic Research Papers*, 51(11) :1685–1708. doi:10.1016/j.dsr.2004.06.008. 34

Pyke, G. (1984). Optimal Foraging Theory - a Critical-Review. *Annual Review of Ecology and Systematics*, 15 :523–575. doi:10.1146/annurev.es.15.110184.002515. 19, 76

R Core Team. (2014). *R : A Language and Environment for Statistical Computing*. R Foundation for Statistical Computing, Vienna, Austria, url : http://www.R-project.org/. 42, 55, 80

Ramasco, V., Barraquand, F., Biuw, M., McConnell, B., and Nilssen, K. T. (2015). The intensity of horizontal and vertical search in a diving forager : the harbour seal. *Movement Ecology*, 3 (1) :15. doi:10.1186/s40462-015-0042-9. 78

Reisinger, R. R., de Bruyn, P. J. N., and Bester, M. N. (2011). Predatory impact of killer whales on pinniped and penguin populations at the subantarctic prince edward islands : fact and fiction. *Journal of Zoology*, pages no–no. doi:10.1111/j.1469-7998.2011.00815.x. 122, 165

Reynolds, J. D., Dulvy, N. K., Goodwin, N. B., and Hutchings, J. A. (2005). Biology of extinction risk in marine fishes. *Proceedings of the Royal Society of London B : Biological Sciences*, 272 (1579) :2337–2344. doi:10.1098/rspb.2005.3281. 12

Rice, J. (1995). Food web theory, marine food webs, and what climate change may do to northern marine fish populations. In *Climate Change and Northern Fish Populations*, pages 561–568. NRC Research Press. 7

Richard, G., Vacquié-Garcia, J., Jouma'a, J., Picard, B., Génin, A., Arnould, J. P. Y., Bailleul, F., and Guinet, C. (2014). Variation in body condition during the post-moult foraging trip of southern elephant seals and its consequences on diving behaviour. *The Journal of Experimental Biology*, 217(14) :2609–2619. doi:10.1242/jeb.088542. 56, 69, 70, 81, 162, 168

Richard, G., Cox, S. L., Picard, B., Vacquié-Garcia, J., and Guinet, C. (2016). Southern elephant seals replenish their lipid reserves at different rates according to foraging habitat. *PLOS ONE*, 11(11) :e0166747. doi:10.1371/journal.pone.0166747. 162, 172

Robinson, P. W., Tremblay, Y., Crocker, D. E., Kappes, M. A., Kuhn, C. E., Shaffer, S. A., Simmons, S. E., and Costa, D. P. (2007). A comparison of indirect measures of feeding behaviour based on ARGOS tracking data. *Deep Sea Research Part II : Topical Studies in Oceanography*, 54 (3–4) :356–368. doi:10.1016/j.dsr2.2006.11.020. 51, 52, 77

Robinson, P. W., Simmons, S. E., Crocker, D. E., and Costa, D. P. (2010). Measurements of foraging success in a highly pelagic marine predator, the northern elephant seal. *Journal of Animal Ecology*, 79(6) :1146–1156. doi:10.1111/j.1365-2656.2010.01735.x. 59, 77

Rodhouse, P. G., Arnbom, T. R., Fedak, M. A., Yeatman, J., and Murray, A. W. A. (1992). Cephalopod prey of the southern elephant seal, *Mirounga leonina* L. *Canadian Journal of Zoology*, 70(5) :1007–1015. doi:10.1139/z92-143. 31

Rodhouse, P. G. and White, M. G. (1995). Cephalopods Occupy the Ecological Niche of Epipelagic Fish in the Antarctic Polar Frontal Zone. *Biological Bulletin*, 189(2) :77–80. doi:10.2307/1542457. 53

Roe, H. S. J. (1974). Observations on the diurnal vertical migrations of an oceanic animal community. *Marine Biology*, 28(2) :99–113. doi:10.1007/BF00396301. 13, 33

Rombouts, I., Beaugrand, G., Fizzala, X., Gaill, F., Greenstreet, S. P. R., Lamare, S., Le Loc'h, F., McQuatters-Gollop, A., Mialet, B., Niquil, N., Percelay, J., Renaud, F., Rossberg, A. G., and Féral, J. P. (2013). Food web indicators under the Marine Strategy Framework Directive : From complexity to simplicity ? *Ecological Indicators*, 29 :246–254. doi:10.1016/j.ecolind.2012.12.021. 12

Ropert-Coudert, Y., Kato, A., Liebsch, N., Wilson, R. R., Müller, G., and Baubet, E. (2004). Monitoring jaw movements : A cue to feeding activity. *Game & wildlife science*, 21(1) :1–19. ISSN 1622-7662, url : `http://cat.inist.fr/?aModele=afficheN&cpsidt=16209506`. 160

Ropert-Coudert, Y. and Wilson, R. P. (2004). Subjectivity in bio-logging : do logged data mislead ? *Memoirs of the National Institute of Polar Research : Special Issue*, 58 :23–33. 97

Ropert-Coudert, Y. and Wilson, R. P. (2005). Trends and perspectives in animal-attached remote sensing. *Frontiers in Ecology and the Environment*, 3(8) :437–444. doi:10.1890/1540-9295(2005)003[0437 :TAPIAR]2.0.CO ;2. 12, 13, 94, 103, 168, 169

Ropert-Coudert, Y., Kato, A., Baudat, J., Bost, C.-A., Maho, Y. L., and Naito, Y. (2001). Time/-depth usage of Adélie penguins : an approach based on dive angles. *Polar Biology*, 24(6) : 467–470. doi:10.1007/s003000100235. 52, 166

Roquet, F., Park, Y.-H., Guinet, C., Bailleul, F., and Charrassin, J.-B. (2009). Observations of the Fawn Trough Current over the Kerguelen Plateau from instrumented elephant seals. *Journal of Marine Systems*, 78(3) :377–393. doi:10.1016/j.jmarsys.2008.11.017. 17, 18, 36, 103

Roquet, F., Williams, G., Hindell, M. A., Harcourt, R., McMahon, C., Guinet, C., Charrassin, J.-B., Reverdin, G., Boehme, L., Lovell, P., and Fedak, M. (2014). A Southern Indian Ocean database of hydrographic profiles obtained with instrumented elephant seals. *Scientific Data*, 1 :140028. doi:10.1038/sdata.2014.28. 17, 18, 103, 117

Roy, S. and Chattopadhyay, J. (2007). Towards a resolution of 'the paradox of the plankton' : A brief overview of the proposed mechanisms. *Ecological Complexity*, 4(1–2) :26 – 33. doi:10.1016/j.ecocom.2007.02.016. 6

Sabarros, P., Ménard, F., Lévénez, J., Tew-Kai, E., and Ternon, J. (2009). Mesoscale eddies influence distribution and aggregation patterns of micronekton in the mozambique channel. *Marine Ecology Progress Series*, 395 :101–107. doi:10.3354/meps08087. 10

Sabourenkov, E. (1991). Myctophids in the diet of Antarctic predators. *CCAMLR Science - Selected Scientific Papers*, SC-CAMLR-SSP/8 :335–368, url : https://www.ccamlr.org/en/publications/science_journal/selected-scientific-papers-sc-camlr-ssp/8/335-368. 13, 33

Saijo, D., Mitani, Y., Abe, T., Sasaki, H., Goetsch, C., Costa, D. P., and Miyashita, K. (2016). Linking mesopelagic prey abundance and distribution to the foraging behavior of a deep-diving predator, the northern elephant seal. *Deep Sea Research Part II : Topical Studies in Oceanography*. doi:10.1016/j.dsr2.2016.11.007. 157, 172

Sala, E. (2006). Top predators provide insurance against climate change. *Trends in Ecology & Evolution*, 21(9) :479–480. doi:10.1016/j.tree.2006.07.006. 12

Sala, J. E., Quintana, F., Wilson, R. P., Dignani, J., Lewis, M. N., and Campagna, C. (2011). Pitching a new angle on elephant seal dive patterns. *Polar Biology*, 34(8) :1197–1209. doi:10.1007/s00300-011-0981-6. 51, 98, 161

Sato, K., Mitani, Y., Cameron, M. F., Siniff, D. B., and Naito, Y. (2003). Factors affecting stroking patterns and body angle in diving Weddell seals under natural conditions. *Journal of Experimental Biology*, 206(9) :1461–1470. doi:10.1242/jeb.00265. 56, 162

Sato, K., Charrassin, J.-B., Bost, C.-A., and Naito, Y. (2004). Why do macaroni penguins choose shallow body angles that result in longer descent and ascent durations? *Journal of Experimental Biology*, 207(23) :4057–4065. doi:10.1242/jeb.01265. 52

Savoca, M. S. and Nevitt, G. A. (2014). Evidence that dimethyl sulfide facilitates a tritrophic mutualism between marine primary producers and top predators. *Proceedings of the National Academy of Sciences*, 111(11) :4157–4161. doi:10.1073/pnas.1317120111. 167

Scheffer, A., Trathan, P. N., and Collins, M. (2010). Foraging behaviour of King Penguins (Aptenodytes patagonicus) in relation to predictable mesoscale oceanographic features in the Polar Front Zone to the north of South Georgia. *Progress in Oceanography*, 86(1–2) : 232–245. doi:10.1016/j.pocean.2010.04.008. 77

Schoener, T. W. (1971). Theory of Feeding Strategies. *Annual Review of Ecology and Systematics*, 2(1) :369–404. doi:10.1146/annurev.es.02.110171.002101. 19

Schreer, J. F., Kovacs, K. M., and O'Hara Hines, R. J. (2001). Comparative diving patterns of pinnipeds and seabirds. *Ecological Monographs*, 71(1) :137–162. doi:10.1890/0012-9615(2001)071[0137 :CDPOPA]2.0.CO ;2. 53

Schusterman, R. J., Kastak, D., Levenson, D. H., Reichmuth, C. J., and Southall, B. L. (2000). Why pinnipeds don't echolocate. *The Journal of the Acoustical Society of America*, 107(4) : 2256–2264. doi:10.1121/1.428506. 95

SEaOS. (2016). Southern Elephant Seals as Oceanographic Samplers : The Life of the Southern Elephant Seal, url : http://biology.st-andrews.ac.uk/seaos/naturalhistory.htm. 30

Senina, I., Sibert, J., and Lehodey, P. (2008). Parameter estimation for basin-scale ecosystem-linked population models of large pelagic predators : Application to skipjack tuna. *Progress in Oceanography*, 78(4) :319–335. doi:10.1016/j.pocean.2008.06.003. 122

Sergio, F., Caro, T., Brown, D., Clucas, B., Hunter, J., Ketchum, J., McHugh, K., and Hiraldo, F. (2008). Top Predators as Conservation Tools : Ecological Rationale, Assumptions, and Efficacy. *Annual Review of Ecology, Evolution, and Systematics*, 39 :1–19. ISSN 1543-592X, url : http://www.jstor.org/stable/30245151. 12

Shephard, S., Fung, T., Houle, J. E., Farnsworth, K. D., Reid, D. G., and Rossberg, A. G. (2012). Size-selective fishing drives species composition in the Celtic Sea. *ICES Journal of Marine Science : Journal du Conseil*, 69(2) :223–234. doi:10.1093/icesjms/fsr200. 12

Shin, Y.-J. and Cury, P. (1999). OSMOSE : A Multispecies Individual-Based Model to Explore the Functional Role of Biodiversity in Marine Ecosystems. In *Ecosystem Approaches for Fisheries Management*, pages 593–607. Alaska Sea Grant, University of Alaska Fairbanks. ISBN 978-1-56612-061-6. doi:10.4027/eafm.1999.43. 22

Shin, Y.-J., Shannon, L. J., and Cury, P. M. (2004). Simulations of fishing effects on the southern Benguela fish community using an individual-based model : learning from a comparison with ECOSIM. *African Journal of Marine Science*, 26(1) :95–114. doi:10.2989/18142320409504052. 22

Shin, Y.-J. and Cury, P. (2001). Exploring fish community dynamics through size-dependent trophic interactions using a spatialized individual-based model. *Aquatic Living Resources*, 14 (2) :65–80. doi:10.1016/S0990-7440(01)01106-8. 22

Shiomi, K., Sato, K., Mitamura, H., Arai, N., Naito, Y., and Ponganis, P. J. (2008). Effect of ocean current on the dead-reckoning estimation of 3-D dive paths of emperor penguins. *Aquatic Biology*, 3(3) :265–270. doi:10.3354/ab00087. 78

Sibert, J., Senina, I., Lehodey, P., and Hampton, J. (2012). Shifting from marine reserves to maritime zoning for conservation of Pacific bigeye tuna (Thunnus obesus). *Proceedings of the National Academy of Sciences*, 109(44) :18221–18225. doi:10.1073/pnas.1209468109. 122

Signal developers. (2013). *signal : Signal processing*. 55, 80, 110

Sih, A. (2005). Predator-prey space use as an emergent outcome of a behavioral response race. In *Ecology of Predator-Prey Interactions*, pages 240–255. Oxford University Press, USA, oxford university press, usa edition. ISBN 9780195171204. 20, 76

Sih, A. (1984). The Behavioral Response Race Between Predator and Prey. *The American Naturalist*, 123(1) :143–150. ISSN 0003-0147. 20, 77

Simon, M., Johnson, M., Tyack, P., and Madsen, P. T. (2009). Behaviour and kinematics of continuous ram filtration in bowhead whales (Balaena mysticetus). *Proceedings of the Royal Society of London B : Biological Sciences*, 276(1674) :3819–3828. doi:10.1098/rspb.2009.1135. 46

Simpkins, M. A., Kelly, B. P., and Wartzok, D. (2001). Three-dimensional analysis of search behaviour by ringed seals. *Animal Behaviour*, 62(1) :67–72. doi:10.1006/anbe.2000.1734. 78, 153

Slip, D. J. (1995). The diet of southern elephant seals (Mirounga leonina) from Heard Island. *Canadian Journal of Zoology*, 73(8) :1519–1528. doi:10.1139/z95-180. 31, 32, 34

Slip, D., Hindell, M. A., and Burton, H. R. (1994). Diving Behavior of Southern Elephant Seals from Macquarie Island : An Overview. In *Elephant Seals : Population Ecology, Behavior, and Physiology*, pages 253–270. University of California Press. 28

Sokolov, S. and Rintoul, S. R. (2007). Multiple jets of the antarctic circumpolar current south of australia. *Journal of Physical Oceanography*, 37(5) :1394–1412. doi:10.1175/jpo3111.1. 36

Sparling, C. E., Georges, J.-Y., Gallon, S. L., Fedak, M., and Thompson, D. (2007). How long does a dive last? Foraging decisions by breath-hold divers in a patchy environment : a test of a simple model. *Animal Behaviour*, 74(2) :207–218. doi:10.1016/j.anbehav.2006.06.022. 52

Stearns, S. C. and Schmid-Hempel, P. (1987). Evolutionary insights should not be wasted. *Oikos*, 49(1) :118. doi:10.2307/3565561. 165

Stephens, D. W. and Krebs, J. R. (1986). *Foraging Theory*. Princeton University Press. ISBN 0-691-08442-4. 20, 50, 76

Stokes, T. K. (1992). An overview of the North Sea multispecies modelling work in ICES. *South African Journal of Marine Science*, 12(1) :1051–1060. doi:10.2989/02577619209504761. 9

Stommel, H. (1963). Varieties of oceanographic experience : The ocean can be investigated as a hydrodynamical phenomenon as well as explored geographically. *Science*, 139(3555) : 572–576. doi:10.1126/science.139.3555.572. 5

Sullivan, C. W., Arrigo, K. R., McClain, C. R., Comiso, J. C., and Firestone, J. (1993). Distributions of phytoplankton blooms in the southern ocean. *Science*, 262(5141) :1832–1837. doi:10.1126/science.262.5141.1832. 37

Takahashi, A., Sato, K., Naito, Y., Dunn, M. J., Trathan, P. N., and Croxall, J. P. (2004). Penguin–mounted cameras glimpse underwater group behaviour. *Proceedings of the Royal Society of London B : Biological Sciences*, 271(Suppl 5) :S281–S282. doi:10.1098/rsbl.2004.0182. 74

Takahashi, A., Matsumoto, K., Hunt Jr., G. L., Shultz, M. T., Kitaysky, A. S., Sato, K., Iida, K., and Watanuki, Y. (2008). Thick-billed murres use different diving behaviors in mixed and stratified waters. *Deep Sea Research Part II : Topical Studies in Oceanography*, 55(16–17) : 1837–1845. doi:10.1016/j.dsr2.2008.04.005. 94

Teo, S. L. H., Kudela, R. M., Rais, A., Perle, C., Costa, D. P., and Block, B. A. (2009). Estimating chlorophyll profiles from electronic tags deployed on pelagic animals. *Aquatic Biology*, 5(2) : 195–207. doi:10.3354/ab00152. 104, 106, 113, 118, 120, 155, 156

Thomalla, S. J., Waldron, H. N., Lucas, M. I., Read, J. F., Ansorge, I. J., and Pakhomov, E. (2011). Phytoplankton distribution and nitrogen dynamics in the southwest indian subtropical gyre and Southern Ocean waters. *Ocean Sci.*, 7(1) :113–127. doi:10.5194/os-7-113-2011. 5, 6

Thompson, D. and Fedak, M. A. (2001). How long should a dive last ? A simple model of foraging decisions by breath-hold divers in a patchy environment. *Animal Behaviour*, 61 : 287–296. doi:10.1006/anbe.2000.1539. 52

Thums, M., Bradshaw, C. J. A., and Hindell, M. A. (2011). In situ measures of foraging success and prey encounter reveal marine habitat-dependent search strategies. *Ecology*, 92 (6) :1258–1270. doi:10.1890/09-1299.1. 150, 160

Treep, J., Bohrer, G., Shamoun-Baranes, J., Duriez, O., de Moraes Frasson, R. P., and Bouten, W. (2016). Using high-resolution GPS tracking data of bird flight for meteorological observations. *Bulletin of the American Meteorological Society*, 97(6) :951–961. doi:10.1175/bams-d-14-00234.1. 169

Tremblay, Y. and Cherel, Y. (2000). Benthic and pelagic dives : a new foraging behaviour in rockhopper penguins. *Marine Ecology Progress Series*, 204 :257–267. doi:10.3354/meps204257. 00107. 52

Turner, M. G. (1989). Landscape Ecology : The Effect of Pattern on Process. *Annual Review of Ecology and Systematics*, 20(1) :171–197. doi:10.1146/annurev.es.20.110189.001131. 2, 158

Tyler, E. H. M., Somerfield, P. J., Berghe, E. V., Bremner, J., Jackson, E., Langmead, O., Palomares, M. L. D., and Webb, T. J. (2011). Extensive gaps and biases in our knowledge of a well-known fauna : implications for integrating biological traits into macroecology. *Global Ecology and Biogeography*, 21(9) :922–934. doi:10.1111/j.1466-8238.2011.00726.x. 10, 12, 14

Vacquié-Garcia, J., Guinet, C., Dragon, A., Viviant, M., Ksabi, N. E., and Bailleul, F. (2015). Predicting prey capture rates of southern elephant seals from track and dive parameters. *Marine Ecology Progress Series*, 541 :265–277. doi:10.3354/meps11511. 145

Vacquié-Garcia, J. (2014). *Variation spatio-temporelle de l'activité d'alimentation des éléphants de mer en relation avec les paramètres physiques et biologiques de l'environnement*. Toulouse 3, url : `http://www.theses.fr/2014TOU30110`. 106

Vacquié-Garcia, J., Royer, F., Dragon, A.-C., Viviant, M., Bailleul, F., and Guinet, C. (2012). Foraging in the Darkness of the Southern Ocean : Influence of Bioluminescence on a Deep Diving Predator. *PLoS ONE*, 7(8) :e43565. doi:10.1371/journal.pone.0043565. 33, 72, 93, 95, 104, 106, 108, 111, 116, 155, 168, 169, 214, 215

Vacquié-Garcia, J., Guinet, C., Laurent, C., and Bailleul, F. (2015). Delineation of the southern elephant seal ?s main foraging environments defined by temperature and light conditions. *Deep Sea Research Part II : Topical Studies in Oceanography*, 113 :145–153. doi:10.1016/j.dsr2.2014.10.029. 43, 44, 55, 56, 80, 96, 110, 168, 172, 214

van den Hoff, J., Burton, H., and Davies, R. (2003). Diet of male southern elephant seals (Mirounga leonina L.) hauled out at Vincennes Bay, East Antarctica. *Polar Biology*, 26(1) : 27–31. doi:10.1007/s00300-002-0447-y. 32

Vance, T. C. and Doel, R. E. (2010). Graphical methods and cold war scientific practice : The stommel diagram's intriguing journey from the physical to the biological environmental sciences. *Historical Studies in the Natural Sciences*, 40(1) :1–47. doi:10.1525/hsns.2010.40.1.1.5

Venables, W. N. and Ripley, B. D. (2007). *Modern applied statistics with S*. Statistics and computing. Springer, New York, NY, 4. ed., corr. print edition. ISBN 0-387-95457-0 978-0-387-95457-8. 60, 86

Vergassola, M., Villermaux, E., and Shraiman, B. I. (2007). 'Infotaxis' as a strategy for searching without gradients. *Nature*, 445(7126) :406–409. doi:10.1038/nature05464. 167

Viviant, M., Trites, A. W., Rosen, D. A. S., Monestiez, P., and Guinet, C. (2010). Prey capture attempts can be detected in Steller sea lions and other marine predators using accelerometers. *Polar Biology*, 33(5) :713–719. doi:10.1007/s00300-009-0750-y. 43, 44, 51, 78, 103

Viviant, M., Monestiez, P., and Guinet, C. (2014). Can We Predict Foraging Success in a Marine Predator from Dive Patterns Only ? Validation with Prey Capture Attempt Data. *PLoS ONE*, 9(3) :e88503. doi:10.1371/journal.pone.0088503. 52, 77

Volker, H. S., Alberto, C. N. G., Raymond, T. P., Haika, I. F., Inga, H., John, T. A., Jane, F. R., Harry, L., and Victor, S. (2002). Mesoscale frontal dynamics : shaping the environment of primary production in the antarctic circumpolar current. *Deep Sea Research Part II : Topical Studies in Oceanography*, 49(18) :3735 – 3769. doi:10.1016/S0967-0645(02)00109-1. 6, 11, 73, 77, 115, 122

Waluda, C. M., Rodhouse, P. G., Trathan, P. N., and Pierce, G. J. (2001). Remotely sensed mesoscale oceanography and the distribution of illex argentinus in the south atlantic. *Fisheries Oceanography*, 10(2) :207–216. doi:10.1046/j.1365-2419.2001.00165.x. 10

Watanabe, H., Moku, M., Kawaguchi, K., Ishimaru, K., and Ohno, A. (1999). Diel vertical migration of myctophid fishes (Family Myctophidae) in the transitional waters of the western North Pacific. *Fisheries Oceanography*, 8(2) :115–127. doi:10.1046/j.1365-2419.1999.00103.x. 13, 33

Watanabe, H., Kubodera, T., Moku, M., and Kawaguchi, K. (2006)a. Diel vertical migration of squid in the warm core ring and cold water masses in the transition region of the western North Pacific. *Marine Ecology Progress Series*, 315 :187–197. doi:10.3354/meps315187. 13, 33

Watanabe, Y., Baranov, E. A., Sato, K., Naito, Y., and Miyazaki, N. (2006)b. Body density affects stroke patterns in Baikal seals. *Journal of Experimental Biology*, 209(17) :3269–3280. doi:10.1242/jeb.02402. 56, 161, 162

Watanabe, Y. Y. and Takahashi, A. (2013). Linking animal-borne video to accelerometers reveals prey capture variability. *Proceedings of the National Academy of Sciences*, 110(6) :2199–2204. doi:10.1073/pnas.1216244110. 51, 99, 103

Weimerskirch, H. (2007). Are seabirds foraging for unpredictable resources ? *Deep Sea Research Part II : Topical Studies in Oceanography*, 54(3–4) :211–223. doi:10.1016/j.dsr2.2006.11.013. 167

Weimerskirch, H., Pinaud, D., Pawlowski, F., and Bost, C.-A. (2007). Does Prey Capture Induce Area-Restricted Search ? A Fine-Scale Study Using GPS in a Marine Predator, the Wandering Albatross. *The American Naturalist*, 170(5) :734–743. doi:10.1086/522059. 152, 167

Wensveen, P. J., Thomas, L., and Miller, P. J. O. (2015). A path reconstruction method integrating dead-reckoning and position fixes applied to humpback whales. *Movement Ecology*, 3 (1) :1–16. doi:10.1186/s40462-015-0061-6. 78, 81, 98

Widder, E., Robison, B., Reisenbichler, K., and Haddock, S. (2005). Using red light for in situ observations of deep-sea fishes. *Deep Sea Research Part I : Oceanographic Research Papers*, 52 (11) :2077–2085. doi:10.1016/j.dsr.2005.06.007. 165

Wiebe, P. H. (1971). A Computer Model Study of Zooplankton Patchiness and Its Effects on Sampling Error1. *Limnology and Oceanography*, 16(1) :29–38. doi:10.4319/lo.1971.16.1.0029. 16

Wiegert, R. and Owen, D. (1971). Trophic structure, available resources and population density in terrestrial vs. aquatic ecosystems. *Journal of Theoretical Biology*, 30(1) :69–81. doi:10.1016/0022-5193(71)90037-3. 6

Wiens, J. A. (1989). Spatial Scaling in Ecology. *Functional Ecology*, 3(4) :385–397. doi:10.2307/2389612. 158, 167

Wildlife Computers. (2016)a. Daily Diary Specifications. `http://wildlifecomputers.com/our-tags/daily-diary/`. 106

Wildlife Computers. (2016)b. TDR10 Specifications. `http://wildlifecomputers.com/our-tags/tdr10/`. 106

Williams, A. and Koslow, J. A. (1997). Species composition, biomass and vertical distribution of micronekton over the mid-slope region off southern Tasmania, Australia. *Marine Biology*, 130(2) :259–276. doi:10.1007/s002270050246. 72, 96

Williams, T. M., Davis, R. W., Fuiman, L. A., Francis, J., Le, B. J., Boeuf, Horning, M., Calambokidis, J., and Croll, D. A. (2000). Sink or Swim : Strategies for Cost-Efficient Diving by Marine Mammals. *Science*, 288(5463) :133–136. doi:10.1126/science.288.5463.133. 20

Wilson, R., Steinfurth, A., Ropert-Coudert, Y., Kato, A., and Kurita, M. (2002). Lip-reading in remote subjects : an attempt to quantify and separate ingestion, breathing and vocalisation in free-living animals using penguins as a model. *Marine Biology*, 140(1) :17–27. doi:10.1007/s002270100659. 52, 77

Wilson, R. P., Shepard, E. L. C., and Liebsch, N. (2008). Prying into the intimate details of animal lives : use of a daily diary on animals. *Endangered Species Research*, v4 :123–137. doi:10.3354/esr00064. 78

With, K. A. (1994). Using fractal analysis to assess how species perceive landscape structure. *Landscape Ecology*, 9(1) :25–36. doi:10.1007/BF00135076. 168

Worthy, G. a. J., Morris, P. A., Costa, D. P., and Boeuf, B. J. L. (1992). Moult energetics of the northern elephant seal (Mirounga angustirostris). *Journal of Zoology*, 227(2) :257–265. doi:10.1111/j.1469-7998.1992.tb04821.x. 30

Young, J. W., Hunt, B. P. V., Cook, T. R., Llopiz, J. K., Hazen, E. L., Pethybridge, H. R., Ceccarelli, D., Lorrain, A., Olson, R. J., Allain, V., Menkes, C., Patterson, T., Nicol, S., Lehodey, P., Kloser, R. J., Arrizabalaga, H., and Anela Choy, C. (2015). The trophodynamics of marine top predators : Current knowledge, recent advances and challenges. *Deep Sea Research Part II : Topical Studies in Oceanography*, 113 :170–187. doi:10.1016/j.dsr2.2014.05.015. 172

Zeileis, A., Kleiber, C., and Jackman, S. (2008). Regression Models for Count Data in R. *Journal of Statistical Software*, 27(8). doi:10.18637/jss.v027.i08. 86

Zhang, X. and Dam, H. G. (1997). Downward export of carbon by diel migrant mesozooplankton in the central equatorial Pacific. *Deep Sea Research Part II : Topical Studies in Oceanography*, 44(9) :2191–2202. doi:10.1016/S0967-0645(97)00060-X. 14, 33

Table des figures

Liste des tableaux

Annexe

A

Informations supplémentaires du chapitre 2

```r
# 1. L'ABC de tout langage ####
cat("Hello world!")

# 2. Archétype de la fonction recursive ####
factorial <- function(x) if (x == 0) 1 else x * factorial(x - 1)

# 3. Une fonction peut en cacher une autre ####
empower <- function(n) function(x) x^n
square <- empower(2)
square_root <- empower(1/2)

# 4. ... symbolise une liste d'arguments ####
compose <- function(f, g, ...) function(...) f(g(...))
identity <- compose(square, square_root)

# 5. Une redéfinition sournoise de la fonction parenthèse ####
# Crédit: Hadley Wickham, http://adv-r.had.co.nz
"(" <- function(x, y) if (runif(1) < 0.1) x else x + 1
(1 + 1) # = 3 ?
```

Aperçu du langage R.

A.1 Overview of the rbl package

A.1.1 Introduction

This is a R package to make dealing with diving predator bio-logging data a easier. Most of the functions in this package were coded to work with Southern Elephant Seal high sampling frequency datasets that I use on a daily basis but they should be relevant for the analysis of the behaviour of other diving predators (such as penguins, turtles, other seals, whales ...) and also provides tools to deal with low resolution data (such as "brokenstick-abstracted" dives profiles). The motivations for developing this package were to better organise code (avoiding copy/paste of regularly used code snippets, keep track of the changes affecting code), to facilitate sharing of this work or and referring to it and to help harmonizing the methods over time, over study species an over research teams. This open source package is also the opportunity to create a place where other people working on diving predators and bio-logging data can coordinate their efforts.

A.1.2 Principle

Fields of application

For now, most tools are designed to help with high sampling frequency time–depth data and acceleration data. These tools cover a range of applications such as

- Fixing issues in the raw data : Timestamp issues, Depth offset over time, ...
- Filtering useful signals from the data : Prey Catch Attempts (Vacquié-Garcia et al., 2015), Static & Dynamic acceleration, Bioluminescent events (Vacquié-Garcia et al., 2012), ...
- Identifying specific parts in a dataset : Dives, Dives phases, Drifting periods, ...
- Implementing relevant algorithms for diving predator data : Brokenstick Models (Fedak et al., 2002), Dive Zone Index (Photopoulou et al., 2015), Wiggles (Halsey et al., 2007),Time At Depth (Fedak et al., 2001), ...
- Proposing a standard format for "Diving Predator datasets" : see subsection A.1.3

- Facilitating data manipulation, visualization of animal behaviour : by providing methods dedicated to specific object classes (subsection A.1.3) and functions with simple syntax (A.1.4)

Design

The behaviour of diving predators such as the elephant seal is structured at different spatio-temporal scales. As diving predators are constrained to breathe at surface but to forage at depth, dive is a key functional unit to interpret their behaviour. Within these dives and the descent, bottom and ascent phases have distinct purposes such as foraging or resting (bottom phase) or transiting between foraging ground and the surface (descent and ascent phases). As a results, understanding the underwater behaviour often implies to decompose the dives into dives phases. Therefore dealing with bio-logging or telemetry data from diving predators generally implies to make analysis at the scale of a dive or a dive phase . The package provides three types of functions to assist with this.

"Raw processing" functions (type 1) These functions are used once on the entire dataset to process the raw data. For instance : Time–Depth correction, delineation of dive and dive phases, extraction of static and dynamic acceleration, detection prey encounter events ...

"Small processing" functions (type 2) Functions to be used, more interactively, at the dive scale or on a specific dive phase. Conversely to the previous category, these functions take as input a small fraction of the dataset. They are generally aimed at extracting meaningful information about animal behaviour rather than correcting issues in the dataset. For instance : brokenstick algorithm to abstract a high frequency time-depth dive profile, calculate Time At Depth, delineate "wiggles" during the bottom phase, identify bioluminescent events (see Vacquié-Garcia et al. (2012)). Since the data correction is handled separately, the code organized in small single purpose functions which are easier to read and understand. Therefore they are easier to maintain and to adapt for specific needs.

"Interactive" functions (type 3) These functions to apply the latter "Small processing" functions on the desired portions of the dataset with a simple syntax. This allows

to avoid loops, copy/pasting of code, improve readability and ease of manipulation of these data.

A.1.3 Data format : description of the ses object class

While functions belonging to type (1) just imply a raw data table (hereafter called tdr table) the functions of types (2) and (3) rely on a specific formatting of the data. As a consequence, it may require some effort to format the data appropriately prior to using functions of types (2 & 3) but this is explained later in A.1.4. For this reason, we provided a complete dataset example with the package[1].
A specific S3 class has been created : the ses class (for Southern Elephant Seal). These objects are just standard R lists with a "ses" label allowing R to recognize that some dedicated functions can be used when they exist. A ses object is designed to encapsulate the archive data from various loggers such as CTD-SRDLs (Sea Mammal Research Unit, St Andrew University), MK9 and MK10 (Wildlife Computers, USA).

Example dataset

```
# Load package and example dataset
require("rbl")
data(exses)

class(exses)
# [1] "ses"  "list"
is.ses(exses)
# [1] TRUE

# Slots
names(exses)
# [1] "name"     "hash"     "tdr"      "stat"
# [5] "delim"    "no_dive"  "bsm"      "drift"    "dzi"
```

Description of main ses slots

`name` The name of the dataset, e.g. the identity of the animal.

`hash` The MD5 checksum of the raw data files (but any character string works). Using MD5 checksum allows to trace back the original data files used to produce the

[1] this makes downloading lasts 5–10 minutes.

ses object regardless of changes in the file names.

tdr The high resolution data, typically at 1 Hz (obtained from the archive downloaded from the tag). The two first columns must be the time (in POSIXct format, and UTC time zone) and the depth (increasing downward). This data.frame has a tdr class with dedicated methods for functions such as plot.

stat Dive summary statistics such as dive duration, dive maximum depth etc ... The first column should be the dive number (no_dive). This data.frame has a stat class.

delim A table with the dive (columns 1 and 2) and bottom phase (columns 4 and 5) delineation information. This table links together the tdr and stat tables with dive and dive phases locations (tdr table row numbers) and their identifier (no_dive). Rows with dive numbers (columns 3) ≤ 0 relate to surface periods while rows with dive numbers > 0 relate to underwater periods (dives). A warning column (columns 6) keep track of potential issues encountered during the delineation processing. Additional information such as the parameters used in the delineation processing are available in the attributes of the object (accessible using the base function attributes).

no_dive *Optional*. This is a vector of the dive numbers (no_dive) to be used by default by the type (3) functions. If this slot does not exists then all the dives numbers listed in the delim table will be used instead.

bsm *Optional*. This is a list of dives abstracted with the brokenstick algorithm. The element of this list have a bsm class with dedicated methods for many functions such as plot, predict, coefficients, residuals, as.data.frame ...

drift *Optional*. This is a table providing descriptive statistics of all the brokenstick segments from the previous slot (a kind of stat table for bsm objects). This table is useful with elephant seal in order to identify the drift dives.

dzi *Optional*. This is a list of the abstracted brokenstick profiles processed with the dive_zone_index function (see Photopoulou et al. (2015) for method explanation).

The element of this list have a dzi class with dedicated methods for functions such as plot.

Minor S3 classes implemented in the package

```
# Additional S3 class implemented in the package
class(exses$tdr)
# [1] "tdr"        "data.frame"
class(exses$stat)
# [1] "stat"       "data.frame"
class(exses$bsm[[1]])
# [1] "bsm"  "list"
class(exses$dzi[[1]])
# [1] "dzi"  "list"
```

More ses slots

There are other slots you may encounter in some datasets, they provide additional metadata :

`commit` An identifier of the rbl package version used to process the raw data files. Refers to commit SHA1 checksums listed on the on-line repository.

`sex` Sex of the individual.

`length` Nose to tail length of the individual (in m). Two values indicate measures at tags deployment and retrieval (in that order).

`weight` Weight of the individual (in kg). Two values indicate measures at tags deployment and retrieval (in that order).

`tags` Tags identifiers and "tagware" version number. When several tag where synchronized the tag serving as clock reference is indicated here.

`loc_type` Are the location collected with ARGOS o GPS or both ?

`locs` All locations with their status (kept of removed) and the animal depth at the time of the location.

A.1.4 Usage examples

This section aims at giving practical examples of the three types of functions described in subsection A.1.2.

"Raw processing" (type 1) functions

Dive and bottom phase delineation Dive and dive phases delineation is a typical example[2] a function is applied to the entire dataset once and is unlikely to be used multiple times on a same dataset. The functions presented in the this subsection are primarily designed to deal with the different type of data ("ses", "tdr" etc), to perform some verifications and to save processing parameters information in the attribute of the output.

```
# Dives and dives' phases delineation

# Suppose we have a raw dataset
data(exses)
raw_data <- data.frame(exses$tdr[  , 1:4])
str(raw_data)
# 'data.frame': 423501 obs. of  4 variables:
#  $ time : POSIXct, format: "2011-10-31 13:55:00" "2011-10-31 13:55:01"
    ...
#  $ depth: num  2.5 1.5 1.5 1.5 2.5 1.5 1.5 1.5 2.5 2.5 ...
#  $ temp : num  3.85 3.85 3.85 3.8 3.8 4.15 4.25 4.05 4 4 ...
#  $ light: num  169 169 169 169 169 ...

# We can delineate dives:
delim <- dive_delim(raw_data)
# or bottom given a dive delim:
delim <- bottom_delim(raw_data, dvs = delim)
# or dives and bottoms at once:
delim <- bottom_delim(raw_data)

# When a "ses" class object is provided a specific methods will be used
delim_ses <- bottom_delim(exses)
```

Time and depth correction

```
# Correct drift in the depth readings
raw_data$depth <- correct_depth(raw_data$depth, plt = TRUE)
```

[2] see "Raw processing"

```
# Fill the gaps in the tdr table, remove duplicated timestamps
cor_data <- correct_time(raw_data, verbose = TRUE)

# See also acceleration processing
# functions:
?prey_catch_attempts
?static_acc
?dynamic_acc
?swimming_effort
```

How to create a ses object?

```
ses <- as.ses(
  name = "Example",
  tdr  = cor_data,      # Corrected data
  stat = data.frame(), # A slot may be left empty...
  delim = bottom_delim(cor_data)
)
# ... and be filled later:
ses$stat <- data.frame(no_dive = unique(abs(ses$delim$no_dive)) %w/o% 0)
```

"Small processing" (type 2) functions

Workflow with bio-logging data collected by diving predators is likely to imply calculations at the dive scale or in some specific parts of the dives (see subsection A.1.2). Because of this many function are designed to work at the dive scale. In this way, the functions are very short and self explanatory. Bottom phase delineation is again a good example[3]. The source code of the some of the methods available to delineate the bottom is presented in the following snippet.

```
# Package source code for bottom delineation (type 2 functions):

# using brokenstick algorithm
bottom_delim_bsm <- function(time, depth = NULL, npts = 6) {
  bsm <- try(brokenstick(time, depth, npts), TRUE)
  if (is.error(bsm)) list(st = NA, ed = NA, success = FALSE)
  else list(st = bsm$pts[2], ed = bsm$pts[npts - 1], success = TRUE)
}
```

[3]This may seem confusing given the subsection A.1.4 ... The type 1 functions of subsection A.1.4 are actually dispatching the work to A.1.4 function according to the input object class.

```
# using a simple depth threshold
bottom_delim_std <- function(depth, ledge = 0.80) {
  x <- abs(depth)
  ledge_depth <- max(x, na.rm = TRUE) * ledge
  rk <- which(x >= ledge_depth)
  if (length(rk) == 0) rk <- which.max(x) + c(-1, 1)
  setNames(as.list(range(rk)), c("st", "ed"))
}

# Other examples for bottom delineation:
?bottom_delim_vspd
?bottom_delim_halsey

# Other examples
?brokenstick ; ?entropy ; ?time_at_depth ; ?BioPIC
# BUT MORE IMPORTANTLY: user-defined functions !
```

"Interactive" (type 3) functions

The ses data format and the type 2 functions are more useful when used with the few type 3 functions presented in this subsection. These are the two functions repeatedly used in the workflow :

1. `tdrply`
2. `tdrexpand`

`tdrply` This function aims at applying a function to specific portions of the `tdr` table with a simple syntax inspired from the `*apply` family R functions. This have many advantages such as making the code easier to read or write and avoiding repetitive copy/pasting of code chunks. Symbols can be used to refer to specific parts of a dive cycle :

- `"~!_/-"` represent a complete dive cycle.
- `"!_/"` select dives.
- `"!"`, `"_"` and `"/"` respectively select descent, bottom and ascent phases.
- `"~"` select surface periods preceding the dives.

- "-" select surface periods following the dives.

Then, any combination can be created from these symbols : "!/" select descents and ascents and merge them into a single table while "!&/" (AND operator) select descents and ascents but keep them separated into distinct tables. Specific dives can be referred to using their dive number (no_dive). Brackets and OR operators are also implemented to create more complex expressions (see ?tdrply for examples).

```
# Declare a default ses to avoid writing it in every call to tdrply
ind(ses)

# Extract bottom of the dive number 65 of ses
dv_btt <- tdrply(identity, ty = "_", no = 65)
```

Here is another example showing the usage of the AND operator :

```
# Maximum depth of the dive number 50
tdrply(max, "depth", ty = "!_/", no = 50, na.rm = TRUE)
#   !_/#50
# 839.5223

# Not the same as: (note output names ans structure)
tdrply(max, "depth", ty = "!&_&/", no = 50, na.rm = TRUE)
#     !#50     _#50     /#50
# 713.5208 839.5223 546.5322

# Not the same as: (note output names ans structure)
tdrply(max, "depth", ty = c("!", "_", "/"), no = 50, na.rm = TRUE)
# $dsc
#     !#50
# 713.5208
#
# $btt
#     _#50
# 839.5223
#
# $asc
#     /#50
# 546.5322

# Add a new dive stat to the stat table
# defaults: ty = "!_/", no = NULL (all dives)
```

```
ses$stat$max_depth <- tdrply(max, "depth", na.rm = TRUE)
```

Here is an example showing a more complex task :

```
# Create 8 breakpoints brokenstick abtracted dive profiles,
# for dives number 50 to 53:
bsm <- tdrply(brokenstick, c("time", "depth"), no = 50:53, npts = 8)

# Plot them, see Figure 1
par(mfrow = c(2, 2))
lapply(bsm, plot, data = TRUE, enumerate = TRUE) # calls plot.bsm
```

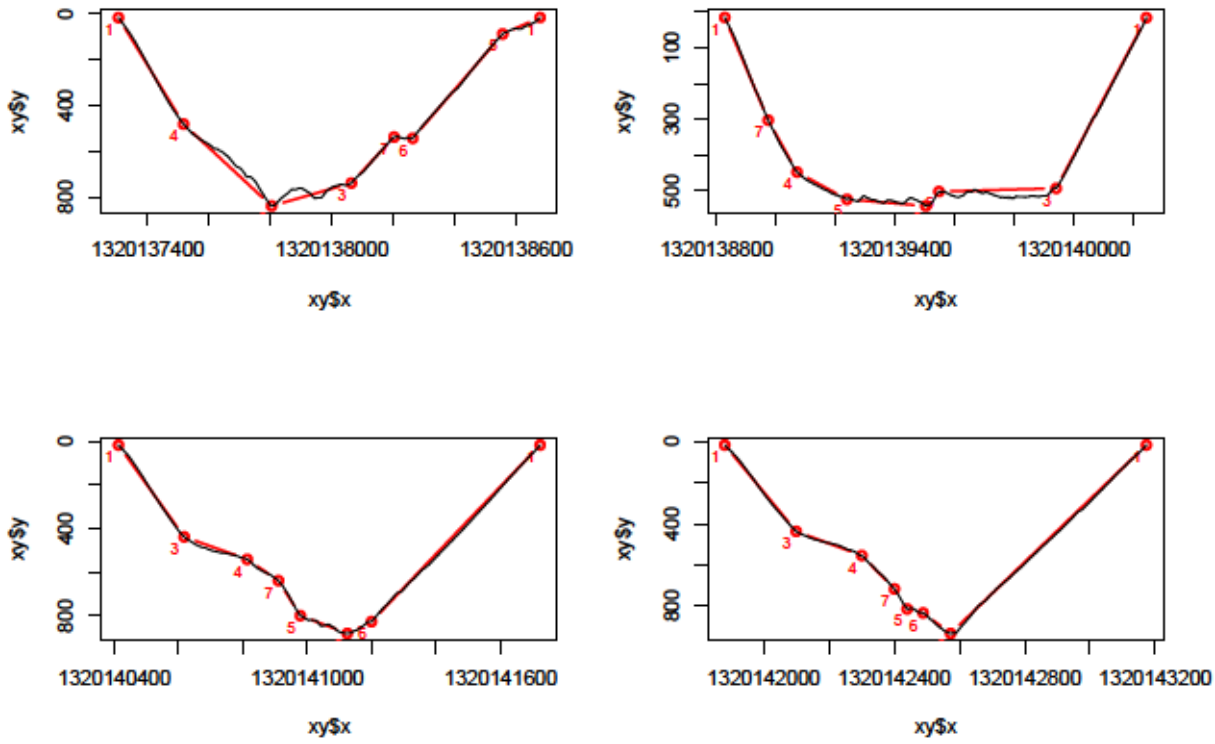

Figure A.1: Broken-stick abstracted dive profiles

Alternatively, any data frame with row numbers in the first and second column can be provided to the `ty` argument. This type of input will be treated as row numbers of `tdr` table. Using dive numbers (`no` argument) and symbols (`ty` argument) instead of subsets of `delim` table directly allows to keep consistent naming of the output. For instance, referring to the surface period that precedes the dive number 100 will be

noted as ty = "~", no = 100 even when user has deleted some rows of delim table and the output of tdrply will be named accordingly ("~#100"). This may help to avoid some errors or to locate them faster.

tdrexpand This function perform the reverse operation that is to say extending a statistic over specific parts of the tdr table. It may be the time to give a concrete data processing example : identify and display drift dives from the example dataset.

```
data(exses)
ind(exses)

# Identify drifting periods in exses$drift
is_drift <- with(exses$drift,
                 dur >= 100 &
                 drift_rate %bw% c(-0.4, 0.6) &
                 abs(roll) >= 90)
# Save the result
exses$drift <- exses$drift[is_drift, ]

# The first two columns are the row numbers delineating the segments
# the third column is an ID number of the segments
str(exses$drift[ , 1:3])
# 'data.frame': 46 obs. of  2 variables:
#  $ st_idx:     int  27848 29439 30537 31851 33289
#  $ ed_idx:     int  28231 29829 31142 32624 34159
#  $ no_seg_tot: int  421   428   434   441   445
```

This is the kind of data frame that can be provided to tdrply or tdrexpand.

```
# Annotate tdr  with the result using tdrexpand
exses$tdr$is_drift <- tdrexpand(rep(TRUE, nrow(exses$drift)),
                                ty = exses$drift, na_value = FALSE)

# Plot some random drift dives, see Figure 2
par(mfrow = c(3,5))
smpl <- sample(unique(exses$drift$no_dive), size = 15, replace = FALSE)
tdrply(plot, # calls plot.tdr, uses a third variable for colors
        cl = c("time", "depth", "is_drift"),
        no = smpl,
        # Sent to plot function via ...
        pch = 20, cex = 0.5,
        # see more on "la" in ?tdrply
```

```
        la = list(main = paste("Dive␣#", smpl)))

# NB: ty = exses$drift can be used in the same way with tdrply
# to perform any calculation on the drifting periods.
# For instance, check that drifting periods have no prey catch attempt
tdrply(any, "is_pca", ty = exses$drift[1:5, ])
# cst#421 cst#428 cst#434 cst#441 cst#445
#   FALSE   FALSE   FALSE   FALSE   FALSE

# The output is named using "cst" (for custom)
# the third column (if provided)
```

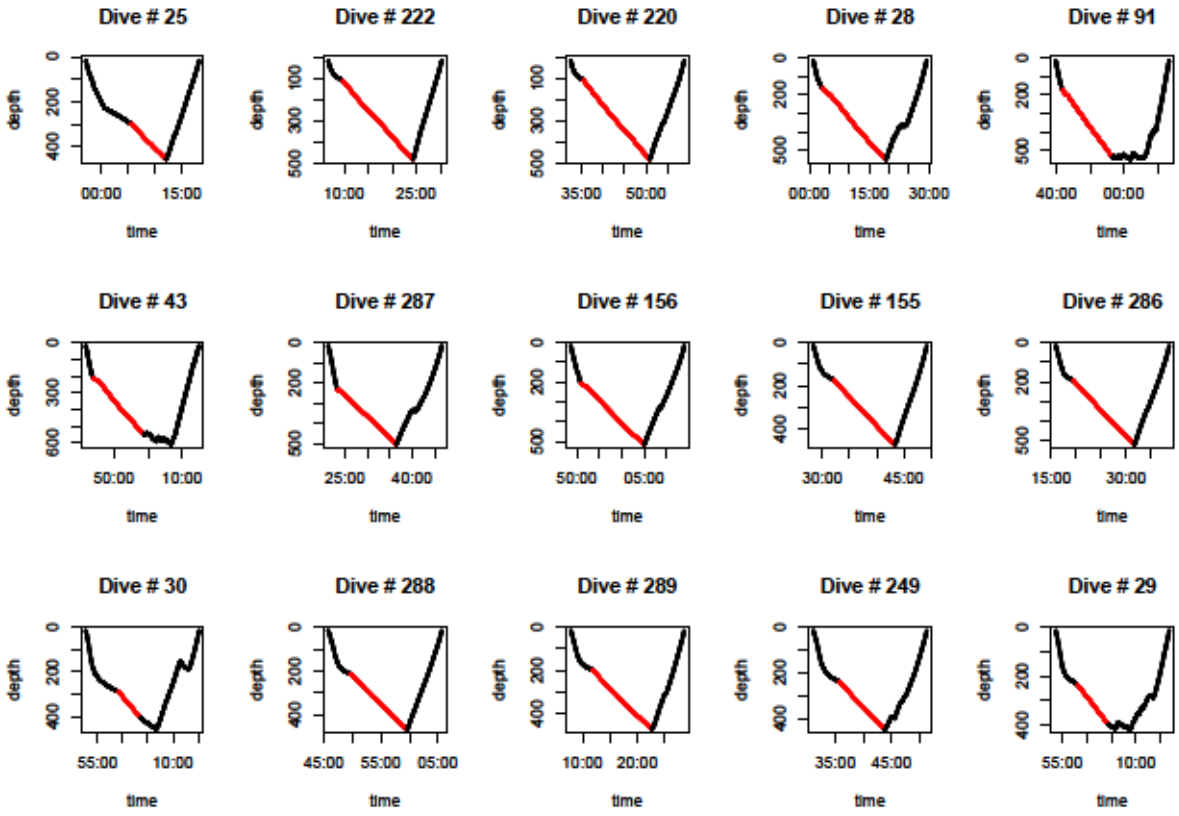

Figure A.2: Some dive portions identified as drifts

A.1.5 Installation

Example with version v0.1.28 of the package. Please visit the "Releases" page to get the last version available.

Windows

```
# Download binary from github
pkg_url <- "https://github.com/SESman/rbl/releases/download/v0.1.28/rbl_
    0.1.28.zip"
download.file(pkg_url, "rbl.zip")

# Install dependencies (listed in DESCRIPTION file)
pkg_dep <- c("data.table", "RcppRoll", "signal", "sqldf", "fields")
install.packages(pkg_dep)

# Local install of "rbl"
install.packages("rbl.zip", repos = NULL)
```

Linux and Mac

```
# Download source code from github
pkg_url <- "https://github.com/SESman/rbl/archive/v0.1.28.tar.gz"
download.file(pkg_url, "rbl.tar.gz")

# Install dependencies (listed in DESCRIPTION file)
pkg_dep <- c("data.table", "RcppRoll", "signal", "sqldf", "fields")
install.packages(pkg_dep)

# Local install of "rbl"
install.packages("rbl.tar.gz", repos = NULL, type = "source")
```

A.1.6 Conclusion

A lot of work has been done to develop some methods or to implement already existing one which but is not presented here because it is not fundamental to explain how the package works. I would suggest the users to visit the source code repository to browse the code in order to get a more detailed view of the package features and to read the original articles listed in the Reference section. It is to be noted that the current default settings are most likely adapted to southern elephant seals. This works aims at becoming a collaborative project so do not hesitate to give some feedback on the pros and cons of the package design and let me know the settings suitable to your study species so that the functions' documentation can be enriched with these information. You may ask questions, make bug reports and even further contribute to

the coding by visiting https://github.com/SESman/rbl.

A.2 rbl manual

Package 'rbl'

November 23, 2016

Title Biologging tools for diving predators in R

Description This is a R package to help working with biologging data focused on diving predators.

Version 0.1.29

Date 2016-04-30

Author Yves Le Bras <yveslebras.fr@gmail.com>

Maintainer Yves Le Bras <yveslebras.fr@gmail.com>

URL https://github.com/SESman/rbl

BugReports https://github.com/SESman/rbl/issues

Depends R (>= 3.1.1)

Suggests knitr,sp,testthat,manipulate

Imports data.table,RcppRoll,signal,sqldf,fields

License MIT + file LICENSE

LazyData true

Roxygen list(wrap = FALSE)

VignetteBuilder knitr

RoxygenNote 5.0.1

R topics documented:

`at_ker` *Test if animal is located around Kerguelen*

Description

Test if animal is located around Kerguelen

Usage

```
at_ker(lon, lat, r = 130)
```

Arguments

`lon`	longitude
`lat`	latitude
`r`	radius

Details

Kerguelen location taken at (49.353282 deg. S,69.354630 deg. E)

`biolum_events` *Identify potential bioluminescence emission events*

Description

Identify potential bioluminescence emission events

Usage

```
biolum_events(x, sensitivity = 1.26, max_light = exp(-20))
```

Arguments

`x`	a data.frame such as returned by `BioPIC` output
`sensitivity`	A threshold to decide if a signal peak is high enought. See details.
`max_light`	Max light level (W/cm^2) where a event can be detected. Set to NULL to disable.

Details

Sensor sensitivity threshold: The minimum ratio between two measures to be considered significantly different. In laboratory experiments, the sensors measured light intensity +- 2 units while submitted to a constant light intensity. Translating the sensor log-scale units to SI linear scale units this accuracy measure translates into a minimum ratio of 1.26

Examples

```
## Not run:
data(exses)
exses$tdr$light_si <- SI_light(exses$tdr$light)
biolum_tbl <- tdrply(BioPIC, obj = exses)
ble_tbl <- Reduce(rbind, lapply(biolum_tbl, biolum_events))

## End(Not run)
```

`BioPIC` *BioPIC: bioluminescent event detection tool*

Description

Adaptation of BioPIC method with 1 Hz sampling frequency datasets and of post-peak attenuation (related to sensor and not depth)

Usage

```
BioPIC(x, lightSI.nm = "light_si", nms = c("alpha", "lessK", "Ia"))
```


Arguments

`x`	a TDR data sample
`lightSI.nm`	The name of the TDR column with light values in W/cm^2.
`nms`	The names of the output variables.

References

Vacquie-Garcia, J., Royer, F., Dragon, A.-C., Viviant, M., Bailleul, F. & Guinet, C. (2012) Foraging in the Darkness of the Southern Ocean: Influence of Bioluminescence on a Deep Diving Predator. PLoS ONE, 7, e43565.

Examples

```
data(exses)
dv <- tdrply(identity, no = 100, obj = exses)[[1]]
dv$light_si <- SI_light(dv$light)
biolum_tbl <- BioPIC(dv)
```

`bottom_delim` *Find the dives' bottom start and end*

Description

Find the dives' bottom start and end

Usage

```
bottom_delim(obj, method = c("vspd", "haslsey", "bsm", "std"), dvs = NULL,
  ...)
```

Arguments

`obj`	An object of class `'ses'` or `'tdr'`. In the first case the function just returns the delim table of the object if it exists else it computes the delim table from the TDR data. with time and depth variables named "time" and "depth".
`method`	the method to used. See help for functions in see also section to get details about possible options. When `"vspd"` or `"halsey"` methods fails `"std"` is used instead.
`dvs`	a delim table such as return by `dive_delim`. If NULL `dive_delim` will be used with default arguments to compute one.
`...`	arguments to be passed to `bottom_delim_vspd`, `bottom_delim_halsey`, `bottom_delim_bsm` or `bottom_delim_std` according to the specified method.

Examples

```
data(exses)
dvs_vspd   <- bottom_delim(exses$tdr)
dvs_halsey <- bottom_delim(exses$tdr, method = "halsey")
dvs_bsm    <- bottom_delim(exses$tdr, method = "bsm")
dvs_std    <- bottom_delim(exses$tdr, method = "std")

# Example using the four methods
n_dv <- 300
opar <- par(no.readonly = TRUE) ; par(mfrow = c(2, 2))
exses$delim <- dvs_vspd
tdrply(plot, 1:2, no = n_dv, obj = exses, main = 'method = "vspd"')
tdrply(points, 1:2, ty = "_", no = n_dv, obj = exses, col = "red")
exses$delim <- dvs_halsey
tdrply(plot, 1:2, no = n_dv, obj = exses, main = 'method = "halsey"')
tdrply(points, 1:2, ty = "_", no = n_dv, obj = exses, col = "red")
exses$delim <- dvs_bsm
tdrply(plot, 1:2, no = n_dv, obj = exses, main = 'method = "bsm"')
tdrply(points, 1:2, ty = "_", no = n_dv, obj = exses, col = "red")
exses$delim <- dvs_std
tdrply(plot, 1:2, no = n_dv, obj = exses, main = 'method = "std"')
tdrply(points, 1:2, ty = "_", no = n_dv, obj = exses, col = "red")
par(opar)
```

---

broadness_index *Broadness index*

Description

The duration of the bottom phase divided by the duration of the dive

Usage

```
broadness_index(x = ind(), time_col = 1)
```

Arguments

x	input data, a ses object.
time_col	Character or numeric giving the column of the TDR table that stores the timestamps.

Details

The index ranges from 0 (short bottom) to 1 (long bottom).

References

Halsey, L.G., Bost, C.-A., Handrich, Y. (2007) A thorough and quantified method for classifying seabird diving behaviour. Polar Biology, 30, 991-1004.

Examples

```
data(exses)
exses$stat$brd <- broadness_index(exses)

plot(brd ~ time, exses$stat)
```

---

brokenstick *Fitting brokenstick models*

Description

brokenstick is used to fit brokenstick models on two-dimensional data such as Time-Depth, Depth-Temperature or Depth-Light profiles. Brokenstick models are useful for compressing or extracting the shape of high resolution profiles.

Usage

```
brokenstick(x, y, npts = 6, start = NULL, na.action, allow.dup = FALSE,
  not.inj.action = c("ignore", "null", "error"), sort.data = FALSE, ...)
```

Arguments

x	The x data. Note that the x values have to be sorted. Can also be a list of x and y (processed by xy.coords). Alternatively, it can also be an object of class "formula".
y	The y data. (processed by xy.coords). Alternatively, if x is a 'formula', y can also be an optional data frame, list or environment (or object coercible by as.data.frame to a data frame) containing the variables in the model. If not found in data, the variables are taken from environment (formula), typically the environment from which brokenstick is called.
npts	The number of points for the brokenstick model to fit. See optBrokenstick for a version of brokenstick which figures out this number of points automatically.
start	Some starting points to start the algorithm with.
na.action	A function which indicates what should happen when the data contain NAs. The default is set by the na.action setting of options, and is na.fail if that is unset. The "factory-fresh" default is na.omit. Another possible value is NULL, no action. Value na.exclude can be useful.
allow.dup	If TRUE the algorithm will not stop when duplicated breakpoints are found. The output will contain a slot called dup, a data.frame with the breakpoint number of the duplicates (dup.no) and the breakpoint number of the its clone among real breakpoints (pts.no)
not.inj.action	What should be done when f: y -> x is not injective.
sort.data	Should the data be sorted according to x values (when they are not) before fitting the broken-stick model.
...	Further arguments to be passed to bsmfit such as eco.mem.

Details

See bsmfit, the function called by brokenstick on each iteration to fit the model with specified points.

Value

A bsm object with (depending on eco.mem):

- pts.x The x values of the brokenstick points (eco.mem inefficient).
- pts.y The y values of the brokenstick points (eco.mem inefficient).
- slope The slopes of each "stick" of the model (eco.mem inefficient).
- intercept The intercept of each "stick" of the model (eco.mem inefficient).
- pts (eco.mem < 4) The index of the brokenstick points.
- na.action Information from the action which was applied to object if NAs were handled specially. (eco.mem inefficient)
- residuals (eco.mem < 3) The model's residuals.
- fitted.values (eco.mem < 2) The fitted values.
- data (eco.mem < 1) The input data used for fitting.
- pts.no The iteration number of points. (eco.mem inefficient)

See Also

optBrokenstick and predict.bsm, residuals.bsm, update.bsm, summary.bsm, coef.bsm, plot.bsm, as.data.frame.bsm for other functions with a S3 method for bsm objects.

Examples

```
data(exses)
dv <- tdrply(identity, 1:2, no = 100, obj = exses)[[1]]

# Syntax
bsm <- brokenstick(dv$time, dv$depth)
bsm <- brokenstick(dv) # if two columns
bsm <- brokenstick(depth ~ time, dv)
bsm <- with(dv, brokenstick(depth ~ time))
```

---

compose *Function composition*

Description

Function composition

Usage

```
compose(...)
```

Arguments

...	functions to be composed

Details

see the infix version %c%

Value

compose returns the composed of functions listed in .... Pay attention to the order, compose(f, g) returns g(f()).

Examples

```
f <- compose(is.na, sum)
f(c(1, NA, NA))
```

---

correct_depth *Correct depth sequence from drift of values over time*

Description

Correct depth sequence from drift of values over time

Usage

```
correct_depth(x, dur = 5000, plt = FALSE, span = 0.15, ...)
```

Arguments

x	The depth sequence.
dur	A window width for rolling functions. Make sure to choose that argument so that the animal went back to the surface at least once in this window.
plt	Should a plot about processing should be drawn ?
span	Argument passed to loess.
...	Other arguments to be passed to loess.

Examples

```
# correct_depth(exses$tdr$depth, plt = TRUE)
```

---

correct_time *Fix jumps and duplicates in TDR time stamps*

Description

Fix jumps and duplicates in TDR time stamps

Usage

```
correct_time(obj, time_seq = 1, verbose = FALSE)
```

Arguments

obj	The TDR dataset
time_seq	A variable to use in order to subset obj and extract the time column. The time variable has to be in POSIXct format.
verbose	A logical indicating if the function should be verbose.

Details

Output rows will be chronologically ordered. Table with time stamp and number of replicate of duplicates is returned in attributes, as well as a data frame listing "time jumps".

Author(s)

Simon Wotherspoon, Yves Le Bras

Examples

```
data(exses)
tmp <- rbind(exses$tdr[c(1,1,2), ], exses$tdr[-c(10, 20:30), ])
tmp <- correct_time(tmp)
attr(tmp, "correct_time")
```

---

curry *Curry*

Description

Curry

Usage

```
curry(FUN, ...)
```

Arguments

FUN	a function
...	arguments to be set

Examples

```
f <- curry(mean, na.rm = TRUE)
f(c(1, NA))
```

---

delta *Compute difference between extremes in a set of observations*

Description

Compute difference between extremes in a set of observations

Usage

```
delta(x, ord = TRUE, na.rm = TRUE)
```


Arguments

x	observations
ord	If TRUE, the output depends on the ranks of observations: `delta = Last_Extreme - First_Extreme` and therefore returns a negative value if `max(x)` is enccountered before `min(x)` in x values.
na.rm	a logical value indicating whether NA values should be stripped before the computation proceeds.

Examples

```
data(exses)
dives_phases_durations <- tdrply(delta, "time", c("!", "_", "/", "!_/"), obj = exses)
```

---

depth_consistency_index *Depth consistency index between two dives*

Description

dri_dive2 * (max_depth_dive2 - max_depth_dive1) / max_depth_dive2

Usage

```
depth_consistency_index(x = ind(), depth_col = 2, fmt = c("vector",
  "matrix"), na.pad = TRUE, ...)
```

Arguments

x	input data, a ses object.
depth_col	Character or numeric giving the column of the TDR table that stores the depth sequence
fmt	Should the function return a vector with pairwise comparison of dive taken in chronologic order or a dissimilarity matrix ?
na.pad	If TRUE and `fmt = "vector"` then a NA is appended to the beginning of the result so that the output can be directly allocated to the dive statistics table. If TRUE and `fmt = "matrix"` then the upper triangle of the matrix is filled with NA to save memory.
...	Arguments to be passed to `depth_range_index`.

Details

Low values indicate high consistency between the vertical areas vistited in the bottom of the two dives (depth range and maximum depth). Low values can incitate benthic dives.

References

Halsey, L.G., Bost, C.-A., Handrich, Y. (2007) A thorough and quantified method for classifying seabird diving behaviour. Polar Biology, 30, 991-1004.

Examples

```
data(exses)
exses$stat$dci <- depth_consistency_index(exses)
hist(exses$stat$dci)
plot(dci ~ time, exses$stat)

Mdci <- depth_consistency_index(exses, fmt = "matrix", na.pad = FALSE)
image(log(Mdci + 0.001)) # Red for values close to 0
```

---

depth_range_index *Depth Range Index*

Description

Vertical extent of the bottom phase

Usage

```
depth_range_index(x = ind(), depth_col = 2, probs = c(0, 1),
  index = TRUE)
```

Arguments

x	input data, a ses object.
depth_col	Character or numeric giving the column of the TDR table that stores the depth sequence
probs	numeric vector of length 2 giving the quantiles probabilities to be used to compute the range. Default to min and max (c(0, 1)). c(0.1, 0.9) can be usefull in order to get estimates robust to wrong bottom delimitation or unusually high wiggles.
index	Should the depth range be divided by the dive maximum depth (index ranging between 0 and 1) or the absolute values be returned ?

Details

The index ranges from 0 (perfectly flat bottom) to 1 (large vertical width bottom).

References

Halsey, L.G., Bost, C.-A., Handrich, Y. (2007) A thorough and quantified method for classifying seabird diving behaviour. Polar Biology, 30, 991-1004.

Examples

```
data(exses)
exses$stat$dri <- depth_range_index(exses)

plot(dri ~ time, exses$stat)
```


---

dive_delim *Find the dives start and end*

Description

Find the dives start and end

Usage

```
dive_delim(obj, thres.dur = c(300, 3000), thres.depth = 15, warn = TRUE,
  ...)
```

Arguments

obj	An object of class 'ses', 'statdives' or 'tdr' with time and depth variables named "time" and "depth".
thres.dur	The minimum time (seconds) a dive should last to be considered as a dive. If thres.dur has two elements the second is the maximum time (seconds) a dive should last to be considered as a dive. If thres.dur = NULL then this threshod is ignored.
thres.depth	The depth threshold (in sensor units): diving period implies greater values.
warn	Should a Warning column be added ?
...	Other arguments

Value

A data frame with the following variable: indice of period start, indice of period end, type of period, duration (s), the dive number and a optional Warning column. Attributes of the data frame include some information about the processing.

See Also

bottom_delim

Examples

```
data(exses)
dvs <- dive_delim(exses$tdr)

# Processing info
table(dvs$warning)
attr(dvs, "thres.depth")
attr(dvs, "thres.dur")
```

dive_zone_index *Compute goodness of fit of brokenstick models: Dive Zone Index (DZI)*

Description

An index of the goodness of fit for brokenstick models. Value of the dive zone index ranges from 0 (perfect fit) to 1. See original article in references.

Usage

```
dive_zone_index(x, iter = NULL, n = NULL)
```

Arguments

x	a bsm object as returned by brokenstick or optBrokenstick.
iter	the iteration number for which the DZI is to be computed. If iter = NULL then it is set to last BSM iteration.
n	Optional. The number of points to use when calculating the dive zone limits. if NULL then n is set to the number of record in the dataset used to fit the BSM (when available) or 500 (when not available)

Details

If the original TDR data are not available to the function the DZI of the last BSM iteration will be computed using the maximum residual from the previous iteration.

Value

A dzi object with:

- dzi The dive zone index obtained at each iteration.
- max_res The maximum residuals at each iteration.
- dz_Lbnd Dive zone lower bound.
- dz_Ubnd Dive zone upper bound.
- dz_width The difference between the two previous slots i.e. the vertical width of the dive zone.
- dz_Xval A vector giving the x values corresponding to dz_Lbnd, dz_Ubnd and dz_width.
- no_seg A vector giving the number of BSM segments to which the dz_Xval belong.
- seg_width Vertical width covered by BSM segments.
- seq_length Duration of BSM segments.
- pts.x, pts.y, pts.no Breakpoints information inherited from x.
- data The raw data of input BSM when available.

References

Photopoulou, T., Lovell, P., Fedak, M. A., Thomas, L. and Matthiopoulos, J. (2015). Efficient abstracting of dive profiles using a broken-stick model. Methods Ecol Evol 6, 278-288. Github repo: https://github.com/theoniphotopoulou/brokenstickmodel.git

Examples

```
data(exses)
dv <- tdrply(identity, 1:2, no = 100, obj = exses)[[1]]
bsm <- brokenstick(dv)
dzi <- dive_zone_index(bsm)

dzi
str(dzi)
plot(dzi)
```

drift_stat *Use brokensticks to identify potential drifts*

Description

drift_stat takes an object and return a data frame of all the brokenstick segments along the trip with statistics such as their vertical speed (average and standard deviation), their duration and so on. This data frame is to be filtered to identify drift segments.

Usage

```
drift_stat(object, thres.bsm = 5, bsm = NULL)
```

Arguments

object	a SES object including a TDR dataset, a "dives statistics" table and a "delim" table.
thres.bsm	a threshold to use with max_dist_cost when running optBrokenstick.
bsm	A list of brokenstick models to use directly instead of computing a new one with thres.bsm as parameter.

Details

To get average pitch and roll angles (degrees), the TDR table must include static acceleration with variable names "axG", "ayG" and "azG". Similarly, for swimming effort and PCA rate, the TDR table must have columns "swm_eff" (numeric) and "is_pca" (logical). Use functions static_acc, swimming_effort and prey_catch_attempts to compute these variables from the raw acceleration readings.

Value

A data frame of all brokenstick segments with start and end index of the segment, no_seg_tot and ID number of the segement, no_seg_dive the number of the segment within its dive, no_dive the ID of the dive conataining the segment, time the starting time of segment, drift_rate the vertical speed of the segment, dur the duration of the segment, min_depth and max_depth the minimum and maximum depths of the segment, acceleration statistics (if acceleration data available) average roll, pitch and swimming effort and PCA rate, the mean squared residuals of the segment.

Examples

```
data(exses)
ind(exses)
exses$drift <- drift_stat(exses)

# Filter drift segments from drift_stat output table
is_drift <- with(exses$drift, dur >= 100 & drift_rate %bw% c(-0.4, 0.6) & abs(roll) >= 90)
tmp <- exses$drift[is_drift, ]

# Time series are good way to check drift segments selection
plot(drift_rate ~ time, tmp, ylim = c(-0.4, 0.6))

# Various ways to save result to slots of exses
exses$drift         <- tmp
exses$no_drift_dive <- unique(tmp$no_dive)
exses$tdr$is_drift  <- tdrexpand(rep(TRUE, nrow(tmp)), ty = tmp, na_value = FALSE)
exses$stat$is_drift <- exses$stat$no_dive %in% exses$no_drift_dive

# Plot a sample
par(mfrow = c(3,3))
no_drft <- sample(exses$no_drift_dive, 9, replace = FALSE)
tdrply(plot, c("time", "depth", "is_drift"), no = no_drft, la = list(main = no_drft))
par(mfrow = c(1,1))
```

---

dynamic_acc *Dynamic (Body) acceleration DBA*

Description

DBA is calculated by smoothing data for each axis to calculate the static acceleration (static_acc), and then subtracting it from the raw acceleration.

Usage

```
dynamic_acc(x, fs = 16, agg_1hz = TRUE, ...)
```

Arguments

x	3 axes acceleration table with time in the first column and acceleration axes in the following columns. Variables must be entitled "time" for time, "ax", "ay", and "az" for x, y and z accelerometer axes.
fs	sampling frequency of the input data (Hz).
agg_1hz	Should the input be aggregated to 1 Hz ?
...	Parameters to be passed to static_acc (e.g fc).

Details

This filtered acceleration can be used to compute ODBA and VeDBA.

Value

returns a data.frame with time, and X, Y and Z static accelearyion at 1 Hz.

---

eco.mem *Subset the slots of bsm objects*

Description

bsm objects, depending on the eco.mem argument used when they were fitted using the brokenstick function, can contain numerous slots (detailed in brokenstick) keeping information about the high sampling frequency data. These information are usefull to get accurate computations in numerous cases but need to be ignored in order to mimic abstracted dive profiles such as those obtained by CTD-SRDL tags. This function is a utility that allows to ignore these high sampling fequency information.

Usage

```
eco.mem(x, n = 4, type = c("ignore", "delete", "reset"))
```

Arguments

x	a bsm object or a list of bsm objects.
n	set the number of slot to ignore as the eco.mem argument in the brokenstick function. The default n = 4 returns abstracted dive profiles as if they were obtained from CTD-SRDL tags.
type	A character indicating how the slots are to be handled. "ignore" put aside the solot (rename) so they are ignored by other bsm processing functions but do not remove them. "delete" delete them so that less memory is used to store the object. "reset" reverse the "ignore" operation.

Examples

```
data(exses)
bsm <- tdrply(brokenstick, 1:2, obj = exses)

x <- eco.mem(bsm[[1]], type = "ignore")
try(predict(x)) # error
x <- eco.mem(x, type = "reset")
predict(x) # return fitted values of sampled time stamps
identical(bsm[[1]], x)

object.size(x)
object.size(eco.mem(x, type = "delete"))

# Works on lists
bsm <- eco.mem(bsm, type = "ignore")
```

`entropy` *Shannon entropy index on time at depth proportions*

Description

Shannon entropy index on time at depth proportions

Usage

```
entropy(x, base = 2, scale = FALSE)
```

Arguments

`x`	a character vector naming the depth layers.
`base`	base argument passed to `log`.
`scale`	if TRUE the output is divided by the `log(N)` where N is the number of layers so that outpout lies between 0 and 1.`log(N)` is the minimum entropy for sample with N layers where each observation of sample is unique i.e all probability are equal.

Examples

```
data(exses)
ind(exses)

brks <- do.call(seq, as.list(c(range(exses$tdr$depth, na.rm = TRUE), by = 2)))
exses$tdr$depth_cat <- as.character(cut(exses$tdr$depth, brks))
plot(tdrply(entropy, "depth_cat", ty = "!_/"), exses$stat$pca)
```

`exses` *An tiny dataset (about 10 days) of an SES equipped with an accelerometer*

Description

An tiny dataset (about 10 days) of an SES equipped with an accelerometer

Usage

```
data(exses)
```

Format

An object of class `'ses'`.

See Also

`as.ses`

`first` *Return first or last element of a list of vector*

Description

Return first or last element of a list of vector

Usage

```
first(x)

last(x)
```

Arguments

`x`	a list of vector

Examples

```
first(1:10)
last(1:10)
```

`front` *Add averaged oceonagraphic fronts to an existing plot*

Description

Add averaged oceonagraphic fronts to an existing plot

Usage

```
front(name = c("SACCF", "PF", "SAF", "SSTF"), col = 1:4, lwd = 2,
  rescaleLon = NULL, rescaleLat = NULL, ...)
```

Arguments

`name`	The name of the front(s) to add. To choose in `c('SACCF', 'PF', 'SAF', 'SSTF', 'NSTF')`
`col`	The colors associated with names.
`lwd`	The width of the line.
`rescaleLon`	If not `NULL` then `rescale` is called with these provided arguments.
`rescaleLat`	If not `NULL` then `rescale` is called with these provided arguments.
`...`	Other atguments to be passed to `lines`.

Details

See the documentation of the `sofronts` dataset for more information about the data.

Examples

```
plot(c(40, 120), c(-80,-30), type = 'n', xlab = '', ylab = '')
front()
```

ind — *Set and get the current individual*

Description

Set and get the current individual

Usage

```
ind(value, cache = FALSE)
```

Arguments

value	If provided this value becomes te current individual. If omited the function return the last declared individual.
cache	Should the object be copied in a cache rather than a link to the object ?

See Also

ind is convenient to use with tdrply.

Examples

```
data(exses)
ind(exses)
exses$test <- "test!"
identical(ind(), exses)
```

isobath — *Add isobaths to an existing plot (Kerguelen area)*

Description

Add isobaths to an existing plot (Kerguelen area)

Usage

```
isobath(depths = -1000, lty = 2, col = "gray", plot = TRUE, ...)
```

Arguments

depths	The isobath(s) which is(are) desired.
lty	The line type.
col	The line color.
plot	Should the lines be drawn ?
...	Other arguments to be passed to lines.

Details

Isobath at -1000 m corresponds approximatively to the Kerguelen shell boarder. See the documentation of the kerbathy dataset for more information about the data.

Examples

```
## Not run:
# Require package 'sp'
plot(c(68, 80), c(-54,-48), type = 'n', xlab = '', ylab = '')
isobath()

## End(Not run)
```

is_day — *Use time and location to find if events occured during the day or the night*

Description

Use time and location to find if events occured during the day or the night

Usage

```
is_day(time, lat, lon, elevlim = c(-18, 18), type = c("character",
  "logical"))
```

Arguments

time	a POSIXlt, POSIXct or data.frame. If a data frame order of columns must be from Year to Second (6 columns).
lat	numeric vector of latitudes.
lon	numeric vector of longitudes.
elevlim	Sun elevation thresholds to distinguish between day and night
type	Should the output type be logical (TRUE for days, FALSE for night and NA otherwise) OR character ("Day", "Night", "Transition" and NA for missing locations).

See Also

sun_position

Examples

```
## Not run:
do.call(is_day, exses$stat[ , c("time", "lat", "lon")])

## End(Not run)
```

is_dive_truncated *Check if a dive profile is complete or truncated*

Description

Check if a dive profile is complete or truncated

Usage

```
is_dive_truncated(x, max_diff = 5, error = FALSE)
```

Arguments

x	The depth sequence of a dive profile.
max_diff	The maximum depth difference tolerated between the start and the end of the dive before the dive is considered as truncated.
error	Should the function give an error if a truncated dive is encountered ?

Examples

```
## Not run:
data(exses)
tdrply(is_dive_truncated, "depth", error = TRUE, obj = exses)

## End(Not run)
```

kerbathy *Bathymetry of the Kerguelen area*

Description

This dataset is a imported shapefile containing the Hi-Res. isobath of the Kerguelen area. Available isobaths from -200 m to -4400 meters by 200 m steps.

Usage

```
data(kerbathy)
```

Format

A SpatialLinesDataFrame (S4 object of sp package)

References

https://www.ga.gov.au/products/servlet/controller?event=GEOCAT_DETAILS&catno=71552

See Also

isobath

optBrokenstick *Fitting automatic brokenstick models*

Description

optBrokenstick is similar to brokenstick except that a cost function can be used to determine the optimal number of points.

Usage

```
optBrokenstick(x, y = NULL, threshold, cost = max_dist_cost, npmin = 2,
  npmax = Inf, start = NULL, na.action, ...)
```

Arguments

x	The x data. Note that the x values have to be sorted. Can also be a list of x and y data as returned by xy.coords.
y	The y data.
threshold	A threshold value for the cost function to be used instead of the minimum. If provided the search of a local minimum in the cost function is abandoned.
cost	The cost function to use. Two included in the package dist_per_pt_cost and max_dist_cost. Feel free to use a custom one.
npmin	Minimun number of points.
npmax	Maximum number of points.
start	Some starting points to start the algorithm with.
na.action	A function which indicates what should happen when the data contain NAs. The default is set by the na.action setting of options, and is na.fail if that is unset. The "factory-fresh" default is na.omit. Another possible value is NULL, no action. Value na.exclude can be useful.
...	Further arguments to be passed to bsmfit such as eco.mem.

Value

Same as brokenstick with the value of the cost function.

See Also

brokenstick and predict.bsm, residuals.bsm, update.bsm, summary.bsm, coef.bsm, plot.bsm, as.data.frame.bsm for other functions with a S3 method for bsm objects.

Examples

```
data(exses)
dv <- tdrply(identity, 1:2, no = 100, obj = exses)[[1]]
plot(depth ~ time, dv, ylim = rev(range(dv$depth)), type = 'l')
bsm <- optBrokenstick(dv)
plot(bsm, add = TRUE)
bsm <- optBrokenstick(dv, threshold = 20, cost = max_dist_cost)
plot(bsm, add = TRUE, col = 'blue', enumerate = TRUE)
```

overall_DBA — *Overall Dynamic Body Acceleration (ODBA)*

Description

Overall Dynamic Body Acceleration (ODBA)

Usage

```
overall_DBA(object)
```

Arguments

object	A data frame or TDR table including dynamic acceleration variables entitled "axD", "ayD", and "azD" for X, Y, and Z axes of the accelerometer.

Value

A vector of ODBA of the same length as object.

pca_count — *Count the number of Prey Catch Attemps (PCA)*

Description

Count the number of Prey Catch Attemps (PCA)

Usage

```
pca_count(x)
```

Arguments

x	a logical vector indicating at each timestamp if it was associated to a PCA event.

Details

A continuous succession of TRUE is considered as a single PCA.

Examples

```
data(exses)
btt_pca <- tdrply(pca_count, "is_pca", ty = "_", obj = exses)
```


pitch — *Attitude angles from static accelation*

Description

Attitude angles from static accelation

Usage

```
pitch(object)

roll(object)
```

Arguments

object	A data frame or TDR table including static acceleration variables entitled "axG", "ayG", and "azG" for X, Y, and Z axes of the accelerometer.

Details

For roll angle, the x axe is not necessary.

Value

A vector of pitch/roll of the same length as object.

plot.dzi — *Plot method for "dzi" objects*

Description

Plot method for "dzi" objects

Usage

```
## S3 method for class 'dzi'
plot(x, dz_col = "lightblue", dz_border = "blue",
  enumerate = TRUE, ...)
```

Arguments

x	a "dzi" object
dz_col	color of dive zone area
dz_border	color of the border of the dive zone area
enumerate	should the order of BSM break points be enumerated.
...	Arguments to be passed to methods, such as graphical parameters (see par).

prey_catch_attempts *Identify Prey Catch attempts*

Description

Identify Prey Catch attempts

Usage

```
prey_catch_attempts(x, fs = 16, fc = 2.64)
```

Arguments

x	3 axes acceleration table with time in the first column and acceleration axes in the following columns. Variables must be entitled "time" for time, "ax", "ay", and "az" for x, y and z accelerometer axes.
fs	sampling frequency of the input data (Hz).
fc	Cut-off frequency for the butterworth high pass filter (Hz)

Value

returns a logical vector of prey catch attempts at 1 Hz frequency. Value is TRUE if the record belong to prey catch attempt FALSE otherwise.

prof *Compute temperature profile from TDR recordings*

Description

Compute temperature profile from TDR recordings

Usage

```
prof(x, y = NULL, by = 5, na.rm = FALSE)
```

Arguments

x	the x variable.
y	The y variable.
by	To specify how to bin the x data.
na.rm	Should the NAs be removed from the output ?

Examples

```
data(exses)
temp_profiles <- tdrply(prof, c("depth", "temp"), by = 10, obj = exses)
plot(temp_profiles[["!_/#33"]], type = 'b')
```


read.wcih *Import data from Wildlife Computers ".tab" text files*

Description

Import data from Wildlife Computers ".tab" text files

Usage

```
read.wcih(x, dt = TRUE, ...)
```

Arguments

x	filename to be imported or a TDR dataset to be formated.
dt	if TRUE function will return a data.table object, else, a data.frame.
...	Arguments to be passed to `file` such as encoding.

Details

Wildlife Computers > Instrument helper > Save instrument readings > R format

resize *Resize an individual*

Description

resize cuts a ses object: given a set of dives to discard, it remove the according rows from the TDR dataset and the statdive table. The dive and bottom delimitation ("delim" table) is updated as well.

Usage

```
resize(x, no_dv_min = 1, no_dv_max = max(x$delim$no_dive), rm = NULL)
```

Arguments

x	An object of class ses.
no_dv_min	The number of the first dive to keep.
no_dv_max	The number of the last dive to keep.
rm	Optional. A logical vector of length = nrow(x$delim), where TRUE indicate that dives are to be removed.

Examples

```
data(exses)
range(exses$tdr$time)
range(abs(exses$delim$no_dive))
range(exses$stat$no_dive)

new.ses <- resize(exses, 50, 55)
range(new.ses$tdr$time)
range(abs(new.ses$delim$no_dive))
range(new.ses$stat$no_dive)
```

`SI_light` *Convert Wildlife Computers light values from/to linear W/cm^2 units*

Description

Use the equation provided by the manufacturer, Wildlife Computers.

Usage

```
SI_light(x)

WC_light(x)
```

Arguments

x	raw/transformed sensor readings

`sofronts` *Southern ocean climatologic fronts*

Description

This dataset contains the coordinates of the the major front of the southern ocean: SACCF (Southern Antarctic Circumpolar Current Front), PF (Polar Front), SAF (Sub-Antarctic Front), SSTF (Southern Sub Tropical Front) and NSTF.

Usage

```
data(sofronts)
```

Format

A data frame of 9212 rows and 3 variables.

Details

The SSTF position is defined by the intersection between the 11 deg. C isotherm and the 150 m isobath. It represents the limits between the northern warm and salty waters (Atlantic, Indian and Pacific oceans) and the colder and less salty water from the sub-antarctic area. It is considered as the northern limit of the antarctic circumpolar current (but not of the Southern Ocean which has as been arbitrarily defined to the 40 deg. S

The SAF position is defined by the maximum meridian temperature gradient between 3 deg. and 8 deg. C at 300 m. It is associated with strong currents. Around Kerguelen it deviates to the north, thus reducing the extent of the sub-antarctic area and increasing that of the polar-frontal area.

The PF position is defined as the northern limit of the minimum subsurface temperature lower than 2 deg. C. It represents the lower trace of the winter-mixed layer, which the upper part warms up during summer. It is associated with strong currents.

The SACCF front is defined as the southern limit of the Antarctic circumpolar current. It represents the border between the antarctic (to the north) and continental (to the south) areas.

Content:

- Lon Longitude
- Lat Latitude
- name The front name.

References

Belkin, I.M. (1988) Main hydrological features of the Central South Pacific, in: Ecosystems of the Subantarctic Zone of the Pacific Ocean, edited by M.E. Vinogradov and M.V. Flint, Nauka, Moscow, 21 28 [Translated as "Pacific Subantarctic Ecosystems", pp.12-17, New Zealand Translation Centre Ltd., Wellington, 1996].

Belkin, I.M. (1993) Frontal structure of the South Atlantic, in: Pelagic Ecosystems of the Southern Ocean, edited by N.M. Voronina, pp. 40 53 (in Russian), Nauka, Moscow.

Belkin, I.M., and A.L. Gordon (1996) Southern Ocean fronts from the Greenwich meridian to Tasmania, J. Geophys. Res., 101(C2), 3675-3696.

Wessel, P., and W. H. F. Smith (1996) A Global Self-consistent, Hierarchical, High-resolution Shoreline Database, J. Geophys. Res., 101(B4), 8741-8743.

See Also

`front`

`static_acc` *Static acceleration*

Description

The raw acceleration is first filtered using a low pass butterworth filter. Then , the extracted signal can be scaled so that the norm of the the vector G is 1 at each second.

Usage

```
static_acc(x, fs = 16, fc = 0.2, Gscale = TRUE, agg_1hz = TRUE)
```

Arguments

x	3 axes acceleration table with time in the first column and acceleration axes in the following columns. Variables must be entitled "time" for time, "ax", "ay", and "az" for x, y and z accelerometer axes.
fs	sampling frequency of the input data (Hz).
fc	Cut-off frequency for the butterworth low pass filter (Hz)
Gscale	Should the values be scaled by the norm of the static acceleration vector ?
agg_1hz	Should the input be aggregated to 1 Hz ?

Details

This filtered acceleration can be used to compute pitch and roll angles

Value

returns a data.frame with time, and X, Y and Z static accelearyion at 1 Hz.

---

straightness *Compute straighness index*

Description

`straightness` compute a straightness index between 0 and 1 by making the ration `L / l` where `L` is the cumulated distance between brokenstick points and and where `l` the cumulated distance between each y data points.

Usage

```
straightness(x, y = NULL, npts = 3)

sinuosity(x, y = NULL, npts = 3)
```

Arguments

x	The x data (time).
y	The y data (depth).
npts	The number of points to use. 2 is the minimum (from the start to the end of data). Each new point adds a step (using the `brokenstick` algorithm) which is taken into account when computing `L`.

Value

`straightness` returns a number between 0 (maximum sinuosity) to 1 (maximum straightness). `sinuosity` is equivalent to `1 / straightness`.

Examples

```
data(exses)
ind(exses)
sunflowerplot(tdrply(straightness, cl = 1:2, ty = '_'), exses$stat$pca)
```


---

swimming_effort *Compute swimming effort*

Description

Compute swimming effort

Usage

```
swimming_effort(x, fs = 16, fc = c(0.4416, 1.0176), rms = FALSE)
```

Arguments

x	3 axes acceleration table with time in the first column and acceleration axes in the following columns. Variables must be entitled "time" for time, "ax", "ay", and "az" for x, y and z accelerometer axes.
fs	sampling frequency of the input data (Hz).
fc	Cut-off frequencies for the butterworth band pass filter (Hz)
rms	Should the root mean square be used (instead of mean of absolute values) when averaging the acceleration to 1 Hz ?

Details

Only Y accelerometer axe is used to compute swimming effort.

Value

returns a vector of swimming effort values at 1 Hz.

---

symmetry_index *Dive/bottom symmetry index*

Description

Based on the moment where animal reaches the dive maximum depth.

Usage

```
symmetry_index(x = ind(), type = c("_", "!_/"), time_col = 1,
  depth_col = 2)
```

Arguments

x	input data, a ses object.
type	Should the index be computed on the bottom phase only (`type = "_"`) or on the complete dive profile (`type = "!_/"`)
time_col	Character or numeric giving the column of the TDR table that stores the timestamps.
depth_col	Character or numeric giving the column of the TDR table that stores the depth sequence

Details

The index ranges from 0 (skewed to the left) to 1 (skewed to the right).

References

Halsey, L.G., Bost, C.-A., Handrich, Y. (2007) A thorough and quantified method for classifying seabird diving behaviour. Polar Biology, 30, 991-1004.

Examples

```
data(exses)
exses$stat$btt.sym <- symmetry_index(exses)
exses$stat$dv.sym <- symmetry_index(exses, type = "!_/")

plot(exses$stat[ , c("time", "btt.sym", "dv.sym")])
```

---

tdrexpand — *Expand a summary variable to the length of TDR data*

Description

Expand a summary variable to the length of TDR data

Usage

```
tdrexpand(x, ty = "!_/", na_value = NA, obj = ind(), ...)
```

Arguments

x	variable to expand.
ty	a kind of regular expression that explains how to duplicate x values along TDR rows.
na_value	the NA value to be used (0 is can be useful).
obj	a "ses" object
...	arguments to be passed to `merge.data.table`.

Value

a vector of the same length as the number of rows in the tdr table of "obj".

See Also

`tdrply`

Examples

```
data(exses)
ind(exses)
exses$tdr$no_btt <- tdrexpand(exses$stat$no_dive, "_")
exses$tdr$no_dive  <- tdrexpand(exses$stat$no_dive, "!_/")
```


---

tdrply — *Apply function to subsets of a TDR dataset*

Description

`tdrply` is a functional programing utility to apply functions to specific parts and variables of TDR datasets. It is based on a call to `mapply`.

Usage

```
tdrply(f, cl = ., ty = "!_/", no = NULL, la = NULL, no_match = "na",
  obj = ind(), ...)
```

Arguments

f	function(s) to apply. The function has to be written considering that it's first argument will be a subset of the TDR data (columns according to `cl`, rows according to `ty`).
cl	character of numeric, the columns to select in the `tdr` table. Enter `cl = NULL` or `cl = .` (default) to keep all columns.
ty	a kind of regular expression to subset diving periods of `tdr` table. The pattern can be any part of this dive cycle representation `'-!_/~'`: • `'-'` surface preceding the dive • `'!'` descent of the dive • `'_'` bottom of the dive • `'/'` ascent of the dive • `'~'` surface following the dive Several symbols can be juxtaposed to bluid more complex groups e.g. `ty = "!_/"` (default which represents a dive). `tdrply` return the result of `f` for each group. `'&'` operator can be used to provide several groups in a same `ty` expression. `'|'` operator can be used within a group in order to match a group in priority but provide rescue cases (e.g `'-|~'` matches `'-'` first but will also match `'~'` if `'-'` is not found). `'()'` are implemented so `'(-|~_)'` is different from `'(-|~)_'`).
no	the dive numbers to process. Keep default `no = NULL` for all dives available in the `delim` table of `obj`. Negative values can be used to exlude dives; `-0` syntax is accepeted to remove the dive number 0.
la	list of additional arguments of `f` whose values depend on the period involved.
no_match	how to handle no match or partial match. See last example for details.
obj	a "ses" object.Optional if a default individual has been declared with `ind`.
...	additional arguments to be passed to `f`. Arguments passed through `...` are recycled for each group defined by `ty` and `no`.

See Also

`tdrexpand`

Examples

```
data(exses)
ind(exses)

## Apply function to each dive
tdrply(function(x) max(x$depth, na.rm = TRUE))
# or, using "cl" to subset columns and "..." to set "na.rm"
tdrply(max, "depth", na.rm = TRUE)
# other examples with "cl" and "..."
bsm <- tdrply(brokenstick, 1:2, npts = 10)
tdrply(plot, 1:2, no = 33) ; plot(bsm[["!_/#33"]], add = TRUE, enumerate = TRUE)

# use "no" to specify what dive numbers should be processed
(tmp <- tdrply(max, "depth", no = 111, na.rm = FALSE)) # dive no 111 only
tdrply(max, "depth", no = -111, na.rm = FALSE) # all dives but no 111
tdrply(max, "depth", no = exses$stat$max_depth == tmp, na.rm = FALSE) # logicals are accepeted

## How to use "ty": few examples
# apply "f" to each group delimited by &
tdrply(max, "light", ty = "!&_&/", no = 50:51)
# apply "f" previous surface or, if not found, next surface
tdrply(max, "light", ty = "-|~", no = 50:51)
# mix operators and use parentheses as desired
tdrply(max, "light", ty = "_!&_/&_(-|~)", no = 50:51)
# When "ty" syntax is not enought just give a data frame instead
df <- data.frame(start = seq(1, 5000, 1000),
                 end = seq(1001, 6000, 1000))
tdrply(max, "depth", df) # notice that names start with "cst" as "custom"
# An id for output names can be provided in third column
(df$id <- sample(10:20, 5, replace = FALSE))
tdrply(max, "depth", df)

## Provide different arguments to each group with "la" (List of Arguments)
opar <- par(no.readonly = TRUE); par(mfrow = c(2, 2))
tdrply(plot, 1:2, no = 50:53, la = list(col = 1:4))
par(opar)

## Not run:
## tdrply is vectorized over "f"
funs <- c(min_depth = min, max_depth = max)
tmp <- tdrply(funs, "depth", "_", no = 50:53, na.rm = TRUE)
as.data.frame(tmp)

## tdrply is vectorized over "ty" as well
tmp <- tdrply(funs, "depth", c("!", "/", surf = "-~"), no = 50:53, na.rm = TRUE)
as.data.frame(unlist(tmp, recursive = FALSE))

## Assuming that some dive bottom could not be properly defined
exses$delim[exses$delim$no_dive == 111, c("btt_st_idx", "btt_ed_idx")] <- c(NA, NA)
# choose how to handle missing periods using "no_match".
# a warning is printed anyway
tdrply(max, "depth", ty = "_", no = 110:112, no_match = "na") # default
tdrply(max, "depth", ty = "_", no = 110:112, no_match = "ignore")
tdrply(max, "depth", ty = "_", no = 110:112, no_match = "error")
# but not if the missing period can be ignored e.g:
tdrply(max, "depth", ty = "!_/", no = 110:112, no_match = "error")
```



```
## End(Not run)
```

`time_at_depth` *Compute the time-at-depth index (TAD) of a dive*

Description

Compute the time-at-depth index (TAD) of a dive

Usage

```
time_at_depth(x, ...)

## Default S3 method:
time_at_depth(x, ...)

## S3 method for class 'tdr'
time_at_depth(x, depth_col = "depth", ...)

## S3 method for class 'bsm'
time_at_depth(x, ...)

## S3 method for class 'ses'
time_at_depth(x = ind(), depth_col = 2, ...)
```

Arguments

x	input data corresponding to a dive or a ses object. Can be a numeric vector of depth records (`time_at_depth.default`), a subset of a tdr table (`time_at_depth.tdr`) or a bsm object (`time_at_depth.bsm`).
...	for S3 methods compatibility.
depth_col	a numeric or a character indicating which column of the TDR table stores the depth records.

Details

The index ranges between 0.5 ("V" shaped dive) to 1 ("U"/square shaped dive).

Examples

```
data(exses)
bsm_6pts <- tdrply(brokenstick, 1:2, obj = exses)
# These 3 lines return the exact same result
tad_highres <- tdrply(time_at_depth, 2, obj = exses)
tad_highres <- tdrply(time_at_depth, 1:2, obj = exses)
tad_highres <- sapply(bsm_6pts, time_at_depth) # because the "data" slot is used
exses$stat$tad <- tad_highres <- time_at_depth(exses)

# When the "data" slot is not available
tad_lowres <- sapply(eco.mem(bsm_6pts), time_at_depth) # data slot is not used
plot(tad_highres, tad_lowres) ; abline(0, 1, col = "red", lwd = 3)
plot(tad ~ time, exses$stat)
```

vectorial_DBA *Vectorial Dynamic Body Acceleration (VeDBA)*

Description

Vectorial Dynamic Body Acceleration (VeDBA)

Usage

```
vectorial_DBA(object)
```

Arguments

object	A data frame or TDR table including dynamic acceleration variables entitled "axD", "ayD", and "azD" for X, Y, and Z axes of the accelerometer.

Value

A vector of VeDBA of the same length as object.

which.dive *Find to which specific dive/surface a instant belongs to*

Description

Find to which specific dive/surface a instant belongs to

Usage

```
which.dive(x, object = ind())
```

Arguments

x	The time (format POSIXct) or a integer giving the row number.
object	A ses object such as returned by as.ses.

wiggles *Count/Extract wiggles in 2D dataset.*

Description

According to Halsey et al. 2007 (see references): Wiggles are a particular pattern in the dive profile over time during a dive where an increase in depth over time changes to a decrease in depth and then back to an increase in depth. This creates a short period in the dive profile that is concave in shape. Wiggles are defined as elements of the dive profile during which at three points the vertical speed passes below 0 m/s. (NB: If useful, certain wiggles could be ignored, e.g. using a threshold based on their depth range or duration.). This function implements this definition of the wiggle and is primarily intended to be used on dive profile but it can be useful to extract the inversions in any kind of 2D data having a monotonous x variable.

Usage

```
wiggles(x, y = NULL, thres.y = 2.5, thres.x = c(10, Inf), step = NULL,
  step.thres.y = NULL, step.thres.x = c(10, Inf), output = c("wig-count",
  "stp-count", "table"), plt = FALSE, bsm = NULL)
```

Arguments

x	The x data. A monotonous variable such as the time sequence of a TDR dataset. Can also be a list of x and y (processed by xy.coords). If x is a data frame with motre than two columns the fist two columns are used.
y	The y data.
thres.y	minimum y difference within a wiggle for it to be taken into account. The default values are usually appropriate if Y is a depth variable from a southern elephant seal dataset. If one value is provided wiggles are kept if the y differences are greater than this threshold. If two values are provided wiggles are kept when the y differences lie between these thresholds. This threshold is used by optBrokenstick in conjunction with max_dist_cost so it can not be set to NULL unless a value is passed to the bsm argument.
thres.x	minimum x difference within a wiggle for it to be taken into account. The default value is usually appropriate if X is a time variable from a southern elephant seal dataset. If one value is provided wiggles are kept when the x differences are greater than this threshold. If two values are provided wiggles are kept if the x differences lie between these thresholds. NULL is equivalent to c(0, Inf).
step	A vertical speed threshold defining "steps" (0.35 m/s for king penguin). If NULL then steps are ignored.
step.thres.y	similar to thres.y but applies to steps only.
step.thres.x	similar to thres.x but applies to steps only.
output	Should the function return the number of wiggles ("wig-count"), the number of steps ("stp-count") or a data frame with width, height and height/width ratio for each transit/step/wiggle identified ("table").
plt	Should graphics about processing be plotted ?
bsm	To speed up the process you can provide a brokenstick model to use directly instead of computing a new one from x and y data.

References

Halsey, L.G., Bost, C.-A., Handrich, Y. (2007) A thorough and quantified method for classifying seabird diving behaviour. Polar Biology, 30, 991-1004.

Examples

```
data(exses)

# Number of wiggles can be used as a proxy of the foraging activity
sunflowerplot(tdrply(wiggles, ty = '_', obj = exses), exses$stat$pca)
sunflowerplot(tdrply(wiggles, ty = '_', obj = exses, step = 0.35), exses$stat$pca)

# Identifying steps as well
tdrply(wiggles, c("time", "depth"), ty = '_', no = 65, obj = exses,
       step = 0.35, output = "table", plt = TRUE)
```

Index

ANNEXE

B

Informations supplémentaires du chapitre 3

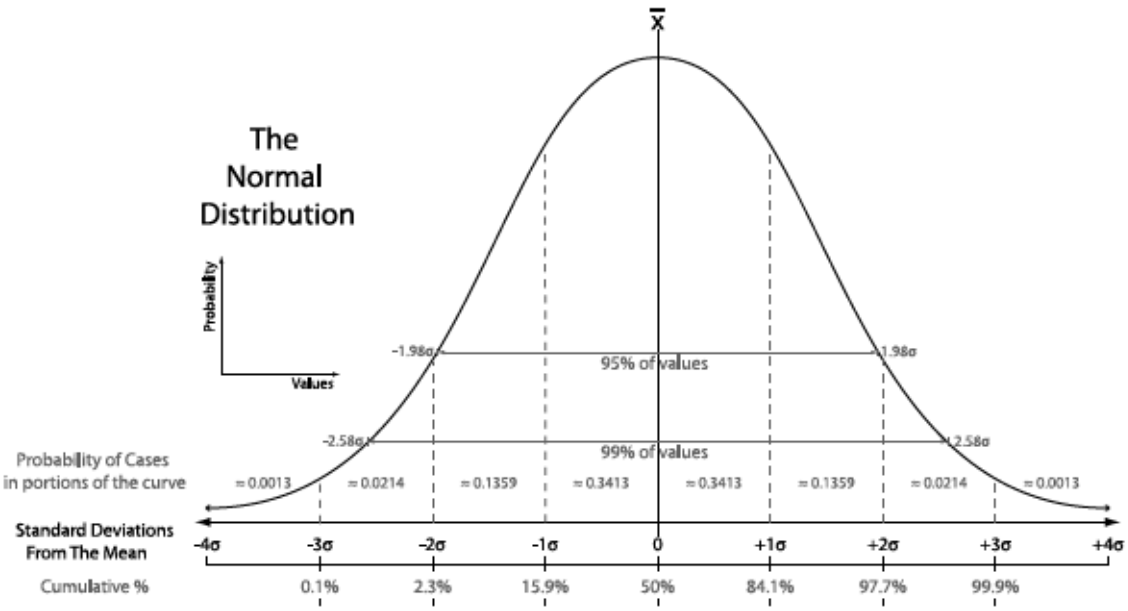

Parmi toutes les densités de probabilité de moyenne μ, de variance σ^2 finie et de support $\mathbb{R}$, l'unique qui maximise l'entropie est celle de la loi normale $N(\mu, \sigma)$. Toute somme de variables aléatoires indépendantes et identiquement distribuées tend vers une variable aléatoire normale (Laplace, 1809).

S1 Appendix: Diving behaviour and device deployment details for the 9 post-breeding female SES

Device deployment details

Device deployment table

Individual	"TDR" device	Head/Back mounted	Location device (all head-mounted)	Weight (kg)	Length (cm)	Recording duration (days)
	TDR10-DD	Back	SPLASH10-F	425	278	71
2010-21	SPLASH10-F	Head				
	TDR10-ACC	Head				
2012-09	TDR10-DD	Back	SPLASH10-F	328	257	33
2012-14	TDR10-DD	Back	CTD-SRDL	258	236	19
2012-15	TDR10-DD	Back	CTD-SRDL	275	234	15
2013-10	TDR10-DD	Back	CTD-SRDL	300	244	50
2013-11	TDR10-DD	Back	CTD-SRDL	277	238	62
2013-16	TDR10-DD	Back	SPOT	236	227	17
2014-24	TDR10-DD	Back	CTD-SRDL	310	255	26
2014-35	TDR10-DD	Back	CTD-SRDL	200	216	23

Links to tags' manufacturer websites

Wildlife Computers tags:

TDR10-DD	http://wildlifecomputers.com/our-tags/daily-diary/
SPLASH10-F	http://wildlifecomputers.com/our-tags/splash/
SPOT	http://wildlifecomputers.com/our-tags/spot/
TDR10-ACC	(not commercialized anymore)

Sea Mammal Research Unit, University of St Andrews: http://www.smru.st-andrews.ac.uk/Instrumentation/SRDL/

CTD-SRDL

B.1. Diving behaviour and device deployment details for the 9 post-breeding female SES 251

Dive statistics for all individuals and all dives together

n dives = 20189, 8.04% of drift dives.

Overall maxmimum depth recorded = 1307 m

Number of dives in Day/Night
Day :10528
Night : 4176
Transition: 5320
NA's : 165

	Number of PEE at bottom	Bottom duration (s)
nbr.val	20189	20189
nbr.null	3844	0
nbr.na	0	0
min	0	1
max	42	4217
range	42	4216
sum	128391	9623049
median	5	462
mean	6.359	476.6
SE.mean	0.04451	1.74
CI.mean.0.95	0.08724	3.412
var	39.99	61159
std.dev	6.324	247.3
coef.var	0.9944	0.5188

	Horizontal speed at surface (km/h)	Median depth at bottom (m)
nbr.val	20015	20189
nbr.null	13	0
nbr.na	174	0
min	0	31.47
max	664.1	1203
range	664.1	1171
sum	102851	8251604
median	3.248	391.4
mean	5.139	408.7
SE.mean	0.0615	1.354
CI.mean.0.95	0.1205	2.654
var	75.71	37014
std.dev	8.701	192.4
coef.var	1.693	0.4707

	Bottom vertical extent (m)	Bottom time doing wiggles (%)
nbr.val	20189	20189
nbr.null	0	3032
nbr.na	0	0
min	1.023e-06	0
max	733.5	100
range	733.5	100
sum	1183168	865823
median	48.5	44.39
mean	58.6	42.89
SE.mean	0.3052	0.1998
CI.mean.0.95	0.5983	0.3917
var	1881	806.3
std.dev	43.37	28.4
coef.var	0.7401	0.6621

	Bottom time doing steps (%)	Descent pitch angle (degree)
nbr.val	20189	20177
nbr.null	1411	0
nbr.na	0	12
min	0	0.01534
max	100	84.98
range	100	84.97
sum	544118	964088
median	20.59	49.3
mean	26.95	47.78
SE.mean	0.1639	0.1142
CI.mean.0.95	0.3213	0.2238
var	542.6	263
std.dev	23.29	16.22
coef.var	0.8643	0.3394

B.1. Diving behaviour and device deployment details for the 9 post-breeding female SES 253

	Ascent pitch angle (degree)	Pitch angle variability at bottom
nbr.val	20178	20116
nbr.null	0	0
nbr.na	11	73
min	0.09414	7.627e-05
max	85.7	0.5756
range	85.6	0.5756
sum	1107008	2657
median	56.29	0.1255
mean	54.86	0.1321
SE.mean	0.1022	0.0005017
CI.mean.0.95	0.2003	0.0009834
var	210.8	0.005063
std.dev	14.52	0.07116
coef.var	0.2646	0.5387

	Pitch angle variability at bottom	Heading angle variability at bottom
nbr.val	20116	20116
nbr.null	0	0
nbr.na	73	73
min	7.627e-05	0.0001091
max	0.5756	0.9955
range	0.5756	0.9954
sum	2657	8101
median	0.1255	0.3743
mean	0.1321	0.4027
SE.mean	0.0005017	0.001649
CI.mean.0.95	0.0009834	0.003233
var	0.005063	0.05473
std.dev	0.07116	0.2339
coef.var	0.5387	0.5809

	Dive duration (s)
nbr.val	20189
nbr.null	0
nbr.na	0
min	306
max	5064
range	4758
sum	22264654
median	1096
mean	1103
SE.mean	2.17
CI.mean.0.95	4.252
var	95025
std.dev	308.3
coef.var	0.2795

Prey Encounter Events (PEE) in non-drift dives

- Percentage of non-drift dives with PEE = 91.08 %.
- Percentage of PEE in descent = 10.48 %.
- Percentage of PEE in bottom = 78.03 %.
- Percentage of PEE in ascent = 11.49 %.

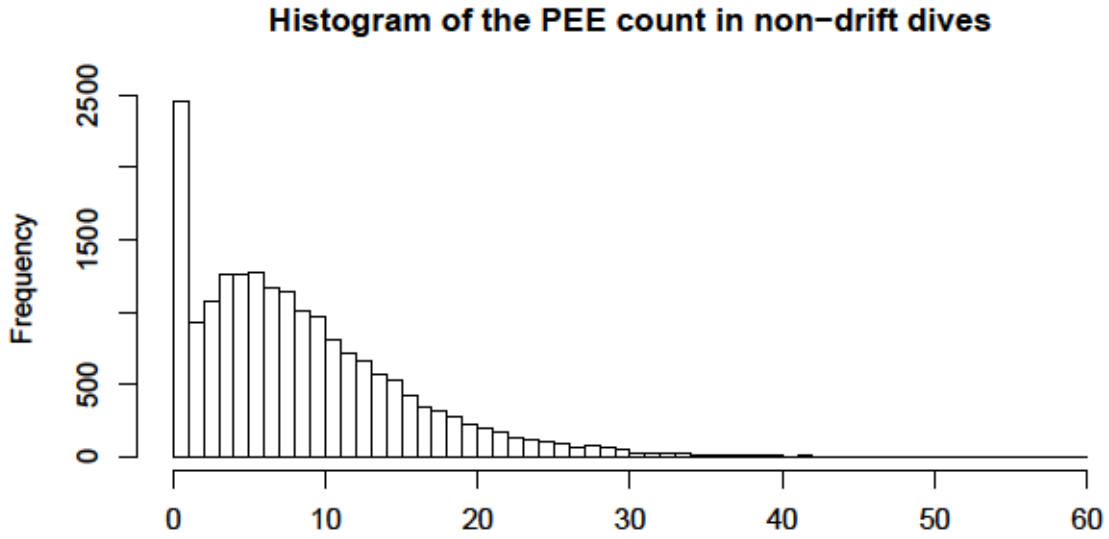

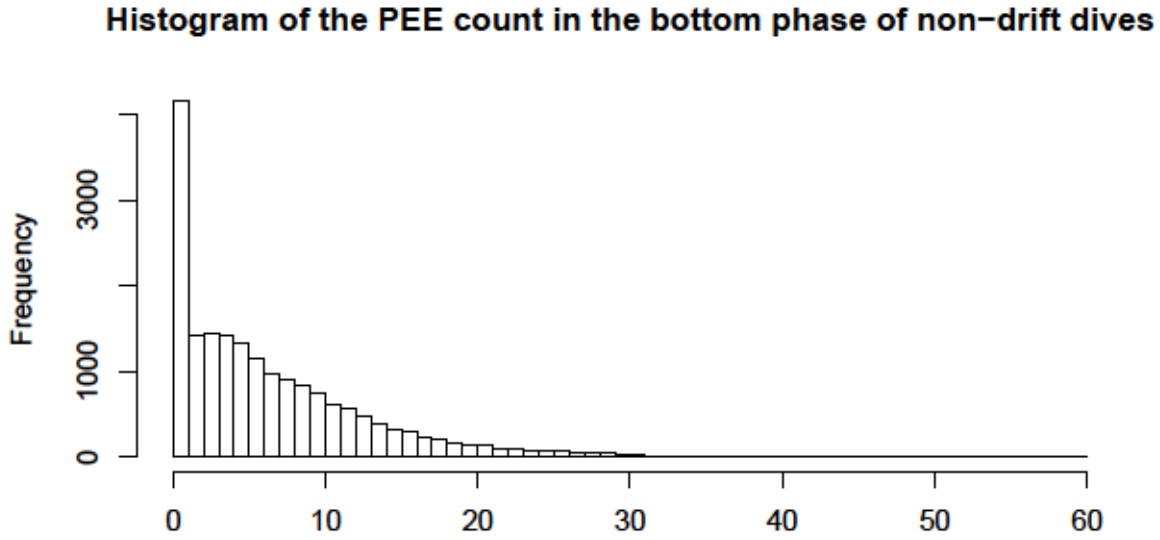

S2 Appendix: Detection of Prey Encounter Events (PEE)

Can we detect PEE using a back-mounted accelerometer?

We used back-mounted to detect PEE instead of head-mounted accelerometers (Wildlife Computers Daily Diary Tags, see device deployement details in the S1 appendix). Here we provide the evidence that this approach yields results very similar to head-mounted accelerometers.

An individual (2010-21) was equipped with two accelerometers, on its head and back, allowing comparison of the results of PEE detection method according to the logger attachment. Each accelerometer has its own clock. A small difference between the clock's internal frequencies lead to a drift between the time of the loggers. Cumulated over weeks the lag between the loggers' time is large enought to be an issue when comparing events at fine temporal scales. Synchronization (Figure 1) is accomplished by finding the time lags which maximize the cross-correlation between the depth sequences of two loggers in regularly-spaced intervals along the time series.

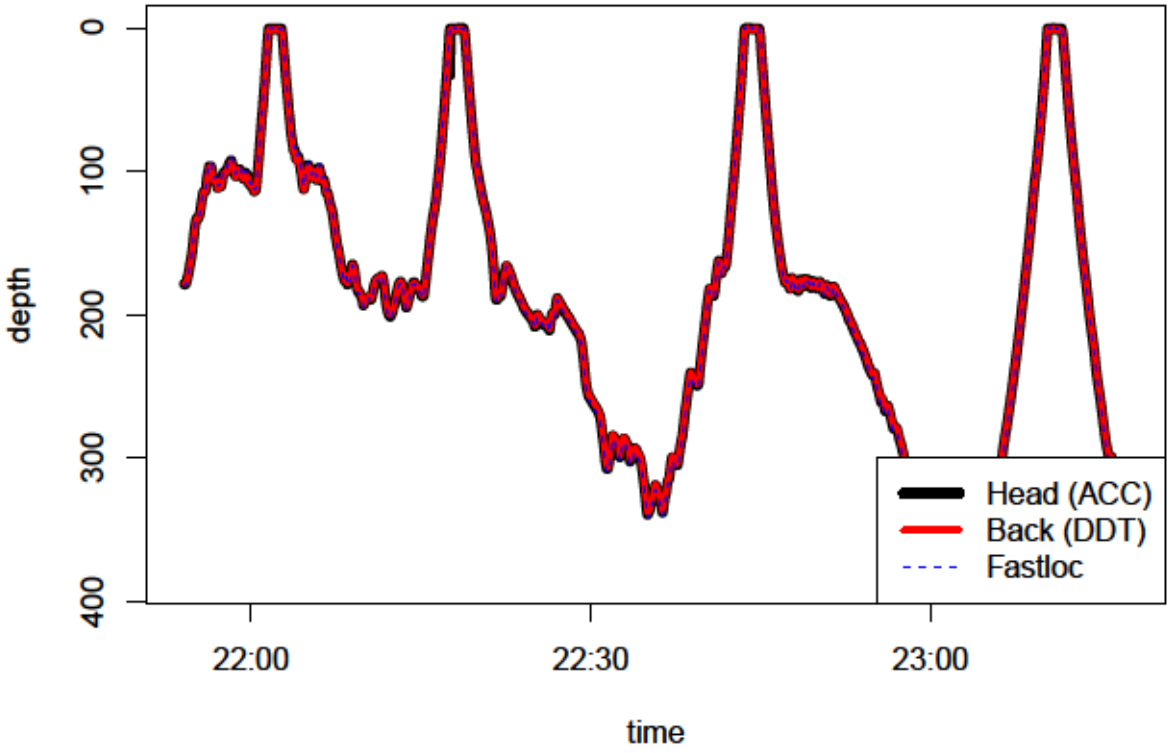

Figure 1: Random sample of the datasets showing synchronization of the devices attached to the individual 2010-21: the two accelerometers (ACC and DDT) and the location collector device (Fastloc). Pearson's product moment correlation coefficient (cor.test) between the two accelerometers time-depth sequences > 0.9999.

A PEE is occuring when the 3 axes of the accelerometer are simultaneouly flagged in a "high-state" according to a 2-means clustering applyied to each axe (See methods in the article methodology, code provided at the end of this this appendix). Comparison of the 2-mean classification results obtained for the two datasets (**at 1 Hz** which requires an accurate synchronization) indicates a Pearson's correlation coefficient of 65 %. Measures consecutively flagged as part of PEE are considered as belonging to a same PEE. Here we provide a comparison of the **count of PEE per dive** which is more robsut to time lag between datasets and is more similar to the metric used in the paper analyses. From the quantile-quantile plot it is noticeable that the PEE count according to the two accelerometers tend to differ in the range of high values (> 20) where some PEE are not detected with the back-mounted accelerometer (Figure 2, left). While PEE detection is expected to work best with head-mounted accelerometers, the results obtained with back mounted accelerometer are really close. The difference mentionned in the range of high PEE counts is not really noticeable on a classic scatter plot (Figure 2, right). The overall Pearson's product moment correlation coefficient between the two PEE count data series is equal to 93 %.

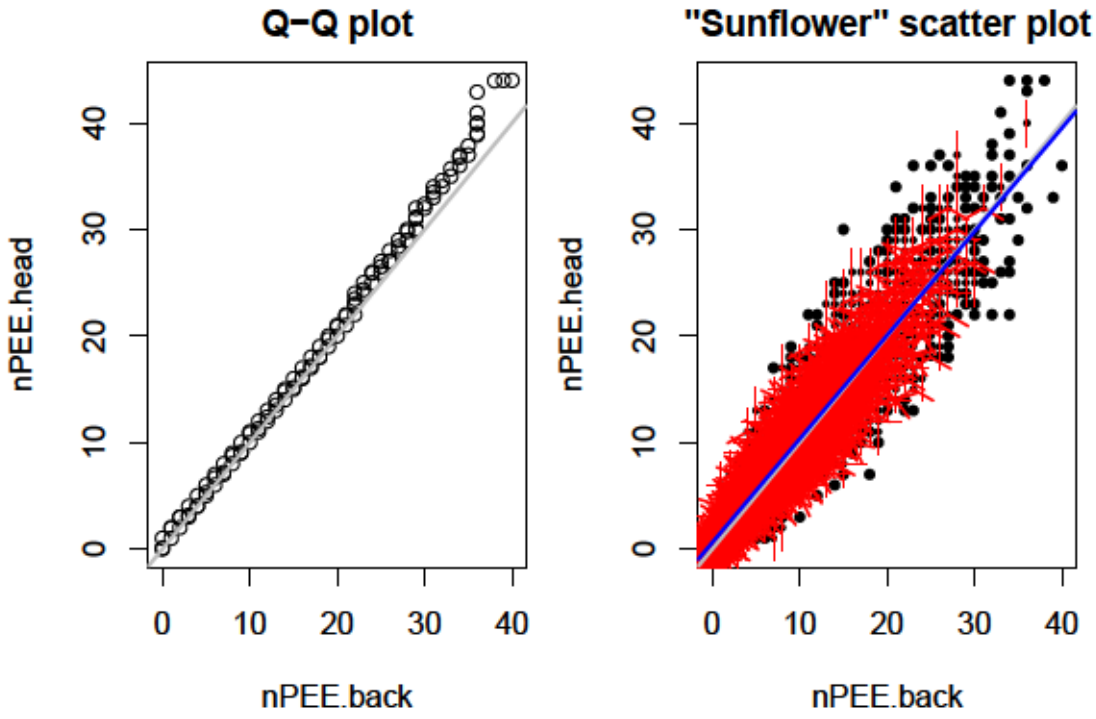

Figure 2: Left: Quantile-Quantile plot of the PEE count per dive calculated on the two datasets. Right: Sunflowerplot between PEE count per dive calculated on the two datasets. Black dot indicates 1 observation. Red ticks indicates the number of superimposed observations. Grey line stands for identity (y = x). Blue line displays the best linear regression fit (see estimated parameters in Table 1).

	Estimate	Std. Error	t value	Pr(>|t|)
(Intercept)	0.598	0.07142	8.373	7.482e-17
nb PEE back	0.9733	0.005713	170.4	0

Table 1: Coefficients of the linear regression fit between nPPE.head and nPEE.back (blue line on Figure 2-right, r-squared = 87 %).

R code for Prey Encounter Events detection

```r
#' Identify Prey Catch Attempts / Prey Encounter Events
#'
#' @param x Data table with time in 1st column and 3D acceleration
#' in the next columns. Variables must be named "time", "ax", "ay", and "az"
#' @param fs sampling frequency of the input data (Hz).
#' @param fc Cut-off frequency for the butterworth high pass filter (Hz)
#' @return returns a logical vector of prey catch attempts at 1 Hz frequency.
#' @source Source code rbl package: \url{https://github.com/SESman/rbl}
prey_catch_attempts <- function(x, fs = 16, fc = 2.64) {
  stopifnot(require("data.table"))
  stopifnot(require("signal"))
  stopifnot(require("RcppRoll"))
  # Generate Butterworth filter
  # Critical frequencies of the filter: f_cutoff / (f_sampling/2)
  bf_pca  <- butter(3, W = fc / (0.5*fs), type = 'high')
  # Apply filter
  if (!is.data.table(x)) x <- data.table(x, key = "time")
  .f <- function(x) as.numeric(filtfilt(bf_pca, x))
  x <- x[ , 2:4 := lapply(.SD, .f), .SDcols = 2:4]
  gc()

  # 1 s fixed window standard deviation + aggregate data to 1 Hz
  x <- x[ , lapply(.SD, sd, na.rm = TRUE), by = time]
  # In case of NAs set ACC to zero
  nas <- lapply(x[ , 2:4, with = FALSE], is.na)
  nas_vector <- Reduce("|", nas)
  if (any(nas_vector)) {
    warning("NAs found and replaced by 0. NA proportion:", mean(nas_vector))
    x$ax[nas$ax] <- 0
    x$ay[nas$ay] <- 0
    x$az[nas$az] <- 0
  }
  gc()

  # 5 s moving window standard deviation
  .f <- function(x) c(0,0,roll_sd(x, 5),0,0)
  x <- x[ , 2:4 := lapply(.SD, .f), .SDcols = 2:4]
  gc()

  # kmean clutering: "high" = TRUE vs "low" = FALSE
  .f <- function(x) {
    km_mod <- kmeans(x, 2)
    high_state <- which.max(km_mod$centers)
    as.logical(km_mod$cluster == high_state)
  }
  x <- x[ , 2:4 := lapply(.SD, .f), .SDcols = 2:4]

  # Aggregate and return to data.frame
  # records classified as PCA if the three axis are simultaneously in high state
  Reduce("&", x[ , time := NULL])
}
```

S3 Appendix: Surface horizontal speed

Relationship with bottom prey encounter event (PEE) rate

Transit rate (or horizontal speed measured from the ARGOS/GPS track) is known to decrease with the foraging activity. For elephant seals this relashionship have been used to infer the location of Areas of Restricted Search were the animals were assumed to be foraging. We define the "surface horizontal speed" as the average horizontal speed during a dive. It is measured fom GPS location collected during the surface periods imediatly preceding and following a dive. Here we present relashionship between the "surface horizontal speed" and the PEE rate for the two individuals equipped with GPS loggers (2012-09 and 2010-21), that we used to describe the effect of diving behaviours on the horizontal speed at surface (model 2).

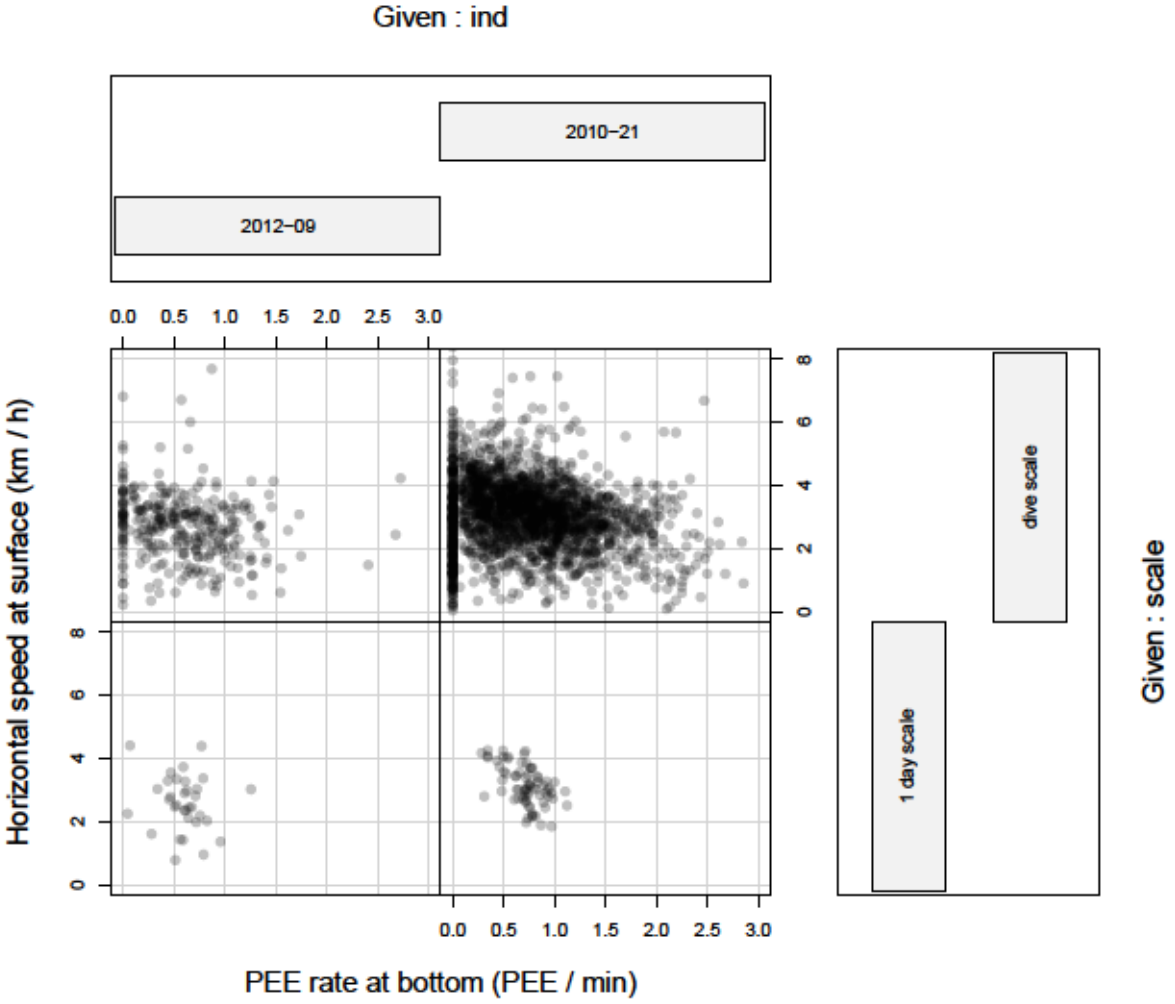

Figure 1: Relashionship between the surface horizontal speed and the PEE rate at dive scale and 1 day scale Dive scale: each point was obtained from a dive surrounded by two observed GPS locations. One day scale: each point is obtained by averaging the dive scale observations every 24 hours.

Does the selection of GPS-located dive induce some bias toward long surface durations ?"

In order to investigate how horizontal surface speed relates to diving behavior (model 2), we selected only dives associated with GPS locations in the surface periods preceding and following the dive. Here we test if this selection could introduce some bias toward dives with longer surface periods.

The duration of surface periods with successful GPS location was found to last longer than surface periods without GPS location by 7 seconds (Table 1). We acknowledge that we did not account for this bias in our study.

```
## About surface duration and amount of GPS-located dives:
##  Percentage of dives with a location in the preceding surface:  59.60723 %
##  Percentage of dives with a location in preceding & following surface:  39.37156 %

##   Quantiles of surface duration (s):

##      0%      1%      5%     95%     99%    100%
##   21.00   84.00   93.00  162.00 1409.73 9330.00

##  Average surface duration:  158.6743 s
##  Standard deviation of surface duration:  382.7328 s
```

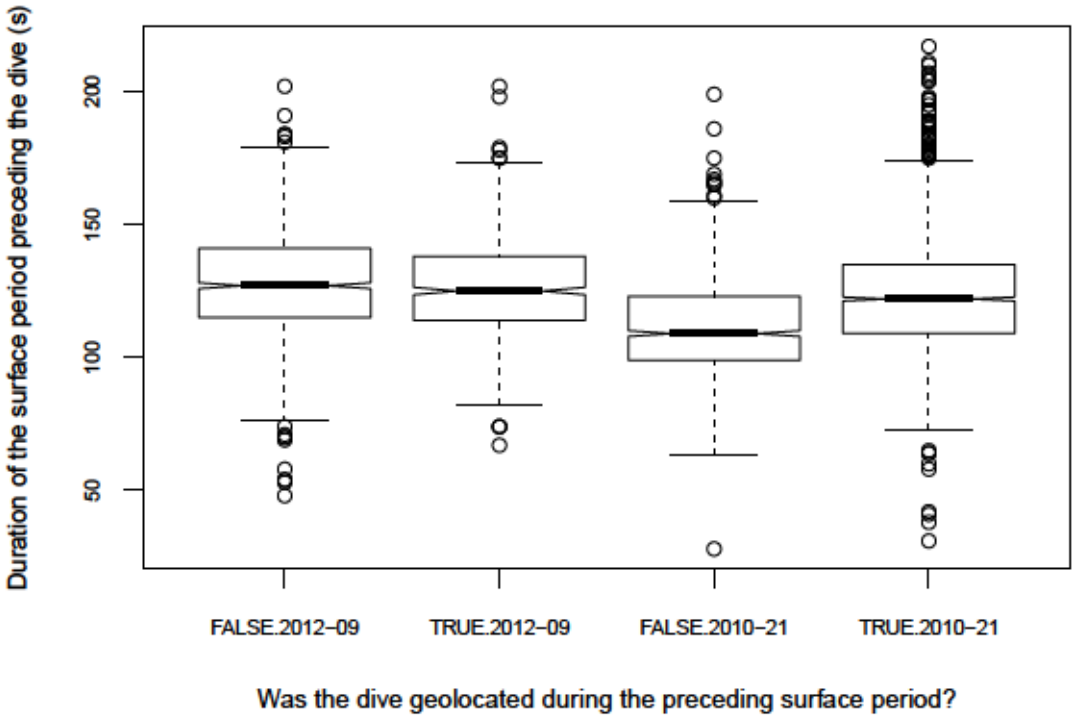

Figure 2: Comparison of surface period duration in relation with the collection of a GPS location (for the two individual equipped with GPS). 2012-09 and 2010-21 are the identifier of the two individuals equipped with GPS loggers.

Table 1: Fixed effects: psf.dur ~ is_geoloc

	Value	Std.Error	DF	t-value	p-value
(Intercept)	119.8	5.186	6213	23.1	2.339e-113
is_geolocTRUE	6.837	0.5143	6213	13.29	8.687e-40

Table 2: Standardized Within-Group Residuals

Min	Q1	Med	Q3	Max
-4.855	-0.6853	-0.07492	0.6372	4.859

Table 3: Summary of the mixed model Surface duration = f(GPS-location, individual) where individual is a random intercept effect.

	Observations	Groups	Log-restricted-likelihood
ind	6216	2	-27170

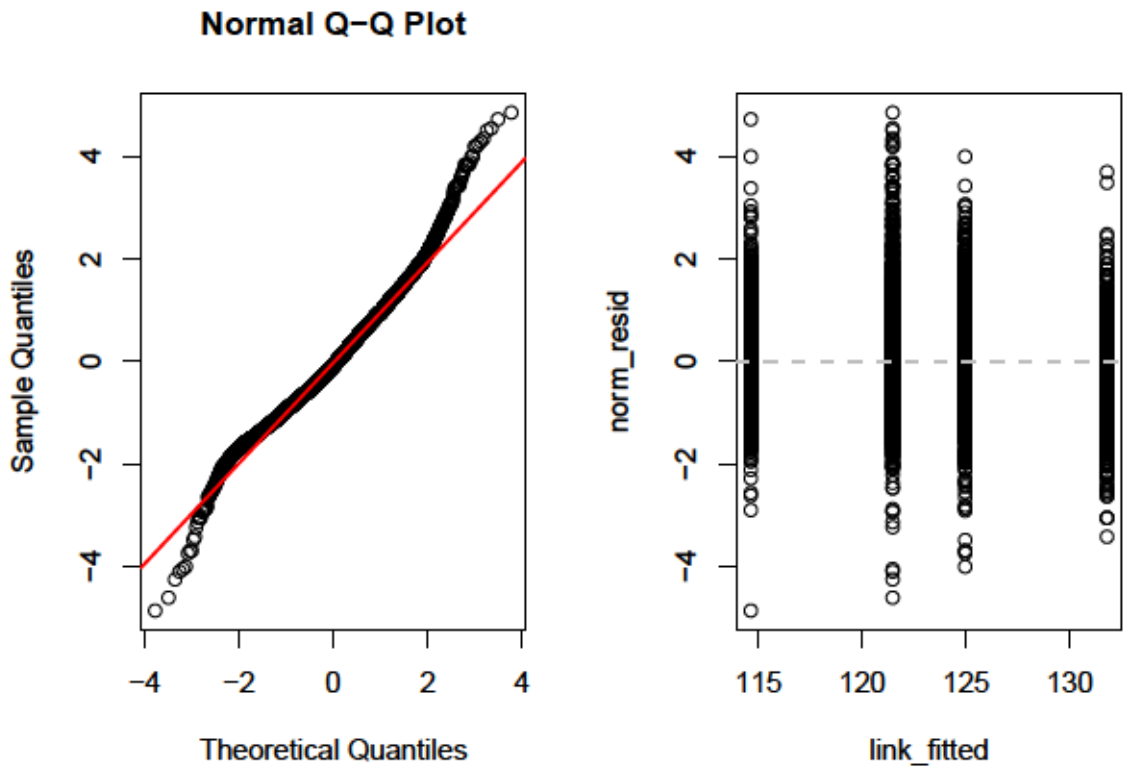

Figure 3: Model residuals

S4 Appendix: Influence of vertical speed on swimming effort during transit phases

This appendix is a complement to the previous analysis about the transit speed adjustments (models 3 & 4). Our goal is to detail how the vertical speed adjustements made by SES during their transit phases impact on the swimming effort required to acomplish these transits.

Data summary per phase

- **Ascent**:

dur	max_depth	tot_swm_eff	vert_spd
Min. : 22.0	Min. : 56.55	Min. : 36.01	Min. :0.1565
1st Qu.:203.0	1st Qu.: 271.23	1st Qu.: 255.97	1st Qu.:1.2186
Median :299.0	Median : 387.46	Median : 390.54	Median :1.3954
Mean :315.4	Mean : 411.42	Mean : 402.94	Mean :1.3640
3rd Qu.:417.0	3rd Qu.: 546.60	3rd Qu.: 532.87	3rd Qu.:1.5545
Max. :970.0	Max. :1051.43	Max. :1031.96	Max. :2.9047

- **Descent**:

dur	max_depth	tot_swm_eff	vert_spd
Min. : 41.0	Min. : 48.05	Min. : 3.182	Min. :0.1745
1st Qu.:177.0	1st Qu.: 259.50	1st Qu.: 20.096	1st Qu.:1.2199
Median :271.0	Median : 373.13	Median : 32.592	Median :1.5391
Mean :289.7	Mean : 398.09	Mean : 45.754	Mean :1.5021
3rd Qu.:379.0	3rd Qu.: 532.13	3rd Qu.: 54.272	3rd Qu.:1.8176
Max. :987.0	Max. :1051.43	Max. :372.188	Max. :2.7342

Exploratory plots

1. Swimming effort is higher in ascent than in descent (Figure 1 & 2).
2. Effect of transit duration is stronger for ascent phases (Figure 1). This is logical because, according to the previous point, the ascent phase requires a greater swimming effort. Yet, considering a multiplicative effect of duration (Figure 2 where trends according to duration are very similar for ascent and descent), the transit duration has roughly the same effect in ascent and descent phases.
3. The effect of vertical speed seems to accentuate for longer transit time (graphic 1). Again, this is logical because the variations of swimming efforts due to changes in the vertical speed are magnified over the complete transit duration. Again, this is not noticeable when considering a multiplicative effect (for a given phase, on Figure 2, the slopes according to vertical speed are similar across the different durations).
4. For descents, a "$>$" shape is noticeable (Figure 2) and seems to indicate that increases in descent vertical speed could be either performed passively (e.g. by pitch angle adjustments) or actively (e.g. by intensifying swimmming effort). However, in the following analyses we will focus on the global effect of the changes of vertical speed on the swimming effort without distinguishing the different possible mecanisms controling the transit rate.

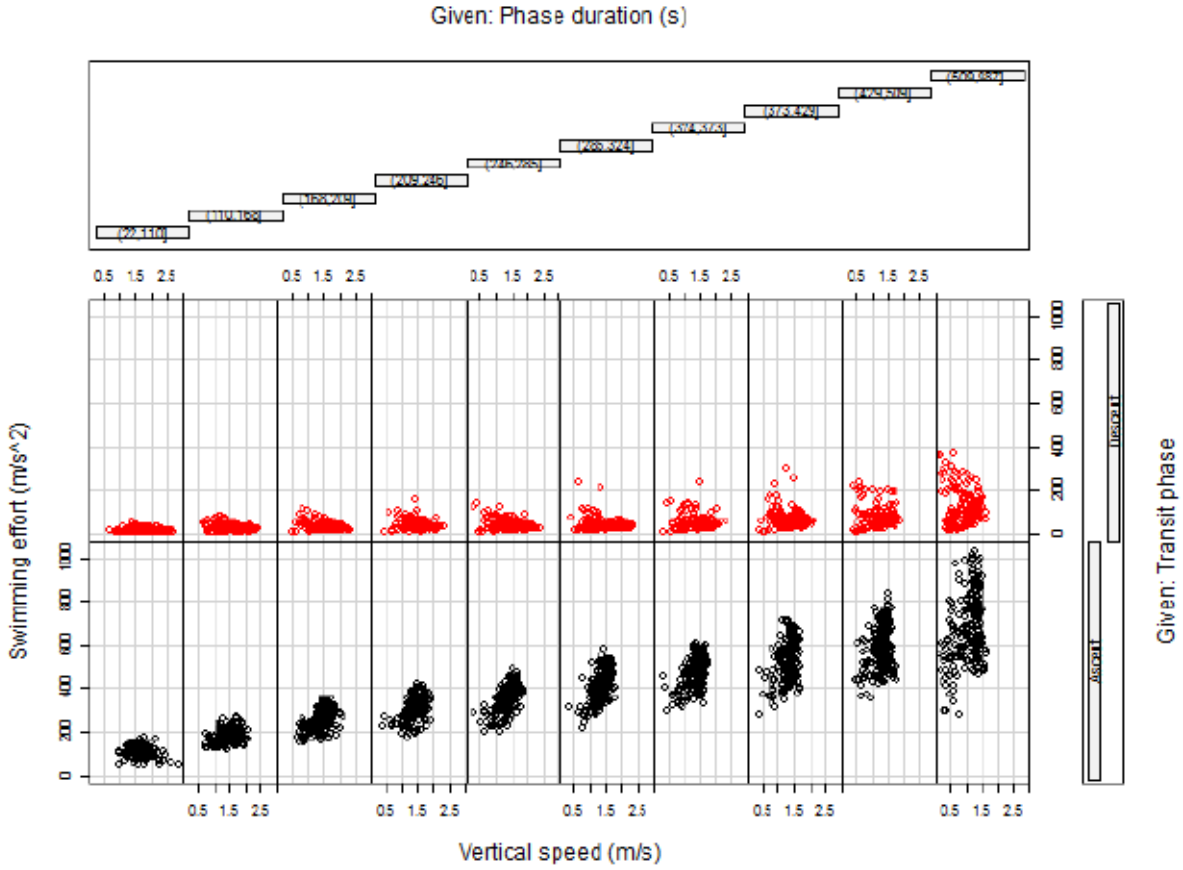

Figure 1: Relationship between swimming effort, vertical spped and phase duration in the descent and ascent phases of SES dives. Ascent phase observation in black, Descent phase observations in red.

```
##
##  Missing rows: 1666
```

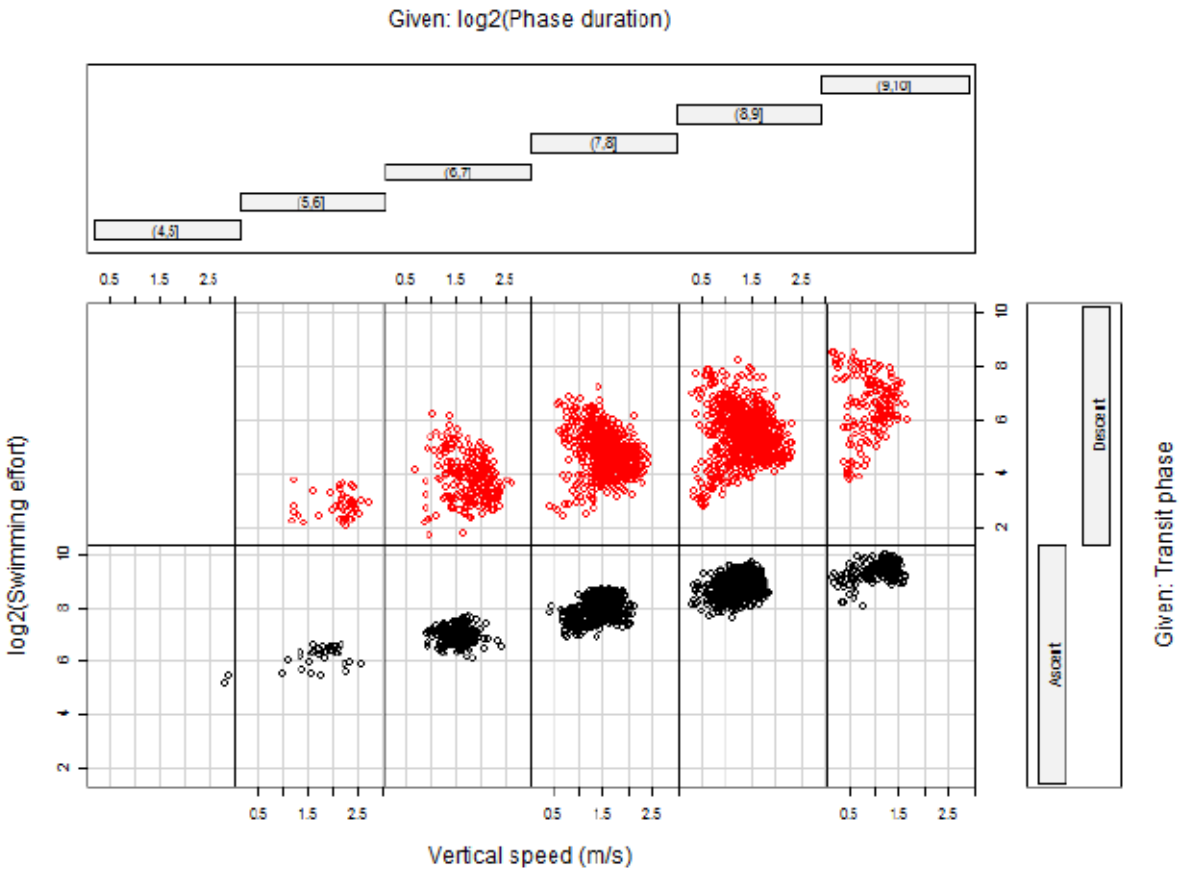

Figure 2: Relationship between swimming effort (log scale), vertical spped and phase duration (log scale) in the descent and ascent phases of SES dives. Ascent phase observation in black, Descent phase observations in red.

Statistical analysis

Theorical considerations (and the previous comparison between Figure 1 & 2) would recommend to model log-transformed swimming effort as a function of log-transformed duration. However, because it allows us to model the effect of depth using a simple interaction term and because the first exploratory plot (graphic 1) provides the evidence that a linear (additive) effect of duration on the swimming effort yield in a reasonale fit, we opt for a model with simple linear additive effects. So far the data presented represented oly one dive evry ten. The model selection is based on the same data.

In a first step we selected the explanary variables to be used in the model. The variance inflation factor provided a simple criterion.

Table 3: Variance Inflation Factor (VIF) table of the potential explanatory variables. Maximum depth was removed from potential explanatory variables. No information is lost because one variable is function of the others (e.g. Vertical speed = maximum depth / duration).

Variables	VIF
dur	9.061
max_depth	7.013
vert_spd	3.741

Table 4: This is the final VIF table. All VIF < 5.

Variables	VIF
dur	1.301
vert_spd	1.301

Then we used a stepwise AIC model selection procedure. Starting from the null model the algorithm was allowed adding or droping a variable at any step untils it reaches the null model (all variables dropped), the full model (effect of the phase factor, of the phase duration and of the vertical speed as well as of the interaction between duration and vertical speed) or it minimizes the AIC. In R syntax the full model specification was `tot_swm_eff ~ phase + (phase:dur) * (phase:vert_spd)`. Each time the spetwise algorithm reached a minimum, the correponding model was re-adjusted with the REML algorithm which is supposed to provide better parameter estimates.

However, the model we obtained after this step had serious heteroskedasticity issues as well as a residual normality issue. Thus, we tested varius correlation structure to handle the heteroskedasticity of our data. The package "nlme" provides many tools to help with this task. Among the various family tested ("varIdent", "varFixed", "varPower" and "varExp" and "varConstPower") we had the higher success with the "varConstPower" family where the "Power" was able to handle the continuous increase of variance with the predicted values and the "Constant" part the estimation of different parameter for ascent and descent phases. This step lowered the AIC by 100 points. The stepwise algorithm was implemented again using this correlation structure.

Once the variance structure was selected we tested if random effects could improve our model (lowering the AIC). Among the combinations of random slopes and intercepts that we tried to fit, the most complex (in terms of number of parameters) failed to converge (even when increasing by four times the number of maximum iterations allowed to likelihood maximization). The smaller AIC was obtained when setting the phase as random slope and intercept. The stepwise AIC selection was implemented again using the correlation structure and these random effects yielding the final model that we will now present.

Table 5: Fixed effects: tot_swm_eff ~ phase + phase:dur + phase:vert_spd + phase:dur:vert_spd

	Value	Std.Error	DF	t-value	p-value
(Intercept)	-21.41	10.1	3826	-2.12	0.03407
phaseDescent	33.37	10.12	3826	3.298	0.0009823
phaseAscent:dur	0.7676	0.02169	3826	35.38	1.659e-237
phaseDescent:dur	0.1589	0.01397	3826	11.37	1.699e-29
phaseAscent:vert_spd	9.228	3.045	3826	3.03	0.002461
phaseDescent:vert_spd	-6.259	1.523	3826	-4.109	4.05e-05
phaseAscent:dur:vert_spd	0.4151	0.0157	3826	26.44	1.281e-141
phaseDescent:dur:vert_spd	-0.01203	0.008303	3826	-1.449	0.1473

Table 6: Standardized Within-Group Residuals

Min	Q1	Med	Q3	Max
-4.233	-0.614	-0.06028	0.5712	7.189

Table 7: Linear mixed-effects model fit by REML : tot_swm_eff ~ phase + phase:dur + phase:vert_spd + phase:dur:vert_spd

	Observations	Groups	Log-restricted-likelihood
ind	3842	9	-18571

The coefficients estimates and t-statistics for the last model fitted presented in Table 5. The squared Pearson correlation coefficient between predicted and observed response is equal to 0.9530408.

Result & discussion

Discussion about the effects of covariate directly from this summary table is difficult because of the numerous interaction terms. For the sake of clarity, we will present and discuss the result using graphics.

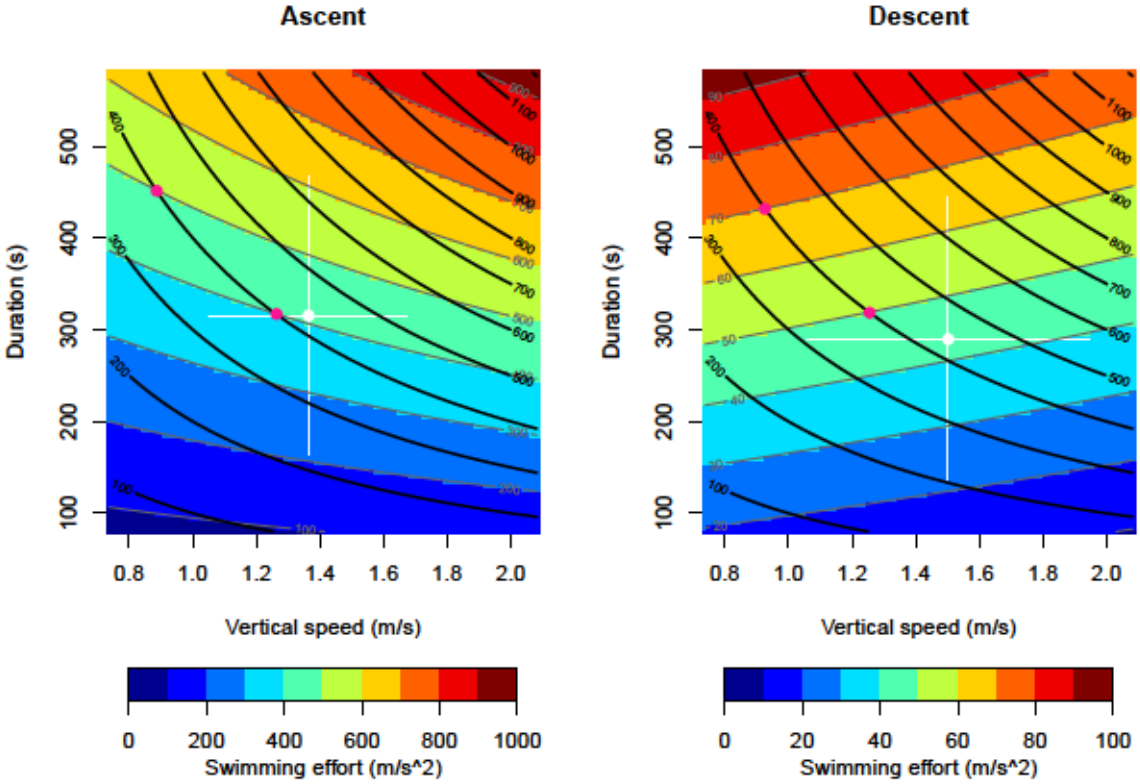

Figure 3: Image plots of model preditions for ascent and descent phases. The thin grey lines are "iso swimming effort" contour lines. The thick black lines are "iso depth" contour lines. To help with the location of likely occuring values of the covariates, the white dot indicates the average vertical speed and phase duration in our observations dataset. White segments display the +- 1 SD range around these means.

In both ascents and descents the duration is the main determinant of the cumulated swimming effort deployed by the seals to perform their transit. The effect of the vertical speed on the swimming effort qualitatively differs according to ascent or descent. Indeed, the ascent phase has greater swimming effort requirements than the descent phase. For a given duration, increasing the vertical speed implies a greater swimming effort in ascent but tend to be associated with a smaller swimming effort in descent (yet, this coefficient is not significant, see "phaseDescent:dur:vert_spd" in the previous model summary table). This leads to greater overall swimming efforts in ascent compared to descents (as highlighted on the figure by the color scales and white dots). This can be explained by the fact that all our individuals are post-breeding female SES, hence negatively buoyant, which can speed up their descent rate by increasing their diving angle while gliding down to the bottom of their dive.

The duration and the vertical speed are physically related. As SES increase their speed to transit from/to surface to/from the bottom of a dive, the duration of their transit is diminuished. More pragmatically, we can look at the changes of swimming effort according to transit speed *given a target depth* by following the path of "iso-depth" lines. For example, considering a SES diving at 400 m to perform the bottom phase:

- **In ascent:** According to the model, a vertical speed of 0.89 m/s would imply a swimming effort of 500 m/s^2 (pink point on the left) and a vertical speed of 1.26 m/s would imply a swimming effort of 400 m/s^2 (pink point on the right). This increase of the vertical speed by 42 % translates into a decrease of the total swimming effort of 20 %.
- **In descent:** This principle applies again with more strength. A vertical speed of 0.93 m/s would require a swimming effort of 70 m/s^2 and vertical speed of 1.26 m/s would require a swimming effort of

50 m/s^2. This increase of the vertical speed by 36 % translates into a decrease of the total swimming effort of 29 %.

- The larger is the gradient of swimming effort along the "iso-depth" path, the greater are the savings of swimming effort with increasing vertical speed. According to this model, the beneficial compensation effect of a reduced duration with increasing speed is attenuated toward fast vertical speeds and short phase durations, particularly during ascent phases.

To sumarize: When negatively buoyant SES speed up their ascent rate, they increase their *swimming effort per unit of time* but the overall savings of transit duration compensate for it and transforms in a reduced or similar swimming effort cumulated over the whole period. In descent, the same compensation phenomenon occurs with more strength since the cost of an increased vertical speed in terms of swimming effort per unit of time is lower than in ascent.

Model diagnostic plot

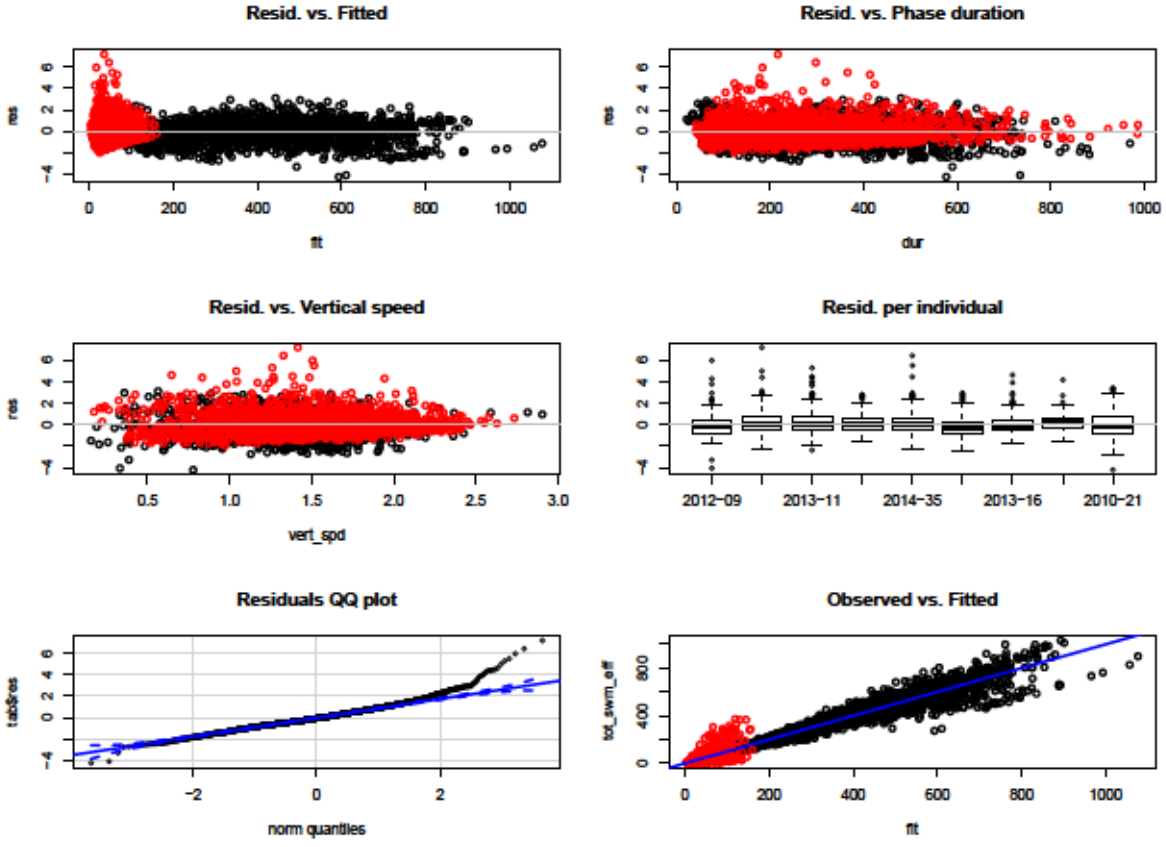

Figure 4: Diagnostic plot of the final model

Annexe

C

Informations supplémentaires du chapitre 4

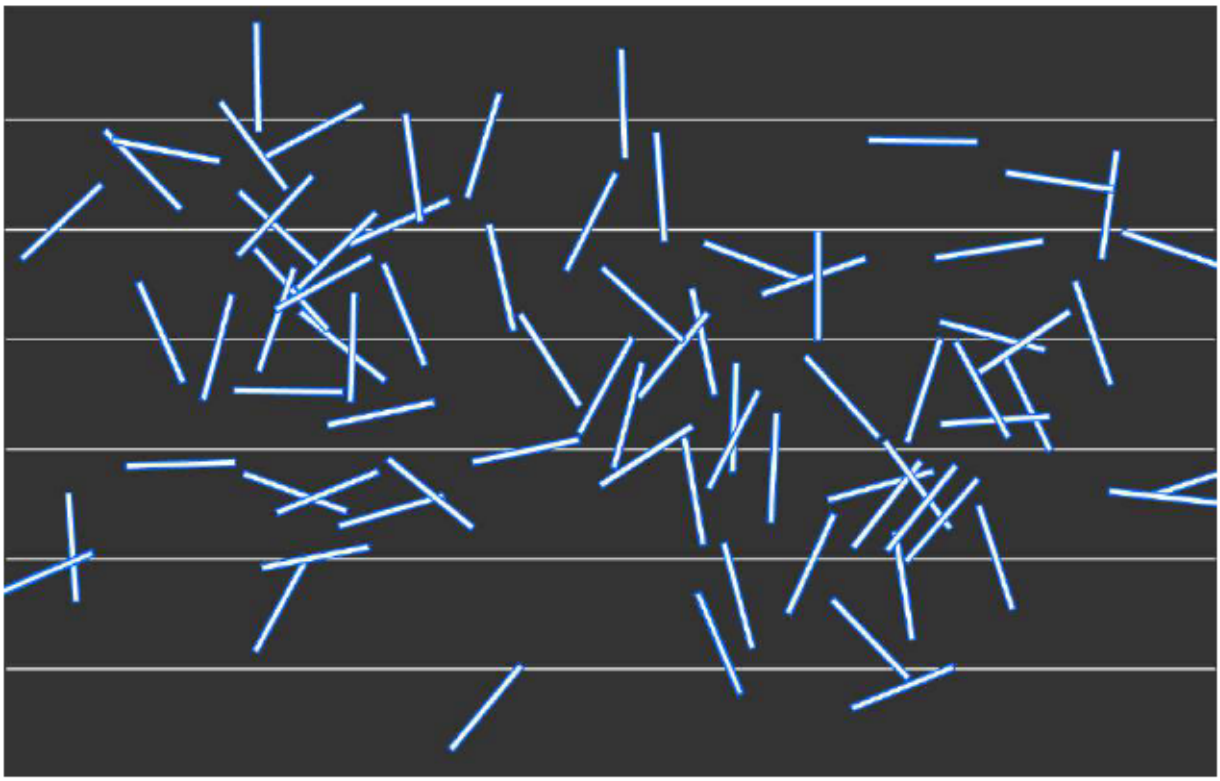

La méthode de Buffon pour estimer π : lancer n aiguilles de longueur l sur un parquet dont les lattes ont une largeur L, soit p la proportion d'aiguilles chevauchant une rainure du parquet : $\lim_{n\to+\infty} 2l/pL = \pi$.

Dans cette simulation, $n = 78$, $p = 49/78$, $l = L$ and $\pi \approx 3.18$.

"Water volume prospected by elephant seals"

Monte Carlo Integration: motivations and principle

We called "volume of water prospected by SES" the volume of water where the SES would have been able to locate prey items. The longer is the SES path, the larger is this volume. However, this volume also depends (i) on the range of the SES perception, and (ii) on the tortuosity of the trajectories. Similarly to the two-dimentional case at surface where tortuous tracks are associated with "Areas of Restricted Search", increasing 3D paths tortuousity implies prospection of smaller water volumes.

Because the SES path at the bottom of their dives can have complex shapes it is not possible to apply a general formula. The convex hull volume did not yield satifying results. Indeed, it appeared that the convex full volume greatly varies according to the location of a few points at the extremities of the trajectories, and it does not take into account the limitated abilities of SES to locate prey at great distances. Hence, we used a numerical method called Monte Carlo Integration (MCI) to assess the volume of water prospected by SES. A simple illustration of the principle of this method in 2D is presented on the figure 1 taken from wikipedia.

To implement MCI assessment of the volume prospected by SES at the bottom of dives, we made the assumption that SES could locate prey all around them, up to a given distance which is hereafter called "detection radius". The calculation of the volume is then a simple application of the example presented on the figure 1 with a third dimension: the square becomes a cuboid that encompass the trajectory of SES and whose volume is easy to calculate, the circle becomes a sphere whose radius is equal to the detection distance. The prospected water volume is calculated by taking the volume of the cuboid multiplied by the proportion of random points located within a given distance (dtection radius) from *any* specific SES location.

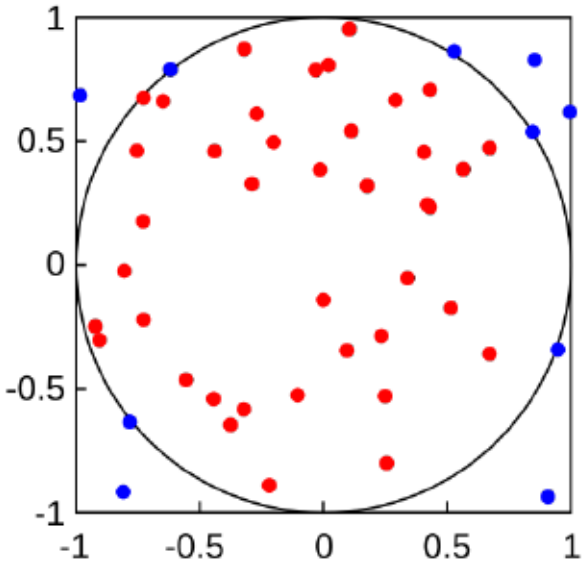

Figure 1: Illustration of Monte Carlo integration to assess π. Figure taken from the Wikipedia article entitled "Monte Carlo integration". Original caption: "In this example, the domain D is the inner circle and the domain E is the square. Because the square's area (4) can be easily calculated, the area of the circle ($\pi * 1^2$) can be estimated by the ratio (0.8) of the points inside the circle (40) to the total number of points (50), yielding an approximation for the circle's area of $4 * 0.8 = 3.2 \sim \pi * 1^2$"

R code implementation

```r
#' Assessement of prospected volume underwater using Monte Carlo integration
#'
#' @param x A data frame with the 3D coordinates of the animal locations (in meters).
#' @param n_sample Number of random points to use, higher values yield more accurate estimates.
#' @param radius Detection radius (in meters).
#' @return Estimate of the prospected volume in m^3
MCi_volume <- function(x, n_sample, radius) {
  stopifnot(require("fields")) # rdist function
  stopifnot(require("rbl"))    # "first" & "last" functions
  # Get limits of the cuboid enclosing bottom track +- "radius"
  cuboid_limits <- Map("+", lapply(x, range), list(radius * c(-1,1)))
  cuboid_volume <- prod(sapply(cuboid_limits, diff))
  # Generate uniformely distributed random points in the cuboid
  random_pts <- as.data.frame(
    Map(runif,
        n = n_sample,
        min = sapply(cuboid_limits, first),
        max = sapply(cuboid_limits, last))
  )
  # Proportion of random points located within "radius" m from any track location
  dist_matrix <- rdist(x, random_pts)
  pts_withinVol_proportion <- mean(apply(dist_matrix <= radius, 2, any))
  cuboid_volume * pts_withinVol_proportion
}
```

Reliability of the method according to detection radius and sampling effort

Experiment setup

Here, we perform an experiment to visualize how volume estimates vary (i) from a dive to another, (ii) according to the sampling effort, (iii) according to the detection radius.

- We select the bottom phases of a random sample of 48 dives from our dataset.
- For each of these bottom phases and each detection radius (1.5, 9 and 18 meters), we assess the volume of water prospected along the 3D path of SES 25 times using MCI and various sampling effort. This allows us to visualize how the the means and variances of the prospected water volume estimates behave according to the sampling effort, for a given radius and a given bottom phase.

Results of the experiment

The figure 2 presents the raw results (volume estimates) for the 9 m radius, using boxplots. As expected, the sampling effort used during the MCI has a great impact on the variance of the estimates but a lower impact on the mean/median estimation. The MCI method is unbiased, but its accuracy is very sensitive to the sampling effort.

Figure 2: Boxplots of the estimated prospected volumes according to the number of random points used in MCI (radius = 9 m). Notice that X axis is in log-scale and that Y axis scale varies according to dive ID.

The results of the entire experiment are summarized on figures 3 and 4 using the variation coefficient (sample standard deviation / sample mean), which can be considered as the measurement error of the MCI method. There is roughtly a linear relationship in log-log scale between the sampling effort and the method accuracy. The intercept of the relationship depends on the detection radius and on the bottom phase whose volume is being assessed. The detection radius has a large impact on the variation coefficient, with larger radius yielding better accuracy. This highlights that higher sampling effort is necessary for the smallest radius we used in the study (1.5 meter). The slopes of the relationships are similar between the various detection radius and bottom phases. These graphics allowed us to adjudciate that a sampling effort of 500,000 points was sufficient for the 9 and 18 meter radius. This sampling effort was doubled for the 1.5 meter radius. The next sections provide additional details on this subject.

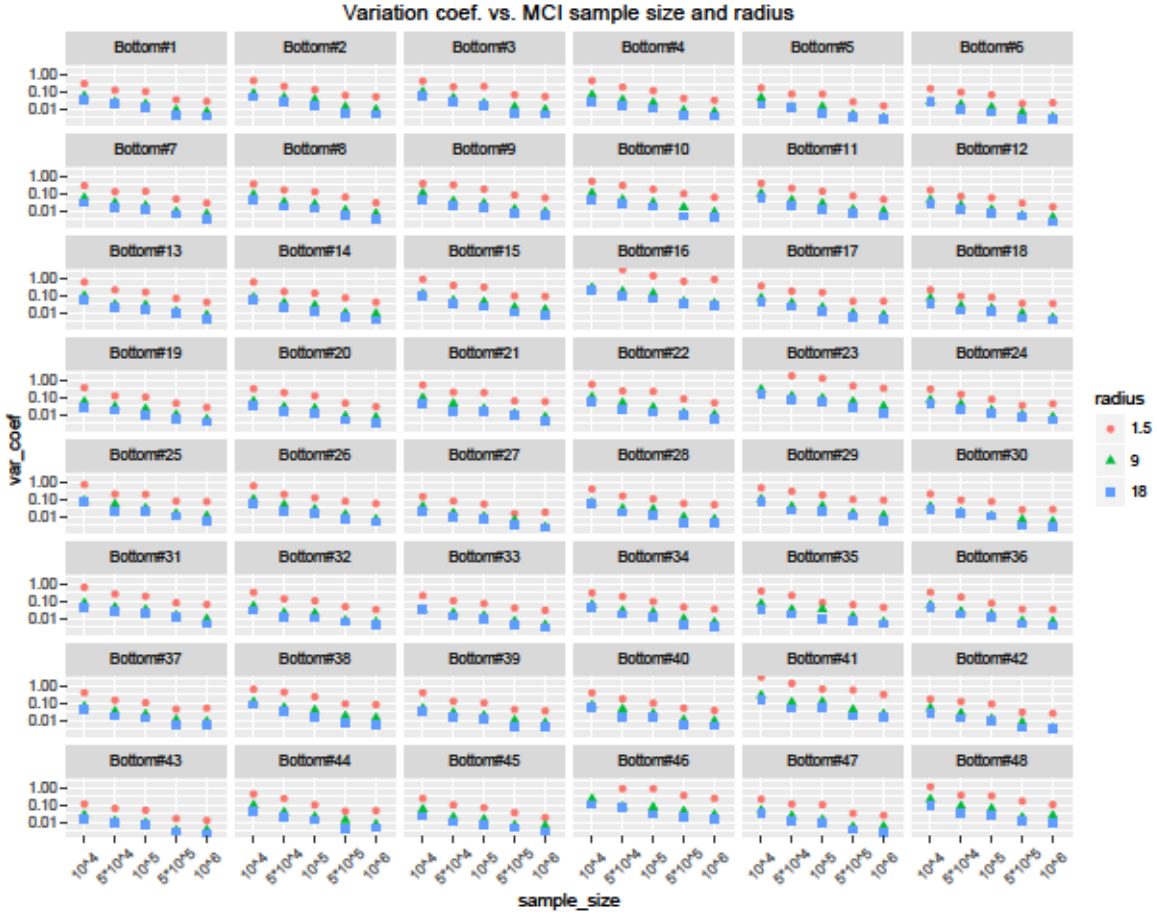

Figure 3: Variation coefficient of the estimated prospected volumes according to the number of random points used in MCI, and according to the detection radius. X and Y axis in log-scales (base 2 and base 10).

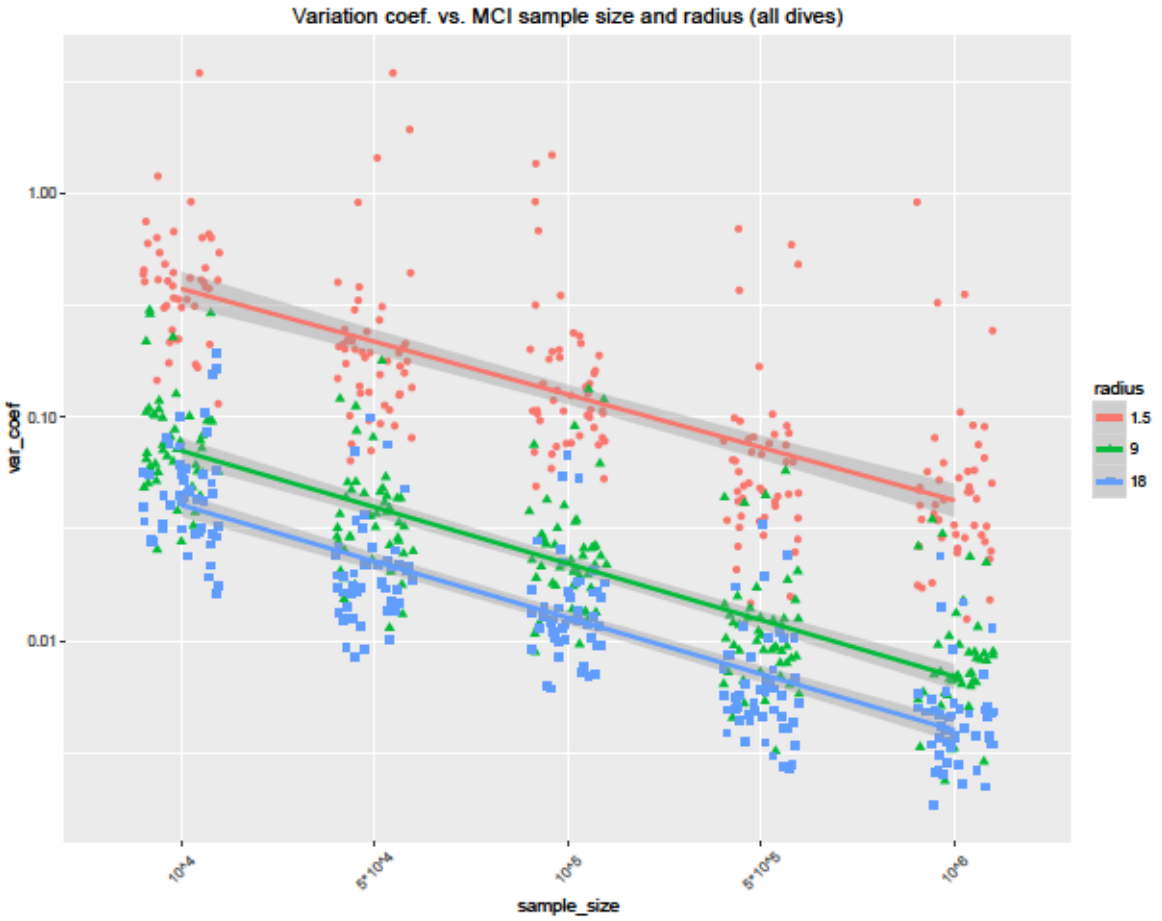

Figure 4: Variation coefficient of the estimated prospected volumes according to the number of random points used in MCI, and according to the detection radius. X and Y axis in log-scales (base 2 and base 10). Some horizontal jitter have been added to avoid points to overlap and provide better readalibity

Coefficient of variation for the settings used in main paper analyses

This section provides summary statistics (mean and 95 % quantile), as well as raw numeric values, of the variation coefficient obtained for MCI settings used in the study (tables 1, 2 and 3). These results reveal that prospected volume estimates are accurate for n = 500000 random points in the MCI if the detection radius is at least 9 meters (tables 1 & 2). For the radius = 1.5 m, the sample size has to be doubled to reach a decent accuracy (table 3).

Table 1: Values for radius = 18 m, n = 5*10^5 random points, NA indicates that all replicates estimated volume to 0. Mean variation coefficient = 0.0073, Quantile 95% = 0.0188

bottom_id	var_coef	bottom_id	var_coef	bottom_id	var_coef
Bottom#1	0.004101	Bottom#17	0.005722	Bottom#33	0.00444
Bottom#2	0.005668	Bottom#18	0.004919	Bottom#34	0.003878
Bottom#3	0.006016	Bottom#19	0.005257	Bottom#35	0.006803
Bottom#4	0.004061	Bottom#20	0.004919	Bottom#36	0.004885
Bottom#5	0.003396	Bottom#21	0.008449	Bottom#37	0.005278
Bottom#6	0.002665	Bottom#22	0.008656	Bottom#38	0.007579
Bottom#7	0.006112	Bottom#23	0.02433	Bottom#39	0.004309
Bottom#8	0.00504	Bottom#24	0.006446	Bottom#40	0.005574
Bottom#9	0.006666	Bottom#25	0.01031	Bottom#41	0.01745
Bottom#10	0.004944	Bottom#26	0.006556	Bottom#42	0.003551
Bottom#11	0.007439	Bottom#27	0.003053	Bottom#43	0.002736
Bottom#12	0.004713	Bottom#28	0.004591	Bottom#44	0.004435
Bottom#13	0.0086	Bottom#29	0.01029	Bottom#45	0.004606
Bottom#14	0.005738	Bottom#30	0.002811	Bottom#46	0.01946
Bottom#15	0.01035	Bottom#31	0.01093	Bottom#47	0.003518
Bottom#16	0.03303	Bottom#32	0.005955	Bottom#48	0.01164

Table 2: Values for radius = 9 m, n = 5*10^5 random points, NA indicates that all replicates estimated volume to 0. Mean variation coefficient = 0.0132, Quantile 95% = 0.043

bottom_id	var_coef	bottom_id	var_coef	bottom_id	var_coef
Bottom#1	0.00835	Bottom#17	0.009097	Bottom#33	0.006644
Bottom#2	0.01269	Bottom#18	0.009049	Bottom#34	0.008996
Bottom#3	0.01298	Bottom#19	0.009441	Bottom#35	0.01274
Bottom#4	0.007965	Bottom#20	0.007978	Bottom#36	0.006943
Bottom#5	0.004534	Bottom#21	0.01108	Bottom#37	0.01025
Bottom#6	0.006385	Bottom#22	0.01205	Bottom#38	0.01734
Bottom#7	0.008539	Bottom#23	0.05756	Bottom#39	0.009557
Bottom#8	0.01062	Bottom#24	0.009453	Bottom#40	0.009992
Bottom#9	0.01237	Bottom#25	0.014	Bottom#41	0.04134
Bottom#10	0.01581	Bottom#26	0.01257	Bottom#42	0.007243
Bottom#11	0.01174	Bottom#27	0.005787	Bottom#43	0.003215
Bottom#12	0.005374	Bottom#28	0.00908	Bottom#44	0.01256
Bottom#13	0.0118	Bottom#29	0.01524	Bottom#45	0.006279
Bottom#14	0.009319	Bottom#30	0.006417	Bottom#46	0.04384
Bottom#15	0.02054	Bottom#31	0.01458	Bottom#47	0.005257
Bottom#16	0.04485	Bottom#32	0.007271	Bottom#48	0.01874

Table 3: Values for radius = 1.5 m, n = 10^6 random points, NA indicates that all replicates estimated volume to 0. Mean variation coefficient = 0.0779, Quantile 95% = 0.2967

bottom_id	var_coef	bottom_id	var_coef	bottom_id	var_coef
Bottom#1	0.02778	Bottom#17	0.0472	Bottom#33	0.02973
Bottom#2	0.05241	Bottom#18	0.03461	Bottom#34	0.0348
Bottom#3	0.0536	Bottom#19	0.0265	Bottom#35	0.04319
Bottom#4	0.03284	Bottom#20	0.0289	Bottom#36	0.03298
Bottom#5	0.01527	Bottom#21	0.05794	Bottom#37	0.05072
Bottom#6	0.02323	Bottom#22	0.04855	Bottom#38	0.08086
Bottom#7	0.02895	Bottom#23	0.3546	Bottom#39	0.03495
Bottom#8	0.02995	Bottom#24	0.04275	Bottom#40	0.03699
Bottom#9	0.05712	Bottom#25	0.07542	Bottom#41	0.3251
Bottom#10	0.06254	Bottom#26	0.05729	Bottom#42	0.02522
Bottom#11	0.0464	Bottom#27	0.01773	Bottom#43	0.01253
Bottom#12	0.01724	Bottom#28	0.04881	Bottom#44	0.04635
Bottom#13	0.04065	Bottom#29	0.09085	Bottom#45	0.01819
Bottom#14	0.04043	Bottom#30	0.02593	Bottom#46	0.244
Bottom#15	0.09213	Bottom#31	0.06581	Bottom#47	0.02475
Bottom#16	0.916	Bottom#32	0.03257	Bottom#48	0.1053

Influence of the dive bottom phase ID with mixed models

We implemented a selection of mixed models in order to focus on the impact of the dive ID on the variation coefficient (CV), given a detection radius and sample size in MCI.

Conclusions:

- We found that dive ID only impact the intercept of the CV-Sample size relationship, that is the base level of the CV, but not the speed at which the CV decreases with inceasing sample size. When sample size is multiplied by 10 ($+1 = log_{10}(10)$), CV is approximatively divided by 3 ($-0.5 \sim log_{10}(1/3)$, see fixed effects summary and figure 4 for their graphical representation). Extrapolating this relationship, it appears that it is not technically achievable to us (due to computation time and RAM) to increase the sample size for the smallest radius so that the corresponding CV reaches the level obtained for other radii.
- Additionaly, the random effect of the dive ID is much larger for the small radius (1.5 meter, std. dev. = 0.34), for which the intercepts are about three times more variable (see random effects summary and tables 1 2 and 3). As a consequence the distance between the average variation coefficient and the 95% quantile is larger for the 1.5 meter detection radius (tables 1, 2 and 3).

Details:

From figures 3 and 4, the list of model to test is quite small. Here are provided the details about the model selection and the model estimates for the best candidate.

```
# Selecting random part of the mixed model with full fixed effects
# No random effect
full.random0 <- lm(log10_var_coef ~ 1 + radius * log10_sampling,
                   data = vol_stats)
# Random intercept only
full.random1 <- lmer(log10_var_coef ~ (1 | bottom_id)
                     + radius * log10_sampling,
```

```
                          data = vol_stats, REML = FALSE)
# Random log10_sampling slope and intercept
full.random2 <- lmer(log10_var_coef ~ (1 + log10_sampling | bottom_id)
                          + radius * log10_sampling,
                          data = vol_stats, REML = FALSE)
# Random radius "slope" and intercept
full.random3 <- lmer(log10_var_coef ~ (1 + radius | bottom_id)
                          + radius * log10_sampling,
                          data = vol_stats, REML = FALSE)
# Random radius & log10_sampling slopes and intercept
# This model fails to converge: "degenerate Hessian with 1 negative eigenvalues" warning
full.random4 <- lmer(log10_var_coef ~ (1 + radius + log10_sampling | bottom_id)
                          + radius * log10_sampling,
                          data = vol_stats, REML = FALSE)
# Compare AIC
AIC(full.random0, full.random1, full.random2, full.random3, full.random4)
```

```
##              df        AIC
## full.random0  7   176.5287
## full.random1  8 -1208.3033
## full.random2 10 -1207.0704
## full.random3 13 -1503.2449
## full.random4 17 -1497.3354
```

```
# Select fixed effects using random effect structure #3
nointeraction.random3 <- lmer(log10_var_coef ~ (1 + radius | bottom_id)
                                   + radius + log10_sampling,
                                   data = vol_stats, REML = FALSE)
# Compare AIC
AIC(full.random3, nointeraction.random3)
```

```
##                          df       AIC
## full.random3             13 -1503.245
## nointeraction.random3    11 -1506.798
```

```
# Print final model estimates
mod.final <- update(nointeraction.random3, REML = TRUE)
summary(mod.final)
```

```
## Linear mixed model fit by REML ['lmerMod']
## Formula:
## log10_var_coef ~ (1 + radius | bottom_id) + radius + log10_sampling
##    Data: vol_stats
##
## REML criterion at convergence: -1498.4
##
## Scaled residuals:
##      Min       1Q   Median       3Q      Max
## -2.70544 -0.62681  0.03389  0.64690  2.98103
##
## Random effects:
##  Groups    Name        Variance Std.Dev. Corr
```

```
##  bottom_id (Intercept) 0.116178 0.34085
##            radius9     0.011504 0.10726  -0.95
##            radius18    0.015822 0.12579  -0.99  0.99
##  Residual              0.004646 0.06817
## Number of obs: 717, groups:  bottom_id, 48
##
## Fixed effects:
##                 Estimate Std. Error t value
## (Intercept)     1.667126   0.052655   31.66
## radius9        -0.768467   0.016694  -46.03
## radius18       -1.010172   0.019200  -52.61
## log10_sampling -0.502632   0.003579 -140.44
##
## Correlation of Fixed Effects:
##             (Intr) radis9 rads18
## radius9     -0.848
## radius18    -0.894  0.926
## lg10_smplng -0.346  0.003  0.003
```

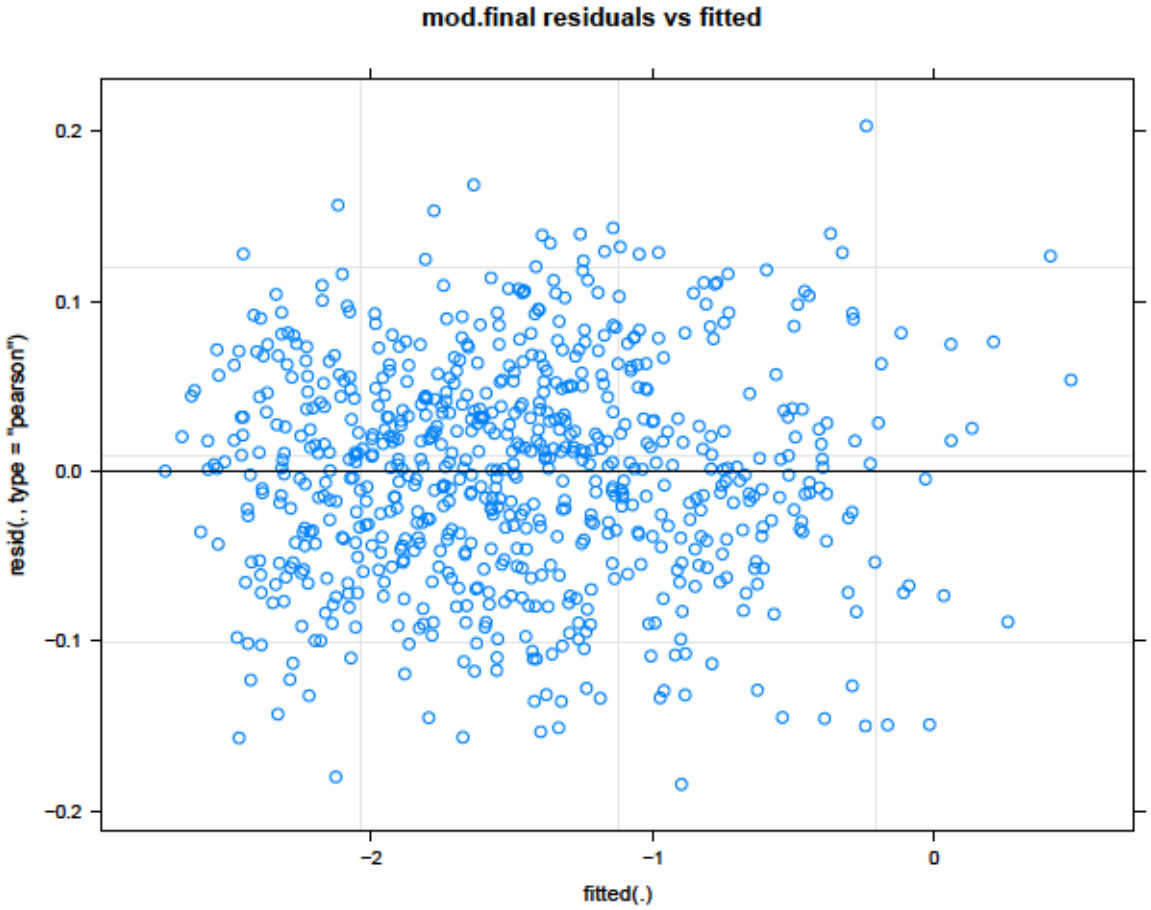

Figure 5: Model residuals

Partial regression lines for 1.5 m and 9 m radii models

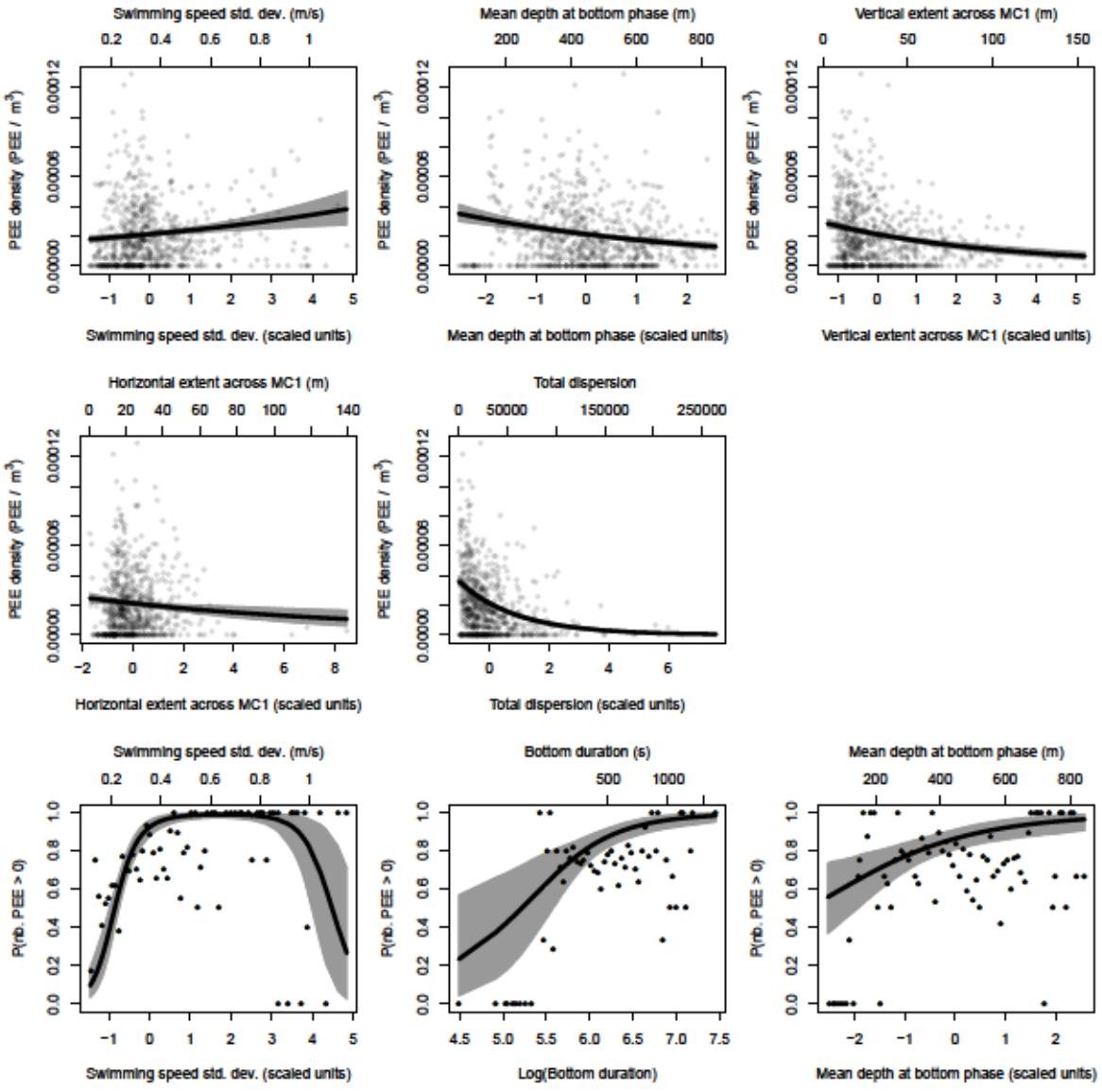

Figure 1: **Estimated relationships between the PEE density proxy and the descriptive parameters of the bottom phase trajectories. Results obtained for 9 m radius.** The top five graphics present the estimated effect of the count model and the bottom three graphics the estimated effects of the zero excess model. The tick black curves display the expected means at population level and the grey shades surrounding them stand for the 95% confidence interval of the expected mean.

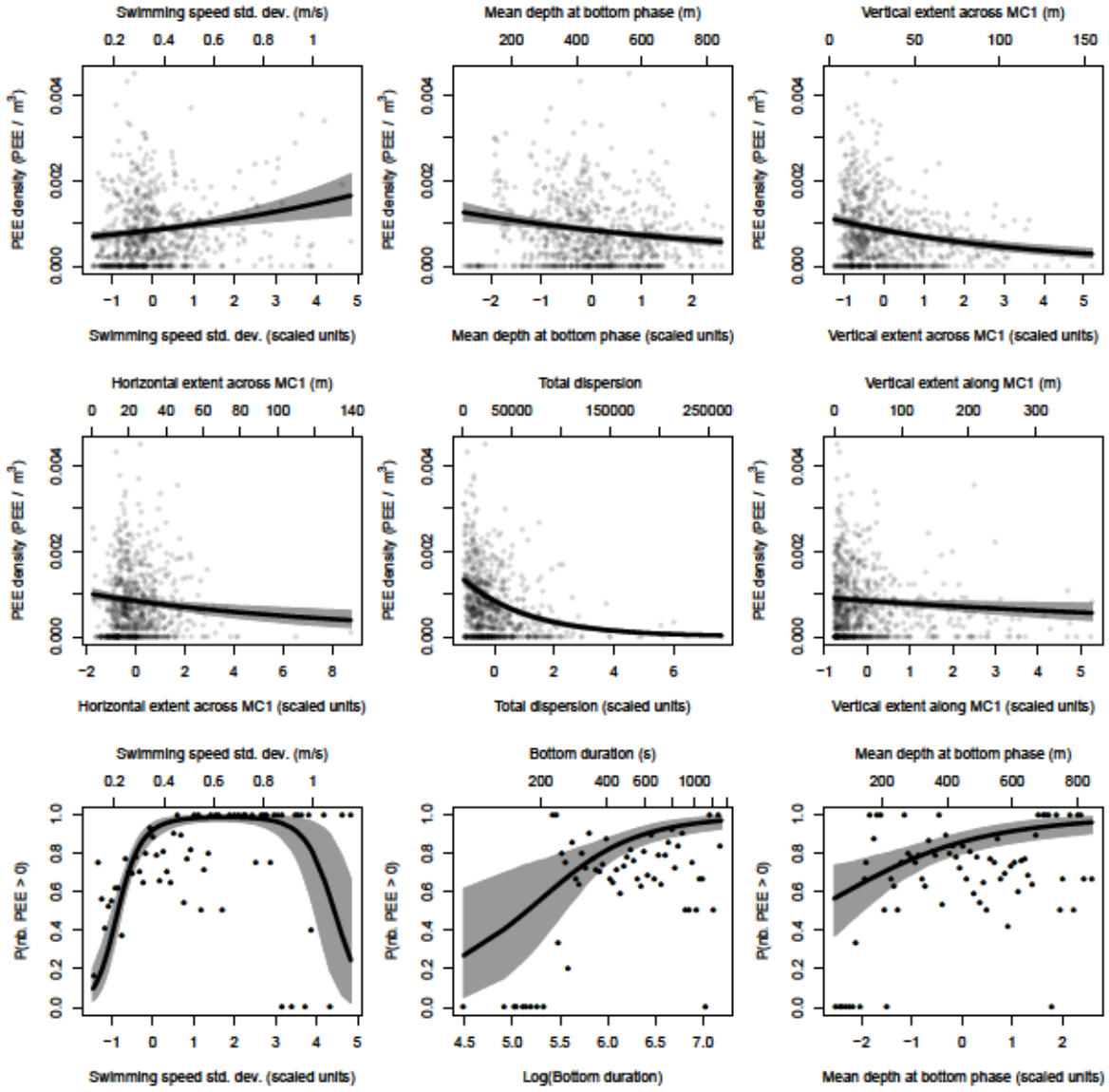

Figure 2: **Estimated relationships between the PEE density proxy and the descriptive parameters of the bottom phase trajectories. Results obtained for** 1.5 m **radius.** The top six graphics present the estimated effect of the count model and the bottom three graphics the estimated effects of the zero excess model. The tick black curves display the expected means at population level and the grey shades surrounding them stand for the 95% confidence interval of the expected mean.

Annexe

D

Informations supplémentaires du chapitre 5

Coucher de soleil romantique à Kerguelen. Crédit : J. Laborie.

Appendix A: Light sensor response to decreasing light intensity

Slow sensor response to decreasing light intensity

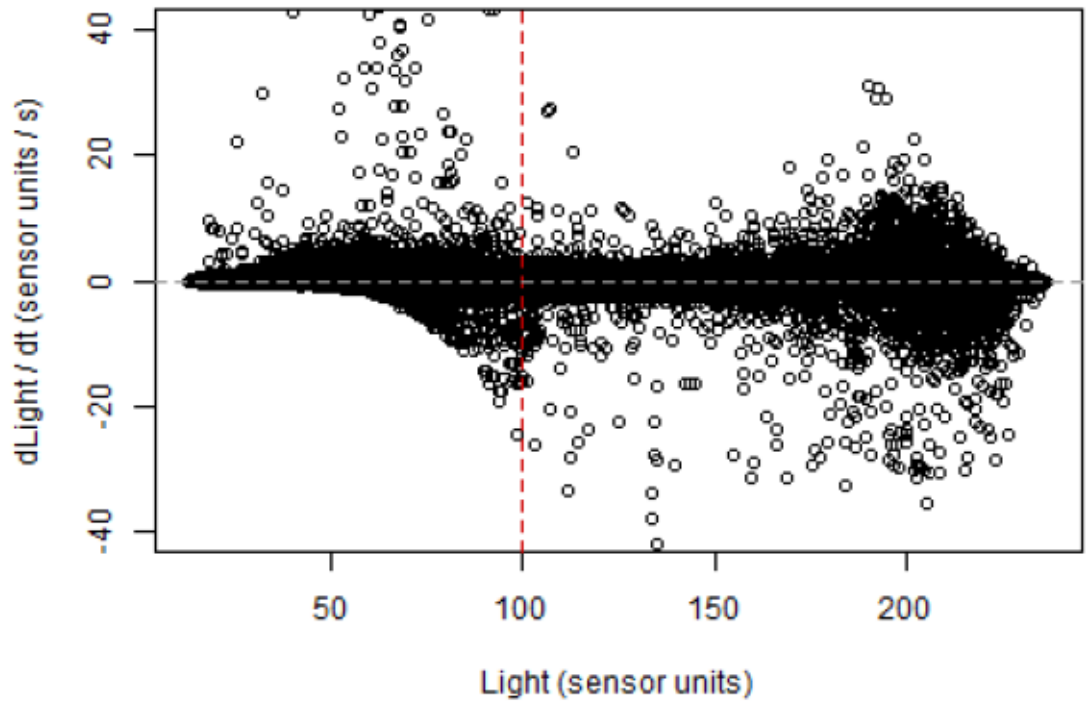

Figure 1: Graphical evidence of the sensor delayed response: dL/dt appears to be constrained in the lower left corner. Red line indicates L = 100.

Scatter plot displays a noticeable feature in the the lower left corner (Figure 1). Indeed, the negative values derivative of the light readings are clearly limited according to a function of the light instensityin range of low sensor values (< 100). To model this relationship between the lower limit of the derivative and the light intensity we tested cusstom equations. The best-fitting curve was estimated by least squared method using the `nls` function).

Modeling sensor sensor response

```
# Select observation with dL/dt < 0
idx <- which(ses$tdr$diff_light < 0)
# Find the quantile 1 / 1000 along binned L values
ses$tdr$light_previous_sec <- c(NA, ses$tdr$light[-nrow(ses$tdr)])
ses$tdr$light_cat <- cut(ses$tdr$light_previous_sec, seq(0, 250, by = 3))
tbl <- merge(
  aggregate(diff_light ~ light_cat, ses$tdr[idx, ], quantile, probs = 0.001),
  aggregate(cbind(light = light_previous_sec) ~ light_cat, ses$tdr[idx, ], mean)
)
tbl_subset <- tbl[tbl$light <= 100, ]

# Estimate parameters of the dL/dt = f(L) relationship with nls
fmla1.1 <- formula(exp(diff_light) ~ exp(K - exp(a * light + b))) # more weigth for small values
fmla1.2 <- formula(    diff_light  ~     K - exp(a * light + b))
fmla2   <- formula(exp(diff_light) ~ a / (1 + exp(-b * (light - c))))
sensor_mod1.1 <- nls(fmla1.1, tbl_subset, start = list(a = 0.20, b = -10, K = -0.70))
sensor_mod1.2 <- nls(fmla1.2, tbl_subset, start = list(a = 0.20, b = -10, K = -0.70))
sensor_mod2   <- nls(fmla2  , tbl_subset, start = list(a = 0.6, b = -0.2, c = 50))
```

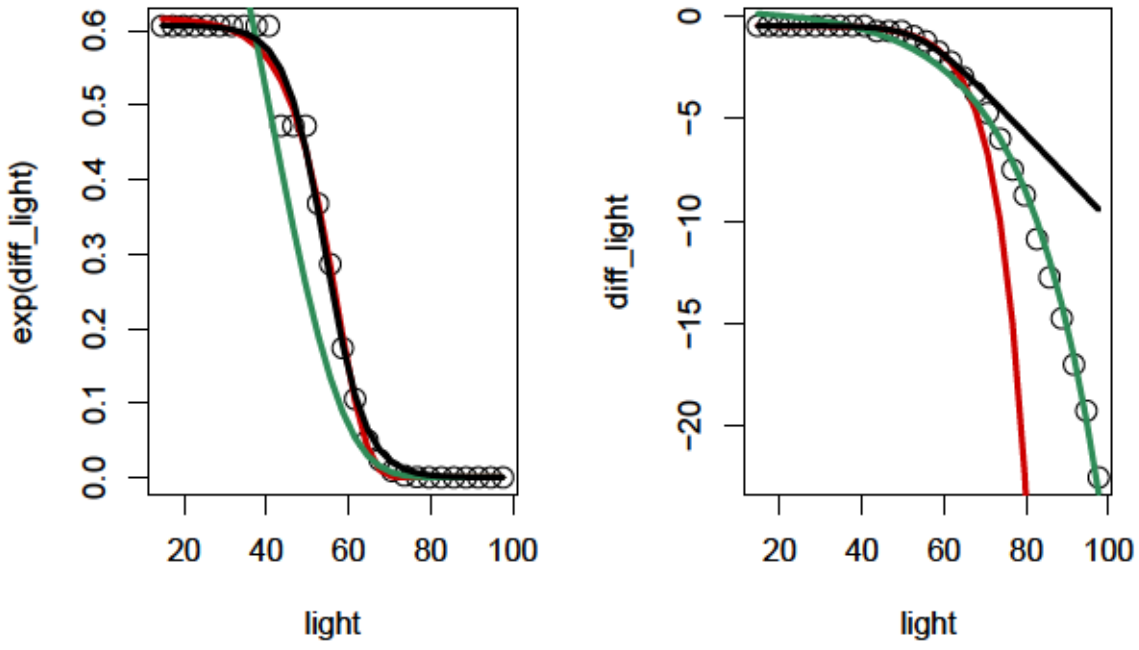

Figure 2: Fitted curves for model 1.1 (red curve) 1.2 (green curve) and 2 (black curve)

While model 2 provides a better fit for low values (light < 50), model 1 (1.1 or 1.2) provides an overall better fit in comparison to model 2. However, the parameter estimation is sensitive to the relative weight allocated

to small light values (red curve) and high values (green curve). We heuristically solved this issue by switching from one model to another according to light values as presented in the following code snippet.

```
# Model 1.2 for low values
mod1_low <- coef(sensor_mod1.1)
pred_low <- function(x) mod1_low[3] - exp(mod1_low[1] * x + mod1_low[2])
# Model 1.2 for high values
mod1_high <- coef(sensor_mod1.2)
pred_high <- function(x) mod1_high[3] - exp(mod1_high[1] * x + mod1_high[2])

# Find switching point
require("rootSolve")
root_fun <- function(x) pred_low(x) - pred_high(x) # plot(0:100, root_fun(0:100))
x_switch <- max(uniroot.all(root_fun, interval = c(0, 100))) # Second root wanted

# Final model
sensor_pred <- function(x) ifelse(x < x_switch, pred_low(x), pred_high(x))
```

Result

```
# Plot predictive model
par(mfrow = c(1, 1), mar = c(4.6, 4.1, 0.6, 0.6))
plot(ses$tdr$light[smpl-1], ses$tdr$diff_light[smpl],
     xlab = "Light (sensor units)",
     ylab = "dLight / dt (sensor units / s)", ylim = c(-40, 40))
lines(5:150, sensor_pred(5:150), lwd = 3, col = "red")
```

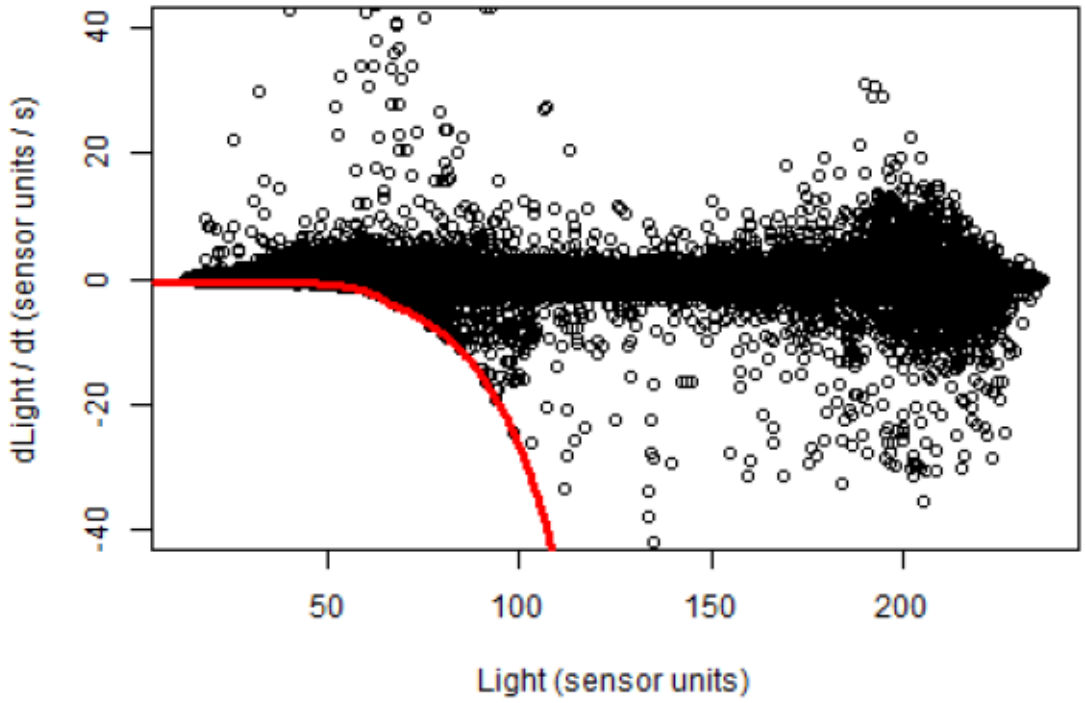

Figure 3: Predicted limitation of light decrease with random sample of the dataset.

This model was then used to test whenever or not a light measure is likely to reflect the actual light instensity in the environment or to result from the sensor limitations. To achieve that we used a affine approximation to approximate L_{t+1} (thus noted $\hat{L}_{t+1}$) given the previous measure L_t: $L_{t+1} \simeq L_t + dL/dt = L_t + f(L_t) = \hat{L}_{t+1}$. We considered that L_{t+1} resulted from sensor limitations - and consequently not refected the real ambiant light intensity - when $|\hat{L}_{t+1} - L_{t+1}| < 2$ (significant difference between observed) and $L_{t+1} - L_t < 0$ (decreasing light intensity). Given the equation provided in the main paper to convert the sensor raw values (L) to international system units (I) these inequalities translates into: $1.26^{-1} < \hat{I}_{t+1}/I_{t+1} < 1.26$ and and $I_{t+1} - I_t < 0$. An example of the result of this test is provided in the figure 1 of the study.

Appendix B: R code used to process light data

Light attenuation coefficient

```r
#' Calculate light attenuation coefficient profile
#'
#' @param x A depth-light profile with at least two variables named
#' \code{"depth"} and \code{"light_si"} (light intensity in W/cm^2).
#' @param cnd A logical indicating (with \code{FALSE}) if some part of the profiles
#' should be omitted regarding light attenuation calculation. Set to \code{TRUE}
#' to ignore this step.
#' @return a data frame with the original depth-light profile with new columns:
#' log tranformed light, monotone smooth of light (fitted with cobs) and
#' light absorption.
#' @details
#' About Wildlife computers mk9/mk10 light sensors:
#' These light intensity sensors are mainly sensitive to blue light.
#' The measures are graduated on a logarithmic scale by 0.25 units and can be converted
#' to w/cm^2 like so \code{light_Wpercm2 <- 10^((light_sensor_unit - 250) / 20)}. The
#' measurement error due to the sensor scale system is about 6\% of the reading value.
light_absorption <- function(x, cnd = NULL) {
  # Dependencies
  stopifnot(require("cobs")) # COnstrained B-Splines, used to get shape of light profile
  stopifnot(require("rbl"))  # functions like is.error, %else%, etc...

  # Data formatting
  if (is.null(x) || nrow(x) == 0 || is.error(x) || length(x) == 0) return(NULL)
  x <- x[order(x$depth), ]
  x$light_abs <- x$light_smth <- NA
  x$light_log <- try(log10(x$light_si), TRUE) %else% {
    x$light_log <- NA
    return(x) # return input, with new vars filled with NAs
  }
  x.bak <- x
  x <- na.omit(x[ , c("depth", "light_si", "light_log")])
  if (nrow(x) <= 3) return(x.bak) # return input, with new vars filled with NAs

  # Fit cobs to the light_log profile
  # Smoothing is needed to
  #   1. reduce influence of posture changes (using constraint = "decrease")
  #   2. reduce noise
  # Choice of the number of knots is important to avoid artefacts
  # caused by discontinuity of derivative around knots.
  # Start with maximum number of knots (cobs can then select knots using AIC):
  nk <- nk_ini <- nrow(x) - 1
  # Loop with error handling
  niter <- 0     # Avoid infinite loop
  exit_code <- 2 # Allows testing f cobs returns an error or warnings
  while (exit_code != 1 && niter < nk_ini) {
    .lo <- tryCatch(
      # The fitted curve must be monotonically decreasing.
```

```
      # cobs are the only computationally efficient smooths in this case.
      cobs(x$depth, x$light_log,
           constraint = "decrease",
           nknots = nk, method = "unif",
           print.mesg = FALSE),
      error = function(e) e, warning = function(w) w
    )
    exit_code <- try(.lo$ifl, silent = TRUE) %else% -1

    if (is(.lo, "error") || exit_code < 1) {
      # Most frequent source of error is the number of knots is to high
      nk <- nk - 1
    } else if (is(.lo, "warning") || exit_code > 1) {
      # Most frequent source of warning is the number of knots is to low
      nk <- nk + 1
    }

    niter <-  niter + 1
  }

  # If previous loop fails to fit a valid smooth, return input, with new vars filled with NAs
  if (is(.lo, "error")) {
    warning("Could not adjust cobs smoothing curve.")
    x.bak$light_abs <- x.bak$light_smth <- NA
    return(x.bak)
  }

  # We go back to full-size dataset and calculate attenuation coefficient
  x <- x.bak
  tmp <- try(predict(.lo, z = x$depth), silent = TRUE)
  if (is.error(tmp)) {
    x$light_abs <- x$light_smth <- NA
    return(x)
  }
  x$light_smth <- tmp[ , "fit"]
  # K = -(log10(I_out) - log(I_in)) / (z_out - z_in)
  x$light_abs <- c(NA, -diff(x$light_smth)) / c(NA, diff(x$depth))
  # K should be >= 0
  x$light_abs <- ifelse(x$light_abs < 0, 0, x$light_abs)

  # Make sure that attenuation is not returned for inappropriate locations
  # in our case K only calculated for "domain B" which is informed by
  # a "absorption_ok" in the input
  if (!is.null(cnd) && any(!cnd)) {
    cnd <- cnd | is.na(x$light_si)
  } else {
    cnd <- is.na(x$absorption_ok) | (x$absorption_ok == 0) %in% TRUE | is.na(x$light_si)
  }
  x$light_smth[cnd] <- NA
  x$light_abs[cnd] <- NA

  x
}
```

Detection of bio-luminescent events

This code is based on the work by Vacquié-Garcia et al (2012) (DOI: 10.1371/journal.pone.0043565). This code is already available online in the "rbl" project page. As such, functions code and examples contains calls to other functions from this R package.

```
## These are small utilities to work with light data from Wildlife computers tags

#' Reciprocal function of base::log10
#' @param x numeric vector
exp10 <- function(x) exp(x * log(10))

#' Convert Wildlife Computers light values from/to linear W/cm^2 units
#' @param x raw sensor readings
SI_light <- function(x) {
  10^((x - 250) / 20) # Equation provided by Wildlife Computers.
}

#' @rdname SI_light
#' @param x Light values in W/cm^2
WC_light <- function(x) {
  20 * log10(x) + 250
}
```

```
## Functions for step 1: Running "BioPIC" on Time-Light dives profiles

#' BioPIC: bioluminescent event detection tool
#'
#' Adaptation of BioPIC method with 1 Hz sampling frequency datasets and
#' of post-peak attenuation (related to sensor and not depth)
#'
#' @param x a TDR data sample
#' @param nms The names of the output variables.
#' @inheritParams biopic.qr
#' @references
#' Vacquié-Garcia, J., Royer, F., Dragon, A.-C., Viviant, M., Bailleul, F.
#' & Guinet, C. (2012) Foraging in the Darkness of the Southern Ocean:
#' Influence of Bioluminescence on a Deep Diving Predator. PLoS ONE, 7, e43565.
#' @examples
#' \dontrun{
#' data(exses)
#' biolum_dvs <- tdrply(BioPIC, obj = exses)
#' }
BioPIC <- function(x, lightSI.nm = "light_si", nms = c("alpha", "lessK", "Ia")) {
  x[ , nms] <-  NA
  nr <- nrow(x)
  for (ii in seq(6, nr - 5)) { # Apply rolling biopic.qr
    x[ii, nms] <- biopic.qr(x[seq(ii - 5, ii + 5), ], lightSI.nm)
  }
  attr(x, "biopic") <- list("lightSI.nm" = lightSI.nm, "bioPIC.nms" = nms)
  x
}
```

```r
#' BioPIC QR decomposition on a TDR sample
#'
#' @param x A data subset of fixed width of 11 seconds/lines.
#' @param lightSI.nm The name of the TDR column with light values in W/cm^2.
#' @references
#' Vacquié-Garcia, J., Royer, F., Dragon, A.-C., Viviant, M., Bailleul, F.
#' & Guinet, C. (2012) Foraging in the Darkness of the Southern Ocean:
#' Influence of Bioluminescence on a Deep Diving Predator. PLoS ONE, 7, e43565.
biopic.qr <- function(x, lightSI.nm = "light_si") {
  Amat <- log10(x[ , lightSI.nm])
  # Build the Q matrix (w rows X length(R) columns)
  Qmat <- matrix(c(
    0, 0, 1, 0, 0, 1, 0, 0, 1, 0, 0, 1, 0, 0, 1,  # log(It) = log(Ia)
    1, 0, 1,                                      # log(It) = log(alpha) + log(Ia)
    1, 1, 1, 1, 2, 1, 1, 3, 1, 1, 4, 1, 1, 5, 1), # log(It) = log(alpha) -K*t + log(Ia)
    nrow = 11, byrow = TRUE)
  Rmat <- try(qr.solve(Qmat, Amat), silent = TRUE) # A = QR. qr.solve() finds R given A&Q
  if (is.error(Rmat)) {
    Rmat <-rep(NA, 3)
  } else {
    Rmat[c(1, 3)] <- exp10(Rmat[c(1, 3)])
  }
  Rmat # alpha, lessK & Ia
}
```

```r
## Function for step 2: Identify bioluminescent events from "BioPIC" output

#' Identify potential bioluminescence emission events
#'
#' @param x a data.frame such as returned by \code{\link{BioPIC}} output
#' @param sensitivity A threshold to decide if a signal peak is high enought. See
#' details.
#' @param max_light Max light level (W/cm^2) where a event can be detected. Set to
#' NULL to disable.
#' @details Sensor sensitivity threshold: The minimum ratio between two measures
#' to be considered significantly different. In laboratory experiments, the
#' sensors measured light intensity +- 2 units while submitted to a constant
#' light intensity. Translating the sensor log-scale units to W/cm^2
#' this accuracy measure translates into a minimum ratio of 1.26.
#' @examples
#' \dontrun{
#' data(exses)
#' biolum_dvs <- tdrply(BioPIC, obj = exses)
#' ble_tbl <- Reduce(rbind, lapply(biolum_dvs, biolum_events))
#' }
biolum_events <- function(x, sensitivity = 1.26, max_light = NULL) {
  # Retrieve info
  alpha <- attr(x, "biopic")$bioPIC.nms[1]
  light <- attr(x, "biopic")$lightSI.nm[1]

  # Increasing light periods
  is_potble <- is.finite(x[ , alpha]) & x[ , alpha] > 1 # Alpha is valid and > 1
  potble <- per(is_potble)
```

```
  potble <- potble[potble$value %in% TRUE, ]

  # Compute peak light ratio
  potble$st_idx <- potble$st_idx
  potble$start_time  <- x[potble$st_idx, 1]
  potble$end_time    <- x[potble$ed_idx, 1]
  potble$start_light <- x[potble$st_idx, light]
  peakmax_idx <- mapply(function(st, ed) which.max(x[st:ed, light]), potble$st_idx, potble$ed_idx)
  peakmax_idx <- peakmax_idx + potble$st_idx - 1
  potble$peakmax_time  <- x[peakmax_idx, 1]
  potble$peakmax_light <- x[peakmax_idx, light]
  potble$peak_ratio <- potble$peakmax_light / potble$start_light

  # Filter
  cnd <- potble$peak_ratio >= sensitivity
  cnd <- "if"(is.null(max_light), cnd, cnd  & potble$peakmax_light <= max_light)
  potble[cnd, -(1:4)]
}
```

Appendix C: Day/Night delineation thresholds

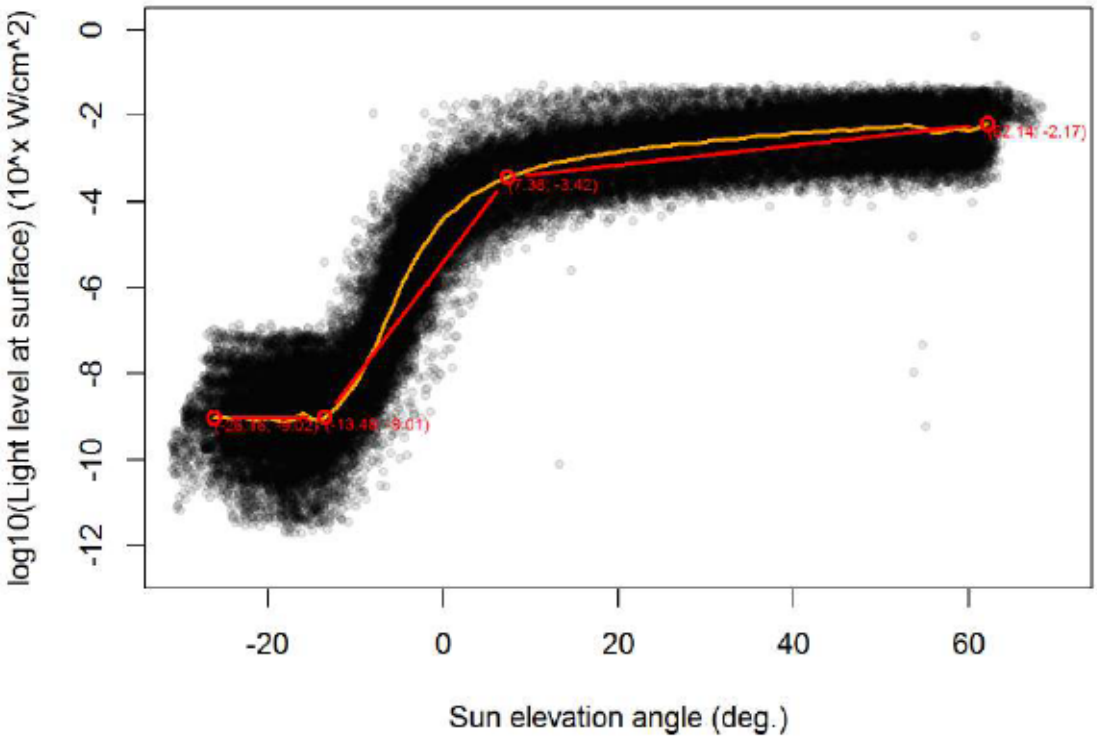

Figure 1: Light level measured during surface periods against solar elevation calculated from time, latitude and longitude (n = 52215). Orange line stands for a loess smooth with a span of 5 sun elevation degrees. Red points and segments indicate main inflexion points according to brokenstick algorithm. From this figure, we chose sun elevation thresholds of -13 and 7 degrees to assign night or day flags to dives.

ANNEXE

E

Article 4 : Guinet *et al.* (2014)

4. Guinet Christophe, Vacquié-Garcia Jade, Picard Baptiste, Bessigneul Guillaume, Le Bras Yves, Dragon Anne-Cécile, Viviant Morgane, Arnould John P. Y., Bailleul Fédéric. (2014). "Southern elephant seal foraging success in relation to temperature and light conditions : insight into prey distribution". *Marine Ecology Progress Series*. **499**. 285-301. doi: 10.3354/meps10660

Vol. 499: 285–301, 2014
doi: 10.3354/meps10660

MARINE ECOLOGY PROGRESS SERIES
Mar Ecol Prog Ser

Published March 3

FREE ACCESS

Southern elephant seal foraging success in relation to temperature and light conditions: insight into prey distribution

Christophe Guinet[1,*], Jade Vacquié-Garcia[1], Baptiste Picard[1], Guillaume Bessigneul[1], Yves Lebras[1], Anne Cécile Dragon[1,2], Morgane Viviant[1], John P. Y. Arnould[3], Frédéric Bailleul[1]

[1]Centre d'Etudes Biologiques de Chizé, CNRS, 79360 Villiers en Bois, France
[2]LOCEAN-UPMC, 4 Place Jussieu, Boite 100, 75252 Paris Cedex 05, France
[3]School of Life and Environmental Sciences, Faculty of Science & Technology, Deakin University, 221 Burwood Highway, Burwood, VIC 3125, Australia

ABSTRACT: The distribution of southern elephant seal *Mirounga leonina* prey encounter events (PEEs) was investigated from the foraging behaviour of 29 post-breeding females simultaneously equipped with a satellite tag, a time–depth recorder and a head-mounted accelerometer. Seal diving depth and PEE were related to water temperature at 200 m (T_{200}), and light level at the surface (L_0) and at depth. Approximately half (49%) of all dives were located in waters encompassed between the southern Antarctic Circumpolar Current Front and the Polar Front. Seals dived significantly deeper during the day than at night. Diving and PEE depth increased with increasing T_{200} and for a given T_{200} according to L_0 and the percentage of surface light reaching 150 m. On average, 540 PEEs per day were recorded. Seals exhibited more PEEs per unit of time spent diving during the twilight period compared with at night, and were least successful during daylight hours. Elephant seals forage in T_{200} ranging between −1 and 13°C; however, few PEEs were recorded at depths shallower than 400–500 m at night when the T_{200} exceeded 8°C. The diet of female Kerguelen elephant seals appears to be dominated by myctophids (lanternfish), and according to the average mass of their most likely myctophid prey (9 g, *Electrona calsbergi* and *E. antarctica*; 30 g *Gymnoscopelus nicholsi* and *G. piabilis*), we estimate that seals consumed 4.8–16.1 kg of fish daily. Despite lower catch rates in warmer waters, no relationship was found between the mean T_{200} at the scale of the foraging trip and daily or absolute mass gain, suggesting that elephant seals are compensating for lower catch rates by consuming larger/richer prey items in those waters.

KEY WORDS: Southern elephant seals · Foraging success · Light · Temperature · Diving behaviour · Prey

INTRODUCTION

An increasing number of studies show that, along with the measurement of concomitant oceanographic data, the behaviour of top marine predators can provide valuable insights into the habitat in which they forage (e.g. Biuw et al. 2007, 2010). Accordingly, the development of miniaturised electronic devices has opened a new era of research on the foraging behaviour of marine predators and allows the acquisition of huge quantitative data sets of behaviour from animals moving freely in their natural environment (Ropert-Coudert & Wilson 2005). Behavioural (location, diving depth, prey capture) and environmental

*Corresponding author: guinet@cebc.cnrs.fr

(temperature, salinity, light, fluorescence) parameters can be continuously recorded by high-resolution multi-channel data loggers. This enables studies of the conditions under which animals live, as well as the ability to monitor their environment (Boehlert et al. 2001).

Among top marine predators, air-breathing diving species such as seals are particularly well-suited for the bio-acquisition (i.e. bio-logging) of movement, behavioural, physiological as well as environmental data using miniaturised animal-attached tags (Rutz & Hays 2009). Their large size allows them to carry electronic devices with minimal disturbance, and researchers can handle them while they are on land in their breeding colonies. Furthermore, while investigating at-sea seal ecology, measurements of oceanographic parameters within the water column have also been obtained. Consequently, foraging, diving predators have provided new and original information about physical (Charrassin et al. 2008, Costa et al. 2008, Roquet et al. 2009) and biological oceanography (Guinet et al. 2013) in often inaccessible regions.

In recent years, one of the most exciting applications of bio-logging is the determination of the distribution and availability of prey of which we have very little knowledge. Until recently, the main limitation was an *in situ* measure of direct prey ingestion. Early devices to record predation events of seabirds and marine mammals included stomach (Wilson et al. 1992) and oesophageal temperature sensors (Ancel et al. 1997, Charrassin et al. 2001), which detected temperature changes induced by prey ingestion. However, these temperature loggers have certain limits, as they are restricted to endotherms feeding on ectothermic prey and are quite invasive. Furthermore, stomach temperature recorders fail to detect multiple rapid ingestions of small prey and are often regurgitated prematurely (Ropert-Coudert et al. 2004, Liebsch et al. 2007). External loggers such as the Inter-Mandibular Angle Sensor (IMASEN) record the mouth-opening angle of predators (Wilson et al. 2002), but are sometimes difficult to apply on animals with flexible lips (Ropert-Coudert et al. 2004, Liebsch et al. 2007). Recent studies in free-ranging diving pinnipeds have overcome this methodological issue by using head- or jaw-mounted accelerometers to detect prey encounter events (PEEs) (Suzuki et al. 2009, Naito et al. 2010, 2013, Viviant et al. 2010, Gallon et al. 2013, Iwata et al. 2012). This has enabled investigations into fine-scale temporal and spatial changes in the foraging of an increasing number of pinniped species, including the southern elephant seal *Mirounga leonina* (SES hereafter) – the largest and deepest-diving pinniped.

Both its abundance and body mass make the SES a major consumer of Southern Ocean (SO) marine resources (Guinet et al. 1996, Hindell et al. 2003). It was previously thought that SES primarily fed on squid, but a recent isotopic investigation challenged this view and, instead, indicated that female SES from the Kerguelen Islands mainly feed on myctophid fish (i.e. lanternfish) (Cherel et al. 2008). Indeed, myctophid (the abundant *Electrona antarctica*, *E. carlsbergi* and *Gymnoscopelus nicholsi*) otoliths have been found in stomachs of SES from the Kerguelen sector (Slip 1995) and elsewhere (Daneri & Carlini 2002).

Satellite tracking data show that SES are broad-ranging animals during their post-breeding and post-moult migrations, with adult females from the Kerguelen Islands foraging mainly in oceanic waters of the Antarctic and Polar Frontal Zones (Bailleul et al. 2010). While at sea, SES dive repeatedly to mesopelagic depths (300–500 m, up to 2000 m) and tend to follow the nycthemeral vertical migration of their mesopelagic prey, diving generally deeper during the day (Hindell et al. 1991, McIntyre et al. 2010). In a recent study, Jaud et al. (2012) found that light level at depth explained 70% of the variation in diving depth of the SES during daylight hours while no significant effect was detected at night. Furthermore, light level at depth in oceanic waters was explained to a large extent by phytoplankton concentration: the higher the phytoplankton concentration, the less light and the shallower the dives of SES (Jaud et al. 2012).

The objectives of this study were to investigate the variation in diving behaviour and prey encounter event rates of female SES to better characterise their prey in terms of likely size and distribution according to environmental conditions such as sea temperature and light level along a north–south gradient ranging from subtropical waters to Antarctica.

MATERIALS AND METHODS

Animal handling and instrumentation

During October/November each year from 2008 to 2012, post-breeding SES females were captured on the Kerguelen Islands (49° 20' S, 70° 20' E). Individuals were anaesthetised using a 1:1 combination of tiletamine and zolazepam (Zoletil 100), which was injected intravenously (McMahon et al. 2000). In general, post-breeding females forage at sea for durations

varying from 65 to 80 d, departing late October before returning to land throughout January to moult. A total of 34 SES females were equipped with a range of satellite tags and data loggers (see Table 1).

Eighteen seals were equipped with GPS loggers in combination with Argos satellite loggers and archival data loggers (SPLASH10-Fast-Loc GPS, Wildlife Computers). SPLASH10 devices transmitted Argos location data and collected GPS location data. The sampling interval of GPS locations was set to a minimum of 20 min, slightly shorter than the average dive duration of post-breeding females (Hindell et al. 1991, McIntyre et al. 2011a), to maximise the chance of obtaining a GPS location every time individuals surfaced between dives. An additional logger, a time–depth recorder (TDR) included in the SPLASH10 devices, collected and archived pressure, light and temperature levels at 1 or 2 s intervals.

Sixteen seals were equipped with conductivity–temperature–depth satellite-relay data loggers (CTD-SRDLs, Sea Mammal Research Unit, University of St Andrews) combined with either TDR loggers (MK9, Wildlife Computers), set to sample and archive pressure, light and temperature levels every 1 or 2 s, or TDR–accelerometer data loggers (MK10-X, Wildlife computers), sampling acceleration as well as pressure. The acceleration was measured on 3 axes: longitudinal (surge), vertical (heave) and lateral (roll) axes were used to separate dynamic accelerations from gravitational acceleration. Acceleration was sampled at 16 Hz and pressure every second. The SPLASH 10, MK10-X and MK9 TDR loggers were set to sample depth (0–1500 m, ±1 m), water temperature (–40 to +60°C, ±0.1°C) and light (5 × 10^{-2} to 5 × 10^{-12} W cm^{-2} in blue wavelength) every 1 or 2 s. Light values are converted on-board via a log transformation to compress the light measurements to a 3 digit value.

Data loggers were glued on the head of the seals, using quick-setting epoxy (Araldite AW 2101, Ciba), after cleaning the fur with acetone. Upon returning from their foraging trip, females were located via Argos data, recaptured and weighed, and loggers were retrieved.

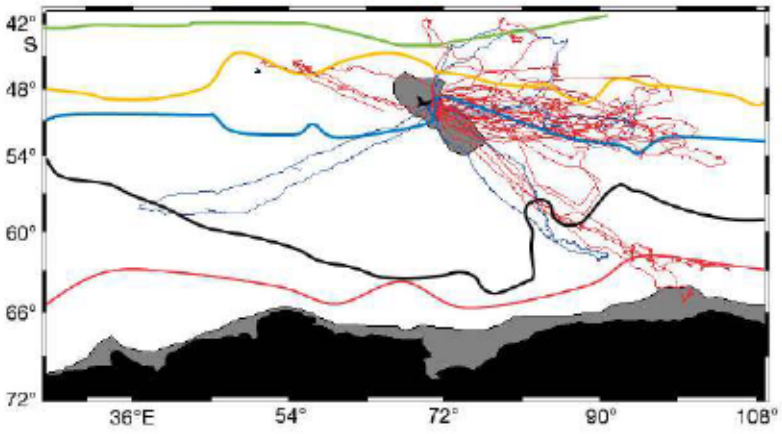

Fig. 1. Tracks of the 29 post-breeding southern elephant seal females for which high-resolution data were recovered. The blue section of track corresponds to the period when accelerometry data were collected. The main frontal structures are reported from south to north: Antarctic divergence (red), Southern Antarctic Circumpolar Current Front (black), Polar Front (blue), Subantarctic Front (orange) and the Subtropical Front (green). Shelf area from the coast to the –1000 m isobaths is indicated in grey

Data processing and analysis

Female SES from the Kerguelen Island population forage mainly in pelagic waters but also to a lesser extent on the Kerguelen and Antarctic continental shelves (i.e. the main foraging habitat of Kerguelen Island sub-adult and adult males; Bailleul et al. 2010, Dragon et al. 2010, Authier et al. 2012). As part of this work we focused on the pelagic portion of the tracks by excluding data from areas where water depths were <1000 m (Fig. 1), based on National Geophysical Data Centre ETOPO2 Global 2 Elevations (www.ngdc.noaa.gov/mgg/global/etopo2.html), to exclude all locations on the Kerguelen and Crozet plateaus where SES are known to conduct benthic dives (Bailleul et al. 2010).

Pressure sensor data were analysed from MK9 and SPLASH10 TDRs to obtain dive depth profiles. For the purpose of this study, and based on the sensor's absolute accuracy, only excursions below a depth of 15 m were analysed. Bottom depth, light and the temperature profiles associated with each dive were extracted (see Dragon et al. 2012 for details). Each dive was divided into a descent, ascent and bottom phase. The bottom phase corresponds to the period between the end of the descent and the beginning of the ascent. The different dive phases were defined according to Dragon et al. (2012) using a custom-written MATLAB code (version 7.0.1; available on request). In the present study, the diving depth is defined as the mean depth during the bottom phase of the dive.

Data from the accelerometer were processed according to Viviant et al. (2010) and Gallon et al. (2013) using custom-written MATLAB code (available on request). Identifying individual feeding events from the accelerometry data was performed according to the following procedures. Firstly, the 3 accelerometer time series were filtered with a high-pass filter of 0.33 critical frequency for data sampled at 16 Hz to remove the remaining noise corresponding to swimming movement, highlighting the peaks in acceleration that represent head movements. Rapid head movements were used to identify possible PEEs. The 0.33 filter was defined visually on power spectral density of acceleration on the 3 axes.

Secondly, the standard deviation along a fixed 1 s window over each time series axis was calculated to sum accelerations at a 1 s scale. The standard deviation along a 5 s moving window, over each standard deviation time series, was then calculated for each axis to highlight extreme standard deviation and consequently significant accelerations. The threshold distinguishing those extreme events was defined using the *kmeans* function (MATLAB, tool box statistics) and was calculated for each seal and for each axis independently. Only head movement events that could be detected simultaneously on the 3 axes were considered as a true PEE; others were considered to be related to dives where animals did not alter their swimming behaviour whilst travelling underwater. Continuous values at 1 Hz above the threshold were considered as unique PEEs. Events separated by periods longer than 1 s below the threshold value for any given axes were considered as a different PEE. The number, timing and depth location of PEEs were determined for each dive. In the present study, a PEE does not mean that the seal was feeding with certainty, but should be considered as a relative index of a prey encounter during the dive.

From these data we then calculated PEE per unit time (PEE rate) at 2 scales: (1) the complete dive and (2) the bottom phase of the dive. The latter removes the effect of the vertical accessibility of the prey, since a seal has to undertake a longer vertical transit when it dives deeper and consequently has less time to spend at the bottom of the dive (i.e. where most PEEs are expected to occur).

For each animal, the temperature profile associated with each dive was extracted from MK9, TDR10-X and SPLASH 10 TDR data. At any given latitude, but different longitudes, water masses with very different temperature profiles can be observed depending on the location of the main frontal structures (see Fig. 1). Dives were therefore ranked regardless of their latitude, in a decreasing order, according to their water temperature at 200 m (T_{200}), to reflect a general north–south gradient. Profiles were then regrouped into 1°C T_{200} classes. Each 1°C class was defined according to its lower boundary (i.e. −1°C defining the [−1°C; 0°C[temperature class). Then, for all the dives belonging to a given T_{200} class, the mean temperature for 5-m depth bins was calculated over the whole depth range. This provides a mean temperature profile for a given temperature scenario at 200 m. These mean temperature profiles were used for figure representation and statistical comparisons between the different 1°C T_{200} classes: day–night difference in the mean diving depth and comparison of PEEs per minute spent diving or spent at the bottom of the dive. Dives shallower than 200 m were allocated to a T_{200} category according to the T_{200} encountered during previous and/or following dives with a diving depth exceeding 200 m.

The SO fronts are narrow regions of sharp horizontal gradients of water properties that mark the boundaries of different water masses (Fig. 1). These structures are defined by representative values of temperature and salinity at approximately 200 m depth, where each front is generally best marked. The water mass the seal was diving in was identified using the T_{200}, as indicated by Park et al. (1991, 1998) and Orsi et al. (1995). Going north from the Antarctic continent, the Antarctic Divergence (AD) has been identified with the most shoreward penetration of the 0.8°C isotherm at depths below the Winter Water. The Southern Antarctic Circumpolar Current Front (SACCF) is defined by a temperature of 1.6°C and a salinity of 34.6 PSU at 200 m depth (Park et al. 1998). The Polar Front (PF) is approximated by the northern limit of the subsurface temperature minimum of 2.8°C at the 100–300 m depth layer (Park et al. 1993, Belkin & Gordon 1996). Although the Subantarctic Front (SAF) is less well defined, values of 6.8°C are considered as subsurface expressions of this front in the Indian sector (Park et al. 1993) and, therefore, we used 7°C at 200 m as the SAF limit. Values of 10.8°C at 200 m depth are adopted to define the Subtropical Front (STF) (Park et al. 1993); therefore, we used 11°C at 200 m as the STF limit in this study. We defined the Polar Frontal Zone as the area located between the STF (northern limit) and the PF (southern limit), and the Antarctic Circumpolar Current (ACC) zone is defined as the area between the SAF and the SACCF.

Light levels within the water column vary greatly according to a number of factors, such as sun angle, cloud cover and phytoplankton concentration within oceanic waters. This latter factor explains approxi-

mately 50% of the variation of light attenuation within the water column (Jaud et al. 2012). For each dive record from the MK9, MK10 X and SPLASH10 TDR data, we calculated the level of light available at each depth measurement along the entire dive. Surface light level (L_0) was calculated as the mean light reading during the surface interval after the dive. The percentage of surface light reaching 150 m (L_{150}/L_0), corresponding in general to the euphotic depth in the SO (Knox 2007), was calculated during the ascent phase of the dive prior to surfacing. To assess the effect of phytoplankton and particle concentration on light level available at depth, light at depth was expressed as a percentage of L_0.

Each dive was attributed to one of 3 periods: day, night or twilight. This was defined according to the solar angle, taking into account the geographical location of the seal provided by the Argos/GPS data and the time at the beginning of the dive. Day was defined when the sun was above the horizon (0°); twilight, when the sun was between 0° and 6° below the horizon; and night, when the sun was more than 6° below the horizon. The twilight period used in our study corresponds to civil dawn and dusk, i.e. the time at which there is enough light for objects to be distinguishable in the air and the light is therefore likely to influence the vertical distribution of biological organisms within the water column. The sun angle according to the geographical location and time was calculated using the *suncycle* function in MATLAB.

Statistical analyses

The relationships between (1) bottom duration according to dive duration and diving depth, (2) dive duration according to T_{200}, diving depth, the number of days elapsed since departure from the colony, L_0, L_{150}/L_0 for day, night and twilight periods and (3) the mean depth at the bottom of the dive and PEE depth according to T_{200}, L_0 and L_{150}/L_0 for day and night (the same analysis was performed north and south of the SAF, i.e. for T_{200} higher and lower than 7°C) were analysed using a linear mixed model (package nlme in R; R Development Core Team 2009). Light level analyses were performed only during day and night. Indeed during twilight, light level varies to a great extent and is known to induce very large variation in elephant seal diving behaviour. Instead, this study aimed to assess whether female SES diving behaviour responds to small changes in L_0 and L_{150}/L_0 during either the day or the night. The variation in PEE according to diving depth, with dive duration or bottom time accounted for in the model, was analysed using a generalised linear mixed model with multivariate normal random effects, using penalized quasi-likelihood (package GlmmPQL in R; R Development Core Team 2009) on night, day and twilight separately. Individual seal was included as a random factor to take into account inter-individual variability. An autoregressive variance–covariance matrix (cor AR1 in R; R Development Core Team 2009) representing first-order autocorrelation structure was used to model the serial correlation among observations for each individual (Zuur et al. 2009). All variables were standardised (centred and scaled) to facilitate model convergence and to be able to compare the respective contribution of the predictors (Zuur et al. 2009). Using GLmmPQL, model selection can only be performed according to p-values. We implemented a stepwise procedure, with the threshold set at $p = 0.05$. Data are presented as means ± SD. The variation in PEE rate throughout the dive and at the bottom of the dive and according to T_{200} classes was compared between day, night and twilight using a Wilcoxon test.

RESULTS

The mean mass and length of the 34 post-breeding females prior to their departure were 296 ± 54 kg and 242 ± 15 cm, respectively. Among these 34 equipped seals, all but 3 were recaptured and high-resolution diving data were successfully recovered for 29 of 31 remaining females. The mean foraging trip duration was 82 ± 9 d (n = 31; Table 1), the mean recovery mass was 363 ± 55 kg (n = 25); therefore, the mean overall mass gain was 75 ± 36 kg while the daily mass gain was 0.9 ± 0.4 kg per day spent at sea (n = 25; Table 1).

The tracks of the 29 SES females for which we had high-frequency measurements of pressure, temperature and light are shown in Fig. 1. These tracks extended from the subtropical zone to the Antarctic shelf. On average, SES performed 66 ± 9 dives daily. Among those, PEE data were obtained for 12 SES along their track (see Fig. 1, Table 1). An example of data obtained for one complete foraging trip is presented in Fig. 2.

Dive, light and temperature distribution

Seals ranged from the AD to the STF front (Figs. 1 & 3). Among the 106 313 dives performed by the 29 post breeding SES females, 62.2, 29.9 and 7.9%

Table 1. Female southern elephant seal identity, deployment and recovery dates, foraging trip duration, mass, standard body length, mean 200 m temperature (T_{200}) and equipment type deployed

Seal ID	Deployment	Recovery	Trip (d)	Departure mass (kg)	Return mass (kg)	Mass gain (kg)	Daily mass gain (kg)	Length (cm)	T_{200} (°C)	Argos-CTD	Splash-10-F	TDR-MK9	TDR-MK 10-X
2008-8	13.10.2008	05.01.2009	84	231.6				225.0	3.0		X		
2009-1	15.10.2009	12.01.2010	89	273.5	294.0	20.5	0.2	225.0	3.5	X		X	
2009-2	15.10.2009	30.12.2009	76	267.5	310.0	42.5	0.6	235.0	5.9	X		X	
2009-3	16.10.2009	11.01.2010	87	268.0	300.0	32.0	0.4	228.0	3.0	X		X	
2009-4	16.10.2009	06.01.2010	82	269.5	370.0	100.5	1.2	230.0	3.1	X		X	
2009-5	17.10.2009	12.01.2010	87	397.5				276.0	0.4		X		
2009-6	19.10.2009	05.01.2010	78	319.5	440.0	120.5	1.5	258.0	5.6		X		
2009-8	20.10.2009	20.01.2010	92	314.5	395.0	80.5	0.9	250.0	1.3	X		X	
2009-9	24.10.2009	10.01.2010	78	272.5	332.5	60.0	0.8	237.0	2.8		X		
2009-10	25.10.2009	20.01.2010	87	321.5	370.0	48.5	0.6	249.0	2.8		X		
2009-11	25.10.2009	12.01.2010	79	300.0	375.0	75.0	0.9	219.0	2.8		X		
2010-8	15.10.2010	29.01.2011	106	237.5	295.0	57.5	0.5	238.0	1.1	X		X	
2010-9	26.10.2010	11.01.2011	77	379.5	430.0	50.5	0.7	255.0	3.4	X		X	
2010-10	16.10.2010	15.01.2011	91	214.0	321.5	107.5	1.2	231.0		X		X	
2010-11	18.10.2010	03.01.2011	77	314.5	392.0	77.5	1.0	260.0	3.3	X		X	
2010-12	16.10.2010			427.0				280.0		X		X	
2010-13	15.10.2010	23.01.2011	100	384.8	448.0	63.2	0.6	261.0	1.6	X		X	
2010-14	18.10.2010	15.01.2011	89	283.5				236.0		X		X	
2010-15	24.10.2010	02.01.2011	70	330.5				270.0	1.2	X	X	X	X
2010-18	26.10.2010	03.01.2011	69	331.0	352.5	21.5	0.3	246.0	7.5		X		X
2010-19	31.10.2010	20.01.2011	81	395.0				266.0	1.2		X		X
2010-20	01.11.2010	15.01.2011	75	342.8	481.0	138.2	1.8	255.0	5.3		X		X
2010-21	18.11.2010	02.01.2011	45	376.5	425.0	48.5	1.1	218.0	1.0		X		X
2011-14	25.10.2011	26.01.2012	93	252.0	305.0	53.0	0.6	240.0	3.2	X			X
2011-16	26.10.2011	20.01.2012	86	255.0	425.0	170.0	2.0	254.0	3.0		X		X
2011-17	26.10.2011	19.01.2012	85	225.0	329.0	104.0	1.2	225.0	1.8	X			X
2011-18	26.10.2011	17.01.2012	83	245.0	327.0	82.0	1.0	238.0	2.8		X		X
2011-21	28.10.2011	31.01.2012	95	245.0				225.0	4.5		X		X
2011-22	28.10.2011	20.01.2012	84	296.0	367.0	71.0	0.8	256.0	2.0	X			X
2011-26	30.10.2011	26.01.2012	88	255.0				232.0	2.8		X		X
2011-27	30.10.2011	16.01.2012	78	236.0	307.0	71.0	0.9	235.0	8.1		X		X
2011-28	30.10.2011	14.01.2012	76	249.0	328.0	79.0	1.0	240.0	3.6		X		X
2011-29	03.11.2011			262.0				230.0			X		X
2011-30	27.10.2011			300.0				240.0		X			X
Mean			83	296.2	366.4	75.4	0.9	243.0	3.2				
SD			11	56.5	56.3	35.9	0.4	16.4	1.9				

dives were performed during day, night and twilight, respectively. The mean dive duration and mean diving depth were 21.4 ± 4.8 min and 519.2 ± 208.3 m for day; 16.7 ± 4.2 min and 384.4 ± 199.2 m for night; and 18.6 ± 3.8 min and 391.5 ± 196.3 m for twilight, respectively. The bottom duration of a dive was found to increase with dive duration but to decrease with increasing diving depth (Table 2). Dive duration increased with the number of days elapsed since departure from land. T_{200} exercised a different effect between day and night. During the day, for a given diving depth, seals increased their dive duration with increasing T_{200} while a negative effect was found at night and no relationship for twilight (Table 3).

The vast majority of dives (88.8%) were concentrated in water masses having a T_{200} encompassed between the AD and the SAF (Fig. 3). However, it is worth noting that 49.0% of the dives were distributed within water masses with a T_{200} ranging between 1 and 3°C, revealing that while foraging within the ACC zone, post-breeding female SES favoured water masses located primarily south of the PF. Approximately one-third (35.5%) of the dives were located in water masses encompassed between the PF and SAF. Only 6.0% of the dives were between the SAF and STF, with just 3.5% just north of the STF and 1.8% south of the AD (Fig. 3).

Diving depth increased with increasing L_0, L_{150}/L_0, as well as T_{200} both during day and night. Daytime

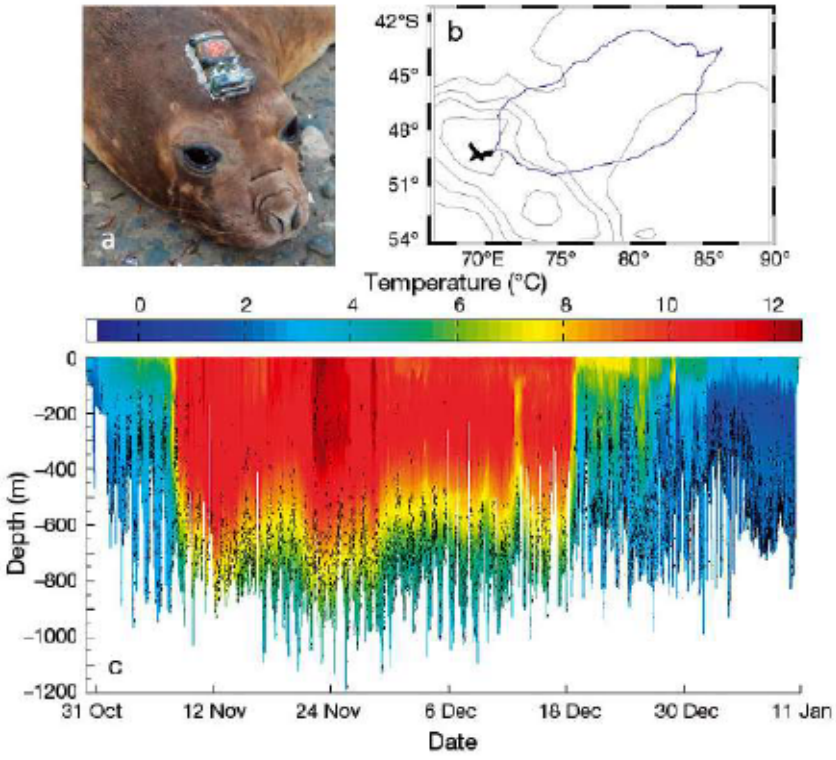

Fig. 2. An example of one female southern elephant seal (a) equipped with a SPLASH 10 tag combined with a head-mounted accelerometer enabling the reconstruction of the (b) seal track as well as (c) the distribution of prey encounter events (PEEs; black circles) according to depth and temperature monitored along the track of the animal

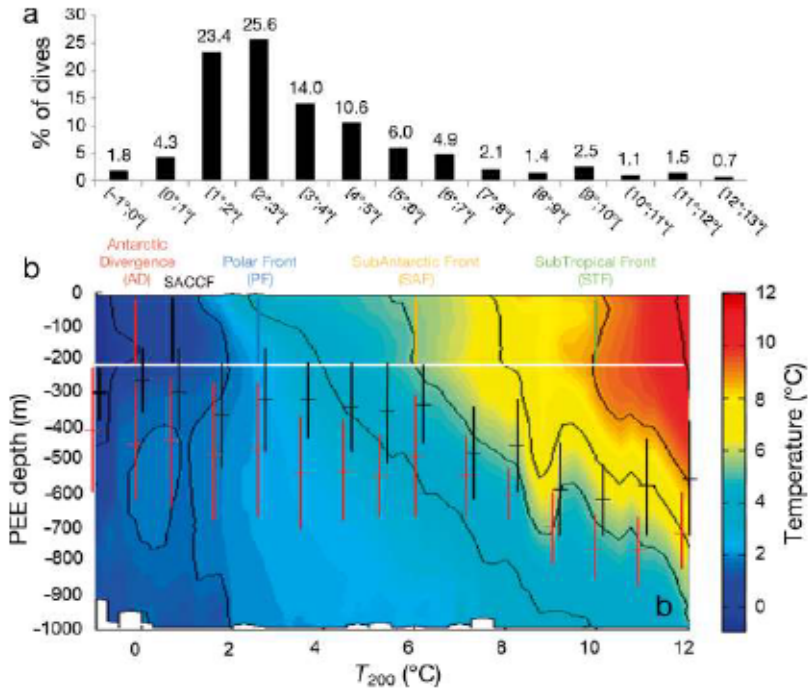

Fig. 3. A temperature transect reconstructed according to the temperature profiles ranked according to temperature at 200 m (T_{200}). (a) The percentage of dives for the 29 southern elephant seals taking place for each 1°C temperature class. Number on top of bar is the % of dives observed for each class. (b) The main frontal structures are located along this transect according to their T_{200} signature (white line, see Fig. 1 for details). Mean (±SD) prey encounter event (PEE) depth during day (red) and night (black) obtained from the 12 seals equipped with head-mounted accelerometers for each 1°C temperature class overlaid on the temperature transect constructed from the data collected by the 29 seals. SACCF: Southern Antarctic Circumpolar Current Front

PEE depth increased with increasing L_0, L_{150}/L_0 and T_{200}, while no effect of T_{200} was detected at night (Table 4).

The difference in mean diving depth between day and night varied more to the south than to the north of the SAF (Fig. 4). Consequently, there was less difference between the depths of day and night dives as the individuals headed towards the STF (Fig. 4). This was particularly noticeable for T_{200} exceeding 7°C (i.e. north of the SAF), for which PEE depth tended to increase rapidly with increasing T_{200}, during both the day and the night (Fig. 4). Indeed, mean diving depth increased significantly with increasing T_{200} during the day but not at night south of the SAF (T_{200} < 7°C). The same significant effect of T_{200} on diving depth was found north of the SAF (T_{200} > 7°C; Table 5), but during both day and night. Furthermore, diving depth was positively related to increasing L_0 north and south of the SAF during both day and night. In addition, diving depth was also related to L_{150}/L_0 during day and night south of the SAF and only at night north of the SAF (Table 5).

Variation in foraging success

For the 12 SES equipped with head-mounted accelerometers, the PEE

events were extracted along the track (time) and related to the corresponding pressure and T_{200} measurements (see Fig. 3). A total of 204 045 PEEs were detected, with 63.3, 26.1 and 10.6 % occurring during day, night and twilight, respectively. A total of 73, 14 and 13 % of the PEEs took place at the bottom, during the descent and during the ascent of the dive, respectively. When considering the PEE per unit of time spent diving or spent at the bottom of the dive, seals were found to be significantly more efficient during twilight compared with at night (dive: $W = 7\,075\,193$, $p < 0.001$; bottom: $W = 7\,680\,996$, $p < 0.001$) or during the day (dive: $W = 44\,313\,536$, $p < 0.001$; bottom: $W = 49\,752\,533$, $p < 0.001$), and they were also more efficient during the night compared with during the day (dive: $W = 19\,339\,935$, $p < 0.001$; bottom: $W = 19\,852\,229$, $p < 0.001$; see Fig. 5).

Drift dives, which are considered essentially as non-foraging dives and function as periods of recovery (Crocker et al. 1997), had very few prey captures (0.39 ± 1.93 PEEs per drift dive, n = 501). Excluding these dives, an average of 8.2 ± 6.6 PEEs were recorded per dive (n = 25 761). The mean PEE depth was 467 ± 211, 304 ±138 and 308 ± 151 m for day, night and twilight, respectively.

A visual examination of PEE depth distribution reveals that it varied between day and night and according to T_{200} (Fig. 6). For T_{200} ranging between 0 and 7°C, the PEE tended to exhibit a bimodal distribution both during day and night. However, both modes are shallower at night compared with the daylight hours. In contrast, for T_{200} higher than 7°C, individuals were capturing prey much deeper both at night and during the day. Furthermore, PEE depth distribution was unimodal and very deep (500–800 m), which tended to be slightly shallower at night compared with during daylight hours.

The number of PEEs for a complete diving event was negatively related to both dive duration and diving depth regardless of the time period (day, night or twilight). The number of PEEs at the bottom of the dive was negatively related to diving depth during both day and

Table 2. Bottom duration according to dive duration and diving depth. ***p < 0.001

Model	Parameter	Estimate	t
Bottom duration	Dive duration	307.65	858.06***
	Diving depth	–271.94	–800.29***

Table 3. Dive duration of female southern elephant seals according to 200 m temperature (T_{200}), diving depth and number of days elapsed since departure for day, night and twilight. **p < 0.01; ***p < 0.001

Model	Parameter	Day		Night		Twilight	
		Estimate	t	Estimate	t	Estimate	t
Dive duration	T_{200}	18.73	7.31**	–31.42	–7.30**	–	ns
	Diving depth	35.01	32.27***	40.71	26.53***	45.13	15.67***
	Days since departure	67.49	31.62***	61.89	24.75***	63.84	14.50***

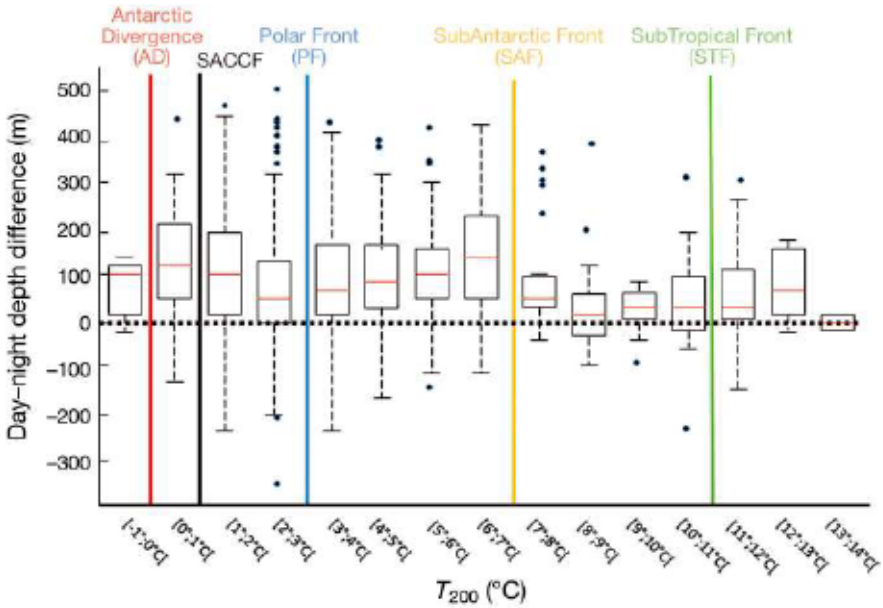

Fig. 4. Box plot of the mean depth differences between day and night dive according to each 1°C temperature at 200 m (T_{200}) class. Horizontal lines represent the median, the box represents the 0.75 to 0.25 quartiles, and whiskers represent 1.5 times the interquartile range (IQR). Small circles represent outliers (i.e. values exceeding 1.5 times IQR). SACCF: Southern Antarctic Circumpolar Current Front.

Table 4. Variation in diving depth and prey encounter event (PEE) depth of female southern elephant seals according to surface light (L_0), the percentage of surface light reaching 150 m (L_{150}/L_0) and 200 m temperature (T_{200}), for day and night. ***p < 0.001

Model	Parameter	Day		Night	
		Estimate	t	Estimate	t
Diving depth	L_0	36.81	25.66***	25.57	10.54***
	L_{150}/L_0	30.80	19.64***	32.25	15.97***
	T_{200}	32.83	16.81***	29.98	11.68***
PEE depth	L_0	36.76	28.32***	–	ns
	L_{150}/L_0	38.94	26.55***	16.16	9.87***
	T_{200}	37.49	18.90***	31.43	14.85***

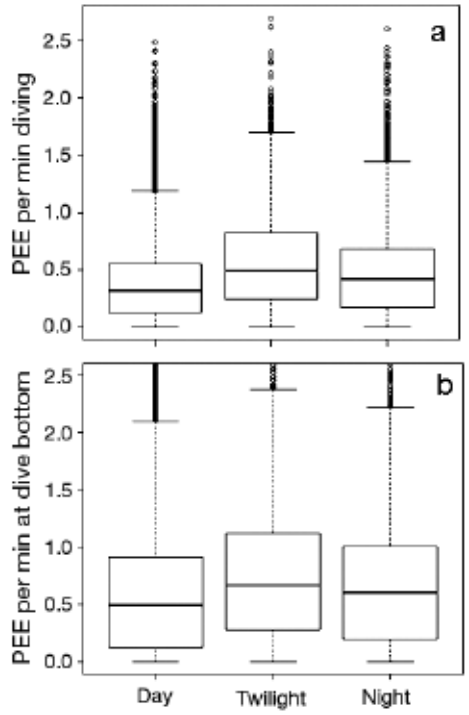

Fig. 5. (a) Box plot of prey encounter events (PEE) per minute spent diving for day, night and twilight periods. (b) Box plot of PEE per minute spent at the bottom of the dive for day, night and twilight periods (see text for details). See Fig. 4 for further details

night, but was positively related to the duration of the bottom phase of the dive during day and twilight periods (no effect was detected at night). Furthermore, PEEs for a complete dive and at the bottom of the dive were negatively related to the L_{150}/L_0, with no effect of L_0, during the day but positively related to both L_0 and L_{150}/L_0 during night and twilight (Table 6).

PEEs per unit of time spent diving or at the bottom of the dive were also found to vary significantly according to the water masses visited by the SES. Compared to what is expected from an even distribution of PEE rate according to T_{200}, individuals were performing more PEEs per unit of time for the following T_{200} water classes: –1°C, 0°C, 2°C, 3°C, 4°C, 5°C, 6°C and 7°C (Fig. 7). However, no relationship was found between either the absolute or the daily mass gain and the mean T_{200} of the water masses visited by the seal ($r^2 < 0.01$, $p > 0.9$ in both cases).

DISCUSSION

The results of the present study clearly demonstrate that during late spring and early summer the diving behaviour and foraging success of SES females were profoundly affected by the physical properties of the water masses visited. Indeed, these results show that at depth, water temperature, surface light level and the percentage of surface light reaching 150 m (used as an indicator of phytoplankton concentration) influence the SES foraging during day, night and twilight periods. Correspondingly, these data reveal the vertical distribution of the SES prey guild in relation to environmental variables.

Firstly, SES females dive deeper as T_{200} increases, indicating that the vertical accessibility of the prey decreases from the AD to subtropical waters. This finding is consistent with previous studies indicating that SES are diving deeper in warmer waters (Biuw et al. 2007, McIntyre et al. 2011b). Interestingly, when controlling for T_{200}, the deeper the SES dive,

Table 5. Variation in diving depth of female southern elephant seals according to surface light (L_0), the percentage of surface light reaching 150 m (L_{150}/L_0) and 200 m temperature (T_{200}) south and north of the Subantarctic Front for day and night. *p < 0.05; **p < 0.01; ***p < 0.001; ns: not significant

Model	Parameter	T_{200} < 7°C				T_{200} > 7°C			
		Day		Night		Day		Night	
		Estimate	t	Estimate	t	Estimate	t	Estimate	t
Diving depth	L_0	38.69	25.51***	24.97	8.67**	24.41	6.09**	23.07	8.27**
	L_{150}/L_0	33.58	20.73***	29.05	14.65***	–	ns	29.45	7.33**
	T_{200}	18.64	10.46***	–	ns	233.5	3.59*	21.02	4.54**

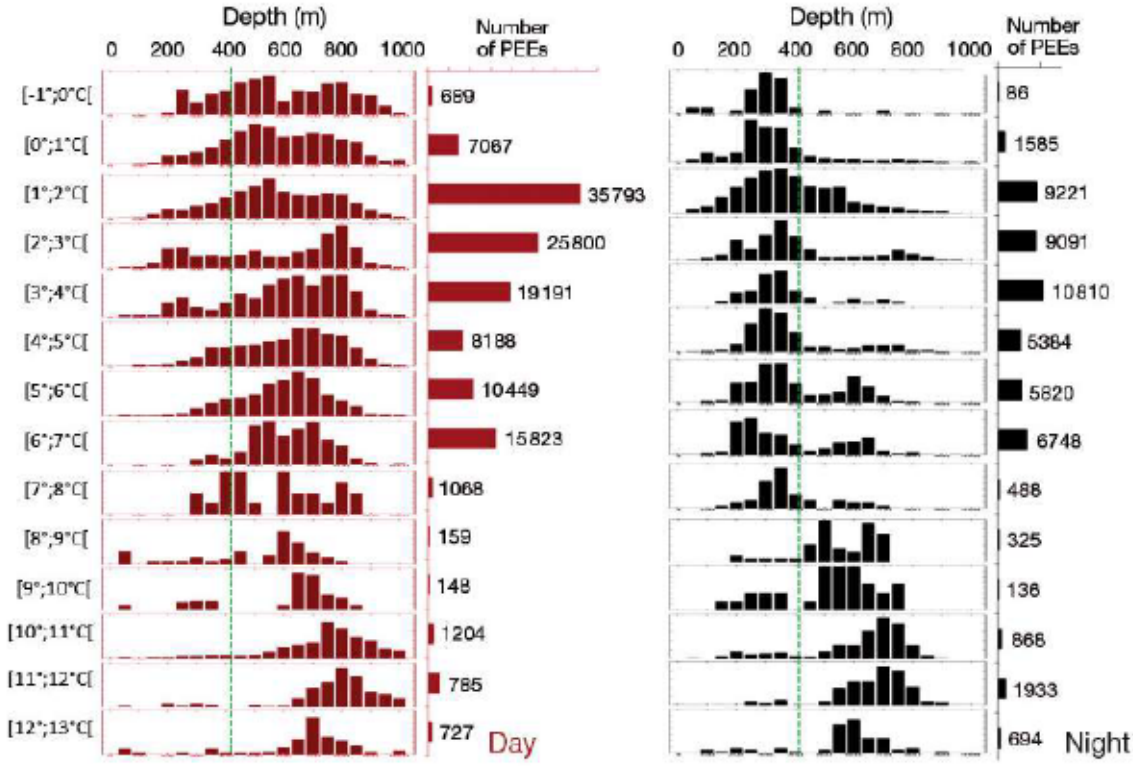

Fig. 6. Depth distribution of prey encounter events (PEEs) according to 50 m depth class during day (red) and night (black) according to each 1°C temperature at 200 m (T_{200}) class. The number of PEEs during day and night for each T_{200} class is indicated

the fewer prey they capture for a given bottom duration, suggesting a general decrease in prey density with increasing depth (Table 6). For waters with a T_{200} warmer than 7°C, a significant decrease in PEEs per unit of time spent diving or at the bottom of the dive was found, suggesting that lower prey densities and at greater depth were found north of the SAF. Furthermore, as SES dive deeper, swimming costs associated with the bottom-surface transit increase and, as a consequence, the amount of time the seal is able to allocate to foraging at the bottom of the dive (i.e. the efficient foraging part of the dive) decreases with increasing diving depth. Furthermore, when considering a complete dive, and contrary to our

Table 6. Variation of the number of prey encounter events (PEE) by female southern elephant seals during the dive and at the bottom of the dive scale according to dive metrics and environmental conditions (surface light [L_0], the percentage of surface light reaching 150 m [L_{150}/L_0] and 200 m temperature [T_{200}]). *p < 0.05; **p < 0.01; ***p < 0.001; ns: not significant

Model	Parameter	Day		Night		Twilight	
		Estimate	t	Estimate	t	Estimate	t
PEE dive	T_{200}	–	ns	–	ns	–	ns
	L_0	–	ns	0.220	11.75***	0.090	6.05**
	L_{150}/L_0	–0.110	–10.96***	0.210	10.42***	0.052	2.65*
	Dive duration	–0.070	–7.79**	–0.171	–12.21***	–0.600	–3.31**
	Diving depth	–0.150	–20.33***	–0.029	–2.67*	–0.210	–11.55***
PEE bottom	T_{200}	–	ns	–	ns	–	ns
	L_0	–	ns	0.289	13.69***	0.114	6.82**
	L_{150}/L_0	–0.080	–6.56**	0.280	12.87***	0.115	5.47**
	Bottom duration	0.079	8.06**	–	ns	0.060	2.66*
	Diving depth	–0.38	–38.60***	–0.360	–25.97***	–0.51	–19.61***

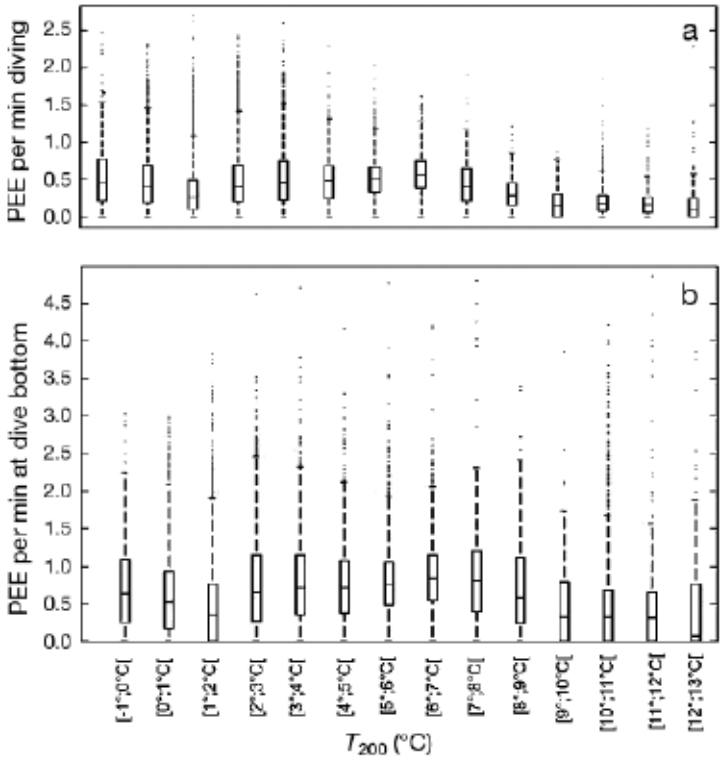

Fig. 7. (b) Box plot of prey encounter events (PEEs) per minute spent diving according to each 1°C temperature at 200 m (T_{200}) class. (b) Box plot of PEEs per minute spent at the bottom of the dive according to each 1°C T_{200} class. See Fig. 4 for further details

expectation, the number of PEEs decreases with increasing dive duration, suggesting that successful foraging dives were energetically more costly (i.e. higher swimming effort) than unsuccessful ones, forcing the seals to come back earlier to the surface. An alternative and non-exclusive hypothesis is that elephant seals modify their dive duration by changing the ascent or descent behaviour (i.e. by descending and ascending more rapidly to the surface) when they encounter high-quality prey patches, as reported in king penguins (Hanuise et al. 2013). Furthermore, when controlling for diving depth, the number of PEEs at the bottom of the dive increases with bottom duration during the day and twilight periods, but not at night, indicating that seals adjust the amount of time allocated to the efficient phase of their dive (bottom) in relation to prey density when generally diving deeper during the day and twilight compared with shallower night dives. Future studies should investigate how these observed variations match with the predictions of the optimal diving theory (Carbone & Houston 1994).

PEEs both during the whole dive and at the bottom of the dive were not related to T_{200}, suggesting that T_{200} has a general effect on prey vertical accessibility but not on foraging success when controlling for dive duration and diving depth. Correspondingly, in the present study, very few seals foraged in water with T_{200} exceeding 7°C (i.e. north of the SAF). Such a behavioural change associated with the SAF is consistent with previous studies indicating that the SAF represents an important biogeographic boundary regarding the latitudinal distribution of warm-water zooplankton (Ansorge et al. 1999) and myctophid species (Koubbi 1993, Koubbi et al. 2011), as well as top marine predators such as seabirds (Bost et al. 2009).

Individuals were found to exhibit lower PEE rates in water masses with T_{200} ranging between 1 and 2°C, corresponding to the zone encompassed between the PF and the SACCF. This is consistent with the finding of Biuw et al. (2007) that SES exhibited negative changes in body condition while migrating between the PF and the SACCF. In the Indian Ocean sector, this zone broadens latitudinally in the Kerguelen region (Orsi et al. 1995) and this sector seems to represent a large region of unfavourable foraging conditions for SES. Despite our results supporting previous findings that dive capacity increases throughout the duration of the foraging trips (Bennett et al. 2001, Hassrick et al. 2010, McIntyre et al. 2011b), both T_{200} and diving depth were also found to influence dive duration in the present study.

For T_{200} lower than 7°C, T_{200}, L_0 and L_{150}/L_0 had a positive effect on the diving depth of SES during the day. No effect of T_{200} was found at night (Table 5). As L_0 is mostly related to both cloud cover and sun angle during the day and cloud cover and moon light at night, the present study emphasises the critical effect of light, mediated through its effect on the distribution of SES prey, on the diving behaviour of SES both during the day, as previously found by Jaud et al. (2012), and at night.

Light level at depth depends on the amount of light reaching the surface of the ocean and the intensity of light attenuation within the water column. In oceanic waters, phytoplankton concentra-

tion is a critical factor controlling most of the surface light attenuation within the water column and, therefore, light levels below the euphotic layer (Morel 1988). Light level at 150 m, combining the effect of surface light and light attenuation within the first 150 m of the water column, has been found to explain nearly 70% of the variation in the daylight diving depth of seals foraging between the PF and the SAF (Jaud et al. 2012). In the present study, with a larger data set we were able to show that SES also modified their diving behaviour at night according to both L_0 and L_{150}/L_0, diving deeper when more light was available at the surface and when that light was less attenuated within the water column, suggesting that in clearer waters with lower phytoplankton concentrations seals had to dive deeper to reach their prey. This finding was consistent with the results obtained by Dragon et al. (2010) showing that the diving depth of SES was negatively related to remotely sensed surface chlorophyll *a* concentration.

The fact that light levels at the surface had an effect on the diving depth of SES at night suggests that variation of moonlight intensity in relation to moon cycle controls the vertical extent of the nycthemeral migration of SES prey and, therefore, their vertical accessibility, with prey items migrating closer to the ocean surface during the darkest nights. A similar effect of moonlight on diving behaviour has previously been observed in Galapagos fur seals *Arctocephalus galapagoensis* (Horning & Trillmich 1999) and northern fur seals *Callorhinus ursinus* (Lea et al. 2010). Several studies have shown that the extent of the vertical, nocturnal migration of zooplankton is related to changes in L_0 and water transparency, and that L_0 is dependent on the moon phase and/or cloud cover (Rudstam et al. 1989, Dodson 1990). Indeed, light is an essential factor for the vertical distribution of a broad range of mesopelagic marine animals, ranging from zooplankton (Liu et al. 2003) to fish (Batty et al. 1990), which distribute themselves according to precise light isolines, with threshold light intensity ('barrier isolume') found to initiate an avoidance reaction by these organisms (Boden & Kampa 1967, Kampa 1976, Gal et al. 1999, Cotté & Simard 2005).

The strong influence of light on the diving behaviour of SES leads us to hypothesise that the large variability in diving depth observed in water for a given T_{200} south of the SAF is likely to be explained by high variability in the amount of light available at depth in response to variations in cloud cover, phytoplankton concentration and sunlight or moonlight. Therefore, while the change in phytoplankton concentration in summer is likely to have an effect on the overall SO productivity and the amount of prey available to SES several months later, it also exerts substantial influence on the vertical accessibility of SES prey. This has direct consequences on the foraging efficiency of these predators, as the deeper they dive, the less efficient (in terms of PEE events per unit of time) they are.

Interestingly, the influence of light on PEEs differed temporally. Surface light (L_0) had no effect on PEEs during the day, but had a positive effect during the night and twilight periods (see Table 6). Similarly, L_{150}/L_0 had a negative effect on PEEs during the day but a positive effect at night and twilight. L_{150}/L_0 is related to the concentration of particles (including phytoplankton) present in the water (Jaud et al. 2012). Therefore, the negative relationship found between L_{150}/L_0 and PEEs would suggest that SES are more successful during the day in areas where higher concentration of particles such as phytoplankton but also possibly zooplankton are encountered. In contrast, both L_0 and L_{150}/L_0 were found to have a positive effect on PEEs during twilight and at night. This suggests that light level within the water column could indirectly impact the foraging success of SES, potentially by influencing the distribution, availability and/or detectability of prey on clear nights and in clear waters.

SES dive generally to shallower depths at night than during daylight hours (Hindell et al. 1991, Biuw et al. 2007); in some instances they have been observed to dive to greater depths at night compared with the day, suggesting that they might be foraging on different prey resources on those occasions (McIntyre et al. 2011a). Consistent with Biuw et al. (2007), the greatest differences between day and night diving depths observed in the present study were between the SAF and the SACCF (i.e. the ACC zone). A noticeable exception was in both Antarctic waters and waters north of the SAF, where the diurnal variation diminished. Reduced differences in diving depth between day and night were observed for high and low T_{200}. However, the factors responsible for these differences between Antarctic and subtropical waters are likely to be different. For the subantarctic–subtropical zone, the contribution of L_0 and L_{150}/L_0 to the variation in diving depth was found to be lower to the north than to the south of the SAF. We interpret this result as the consequence of the deepening of SES females dives in search of prey found in deeper, colder waters. The 8°C isotherm appears to represent the upper limit of the vertical distribution

of most of the SES's prey (see Figs. 2, 3) and the diving depth of SES deepens with this isotherm from the SAF to the STF (Fig. 3). Indeed, as light levels decrease exponentially with depth, the influence of light levels should decrease north of the SAF at all times due to the increased diving depth required to reach the SES's prey; as a consequence, the diurnal differences in dive depth should decrease, as observed. A reduced diurnal difference in the diving depths of SES was also observed in Antarctic waters. This is consistent with a previous report (Biuw et al. 2007) that interpreted this as indicating animals foraging benthically on the Antarctic Shelf. However, all SES females in our study foraged in oceanic waters associated with the AD, well off the Antarctic Shelf. Therefore, the reduced diurnal difference in diving depth (Fig. 4) suggests that SES females were feeding on prey remaining close to the surface during daylight hours.

The SO is characterised by broad concentric bands of water masses around the Antarctic continent, with each zone maintaining its unique physical properties (e.g. Orsi et al. 1995, Belkin & Gordon 1996). This has 2 implications. Firstly, the concentric nature of the current and water masses of the SO ensures circumpolar continuity of its ecosystems and zooplankton and fish species (Baker 1954). Therefore, our findings regarding the vertical distribution of SES prey could be extrapolated to other parts of the SO. Secondly, the T_{200} gradient used in our study largely reflects the latitudinal structuring of the SO from subtropical to Antarctic waters.

The first assumption of our study is that female SES diet is dominated by myctophid fish. Recent studies suggest that myctophids are likely to represent a major proportion of the SES female diet (Cherel et al. 2008, Bailleul et al. 2010) and 3 of the dominant myctophid species in the SO (*Electrona antarctica*, *E. calsbergi* and *Gymnoscopelus nicholsi*) have previously been found in stomach contents of SES (Slip 1995, Daneri & Carlini 2002). Furthermore, a recent study using a head-mounted camera on northern elephant seals (Naito et al. 2013) identified 2 small mesopelagic fishes as prey items, a myctophid and a bathypelagid, suggesting that elephant seals, despite their large size, are feeding on abundant but small prey items. Indeed, myctophid fish are a high-calorific prey (9.3 kJ g^{-1} wet mass) when compared with icefish (5.4 kJ g^{-1} wet mass) and prey items such as squid (1.7–4.5 kJ g^{-1} wet mass; Lea et al. 2002a,b). However, we acknowledge that other prey items such as squids are also likely consumed by SES.

The second assumption of our study is that a PEE provides a robust proxy for actual prey encounters. According to the calculated mean catch rate of 8.2 prey items per dive, we estimate that on average a SES female performing approximately 66 dives per day will catch approximately 540 prey items daily. Assuming that *Electrona calsbergi*, *E. antarctica*, *Gymnoscopelus nicholsi* and *G. piabilis* represent the major prey items within the ACC zone and that their mass generally ranges between 9 g (*Electrona calsbergi*, *E. antarctica*) and 30 g (*G. nicholsi*, *G. piabilis*; C. A. Bost & Y. Cherel pers. comm.), we estimate that a range of 4.8–16.1 kg of fish are ingested daily per seal. These values are not inconsistent with the daily mass gains (mean 0.9 ± 0.4 kg, range: 0.2–2 kg) observed in the post-breeding females in our study using a mean 10% energy transfer efficiency to body mass growth (see Ashwell Erickson & Elsner 1981, Rosen & Trites 1999, Jeanniard du Dot et al. 2008). These estimates are consistent with those based on calculations using at-sea field metabolic rates and photographs obtained by head-mounted cameras (Naito et al. 2013), revealing that northern elephant seal females feed on small mesopelagic prey (10–20 g), catching 430 to 860 prey items and an estimated ingested mass ranging between 4.3 and 17.2 kg of prey daily.

The SO mesopelagic ichthyofauna is dominated by myctophids (Kock 1992), with approximately 35 species (Hulley 1990) and a crude estimated biomass ranging between 70 and 340 million tonnes (Lubimova et al. 1987, Sabourenkov 1991). Previous studies suggest that temperature, light and oxygen content of the water are key environmental factors controlling their distribution (Hulley & Lutjeharms 1995).

Four species of myctophids contribute the bulk of the SO fish biomass: *Krefftichthys anderssoni*, *Electrona antarctica*, *E. carlsbergi* and *Gymnoscopelus nicholsi* (Sabourenkov 1991). Despite their ecological significance and considerable biomass, remarkably little is known about the basic biology of myctophids (Collins et al. 2008). While they are known to perform daily vertical migrations in the water column, remaining at deep depths during the day and feeding in shallower depths at night (Gjosaeter & Kawaguchi 1980), there is a major lack of knowledge regarding myctophid habitats and environmental factors controlling their distribution (Gjosaeter & Kawaguchi 1980, Catul et al. 2011). Assuming that myctophids represent the main component of SES female diet, the fine-scale monitoring of SES foraging behaviour according to environmental factors provides indirect

information on the myctophid vertical distribution in relation to temperature and light conditions along a north–south latitudinal gradient.

Our results suggest that SES may target different communities of myctophids at different depths north of the SAF. Indeed, as part of the ICHTYOKER transect run between Kerguelen and St. Paul Island, data from trawls at night to depths ranging between 0 and 330 m in waters with a temperature range of 11–17°C revealed a myctophid community dominated by *Symbolophorus barnardi*, *Lampanyctus australis*, *Electrona paucirastra* and *Lampichthys procerus* (G. Duhamel, P. Prouvost, J. Boutain unpubl. data). These fish species were more abundant in the northern vicinity of the STF. Therefore, the fact that SES dive to deeper depths to reach water temperatures lower than 8°C suggests that they target a different assemblage of myctophids. This community is likely to be dominated by *Electrona calsbergi*, *E. subaspera*, *Gymonoscopelus piabilis*, *G. fraseri* and *G. bolini*, and this mycthophid community distribution deepens with increasing temperature north of the SAF (Hulley 1981).

As mentioned earlier, a reduced diurnal difference in the diving depths of SES was also detected in Antarctic waters. This behaviour was also detected on very few occasions between the SACCF and the PF. In Antarctic waters, *Electrona carlsbergi*, a schooling species (Zasel'sliy et al. 1985), is commonly encountered close to the surface during the day (Hulley 1986, Fielding et al. 2012). *Electrona antarctica*, a non-schooling species, which is slightly larger than *E. carlsbergi*, is also found in SES stomach contents and may also represent an important prey item, along with *E. carslbergi*.

The difference in schooling behaviour of *Electrona* species might influence the foraging strategy of SES. Indeed, 3-dimensional reconstruction of dive tracks reveals that the sinuosity of the path at the bottom of the dive increases with the number of PEEs. Individuals exhibit an area-restricted search behaviour at the bottom of their dive and for several consecutive dives when large numbers of PEEs occur (C. G., J. V.-G., Y. L., J. Jouma'a unpubl. data), suggesting that SES are targeting schooling resources in these dives. However, on a few dives, large numbers of PEEs were observed despite the fact that the seals were travelling in a nearly constant direction, suggesting a more dispersed prey resource, possibly *E. antarctica*. In Antarctic waters, krill is also observed within the first 100 m of the water column, and could be targeted by some seals feeding close to the surface during the day, as krill is suspected to be preyed upon by some seals (Y. Cherel pers. comm.).

The lack of relationship between the mean T_{200} encountered by the SES during their foraging trip and either the absolute mass gain or the daily mass gain is supportive of a change in prey quality and/or size according to the water masses visited. This suggests that the lower catch rate observed in warmer waters, as well as the greater proportion of the swimming effort allocated to a greater diving depth to access those prey, might be compensated by the consumption of larger and/or higher quality prey in those water masses. For example, larger myctophids such as *Gymonoscopelus piabilis*, *G. nicholsi* and possibly *G. bolini* may represent a major component of SES female diet in these warmer northern waters. Indeed, in a recent study, G. Richard, J. V.-G. J. Jouma'a, C. G. (unpubl. data) found that the decrease in SES density (i.e. increase of lipid content) was positively related to the number of PEEs and was found to vary according to the foraging habitat. SES foraging north of the SAF improved their body condition at a similar rate compared with those foraging further south, despite a lower PEE rate and a greater swimming effort due to greater diving depth. This result is supportive of the hypothesis that SES females foraging north of the SAF were likely to feed on larger prey items, such as *Gymnoscopelus* spp., compared with those foraging south of the SAF.

Another interesting finding of this study regarding foraging success was that PEE rate both during the dive and at the bottom of the dive varied according to diurnal rhythm, with SES being more efficient during twilight compared with at night and during the day. Individuals were also found to have a significantly higher PEE rate at night compared with during the day. While we were expecting a lower foraging efficiency during daytime dives (complete dive) due to the greater diving depths recorded, we were not expecting such differences when only taking into account the PEE rate calculated at the bottom of the dive. In fact, we were expecting the opposite relationship, with a greater success rate during the bottom phases of daytime dives. Indeed, while some myctophids species are known to be actively feeding during both day and night, several studies have shown that during the day myctophids tend to aggregate in denser schools, behaving more lethargically, possibly making them more vulnerable to predation (Barham 1966, Kinzer et al. 1993, Kaartvedt et al. 2009). The present study suggests the opposite, indicating that elephant seals might be more efficient when their prey is supposedly actively foraging at night closer to the surface or performing nycthemeral migrations. Therefore, we hypothesise that actively,

vertically migrating (at dusk and dawn) and/or foraging myctophids (at night) are easier to detect and/or locate, either because they reach aggregation levels allowing the maximization of encounter rates by predators or because their active behaviour makes them more vulnerable to predation. Actively moving prey might be easier to locate by the foraging seals. Indeed, as prey move they create hydrodynamic trails likely to be detected by SES through their vibrissae (Dehnhardt et al. 2001).

Alternatively, a recent modelling study has shown that predators reach their maximum PEE efficiency at intermediate aggregation levels of prey, with highly aggregated patches being too difficult to locate, while dispersed prey are diluted in the environment and do not allow the predator to be efficient (Massardier 2013).

Prey may also produce sounds detected by elephant seals, which are known to have excellent underwater hearing ability (Kastak & Schusterman 1998). Indeed, over a 12-yr study, McCauley & Cato (pers. comm.) found recently that fish choruses, most likely to be myctophids, always occurred shortly after dusk and pre-dawn, with most energy in the 1–3 kHz range. Furthermore, while active, myctophids might be more likely to signal their presence by producing bioluminescence that seals could detect visually (Vacquié-Garcia et al. 2012). Such hypotheses should be further investigated in future studies and should provide new and valuable insights into the ecology and distribution of SES prey.

Acknowledgements. This study is part of a national research program (no. 109, H. Weimerskirch and the observatory Mammifères Explorateurs du Milieu Océanique, MEMO SOERE CTD 02) supported by the French Polar Institute (Institut Paul Emile Victor, IPEV). This work was carried out in the framework of the ANR Blanc MYCTO-3D-MAP and ANR VMC 07: IPSOS-SEAL programs and CNES-TOSCA program ('Élephants de mer océanographes'). The authors also thank the Total Foundation for financial support. All animals in this study were treated in accordance with the IPEV ethical and Polar Environment Committees guidelines. We thank all the people who contributed to the field work and data processing, with special thought to M. Authier, A. Chaigne, Q. Delorme, N. El Skaby, J. C. Vaillant and F. Vivier. We are extremely grateful to the 3 anonymous referees for their constructive suggestions and the detailed corrections provided.

LITERATURE CITED

Ancel A, Horning M, Kooyman GL (1997) Prey ingestion revealed by oesophagus and stomach temperature recordings in cormorants. J Exp Biol 200:149–154

Ansorge IJ, Froneman PW, Pakhomov EA, Lutjeharms JRE, Perissinotto R, van Ballegooyen RC (1999) Physical-biological coupling in the waters surrounding the Prince Edward Islands (Southern Ocean). Polar Biol 21:135–145

Ashwell Erickson S, Elsner R (1981). The energy cost of free existence for Bering Sea harbour and spotted seals. In: Hood DW, Calder JA (eds) Eastern Bering Sea Shelf: oceanography and resources, Vol II. University of Washington Press, Seattle, WA, p 869–899

Authier M, Ponchon A, Martin C, Bentaleb I, Guinet C (2012) Foraging fidelity as a recipe for a long life: foraging strategy and longevity in male southern elephant seals. PLoS ONE 7:e32026

Bailleul F, Authier M, Ducatez S, Roquet F, Charrassin JB, Cherel Y, Guinet C (2010) Looking at the unseen: combining animal bio-logging and stable isotopes to reveal a shift in the ecological niche of a deep-diving predator. Ecography 33:709–719

Baker A (1954) The circumpolar continuity of Antarctic plankton species. Discov Rep 27:201–218

Barham EG (1966) Deep scattering layer migration and composition: observations from a diving saucer. Science 151: 1399–1403

Batty R, Blaxter J, Richard J (1990) Light intensity and the feeding behaviour of herring, *Clupea harengus*. Mar Biol 107:383–388

Belkin IM, Gordon AL (1996) Southern Ocean fronts from Greenwich meridian to Tasmania. J Geophys Res 101: 3675–3696

Bennett KA, McConnell BJ, Fedak MA (2001) Diurnal and seasonal variations in the duration and depth of the longest dives in southern elephant seals (*Mirounga leonina*): possible physiological and behavioural constraints. J Exp Biol 204:649–662

Biuw M, Boehme L, Guinet C, Hindell M and others (2007) Variations in behaviour and condition of a Southern Ocean top predator in relation to *in situ* oceanographic conditions. Proc Natl Acad Sci USA 104:13705–13710

Biuw M, Nøst OA, Stien A, Lydersen C, Kovacs K (2010) Effect of hydrographic variability on the spatial, seasonal and diel diving patterns of southern elephant seals in the eastern Weddell sea. PLoS ONE 5:e13816

Boden BP, Kampa EM (1967) The influence of natural light on the vertical migrations of an animal community in the sea. Symp Zool Soc 19:15–26

Boehlert GW, Costa DP, Crocker DE, Green P, O'Brien T, Levitus S, Le Boeuf BJ (2001) Autonomous pinniped environmental samplers: using instrumented animals as oceanographic data collectors. J Atmos Ocean Technol 18:1882–1893

Bost CA, Cotté C, Bailleul F, Cherel Y and others (2009) The importance of oceanic fronts to marine birds and mammals of the southern oceans. J Mar Syst 78:363–376

Carbone C, Houston AI (1994) Patterns in the diving behavior of the pochard, *Aythya ferina*: a test of an optimality model. Anim Behav 48:457–465

Catul V, Gauns M, Karuppasamy PK (2011) A review on mesopelagic fishes belonging to family Myctophidae. Rev Fish Biol Fish 21:339–354

Charrassin JB, Kato A, Handrich Y, Sato K and others (2001) Feeding behaviour of free-ranging penguins determined by oesophageal temperature. Proc Biol Sci 268:151–157

Charrassin JB, Hindell M, Rintoul SR, Roquet F and others (2008) Southern Ocean frontal structure and sea-ice formation rates revealed by elephant seals. Proc Natl Acad Sci USA 105:11634–11639

Cherel Y, Ducatez S, Fontaine C, Richard P, Guinet C (2008) Stable isotopes reveal the trophic position and mesopelagic fish diet of female southern elephant seals breeding on the Kerguelen Islands. Mar Ecol Prog Ser 370: 239–247

Collins MA, Xavier JC, Johnston NM, North AW and others (2008) Patterns in the distribution of myctophid fish in the northern Scotia Sea ecosystem. Polar Biol 31:837–851

Costa DP, Klinck JM, Hofmann EE, Dinniman MS, Burns JM (2008) Upper ocean variability in West Antarctic Peninsula continental shelf waters as measured using instrumented seals. Deep-Sea Res II 55:323–337

Cotté C, Simard Y (2005) Formation of dense krill patches under tidal forcing at whale feeding hot spots in the St. Lawrence Estuary. Mar Ecol Prog Ser 288:199–210

Crocker DE, Le Boeuf BJ, Costa DP (1997) Drift diving in female northern elephant seals: implication for food processing. Can J Zool 75:27–39

Daneri GA, Carlini AR (2002) Fish prey of southern elephant seals, *Mirounga leonina*, at King George Island. Polar Biol 25:739–743

Dehnhardt G, Mauck B, Hanke W, Bleckmann H (2001) Hydrodynamic trail following in harbor seals (*Phoca vitulina*). Science 293:102–104

Dodson S (1990) Prediciting diel vertical migration of zooplankton. Limnol Oceanogr 35:1195–1200

Dragon AC, Monestiez P, Bar-Hen A, Guinet C (2010) Linking foraging behaviour to physical oceanographic structures: southern elephant seals and mesoscale eddies east of Kerguelen Islands. Prog Oceanogr 87:61–71

Dragon AC, Bar-Hen A, Monestiez P, Guinet C (2012) Horizontal and vertical movements as predictors of foraging success in a marine predator. Mar Ecol Prog Ser 447: 243–257

Fielding S, Watkins JL, Collins MA, Enderlein P, Venables HJ (2012) Acoustic determination of the distribution of fish and krill across the Scotia Sea in spring 2006, summer 2008 and autumn 2009. Deep-Sea Res II 59–60: 173–188

Gal GL, Ellis R, Rudstam LG, Mohammadian AM (1999) Light and diel vertical migration: spectral sensitivity and light avoidance by *Mysis relicta*. Can J Fish Aquat Sci 56: 311–322

Gallon S, Bailleul F, Charrassin JB, Guinet C, Bost CA, Handrich Y, Hindell M (2013) Identifying foraging events in deep diving southern elephant seals, *Mirounga leonina*, using acceleration data loggers. Deep-Sea Res II 88-89:14–22

Gjosaeter J, Kawaguchi K (1980) A review of the world resources of mesopelagic fish. FAO Fish Tech Pap 193: 1–151

Guinet C, Cherel Y, Ridoux V, Jouventin P (1996) Consumption of marine resources by seabirds and seals in Crozet and Kerguelen waters: changes in relation to consumer biomass 1962–1985. Antarct Sci 8:23–30

Guinet C, Walker E, Monestiez P, Xing X and others (2013) Assessment of phytoplankton concentration in the Southern Ocean by elephant seal equipped with a new generation of CTD-fluorescence tags. Earth Syst Sci Data 5:15–29

Hanuise N, Bost CA, Handrich Y (2013) Optimization of transit strategies while diving in foraging king penguins. J Zool 290:181–191

Hassrick JL, Crocker DE, Teutschel NM, McDonald BI, Robinson PW, Simmons SE, Costa DP (2010) Condition and mass impact oxygen stores and dive duration in adult female northern elephant seals. J Exp Biol 213: 585–592

Hindell MA, Slip DJ, Burton HR (1991) The diving behaviour of adult male and female southern elephant seals, *Mirounga leonina* (Pinnipedia: Phocidae). Aust J Zool 39: 595–619

Hindell MA, Bradshaw CJA, Sumner MD, Michael KJ, Burton HR (2003) Dispersal of female southern elephant seals and their prey consumption during the austral summer: relevance to management and oceanographic zones. J Appl Ecol 40:703–715

Horning M, Trillmich F (1999) Lunar cycles in diel prey migrations exert a stronger effect on the diving of juveniles than adult Galapagos fur seals. Proc R Soc Lond B Biol Sci 266:1127–1132

Hulley PA (1981) Results of the research cruises of FRV 'Walther Herwig' to South America. LVIII. Family Myctophidae (Osteichthyes, Myctophiformes). Arch FischWiss 31:1–300

Hulley PA (1986) Myctophidae. In: Smith MM, Heemstra PC (eds) Smiths' sea fishes. Springer-Verlag, Berlin, p 282–321

Hulley PA (1990) Family Myctophidae. In: Gon O, Heemstra PC (eds) Fishes of the Southern Ocean. JLB Smith Institute of Ichthyology Publishers, Grahamstown, p 146–178

Hulley PA, Lutjeharms JRE (1995) The south-western limit for the warm-water, mesopelagic ichthyofauna of the Indo-West-Pacific: lanternfish (Myctophidae) as a case study. S Afr J Mar Sci 15:185–205

Iwata T, Sakamoto KQ, Takahashi A, Edwards EWJ, Staniland IJ, Trathan PN, Naito Y (2012) Using a mandible accelerometer to study fine-scale foraging behavior of free-ranging Antarctic fur seals. Mar Mamm Sci 28: 345–357

Jaud T, Dragon AC, Garcia JV, Guinet C (2012) Relationship between chlorophyll a concentration, light attenuation and diving depth of the southern elephant seal *Mirounga leonina*. PLoS ONE 7:e47444

Jeanniard du Dot T, Rosen DAS, Trites AW (2008) Steller sea lions show diet-dependent changes in body composition during nutritional stress and recover more easily from mass loss in winter than in summer. J Exp Mar Biol Ecol 367:1–10

Kaartvedt S, Røstad A, Klevjer TA, Staby A (2009) Use of bottom-mounted echo sounders in exploring behavior of mesopelagic fishes. Mar Ecol Prog Ser 395:109–118

Kampa EM (1976) Photoenvironment and vertical migrations of mesopelagic marine animal communities. In: De Coursey PJ (ed) Biological rhythms in the marine environment. Belle W Baruch Library in Marine Sciences, University of South Carolina Press, Columbia, SC, p 257–272

Kastak D, Schusterman RJ (1998) In-air and underwater hearing sensitivity of a northern elephant seal (*Mirounga angustirostris*). Can J Zool 77:1751–1758

Kinzer J, Bottger-Schnack R, Schulz K (1993) Aspects of horizontal distribution and diet of myctophid fish in the Arabian Sea with reference to the deep water oxygen deficiency. Deep-Sea Res II 40:783–800

Knox GA (2007) Biology of the Southern Ocean, 2nd edn. CRC Press, Boca Raton, FL

Kock KH (1992) Antarctic fish and fisheries. Cambridge University Press, Cambridge

Koubbi P (1993) Inflence of the frontal zones on ichthyo-

plankton and mesopelagic assemblages in the Crozet Basin (Indian sector of the Southern Ocean). Polar Biol 13:557–564

Koubbi P, Moteki M, Duhamel G, Goarant A and others (2011) Ecoregionalization of myctophid fish in the Indian sector of the Southern Ocean: results from generalized dissimilarity models. Deep-Sea Res II 58:170–180

Lea MA, Cherel Y, Guinet C, Nichols PD (2002a) Antarctic fur seals foraging in the Polar Frontal Zone: inter-annual shifts in diet as shown from fecal and fatty acid analyses. Mar Ecol Prog Ser 245:281–297

Lea MA, Nichols PD, Wilson G (2002b) Fatty acid composition of lipid-rich myctophids and mackerel icefish (*Champsocephalus gunnari*) Southern Ocean food-web implications. Polar Biol 25:843–854

Lea MA, Johnson D, Melin S, Ream R, Gelatt T (2010) Diving ontogeny and lunar responses in a highly migratory mammal, the northern fur seal *Callorhinus ursinus*. Mar Ecol Prog Ser 419:233–247

Liebsch N, Wilson RP, Bornemann H, Adelung D, Plötz J (2007) Mouthing off about fish capture: jaw movement in pinnipeds reveals the real secrets of ingestion. Deep-Sea Res II 54:256–269

Liu SH, Sun S, Han BP (2003) Diel vertical migration of zooplankton following optimal food intake under predation. J Plankton Res 25:1069–1077

Lubimova TG, Shust KV, Popkov VV (1987) Specific features in the ecology of Southern Ocean mesopelagic fish of the family Myctophidae. Biological resources of the Arctic and Antarctic (collected papers). Nauka Press, Moscow, p 320–337 (in Russian)

Massardier L (2013) Etude de la faisabilité du couplage d'un modèle océanique et d'un modèle individu centré en vue de la simulation du comportement de grands prédateurs en zone australe. MSc thesis, Université Nice Sophia Antipolis

McIntyre T, De Bruyn PJN, Ansorge IJ, Bester MN, Bornemann H, Plötz J, Tosh CA (2010) A lifetime at depth: vertical distribution of southern elephant seals in the water column. Polar Biol 33:1037–1048

McIntyre T, Bornemann H, Plötz J, Tosh CA, Bester MN (2011a) Water column use and forage strategies of female southern elephant seals from Marion Island. Mar Biol 158:2125–2139

McIntyre T, Ansorge IJ, Bornemann H, Plötz J, Tosh CA, Bester MN (2011b) Elephant seal dive behaviour is influenced by ocean temperature: implications for climate change impacts on an ocean predator. Mar Ecol Prog Ser 441:257–272

McMahon CR, Burton H, Slip D, McLean S, Bester M (2000) Field immobilisation of southern elephant seals with intravenous tiletamine and zolazepam. Vet Rec 146: 251–254

Morel A (1988) Optical modeling of the upper ocean in relation to its biogenous matter content (case I waters). J Geophys Res 93:10749–10768

Naito Y, Bornemann H, Takahashi A, McIntyre T, Plotz J (2010) Fine-scale feeding behaviour of Weddell seals revealed by mandible accelerometer. Polar Sci 4: 309–316

Naito Y, Costa DP, Adachi T, Robinson PW, Fowler M, Takahashi A (2013) Unravelling the mysteries of a mesopelagic diet: a large apex predator specializes on small prey. Funct Ecol 27:710–717

Orsi AH, Whiteworth IT, Nowlin WD Jr (1995) On the meridional extent and fronts of the Antarctic Circumpolar Current. Deep-Sea Res I 42:641–673.

Park YH ,Gambéroni L, Charriaud E (1991) Frontal structure, transport and variability of the Antarctic Circumpolar Current in the South Indian Ocean sector, 40°–80°E. Mar Chem 35:45–62

Park YH, Gambéroni L, Charriaud E (1993) Frontal structure, water masses, and circulation in the Crozet Basin. J Geophys Res 98:12361–12385

Park YH, Charriaud E, Fieux M (1998) Thermohaline structure of the Antarctic surface water/winter water in the Indian sector of the Southern Ocean. J Mar Syst 17:5–23

R Development Core Team (2009) R: a language and environment for statistical computing. R Foundation for Statistical Computing, Vienna

Ropert-Coudert Y, Wilson RP (2005) Trends and perspectives in animal-attached remote sensing. Front Ecol Environ 3:437–444

Ropert-Coudert Y, Kato A, Liebsch N, Wilson RP, Müller G, Baubet E (2004) Monitoring jaw movements: a cue to feeding activity. Game Wildl Sci 20:1–19

Roquet F, Park YH, Guinet C, Bailleul F, Charrassin JB (2009) Observations of the Fawn Trough Current over the Kerguelen Plateau from instrumented elephant seals. J Mar Syst 78:377–393

Rosen DAS, Trites AW (1999) Metabolic effect of low-energy diet on Steller sea lions, *Eumetopias jubatus*. Physiol Biochem Zool 72:723–731

Rudstam LG, Danielsson K, Hansson S, Johansson S (1989) Diel vertical migration and feeding patterns of *Mysis mixta* (Crustacea, Mysidacea) in the Baltic Sea. Mar Biol 101:43–52

Rutz C, Hays GC (2009) New frontiers in biologging science. Biol Lett 5:289–292

Sabourenkov E (1991) Myctophids in the diet of Antarctic predators. CCAMLR Selected Sci Pap 1991:335–368

Slip DJ (1995) The diet of southern elephant seals (*Mirounga leonina*) from Heard island. Can J Zool 73: 1519–1528

Suzuki I, Naito Y, Folkow LP, Miyazaki N, Blix AS (2009) Validation of a device for accurate timing of feeding events in marine animals. Polar Biol 32:667–671

Vacquié-Garcia J, Royer F, Dragon AC, Viviant M, Bailleul F, Guinet C (2012) Foraging in the darkness of the Southern Ocean: influence of bioluminescence on a deep diving predator. PLoS ONE 7:e43565

Viviant M, Trites AW, Rosen DAS, Monestiez P, Guinet C (2010) Prey capture attempts can be detected in Steller sea lions and other marine predators using accelerometers. Polar Biol 33:713–719

Wilson RP, Cooper J, Plötz J (1992) Can we determine when marine endotherm feed? A case study with seabirds. J Exp Biol 167:267–275

Wilson RP, Steinfurth A, Ropert-Coudert Y, Kato A, Kurita M (2002) Lip-reading in remote subjects: an attempt to quantify and separate ingestion, breathing and vocalisation in free-living animals using penguins as a model. Mar Biol 140:17–27

Zasel'sliy VS, Kudrin BD, Poletayev VA, Chechenin S (1985) Some features of the biology of *Electrona carlsbergi* (Taning) (Myctophidae) in the Atlantic sector of the Antarctic. J Ichthyol 25:163–166

Zuur AF, Ieno EN, Walker NJ, Saveliev AA, Smith GM (2009) Mixed effects models and extensions in ecology with R. Springer, New York, NY

Editorial responsibility: Peter Corkeron, Woods Hole, Massachusetts, USA

Submitted: January 16, 2013; Accepted: November 20, 2013
Proofs received from author(s): February 14, 2014

ANNEXE

F

Article 5 : Jouma'a *et al.* (2015)

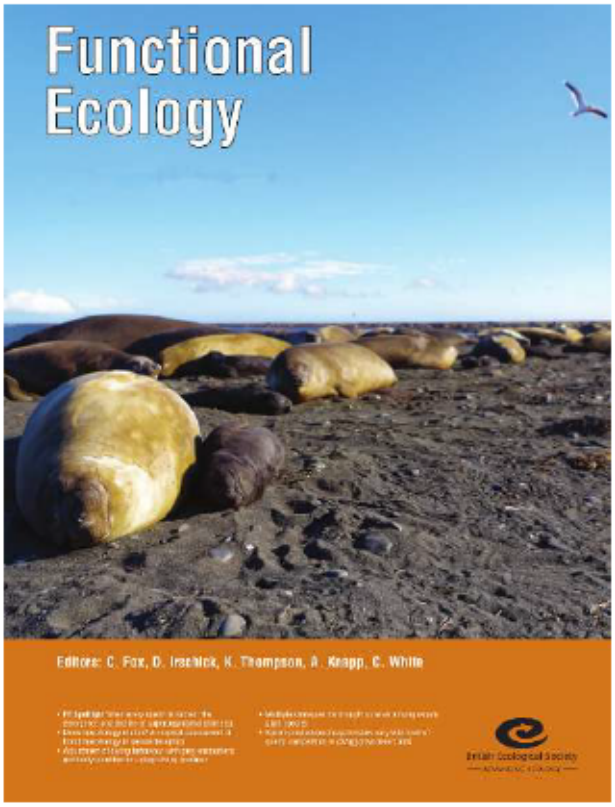

Éléphants de mer en mue. Crédit : J. Jouma'a

5. Jouma'a Joffrey, Le Bras Yves, Richard Gaëtan, Vacquié-Garcia Jade, El Ksabi Nory, Picard Baptiste, Guinet Christophe. (2016). Adjustment of diving behaviour with prey encounters and body condition in a deep diving predator : the Southern Elephant Seal. *Functional Ecology*. **30**(4). 636-648. doi: 10.1111/1365-2435.12514

Functional Ecology

Functional Ecology 2016, **30**, 636–648 doi: 10.1111/1365-2435.12514

Adjustment of diving behaviour with prey encounters and body condition in a deep diving predator: the Southern Elephant Seal

Joffrey Jouma'a*, Yves Le Bras, Gaëtan Richard, Jade Vacquié-Garcia, Baptiste Picard, Nory El Ksabi and Christophe Guinet*

CEBC, UMR 7372 ULR-CNRS, 79360 Villiers en Bois, France

Summary

1. Optimal diving models have been developed to investigate how air-breathing predators should adjust their diving behaviour to optimize their foraging efficiency. Using time-depth recorders and 3D accelerometers, we addressed this question on six free-ranging Southern Elephant Seal (SES) females equipped on Kerguelen Island.

2. We hypothesize that seals would initially increase their foraging time with distance to the foraging patches before reducing it for physiological reasons, regardless of the prey encountered. We expect that SES spends more time at depths where more Prey Catch Attempts (PCA) occur, that is at the bottom. We also hypothesize that bottom time should be related to both the seal body density and the swimming effort dedicated to catching prey, as we expect seals to be more active when catching prey. Finally, because oxygen is acquired at the surface only, we expect that recovery times increase with the duration of the previous dives.

3. A total of 72·6% of PCA detected by accelerometer occurred at the bottom of the dive. At shallow depths (< 300 m), seals spent more time at the bottom in dives where PCA occurred compared to non-PCA dives. At deeper depths, SES had shorter bottom times in PCA dives due to higher swimming effort. When only dives associated with PCA were considered, the time spent at the bottom increased with the number of PCA. In addition, the closer the seal was to neutral buoyancy, the longer was the bottom duration. Body density, that is buoyancy, was found to be a critical factor in controlling variations in the dive duration through the swimming effort to access the prey at the bottom of the dive. Finally, post-dive surface intervals were related to the duration and swimming effort of the previous dive.

4. This study reveals how a marine top predator adjusts the time spent at the bottom depending on its body density, prey encounter rate and prey accessibility. It also highlights that using the duration of the foraging phase as a proxy of foraging success can be seriously misleading in SES. Finally, the need to use an energetic approach with bio-logging technology to study behavioural ecology is emphasized.

Key-words: bio-logging, buoyancy, foraging behaviour, marine mammal, optimal diving theory

Introduction

Many animals are bound to a specific site which they have to return to, often for catching their prey or feeding their offspring, like seabirds returning to the colony to feed their chicks. They are thus limited to areas around this central place to find resources. This specificity leads to particular temporal and energetic constraints, due to energy expenditure to travel to and from this central place and/or a limited time available for feeding before returning to the central place (Pyke 1984; Kacelnik, Houston & Schmid-Hempel 1986). In an aquatic environment, dives performed by air-breathing predators can be considered as a special case of the central place foraging theory (Houston & McNamara 1985). Because they are physiologically constrained to come up to the surface to renew their oxygen supply, it induces complex decisions rule in order to optimize resource acquisition.

*Correspondence authors. E-mails: christophe.guinet@cebc.cnrs.fr; joffreyjoumaa@icloud.com

The number of encountered prey was generally assumed to be proportional to the time spent searching since there are few data on the quality of the patches encountered by animal. The first studies on optimal diving behaviours therefore examined strategies that maximize time spent at the foraging patch, and it was expected that the decision to end a dive was entirely based on oxygen reserves (Kramer 1988; Houston & Carbone 1992; Thompson, Hiby & Fedak 1993; Carbone & Houston 1994). The main prediction of this assumption is that breath-holding divers should stay at depth as long as their oxygen store allows it. The duration of most dives was therefore expected to approach the aerobic dive limit (Thompson & Fedak 2001), which is the dive duration at which all the usable oxygen stores have been used (Houston 2011). However, models based on this theory were unrealistic because many species end most of their dives before reaching this limit (Costa, Gales & Goebel 2001; Costa *et al.* 2004).

Although the diving performance of an air-breathing animal clearly depends on its physiological abilities, it was found that other factors play important roles in the decision to stay or leave a patch, such as predation risk (Heithaus & Frid 2003), distribution, abundance, depth and energy content of the prey (Ydenberg & Clark 1989; Thompson & Fedak 2001; Cornick & Horning 2003; Sparling *et al.* 2007). Thompson & Fedak's (2001) model examined how breath-holding predators adjust their dive time budget in relation to depth and patch quality, whilst taking into account the oxygen balance. They showed that there is a net benefit to ending dives early, without fully depleting their oxygen stores, if no prey is encountered. This benefit is higher in lower density patches and reduced in the deepest dives. Thompson, Hiby & Fedak (1993) showed that in deep dives, animals swim with the minimum cost of transport during the transit phase, suggesting that the costs associated with deepest dives can be minimized by behavioural mechanisms.

Animals can adjust their swimming effort finely through variations in stroke frequency and body angle (Sato *et al.* 2003; Fossette *et al.* 2010; Miller *et al.* 2012) to reduce oxygen consumption and maximize time at depth. However, they are also affected by intrinsic parameters such as buoyancy, which is determined by body composition, and more specifically, by the percentage of adipose tissue (Crocker, Le Boeuf & Costa 1997; Beck, Bowen & Iverson 2000; Sato *et al.* 2003). Several studies highlight the influence of buoyancy on different aspects of diving behaviour, such as rate of ascent and descent (Webb *et al.* 1998; Beck, Bowen & Iverson 2000; Sato *et al.* 2003; Adachi *et al.* 2014). In a recent study on southern elephant seal, *Mirounga leonina* (SES hereafter), Richard *et al.* (2014) showed that, in negatively buoyant SES, 1% variation in buoyancy resulted in a 20% variation of swimming effort, during the ascent phase. Therefore, taking into account buoyancy appears to be essential for the prediction of the optimal diving behaviour.

This result reflects the recent development of bio-logging. Today, mouth-opening and head movement can be detected using Hall sensors (Wilson *et al.* 2002) or accelerometers (Okuyama *et al.* 2009; Suzuki *et al.* 2009; Naito *et al.* 2010, 2013; Viviant *et al.* 2010) to provide a set of new proxies for prey encounter rates. Furthermore, accelerometers can be also used to monitor swimming effort as well as animal posture such as pitch in water. Changes in Prey Catch Attempts (PCA hereafter) and swimming behaviour can then be monitored throughout the dive when pressure sensors are added. With these series of information (occurrence and number or history of PCA), we can indirectly assess the quality of the area visited by animals and investigate the fine-scale behavioural responses of diving predators in relation to the habitat quality.

As part of this study, we investigated how a free-ranging marine predator, the southern elephant seal, adjusts its diving behaviour to recent prey encounters, distance to prey patches (depth) and its buoyancy. Knowing that time spent at the bottom of a dive corresponds to the main foraging time of SES (Guinet *et al.* 2014) we make the following predictions:

1. Seals should first increase their foraging time with increasing distance, that is dive depth, to the foraging patch and then decrease it, whether they encounter prey or not (Houston & Carbone 1992).
2. In agreement with Thompson & Fedak's prediction (2001) for a given diving depth, seals should increase their bottom time when more PCA occur at the dive's bottom phase compared to when no PCA occur.
3. The amount of time the seal allocates to foraging at the bottom of their dive should be related to both its body density and to its swimming effort to catch prey as we expect that seals are more active when catching prey. Furthermore, individuals closer to neutral buoyancy should be able to allocate more time at the bottom of their dive because the round trip cost of transport is minimum at neutral buoyancy (Miller *et al.* 2012; Adachi *et al.* 2014), and as a consequence, the amount of energy spent by the individual and the amount of oxygen consumed are both reduced (Tucker 1975).
4. Because oxygen is acquired at the surface with diminishing returns, that is nonlinear (Butler & Jones 1997), recovery times increase with the duration of the preceding dive (Kooyman & Ponganis 1998). Thus, shallow dives yield a higher net rate of oxygen acquisition and deeper dives result in a higher proportion of time spent recuperating at the surface (Kramer 1988). To maximize the proportion of time spent in the food patch, we predict that surface time should increase with target depth (Houston & Carbone 1992).

Materials and methods

ETHICS STATEMENTS

The Ethics Committee of the French Polar Institute (IPEV) validated all scientific procedures applied on elephant seals. All

animals in this study were handled and cared for in total accordance with its guidelines and recommendations.

DEPLOYMENT OF DEVICES AND DATA COLLECTION

We used data from six post-breeding females SES (mean mass = 309 ± 68 kg; mean length = 247 ± 17 cm, Table 1) equipped on the Kerguelen Islands (49°20′S, 70°20′E) with an Argos-GPS satellite tag (Splash 10-F; Wildlife Computers, Redmond, WA, USA) combined with a time-depth recorder–accelerometer (TDR-MK10-X; Wildlife Computers). The six Splash-10-F tags were glued to the fur on the seals' heads. In 2010, three time-depth recorder–accelerometers were also glued on the head of three different seals, with another time-depth recorder–accelerometer (MK10-X; Wildlife Computers) on the back of one of them. The following year, two MK10-X were deployed on the animals' backs and one on the head, again on three different seals. Pressure was sampled at 1 Hz by TDR, ± 1% of reading. Data loggers were set to collect and archive pressure every second, while triaxial acceleration was sampled at 16 Hz.

The seals were captured with a canvas head-bag and anaesthetized using a 1:1 combination of Tiletamine and Zolazepam (Zoletil 100) injected intravenously (McMahon *et al.* 2000; Field *et al.* 2002). Data loggers were glued using a quick-setting epoxy glue (Araldite AW 2101), after the fur was cleaned with acetone. The loggers were then recovered when females SES returned to shore to moult (i.e. January–February following deployments). Seals ashore were located using their Argos locations.

All scripts used thereafter for data treatment and analysis are available upon request.

DIVE CYCLE STATISTICS

A dive cycle is defined as a dive (descent, bottom and ascent phases) followed by a period of time spent at the surface. Because there is drift over time in pressure transducers in TDR, due to different factors during a dive, a zero offset correction of depth was applied to our data set using a custom script performed with a commercial software package (MATLAB 8.1; The MathWorks, Natick, MA, USA). Only dives deeper than 15 m were kept for analysis, otherwise seals were considered to be at the surface. This threshold was chosen to avoid subsurface movements to be identified as dives. Each dive was then divided into three different phases: descent, bottom and ascent phases by using a vertical speed criterion chosen after a sensitivity analyses. Descent and ascent phases were characterized as a period when the vertical speed from or towards the surface, fitted to a polynomial of degree 4, was >0·75 m s^{-1}. This is similar to the approach of Luque (2007) in its R package `diveMove`, but differs from most studies which determine the bottom time from the moment when a certain percentage of the maximum dive depth is achieved (Lesage, Hammill & Kovacs 1999; Insley *et al.* 2008). Here, the bottom phase refers to a period between the descent and ascent phase where the fitted curve of the vertical speed was lower than 0·75 m s^{-1}, in absolute terms. Time spent at the surface is the time lapse between two dives. This definition of the surface time results in a conservative definition of a dive, which avoids considering small subsurface excursions as dives. However, it also introduces consistent overestimation of time spent loading oxygen at the surface, as it includes the periods of descent and ascent above 15 m. Diving variables were calculated for each dive with MATLAB, using custom dive-analysis scripts. The selected diving variables were maximum depth (m), dive duration (s), time spent during descent, bottom and ascent phases (s). Data from the accelerometers were used to estimate stroke rate (Sato *et al.* 2003) and the intensity of the hind flipper movement, and subsequently used to calculate a swimming effort index (eqn 1), by using a 0·6 Hz-wide band pass centred on the second peak identified from the power spectral density.

$$\text{Swimming effort} = \frac{\sum|\text{peaks}|}{\Delta t} \qquad \text{eqn 1}$$

The swimming effort (m s^{-3}) was defined as the summed value of absolute acceleration peaks, Σ|peaks| (m s^{-2}), over the relevant periods Δ*t* (s) (Richard *et al.* 2014). Hereafter, the total swimming effort is defined as the sum of the absolute lateral acceleration (m s^{-2}) only, that is without considering effort duration. Dive angles, defined as angles from the horizontal plane, were then calculated according to Tuck (2007) by using static acceleration obtained with a low-pass filtering (cut-off frequency of 0·2 Hz) applied to the three axes (eqn 2).

$$\text{Pitch} = \arctan\left(\frac{x}{\sqrt{(y^2 + z^2)}}\right) \qquad \text{eqn 2}$$

BODY DENSITY

Body density variation over time was estimated according to methodology outlined by Richard *et al.* (2014). For each drift dive, a drift rate was determined by calculating the slope between depth and time using linear regression (Biuw *et al.* 2003; Bailleul *et al.* 2007; Mitani *et al.* 2010). If there were several drift dives, the drift rate was averaged by day. A model was then built to monitor these daily drift rate variations with changes in daily average swimming speed during the descent phase (Richard *et al.* 2014). Using this relationship, variations in daily drift rate were then calculated for every daily average descent swimming speed calculated from others dives. Finally, based on the drift dives model developed by Biuw *et al.* (2003), we then used the change in drift rate to assess body density variations. This method provided us daily estimates of body density for each animal.

PATCH QUALITY

The patch quality was assessed by considering the number of PCA per unit of time spent in the bottom phase of the dive (as detected

Table 1. Descriptive information about the six post-breeding females SESs

Seal ID	Body mass (kg)	Size (cm)	Departure date	Days recorded	Number of dives	Number of drift dives
10A5015	377	266	11/21/2010	74	4515	90
10A5017	245	225	10/29/2011	54	3768	48
10A5019	249	240	10/31/2011	56	3707	123
10A5022	255	232	10/31/2011	58	3727	61
78524	331	266	10/28/2010	61	3361	125
78525	395	252	11/01/2010	81	4118	49

by acceleration). PCA rate was considered to be a good proxy for prey encounter rate; we assume prey encounter rate is positively correlated with improved patch quality. Dynamic accelerations resulting from strokes and rapid head movements were extracted from the three axes with an order 3 high-pass digital Butterworth filter with a normalized cut-off frequency of 0·33 Hz (performed with `butter` function). For each axis, a fixed window of one-s was used to calculate the standard deviation every second. Signals reduced in this way were smoothed using a moving standard deviation with a window size of 5 s. Finally, a 2-mean clustering was performed for each signal. *1* was associated with data from the higher cluster and *0* to the others. Possible PCAs occur when a *1* was found in the three axes. A continuous succession of *1* was identified as a single PCA.

DATA ANALYSIS

All statistical analyses were conducted using R (R Development Core Team 2014). Linear mixed-effects models were fit with the `nlme` package (Pinheiro *et al.* 2013). Individuals were included as random factors, and we accounted for the temporal correlation in our data using an autoregressive variance–covariance matrix (corAR1). Drift dives were identified using Dragon *et al.*'s (2012) method. These dives which are not thought to be foraging dives, but rather recovery dives (Crocker, Le Boeuf & Costa 1997), were excluded from our analyses.

A basic model including all diving variables was constructed to explain bottom time variations in order to test the effect of the number of PCA and the depth on bottom time. Basic models investigated the bottom time duration in relation to dive duration, dive angle, diving depth and swimming effort. The animal's body density was also included to our models due to its important influence on diving behaviour. Following our preliminary analysis, three analyses were conducted: dives with PCA, dives without PCA and all dives. For each analysis, multi-model inference was used to select the best basic model according to Akaike Information Criterion (AIC), using `dredge` function from the `MuMIn` R-package (Barton 2013).

To explore the relationship between bottom times and patch quality, the number of PCA was added to the basic model chosen. Similarly, a quadratic depth term was set as a co-variable, representing an increase, followed by a decrease of bottom time with depth, as predicted in the Houston & Carbone model (1992). We assessed the significance of both parameters by comparing the basic model with the addition of one variable to the basic model, using an ANOVA test. To investigate the variations of bottom time with the availability and the vertical accessibility of prey according to energy spent, a model based only on swimming effort during the bottom phase was built. This parameter was examined in relation to depth, bottom duration, body density and number of PCA.

To identify a possible change in the influence of PCA (occurrence and number of events) and body density on bottom duration and swimming behaviour according to diving depth, simple linear mixed-effects models including the variable considered and the depth were fitted for every 50 m depth class, from 50 to 1050 m. The effects of PCA and body density were assessed by the associated estimate and confidence interval (see Table S4), which were represented on all figures by ribbon graphs.

Finally, we investigated post-dive intervals in relation to the effort expended by SESs in the previous dive, in terms of time, total swimming effort and patch quality explored. Post-dive surface intervals were found to be directly related to the number of breaths taken by SES (Génin *et al.* 2015). All models were evaluated for surface intervals ranging between upper and lower fences ($Q3 + 1{\cdot}5IQR$ and $Q1 - 1{\cdot}5IQR$) where $Q1$ is the lower 25% quantile, $Q3$ is the upper 25% quantile and $IQR = Q3–Q1$, to remove outliers. Less than 3·4% ($n = 782$) of the surface interval data ($n = 23196$) were excluded from the analyses at the dive scale. We focused on recovery periods likely to be related directly to the previous dive. Extended surface intervals may represent other surface behaviours, such as socializing or extended recovery periods at a multi-dive scale.

Results

OVERALL DIVING BEHAVIOUR

A total of 23 196 dives were recorded from the six post-breeding females SESs: 2·1% were drift dives; the other 97·9% were processed to extract the number of PCA, dive angles and swimming effort. Mean dive duration was 20·7 ± 4·8 min, and the maximum dive duration was 56·0 min (Table 2). The overall mean dive depth was 542 ± 226 m reaching up to 1318 m. PCA were detected in 89·0% of non-drift dives. Within those dives, 14·8% of PCA occurred during the descent phase, 12·6% during the ascent and 72·6% during the bottom phase (Table 2).

BASIC MODELS

Although three different analyses were considered, that is situations considering all dives, dives with PCA and dives without, the global model, that is including all variables, was the most parsimonious in each situation (wAIC = 0·94, wAIC = 0·99 and wAIC = 0·62 respectively; see Supporting Information, Table S1). We found a positive relationship between bottom time and dive duration, dive angles and swimming effort. Conversely, we found a negative relationship between bottom time and depth, swimming effort during descent phase and animal's body density (Table 3).

BOTTOM TIME VS. DEPTH RELATED TO PREY AVAILABILITY AND BODY DENSITY

The quadratic depth term emerged as a significant parameter in dives with and without PCA (P-value = 0·004 and P-value < 0·001, respectively; Table 4). However, even if the negative parameter tended to be in agreement with Houston & Carbone (1992) when considering all dives together, this variable was not significant (P-value = 0·302). In PCA dive, bottom time did not change with diving depth up to 550 m and decreased with greater diving depth. In non-PCA, bottom time increased with diving depth up to 550 m and then decreased with increasing diving depth (Fig. 1). For both dives with and without PCA, we therefore observed a break in bottom time, followed by a decrease around 550 m depth (Fig. 1).

Bottom time was significantly shorter when PCA were present (Table 4) compared to dives without PCA in the model that considered all dives. However, when considering diving depth, SESs exhibited longer bottom durations in the presence of PCA until 350 m (Fig. 1). Between

Table 2. Main dive characteristics obtained for the six post-breeding females SESs, drift dives excluded. Mean values are given with ± SD

Seal ID	10A5015	10A5017	10A5019	10A5022	78524	78525
n Dives	4425	3768	3707	3727	3361	4118
Dive time (s)	1269·16 ± 307·76	1070·61 ± 198·45	1157·36 ± 281·87	1190·12 ± 212·46	1376·75 ± 286·89	1350·54 ± 271·27
Max dive time (s)	3027	3004	2968	3114	2801	3362
Bottom time (s)	758·35 ± 243·52	458·75 ± 216·37	571·55 ± 239·39	502·10 ± 270·14	573·78 ± 346·98	792·19 ± 329·49
Descent swimming effort ($m\ s^{-3}$)	0·25 ± 0·09	0·33 ± 0·09	0·25 ± 0·14	0·23 ± 0·10	0·20 ± 0·14	0·20 ± 0·12
Bottom swimming effort ($m\ s^{-3}$)	0·55 ± 0·14	0·85 ± 0·23	0·73 ± 0·21	0·70 ± 0·20	0·69 ± 0·23	0·53 ± 0·16
Ascent swimming effort ($m\ s^{-3}$)	0·78 ± 0·17	1·52 ± 0·21	1·16 ± 0·20	1·32 ± 0·27	1·35 ± 0·20	0·89 ± 0·15
Descent angle (°)	−42·72 ± 11·23	−51·78 ± 11·39	−54·70 ± 12·71	−43·92 ± 10·50	−43·88 ± 9·62	−34·39 ± 9·51
Ascent angle (°)	52·62 ± 14·64	71·54 ± 7·08	69·01 ± 9·06	63·37 ± 11·20	46·52 ± 14·58	53·40 ± 13·93
Dive depth (m)	469 ± 230	563 ± 186	532 ± 215	583 ± 231	643 ± 221	508 ± 234
Max diving depth (m)	1318	1271	1183	1300	1188	1260
n PCA in descent phase	0·79 ± 1·54	1·76 ± 1·95	0·91 ± 1·47	2·28 ± 2·65	0·88 ± 1·47	1·31 ± 2·38
n PCA in bottom phase	8·88 ± 7·33	5·66 ± 4·65	6·62 ± 5·22	8·10 ± 7·98	4·43 ± 5·12	4·53 ± 6·05
n PCA in ascent phase	1·08 ± 1·78	1·29 ± 1·67	0·95 ± 1·39	1·66 ± 1·97	0·91 ± 1·55	1·05 ± 1·86
Surface time (s)	129·39 ± 129·52	143·26 ± 73·26	128·63 ± 72·17	138·85 ± 89·41	172·55 ± 159·48	143·43 ± 51·51

350 and 750 m dives with PCA had a shorter bottom duration compared to dives without. Beyond this depth, the difference is more tenuous, that is PCA estimate closer to 0, but seals spent more time at the bottom in PCA dives (Fig. 1). When only dives with PCA were taken into account, bottom duration was found to be negatively correlated (P-value < 0·001) to PCA occurring in the transit phases but positively (P-value < 0·001) to those occurring at the bottom of the dive (Table 4). The latter pattern is significant for depths ranging between 250 and 950 m (Fig. 2). Outside this depth range, the number of PCA does not significantly influence the time spent at the bottom.

All seals remained negatively buoyant during the time of this study, with seal density ranging from 1036 to 1059 $kg\ m^{-3}$. The negative relationship found in basic models between bottom duration and body density occurred at almost all depth ranges (Fig. 3). Apart from 50 to 250 m and between 550 and 600 m, the closer to neutral buoyancy the SES was, the longer the dive bottom duration was.

SWIMMING EFFORT VS. BODY DENSITY

The total swimming effort increased almost linearly with depth (Fig. 4). However, a shift was observed at 300 m according to seal density. At shallower depth, body density does not influence significantly the total swimming effort. At greater diving depth, seals closer to neutral buoyancy exhibit a smaller swimming effort compared to denser ones (Fig. 4).

The distribution of bottom swimming effort according to depth ranges showed clear differences between dives with and without PCA (Fig. 5; Table 5). Generally, swimming effort at the bottom of the dive increased when PCA were present. However, from 150 m in the absence of PCA, seals clearly decreased their swimming effort at the bottom of their dive. We also found a positive relationship of the bottom swimming effort with maximum depth and body density, and a negative relationship with the bottom time (Table 5).

The model that considers only dives with PCA provides support for an increase of bottom swimming effort with the number of PCA, mediated by seal density (Table 5). In these dives, the seals swimming effort in the bottom phase was also found to increase with their body density.

A shift of the ratio of the total swimming effort at the bottom to the total swimming effort during transit phases, that is descent and ascent phases, is observed for diving depth close to 550 m (see Fig. S1). At this depth, the total bottom swimming effort becomes greater than the total transiting swimming effort. This ratio is also depending on the animal's body density (Table 6), which means the depth limit from which this ratio drops below 1, that is total transiting swimming effort > total bottom swimming effort, is reached sooner for denser (550 m for a seal den-

Table 3. Relationships between bottom time (bottomTime) and its predictors from best model chosen with parsimony (see Table S1) in each situation and associated *P*-value. Co-variables were dive duration (diveTime), maximum depth (maxDepth), ascent and descent angles (ascentAngle, descentAngle), ascent and descent swimming effort (ascentEffort, descentEffort) and body density (bodyDensity)

		All dives (N = 22 700)		Dives with captures (N = 18 770)		Dives without captures (N = 3930)	
Models	Parameters	Estimate	*P*-value	Estimate	*P*-value	Estimate	*P*-value
bottomTime ~	diveTime	266·83 ± 0·91	<0·01	262·08 ± 0·95	<0·01	278·34 ± 2·14	<0·01
	maxDepth	−275·11 ± 0·95	<0·01	−273·84 ± 0·95	<0·01	−288·99 ± 4·48	<0·01
	descentAngle	−24·25 ± 0·70	<0·01	−24·50 ± 0·80	<0·01	−31·15 ± 2·08	<0·01
	ascentAngle	25·48 ± 0·74	<0·01	22·15 ± 0·76	<0·01	49·14 ± 2·93	<0·01
	descentEffort	−5·55 ± 0·64	<0·01	−5·57 ± 0·66	<0·01	−1·69 ± 2·79	0·55
	ascentEffort	15·81 ± 0·81	<0·01	13·91 ± 0·84	<0·01	23·95 ± 2·73	<0·01
	bodyDensity	−3·52 ± 1·10	<0·01	−3·15 ± 1·06	<0·01	−1·42 ± 4·67	0·76

Table 4. Results from ANOVAs between basic models and basic models with a quadratic term of maximum depth ($maxDepth^2$), the number of PCA (PCA count) or the presence of PCA ($PCA_{presence}$) added. For each models, the Akaike's information criterion (AIC) and the Bayesian information criterion (BIC) were calculated. For each co-variable added, the value and the standard deviation associated were calculated (Estimate) as well as the log-likelihood ratio (L.ratio) and associated *P*-value for each ANOVAs performed

Models	Parameters	AIC	BIC	Estimate	L.ratio	*P*-value
bottomTime ~ (All dives)	Basic model	258515·7	258603·8			
	Term added:					
	$maxDepth^2$	258516·7	258612·7	−0·128 ± 0·67	1·07	0·302
	$PCA_{presence}$	258489·2	258585·3	−11·55 ± 2·31	28·49	<0·001
bottomTime ~ (Dives with PCA)	Basic model	229518·5	229605·4			
	Term added:					
	$maxDepth^2$	229512·1	29606·9	1·85 ± 0·68	8·41	0·004
	n PCA in bottom phase	229486·5	229581·3	4·33 ± 0·75	34·03	<0·001
	n PCA in transit phase	229503·7	229598·5	−2·79 ± 0·71	16·77	<0·001
bottomTime ~ (Dives without PCA)	Basic model	27693·1	27755·8			
	Term added:					
	$maxDepth^2$	27683·9	27752·4	−7·46 ± 2·75	11·17	<0·001

sity ranging between 1036 and 1045 kg m^{-3}, see Fig. S1) than lighter animals (600 m for a seal density ranging between 1051 and 1059 kg m^{-3}, see Fig. S1).

SURFACE TIME VS. EFFORT MADE

The selected model that surface intervals were best explained and positively related to the total swimming effort and dive duration (Table 7; wAIC = 0·73, see Table S3). Adding PCA did not improve the model (wAIC = 0·27, see Table S3).

Discussion

Although neither the exact quantity of prey ingested, nor their quality can be assessed, the accelerometer provides a quantitative index of the number of PCA. It allows us to investigate the changes in foraging behaviour of SES females in relation to their dive patterns. This method provides an estimate of where, when and how often foraging events occurred within a dive in these free-ranging marine predators. An increasing body of evidence suggests that diving predators remain within their aerobic dive limit while diving (Costa, Gales & Goebel 2001; Costa *et al.* 2004) as the incurred costs of anaerobic dives are too high to forage efficiently (Kooyman *et al.* 1980, 1983). Only aerobic metabolism allows frequent, repetitive dives as elephant seals do. The current study suggests that to remain within their aerobic limit, SESs optimize their diving behaviour and duration according to a number of parameters including foraging success and buoyancy.

BOTTOM TIME AND DEPTH

Regardless of the prey encounter events, bottom time was found to decrease linearly with depth. However, this relationship was not significant according to the quadratic polynomial relationship as predicted by Houston & Carbone's (1992), which assumes that the foraging time correspond to the bottom duration. When distinguishing dives with and without PCA, the bottom duration was found to vary according to a quadratic polynomial for non-PCA (unsuccessful) dives. Bottom time first increased then

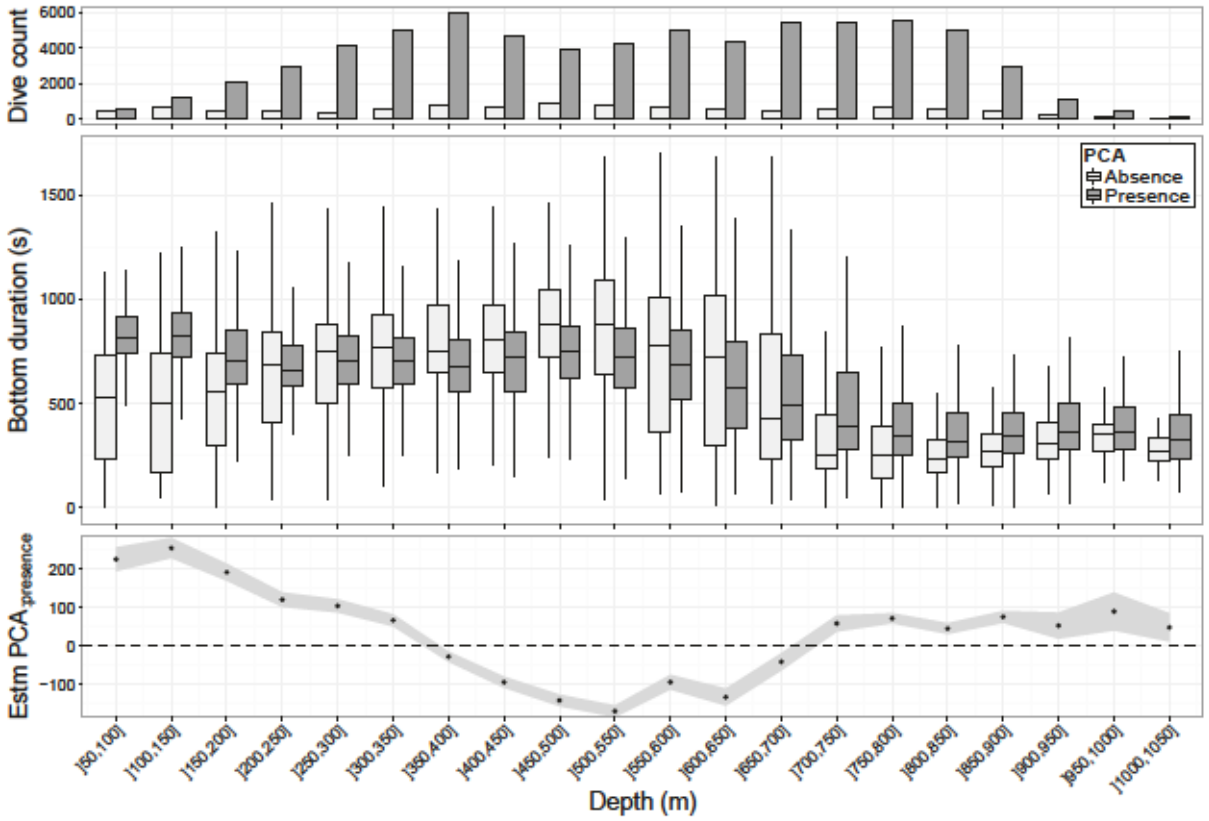

Fig. 1. Bottom duration related to depth and prey availability. The histogram represents the number of dives per boxplots. Between 350 and 700 m, bottom duration is less important when animals catch prey (estimate $PCA_{:presence} < 0$, see Table S4), whereas it is the opposite deeper (estimate $PCA_{:presence} > 0$, see Table S4).

decreased with depth in non-PCA dives. In successful dives, model outcome suggests the opposite: a decrease then an increase (Table 4). This result must be taken with caution due the weakness of the quadratic depth term (estimate = 1·85 ± 0·68 m^2; *P*-value = 0·004). Bottom time remained fairly constant until the seals reached 550 m, whereupon bottom time was negatively related to increasing diving depth (Fig. 1). The patterns found for PCA dives were therefore consistent with studies examining behaviour of diving birds (Carbone & Houston 1994; Cook *et al*. 2008), where a nonlinear relationship of bottom time with depth are also found. At shallow depths, birds maintain low oxygen reserves in order to experience higher rates of oxygen intake. As dive depth increases, birds increase the size of their oxygen stores to allow more foraging time. When approaching the maximum dive duration, they decrease their foraging time at the bottom to compensate for increasing travel time with increasing diving depth (Carbone & Houston 1994). Our results are consistent with such a trade-off between foraging time and travel time. Beyond 550 m dive depth, depending on the seal's body density, the overall transiting swimming effort and therefore the cost to access the prey were found to exceed the swimming effort spent by the seal at the bottom of the dive (Fig. S1). This depth corresponds to the point at which bottom time starts decreasing with increasing dive depth (Fig. 1).

BOTTOM TIME AND PCA

Our results indicate that SES has shorter bottom times in dives when PCA occurred compared to non-PCA dives. This is true between 350 and 700 m, but not for shallower depths where bottom time was longer in the presence of PCA. For dives deeper than 700 m, there was almost no difference in bottom time between dives with and without PCA. Therefore, at shallow and greater depths our results were consistent with Thompson & Fedak's predictions (2001). They suggest that there is a benefit to ending dives earlier when no PCA occur at shallow depths. Regardless of foraging success, seals should also maximize the bottom time for very deep dives to compensate for transit time between the surface and the dive bottom. Other empirical studies agree with these results, such as Sparling *et al.* (2007) on grey seals (*Halichoerus grypus*) and Mori *et al*. (2002) on Brünnich's guillemots, (*Uria lomvia*).

However, between 350 and 700 m, our results differ from predictions. SESs were found to perform longer bottom durations when no PCA occurred. They did it by

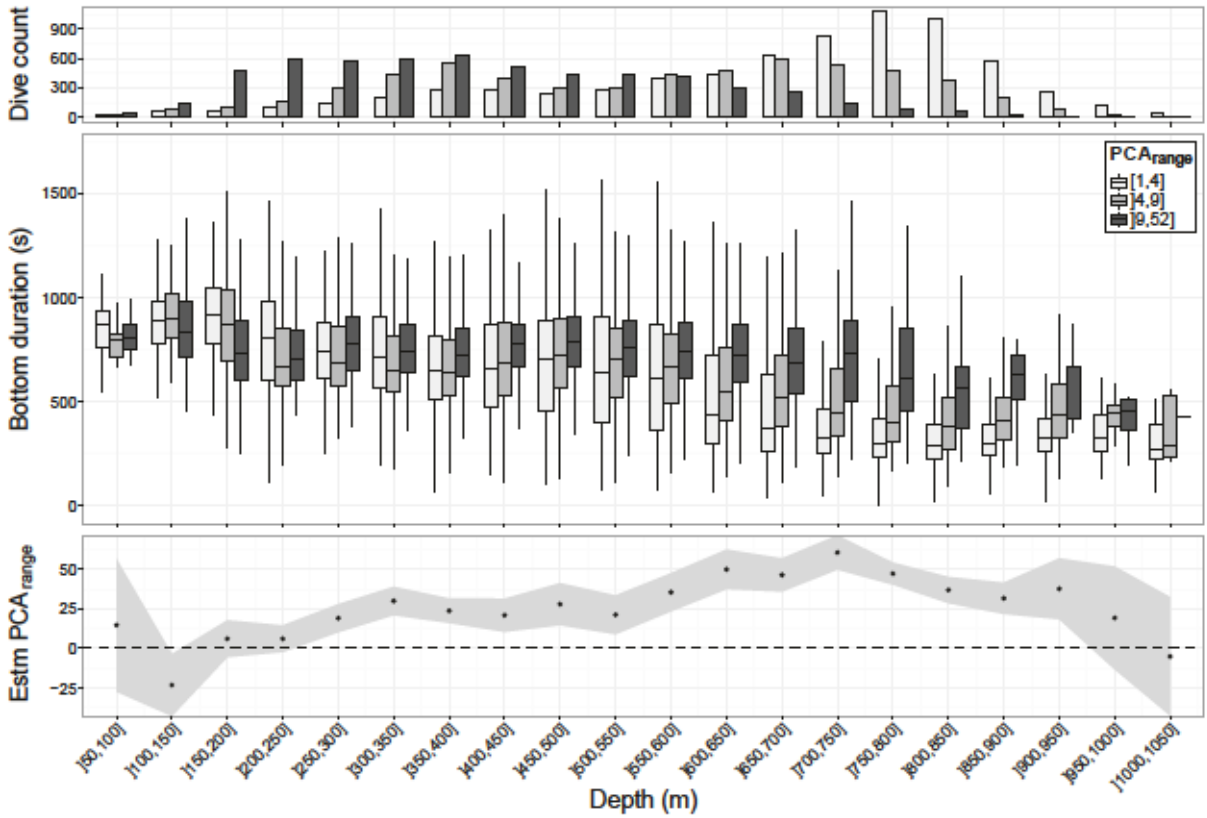

Fig. 2. Bottom duration related to depth and number of PCA at the bottom phase. The histogram represents the number of dives per boxplots. Below 250 m depth, bottom duration increases significantly with the number of PCA (estimate $PCA_{Range} > 0$, see Table S4).

reducing their swimming effort during the bottom phase. It is unclear at this stage whether the reduction in the swimming effort is either related to a searching strategy where the seal ceases to actively swim to investigate their environment using visual or auditory cues, or to a general slow descending behaviour (mainly gliding) as long as they do not encounter prey. Preliminary investigation suggests that negatively buoyant post-breeding seals rely on their negative buoyancy to glide down at a low negative pitch while searching for their prey during the bottom phase of the dive. On average, the end of the bottom phase was 61 ± 109 m deeper than the beginning of the bottom phase in non-PCA dives, while no trends were found in PCA dives. The reduction in energy and oxygen consumption could then allow them to stay at the bottom for longer periods (Boyd 1997; Cornick & Horning 2003). It also provides support for the inclusion of the energetic approach to study optimal foraging in free-ranging animals. This point should be investigated further: if our interpretation is correct, we expect to observe the opposite trend in positively buoyant seals with a decreasing depth between the beginning and the end of the bottom phase in non-PCA dives.

When considering dives where at least one PCA occurred, the more PCA performed by seals at any given bottom depth, the longer the bottom time was. This result is consistent with what Cornick & Horning (2003) found in captive Steller sea lion, *Eumetopias jubatus*. This finding provides further support for the assumption that bottom time is positively related to patch quality. When SESs perform at least one PCA during the bottom phase, bottom time increases significantly with PCA, which is also consistent with Thompson & Fedak's prediction (2001). However, when only dive data are available, it is not possible to distinguish between non-PCA and PCA dives. Consequently, using the duration of the bottom foraging phase according to diving depth as a proxy of foraging success (Boyd, Reid & Bevan 1995; Fedak, Lovell & Grant 2001; Watwood *et al.* 2006) can be seriously misleading in SES. Non-PCA dives will be detected as the most successful dives over a broad range of diving depth. While positive residuals at shallow depths (up to 350 m) are likely to be indicative of higher foraging success, higher bottom duration residuals than expected at depths ranging from 300 to 700 m are likely to be indicative of a poor foraging success. This latter pattern is consistent with what Thums *et al.* (2013) found on adult female southern elephant seals at Macquarie Island.

When PCA occurred in descent and ascent phases, SESs significantly reduced the time they spent at the bottom with increasing numbers of PCA during these transit phases. This suggests that energy expenditure increases

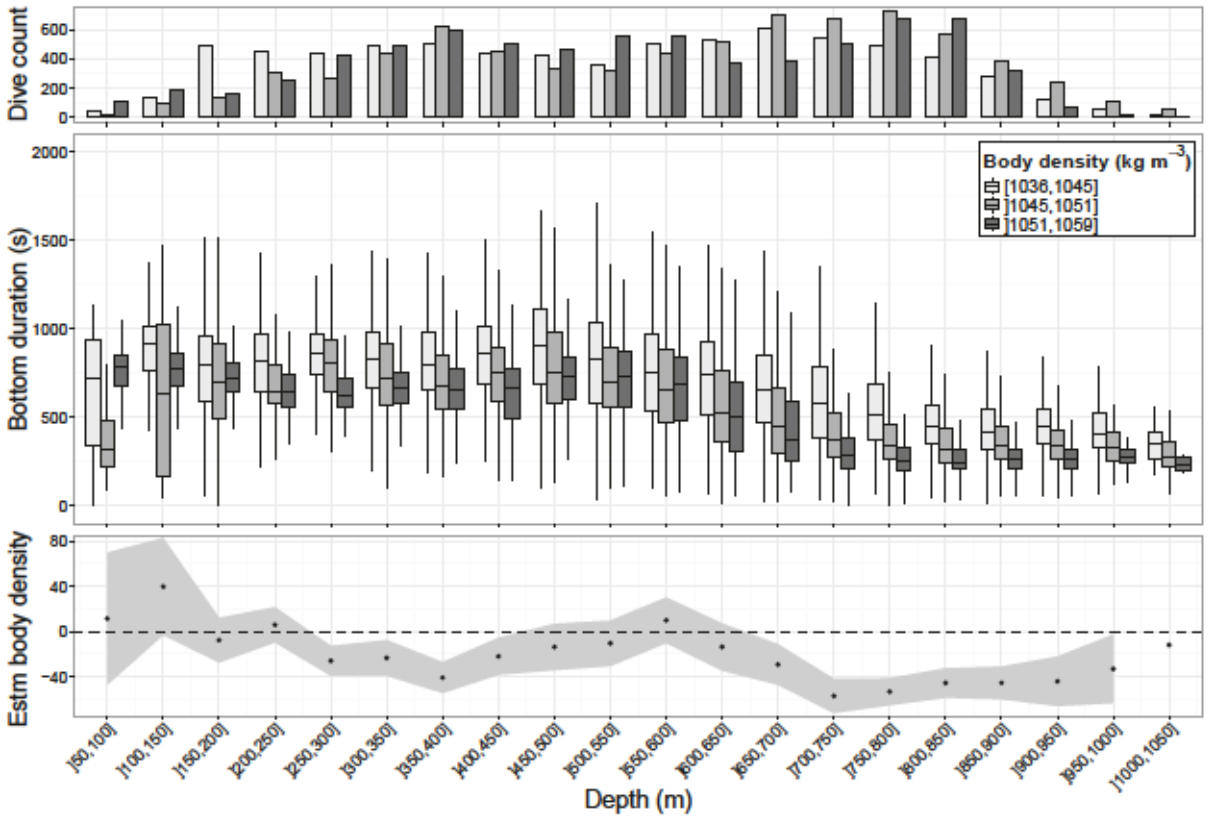

Fig. 3. Bottom duration related to depth and animal's body density. The histogram represents the number of dives per boxplots. Except until 250 m depth and between 450 and 650 m, the fatter a SES, the more it can spend time at the bottom (estimate Body Density < 0, see Table S4).

when the seal is catching prey. This is expected to have direct consequences on the amount of time SESs are able to allocate to stay at the bottom of their dive (McConnell, Chambers & Fedak 1992).

BOTTOM TIME, BODY DENSITY AND SWIMMING EFFORT

The animal's body density, or buoyancy, was an important parameter in controlling the duration of the dive bottom phase. The three basic models (Table 3) provide support for a negative relationship between bottom time and body density, that is the more negatively buoyant the seals, the shorter the bottom duration. This finding is consistent with results found by Beck, Bowen & Iverson (2000) that showed denser grey seals displayed shorter bottom duration compared to fatter seals. Our results are also in accordance with several other studies which show buoyancy as an important variable of diving behaviour (Webb *et al.* 1998; Beck, Bowen & Iverson 2000; Miller *et al.* 2004; Adachi *et al.* 2014; Richard *et al.* 2014) and that the round trip cost of transport is lowest at neutral buoyancy (Miller *et al.* 2012; Sato *et al.* 2013). Negatively buoyant animals are assisted during descent phase by their higher density, but must swim harder during the ascent (Richard *et al.* 2014). Williams *et al.* (2000) showed that several marine mammals used their buoyancy to adopt this energy-conserving strategy.

Seals are subjected to body compression during the whole dive, but particularly at the beginning which may explain inversions of slope for the first depth ranges (Fig. 4). Complete lung collapse is supposed to occur at these depths (Kooyman & Sinnett 1982; Falke *et al.* 1985; McDonald & Ponganis 2012). When their lungs are not completely collapsed, seals which are negatively buoyant but close to neutral buoyancy remain positively buoyant and should provide an overall greater total swimming effort to remain at those depths, compared to more negatively buoyant seals. The opposite relationship is found at greater diving depths, where buoyancy is almost exclusively related to body composition, that is lipid proportion: seals tending to provide higher total swimming effort when they are further from neutral buoyancy.

We found a positive relationship between the swimming effort at the bottom and the number of PCA occurring during the bottom of a dive. In other words, SESs are swimming more actively when catching prey. Seals closer to neutral buoyancy spend more time at the bottom of their dive compared to denser animals which were

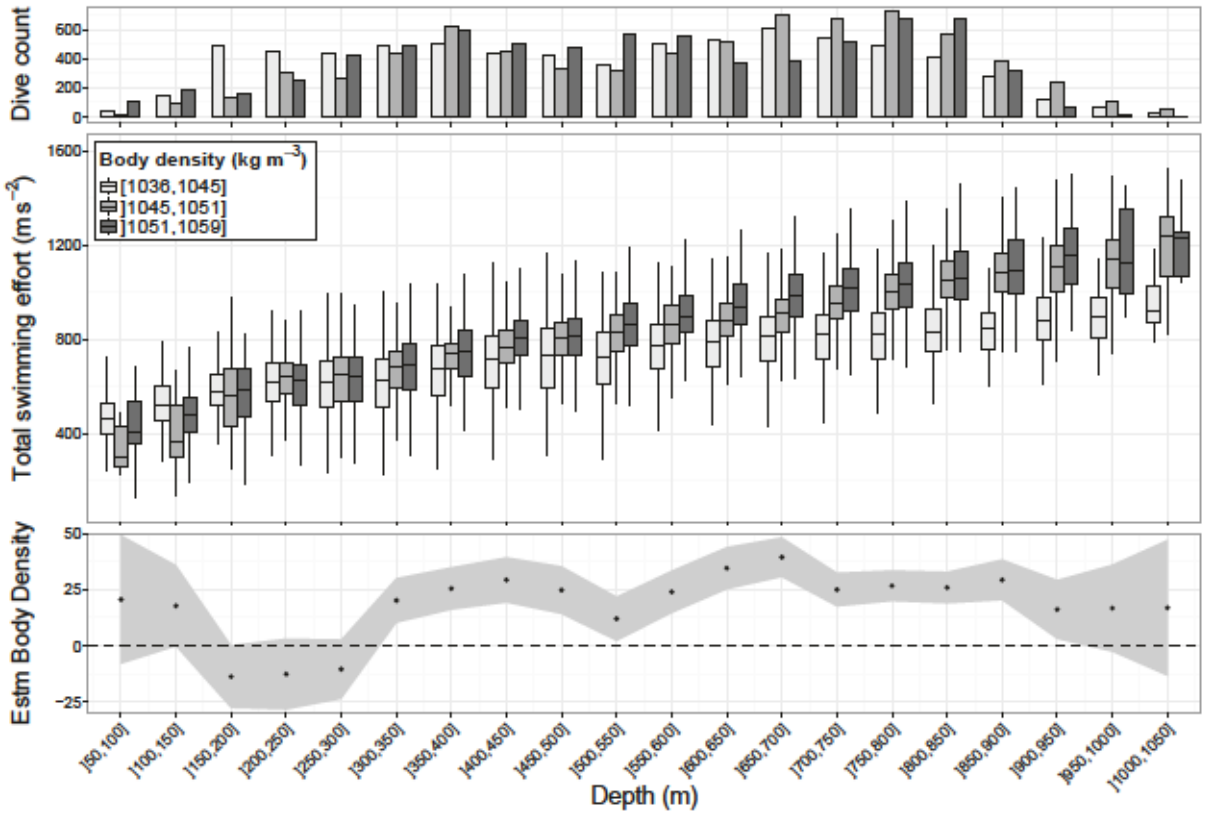

Fig. 4. Total swimming effort related to depth and animal's body density. The histogram represents the number of dives per boxplots. A shift is observed around 300 metres depth; denser animals must provide a higher effort below that depth (estimate Body Density > 0, see Table S4).

Table 5. Relationship for the top-ranked model of the bottom swimming effort (bottomEffort) with bottom time (bottomTime), maximum depth (maxDepth), body density (bodyDensity), presence of PCA (PCA:$_{presence}$) or number of capture attempts (*n* PCA), depending on the situation (all dives or dives with PCA), and associated *P*-value

Models	Parameters	Estimate	*P*-value
bottomEffort	bottomTime	−0·11 ± 0·001	<0·001
(All dives)	maxDepth	0·05 ± 0·001	<0·001
	bodyDensity	0·02 ± 0·002	<0·001
	PCA$_{presence}$	0·05 ± 0·004	<0·001
bottomEffort	bottomTime	−0·12 ± 0·001	<0·001
(Dives with PCA)	maxDepth	0·02 ± 0·001	<0·001
	bodyDensity	0·02 ± 0·001	<0·001
	n PCA	0·05 ± 0·001	<0·001

observed to make a greater swimming effort during the bottom phase to maintain themselves at their preferred foraging depth.

SURFACE TIME AND DIVING BEHAVIOURS

Surface time is expected to vary with increasing dive duration and foraging effort in diving predators. Kramer (1988) claimed that post-dive interval should increase with depth due to the shape of the oxygen uptake function. We found that the time spent at surface replenishing the oxygen stores was positively related to dive duration and total swimming effort exerted during the previous dive. Le Boeuf *et al.* (2000) also found a strong effect of dive duration on surface time, but this was highly variable and depended on the seal studied. That variability observed could be due to the variation of the total swimming effort measured in the current study. Because dive duration and total swimming effort are both positively related to diving depth, the maximum depth reached was also found to positively influence the duration of the surface interval. Despite the fact that the swimming effort at the bottom of the dive was positively related to the number of PCA, the number of PCA itself was not found to be a significant parameter in this model. Similarly, the swimming effort is likely to be related to the seal's buoyancy and was found to contribute significantly to the bottom duration in our study.

Conclusions

This study highlights the importance of using a correct metrics of foraging success to accurately reflect true for-

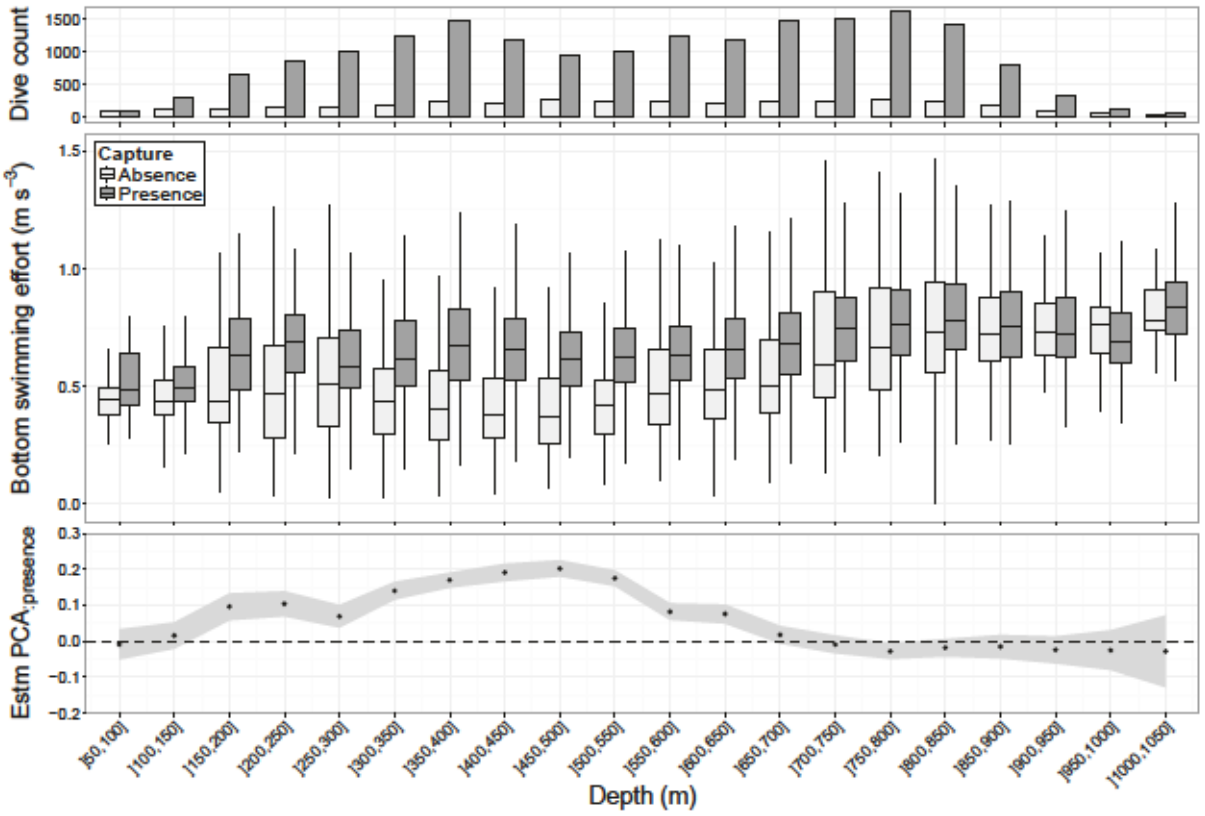

Fig. 5. Bottom swimming effort related to depth and prey availability. The histogram represents the number of dives per boxplots. Below 150 m depth, bottom swimming effort is more important for dives with prey catch attempts (estimate $PCA_{presence} > 0$, see Table S4). This difference disappears beyond 550 m depth.

Table 6. Relationship for the ratio of total bottom swimming effort to total transit swimming effort $\left(\frac{TOTbottomEffort}{TOTtransitEffort}\right)$ with depth (maxDepth) and body density (bodyDensity), and associated *P*-value

Model	Parameters	Estimate	*P*-value
$\frac{TOTbottomEffort}{TOTtransitEffort} \sim$	maxDepth	−0·09 ± 0·01	<0·001
	bodyDensity	−0·07 ± 0·02	0·015

Table 7. Relationship for the top-ranked model of the surface time (surfaceTime) with total swimming effort (diveEffort), dive time (diveTime) of the previous dive, and associated *P*-value

Model	Parameters	Estimate	*P*-value
surfaceTime ~	diveEffort	3·68 ± 0·08	<0·001
	diveTime	2·90 ± 0·13	<0·001

aging success. This is essential to investigate further the relationship between time spent at the bottom and prey acquisition, which is assumed by most of the optimal foraging models developed (Kramer 1988; Houston & Carbone 1992; Thompson, Hiby & Fedak 1993; Carbone & Houston 1996). Finally, this study demonstrates the usefulness of accelerometers to understand diving behaviour. Data from these highlight for the first time the combined effects of buoyancy, prey encounters and diving depth, on variations in swimming effort in a free-ranging marine predator, and consequently, in the control at very fine scale of the diving behaviours in a marine mammal.

Acknowledgements

The authors would like to thank all the persons involved in the tagging and controls of elephant seals on Kerguelen Island and the French Polar Institute (Institut Paul Emile Victor, IPEV), for providing logistic and financial support. This work was carried out in the framework of the ANR Blanc MYCTO-3D-MAP, ANR VMC IPSOS-SEAL programs and CNES-TOSCA program ('Éléphants de mer océanographes'). This study is part of a IPEV program no. 109, (P.I. H. Weimerskirch) and the observatory Mammifères Explorateurs du Milieu Océanique, (MEMO SOERE CTD 02). The authors also thank the Total Foundation for financial support as well as Malcolm O'Toole and Tiphaine Jeanniard du Dot for correcting the English. They would particularly like to thank Patrick Duncan for his writing assistance and his informed proofreading. J.J. was supported by «Direction Générale de l'Armement».

Data accessibility

Data deposited in the Figshare repository: http://dx.doi.org/10.6084/m9.figshare.1452900 (Jouma'a *et al.* 2015).

References

Adachi, T., Maresh, J.L., Robinson, P.W., Peterson, S.H., Costa, D.P., Naito, Y. *et al.* (2014) The foraging benefits of being fat in a highly migratory marine mammal. *Proceedings of the Royal Society of London B: Biological Sciences*, **281**, 20142120.

Bailleul, F., Charrassin, J.-B., Monestiez, P., Roquet, F., Biuw, M. & Guinet, C. (2007) Successful foraging zones of southern elephant seals from the Kerguelen Islands in relation to oceanographic conditions. *Philosophical transactions of the Royal Society of London. Series B, Biological sciences*, **362**, 2169–2181.

Barton, K. (2013) MuMIn: Multi-model inference. R package version 1.9.13.

Beck, C.A., Bowen, W.D. & Iverson, S.J. (2000) Seasonal changes in buoyancy and diving behaviour of adult grey seals. *The Journal of Experimental Biology*, **203**, 2323–2330.

Biuw, M., McConnell, B., Bradshaw, C.J.A., Burton, H. & Fedak, M. (2003) Blubber and buoyancy: monitoring the body condition of free-ranging seals using simple dive characteristics. *The Journal of Experimental Biology*, **206**, 3405–3423.

Boyd, I.L. (1997) The behavioural and physiological ecology of diving. *Trends in Ecology & Evolution*, **12**, 213–217.

Boyd, I.L., Reid, K. & Bevan, R.M. (1995) Swimming speed and allocation of time during the dive cycle in Antarctic fur seals. *Animal Behaviour*, **50**, 769–784.

Butler, P.J. & Jones, D.R. (1997) Physiology of diving of birds and mammals. *Physiological Reviews*, **77**, 837–899.

Carbone, C. & Houston, A.I. (1994) Patterns in the diving behaviour of the pochard, *Aythya ferina*: a test of an optimality model. *Animal Behaviour*, **48**, 457–465.

Carbone, C. & Houston, A.I. (1996) The optimal allocation of time over the dive cycle: an approach based on aerobic and anaerobic respiration. *Animal Behaviour*, **51**, 1247–1255.

Cook, T.R., Lescroël, A., Tremblay, Y. & Bost, C.-A. (2008) To breathe or not to breathe? Optimal breathing, aerobic dive limit and oxygen stores in deep-diving blue-eyed shags. *Animal Behaviour*, **76**, 565–576.

Cornick, L.A. & Horning, M. (2003) A test of hypotheses based on optimal foraging considerations for a diving mammal using a novel experimental approach. *Canadian Journal of Zoology*, **81**, 1799–1807.

Costa, D.P., Gales, N.J. & Goebel, M.E. (2001) Aerobic dive limit: how often does it occur in nature? *Comparative Biochemistry and Physiology. Part A, Molecular & Integrative Physiology*, **129**, 771–783.

Costa, D., Kuhn, C., Weise, M., Shaffer, S. & Arnould, J. (2004) When does physiology limit the foraging behaviour of freely diving mammals?

Crocker, D.E., Le Boeuf, B.J. & Costa, D.P. (1997) Drift diving in female northern elephant seals: implications for food processing. *Canadian Journal of Zoology*, **75**, 27–39.

Dragon, A., BarHen, A., Monestiez, P. & Guinet, C. (2012) Horizontal and vertical movements as predictors of foraging success in a marine predator. *Marine Ecology Progress Series*, **447**, 243–257.

Falke, K.J., Hill, R.D., Qvist, J., Schneider, R.C., Guppy, M., Liggins, G.C. *et al.* (1985) Seal lungs collapse during free diving: evidence from arterial nitrogen tensions. *Science*, **229**, 556–558.

Fedak, M.A., Lovell, P. & Grant, S.M. (2001) Two approaches to compressing and interpreting time-depth information as collected by time-depth recorders and satellite-linked data recorders. *Marine Mammal Science*, **17**, 94–110.

Field, I.C., Bradshaw, C.J.A., McMahon, C.R., Harrington, J. & Burton, H.R. (2002) Effects of age, size and condition of elephant seals (*Mirounga leonina*) on their intravenous anaesthesia with tiletamine and zolazepam. *The Veterinary Record*, **151**, 235–240.

Fossette, S., Gleiss, A.C., Myers, A.E., Garner, S., Liebsch, N., Whitney, N.M. *et al.* (2010) Behaviour and buoyancy regulation in the deepest-diving reptile: the leatherback turtle. *The Journal of Experimental Biology*, **213**, 4074–4083.

Génin, A., Richard, G., Jouma'a, J., Picard, B., El Ksabi, N., Vacquié Garcia, J. *et al.* (2015) Characterization of postdive recovery using sound recordings and its relationship to dive duration, exertion and foraging effort of southern elephant seals (*Mirounga leonina*). *Marine Mammal Science*. doi: 10.1111/mms.12235

Guinet, C., Vacquié-Garcia, J., Picard, B., Bessigneul, G., Lebras, Y., Dragon, A.C. *et al.* (2014) Southern elephant seal foraging success in relation to temperature and light conditions: insight into prey distribution. *Marine Ecology Progress Series*, **499**, 285–301.

Heithaus, M.R. & Frid, A. (2003) Optimal diving under the risk of predation. *Journal of Theoretical Biology*, **223**, 79–92.

Houston, A.I. (2011) Assessing models of optimal diving. *Trends in Ecology & Evolution*, **26**, 292–297.

Houston, A.I. & Carbone, C. (1992) The optimal allocation of time during the diving cycle. *Behavioral Ecology*, **3**, 255–265.

Houston, A.I. & McNamara, J.M. (1985) The variability of behaviour and constrained optimization. *Journal of Theoretical Biology*, **112**, 265–273.

Insley, S., Robson, B., Yack, T., Ream, R. & Burgess, W. (2008) Acoustic determination of activity and flipper stroke rate in foraging northern fur seal females. *Endangered Species Research*, **3**, 147–155.

Jouma'a, J., Bras, Y.L., Richard, G., Vacquié-Garcia, J., Picard, B., Ksabi, N.E. *et al.* (2015) Data from: adjustment of diving behaviour with prey encounters and body condition in a deep diving predator: the Southern Elephant Seal. *Figshare*. doi: 10.6084/m9.figshare.1452900.

Kacelnik, A., Houston, A.I. & Schmid-Hempel, P. (1986) Central-place foraging in honey bees: the effect of travel time and nectar flow on crop filling. *Behavioral Ecology and Sociobiology*, **19**, 19–24.

Kooyman, G.L. & Ponganis, P.J. (1998) The physiological basis of diving to depth: birds and mammals. *Annual Review of Physiology*, **60**, 19–32.

Kooyman, G.L. & Sinnett, E.E. (1982) Pulmonary shunts in harbor seals and sea lions during simulated dives to depth. *Physiological Zoology*, **55**, 105–111.

Kooyman, G.L., Wahrenbrock, E.A., Castellini, M.A., Davis, R.W. & Sinnett, E.E. (1980) Aerobic and anaerobic metabolism during voluntary diving in Weddell seals: evidence of preferred pathways from blood chemsitry and behavior. *Journal of Comparative Physiology*, **138**, 335–346.

Kooyman, G.L., Castellini, M.A., Davis, R.W. & Maue, R.A. (1983) Aerobic diving limits of immature Weddell seals. *Journal of Comparative Physiology*, **151**, 171–174.

Kramer, D.L. (1988) The behavioral ecology of air breathing by aquatic animals. *Canadian Journal of Zoology*, **66**, 89–94.

Le Boeuf, B.J., Crocker, D.E., Grayson, J., Gedamke, J., Webb, P.M., Blackwell, S.B. *et al.* (2000) Respiration and heart rate at the surface between dives in northern elephant seals. *Journal of Experimental Biology*, **203**, 3265–3274.

Lesage, V., Hammill, M.O. & Kovacs, K.M. (1999) Functional classification of harbor seal (*Phoca vitulina*) dives using depth profiles, swimming velocity, and an index of foraging success. *Canadian Journal of Zoology*, **77**, 74–87.

Luque, S.P. (2007) Diving behaviour analysis in R. *R News*, **7**, 8–14.

McConnell, B.J., Chambers, C. & Fedak, M.A. (1992) Foraging ecology of southern elephant seals in relation to the bathymetry and productivity of the Southern Ocean. *Antarctic Science*, **4**, 393–398.

McDonald, B.I. & Ponganis, P.J. (2012) Lung collapse in the diving sea lion: hold the nitrogen and save the oxygen. *Biology Letters*, **8**, 1047–1049.

McMahon, C.R., Burton, H., McLean, S., Slip, D. & Bester, M. (2000) Field immobilisation of southern elephant seals with intravenous tiletamine and zolazepam. *The Veterinary Record*, **146**, 251–254.

Miller, P.J.O., Johnson, M.P., Tyack, P.L. & Terray, E.A. (2004) Swimming gaits, passive drag and buoyancy of diving sperm whales *Physeter macrocephalus*. *The Journal of Experimental Biology*, **207**, 1953–1967.

Miller, P.J.O., Biuw, M., Watanabe, Y.Y., Thompson, D. & Fedak, M.A. (2012) Sink fast and swim harder! Round-trip cost-of-transport for buoyant divers. *Journal of Experimental Biology*, **215**, 3622–3630.

Mitani, Y., Andrews, R.D., Sato, K., Kato, A., Naito, Y. & Costa, D.P. (2010) Three-dimensional resting behaviour of northern elephant seals: drifting like a falling leaf. *Biology Letters*, **6**, 163–166.

Mori, Y., Takahashi, A., Mehlum, F. & Watanuki, Y. (2002) An application of optimal diving models to diving behaviour of Brünnich's guillemots. *Animal Behaviour*, **64**, 739–745.

Naito, Y., Bornemann, H., Takahashi, A., McIntyre, T. & Plötz, J. (2010) Fine-scale feeding behavior of Weddell seals revealed by a mandible accelerometer. *Polar Science*, **4**, 309–316.

Naito, Y., Costa, D.P., Adachi, T., Robinson, P.W., Fowler, M. & Takahashi, A. (2013) Unravelling the mysteries of a mesopelagic diet: a large apex predator specializes on small prey. *Functional Ecology*, **27**, 710–717.

Okuyama, J., Kawabata, Y., Naito, Y., Arai, N. & Kobayashi, M. (2009) Monitoring beak movements with an acceleration datalogger: a useful

technique for assessing the feeding and breathing behaviors of sea turtles. *Endangered Species Research*, **10**, 39–45.
Pinheiro, J., Bates, D., DebRoy, S., Sarkar, D. & R Core team. (2013) Nlme: Linear and Nonlinear Mixed Effects Models.
Pyke, G.H. (1984) Optimal foraging theory: a critical review. *Annual Review of Ecology and Systematics*, **15**, 523–575.
R Development Core Team (2014) *R: A Language and Environment for Statistical Computing*. R Foundation for Statistical Computing, Vienna, Austria.
Richard, G., Vacquié-Garcia, J., Jouma'a, J., Picard, B., Génin, A., Arnould, J.P.Y. *et al*. (2014) Variation in body condition during the post-moult foraging trip of southern elephant seals and its consequences on diving behaviour. *The Journal of Experimental Biology*, **217**, 2609–2619.
Sato, K., Mitani, Y., Cameron, M.F., Siniff, D.B. & Naito, Y. (2003) Factors affecting stroking patterns and body angle in diving Weddell seals under natural conditions. *The Journal of Experimental Biology*, **206**, 1461–1470.
Sato, K., Aoki, K., Watanabe, Y.Y. & Miller, P.J.O. (2013) Neutral buoyancy is optimal to minimize the cost of transport in horizontally swimming seals. *Scientific Reports*, **3**, 2205.
Sparling, C.E., Georges, J.-Y., Gallon, S.L., Fedak, M. & Thompson, D. (2007) How long does a dive last? Foraging decisions by breath-hold divers in a patchy environment: a test of a simple model. *Animal Behaviour*, **74**, 207–218.
Suzuki, I., Naito, Y., Folkow, L.P., Miyazaki, N. & Blix, A.S. (2009) Validation of a device for accurate timing of feeding events in marine animals. *Polar Biology*, **32**, 667–671.
Thompson, D. & Fedak, M.A. (2001) How long should a dive last? A simple model of foraging decisions by breath-hold divers in a patchy environment. *Animal Behaviour*, **61**, 287–296.
Thompson, D., Hiby, A.R. & Fedak, M. (1993) How fast should I swim? Behavioural implications of diving physiology. *Symposium Zoology Society London*, **66**, 349–368.
Thums, M., Bradshaw, C.J.A., Sumner, M.D., Horsburgh, J.M. & Hindell, M.A. (2013) Depletion of deep marine food patches forces divers to give up early (ed G Hays). *Journal of Animal Ecology*, **82**, 72–83.
Tuck, K. (2007) Tilt sensing using linear accelerometers. Freescale Semiconductor, AN3461 Rev. 2.
Tucker, V.A. (1975) The energetic cost of moving about: walking and running are extremely inefficient forms of locomotion. Much greater efficiency is achieved by birds, fish—and bicyclists. *American Scientist*, **63**, 413–419.
Viviant, M., Trites, A.W., Rosen, D.A.S., Monestiez, P. & Guinet, C. (2010) Prey capture attempts can be detected in Steller sea lions and other marine predators using accelerometers. *Polar Biology*, **33**, 713–719.
Watwood, S.L., Miller, P.J.O., Johnson, M., Madsen, P.T. & Tyack, P.L. (2006) Deep-diving foraging behaviour of sperm whales (*Physeter macrocephalus*). *Journal of Animal Ecology*, **75**, 814–825.
Webb, P.M., Crocker, D.E., Blackwell, S.B., Costa, D.P. & Boeuf, B.J. (1998) Effects of buoyancy on the diving behavior of northern elephant seals. *The Journal of Experimental Biology*, **201**, 2349–2358.
Williams, T.M., Davis, R.W., Fuiman, L.A., Francis, J., Le, B.J., Boeuf Horning, M. *et al*. (2000) Sink or swim: strategies for cost-efficient diving by marine mammals. *Science*, **288**, 133–136.
Wilson, R., Steinfurth, A., Ropert-Coudert, Y., Kato, A. & Kurita, M. (2002) Lip-reading in remote subjects: an attempt to quantify and separate ingestion, breathing and vocalisation in free-living animals using penguins as a model. *Marine Biology*, **140**, 17–27.
Ydenberg, R.C. & Clark, C.W. (1989) Aerobiosis and anaerobiosis during diving by western grebes: an optimal foraging approach. *Journal of Theoretical Biology*, **139**, 437–447.

Received 19 August 2014; accepted 2 July 2015
Handling Editor: Daniel Costa

Supporting Information

Additional Supporting information may be found in the online version of this article:

Table S1. Top five ranked linear mixed-effects models by AIC of bottom time as the response variable explained by dive duration, ascent and descent angles, ascent and descent effort, body density and maximum depth.
Table S2. Top five ranked linear mixed-effects models by AIC of bottom swimming effort as the response variable explained by bottom time, body density and maximum depth.
Table S3. Top five ranked linear mixed-effects models by AIC of surface time as the response variable explained by total swimming effort provided during the last dive and the prey capture attempts availability.
Table S4. Estimates and confidence intervals for prey availability, number of prey and the body density in each linear mixed effects models associated to box plot.
Fig. S1. Evolution of the relation between total bottom swimming effort and total transit swimming effort according to depth and animal's body density.

ANNEXE

G

Article 6 : Jouma'a *et al.*, en révision

6. Jouma'a Joffrey, Le Bras Yves, Picard Baptiste, Guinet Christophe. (2016). Three-dimensional assessment of hunting strategies in a deep diving predator. *Marine Ecology Progress Series*. **En révision**

Three-dimensional assessment of hunting strategies in a deep diving predator

Joffrey Jouma'a*, Yves Le Bras, Baptiste Picard & Christophe Guinet

*corresponding author

Joffrey Jouma'a (joffreyjoumaa@icloud.com, orcid.org/0000-0002-2862-0899) Centre d'Etudes Biologiques de Chizé (CNRS - UMR 7372), University of La Rochelle, France

Yves Le Bras, Centre d'Etudes Biologiques de Chizé (CNRS - UMR 7372), University of La Rochelle, France

Baptiste Picard, Centre d'Etudes Biologiques de Chizé (CNRS - UMR 7372), University of La Rochelle, France

Christophe Guinet, Centre d'Etudes Biologiques de Chizé (CNRS - UMR 7372), University of La Rochelle, France

Running title: Hunting strategies in southern elephant seals

Abstract

Despite their crucial role in the understanding of foraging behaviors, only few studies have examined the animals' fine-scale movements in response to the spatial distribution of prey. This is all the more true when studying marine predators where both vertical and horizontal dimensions must be take into account. In the present study, thanks to three-dimensional reconstruction of underwater animal paths, we investigated the relationship between area restricted search (ARSs) and foraging behaviors in terms of diving behaviors and hunting strategies associated with each prey catch in the Southern Elephant Seal. We equipped 6 post-breeding females on Kerguelen Islands with an Acousonde™ recording simultaneously sounds, pressure, acceleration and magnetic field-strength in three dimensions (n = 879 dives). Using the spherical first passage time analysis, we identified ARSs in 46.4% of the dives. They represented 37.8% of the bottom time, but due to a higher prey capture rate, 67.4% of prey catches took place in ARS. These areas, occurring within a sphere of 45.3±28.9 m radius, were characterized by an increase in energy expenditure and a strong variability in the roll and heading compared to non ARS region. From the unsupervised classification performed on acceleration properties, we demonstrated that seals used three hunting strategies to capture prey while foraging inside ARS. We found that 32.8% of prey catch matched a passive-gliding approach from the above. The other two modes corresponded to an actively swimming approach associated with an increase of heading and rolling movements for the first one (56.6% of captures), and to a much larger swimming effort for the second one (10.6% of captures). These data revealed a strong link between seals' fine-scale movements and foraging activity, suggesting that seals fed mainly on patchily distributed resources, with different hunting strategies that may be indicative of several prey types targeted.

Introduction

Movement is a crucial behavioral response to diverse key processes such as feeding, finding mates, avoiding predators, and avoiding harmful environmental conditions. The necessity to better understand the roles and the mechanisms underlying animal movement has led to the development of new tools. The technical advances in bio-logging have greatly improved our ability to monitor the behavior and movements of free-ranging animals, since it allows now to reconstruct the path in three dimension at very fine scale using high sampling frequency (Mitani et al. 2003; Laplanche, Marques, et Thomas 2015). Thanks to these developments, studies focusing on movement behavior raises the scope and scale of questions that can be addressed (Hussey et al. 2015; Hays et al. 2016). Therefore, bio-logging technologies have significantly contributed to filling the gap in our knowledge of animal behavior, by relating movements to physiology (Butler et Jones 1997; Génin et al. 2015), physical environment (Heupel et Simpfendorfer 2008; Ortega et al. 2009) and exploited resources (Barbour et Parker 2014; Guinet et al. 2014; Goldbogen et al. 2015; Kuhn, Sterling, et Zeppelin 2015; Wilmers et al. 2015; Adachi et al. 2016). In this context, loggers deployed on wild animals made possible the recording of information that would have been impossible to get otherwise, without being restricted by visibility, observer bias, or geographic scale (Brown et al. 2013).

Different kinds of loggers are used to study wild animals, such as those recording locations, depth, physiological measurements, or environmental variables (water temperature, salinity or light and fluorescence levels) (Hussey et al. 2015). While the movements of terrestrial organisms are almost exclusively determined by a two-dimensional space, aquatic animals evolve in a domain that includes a vertical dimension, modifying the general approach to space use. Thanks to information on location combined with depth, speed, and animal's orientation, track in three dimensions can be computed using some form of dead reckoning (Wilson et al. 2007), where each position is calculated using these information and a previous determined location. The speed in three dimensions can be directly inferred using a propeller (Watanabe et al. 2011; Adachi et al. 2016), or indirectly from the tag flow noise (Burgess et al. 1998; Simon et al. 2009) whereas the orientation can be calculated by accelerometer and magnetometer data (Mitani et al. 2010; Laplanche, Marques, et Thomas 2015).

By recording a high level of detail (Brown et al. 2013) through the biomechanics (Cooke et al. 2004) and exercise science (Suzuki et al. 2009), acceleration data provide a powerful tool in behavioral studies. First, accelerometers can provide an estimate of the energy expenditure based on the variation in acceleration (Halsey et al. 2011). Additionally, the waveform of the signal informs on the body posture and the animal movements (Shepard et al. 2008). The movements identified using this technique can be used to construct ethograms and differentiate a range of discrete behaviors (Sakamoto et al. 2009; Bom et al. 2014; Berman et al. 2014), by ensuring they are biologically meaningful. To date, three methods have been developed for assigning acceleration data to behavioral categories based on signal properties (Brown et al. 2013). (1) The *manual examination* consists in detecting reference patterns and fixing thresholds (Collins et al. 2015), *e.g.* mouth opening detection interpreted as prey catch attempts (Viviant et al. 2010). (2) The *supervised machine learning algorithms*, based on algorithms which are trained on data generated from known behaviors (Nadimi, Søgaard, et Bak 2008). And (3) the *unsupervised machine learning algorithms* (Sakamoto et al. 2009; Chimienti et al. 2016). This latter method presents the advantage to infer categories

from the dataset itself by finding hidden structure, rather than from a labelled dataset. Considering acceleration data without prior knowledge gives the opportunity to detect in a more objective way new behaviors that no one has observed or described before (Chimienti et al. 2016).

Studies that investigate the foraging ecology of a top marine predator, through both tracking and diving data, can use the first-passage time analysis (FPT) by integrating the vertical dimension (Frédéric Bailleul et al. 2007; Frédéric Bailleul, Lesage, et Hammill 2010; Hoskins, Costa, et Arnould 2015; Adachi et al. 2016). (Fauchald et Tveraa 2003) were the first to investigate the spatial distribution of foraging effort with the FPT as a measure of search effort along a path. This method identifies the spatial scale and position of the area-restricted search (ARS) (Kareiva et Odell 1987), which is a fundamental aspect of movement patterns analyses. (Frédéric Bailleul, Lesage, et Hammill 2010) proposed a new approach to investigate ARS in three-dimensional movements: the spherical first-passage time (SFPT). This method is similar to the FPT, except it considers both the vertical and the horizontal dimensions simultaneously, leading to the concept of time spent inside a sphere rather than a circle.

The purpose of this study was to investigate the hunting behaviors in a deep diving predator, the southern elephant seal *Mirounga leonina* (SES). Using high resolution three dimensional reconstruction of the dive track, we therefore aimed at (1) determining the three-dimensional scale where SESs increase their foraging effort at the dive level, using location and behavioral data, (2) comparing the foraging behaviors inside and outside dive bottom ARS, and (3) at identifying different hunting behaviors within an ARS, using unsupervised classification approach.

Materials and methods

Ethics statements

The Ethics Committee of the French Polar Institute validated all scientific procedures applied on elephant seals. All animals in this study were handled and cared for in total accordance with its guidelines and recommendations.

Deployment of Devices and Data Collection

Six post-breeding female SES (mean mass=277±47 kg; mean length=238±11 cm, Table 1) were equipped on the Kerguelen Islands (49°20'S, 70°20'E) with an Argos-GPS satellite tag (Splash 10-F, Wildlife Computer, USA), and an autonomous acoustic/accelerometer/magnetometer and pressure logger named Acousonde™, model 3A (Acoustimetrics, Greeneridge Scences, Inc, USA). The six Splash 10-F tags were glued to the fur on the seals' heads, whereas the Acousondes™ were glued on the back of the animals on the longitudinal axis, 10 cm behind the scapula. Two animals were equipped in 2011 and the other four in 2012. Data loggers were set to collect and archive pressure every second, while tri-axial acceleration and magnetometer were sampled at 5 Hz. All sensors were calibrated by their respective manufacturers. Because sound recording requires high levels of energy consumption, Acousondes™ were programmed to record sound at a frequency of 6 kHz for three hours every 12 h in 2011 and at a frequency of 12.2 kHz for three hours every 24 h for the four individuals equipped in 2012.

The seals were captured with a canvas head-bag and anaesthetized using a 1:1 combination of Tiletamine and Zolazepam (Zoletil 100) injected intravenously (McMahon et al. 2000; Field et al. 2002). Data loggers were glued using a quick-setting epoxy glue (Araldite AW 2101), after the fur was cleaned with acetone. The loggers were then recovered when female SES returned to shore to molt (*i.e.* January-February following deployments). Seals were located using their Argos locations.

Unless otherwise stated, most of our analyses were conducted using R (R Core Team 2015). All scripts used here for data treatment and analyses are available upon request.

Diving Behavior Parameters

We consider the seal is diving when the depth exceed 15 meters. This threshold was chosen to avoid subsurface movements to be identified as dives. Each dive was then divided into three different phases: descent, bottom and ascent phases by using a vertical speed criterion chosen after a sensitivity analyses. Descent and ascent phases were characterized, as a period when the vertical speed from or towards the surface, fitted to a polynomial of degree 4, was higher than 0.75 m s^{-1}. The bottom phase refers to a period between the descent and ascent phase, where the fitted curve of the vertical speed was lower than 0.75 m s^{-1}, in absolute terms. Using a custom script, this analysis was performed with a commercial software package (MATLAB 8.1; The MathWorks, Natick, MA, USA)

Data from the accelerometers were used to calculate a swimming effort index based on stroke rate and amplitude, by using a band pass filter (lower cut-off frequency: 0.44 Hz; higher cut-off frequency: 1 Hz) on the lateral axis. The swimming effort ($m.s^{-2}$) was then defined as the summed absolute values of the filtered lateral acceleration (Richard et al. 2014; Jouma'a et al. 2016). Acceleration data were also used to calculate a proxy of the energy expenditure called the vector of dynamic body acceleration, named hereafter VEDBA (Qasem et al. 2012). For that purpose, we used a high-pass filter with a cut-off frequency of 0.5 Hz to remove the static acceleration on each channels, and then square root of the three axis sum square following the formula:

$$VEDBA = \sqrt{A_x^2 + A_y^2 + A_z^2}$$

Where *A* refers to the filtered acceleration.

Body orientation in three dimensions, *i.e.* the pitch, the roll and the heading were calculated using the animalTrack R package (Farrell et Fuiman 2013) by using filtered acceleration and geomagnetism obtained with a 0.5 Hz low-pass filtering. Processing acceleration and geomagnetism data with the same filter, limits the occurrence of artefacts in calculated headings (Shiomi et al. 2010). Therefore, in a way to assess the animal movement in three dimensions, the circular average of the pitch as well as the circular variance of the roll and the heading were calculated using respectively the circ.mean and circ.disp function from the CircStats R package (Agostinelli 2012).

Three Dimensional Reconstruction and Speed Estimation

Knowing the depth and the orientation of the animal allows us to reconstruct the path of the animal under water by using the dead_reckoning function from the R package animalTrack (Farrell et Fuiman 2013). Such a reconstruction has to make assumptions of the animal's speed. Here, the speed of the animal has been calculated from the low frequency flow noise

on the acoustic recorder (Fletcher et al. 1996; Burgess et al. 1998; Goldbogen et al. 2006; Simon et al. 2009; Génin et al. 2015). For each individual, the noise power was computed with a 110 Hz low-pass filter during periods under 200 m depth, with an animal's pitch between -90° and -75° and an acceleration on the three axes below 1 $m.s^{-2}$. We used these descent periods for the speed–noise calibration because in this situation, the absolute descent speed of the seal can be easily estimated knowing the pitch and the vertical speed. We then fitted a single-term exponential curve between the flow noise, (Simon et al. 2009), and the absolute descent speed. This relation was used to estimate the swimming speed in any part of the dataset that includes sound recordings.

Spherical First Passage Time

SFPT has been developed in the case of three dimension movements to account for the vertical dimension in ARS scale identification and description (Frédéric Bailleul, Lesage, et Hammill 2010). Based on FPT (Fauchald et Tveraa 2003), the SFPT is defined as the time required to cross a sphere with a given radius (Figure 1). To determine the optimal radius of the sphere used for ARS detection, we tested different radii, range 10 - 300 m by 10 m, and visually chose the one providing the highest contrast in SFPT, *i.e.* a radius of 50 m in this study. Then we used lavielle function from R package adehabitatLT (Calenge 2006) that performs a non-parametric segmentation on time series based on Lavielle's method (Lavielle 2005), to finally identified ARS in SFPT time series. To estimate the scale of an ARS, we considered the radius and the time spent inside a sphere centered on the centroid of the ARS that included 95% of animal's position inside.

Detection of Prey Catch Attempts

Mouth opening events indicative of prey catch attempts can be detected from acceleration data (Naito et al. 2010; Viviant et al. 2010; Gallon et al. 2013). Here we used a method derived from (Viviant et al. 2010), and adapted by (Vacquié-Garcia et al. 2015) to identify rapid head movement, interpreted to be associated with prey encounter events, with a custom script performed with MATLAB. We first applied on the signal a high-pass filter of 2.4 Hz in order to remove noise corresponding to swimming movements. Then, a fixed window of one second was used to calculate the standard deviation every second on each channel. Signals reduced in this way were smoothed using a moving standard deviation with a five-second window size. Finally, a 2-mean clustering was performed on the final three signals. Prey catch attempt was defined as a continuous sequence of samples in which all of the three axes were classified in the high-variance cluster.

Behavioral comparison of foraging effort inside and outside ARS during the bottom phase

For each SESs, in dives where ARS were detected, we first calculated both proportion of prey catch attempts and the associated catch attempts rate occurring during the bottom phase, inside and outside ARS. We focused on the bottom phase to avoid the effect of directed movements associated with the ascent and the descent phase. Then focusing on hunting behavior, defined as the animal's behavior before prey catch attempts, the average speed, swimming effort and VEDBA, as well as the circular variance of the heading and the roll, and the circular mean of the pitch were calculated during the 20 s preceding the catch attempts. Using Wilcoxon-Mann-Whitney tests for unpaired data, we then compared averaged values for each SES of these variables inside vs. outside ARS

Unsupervised Hunting Behavior Classification Inside ARS

To identify different hunting behaviors inside ARS, we based our classification on acceleration signal properties from the three channels by considering an arbitrary time window before prey catch attempts. We present the outputs for a 20 s time window, but a sensitivity analysis revealed a similar classification for a time window ranging from 10 to 40 s (Appendix 1). Beyond 40 s, up to 60 s, the classification was still the same except that the proportion of prey catch attempts in each cluster was different.

The calculated signal properties were the mean, the maximum, the minimum, the skewness and the kurtosis (respectively skewness and kurtosis from moments R package (Komsta et Novomestky 2015)), as well as the main frequency that composed the signal and the associated power spectral density (pspectrum from psd R package (Barbour et Parker 2014)) for each raw acceleration axis. The same parameters were calculated on acceleration data filtered with a 0.5 Hz low-pass and a 0.5 Hz high-pass filter, respectively, to retain both the gravitational part of the signal, and the one due to animal's movements.

A PCA analysis was conducted to create a set of orthogonal variables. The optimal number of factors to extract from the PCA, was determined with the Kaiser's rule (Kaiser 1960) through the nScree function from the R package nFactors (Raiche 2010).

We finally performed an agglomerative hierarchical clustering on results from the factor analysis using HCPC function from FactoMineR R package (Husson et al. 2015), by computing the Euclidian distance matrix and following the Ward's criterion. The suggested partition was the one with the higher relative loss of inertia.

Assuming each cluster is a specific hunting behavior, we described these behaviors in terms of average speed, swimming effort and VEDBA, circular average roll and pitch, circular variance of heading, and average prey capture rate during the time window of 20 s before prey catch attempts.

Results

Detection and scale of ARS

The average percentage of dive with ARS (Table 2) was 46.4±0.9%, range: 34.1 (Seal 6) – 58.7% (Seal 3). Overall, the scale of an ARS was similar for the six elephant seals with an average of 45.3±28.9 m radius, and a median of 36.6 m (Figure 2a). This represents an average of 157.1±115.7 s spent inside the ARS, with a median of 123 s (Figure 2b).

Differences of Foraging Behaviors Inside and Outside ARS

When ARSs were detected within a dive, they represented an average 37.8±7.5% of the bottom time, with an associated mean prey capture attempts rate of 1.2±0.3 per minute (Table 3). Non-ARSs represented 62.2±7.5% of bottom time for each animal, with a significant lower mean capture attempts rate of 0.9±0.4 per minute (Wilcoxon-Mann-Whitney p-value <0.01).

At the bottom phase of these dives, before a prey catch attempt, the average VEDBA, and the circular variance of heading and the roll were significantly different outside and inside ARS (Figure 3, Wilcoxon-Mann-Whitney p-value <0.01). Indeed, during the 20 s preceding

the prey catch attempts, the circular variance of the heading and the roll, and the average VEDBA was higher in ARS than outside. The average swimming effort and the circular mean of the pitch were not significantly different inside vs. outside ARS (Figure 3, Wilcoxon-Mann-Whitney *p-value* > 0.05). The same result was found for the average speed, even if visual inspection tend to suggest a lower average speed inside ARS.

Characterization of Hunting Behaviors Inside ARS at the Bottom

Using the Kaiser's rule to reduce the number of variable as inputs for the classification, we only considered the first 18 scores of the PCA (Appendix 2). The hierarchical clustering (Figure 4), through the higher loss of inertia by partitions, revealed the presence of three related clusters obtained from the factor map. All parameters present in this section were averaged during the 20 s preceding prey catch attempts, which explains high values of capture rate compare to values in Table 3.

The first cluster (n=826, Table 4) was characterized by high values of circular variance for the heading (37.6±118 °) and the roll (32.5±1.1 °), and a circular mean for the pitch near zero degrees (-1.5±2.0 °). It was also associated with a large capture rate of 5.7±2.5 prey catch attempts.min^{-1} and high values of VEDBA (138.15±45.94 m.s-²). Catch attempts contained in the second cluster (n=155) were associated with high values of VEDBA and swimming effort (respectively 132.13±38.83 m.s-^{2} and 124.3±33.1 m.s-²), a circular mean for the pitch of 41.8±1.9 ° and a low capture rate of 3.6±1.5 prey catch attempts.min^{-1}. The last behavior associated with the third cluster (n=479) included catch attempts with low values of swimming effort (45.6±27.8 m.s-²), a circular mean for the pitch of -12.0±3 °, a capture rate of 3.6±1.4 prey catch attempts.min^{-1} and low value for VEDBA (54.77±30.46 m.s-²).

The proportion of these three classes of foraging leading to prey catch attempts is nearly identical for all individuals (Figure 5). The cluster 1 containing the largest proportion of catch attempts, followed by cluster 3 and cluster 2 (respectively 56.6%, 12.8 % and 10.6%).

Discussion

Path reconstruction

Despite recent advances in the bio-logging field, still many biases have to be considered when using new tools to study marine animals' path. When predicting the position of an animal underwater, the term *pseudo-track* is preferred rather than *track* to reinforce the idea that absolute position is unknown (Hazen et al. 2009). Such differentiation is crucial, as the reconstruction process relies on multiple assumptions. For instance, to simplify the reconstruction we assume that the animal frame is the same as the tag frame, which is not always the case (Laplanche, Marques, et Thomas 2015). To make a reliable estimation of the speed, we also assume that recording sound under a certain frequency is proportional to the animal's speed due to the noise of the water flow. However, in some situations like if the seal was swimming in the current direction or moving into a position in which its head creates a depression, diminishing therefore the flow noise over the tag, this estimation can be misleading. As mentioned by (Laplanche, Marques, et Thomas 2015), the implementation of these approximation can have considerable impacts on the estimated track. Nonetheless, new methods based on Bayesian statistics (Laplanche, Marques, et Thomas 2015; Wensveen, Thomas, et Miller 2015) developed to compensate these approximations are time

consuming and still inadequate to analyze very large sample size of dives. Therefore, dealing with a relatively large sample size of dives, we consider the method employed in our study as a likely acceptable trade-off between accuracy and processing time.

Areas of Increased Foraging Effort

A reliable estimation of the animal's track underwater is required to assess and understand the role of marine predators within their ecosystem. Because they perceive and react to the environmental heterogeneity, their reactions detected through changes in movements are usually interpreted as interaction and response to physical and/or biological changes (Gordon 1991; Nathan et al. 2008). In a foraging context, an inaccurate estimation of the scale at which animals are searching could lead to misinterpreting their response to environmental changes or disturbances. By using the spherical first passage (Frédéric Bailleul, Lesage, et Hammill 2010) we accounted for the vertical dimension to improve movement analyses in three-dimensions. Based on tracking and diving data, this is the first study to implement this innovative method for looking at ARS in order to differentiate behavioral states, thanks to unsupervised classification. Our study revealed that SESs perform active search in an optimal sphere of 45.3±28.9 m radius. The smaller radii (9 and 18 m) found by (Adachi et al. 2016) could be due to behavioural differences between both species (*Mirounga angustirostris* vs. *Mirounga leonina*), or between prey targeted. In addition, the method used by (Adachi et al. 2016) is different from ours, since they considered the radius of the sphere used to detect ARS as the actual radius of the ARS. In our study, we showed that using a sphere of 50 m radius for ARS detection allow us to detect ARS within a sphere of a 37 m median radius (Figure 2a). Detected in half of the dives, our ARS represent just 37.8% of bottom times, but due to higher prey capture rate, they represent 67.4% of the whole prey catch attempts performed during the bottom phase of dives. Our results were consistent with those from (Adachi et al. 2016) that most feeding events occurred in ARS zones (78 and 86 % for small and large ARS, respectively). SESs appears therefore to have higher encounter rates in areas representing a small part of the main foraging time, the bottom phase (Guinet et al. 2014; Jouma'a et al. 2016). These results would suggest prey aggregation, which seems to be consistent with the patchy distribution of their main prey, the myctophids (Auster et al. 1992; Cherel et al. 2008). Since the difference in prey encountered rate inside vs. outside ARS is not significant, we would define a prey aggregation as areas where the local prey density is higher than the mean overall prey density in the environment.

Regarding swimming behaviors before prey catch attempts at the bottom level, the hunting behavior inside vs. outside was different. ARS appeared to be zones with a higher swimming activity, where animals seems to reduce speed, with a significant increase of horizontal sinuosity, *i.e.* high values of circular variance for heading, and high values in the circular variance for the roll, meaning that animals tend to have a rotating movement when capturing prey (Figure 3). The increase of sinuosity within an ARS suggests that such behavior results from higher resource concentration as revealed from satellite tracking study in birds (Veit et Prince 1997; Pinaud et Weimerskirch 2005) and mammals (Haskell 1997; Thums, Bradshaw, et Hindell 2011). In this study, we showed that SESs increase their three-dimensional track sinuosity at the dive scale in relation to a higher prey encountered rate (Figure 3; Table 3). This is a finding consistent with the increase of both horizontal and vertical sinuosity detected in relation to the increasing number of prey catch attempts (Le Bras et al. submitted).

We interpret the likely reduction of speed before prey catch attempts within an ARS as a predation strategy consisting in catching prey more accurately inside a patch, by favoring specific hunting strategies over just fast swimming. During the bottom phase, the animal could swim rapidly from a patch to another, capturing prey on its way; then inside ARS, it would reduce its speed while foraging. This tactic of switching from extensive to intensive search mode by regulating speed has also been found in plaice, *Pleuronectes platessa* (Hill, Burrows, et Hughes 2002). Because the horizontal speed of an animal is linked to its swimming effort (Sato et al. 2013), we would then expect higher swimming effort before a catch attempt outside ARS. Such a difference was not observed, and this could be due to our proxy of the speed which is known be limited when animal's sinuosity increase, because of interference noises. Another explanation would be that SES, by reducing its speed, would reallocate energy saved in this case for rolling movements or quick direction changes, potentially responsible for the reduction in travelling speed compared to more linear tracks outside ARS. The fact that pursuing prey inside ARS required more energy, *i.e.* high value of VEDBA, than chasing outside, by increasing sinuosity for instance, could be partly balanced by reducing speed. These hypotheses need however to be taken with caution since no significantly differences in swimming speed were detected outside vs. inside ARS (Figure 3). The other way SESs have to compensate the extra energy required to chase inside ARS, is to be more efficient inside these areas, by catching more prey.

Behavioral Classification

Techniques based on acceleration data for animal movement classification are beginning to emerge in the ecological literature (Shepard et al. 2008; Nathan et al. 2012; Brown et al. 2013; Collins et al. 2015). An increasing number of studies have developed supervised algorithm classification, but only a few suggested using unsupervised method (Sakamoto et al. 2009; Chimienti et al. 2016). Here, like (Sakamoto et al. 2009), the classification was based on *k*-means clustering, except that the number of clusters was estimated using hierarchical clustering on principle components. We believe that our method reduces the decision-biases associated with supervised method. This innovative method enabled to identify objectively three different clusters interpreting as hunting modes in ARS.

The first cluster is likely related to a substantial horizontal sinuosity as though SESs were chasing fishes all round them within the patch, remaining at the same depth, *i.e.* on a horizontal disk indicative that prey are distributed within fine horizontal layers. This hunting mode agreed with findings of Le Bras et al. (submitted) that female elephant seals were found to be more successful when foraging inside a prey patch distributed in narrow vertical layers. During this hunting mode, SESs appear to roll alternating almost from back to belly, which is not observed in any other cluster. These variations in the roll has been documented in northern fur seal (Battaile et al. 2015) and sperm whales (Miller, Johnson, et Tyack 2004). In this latter case, this behavior was associated to active clicking, indicative of prey catch attempts. Here, these variations are in part responsible for the associated high-energy expenditure. Indeed, this hunting mode appeared to be the most costly in energy with the highest average of VEDBA. In addition to three-dimensional movements, this energy expenditure is also due to the swimming effort necessary to maintain these negatively buoyant animals at the same depth (Richard et al. 2014). According to the associated high capture rate (almost twice higher than the others identified modes) we believed that SESs would compensate the energy required to catch these prey, which represents 56.6% of capture attempts, by catching as much prey as possible and potentially by feeding on prey

with high energy density. With their patchy distribution (Auster et al. 1992) and their lethargic behavior (Barham 1971), small myctophids, which are high energy density fishes (Lenky et al. 2011) are the most plausible candidate prey.

We interpreted the second mode as an active chase, as SESs attack from below with a large swimming effort. Here, the energy expenditure is almost exclusively due to the animal's stroke, as if the only purpose of the animal was to charge into prey. Depending on the depth and the prey, SES could in this case use the prey drop shadow to better target them. As the associated prey catch attempt rate was also found to be low, we hypothesized that SESs would compensate the extra energy required to catch fast moving prey while ascending, by favoring large prey, like squids for instance or larger myctophids species such as *Gymnoscopelus bolini*.

Finally, the last cluster reveals a passive hunting mode that would consist of catching prey from above, by gliding down on them at a relatively low angle. All females were found to remain negatively buoyant during post-breeding foraging trips (Richard et al. 2014), particularly during the first weeks following their departure from the colony, and therefore glide when moving down (R. W. Davis et Weihs 2007). This attitude, while being interpreted as an energy-saving strategy, *i.e.* low value for VEDBA, could also be interpreted as opportunistic captures, by catching prey by stealth during the approach phase. In this case, the associated low sinuosity could be perceived as if SESs travelled in a straight direction, gliding down at a low angle and picking low density prey on their way.

These three foraging strategies were also found to be the same outside ARS (Appendix 3), highlighting that hunting behavior is not dependent on the ARS mode. Presumably, areas of increasing foraging effort appear to be contingent upon the prey density.

Foraging Ecology

Marine ecosystems are difficult to access and to study. However, the combination of diving and tracking data from top predators can be extremely useful to improve our understanding of the role and the structure of the marine resources. Following the conceptual framework of the optimal foraging theory (Charnov 1976), predators should adjust their movements to prey encounters or environmental conditions. In a favorable environment, or when prey is encountered, predators are expected to increase their turning rate (C. S. Davis et al. 1991) and decrease their speed (Patlak 1953; Turchin 1991), which was found in southern elephant seal.

As no differences in the proportion of hunting modes were observed between individual, our results on hunting classification could be generalizable, but the small number of individuals do not allow us to conclude at the population level. Here, three different strategies emerge from this analysis. One of them is associated with opportunistic captures and represents 32.8% of prey capture. It consists of catching prey at a lower rate, by adopting some kind of energy-saving strategy. The other two strategies are much more energy consuming, in part because of the swimming effort required for these animals to ascent or to stay at the same depth. In addition to this effort, the energy expenditure was also found to be related to three-dimensional movement for the main hunting behaviors used in 56.6% of the prey catch attempts. We believe the extra energy required by employing this hunting mode would be compensated with a greater number of captured prey; furthermore if these prey have higher energy density. As this strategy seems to be preferred over the others, we believe the

associated energy balance (energy intake *vs.* energy expenditure) is more favorable than the others.

These findings challenge the general assumption that elephant seals mainly adopt energy saving foraging behaviors. Based on previous studies (Adachi et al. 2014; Richard et al. 2014; Maresh et al. 2015; Jouma'a et al. 2016), we believe that SESs adopt an energy saving strategy when transiting between patches, through the minimal cost of transport (Miller et al. 2012), but that are actively moving when foraging within a patch. While this classification is indicative of different foraging strategies, one can consider that it may also be indicative of different prey types. Further investigations, such as these initiated by (Vacquié-Garcia et al. 2015) on the delineation of SESs' foraging environments defined by temperature, light level and depth or (Frederic Bailleul, Vacquie-Garcia, et Guinet 2015) on the dissolved oxygen in water masses visited by SESs would be interesting to assess the distribution and the ecology of their prey.

Acknowledgements

The authors would like to thank all the persons involved in the tagging and controls of elephant seals on Kerguelen Island and the French Polar Institute, for providing logistic and financial support. This work was carried out in the framework of the ANR Blanc MYCTO-3D-MAP, ANR VMC IPSOS-SEAL programs and CNES-TOSCA program ("Éléphants de mer océanographes"). This study is part of IPEV program no. 109, (P.I. H. Weimerskirch) and the observatory Mammifères Explorateurs du Milieu Océanique, (MEMO SOERE CTD 02). The authors also thank the Total Foundation for financial support. They would particularly like to thank Simon Benhamou for his valuable suggestions on the ARS detection part. J.J. was supported by "Direction Générale de l'Armement".

References

Adachi, Taiki, Daniel P. Costa, Patrick W. Robinson, Sarah H. Peterson, Masato Yamamichi, Yasuhiko Naito, et Akinori Takahashi. 2016. « Searching for Prey in a Three-dimensional Environment: Hierarchical Movements Enhance Foraging Success in Northern Elephant Seals ». *Functional Ecology*. doi:10.1111/1365-2435.12686.

Adachi, Taiki, Jennifer L. Maresh, Patrick W. Robinson, Sarah H. Peterson, Daniel P. Costa, Yasuhiko Naito, Yuuki Y. Watanabe, et Akinori Takahashi. 2014. « The Foraging Benefits of Being Fat in a Highly Migratory Marine Mammal ». *Proceedings of the Royal Society of London B: Biological Sciences* 281 (1797): 20142120. doi:10.1098/rspb.2014.2120.

Agostinelli, Claudio. 2012. « CircStats: Circular Statistics, from "Topics in circular Statistics" (2001) ». *R package version 0.2-4*. http://CRAN.R-project.org/package=CircStats.

Auster, Peter J., Carolyn A. Griswold, Marsh J. Youngbluth, et Thomas G. Bailey. 1992. « Aggregations of Myctophid Fishes with Other Pelagic Fauna ». *Environmental Biology of Fishes* 35 (2): 133‑39. doi:10.1007/BF00002187.

Bailleul, Frédéric, Jean-Benoît Charrassin, Pascal Monestiez, Fabien Roquet, Martin Biuw, et Christophe Guinet. 2007. « Successful Foraging Zones of Southern Elephant Seals from the Kerguelen Islands in Relation to Oceanographic Conditions ». *Philosophical Transactions of the Royal Society of London. Series B, Biological Sciences* 362 (1487): 2169‑81. doi:10.1098/rstb.2007.2109.

Bailleul, Frédéric, Véronique Lesage, et Mike O. Hammill. 2010. « Spherical First Passage Time: A tool to investigate area-restricted search in three-dimensional movements ». *Ecological Modelling* 221 (13–14): 1665‑73. doi:10.1016/j.ecolmodel.2010.04.001.

Bailleul, Frederic, Jade Vacquie-Garcia, et Christophe Guinet. 2015. « Dissolved Oxygen Sensor in Animal-Borne Instruments: An Innovation for Monitoring the Health of Oceans and Investigating the Functioning of Marine Ecosystems ». *PLoS ONE* 10 (7): e0132681. doi:10.1371/journal.pone.0132681.

Barbour, Andrew J., et Robert L. Parker. 2014. « Psd: Adaptive, Sine Multitaper Power Spectral Density Estimation for R ». *Computers & Geosciences* 63 (février): 1‑8. doi:10.1016/j.cageo.2013.09.015.

Barham, E. G. 1971. « Deep-sea fishes: lethargy and vertical orientation ». In *Proceedings of an international symposium on biological sound scattering in the ocean*, 100‑116. G. B. Farquhar (ed.). U.S. Gov. Printing Office, Washington, DC.

Battaile, Brian C., Kentaro Q. Sakamoto, Chad A. Nordstrom, David A. S. Rosen, et Andrew W. Trites. 2015. « Accelerometers Identify New Behaviors and Show Little Difference in the Activity Budgets of Lactating Northern Fur Seals (Callorhinus ursinus) between Breeding Islands and Foraging Habitats in the Eastern Bering Sea ». *PLoS ONE* 10 (3): e0118761. doi:10.1371/journal.pone.0118761.

Berman, Gordon J., Daniel M. Choi, William Bialek, et Joshua W. Shaevitz. 2014. « Mapping the Stereotyped Behaviour of Freely Moving Fruit Flies ». *Journal of The Royal Society Interface* 11 (99): 20140672. doi:10.1098/rsif.2014.0672.

Bom, Roeland A., Willem Bouten, Theunis Piersma, Kees Oosterbeek, et Jan A. van Gils. 2014. « Optimizing Acceleration-Based Ethograms: The Use of Variable-Time versus Fixed-Time Segmentation ». *Movement Ecology* 2 (1): 6. doi:10.1186/2051-3933-2-6.

Brown, Danielle D., Roland Kays, Martin Wikelski, Rory Wilson, et A. Peter Klimley. 2013. « Observing the Unwatchable through Acceleration Logging of Animal Behavior ». *Animal Biotelemetry* 1 (1): 1‑16. doi:10.1186/2050-3385-1-20.

Burgess, W. C., P. L. Tyack, B. J. Le Boeuf, et D. P. Costa. 1998. « A programmable acoustic recording tag and first results from free-ranging northern elephant seals ». *Deep Sea Research Part II: Topical Studies in Oceanography* 45 (7): 1327‑51. doi:10.1016/S0967-0645(98)00032-0.

Butler, P. J., et D. R. Jones. 1997. « Physiology of Diving of Birds and Mammals ». *Physiological Reviews* 77 (3): 837‑99.

Calenge, Clément. 2006. « The Package "adehabitat" for the R Software: A Tool for the Analysis of Space and Habitat Use by Animals ». *Ecological Modelling* 197 (3-4): 516-19. doi:10.1016/j.ecolmodel.2006.03.017.

Charnov, Eric L. 1976. « Optimal foraging, the marginal value theorem ». *Theoretical Population Biology* 9 (2): 129-36. doi:10.1016/0040-5809(76)90040-X.

Cherel, Y, S Ducatez, C Fontaine, P Richard, et C Guinet. 2008. « Stable Isotopes Reveal the Trophic Position and Mesopelagic Fish Diet of Female Southern Elephant Seals Breeding on the Kerguelen Islands ». *Marine Ecology Progress Series* 370 (octobre): 239-47. doi:10.3354/meps07673.

Chimienti, Marianna, Thomas Cornulier, Ellie Owen, Mark Bolton, Ian M. Davies, Justin M.J. Travis, et Beth E. Scott. 2016. « The Use of an Unsupervised Learning Approach for Characterizing Latent Behaviors in Accelerometer Data ». *Ecology and Evolution* 6 (3): 727-41. doi:10.1002/ece3.1914.

Collins, Philip M., Jonathan A. Green, Victoria Warwick-Evans, Stephen Dodd, Peter J. A. Shaw, John P. Y. Arnould, et Lewis G. Halsey. 2015. « Interpreting Behaviors from Accelerometry: A Method Combining Simplicity and Objectivity ». *Ecology and Evolution* 5 (20): 4642–4654. doi:10.1002/ece3.1660.

Cooke, Steven J., Scott G. Hinch, Martin Wikelski, Russel D. Andrews, Louise J. Kuchel, Thomas G. Wolcott, et Patrick J. Butler. 2004. « Biotelemetry: A Mechanistic Approach to Ecology ». *Trends in Ecology & Evolution* 19 (6): 334-43. doi:10.1016/j.tree.2004.04.003.

Davis, Cabell S., Glenn R. Flierl, P. H. Wiebe, et P. J. S. Franks. 1991. « Micropatchiness, turbulence and recruitment in plankton ». *Journal of Marine Research* 49 (1): 109-51. doi:10.1357/002224091784968602.

Davis, Randall W, et Daniel Weihs. 2007. « Locomotion in diving elephant seals: physical and physiological constraints ». *Philosophical Transactions of the Royal Society B: Biological Sciences* 362 (1487): 2141-50. doi:10.1098/rstb.2007.2107.

Farrell, Ed, et Lee Fuiman. 2013. « animalTrack: Animal track reconstruction for high frequency 2-dimensional (2D) or 3-dimensional (3D) movement data. » *R package version 1.0.0*. http://CRAN.R-project.org/package=animalTrack.

Fauchald, Per, et Torkild Tveraa. 2003. « Using First-Passage Time in the Analysis of Area-Restricted Search and Habitat Selection ». *Ecology* 84 (2): 282-88.

Field, I C, C J A Bradshaw, C R McMahon, J Harrington, et H R Burton. 2002. « Effects of Age, Size and Condition of Elephant Seals (Mirounga Leonina) on Their Intravenous Anaesthesia with Tiletamine and Zolazepam ». *The Veterinary Record* 151 (8): 235-40.

Fletcher, Stacia, Burney J. Le Boeuf, Daniel P. Costa, Peter L. Tyack, et Susanna B. Blackwell. 1996. « Onboard acoustic recording from diving northern elephant seals ». *The Journal of the Acoustical Society of America* 100 (4): 2531-39. doi:10.1121/1.417361.

Gallon, S., F. Bailleul, J. -B. Charrassin, C. Guinet, C. -A. Bost, Y. Handrich, et M. Hindell. 2013. « Identifying foraging events in deep diving southern elephant seals, Mirounga leonina, using acceleration data loggers ». *Deep Sea Research Part II: Topical Studies in Oceanography*, Fourth International Symposium on Bio-logging Science, 88–89 (avril): 14‑22. doi:10.1016/j.dsr2.2012.09.002.

Génin, Alexandre, Gaëtan Richard, Joffrey Jouma'a, Baptiste Picard, Nory El Ksabi, Jade Vacquié Garcia, et Christophe Guinet. 2015. « Characterization of Postdive Recovery Using Sound Recordings and Its Relationship to Dive Duration, Exertion and Foraging Effort of Southern Elephant Seals (Mirounga Leonina) ». *Marine Mammal Science* 31 (4): 1452–1470. doi:10.1111/mms.12235.

Goldbogen, Jeremy A., John Calambokidis, Robert E. Shadwick, Erin M. Oleson, Mark A. McDonald, et John A. Hildebrand. 2006. « Kinematics of Foraging Dives and Lunge-Feeding in Fin Whales ». *Journal of Experimental Biology* 209 (7): 1231‑44. doi:10.1242/jeb.02135.

Goldbogen, Jeremy A., Elliott L. Hazen, Ari S. Friedlaender, John Calambokidis, Stacy L. DeRuiter, Alison K. Stimpert, et Brandon L. Southall. 2015. « Prey Density and Distribution Drive the Three-dimensional Foraging Strategies of the Largest Filter Feeder ». *Functional Ecology* 29 (7): 951‑61. doi:10.1111/1365-2435.12395.

Gordon, Deborah M. 1991. « Variation and Change in Behavioral Ecology ». *Ecology* 72 (4): 1196‑1203. doi:10.2307/1941093.

Guinet, Christophe, Jade Vacquié-Garcia, Baptiste Picard, Guillaume Bessigneul, Yves Lebras, Anne Ccile Dragon, Morgane Viviant, John P. Y. Arnould, et Frdric Bailleul. 2014. « Southern elephant seal foraging success in relation to temperature and light conditions: insight into prey distribution ». *Marine Ecology Progress Series* 499 (mars): 285‑301. doi:10.3354/meps10660.

Halsey, L. G., C. R. White, M. R. Enstipp, R. P. Wilson, P. J. Butler, G. R. Martin, D. Grémillet, et D. R. Jones. 2011. « Assessing the Validity of the Accelerometry Technique for Estimating the Energy Expenditure of Diving Double-Crested Cormorants Phalacrocorax Auritus ». *Physiological and Biochemical Zoology: PBZ* 84 (2): 230‑37. doi:10.1086/658636.

Haskell, David G. 1997. « Experiments and a model examining learning in the area-restricted search behavior of ferrets (Mustela putorius furo) ». *Behavioral Ecology* 8 (4): 448‑49. doi:doi: 10.1093/beheco/8.4.448.

Hays, Graeme C., Luciana C. Ferreira, Ana M.M. Sequeira, Mark G. Meekan, Carlos M. Duarte, Helen Bailey, Fred Bailleul, et al. 2016. « Key Questions in Marine Megafauna Movement Ecology ». *Trends in Ecology & Evolution*. doi:10.1016/j.tree.2016.02.015.

Hazen, Elliott L., Ari S. Friedlaender, Michael A. Thompson, Colin R. Ware, Mason T. Weinrich, Patrick N. Halpin, et David N. Wiley. 2009. « Fine-scale prey aggregations and foraging ecology of humpback whales Megaptera novaeangliae ». *Marine Ecology Progress Series* 395 (décembre): 75‑89. doi:10.3354/meps08108.

Heupel, Mr, et Ca Simpfendorfer. 2008. « Movement and Distribution of Young Bull Sharks Carcharhinus Leucas in a Variable Estuarine Environment ». *Aquatic Biology* 1 (février): 277‑89. doi:10.3354/ab00030.

Hill, S, M.T Burrows, et R.N Hughes. 2002. « Adaptive Search in Juvenile Plaice Foraging for Aggregated and Dispersed Prey ». *Journal of Fish Biology* 61 (5): 1255‑67. doi:10.1006/jfbi.2002.2145.

Hoskins, Andrew J., Daniel P. Costa, et John P. Y. Arnould. 2015. « Utilisation of Intensive Foraging Zones by Female Australian Fur Seals ». *PLoS ONE* 10 (2): e0117997. doi:10.1371/journal.pone.0117997.

Hussey, Nigel E., Steven T. Kessel, Kim Aarestrup, Steven J. Cooke, Paul D. Cowley, Aaron T. Fisk, Robert G. Harcourt, et al. 2015. « Aquatic Animal Telemetry: A Panoramic Window into the Underwater World ». *Science* 348 (6240): 1255642. doi:10.1126/science.1255642.

Husson, François, Julie Josse, Sébastien Le, et Jérémy Mazet. 2015. « FactoMineR: Multivariate Exploratory Data Analysis and Data Mining ». *R package version 1.31.3*. http://CRAN.R-project.org/package=FactoMineR.

Jouma'a, Joffrey, Yves Le Bras, Gaëtan Richard, Jade Vacquié-Garcia, Baptiste Picard, Nory El Ksabi, et Christophe Guinet. 2016. « Adjustment of Diving Behaviour with Prey Encounters and Body Condition in a Deep Diving Predator: The Southern Elephant Seal ». Édité par Daniel Costa. *Functional Ecology* 30 (4): 636‑48. doi:10.1111/1365-2435.12514.

Kaiser, Henry F. 1960. « The application of electronic computers to factor analysis. » *Educational and Psychological Measurement* 20: 141‑51.

Kareiva, Peter, et Garrett Odell. 1987. « Swarms of Predators Exhibit "Preytaxis" if Individual Predators Use Area-Restricted Search ». *The American Naturalist* 130 (2): 233‑70.

Komsta, Lukasz, et Frederick Novomestky. 2015. « moments: Moments, cumulants, skewness, kurtosis and related tests ». *R package version 0.14*. http://CRAN.R-project.org/package=moments.

Kuhn, Carey E., Jeremy T. Sterling, et Tonya K. Zeppelin. 2015. « Linking Northern Fur Seal Behavior with Prey Distributions: The Impact of Temporal Mismatch between Predator Studies and Prey Surveys ». *Animal Biotelemetry* 3 (1): 9. doi:10.1186/s40317-015-0029-8.

Laplanche, Christophe, Tiago A. Marques, et Len Thomas. 2015. « Tracking Marine Mammals in 3D Using Electronic Tag Data ». *Methods in Ecology and Evolution* 6 (9): 987–996. doi:10.1111/2041-210X.12373.

Lavielle, Marc. 2005. « Using Penalized Contrasts for the Change-Point Problem ». *Signal Processing* 85 (8): 1501‑10. doi:10.1016/j.sigpro.2005.01.012.

Lenky, Crystal, Regina Eisert, Olav T. Oftedal, et Victoria Metcalf. 2011. « Proximate Composition and Energy Density of Nototheniid and Myctophid Fish in McMurdo Sound and the Ross Sea, Antarctica ». *Polar Biology* 35 (5): 717‑24. doi:10.1007/s00300-011-1116-9.

Maresh, Jennifer L., T. Adachi, A. Takahashi, Y. Naito, De Crocker, M. Horning, Tm Williams, et Dp Costa. 2015. « Summing the Strokes: Energy Economy in Northern Elephant Seals during Large-Scale Foraging Migrations ». *Movement Ecology* 3 (1). doi:10.1186/s40462-015-0049-2.

McMahon, C R, H Burton, S McLean, D Slip, et M Bester. 2000. « Field Immobilisation of Southern Elephant Seals with Intravenous Tiletamine and Zolazepam ». *The Veterinary Record* 146 (9): 251‑54.

Miller, P. J. O., M. Biuw, Y. Y. Watanabe, D. Thompson, et M. A. Fedak. 2012. « Sink fast and swim harder! Round-trip cost-of-transport for buoyant divers ». *Journal of Experimental Biology* 215 (20): 3622‑30. doi:10.1242/jeb.070128.

Miller, P. J. O., M. P. Johnson, et P. L. Tyack. 2004. « Sperm Whale Behaviour Indicates the Use of Echolocation Click Buzzes "Creaks" in Prey Capture ». *Proceedings of the Royal Society B: Biological Sciences* 271 (1554): 2239‑47. doi:10.1098/rspb.2004.2863.

Mitani, Yoko, Russel D Andrews, Katsufumi Sato, Akiko Kato, Yasuhiko Naito, et Daniel P Costa. 2010. « Three-Dimensional Resting Behaviour of Northern Elephant Seals: Drifting like a Falling Leaf ». *Biology Letters* 6 (2): 163‑66. doi:10.1098/rsbl.2009.0719.

Mitani, Yoko, Katsufumi Sato, Shinichiro Ito, Michael F. Cameron, Donald B. Siniff, et Yasuhiko Naito. 2003. « A Method for Reconstructing Three-Dimensional Dive Profiles of Marine Mammals Using Geomagnetic Intensity Data: Results from Two Lactating Weddell Seals ». *Polar Biology* 26 (5): 311‑17. doi:10.1007/s00300-003-0487-y.

Nadimi, E. S., H. T. Søgaard, et T. Bak. 2008. « ZigBee-based wireless sensor networks for classifying the behaviour of a herd of animals using classification trees ». *Biosystems Engineering* 100 (2): 167‑76. doi:10.1016/j.biosystemseng.2008.03.003.

Naito, Yasuhiko, Horst Bornemann, Akinori Takahashi, Trevor McIntyre, et Joachim Plötz. 2010. « Fine-scale feeding behavior of Weddell seals revealed by a mandible accelerometer ». *Polar Science*, Antarctic Biology in the 21st Century - Advances in and beyond IPY, 4 (2): 309‑16. doi:10.1016/j.polar.2010.05.009.

Nathan, Ran, Wayne M. Getz, Eloy Revilla, Marcel Holyoak, Ronen Kadmon, David Saltz, et Peter E. Smouse. 2008. « A movement ecology paradigm for unifying organismal movement research ». *Proceedings of the National Academy of Sciences of the United States of America* 105 (49): 19052‑59. doi:10.1073/pnas.0800375105.

Nathan, Ran, Orr Spiegel, Scott Fortmann-Roe, Roi Harel, Martin Wikelski, et Wayne M. Getz. 2012. « Using Tri-Axial Acceleration Data to Identify Behavioral Modes of Free-Ranging Animals: General Concepts and Tools Illustrated for Griffon Vultures ». *The Journal of Experimental Biology* 215 (6): 986‑96. doi:10.1242/jeb.058602.

Ortega, Lori A., Michelle R. Heupel, Philip Van Beynen, et Philip J. Motta. 2009. « Movement Patterns and Water Quality Preferences of Juvenile Bull Sharks (Carcharhinus Leucas) in a Florida Estuary ». *Environmental Biology of Fishes* 84 (4): 361‑73. doi:10.1007/s10641-009-9442-2.

Patlak, Clifford S. 1953. « Random Walk with Persistence and External Bias ». *The Bulletin of Mathematical Biophysics* 15 (3): 311‑38. doi:10.1007/BF02476407.

Pinaud, David, et Henri Weimerskirch. 2005. « Scale-Dependent Habitat Use in a Long-Ranging Central Place Predator ». *Journal of Animal Ecology* 74 (5): 852‑63. doi:10.1111/j.1365-2656.2005.00984.x.

Qasem, Lama, Antonia Cardew, Alexis Wilson, Iwan Griffiths, Lewis G. Halsey, Emily L. C. Shepard, Adrian C. Gleiss, et Rory Wilson. 2012. « Tri-Axial Dynamic Acceleration as a Proxy for Animal Energy Expenditure; Should We Be Summing Values or Calculating the Vector? » *PLoS ONE* 7 (2): e31187. doi:10.1371/journal.pone.0031187.

R Core Team. 2015. « R: A Language and Environment for Statistical Computing ». *R Foundation for Statistical Computing*. https://www.R-project.org/.

Raiche, Gilles. 2010. « nFactors: an R package for parallel analysis and non graphical solutions to the Cattell scree test ». *R package version 2.3.3*. http://CRAN.R-project.org/package=nFactors.

Richard, Gaëtan, Jade Vacquié-Garcia, Joffrey Jouma'a, Baptiste Picard, Alexandre Génin, John P. Y. Arnould, Frédéric Bailleul, et Christophe Guinet. 2014. « Variation in Body Condition during the Post-Moult Foraging Trip of Southern Elephant Seals and Its Consequences on Diving Behaviour ». *The Journal of Experimental Biology* 217 (mai): 2609‑19. doi:10.1242/jeb.088542.

Sakamoto, Kentaro Q., Katsufumi Sato, Mayumi Ishizuka, Yutaka Watanuki, Akinori Takahashi, Francis Daunt, et Sarah Wanless. 2009. « Can Ethograms Be Automatically Generated Using Body Acceleration Data from Free-Ranging Birds? » *PloS One* 4 (4): e5379. doi:10.1371/journal.pone.0005379.

Sato, Katsufumi, Kagari Aoki, Yuuki Y. Watanabe, et Patrick J. O. Miller. 2013. « Neutral Buoyancy Is Optimal to Minimize the Cost of Transport in Horizontally Swimming Seals ». *Scientific Reports* 3 (juillet): 2205. doi:10.1038/srep02205.

Shepard, Emily L. C., Rory P. Wilson, Flavio Quintana, Agustina Gmez Laich, Nikolai Liebsch, Diego A. Albareda, Lewis G. Halsey, et al. 2008. « Identification of animal movement patterns using tri-axial accelerometry ». *Endangered Species Research* 10 (mars): 47‑60. doi:10.3354/esr00084.

Shiomi, K, T Narazaki, K Sato, K Shimatani, N Arai, Pj Ponganis, et N Miyazaki. 2010. « Data-Processing Artefacts in Three-Dimensional Dive Path Reconstruction from Geomagnetic and Acceleration Data ». *Aquatic Biology* 8 (mars): 289‑94. doi:10.3354/ab00239.

Simon, Malene, Mark Johnson, Peter Tyack, et Peter T. Madsen. 2009. « Behaviour and Kinematics of Continuous Ram Filtration in Bowhead Whales (Balaena Mysticetus) ». *Proceedings of the Royal Society of London B: Biological Sciences* 276 (1674): 3819‑28. doi:10.1098/rspb.2009.1135.

Suzuki, Ippei, Yasuhiko Naito, Lars P. Folkow, Nobuyuki Miyazaki, et Arnoldus S. Blix. 2009. « Validation of a Device for Accurate Timing of Feeding Events in Marine Animals ». *Polar Biology* 32 (4): 667‑71. doi:10.1007/s00300-009-0596-3.

Thums, Michele, Corey J. A. Bradshaw, et Mark A. Hindell. 2011. « In situ measures of foraging success and prey encounter reveal marine habitat-dependent search strategies ». *Ecology* 92 (6): 1258‑70. doi:10.1890/09-1299.1.

Turchin, Peter. 1991. « Translating Foraging Movements in Heterogeneous Environments into the Spatial Distribution of Foragers ». *Ecology* 72 (4): 1253‑66. doi:10.2307/1941099.

Vacquié-Garcia, Jade, Christophe Guinet, Cécile Laurent, et Frédéric Bailleul. 2015. « Delineation of the southern elephant seal's main foraging environments defined by temperature and light conditions ». *Deep Sea Research Part II: Topical Studies in Oceanography*, Impacts of climate on marine top predators, 113 (mars): 145‑53. doi:10.1016/j.dsr2.2014.10.029.

Veit, R.R., et P.A. Prince. 1997. « Individual and Population Level Dispersal of Black-Browed Albatrosses Diomedea Melanophris and Grey-Headed Albatrosses D. Chrysostoma in Response to Antarctic Krill ». *Ardea* 85: 129‑34.

Viviant, Morgane, Andrew W. Trites, David A. S. Rosen, Pascal Monestiez, et Christophe Guinet. 2010. « Prey Capture Attempts Can Be Detected in Steller Sea Lions and Other Marine Predators Using Accelerometers ». *Polar Biology* 33 (5): 713‑19. doi:10.1007/s00300-009-0750-y.

Watanabe, Yuuki Y., Katsufumi Sato, Yutaka Watanuki, Akinori Takahashi, Yoko Mitani, Masao Amano, Kagari Aoki, et al. 2011. « Scaling of swim speed in breath-hold divers: Scaling of swim speed ». *Journal of Animal Ecology* 80 (1): 57‑68. doi:10.1111/j.1365-2656.2010.01760.x.

Wensveen, Paul J., Len Thomas, et Patrick J. O. Miller. 2015. « A Path Reconstruction Method Integrating Dead-Reckoning and Position Fixes Applied to Humpback Whales ». *Movement Ecology* 3 (1): 1‑16. doi:10.1186/s40462-015-0061-6.

Wilmers, Christopher C., Barry Nickel, Caleb M. Bryce, Justine A. Smith, Rachel E. Wheat, et Veronica Yovovich. 2015. « The golden age of bio-logging: how animal-borne sensors are advancing the frontiers of ecology ». *Ecology* 96 (7): 1741‑53. doi:10.1890/14-1401.1.

Wilson, R. P., Nikolai Liebsch, Ian M. Davies, Flavio Quintana, Henri Weimerskirch, Sandra Storch, Klaus Lucke, et al. 2007. « All at sea with animal tracks; methodological and analytical solutions for the resolution of movement ». *Deep Sea Research Part II: Topical Studies in Oceanography*, Bio-logging Science: Logging and Relaying Physical and Biological Data Using Animal-Attached Tags Proceedings of the 2005 International Symposium on Bio-logging Science Second International Conference on Bio-logging Science, 54 (3–4): 193‑210. doi:10.1016/j.dsr2.2006.11.017.

Tables

Table 1: Descriptive information about the six post-breeding females SESs

Seal	Body mass (kg)	Size (cm)	*n* days recorded	*n* dives	*n* dives with sound	Departure date	Acousonde ID
1	230	232	24	1945	227	2012-10-28	626019
2	362	235	12	409	60	2012-11-03	626020
3	282	248	4	288	46	2012-10-28	626022
4	292	225	29	1777	212	2012-11-01	626040
5	255	254	13	821	123	2011-10-26	A031
6	245	238	13	1081	211	2011-10-28	A032

Table 2: Descriptive information about ARS for the six post-breeding females SESs

Seal	Time in ARS (s)	Radius ARS (m)	Proportion of dive with ARS (%)
1	131.5±61.5	39.7±19.9	55.5
2	138.6±60.6	42.1±21.8	43.3
3	176.1±121.4	54.9±37.9	58.7
4	182.2±132.9	44.6±30.9	39.6
5	230.3±188.2	63.1±15.9	47.2
6	131.5±91.6	44.7±28.0	34.1

Table 3: Dives ARS proportion and rate of prey catch attempts for each individual during the bottom phase for which ARS were detected.

Seal	ARS		non ARS	
	Proportion (%)	Prey catch attempts.min^{-1}	Proportion (%)	Prey catch attempts.min^{-1}
1	40.0	1.4	60.0	0.7
2	24.6	1.5	75.4	1.5
3	43.5	1.2	56.5	0.4
4	33.8	1.1	66.2	1.2
5	44.5	0.8	55.5	0.6
6	40.2	1.4	59.8	1.0

Table 4: Summary of the behaviour during the 20 s preceding prey catch attempts in the three groups identified from the unsupervised classification. Mean values and circular mean values are respectively given ± standard deviation and circular variance.

Cluster	n	μ VeDBA (m.s^{-2})	μ Swimming effort (m.s^{-2})	μ Speed (m.s-1)	θ_c^2 Roll (°)	μ_c Pitch (°)	θ_c^2 Heading (°)	Prey catch attempts.min-1
1	826	138.15±45.94	80.44±26.03	1.6±0.26	32.49±1.14	-1.47±2.02	37.61±1.08	5.65±2.47
2	155	132.13±38.83	124.31±33.14	1.76±0.3	8.68±1.04	41.76±1.92	12.56±1.39	3.64±1.45
3	479	54.77±30.46	45.57±27.76	1.64±0.34	5.06±0.48	-12.04±2.97	9.65±1.03	3.61±1.43

Figures

Figure 2: a) Density distribution of the radius for a sphere centred on the centroid of each ARS, including 95 % of elephant seal's position, the median is at 36.6 m; b) density distribution of the time spent inside this sphere, the median is at 123 s.

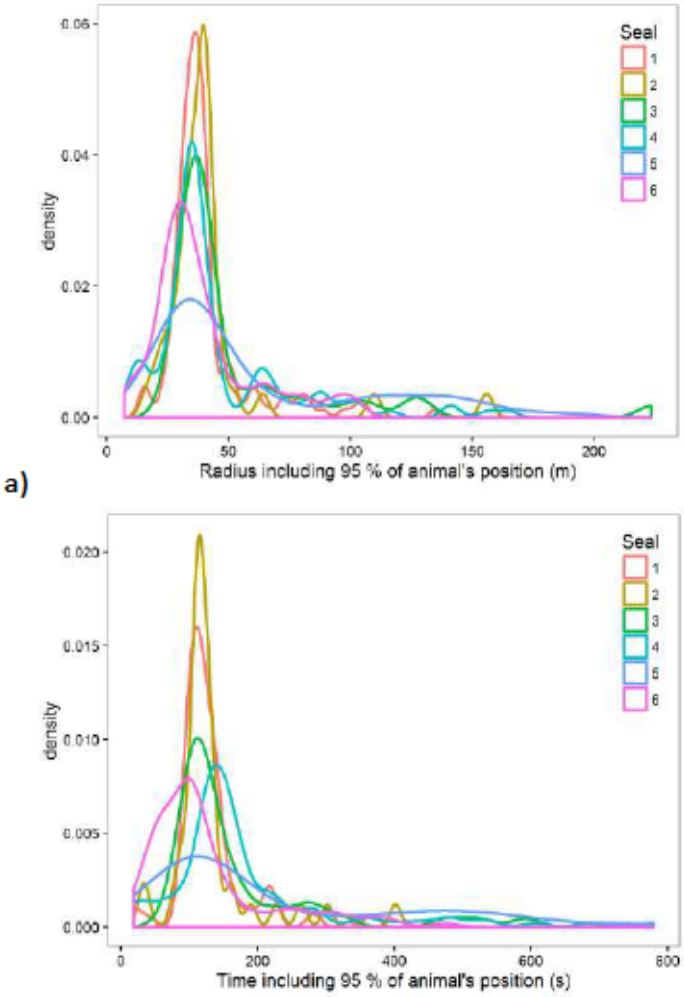

Figure 1: Illustration of the process used to detect areas restricted search (ARS) within a dive (dive 994). Based on Bailleul *et al.* (2010) and L avielle's method, the search area (in red) found for this dive took place in a sphere of 37.9 m radius, where southern elephant seal 1 (SES 1) spent 142 s.

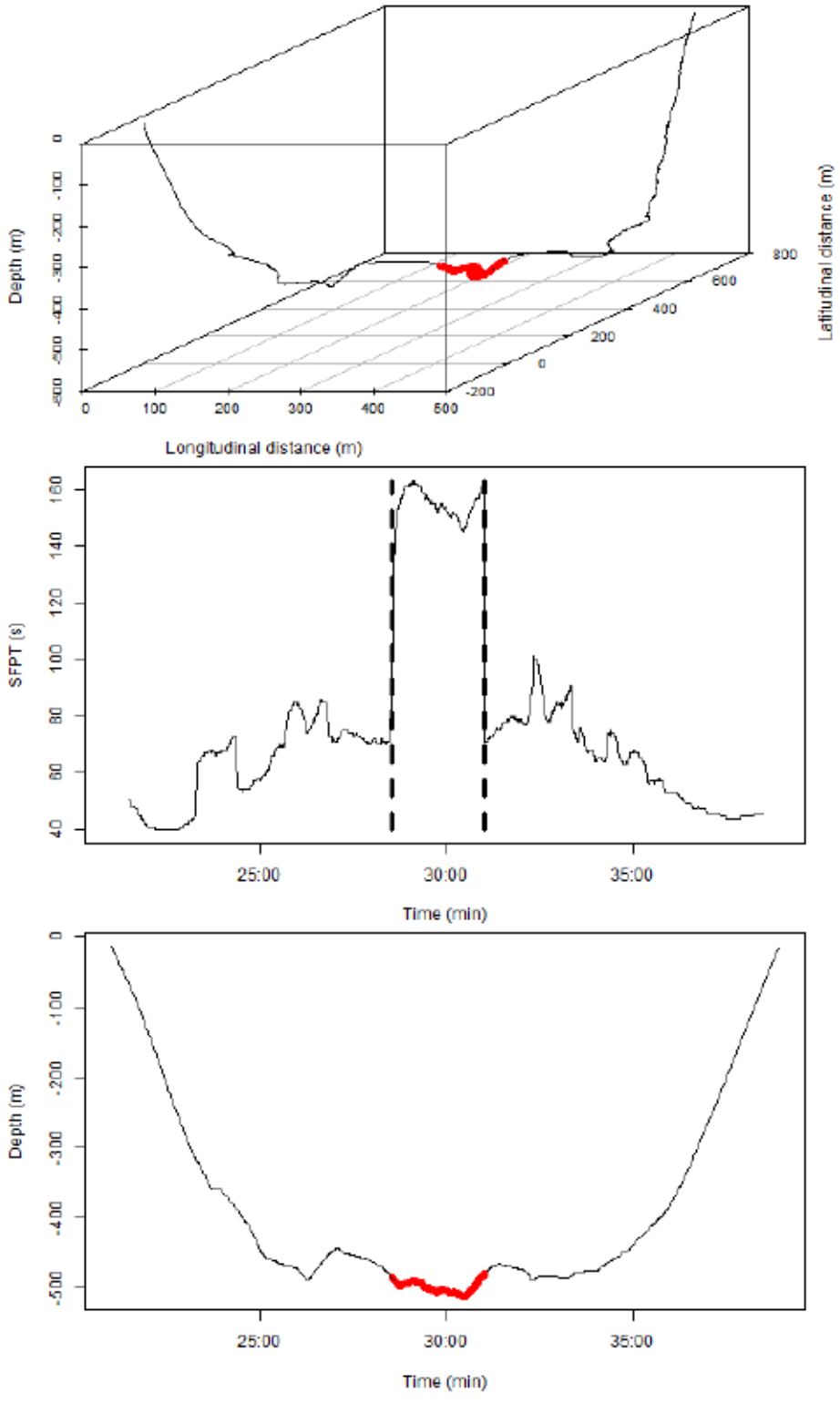

ANNEXE

H

Article 7 : Cazau *et al.* (2017)

7. Cazau Dorian, Bonnel Julien, Jouma'a Joffrey, Le Bras Yves, Guinet Christophe. (2017). Measuring the marine soundscape of the Indian Ocean with Southern Elephant Seals used as acoustic gliders of opportunity. *Journal of Atmospheric and Oceanic Technology*. doi: 10.1175/JTECH-D-16-0124.1

Measuring the Marine Soundscape of the Indian Ocean with Southern Elephant Seals Used as Acoustic Gliders of Opportunity

DORIAN CAZAU AND JULIEN BONNEL

ENSTA Bretagne, Lab-STICC (UMR CNRS 6285), Brest, France

JOFFREY JOUMA'A, YVES LE BRAS, AND CHRISTOPHE GUINET

Centre d'Etudes Biologiques de Chizé, UMR 7372 Université de La Rochelle-CNRS, Villiers-en-Bois, France

(Manuscript received 17 June 2016, in final form 1 September 2016)

ABSTRACT

The underwater ambient sound field contains quantifiable information about the physical and biological marine environment. The development of operational systems for monitoring in an autonomous way the underwater acoustic signal is necessary for many applications, such as meteorology and biodiversity protection. This paper develops a proof-of-concept study on performing marine soundscape analysis from acoustic passive recordings of free-ranging biologged southern elephant seals (SES). A multivariate multiple linear regression (MMLR) framework is used to predict the measured ambient noise, modeled as a multivariate acoustic response, from SES (depth, speed, and acceleration) and environmental (wind) variables. Results show that the acoustic contributions of SES variables affect mainly low-frequency sound pressure levels (SPLs), while frequency bands above 3 kHz are less corrupted by SES displacement and allow a good measure of the Indian Ocean soundscape. Also, preliminary results toward the development of a mobile embedded weather sensor are presented. In particular, wind speed estimation can be performed from the passive acoustic recordings with an accuracy of 2 m s^{-1}, using a rather simple multiple linear model.

1. Introduction

In the frequency band from a few tens of a hertz up to 50 kHz, the dominant sources of ambient noise in the ocean can be broadly divided into sounds resulting from geophony (i.e., sounds from natural physical processes, e.g., wind-driven waves, rainfall, seismicity, breaking waves, current), biophony (i.e., sounds from biological activities, e.g., whale vocalizations, snapping shrimp beds), and anthropophony (i.e., man-made sounds, e.g., commercial shipping, sonar, seismic prospecting, oil and gas surveys) (Knudsen et al. 1948; Wenz 1962). All these sources contribute conjointly to the noise spectrum characteristics (e.g., pressure level, spectral slope) in varying degrees, depending on their strength and conditions prevailing at the measurement location. Thus, the underwater ambient sound field contains quantifiable information about the physical and biological marine environment. To extract this information, passive acoustic systems have been used for monitoring, recording, and interpreting in a continuous and autonomous way the underwater acoustic signal, facilitating an all-weather and all-season ocean monitoring.

The study of ocean ambient noise plays a growing role in many different research fields. In biodiversity, it helps in preserving marine animal ecosystems by better understanding the impacts of human activities on their ecology (Sirovic et al. 2013). In meteorology, global climate models and local weather forecasts rely on field information about weather across oceans. Observations of rain and wind phenomena from underwater noise allow for better study of air–sea interactions, and increase greatly the spatio-temporal resolution provided by satellite (Vagle et al. 1990; Nystuen and Selsor 1997; Ma and Nystuen 2005; Pensieri et al. 2015). In cryogenics, the noise generated by glaciers allows for quantification of melting processes in the Arctic and is a good indicator of rapid climate processes (Urick 1971; Glowacki et al. 2015). In oceanography, measurement and characterization of ambient noise

Corresponding author address: Dorian Cazau, ENSTA Bretagne, Lab-STICC (UMR CNRS 6285), 2 rue François Verny, 29806 Brest CEDEX 09, France.
E-mail: dorian.cazau@ensta-bretagne.fr

DOI: 10.1175/JTECH-D-16-0124.1

are essential to enhance the signal-to-noise ratio of acoustic-based underwater instruments (Rahmati et al. 2014). The need for better assessment of global change and its consequences have drawn attention and highlighted the need for an intense monitoring of underwater noise level and, consequently, for the development of innovative sensors and networks (Duennebier et al. 2002; Johnson and Tyack 2003; Aguzzi et al. 2011; Favali 2013) able to collect and analyze long-term underwater sound data.

Ambient noise studies mostly take place in the northeastern Pacific (Chapman and Price 2011) and Atlantic Oceans (Nieukirk et al. 2004). Previous studies in the Indian Ocean have focused on the northwestern (Wagstaff 2005) and the tropical regions of the Indian Ocean (Miksis-Olds et al. 2013; Hawkins et al. 2014; Tsang-Hin-Sun et al. 2015). Tournadre (2014) showed that the ship traffic has had a global increase in the Indian Ocean in the last two decades. In the Southern Ocean, a recent study highlighted the predominant role of icebergs in the Southern Hemisphere soundscape (Matsumoto et al. 2014). Miksis-Olds et al. (2013) reported that the observed sound floor increases are consistent with concurrent increases in shipping, wind speed, wave height, and blue whale abundance in the Indian Ocean. Nair et al. (2015) developed a semiempirical model to predict surface ambient sound spectra in 1–50 kHz for rainfall rates in 2–200 mm h^{-1} and wind speeds within 2–14 m s^{-1}.

Most often, hydrophones used for marine soundscape studies are bottom mounted, shore terminated, and fixed at a certain depth. Other studies have also used mobile hydrophones, either dragged behind a drifting buoy or boat (Nystuen and Selsor 1997), or attached to vertical profiler float (Ward et al. 2011; Küsel et al. 2011; Barclay and Buckingham 2013). More recently, with the development of miniaturized electronic devices, hydrophones have been embedded in underwater gliders (Baumgartner et al. 2008; Matsumoto et al. 2011; Klinck et al. 2012). These gliders can survey a large area by autonomously navigating the defined area (Rogers et al. 2004; Rudnick et al. 2004), and they have shown great promise in monitoring marine mammals (Baumgartner et al. 2008; Klinck et al. 2012), oceanographic phenomena (Matsumoto et al. 2011), and meteorological surface conditions (Cauchy et al. 2015).

In the same line of technological innovation, the use of animalborne autonomous recording tags, called biologging, is becoming widespread (Ropert-Coudert and Wilson 2005), and allows for the acquisition of huge quantitative datasets for inferences on movement, ecology, physiology, and behavior of animals moving freely in their natural environment. Multichannel dataloggers are used, and data are sampled at high resolution over large temporal and spatial ranges, including geographical areas uncovered by satellite data. In addition to providing parameters related to the animal biological processes, environmental parameters (e.g., temperature, salinity, light, fluorescence) can also be continuously recorded.

In this project, southern elephant seals (SES) of the Kerguelen Islands are used as acoustic gliders of opportunity. SES are wide-ranging animals during their postbreeding and postmoulting migrations. Adult females (*Mirounga leonina*) from the Kerguelen Islands (49°200′S, 70°200′E) forage mainly in oceanic waters of the Antarctic and polar frontal zones (below 60°S) from October to February (Bailleul et al. 2010). Among top marine predators, air-breathing diving species such as SES are particularly well suited for biologging because their large size allows them to carry electronic devices with minimal disturbance. These devices are stuck on SES while they are on land in their breeding colonies. The strong east–west current speeds and the thick ice surface layers in this part of the austral ocean make the use of regular gliders very complicated, while these harsh environmental conditions are not a problem for SES.

So far, these biologged SES have been used to collect measurements of physical (Charrassin et al. 2008; Costa et al. 2008; Roquet et al. 2009) and biological (Guinet et al. 2013) oceanographic parameters, in often inaccessible regions. The SES and their closed-loop migratory route also provide the opportunity for using Acousondes[1] (Acoustimetrics, Greeneridge Sciences, Inc., Felton, California) that can be retrieved at the end of their migration. Acoustic data have already been recorded and used to investigate behavioral and ecophysiological (breathing rate) parameters (Genin et al. 2015). While at sea, SES dive repeatedly to mesopelagic depths (300–500 m up to 2000 m) and tend to follow the diel vertical migration of their mesopelagic prey, diving generally deeper during the day (Guinet et al. 2014). SES regularly perform dives during which they spend a large proportion of time descending passively through the water column (Richard et al. 2014). In the following, this type of dive will be referred to as drift dives.

The main objective of this current study is to demonstrate that marine soundscape can be measured with biologged SES used as acoustic gliders of opportunity. However, the SES movements (e.g., depth/speed variations) impact the measured sound spectra. It is thus first required to identify, characterize, and if possible remove the acoustic noise produced by SES movements that corrupts the measured soundscape. Under the

[1] Acousondes are miniature, self-contained, autonomous acoustic recorder designed for underwater applications.

assumption that different sound sources have unique acoustic signatures, passive acoustics can be used to make a classification of the ambient sound field. In this paper, a multivariate acoustic response in a multivariate multiple linear regression (MMLR) framework is used to decompose the measured ambient noise into different acoustic sources (acting as predictors) related either to the environment or to the SES. The ambient noise is modeled as a multivariate response of spectral parameters, namely, sound pressure levels (SPLs) and spectral slopes (SS), in various frequency bands. These acoustic features have been widely used in studies on marine soundscape and acoustical meteorology (Nystuen and Selsor 1997; Ma and Nystuen 2005; Pensieri et al. 2015). Ancillary datasets on wind speed and on SES diving behavior are used to define the predictors. Once we have fully characterized the acoustic noise induced by the SES displacements, we present results on the measured soundscape, and we focus on the effect of wind speed on the ambient noise level. These measures are compared with those made in other ocean environments at comparable depths, and also with theoretical models.

This paper is organized as follows. Section 1 provides details on acoustic measurements and on the different variables used in the regression framework. Section 2 presents exploratory and qualitative results, with an emphasis on the differences between spectra measured during the drift and active swimming phases of the SES. Then, more quantitative results are presented, in particular to evaluate the accuracy of estimating wind speed from our passive acoustic recordings. Section 3 proposes two general discussions on the relations between the external influence variables and the measured spectra, and on the marine soundscape resulting from our acoustic glider of opportunity.

2. Methods

a. Materials

In the austral winter of 2012, five different postbreeding female SES of similar body conditions were captured and equipped with dataloggers on the Kerguelen Islands. These loggers included an Acousonde 3A device (already used in similar research studies; e.g., Burgess et al. 1998; Burgess 2000) glued on the back of the seal on the longitudinal axis, 10 cm behind the scapula. The Acousonde 3A recorded sound at a sampling frequency F_s of 12.2 kHz with an acoustic sampling resolution of 16 bits, using a built-in low-frequency hydrophone. It also has a high-pass filter at 22 Hz (to remove powerful low-frequency flow noise) and an antialias (low pass) filter at 4640 Hz. The hydrophone response is flat in this band so that overall the useable bandwidth is 22–4640 Hz (more details can be found at http://acousonde.com/faqtechnical.html). Total storage capacity is 64 GB. The unamplified raw sensitivity of the hydrophone is −201 dB (low-power-channel hydrophone) ref 1 V $(\mu Pa)^{-1}$, that is, 0.089 mV Pa^{-1}. There is no onboard signal processing embedded into the Acousonde. The Acousonde's raw data have been converted to pressure data using a MATLAB (MathWorks, Natick, Massachusetts) program provided by Greeneridge Sciences, Inc. (the Acousonde manufacturer). The Acousonde also continuously recorded depth (pressure) and triaxial acceleration with a sampling frequency of 5 Hz.

TABLE 1. Global overview of the passive acoustic recording database, with C as the cumulated duration. Each recording lasts approximately 4 h.

Acousonde	No. of recordings	Period	C (h)
A626019	20	30 Oct–18 Nov 2012	76.4
A626020	13	22 Sep–10 Nov 2012	51.2
A626021	4	30 Oct–2 Nov 2012	16
A626022	5	30 Oct–3 Nov 2012	18.6
A626040	24	31 Oct–23 Nov 2012	95.4

b. Acoustic database

Table 1 provides a global overview of the sound database. The five Acousondes deployed were activated on the field almost at the same time, making their recordings overlap in time. The smaller number of recordings in Acousondes A626021 and A626022 was caused by technological deficiency. To save onboard storage space, a duty cycle was set up in each Acousonde that automatically turned it on for 4 h every 24 h. Each 4-h recording was segmented into 10-s time windows (except for the long-term averaged spectrogram, where we used 30-s time windows), using non-overlapping Hamming windows. We removed all the sound files for which the SES depth was less than 10 m, which includes phases when the SES is on land and phases when the SES is at the surface at sea. All data processing and analysis were conducted using MATLAB. A total of 184.2 h of audio recordings have eventually been used, providing 66 296 observations of 10 s long.

Figure 1 represents the migratory routes followed by the SES during which the Acousondes were active. The spatiotemporal coverage provided by SES routes ranges from 71° to 87° in longitude and from −46° to −52° in latitude.

c. Identification of drift phases

As already done in Dragon et al. (2012), pressure data were used to split the ascent and descent dive phases into two different categories based on diving behavior,

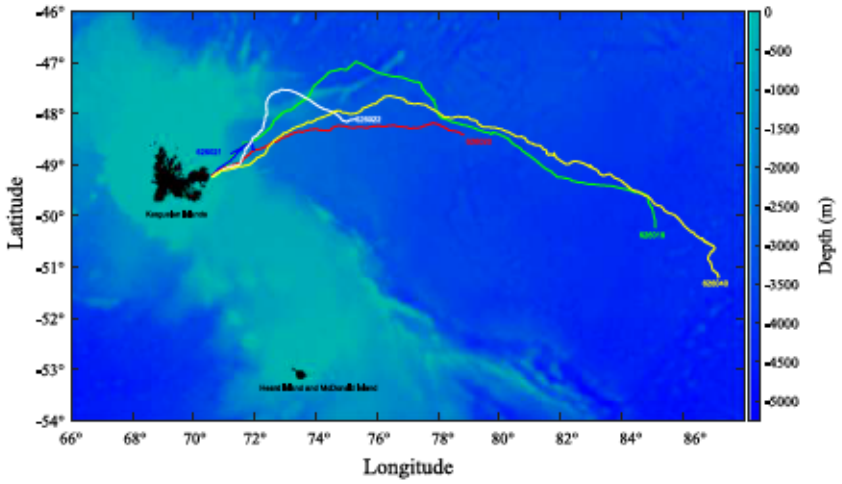

FIG. 1. Migratory routes of five different SES plotted on a map zoomed in on the Kerguelen Islands (49°200′S, 70°200′E), in the Indian Ocean. Details of individual SES are given in Table 1. These trajectories are based on GPS data from an *Argos* GPS satellite tag fixed on each SES. Only the segments of routes during which the Acousondes were active are drawn.

namely, drift dives and active swimming dives. In our study, drift dives are important, as they are expected to offer the cleanest acoustic measures. Drift dive identification was processed in two steps. First, we used first the complete time–depth recorder (TDR), which allowed us to (i) identify drift dives and (ii) isolate the passive drift phases during those dives (Dragon et al. 2012). For each drift dive, a drift rate was determined as the slope coefficient of a linear regression between depth and time (Bailleul et al. 2010; Mitani et al. 2010). In the second step, we used accelerometer data to exclude phases of active swimming during drift phases assessed by the TDR-only data. Active swimming was considered to take place when lateral acceleration exceeded the -0.2 to $0.2\,\mathrm{m\,s^{-2}}$ range. It is noteworthy that a more detailed taxonomy could have been used [e.g., Richard et al. (2014) subdivided the active swimming dives into exploratory dives, shallow active dives, and deep active dives], but in this paper diving characteristics of the SES will be limited to this two-class behavior, for the sake of clarity and conciseness with our acoustical meteorology application.

Table 2 provides statistical information on three different dive phases of SES, namely, surface, drifting, and active swimming phases. The R package Biologging tools[2] were used to estimate automatically the drift phases of SES. Drift phases have an average duration of 2 min. Overall, they cover only 6% of the total recording period, with a higher presence of more active swimming dives (83%). These estimated drift phases have already been used in previous biological studies (Vacquié-Garcia et al. 2012; Guinet et al. 2014; Richard et al. 2014; Genin et al. 2015).

d. Regression variables

Table 3 presents details on the different variables used in the regression analysis. They are detailed in the following.

1) ACOUSTIC VARIABLES

Each 10-s time series has been fast Fourier transformed (FFT) to obtain a 512-point power spectrum. Each spectrum is integrated on one-third octave frequency bands. The SPLs averaged over the one-third octave subband centered around f_c kHz, and the SS between the frequencies f_1 and f_2, have been extracted from the measured spectra; they are labeled SPL(f_c) and SS(f_1-f_2), respectively. SPL measures are computed as

$$\mathrm{SPL}(f_c)^{(m)} = 10\log_{10}\left[\frac{1}{p_{\mathrm{ref}}^2}\sum_{f=f_{\mathrm{lower}}}^{f=f_{\mathrm{upper}}}\frac{P^{(m)}(f)}{B}\right], \quad (1)$$

TABLE 2. Statistics on dive phases, with D as the mean phase duration, C as the cumulated duration, and P_{tot} as the percentage over total acoustic recordings.

Dive phases	D (min)	C (h)	P_{tot} (%)
Surface	2.5	42.5	11
Drift phases	2	22.9	6
Active phases	3	311.8	83

[2] Developed by Yves le Bras (CEBC-CNRS-UMR 7372 Université de La Rochelle, Chizé, France) and available at https://github.com/SESman/rbl.

TABLE 3. Details of variables used in the regression analysis, classified into four categories: acoustics, SES displacements, SES status dive, and environment. All center frequencies f_c in the SPL descriptors have been rounded to a multiple of 10 for clarity in the notation.

Variable categories	Variable description	Variable labels	Units
Acoustics	Sound pressure levels	SPL(0.05), SPL(0.2), SPL(0.5), SPL(1), SPL(1.6), SPL(2.5), SPL(3.2), SPL(4)	dB
	Spectral slope	SS(1–2.5), SS(2.5–4)	dB f^{-1}
SES displacements	Speed	V	m s^{-1}
	Triaxial acceleration	a_x, a_y, a_z	m s^{-2}
	Depth	d	m
Environment	Wind speed	W	m s^{-1}

where $f_{\text{lower}} = f_c 10^{1/20}$ and $f_{\text{upper}} = f_c 10^{(-1)/20}$, $p_{\text{ref}} = 1\ \mu$Pa, and B is the noise power bandwidth of the window function ($B = 1.36$ for a Hamming window). The power spectrum $P^{(m)}(f)$ is defined as

$$P^{(m)}(f) = 2\left|\frac{X^{(m)}(f)}{N}\right|^2, \tag{2}$$

where $X^{(m)}(f)$ is the FFT of the mth segment, given by

$$X^{(m)}(f) = \sum_{n=0}^{N-1} x_{\text{win}}^{(m)}[n] e^{(-i2\pi fn)/N}, \tag{3}$$

where x_{win} is a windowed segment of a time series. SS are calculated using a least squares fit to the SPLs over the specified frequency band. After correlation analysis, it appeared that strong correlations exist between different pairs of acoustic features, implying that knowledge of one necessarily implies knowledge of the other. Then, to reduce the dimension of the acoustic feature vector, we kept only the SPL(f_c) measures per octave and the two slopes that maximize the Pearson correlation coefficient with the regression variables SES and Environment presented in sections 2d(2) and 2d(3), respectively. The acoustic descriptors resulting from this process, listed in Table 3, form a ten-dimensional feature vector over all the observations consisting of the following descriptors: {SPL(0.05), SPL(0.2), SPL(0.5), SPL(1), SPL(1.6), SPL(2.5), SPL(3.2), SPL(4), SS(1–2.5), SS(2.5–5)}. In the following, all f_c values have been rounded to a multiple of 10 for clarity in the notation, and all sound pressure levels are given in dB ref μPa^2.

2) SES DISPLACEMENTS

The raw triaxial acceleration data from the accelerometer of the Acousonde 3A were used and labeled a_x, a_y, and a_z (longitudinal, lateral, and vertical axes, respectively). To estimate swimming speed V, we first need to compute the pitch θ of the seal, defined as the angle θ between the SES body direction and the horizontal, that is,

$$\theta = \arctan\left(\frac{a_x}{\sqrt{a_y^2 + a_z^2}}\right). \tag{4}$$

As explained in Sato et al. (2003) and Aoki et al. (2011), the acceleration data used to compute the pitch using Eq. (4) have been filtered with a low-pass filter at 0.2 Hz in order to isolate the gravity component of the movement. Then V was computed by combining information on the vertical speed and the seal pitch as follows:

$$V = \frac{U_{\text{vert}}}{\sin(\theta)}, \tag{5}$$

where U_{vert} corresponds to the vertical speed (as determined from the depth recorder) of the SES, and V corresponds to the vertical speed corrected by the orientation of the SES given by its pitch. As already reported in past studies (Miller et al. 2004; Richard et al. 2014; Genin et al. 2015), this method is reliable only for steeper body angles (with an absolute body pitch over 30°). As a result, we use this proxy for deep descents and ascents, that is, ending and starting below 400 m deep, respectively, and with an absolute pitch over 30°. Eventually, the variable depth d is directly read from the TDR, with negative values below the ocean surface. Figures 2a–c represent the histograms of speed, acceleration, and depth data, respectively, matched with the analyzed passive acoustic recordings. As expected, higher extrema values of speed and rms acceleration (labeled rms $-$ a) are obtained for active swimming periods (going from a range of [0.15–2] m s^{-1} and [0–6] m s^{-2} to [0.7–3] m s^{-1} and [0–10] m s^{-2}, respectively, for the drift and active swimming phases, respectively), while depth and wind speed are reasonably well balanced between the two categories.

3) ENVIRONMENT

The dataset on wind speed was extracted from the Advanced Scatterometer (ASCAT) retrievals[3] and

[3] Available at ftp://ftp.ifremer.fr/ifremer/cersat/products/gridded/MWF/L3/ASCAT/Daily/Netcdf/.

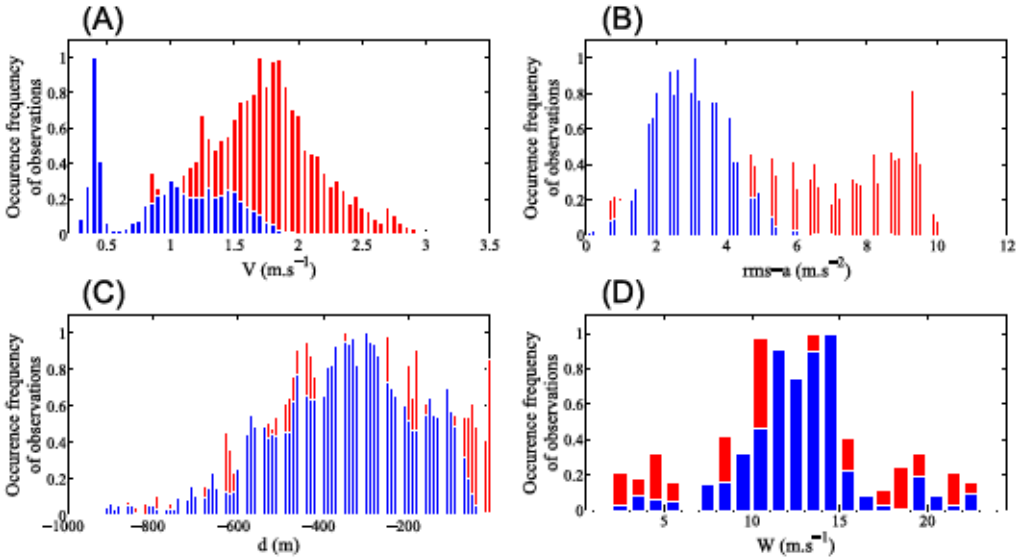

FIG. 2. Histograms of (a) SES swimming speed, (b) acceleration, (c) depth, and (d) wind speed data matched with the analyzed passive acoustic recordings. Each histogram has been individually unitary normalized. Each observation is labeled either as a drift phase (blue) or an active swimming phase (red).

provided gridded daily-averaged wind and wind stress fields over global oceans (Bentamy and Croize-Fillon 2012). The calculation of daily estimates uses ascending and descending available and valid retrievals. The objective method aims to provide daily-averaged gridded wind speed, zonal component, meridional component, wind stress, and the corresponding components at global scale. The error associated with each parameter, related to the sampling impact and wind space and time variability, is provided too. When compared with buoy measurements, this error for wind speed is below 2 ms^{-1} (Bentamy and Fillon 2015). More details about data, the objective method, and computation algorithm can be found in Bentamy and Croize-Fillon (2012). The European Centre for Medium-Range Weather Forecasts (ECMWF) analyses have been used as a temporal interpolation basis of ASCAT retrievals. The resulting fields are 10 m high above the ocean surface, and have spatial resolutions of 0.25° in longitude and latitude, and a 3-h temporal resolution.

An acoustic measurement is a spatially integrated measure, with an area of measurement at the ocean surface (also called the listening area in literature) that depends on the hydrophone depth and on the beam pattern of the ambient noise field. The listening area of a 500-m-depth hydrophone is around 8 km^2 (Nystuen et al. 2015), which is well included in the satellite pixel resolution (around 30 km^2 at the SES latitudes).

Figure 2d represents the histogram of wind speed data matched with the analyzed passive acoustic recordings. From operational point of view, it is more significant to provide the correct classification of wind speed class than wind speed estimates. We thus identified from these data four different classes of wind speeds, labeled W_1 (below 7.5 ms^{-1}), W_2 (between 7.5 and 12.5 ms^{-1}), W_3 (between 12.5 and 17.5 ms^{-1}), and W_4 (higher than 17.5 m s^{-1}). Each class corresponds to an average increase of 5 ms^{-1} in wind speed, except for classes W_2 and W_3. These classes correspond roughly to the sea states of the Beaufort scale from 2 to 5 (light wind) for W_1, from 6 to 7 (high wind) for W_2 and W_3, and from 8 to 9 (gale wind) for W_4 (Knudsen et al. 1948). Sea state 1 has not been used, as noise produced by weak wind speed is too low to be detected (Pensieri et al. 2013).

e. *Multivariate multiple linear regression*

1) MODEL FORMULATION

MMLR is a common statistical tool that informs about the linear relationship between dependent variables (i.e., the response) and independent variables (i.e., the predictors). With multiple response variables available, as in our case, the standard approach to modeling them is to regress each response variable separately on the same set of explanatory variables. However, although it is simple and popular, this univariate response approach may not be optimal, since they do not utilize the joint information among response variables. To solve this multiresponse regression problem, Breiman and Friedman (1997) proposed a method, called the curd

and whey, that uses the relationship among response variables to improve predictive accuracy. They showed that their method can outperform separate univariate regression approaches when there are correlations among the response variables. The multivariate general linear model is

$$\underbrace{\mathbf{Y}}_{(n,r)} = \underbrace{\mathbf{X}}_{(n,p+1)} \underbrace{\boldsymbol{\beta}}_{(p+1,r)} + \underbrace{\mathbf{E}}_{(n,r)}, \quad (6)$$

where $\mathbf{Y}$ is a matrix of n observations on r response variables. The $\mathbf{X}$ is a model matrix with columns for p regressors, including an initial column of ones for the regression constant, also called intercept. The $\boldsymbol{\beta}$ is a matrix of regression coefficients, one column for each response variable. The $\mathbf{E}$ is a matrix of errors that follows a Gaussian law $N(0, \sigma^2)$. Each response (dependent variable) gets its own linear equation of the form $\mathbf{Y}_r \sim \beta_{0p} + \sum_{p=1}^{P} \beta_{rp}\mathbf{X}_p + E_{n,r}$, conjointly estimated along with the other responses, and depending only on the predictors (independent variables), whose contributions are weighted by the regression coefficients β_{rp} (Breiman and Friedman 1997).

Parametric nonlinear models also exist, and represent the relationship between a continuous response variable and one or more continuous predictor variables in the form $\mathbf{Y} = f(\mathbf{X}, \beta) + \mathbf{E}$, where f is any function of $\mathbf{X}$ and $\boldsymbol{\beta}$ that evaluates each row of $\mathbf{X}$ along with the vector $\boldsymbol{\beta}$ to compute the prediction for the corresponding row of $\mathbf{Y}$.

In regression analysis terms, two noncorrelated predictors used in combination would predict unique variance in a response, while two more correlated predictors tend to predict shared variance, and so are less efficient. Prior to MMLR, a principal components analysis (PCA) can then be used to decorrelate predictors. PCA is a dimension reduction method that constructs independent new variables that are linear combinations of the original variables, by reducing redundancy (i.e., increasing standard deviation) between all variable dimensions. PCA was performed to see how our different SES and environmental variables were structured within the dataset, and whether the acoustic variables were responding to this structure. PCA also avoids multicollinearity problems in regression analysis (Zhang et al. 2006). Such problems make regression coefficients become unstable when highly correlated predictors are present. This further justifies the use of PCA in our study.

In this project, two different setups of the MMLR method were used. We first studied the contributions of SES and environment variables (i.e., the predictors $\mathbf{X}$, with $p = 6$) in the multivariate acoustic response characterizing the measured spectra (i.e., the responses $\mathbf{Y}$, with $r = 10$) over all 10-s observations ($n = 66\,296$). Here, predictors are the different physical processes contributing independently to the distribution of acoustic energy in the measured spectra. In the second application, we evaluated the classification accuracy of an MMLR on PCA-processed acoustic measures ($p = 10$) in predicting wind speed ($r = 1$).

Also, all variables were standardized (i.e., zero mean and unitary variance), which allows a better comparison of regression weights between each predictor (especially with variables having different range values, as for depth and wind speed in our study), as the unstandardized weights are a function of the variance of the predictor variables. Standardization removes most of the correlation between linear and higher-order terms, which reduces the chance of adding these terms unnecessarily.

2) EVALUATION METRICS

To assess quantitatively the quality of our regression analysis and estimation, we provided as evaluation metrics the p value and the multiple correlation coefficient squared [ordinary R^2 (%)], also called the coefficient of determination. To further evaluate the impacts of each predictor in the MMLR model, we performed a sequential significance testing of each dependent variable through the metric ΔR_a^2, defined as

$$\Delta R_a^2 = \frac{|R_a^2 - R_a^2(-p)|}{R_a^2}, \quad (7)$$

where R_a^2 refers to the adjusted R^2 metric, and $R_a^2(-p)$ refers to the adjusted R^2 metric obtained with an MMLR performed without the predictor p. This amount of change in R^2 is a measure of the increase in predictive power of a particular dependent variable, given the dependent variable or variables already in the model. In other words, this metric allows for performing significance testing to determine whether the addition of another dependent variable to the regression model significantly increases the value of R^2. Also, the ordinary R^2 value systematically increases with the addition of terms to the regression model; consequently, in order to compare models with different numbers of predictors, we use the adjusted R^2 metric.

3. Results

a. *Exploratory data analysis*

Figure 3 shows a typical long-term spectral average computed over four acoustic recordings (i.e., a total of 16 h of recordings from four different days) from the SES individual A626019. SES variables and wind speed values are superimposed onto this spectrogram. It can

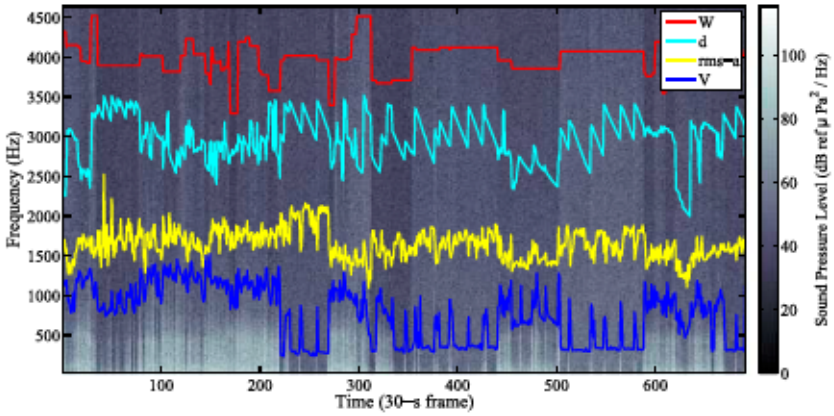

FIG. 3. Long-term spectrogram averaged over four acoustic recordings (i.e., a total of 16 h of recordings from four different days) from SES A626019. It was generated using 2048-point FFTs, Hamming windows, and no overlap, and averaged every 30 s. The four variables V, rms $-$ a, d, and W are superimposed onto the spectrogram with relative linear scales ranging from 0.3 to 2.7 ms^{-1}, 0.2 to 10 ms^{-2}, -150 to 600 m, and 4 to 18 $m\,s^{-1}$, respectively.

be seen that the drift and active swimming phases are clearly identified through the acoustic energy in low-frequency bands that correlate well with the SES speed. Also, acoustic energy in higher-frequency bands appear to be reinforced with higher wind speed, independently from other SES-related variables. In other words, two frequency regions of the spectra are mainly impacted, showing first strong evidence of correlations: a first region in frequency subbands below 2.5 kHz, modulated accordingly to SES speed, and a second region above this frequency that is more dominated by wind speed.

To provide more details on the shape of spectra measured during drift phases, Fig. 4 represents an averaged spectrum computed during temporal phases with values of SES speed and acceleration belonging to their 5th percentiles. In the following, these phases will be referred to as extreme drift phases. Also, this averaged spectrum will be associated with our measured soundscape. Regarding median levels across this acoustic dataset, they ranged between 47 and 70 dB ref $1\,\mu Pa^2\,Hz^{-1}$. The spectrum slope falls off quickly from its highest level at 50 Hz at a rate of about -5 dB per octave up to

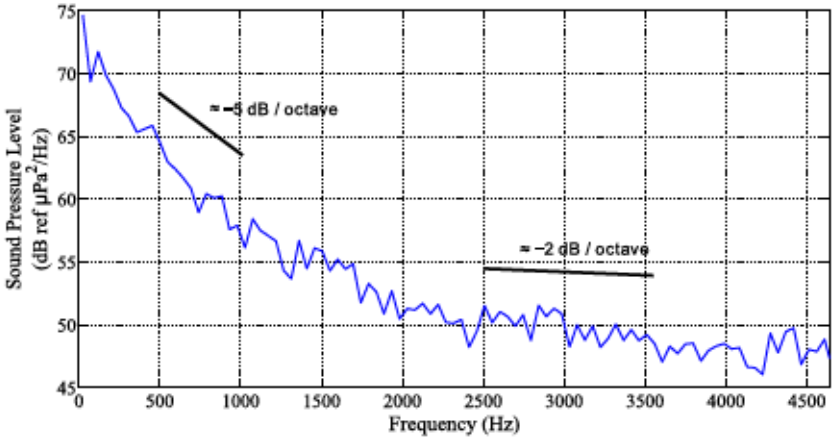

FIG. 4. Averaged spectrum computed during extreme drift phases, i.e., with values of SES speed and acceleration belonging to their 5th percentile. Two representative theoretical SS (dB per octave) are superimposed onto the spectrum. The approximate signs mean that these slopes are only locally correct in frequency (i.e., the first slope is a decrease of -5 dB within the octave 500–1000 Hz, and the second slope is a decrease of -2 dB within the octave 2500–5000 Hz).

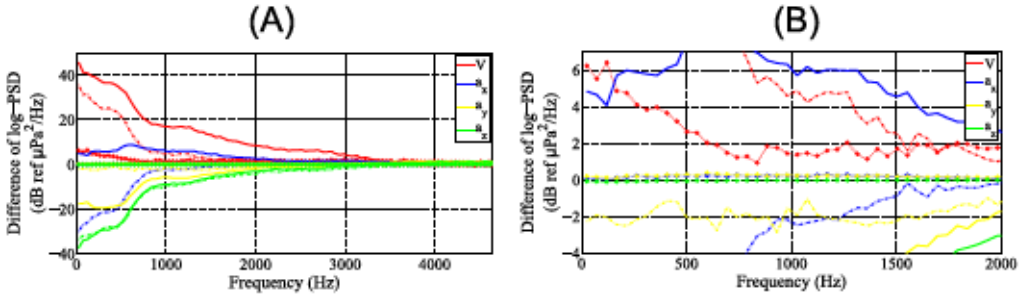

FIG. 5. Differences between averaged logarithmic PSD with values of SES speed and acceleration belonging to their 20th, 60th, and 95th percentiles (dot-plus-circle, dashed–dotted, and solid lines, respectively), and their 5th percentile. (a) The full spectrum, (b) a zoomed-in view of the frequency range [10; 2000] Hz and level range [−8; 8] dB.

2 kHz, where it becomes flatter up to 5000 Hz, assuming a slope of −5 dB per octave.

We then quantified the averaged deformation of spectra due to SES displacements relative to this extreme drifting behavior. In Fig. 5, we computed the differences between averaged logarithmic power spectral density (PSD) with values of SES speed and acceleration belonging to their 20th, 60th, 95th percentiles (dot-plus-circle, dashed–dotted, and solid lines, respectively), and their 5th percentile. From Fig. 5a, we can observe that SES speed strongly impacts the acoustic data for frequencies lower than 2000 Hz, with variations that can reach 40 dB. The three acceleration components contribute to an increase in the measured noise below 800 Hz, with gains from −30 to −10 dB. From Fig. 5b, it can be observed from the dashed–dotted curves that the acoustic distortions from our marine soundscape spectrum above (see Fig. 4) are quite minimal, that is, in the order of magnitude of 5 dB with the SES speed and less than 1 dB with the acceleration variables. Also, we did not find any significant influences of depth on the acoustic features (see Fig. A1).

b. *Correlation analysis*

To provide a more global insight into the correlation structure of our variables, we performed a PCA on the complete variable dataset. Figure 6 shows both the orthonormal principal component coefficients of each variable on the first two principal axes and the principal component scores for each observation (i.e., the coordinates of the original data in the new coordinate system defined by the principal components). In the space of the principal components of the acoustic/SES/environmental variables, the first two principal components distinctly separate the different acoustic features. Indeed, these features move from the first to the second principal axis as their center frequencies increase. In other words, low-frequency SPL observations remain in the bottom-right half-space, while the higher-frequency SPL observations are in the top-right half-space. We can now see how SES and wind speed variables distribute on the fan of SPL values. SES speed V is among low-frequency SPLs with a high score on the first PCA axis and a negative score on the second axis ($PCA_1 = 0.3$; $PCA_2 = -0.1$), while wind speed W contributes much more to the second PCA axis ($PCA_1 = -0.02$; $PCA_2 = 0.48$). The discriminative power over wind speeds with this PCA analysis is revealed by color mapping different classes of wind speed, W_1 to W_4 (defined in section 3) in Fig. 6. This plot illustrates the

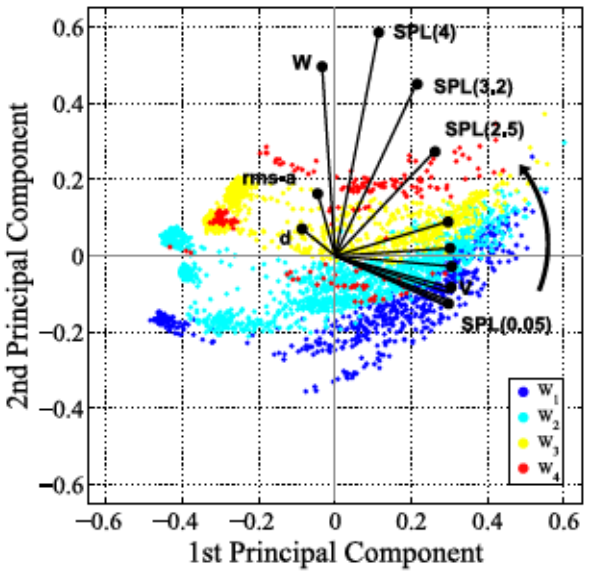

FIG. 6. Orthonormal PCA for each variable (blue lines), and the principal component scores for each observation resulting from the PCA in the first two PCA axes. For the sake of clarity, all the SPL acoustic features are located at their respective black bullet in increasing order, as illustrated by the black arrow. Also, observations are classified into four different classes of wind speeds, W_1–W_4, with different colors.

TABLE 4. Results of the MMLR model for the multivariate acoustic response. SES and environmental variables are taken as predictors. Results are reported in terms of regression coefficients, p values, ordinary R^2, and ΔR_a^2, as described in section 2. All numerical values have been rounded to the closest hundredth. Most significant regression results are in bold, and their P values are labeled with superscript letters.

	Regression coefficients							Ordinary R^2 (%)	ΔR_a^2					
	β_0	V	a_x	a_y	a_z	d	W	All	V	a_x	a_y	a_z	d	W
SPL(0.05)	0.1	**0.33**[a]	0.09	0.11	0.07	−0.02	−0.01	88	**0.76**[b]	0.12	0.1	0.11	<0.01	<0.01
SPL(0.2)	0.13	**0.35**[a]	0.1	0.13	0.08	0.04	0.03	83	**0.74**[b]	0.06	0.03	0.08	<0.01	<0.01
SPL(0.5)	0.04	**0.37**[a]	0.09	0.05	0.04	0.03	0.04	76	**0.88**[b]	0.04	0.02	0.06	<0.01	<0.01
SPL(1)	0.21	**0.24**[c]	−0.03	0.07	0.04	0.07	0.05	54	**0.66**[b]	0.04	0	0.05	0.01	0.1
SPL(1.6)	0.36	**0.17**[c]	0.02	0.03	0.05	0.04	0.07	51	**0.54**[b]	0.01	<0.01	0.02	0.08	0.26
SPL(2.5)	0.3	0.05	0.03	0.01	0.01	−0.01	0.08	45	0.37	0.09	<0.01	<0.01	0.1	**0.41**[b]
SPL(3.2)	0.74	0.04	0.04	0.04	0.02	0.02	**0.15**[c]	37	0.23	0.04	<0.01	<0.01	<0.01	**0.78**[b]
SPL(4)	0.8	0.03	0.01	0.02	0.01	−0.01	**0.16**[a]	41	0.19	0.1	<0.01	<0.01	0.02	**0.84**[b]
SS(1–2.5)	0.42	0.06	0.01	0.05	0.04	0.07	0.08	63	0.34	0.11	0.07	0.05	0.07	0.54
SS(2.5–4)	0.21	0.05	0.02	0.04	0.01	0.04	**0.11**[c]	45	0.26	<0.01	0.04	0.03	0.01	0.72

[a] $P < 0.01$.
[b] $P > 0.05$.
[c] $P < 0.05$.

positive correlation of wind speed over the second PCA axis. These first two principal components explained 80% (first component, 60%; second component, 20%) of the total variable variance.

These correlation tendencies were already highlighted through individual pairwise correlations between the acoustic, SES, and environmental features (see appendix B). To further compare the contributions of SES and environmental variables to the measured spectra, a multivariate regression analysis was eventually conducted. Previous correlation analysis (section 1) showed that our acoustic responses are at least moderately correlated, which is necessary for the multivariate regression analysis to make sense. Also, our acoustic database is assumed to be large enough so this analysis is reliable. We then modeled the multivariate ten-dimensional acoustic response with an MMLR model, and used SES and environment parameters as independent predictors. Table 4 shows the details of this analysis, with the regression coefficients β set up in the multivariate regression equations of the model displayed in the first column, and the evaluation metrics ordinary R^2 and ΔR_a^2 in the other two columns. The same results as in the previous analysis are reached, with this clear duality between the variables SES and wind speeds in explaining acoustic feature variations, largely dominating the other variables of SES depth and acceleration.

SES speed has coefficients at least around 10 times as superior as the other predictors in the response from SPL(0.05) to SPL(0.2). Wind speed becomes prevalent in the higher-frequency SPL responses, which is consistent with the correlation analysis results above. Above SPL(3.2), the coefficients of wind speed are at least around 4 times as superior as the other variables, and as high as 10 times for SPL(4). The acoustic response SPL(4) is predicted by the equation $\mathrm{SPL}(4) = 0.8 + 0.03 \times V + 0.01a_x + 0.02a_y + 0.01a_z - 0.01 \times d + 0.16 \times W$. Also, 41% of the variance in the measure of SPL(4) can be explained by measures of all predictors, with a relative contribution of the wind speed equal to 0.84. Observing the R^2 values, it can be stated that the model better fits the low-frequency data through the SES speed. Regarding depth and acceleration, their contributions remain quite constant in the different acoustic responses and are largely dominated by either the SES speed or the wind speed.

c. *Wind dependence of ambient noise*

1) QUALITATIVE OBSERVATIONS

In Fig. 7, passive acoustic recording spectra have been median averaged on the basis of our four wind speed classes, W_1–W_4, for the drift (Fig. 7a) and active swimming (Fig. 7b) phases. We superimposed onto these spectra the Wenz curves (Wenz 1962), expressed by

$$\mathrm{SPL}(f, U) = \alpha - 5\log_2(f) + 5\log_2(U), \qquad (8)$$

where we used the median of each wind speed class for the value of U, and arbitrarily set α so the first curve fits the first class W_1. Note that because of α, Eq. (8) does not depict exactly Wenz curves. Adding an offset is necessary, probably because the global ambient noise level is site specific. The Wenz curves state that doubling frequency reduces the noise level by 5 dB, and that doubling wind speed (in kt; $1\,\mathrm{kt} = 0.51\,\mathrm{m\,s^{-1}}$) increases the noise level by 5 dB. In Fig. 7, we can see that the averaged measured spectra follow the Wenz predictions. This is particularly true for frequencies above 2.5 kHz, both in terms of noise level (i.e., SPL increases of +5, 3, and

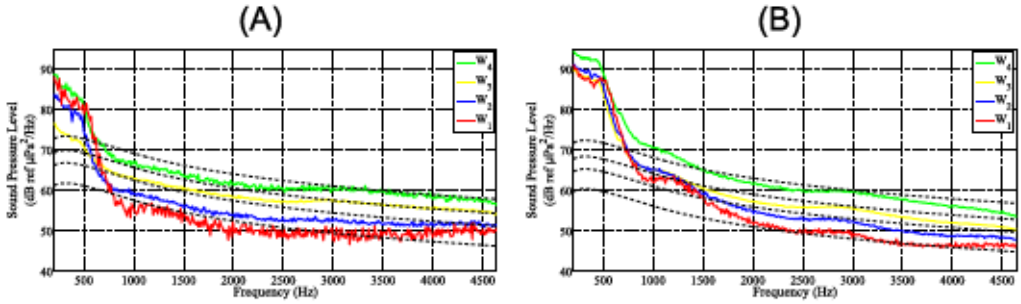

FIG. 7. Representation of four averaged ambient noise spectra corresponding to the different wind speed classes, W_1–W_4, for the (a) drift and (b) active swimming phases. The superimposed black dotted curves correspond to the Wenz curves, computed with the center wind speed value of each interval.

2.5 dB between our four classes at a given frequency) and in terms of spectral slope (for a given wind speed). Differences can also be observed between the measured spectra of the drift and active swimming phases, with a better fit to the Wenz curves for the drift phases. But still a strong discrimination is noticeable between the spectra of the different wind speed classes for both active swimming and drifting behavior.

2) QUANTITATIVE VALIDATION

In a further experiment, a sample fitting verification was performed to testify the effectiveness of different regression classifiers to predict wind speed. These classifiers were tested on a drift-only dataset and on the complete dataset. A fivefold cross validation with a stratified procedure has been applied to each dataset, meaning that each fold contains roughly the same proportions of observations from the different wind speed classes.

As listed in the first column of Table 5, we first tested a simple linear regression model, using the SPL(4) as the single predictor. This descriptor was the most correlated acoustic feature with wind speed ($r = 0.67$, $P < 0.001$, from Fig. B1). We also tested a multiple linear model and a nonlinear regression model, using as predictors the first three principal axes of a PCA performed on the ten-dimensional acoustic vector, labeled PCA_1, PCA_2, and PCA_3, respectively.

As an evaluation metric, we use the rms difference ε_{ws} between the ground truth and the estimated wind speed. The average error $\overline{\varepsilon_{ws}}$ was then computed on the resulting errors in each fold. We also report the median absolute deviation on these tests to assess the statistical significance of our experiments.

An example of wind speed prediction is represented in Fig. 8a using the multiple linear regression model superimposed onto the ground truth. Figure 8b represents the fitting plot of the adjusted model, showing that the model as a whole is significant (i.e., a horizontal line does not fit between the confidence bounds). The slope of this line is the slope of a fit to the predictors projected onto their best-fitting direction—in other words, the norm of the coefficient vector. Wind speed values are displayed in unstandardized (natural) units.

Table 5 displays for each regression model the average error $\overline{\varepsilon_{ws}}$ and coefficient R^2, differentiating the drift and active swimming phases. The regression equations (with their standard deviation over the folds) set during training and used for prediction are $4.74(\pm0.02) + 0.6(\pm0.03)\dot{S}PL(5)$ and $9.6(\pm0.002) + 0.01(\pm0.002)PCA_1 + 0.51(\pm0.006)PCA_2 - 0.42(\pm0.001)PCA_3$ for the simple linear model and the PCA-based multiple linear regression model, respectively. Globally, the classification performance with our models was very satisfactory, with ε_{ws} ranging from 1.9 to 3.4 m s^{-1}. The best-performing model for the drift phases was the PCA-based multiple linear regression model, although no major improvement was brought by any of our classifiers regarding the simple linear regression model. Indeed, taking the complete ten-dimensional

TABLE 5. Performance of different regression classifiers to estimate wind speed. Performance is reported in terms of the wind speed estimation error $\overline{\varepsilon_{ws}}$ (m s^{-1}), with its standard deviation.

Classifiers	Drift phases		Active swimming phases	
	$\overline{\varepsilon_{ws}}$ (±std dev) (m s^{-1})	Ordinary R^2	$\overline{\varepsilon_{ws}}$ (±std dev) (m s^{-1})	Ordinary R^2
Simple linear regression	2.2 ± 0.6	54	3.4 ± 0.8	74
PCA-based multiple linear regression	1.9 ± 0.3	63	2.7 ± 0.3	81
PCA-based nonlinear regression	2.1 ± 0.4	58	2.6 ± 0.5	65

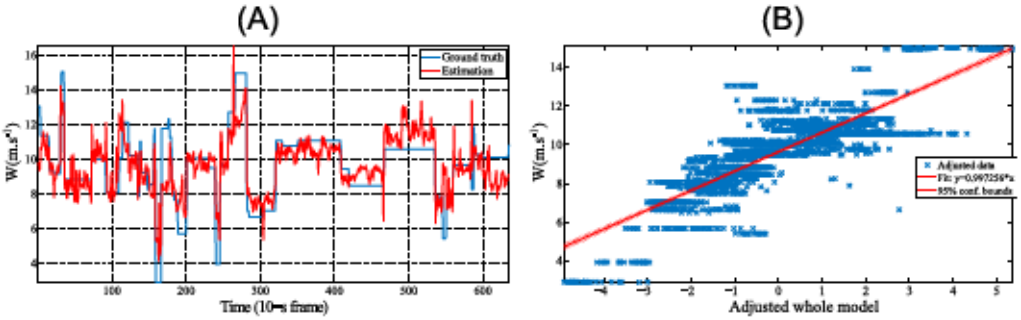

FIG. 8. Predictions of wind speeds obtained with an MMLR model, taking acoustic features as predictors. (a) The ground truth (blue) and the rms error of the model (orange) are superimposed. (b) The fitting plot of the adjusted model is represented.

acoustic feature vector instead of one single SPL feature only reduces ε_{ws} from 2.2 to $1.9^{-1}\,m\,s^{-1}$. Similarly, the increase in model complexity with the nonlinear model did not induce noticeable performance improvement, reducing ε_{ws} from 2.2 to $2.1^{-1}\,m\,s^{-1}$. For the active swimming phases, the use of more complex models brought more significant improvement, reducing the average error ε_{ws} from 3.4 to $2.7^{-1}\,m\,s^{-1}$ and 3.4 to $2.6^{-1}\,m\,s^{-1}$ for the multiple linear and nonlinear regression models, respectively, in reference to the simple linear regression model. For these phases, the multiple linear model includes a more complete modeling of the full spectrum that is beneficial to wind speed estimation. Also, we can note that the PCA-processed acoustic features stabilize wind speed predictions between the different folds.

4. Discussion

Our correlation and regression analysis allowed us to detail the acoustic contributions of different explanatory variables in the overall measured spectra. These variables depend on either the SES (displacements and dive types) or the environment. Our results show that the variables of SES swimming speed and acceleration impacted mostly low-frequency SPLs, with regression coefficients decreasing with the increase of SPL center frequencies (see Table 3). These high low-frequency SPL values most likely result from the turbulent flow noise generated by the SES body when moving in the fluid. Indeed, the turbulence of a flow is characterized by its Reynolds number, which mainly depends on a representative dimension of solid-fluid contact, and the speed of the solid. For the SES, the solid dimension D_h is taken as the dimension of the head, that is, 0.2 m, and with V between 1 and 3 $m\,s^{-1}$. The Reynolds number can then be computed as

$$R = \frac{\rho V D_h}{\mu} \approx 4 \times 10^5 \qquad (9)$$

with $\rho = 1000\,kg\,m^{-3}$ as the water density (rough approximation of the depth-dependent density of ocean water that is denser) and $\mu = 1$ cP is the water viscosity. For Reynolds numbers higher than 16000, a fully developed turbulent flow field is generated around the hydrophone, since the pressure fluctuations in the surrounding fluid are in direct contact with the active area of the hydrophone. As shown in specialized literature (Tennekes and Lumley 1972; Van Dyke 1982), for frequencies in the inertial subrange, the energy spectrum of turbulence is expected to scale with frequency as $f^{-5/3}$, which is equivalent to a spectral slope of −17 dB decade^{-1}. To fully validate the hypothesis of a turbulent flow-generated noise, a comparison of the averaged spectra slope during active swimming phases and the theoretical slope of a chaotic flow noise, following a frequency decrease in $f^{-5/3}$, was performed over the band frequency ranging from 10 to 1000 Hz. A Pearson correlation of $r = 0.86$ ($P < 0.0001$) was found and then showed good agreement with turbulent self-noise. The effect of flow turbulence on the acoustic recordings has already been studied in previous studies. Barclay and Buckingham (2013) proposed a postprocessing method to remove from the computation of spatial coherence the contributions of pseudosound, while Burgess et al. (1998) showed that flow noise could be used as a proxy for the hydrophone carrier speed.

As SES speed and acceleration are highly reduced during drift phases (a strong negative correlation coefficient between drift phases and V, $r = -0.95$, $P < 0.0001$), the self-noise due to pressure fluctuations around the hydrophone is also reduced (Burgess et al. 1998). This tendency has already been documented in different moving hydrophone situations, like with vertical profilers (Barclay and Buckingham 2013). These drift phases then provide clean experimental conditions for acoustic analysis, with a domination of environment-related acoustic events over SES variables.

The SES depth d was seen to have much minor effects on the measured spectra, with regression coefficients inferior to 0.4 ($P < 0.0001$) over the different acoustic descriptors. This result can be explained easily. Indeed, the SES explanatory variables impacting the spectra are directly linked to the SES, and so independent from its depth. Also, our main explanatory variable for the environment, the wind speed, is assumed to be a uniformly distributed surface sound source, with an underwater propagation that is at near-vertical angle, as for most geophysical sound sources (wind/rain/drizzle). Refraction by the sound speed profile of the associated acoustic energy is then negligible, and is consequently independent of depth if absorption is neglected. In our data, absorption effects were not significant in comparison to the other explanatory variables of SES speed and wind speed. This property of depth independence has also been studied by Barclay and Buckingham (2013), validating experimentally Cron and Sherman's (1962) theory that predicts a constant (vertical) directional density function for wind-driven sources.

Our results from the marine soundscape part will be the focus now. To capture a marine soundscape, a full noncorrupted measured spectrum (typically from 10 to 10000 Hz) is needed. According to our correlation analysis, the most corrupted frequency bands are below 1 kHz, with major contributions from V. This ensures us that for low V values, corruption from nonenvironmental sources should be canceled out for these SPL responses. Following this idea, we performed a measure of our marine soundscape using only on the 5th percentile values of the SES speed and acceleration (see Fig. 4), referring to these dives as extreme drifts, when the SES is very slow. These V values range from 0.2 to 0.6 $m\,s^{-1}$ and induce variations strictly inferior to 5 dB in the SPL(0.05) (from Fig. 5), which are negligible regarding SPL variations in the same frequency band from classical acoustic sources present in a marine soundscape [e.g., Tsang-Hin-Sun et al. (2015) reported, for the same geographical area, daily variations in the sound pressure level in the order of 20 dB at 10 Hz and 15 dB at 50 Hz, which are associated with tectonic and shipping noise, respectively]. The spectrum shape obtained during these drift phases is quite similar from standard deep-ocean ambient noise spectra. The deep-water Atlantic curve falls off rapidly from its highest level at 50 Hz at a rate of about −8 dB per octave. It is flat from 200 to 400 Hz and then assumes a slope of −4 dB to 1000 Hz (Perrone 1969; Marshall 2005). Our spectrum shape can also be well approximated by the standard Knudsen–Alford–Emling curves, which are straight lines of constant negative slope of 5 dB per octave over the full frequency range (Knudsen et al. 1948). Considering the median levels of our averaged spectrum, in the Kerguelen Islands region, they were the same order of magnitude as those recently reported in the Indian Ocean by Tsang-Hin-Sun et al. (2015). For example, our SPLs ranged generally from 65 to 75 dB ref 1 $\mu Pa^2\,Hz^{-1}$ in the frequency band [50–100] Hz, whereas levels across the sites studied in Tsang-Hin-Sun et al. (2015) have been reported to be 75–85 dB ref and 65–70 dB ref 1 $\mu Pa^2\,Hz^{-1}$ (with the hydrophone WKER1, moored at 500 m below the sea surface) at 50 and 100 Hz, respectively. These levels are quite coherent with a measure done above the sound fixing and ranging (SOFAR) channel.

Regarding the measurement of wind speed, studies in acoustical meteorology (Vagle et al. 1990; Nystuen and Selsor 1997; Ma and Nystuen 2005; Pensieri et al. 2015) have shown that surface wind speed impacts the linearly ocean ambient noise level in such a way that relatively simple computational approaches (typically a constant threshold set to a one-third octave subband-averaged SPL) are sufficient to predict wind speed from underwater acoustics. Selecting the proper frequency bands is often the critical issue in such studies. It is known that SPL spectra associated with wind result from resonant acoustic radiation from bubbles generated by breaking waves (Medwin and Beaky 1989). The population size distribution of the bubbles defines the shape of the SPL spectra, and this shape of distribution is invariant with wind speed. However, as wind speed increases, the total bubble concentration increases because the fractional area coverage of breaking waves increases. The increase in bubble concentration leads to a concomitant increase in the SPL across all frequencies. This uniform increase as a function of frequency allows the SPL at a single frequency to be used to estimate wind speed. For example, the wind speed algorithm Wind Observations Through Ambient Noise (WOTAN) from Vagle et al. (1990) is based on the SPL at 8 kHz. More recently, Cauchy et al. (2015) applied the WOTAN algorithm to acoustic passive recordings from an underwater glider, with an error of 2 $m\,s^{-1}$ in wind speed estimates. In this paper, we first observed a uniform increase of sound levels with an increasing wind speed over a range of approximately 15 dB (from Fig. 7) that was observed in other studies for similar wind speed values (e.g., Pensieri et al. 2015). We also tested the use of different regression models to predict the wind speed from the acoustic descriptors detailed in Table 4. Our simplest model consists of a linear regression using the acoustic feature SPL(4) as predictor, in a very similar way as the WOTAN algorithm. The classification performance of this simple model was satisfactory, with an accuracy of 2.1 $m\,s^{-1}$ that validates the possibility of predicting wind speed from our spectra using similar methods as those found in literature (although the 8-kHz sample frequency could not be used in our study due to

technological limitations). Our numerical experiments also tested more complex models, such as a multiple linear regression model, using PCA-based acoustic features as predictors and a multiple nonlinear regression model. Using a higher number of acoustic predictors and nonlinear fitting models did not induce significant performance enhancement, leading to the conclusion that the SES passive acoustic recordings do not increase the processing complexity in the task of extracting wind speed information from a measured spectra.

Another interesting finding of our study is that wind speed estimation can be performed quite independently of SES diving behavior. Indeed, the error estimations between the drift and active swimming phases do not show discrepancies statistically significant, with average errors of $\varepsilon_{ws} = 1.9 \pm 0.2\,\mathrm{m\,s^{-1}}$ and $\varepsilon_{ws} = 2.7 \pm 0.3\,\mathrm{m\,s^{-1}}$ for the multilinear regression model. This result can be explained as follows. Noise spectra for hydrophones in the deep ocean show little dependence on wind at frequencies below 400 Hz (Piggott 1964). Most ''meteo bands'' used in studies are between 2 and 10 kHz, which fit well with the frequency subbands identified in our study to extract wind speeds. This result shows great promise in using SES as an acoustic glider for wind speed estimation. Because so few passive drift dives are performed daily (Dragon et al. 2012), wind speed measures would become difficult to assess at a fine temporal scale using only these dives. In contrast, our ability to measure wind speed accurately over all dive phases provides a high-frequency time series, with SES performing approximately 60–70 dives daily (Dragon et al. 2012).

5. Conclusions

Measuring and interpreting marine soundscape require passive acoustic recordings that are free from nonenvironmental noise. This current study explored the possibility of measuring soundscape with recordings from biologged southern elephant seals (SES). This technological approach offers valuable advantages, such as a high temporal resolution in acoustic measurements (in comparison to satellite-based measures). Also, SES allow the exploration of regions that are inaccessible to other technologies (e.g., underwater gliders). Indeed, the strong east–west current speeds and the rough sea state in the Southern Ocean make the use of regular gliders very complicated, while these harsh environmental conditions are not a problem for SES.

In this study, a multivariate multiple linear regression framework was essentially used to discriminate the acoustic contributions between the processes related to SES and the ocean environment. Our results showed that with passive acoustic recordings from a tagged free-ranging SES, minimal sound corruption from the SES could be obtained during extreme drift phases, allowing for the analysis of marine soundscape. Also, in frequency bands higher than 2.5 kHz, wind speed could be estimated using simple classification approaches (such as linear regression models), independently from the SES biological processes.

Future studies should use a more complete recording dataset, including additional environmental (e.g., rain, current, aquatic seisms), anthropological (e.g., ship traffic), and biological (e.g., whale vocalizations) variables that were not significantly present in our current dataset. This will be needed to fully validate our system as an operational measuring system to measure marine soundscape and to explain its characteristics with a full set of acoustic sources. Also, the ability to associate mobile acoustic data with estimates of surface weather conditions allows for a novel approach to studying air–sea interactions, which will need to be tested at a larger scale, that is, using different types of mobile platforms (e.g., gliders, profiling floats), in different ocean environments.

Acknowledgments. The authors are indebted to several researchers of the CEBC (Chizé, France), in particular Gaetan Richard, for assistance in sample preparation, data collection, processing algorithms, as well as numerous exchanges on SES biology. This study was conducted as part of the Institut Polaire program 109 (ecology of seabirds and marine mammals, P. I. H. Weimerskirch). The authors also would like to thank the Direction Générale de l'Armement (DGA, France) for supporting this work, the Fondation Total for funding the Acousonde as part of the Sea Bio-Sound project, the CNES-TOSCA, and the French Polar Institute for logistical and financial support, as well as all the Kerguelen fieldworkers for collecting data.

APPENDIX A

Influence of Depth on the Acoustic Features

Figure A1 shows the effect of depth on the SPL descriptors. We computed the differences between the SPLs above 100 m and at successive depths down to 800 m, averaged over 200 descending dives of the SES. We made the assumption that during the duration of these dives, the ocean ambient noise does not vary significantly. We can observe that the two lowest-frequency SPLs, SPL(0.05) and SPL(0.5), vary accordingly with the SES swimming speed V (represented by the black dashed curve) rather

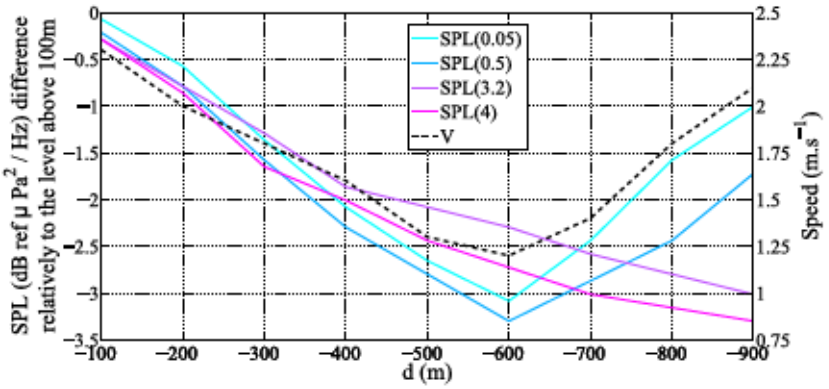

FIG. A1. Effects of depth on the SPL descriptors. The SES speed has also been superimposed onto these curves. Median values have been computed every 100 m in depth *d*.

than with depth, and remain nearly parallel from one depth measure point to another. On the contrary, the two highest-frequency SPLs, SPL(3.2) and SPL(4), have a lower decreasing rate that seems to be more decorrelated to *V* and could traduce some attenuation effects due to absorption or geometrical dispersion. Overall, depth induces some minor acoustic modifications that remain globally inferior to 2 dB above 500 m.

APPENDIX B

Pairwise Correlation and Scattering Plot of Variables

The pairwise correlation between the acoustic, SES, and environmental features was performed using standardized values. Resulting correlation coefficients are provided in Fig. B1 along with scattering plots. Strong

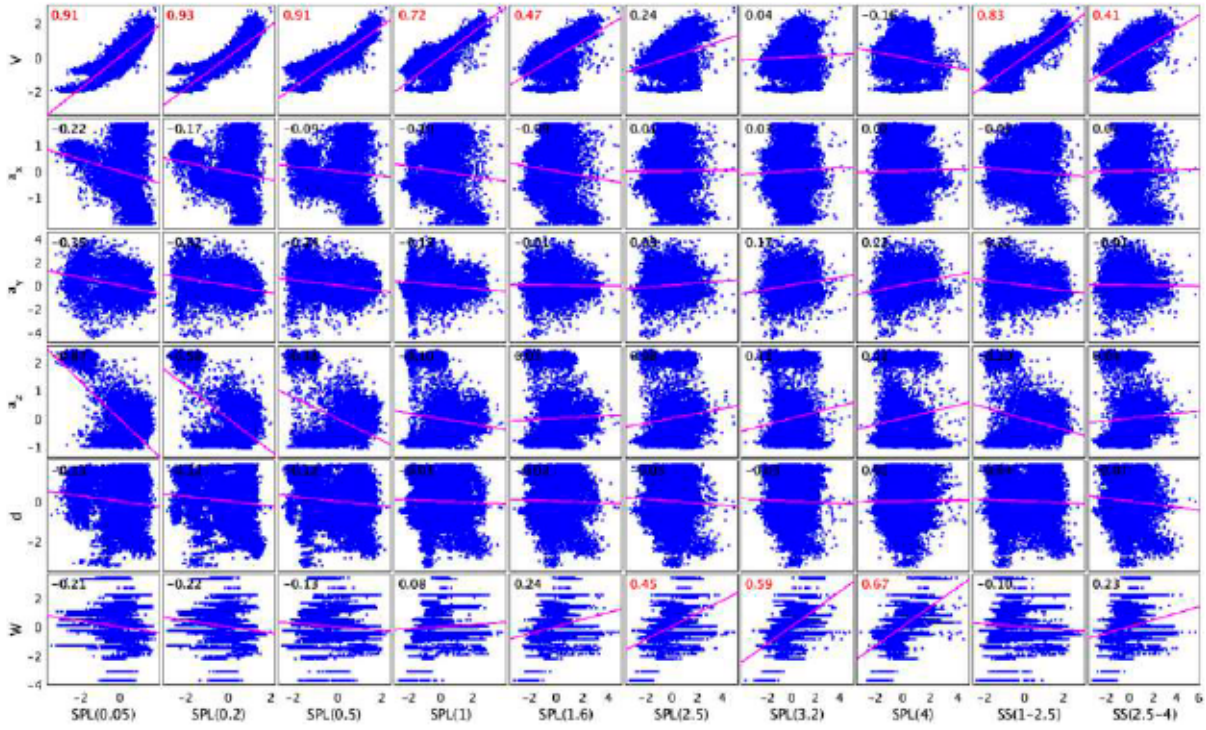

FIG. B1. Scattering plots and pairwise correlations between acoustic variables and SES and environment variables, using standardized values. Pearson correlation coefficients higher than 0.4, and with a *P* value below 0.001 (red).

correlation relations appear between specific parameters, such as SES speed with SPL(0.05), SPL(0.2), and SPL(0.5) ($r > 0.9$, $P < 0.001$), and wind speed with SPL(3.7) and SPL(4) (r of 0.59 and 0.67 with $P < 0.001$, respectively). Other variables, such as SES depth and acceleration, did not show significant correlation with any acoustic features, with coefficients remaining below 0.2 ($P < 0.001$). An analysis of pairwise correlations between SES and environment variables also informed us that they were relatively low ($r < 0.2$, with an average P value < 0.001). Also, we can observe that globally SPL descriptors explain better data variability than SS descriptors.

REFERENCES

Aguzzi, J., and Coauthors, 2011: The new seafloor observatory (OBSEA) for remote and long-term coastal ecosystem monitoring. *Sensors*, **11**, 5850–5872, doi:10.3390/s110605850.

Aoki, K., and Coauthors, 2011: Northern elephant seals adjust gliding and stroking patterns with changes in buoyancy: Validation of at-sea metrics of body density. *J. Exp. Biol.*, **214**, 2973–2987, doi:10.1242/jeb.055137.

Bailleul, F., M. Authier, S. Ducatez, F. Roquet, J. B. Charrassin, Y. Cherel, and C. Guinet, 2010: Looking at the unseen: Combining animal bio-logging and stable isotopes to reveal a shift in the ecological niche of a deep-diving predator. *Ecography*, **33**, 709–719, doi:10.1111/j.1600-0587.2009.06034.x.

Barclay, D. R., and M. J. Buckingham, 2013: Depth dependence of wind-driven, broadband ambient noise in the Philippine Sea. *J. Acoust. Soc. Amer.*, **133**, 62–71, doi:10.1121/1.4768885.

Baumgartner, M. F., S. M. Van Parijs, F. W. Wenzel, C. J. Tremblay, H. C. Esch, and A. M. Warde, 2008: Low frequency vocalizations attributed to sei whales (*Balaenoptera borealis*). *J. Acoust. Soc. Amer.*, **124**, 1339–1349, doi:10.1121/1.2945155.

Bentamy, A., and D. Croize-Fillon, 2012: Gridded surface wind fields from Metop/ASCAT measurements. *Int. J. Remote Sens.*, **33**, 1729–1754, doi:10.1080/01431161.2011.600348.

——, and ——, 2015: Daily ASCAT surface wind fields. IFREMER Tech. Rep., 15 pp.

Breiman, L., and J. H. Friedman, 1997: Predicting multivariate responses in multiple linear regression. *J. Roy. Stat. Soc.*, **59B**, 3–54, doi:10.1111/1467-9868.00054.

Burgess, W. C., 2000: The bioacoustic probe: A general-purpose acoustic recording tag. *J. Acoust. Soc. Amer.*, **108**, 2583–2583, doi:10.1121/1.4743598.

——, P. Tyack, B. Le Boeuf, and D. P. Costa, 1998: A programmable acoustic recording tag and first results from free-ranging northern elephant seals. *Deep-Sea Res. II*, **45**, 1327–1351, doi:10.1016/S0967-0645(98)00032-0.

Cauchy, P., T. Pierre, L. Mortier, and B. Marie-Noelle, 2015: Passive acoustics embedded on gliders—Weather observation through ambient noise. *Proc. Third Underwater Acoustics Conf. and Exhibition (UACE2015)*, Platanias, Crete, Greece, European Acoustics Association, 565–570.

Chapman, N. R., and A. Price, 2011: Low frequency deep ocean ambient noise trend in the Northeast Pacific Ocean. *J. Acoust. Soc. Amer.*, **129**, EL161, doi:10.1121/1.3567084.

Charrassin, J. B., and Coauthors, 2008: Southern Ocean frontal structure and sea-ice formation rates revealed by elephant seals. *Proc. Natl. Acad. Sci. USA*, **105**, 11 634–11 639, doi:10.1073/pnas.0800790105.

Costa, D. P., J. M. Klinck, E. E. Hofmann, M. S. Dinniman, and J. M. Burns, 2008: Upper ocean variability in west Antarctic Peninsula continental shelf waters as measured using instrumented seals. *Deep-Sea Res. II*, **55**, 323–337, doi:10.1016/j.dsr2.2007.11.003.

Cron, B. F., and C. H. Sherman, 1962: Spatial-correlation functions for various noise models. *J. Acoust. Soc. Amer.*, **34**, 1732–1736, doi:10.1121/1.1909110.

Dragon, A.-C., A. Bar-Hen, P. Monestiez, and C. Guinet, 2012: Horizontal and vertical movements as predictors of foraging success in a marine predator. *Mar. Ecol. Prog. Ser.*, **447**, 243–257, doi:10.3354/meps09498.

Duennebier, F. K., and Coauthors, 2002: HUGO: The Hawaii Undersea Geo-Observatory. *IEEE J. Oceanic Eng.*, **27**, 218–227, doi:10.1109/JOE.2002.1002476.

Favali, P., 2013: NEMO-SN1 abyssal cabled observatory in the Western Ionian Sea. *IEEE J. Oceanic Eng.*, **38**, 358–374, doi:10.1109/JOE.2012.2224536.

Genin, A., G. Richard, J. Jouma'a, B. Picard, N. El Ksabi, J. Vacquié-Garcia, and C. Guinet, 2015: Characterization of postdive recovery using sound recordings and its relationship to dive duration, exertion and foraging effort of southern elephant seals (*Mirounga leonina*). *Mar. Mammal Sci.*, **31**, 1452–1470, doi:10.1111/mms.12235.

Glowacki, O., G. B. Deane, M. Moskalik, Ph. Blondel, J. Tegowski, and M. Blaszczyk, 2015: Underwater acoustic signatures of glacier calving. *Geophys. Res. Lett.*, **42**, 804–812, doi:10.1002/2014GL062859.

Guinet, C., and Coauthors, 2013: Calibration procedures and first dataset of Southern Ocean chlorophyll *a* profiles collected by elephant seals equipped with a newly developed CTD-fluorescence tags. *Earth Syst. Sci. Data*, **5**, 15–29, doi:10.5194/essd-5-15-2013.

——, and Coauthors, 2014: Southern elephant seal foraging success in relation to temperature and light conditions: Insight into prey distribution. *Mar. Ecol. Prog. Ser.*, **499**, 285–301, doi:10.3354/meps10660.

Hawkins, R., J. Miksis-Olds, D. L. Bradley, and C. Smith, 2014: Periodicity in ambient noise and variation based on different temporal units of analysis. *Proc. Meet. Acoust.*, **17**, 070035, doi:10.1121/1.4772729.

Johnson, M., and P. Tyack, 2003: A digital acoustic recording tag for measuring the response of wild marine mammals to sound. *IEEE J. Oceanic Eng.*, **28**, 3–12, doi:10.1109/JOE.2002.808212.

Klinck, H., and Coauthors, 2012: Correction: Near-real-time acoustic monitoring of beaked whales and other cetaceans using a Seaglider. *PLoS One*, **7**, 1–8, doi:10.1371/annotation/57ad0b82-87c4-472d-b90b-b9c6f84947f8.

Knudsen, V., R. Alford, and J. Emling, 1948: Underwater ambient noise. *J. Mar. Res.*, **7**, 410–429.

Küsel, E. T., D. K. Mellinger, L. Thomas, T. A. Marques, D. Moretti, and J. Ward, 2011: Cetacean population density estimation from single fixed sensors using passive acoustics. *J. Acoust. Soc. Amer.*, **129**, 3610–3622, doi:10.1121/1.3583504.

Ma, B. B., and J. A. Nystuen, 2005: Passive acoustic detection and measurement of rainfall at sea. *J. Atmos. Oceanic Technol.*, **22**, 1225–1248, doi:10.1175/JTECH1773.1.

Marshall, S., 2005: Depth dependence of ambient noise. *IEEE J. Oceanic Eng.*, **30**, 275–281, doi:10.1109/JOE.2005.850876.

Matsumoto, H., J. H. Haxel, R. P. Dziak, D. Bohnenstiehl, and R. W. Embley, 2011: Mapping the sound field of an erupting

submarine volcano using an acoustic glider. *J. Acoust. Soc. Amer.*, **129**, EL94, doi:10.1121/1.3547720.

——, D. R. Bohnenstiehl, J. Tournadre, R. P. Dziak, J. H. Haxel, T.-K. A. Lau, M. J. Fowler, and S. A. Salo, 2014: Antarctic icebergs: A significant natural ocean sound source in the Southern Hemisphere. *Geochem. Geophys. Geosyst.*, **15**, 3448–3458, doi:10.1002/2014GC005454.

Medwin, H., and M. M. Beaky, 1989: Bubble sources of the Knudsen sea noise spectra. *J. Acoust. Soc. Amer.*, **86**, 1124–1130, doi:10.1121/1.398104.

Miksis-Olds, J. L., D. L. Bradley, and X. M. Niu, 2013: Decadal trends in Indian Ocean ambient sound. *J. Acoust. Soc. Amer.*, **134**, 3464–3475, doi:10.1121/1.4821537.

Miller, P. J. O., M. P. Johnson, P. L. Tyack, and E. A. Terray, 2004: Swimming gaits, passive drag and buoyancy of diving sperm whales *Physeter macrocephalus*. *J. Exp. Biol.*, **207**, 1953–1967, doi:10.1242/jeb.00993.

Mitani, Y., R. D. Andrews, K. Sato, A. Kato, Y. Naito, and D. P. Costa, 2010: Three-dimensional resting behaviour of northern elephant seals: Drifting like a falling leaf. *Biol. Lett.*, **6**, 163–166, doi:10.1098/rsbl.2009.0719.

Nair, N. R., N. Elizabeth Shani, R. Raju, and S. Satheeshkumar, 2015: Underwater ambient noise variability from satellite data—An Indian Ocean perspective. *2015 IEEE Underwater Technology (UT)*, 4 pp., doi:10.1109/UT.2015.7108285.

Nieukirk, S. L., K. M. Stafford, D. K. Mellinger, R. P. Dziak, and C. G. Fox, 2004: Low-frequency whale and seismic airgun sounds recorded in the mid-Atlantic Ocean. *J. Acoust. Soc. Amer.*, **115**, 1832–1843, doi:10.1121/1.1675816.

Nystuen, J. A., and H. D. Selsor, 1997: Weather classification using passive acoustic drifters. *J. Atmos. Oceanic Technol.*, **14**, 656–666, doi:10.1175/1520-0426(1997)014<0656:WCUPAD>2.0.CO;2.

——, M. A. Anagnostou, E. M. Anagnostou, and A. Papadopoulos, 2015: Monitoring Greek seas using passive underwater acoustics. *J. Atmos. Oceanic Technol.*, **32**, 334–349, doi:10.1175/JTECH-D-13-00264.1.

Pensieri, S., R. Bozzano, M. Anagnostou, E. Anagnostou, R. Bechini, and J. Nystuen, 2013: Monitoring the oceanic environment through passive underwater acoustics. *2013 MTS/IEEE OCEANS—Bergen*, 10 pp., doi:10.1109/OCEANS-Bergen.2013.6607995.

——, ——, J. A. Nystuen, E. N. Anagnostou, M. N. Anagnostou, and R. Bechini, 2015: Underwater acoustic measurements to estimate wind and rainfall in the Mediterranean Sea. *Adv. Meteor.*, **2015**, 612512, doi:10.1155/2015/612512.

Perrone, A. J., 1969: Deep-ocean ambient-noise spectra in the northwest Atlantic. *J. Acoust. Soc. Amer.*, **46**, 762, doi:10.1121/1.1911759.

Piggott, C. L., 1964: Ambient sea noise at low frequencies in shallow water of the Scotian Shelf. *J. Acoust. Soc. Amer.*, **36**, 2152, doi:10.1121/1.1919337.

Rahmati, M., P. Pandey, and D. Pompili, 2014: Separation and classification of underwater acoustic sources. *2014 Underwater Communications and Networking*, Sestri Levante, Italy, CMRE, doi:10.1109/UComms.2014.7017145.

Richard, G., J. Vacquié-Garcia, J. Jouma'a, B. Picard, A. Génin, J. P. Y. Arnould, F. Bailleul, and C. Guinet, 2014: Variation in body condition during the post-moult foraging trip of southern elephant seals and its consequences on diving behaviour. *J. Exp. Biol.*, **217**, 2609–2619, doi:10.1242/jeb.088542.

Rogers, E. O., J. G. Genderson, W. S. Smith, G. F. Denny, and P. J. Farely, 2004: Underwater acoustic glider. *2004 IEEE International Geoscience and Remote Sensing Symposium Proceedings*, Vol. 3, IEEE, 2241–2244, doi:10.1109/IGARSS.2004.1370808.

Ropert-Coudert, Y., and R. P. Wilson, 2005: Trends and perspectives in animal-attached remote sensing. *Front. Ecol. Environ.*, **3**, 437–444, doi:10.1890/1540-9295(2005)003[0437:TAPIAR]2.0.CO;2.

Roquet, F., Y.-H. Park, C. Guinet, F. Bailleul, and J.-B. Charrassin, 2009: Observations of the Fawn Trough Current over the Kerguelen Plateau from instrumented elephant seals. *J. Mar. Syst.*, **78**, 377–393, doi:10.1016/j.jmarsys.2008.11.017.

Rudnick, D. L., R. E. Davis, C. C. Eriksen, D. M. Fratantoni, and M. J. Perry, 2004: Underwater gliders for ocean research. *Mar. Technol. Soc. J.*, **34**, 73–84, doi:10.4031/002533204787522703.

Sato, K., Y. Mitani, M. F. Cameron, D. B. Siniff, and Y. Naito, 2003: Factors affecting stroking patterns and body angle in diving Weddell seals under natural conditions. *J. Exp. Biol.*, **206**, 1461–1470, doi:10.1242/jeb.00265.

Sirovic, A., S. M. Wiggins, and E. M. Oleson, 2013: Ocean noise in the tropical and subtropical Pacific Ocean. *J. Acoust. Soc. Amer.*, **134**, 2681–2689, doi:10.1121/1.4820884.

Tennekes, H., and J. L. Lumley, 1972: *A First Course in Turbulence*. MIT Press, 300 pp.

Tournadre, J., 2014: Anthropogenic pressure on the open ocean: The growth of ship traffic revealed by altimeter data analysis. *Geophys. Res. Lett.*, **41**, 7924–7932, doi:10.1002/2014GL061786.

Tsang-Hin-Sun, E., J.-Y. Royer, and E. C. Leroy, 2015: Low-frequency sound level in the southern Indian Ocean. *J. Acoust. Soc. Amer.*, **138**, 3439–3446, doi:10.1121/1.4936855.

Urick, R., 1971: Noise of melting icebergs. *J. Acoust. Soc. Amer.*, **50**, 337–341, doi:10.1121/1.1912637.

Vacquié-Garcia, J., F. Royer, A.-C. Dragon, M. Viviant, F. Bailleul, and C. Guinet, 2012: Foraging in the darkness of the Southern Ocean: Influence of bioluminescence on a deep diving predator. *PLoS One*, **8**, e43565, doi:10.1371/journal.pone.0043565.

Vagle, S., W. G. Large, and D. M. Farmer, 1990: An evaluation of the WOTAN technique for inferring oceanic wind from underwater sound. *J. Atmos. Oceanic Technol.*, **7**, 576–595, doi:10.1175/1520-0426(1990)007<0576:AEOTWT>2.0.CO;2.

Van Dyke, M., 1982: *An Album of Fluid Motion*. 14th ed. Parabolic Press, 176 pp.

Wagstaff, R., 2005: An ambient noise model for the northeast Pacific Ocean basin. *IEEE J. Oceanic Eng.*, **30**, 286–294, doi:10.1109/JOE.2004.836993.

Ward, J., and Coauthors, 2011: Beaked whale (*Mesoplodaon densirostris*) passive acoustic detection in increasing ambient noise. *J. Acoust. Soc. Amer.*, **129**, 662–669, doi:10.1121/1.3531844.

Wenz, G. M., 1962: Acoustic ambient noise in the ocean: Spectra and sources. *J. Acoust. Soc. Amer.*, **34**, 1936–1956, doi:10.1121/1.1909155.

Zhang, Z., J. Neubauer, and D. A. Berry, 2006: Aerodynamically and acoustically driven modes of vibration in a physical model of the vocal folds. *J. Acoust. Soc. Amer.*, **120**, 2841–2849, doi:10.1121/1.2354025.

ANNEXE

I

Article 8 : Jouma'a *et al.*, en prep.

8. Jouma'a Joffrey, Le Bras Yves, Picard Baptiste, Guinet Christophe. (2016). Spatio-temporal variations in field metabolic rate of post-moulting southern elephant seals. **En préparation**

Spatio-Temporal Variations in Field Metabolic Rate of Post-Moulting Southern Elephant Seals

Introduction

To understand and to evaluate the metabolism of a species is one of the fundamental questions in ecology since it allows to link all the components of an ecosystem, from the individual to the population level (Brown *et al.*, 2004). An animal's metabolic rate determines its resource requirements, such as food (Nagy, 1987), but also life history traits as growth rate, lifespan or age at maturity (van Noordwijk & de Jong, 1986; Kozłowski & Wiegert, 1986). At the ecosystems scale, the field metabolic rate (FMR) or animal energy expenditure is a key input in the energy transfer within food webs and across individuals. Assessing these energy requirements provides a broader picture of how organisms are interlinked within an ecosystem, which is essential to evaluate their resilience to anthropogenic disturbance and rapid environmental changes.

Direct monitoring of energy requirements is quite challenging in free-ranging animals, especially for top predators which are often difficult to access. To cope with such difficulties, many studies have focused on indirect information, such as the spatiotemporal distribution of the foraging effort (Guinet *et al.*, 2001; Ainley *et al.*, 2003) or the prey distribution (Eide *et al.*, 2004; Thayer & Sydeman, 2007). The balance between energy expenditure and energy intake drives many aspects of the physiology, biology, and ecology of organisms, affecting therefore their reproduction and survival (Magni *et al.*, 2000; Stubbs & Tolkamp, 2006). While these information are challenging to get for terrestrial animals, it is even more complicated for marine animals since they widely disperse in a three-dimensions habitat.

Deep diving marine mammals require high energy demands in response to high hydrostatic pressure and cold temperatures (Seibel & Drazen, 2007). To keep the energy balance positive, the energy intake has therefore to exceed the foraging cost. This can be done by several behavioural adaptations like swimming at the minimum cost of transport speeds (Miller *et al.*, 2012), adopting a burst-and-glide strategy (Williams *et al.*, 2000), or targeting specific depths (Williams, 1989; Mori, 1998). By adjusting their diving behaviours in such a way, air breathing marine mammals should maximize the difference between the energy expenditure, and the energy intake. The foraging cost can thus be considered as one way to reflect the energy demands through the cost of transport, and the cost of chasing and capturing prey (Elliott *et al.*, 1977; Shipman & Walker, 1989; Gorman *et al.*, 1998; Carbone *et al.*, 2007).

As a central place forager, the southern elephant seal, *Mirounga leonina* (SES hereafter), comes ashore twice a year, once for the reproduction and once for the moult. Right after this second period ashore, embryos are released from diapause and implantation occurs (Gibbney, 1953). During this period, a significant change in the energy balance could then have serious consequences on the survival of the embryo. Keeping a positive energy balance during the post-moulting period appears therefore to be a key component for the allocation of more energy to survival but also to reproduction, resulting in the enhancement of the population's fitness (Costa, 2012).

The use of even more efficient data loggers made it possible to get precious information on both the energy expenditure and the energy intake in wild animals (Charrassin *et al.*, 2001; Wilson *et al.*, 2002, 2006). In SES, the use of accelerometers has eased the acquisition of information on the swimming effort (Richard *et al.*, 2014; Jouma'a *et al.*, 2016), the foraging effort in term of prey catch attempts (Gallon *et al.*, 2013; Vacquié-Garcia *et al.*, 2015) and the animal's body density (Aoki *et al.*, 2011; Richard *et al.*, 2014; Adachi *et al.*, 2014). Despite the large deployment of accelerometers over the past decade, the number of studies focusing on the energy expenditure over the post-moulting trip of this species is very limited. The only studies that tempted to monitor changes in the energy expenditure over the post-moulting period used the number of flipper stroke calculated from acceleration data as a proxy of the FMR in northern elephant seals, *Mirounga angustirostris*, (Maresh *et al.*, 2014, 2015). While the acceleration data recording duration are not mentioned in these studies, the estimation of the energy expenditure is usually restricted to the post-breeding period at sea (Carlini *et al.*, 2005; Richard *et al.*, 2014), as the high-resolution dataset required to estimate such parameter can usually not be recorded during the whole post-moulting season due to battery limitation. One way to estimate the energy expenditure for post-moulting dives without the acceleration data, is therefore to build a predictive model on post-breeding dives of the energy expenditure, derived from the acceleration data, and then uses it to predict on post-moulting dive.

In this context, we used high resolution datasets (time-depth and acceleration) from 8 post-breeding SESs to examine how to best predict variations in the number of flipper strokes, from low-resolution based dive metrics and buoyancy changes. Using this model, we first predicted the number of flipper strokes on the low-resolution dives of 107 post-moulting SESs over an 11 years' period (2004-2015). Then, using the Maresh *et al.* (2014)

equation relating the number of flipper strokes to the energy expenditure, we tested if the energy expenditure in post-moulting SESs' dives varies in space, time and among sex.

Materials & Methods

Ethics Statements

The Ethics Committee of the French Polar Institute validated all scientific procedures applied on elephant seals. All animals in this study were handled and cared for in total accordance with its guidelines and recommendations.

Animal Tagging

The seals were captured with a canvas head-bag and anaesthetized using a 1:1 combination of Tiletamine and Zolazepam (Zoletil 100) injected intravenously (McMahon *et al.*, 2000; Field *et al.*, 2002). Data loggers were glued using a quick-setting epoxy glue (Araldite AW 2101), after the fur was cleaned with acetone. The loggers were then recovered when female SES returned to shore to moult (*i.e.* January-February following deployments). Seals ashore were located using their Argos locations.

Biological Data Collection

Post-breeding Dataset We used a first dataset composed of 8 post-breeding females equipped on the Kerguelen Islands (49°20'S, 70°20'E), in 2010 (n = 3), 2011 (n = 3) and 2014 (n = 2) with SPLASH-10 and TDR-MK10-X (Wildlife Computers). SPLASH-10 loggers archive sampled dive depth at every second, while locations are transmitted directly via the Argos system. TDR-MK10X includes a time-depth recorder sampling at 1 Hz, and a 3D accelerometer, sampling acceleration at 16 Hz. Both data were stored in the logger's memory meaning the tag needs to be recovered to retrieve them.

Post-moulting Dataset The second dataset was composed of 107 post-moulting SESs (64 females and 43 males) also equipped on the Kerguelen Islands of satelliterelay data loggers [SRDLs; Sea Mammal Research Unit (SMRU) Instrumentation, St Andrews, UK] as part of the MEMO Observatory (http://www.insu.cnrs.fr/ node/4125) between 2004 and 2015. The SRLDs recorded high-resolution time-depth profiles at 2 s intervals before being resumed using a broken-stick algorithm on-board which reduced the data to four at-depth and two surface dive inflection points (Fedak *et al.*, 2001; Gordine *et al.*, 2015). The abstracted data were then compressed and relayed via the Argos satellite system (Fedak *et al.*, 2002; Argos, 2011).

Unless otherwise stated, most of our analyses were conducted using R (R Core Team, 2015). All scripts used below for data treatment and analyses are available upon request.

Parameters Calculation

General Approach As body density changes are important in the energy balance of elephant seals, we based our predictive model of the number of flipper strokes (from post-breeding dives), on dive metrics and buoyancy changes. Dive metrics were calculated from high resolution dataset for post-breeding dives, and directly transmitted for post-moulting dives from SRDLs tags. To calculate buoyancy changes in the same way for post-moulting and post-breeding dives, we degraded the highresolution post-breeding dataset to be equivalent to the low-resolution post-moulting dataset (four depth records per dives). Using the same method, we then calculated a proxy of the daily body density changes in both low-resolution datasets (the postmoulting one and the degraded post-breeding one). We were therefore able to build a model on post-breeding dives that will be used to predict on post-moulting dives.

Diving Parameters Dive metrics of low resolution dataset were directly transmitted for post-moulting dives from SRDLs tag, *i.e.* post-dive surface interval, dive duration and the maximum depth (Fedak *et al.*, 2001). For high-resolution dataset of post-breeding dives, data were processed using the rbl R packages available on GitHub (https://github.com/SESman/rbl). Basically, we applied an offset correction of depth measurements to account for the drift that occurred over time, through the offset-correction function. Dives were then identified when deeper than 15 metres using dive_delim function. This threshold was used to avoid subsurface movement to be considered as dives.

Proxy of Buoyancy Changes To calculate buoyancy changes in the same way for post-moulting and post-breeding dives, we degraded the high-resolution postbreeding dives to be equivalent to the low-resolution post-moulting dives based on
Heerah *et al.* (2015) through the brokenstick function in the rbl R package (Le Bras, 2016). Using the method developed by Gordine *et al.* (2015), we then calculated daily values for the drift rate considering only the segment 2, 3 and 4 of each dive. We then calculated the vertical speed associated with each of these segments. We removed any segments with a zero vertical speed, those with an absolute vertical speed higher than 0.6 $m.s^{-1}$, and those shorter than 40 % of the dive duration. To avoid keeping "U"-shaped dives, we calculated for each dive the ratio between the actual dive area (defined in the same way as Fedak *et al.*, 2001) and the rectangle defined by the maximum depth and the dive time. We preferred this metric to the time allocation at depth index (Fedak *et al.*, 2001) to avoid the arbitrary choice

of the animal's speed. We finally kept segments for which this ratio was below 0.75. With the set of remaining segments, we took the daily median of their vertical speed as a proxy of daily changes in buoyancy. This proxy was then modelled using a constrained beta spline (Ng & Maechler, 2007) with the cobs function from the R package of the same name (Ng & Maechler, 2015). To reduce the effect of noise in the data but also to get the trend over the whole trip at sea, the maximum number of knots was set to five. These knots were generated using the quantile method with a level fixed at 80 % (Gordine *et al.* (2015) fixed this level at 20 %, but their definition of the vertical speed was the opposite than ours, which finally results in the same level).

Count Flipper Strokes The number of flipper stroke was obtained from accelerometers deployed on post-breeding animals. For each animal, we randomly select 50 dives over their whole trip at sea. Then using a band-pass filter on the lateral axis, we only kept frequencies including the second peak observed on the power spectral density. To automatically detect the low and high cut-off frequency on the power spectral density (Appendix I, Figure I.1), we used the segmentation of Lavielle on time series (lavielle function in the adehabitatLT R package, Calenge (2006)). The minimum number of observations in each segment was set to 1000 values, with a maximum number of segments of five, and a contrast function based on the variance. The third segment identified was the one related to the animal's stroke, since it overlapped the second peak. This segment was characterized by a minimum and a maximum frequency defined then as the low and high cut-off frequency of the band-pass filter used to isolate frequencies due to animal's flipper stroke. The remaining peaks on the filtered signal with an amplitude greater than a threshold were considered to be flipper strokes and so used in our analyses as a proxy of energy expenditure (Maresh *et al.*, 2014, 2015). Contrary to Maresh *et al.* (2014, 2015), this amplitude threshold was defined for each animal as the quantile 0.5 of the absolute amplitude associated with each flipper stroke.

We believed that counting flipper stroke based on a filter and a threshold calculating at the individual level allows us to partly take into account for small differences in accelerometer placement during attachment, and inherent differences between seals.

Predictive Model

To predict the number of strokes performed in each post-moulting dives, we built a predictive model on post-breeding dives of the count flipper stroke with the postdive surface interval (srf_inter), the dive duration (dv_dur), the maximum depth (max_depth) and a proxy of the buoyancy (buoyancy_proxy) as explanatory variables. To get the overall variation of the body density during a complete trip at sea, we only selected post-breeding animals that

remained at least one month (31 days) at sea. All the variables considered in our models were previously tested for collinearity (Zuur *et al.*, 2010), and revealed a variance inflation factor below 3. Because the script used to identify dives in post-breeding animals may have missed some of them, some estimated surface intervals were unusually long. Based on the histogram of the surface interval, only the dives associated with a surface interval below 350 s were therefore retained (Appendix I, Figure I.2). To reduce the influence of autocorrelations in our data, we subsampled our dataset by taking one dive every 20 dives per individual.

We then used the bam function from the mgcv R package to perform a generalized additive model (Wood *et al.*, 2015), with the individual as a random intercept and a Gaussian distribution. As we wanted the best fit, we allowed for each smooth a degree of freedom up to 20. Models used further could be specified as:

Count flipper stroke ~ alpha + s(dv_dur, k = 20) + s(srf_inter, k = 20) + s(max_depth, k = 20) + s(buoyancy_proxy, k = 20) + s(id, bs = "re")

where *s()* indicated a smooth function based on natural splines, *k* the number of degrees of freedom allowed and *bs* a way to specify a random intercept (Wood, 2016).

Analyses

Data Partioning To explore the variability in the average energy expenditure per dive, we separated animals that went to Antarctica, *i.e.* below -60 ° of latitude, from the others. For the same reason, each trip was segmented into three phases: the outward, the central and the return phase. The central phase was defined as any position located at a distance longer than 80 % of the maximum distance from the departure location. This threshold was chosen after visual inspection of the relation between the distance from the coast and the time spent at sea (Appendix I, Figure I.3). The outward phase was defined from the first location to the first one of the central phase, and the return phase from the last one of the central phase to the last one of each animal's track.

Average Energy Expenditure Variability The average energy expenditure per dive (in J kg^{-1} s^{-1}, noted FMR hereafter) was then calculated using the (Maresh *et al.*, 2014) equation for all post-moulting dives:

$$\text{FMR} = \frac{2.58.S_n}{\text{Dive duration}} \quad (5.1)$$

where S_n is the predicted value of the number of flipper strokes per dive, for post-moulting dives.

A linear mixed-effects model was fitted using the nlme package (Pinheiro *et al.*, 2013) to explore the variability of FMR in relation to four parameters: the destination (Antarctica or others), the trip phase (outward, central or return), the sex and the year. Individuals were included as random factors, and we accounted for the temporal correlation in our data by taking one dive every 20.

To investigate further inter-annual variability of the FMR, we performed a KruskallWallis test considering independently male and female. To account for the high variability in the FMR at the individual level, the median was chosen rather than the average of FMR per individual.

Results

Predictive Model

General Results Among the eight post-breeding female elephant seals used to build the predictive model, an average of (mean ± sd) 3661 ± 955 dives were recorded per individual, for a total 29288 dives. The females spent 65 ± 10 d at sea (Table 5.1), diving at an average maximum depth of 517 ± 84 m. They spend on average 130.9 ± 15.68 s at the surface between two consecutive dives, and dove during 1193.8 ± 159.97 s.

Table 5.1 – Overall information on animals post breeding animals used in the predictive model. Mean values are given with ± sd.

id	*n* days	*n* dives	Departure date	Dive duration (s)	Surface interval (s)	Dive depth (m)	Stroke count per dives
2010-18	60	2544	10/28/2010	1420.67 ± 259.96	159.49 ± 29.99	645.99 ± 199.17	715.71 ± 174.86
2010-19	69	3288	11/05/2010	1368.87 ± 253.64	139.71 ± 20.62	512.83 ± 227.18	959.62 ± 224.05
2010-21	72	3546	11/22/2010	1300.68 ± 281.31	120.56 ± 21.8	482.19 ± 207.33	879 ± 212.21
2011-21	53	3306	10/29/2011	1081.04 ± 194.89	137.67 ± 21.71	566.84 ± 179.61	659.6 ± 124.97
2011-26	58	3290	10/31/2011	1191.97 ± 208.16	133.28 ± 21.67	568.56 ± 226.85	806.83 ± 164.93
2011-28	55	3212	11/01/2011	1168.79 ± 276.95	121.04 ± 17.27	523.87 ± 204.98	827.92 ± 193.61
2014-22	79	5625	10/29/2014	963.91 ± 288.46	107.17 ± 19.91	359.78 ± 148.05	647.84 ± 191.07
2014-23	73	4477	10/29/2014	1054.5 ± 240.82	128.25 ± 14.77	477.12 ± 128.38	782.03 ± 162.81

Table 5.2 – Percent of deviance explained by each term of the predictive model: stroke count ~ alpha + s(dv_dur, k = 20) + s(srf_inter, k = 20) + s(max_depth, k = 20) + s(buoyancy_proxy, k = 20) + s(id, bs = "re")

Covariates	Percent of deviance explained (%)

Stroke count ~	Dive time	20
	Surface interval	2
	Max depth 12 Drift rate 10	
	Random(individual) 16	
Total		60

The predictive model was applied on 107 post-moulting SESs, representing a total of 409531 dives, with an average of 3828 ± 1790 dives recorded per individual (Appendix I, Table 1). These animals spent 204 ± 56 d at sea, and 128 ± 22 s at the surface between two dives. They dove during 1631 ± 340 s at an average maximum depth of 424 ± 110 m.

Power Predictive and Residual Diagnostic The predictive model accounted for 60 % of the deviance, with 16 % of the deviance explained by the individual random effect only (Table 5.2). Our proxy of the buoyancy changes explained 13 %, and the dive duration 20 %. The distribution of residuals is a bit shifted towards positive values, with a heavy tail for negative values, compared to a Gaussian distribution (Figure 5.1). An increase of the number of strokes per dive was found with an increase of the dive duration and the maximum depth, and a decrease with the post-dive surface interval and the body density (Figure 5.2).

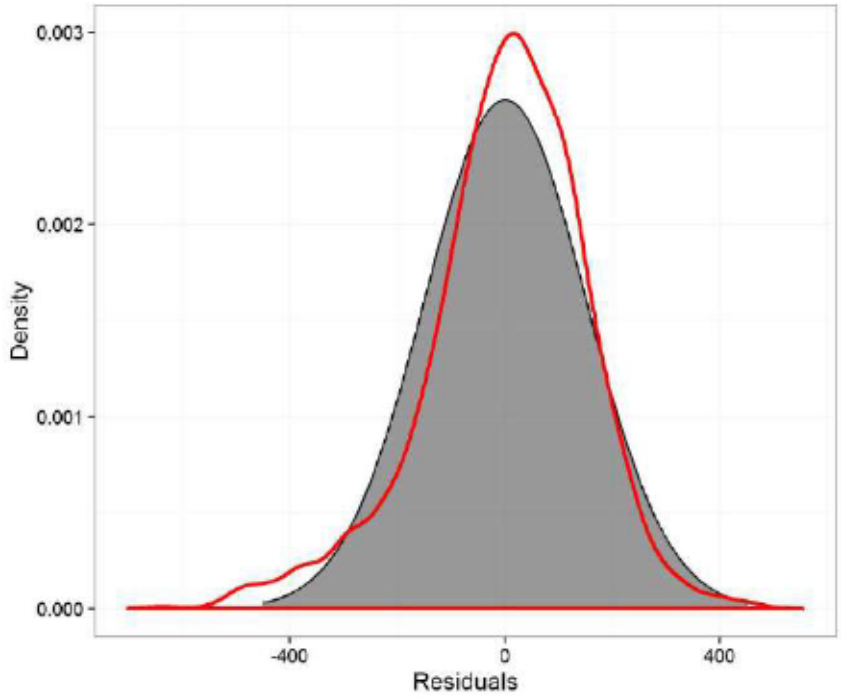

Figure 5.1 – Comparison between the distribution of the residuals from the predictive model (red curve) and a Gaussian distribution. The heavy tail for negative residual values means it overestimates the small numbers of strokes per dives.

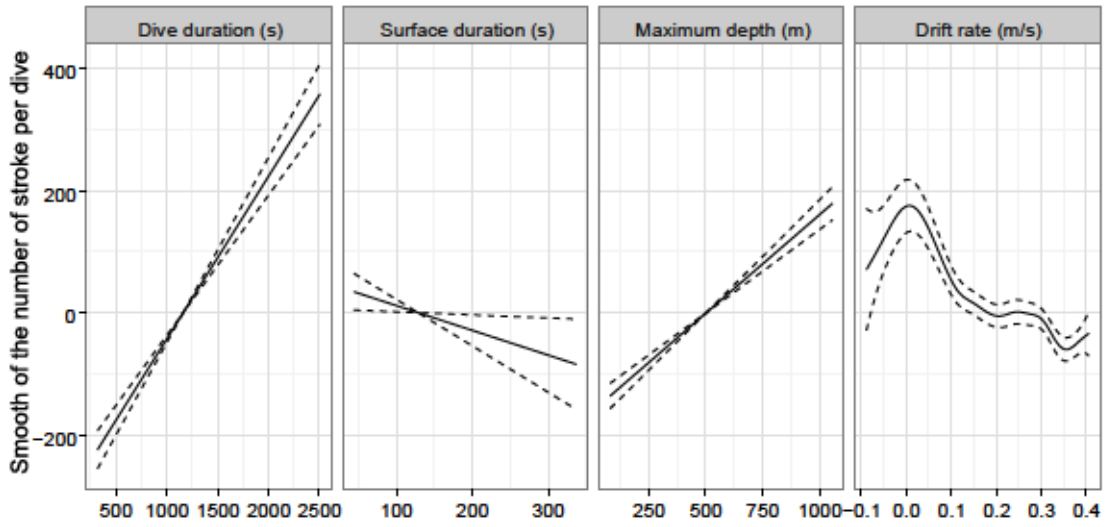

Figure 5.2 – Relationships from the predictive model between the number of flipper stroke per dives and the dive duration, the post-dive surface duration, the maximum depth and the drift rate.

Predictions Analysis

Energy Expenditure & Destination, Sex and Trip Phases Regardless of the destination, the trip phase or the year, the FMR was significantly higher for males than females (105.3 ± 13.7 vs. 80.9 ± 39.2 kJ kg^{-1} d^{-1} respectively; p-value < 0.01, Table 5.3). Similarly, but independently of the sex instead of the destination, animals reaching Antarctica had a significantly higher FMR (108.6 ± 52.1 vs. 71.73 ± 13.7 kJ kg^{-1} d^{-1} respectively; p-value < 0.01, Table 5.3). In the same way, the energy expenditure during the central phase (91.4 ± 62.1 kJ kg^{-1} d^{-1}) of the trip was significantly lower than during the outward phase (109.7 ± 63 kJ kg^{-1} d^{-1}), and significantly higher than the return phase (82.8 ± 61.4 kJ kg^{-1} d^{-1}; both p-value < 0.01, Table 5.3).

Table 5.3 – Relationships between the energy expenditure (FMR) and the destination, the sex, the trip phase and the year, and the associated p-values from a linear mixed effect model with individual as a random intercept. For each qualitative covariate, the estimate represents how stroke count varies with the modality presented here, compared to the one which is not presented. The year covariate was set as a quantitative variable to avoid the multiplicity of the modalities.

	Covariate	Modality	Estimate	p-value
FMR ~	Destination Sex	Antarctica Male	0.31	<0.01
			0.19	<0.01
	Phase of the trip at sea	Outward	0.11	<0.01
		Return	-0.10	<0.01
	Year	-	0.00	0.78

Inter-Annual Variability in Energy Expenditure Without any consideration on the sex, the destination or the trip phase, the covariate year has no effect on the FMR (p-value = 0.78, Table 5.3). However, when distinguishing sexes (Figure 5.3), at least one year differed from the others for males (Kruskal-Wallis chi-squared = 20.50, df = 10, p-value = 0.03) and females (Kruskal-Wallis chi-squared = 24.26, df = 10, p-value < 0.01).

Discussion

This study illustrates the necessity to monitor individual parameters over long-term to get the overall picture of the relationships between biological and physical parameters within an ecosystem. Using a predictive model to estimate the energy

Figure 5.3 – Distribution of the energy expenditure (kJ.kg-¹.d-¹) in post-moulting southern elephant seals (*Mirounga leonina*) from 2004 to 2015 in males and females.

expenditure over an 11-year period, our findings revealed spatial and temporal variability of the energy expenditure, which differs between sexes.

Using the Maresh *et al.* (2014) equation based on the number of strokes as a proxy of the energy expenditure stated several assumptions that need to be clarified. First, it assumes the number of strokes to be comparable between individuals of different ages. This assumption is based on Maresh *et al.* (2014) which found no significant relationships between size or age in the FMR of 12 female northern elephant seals. While differences between sexes were not tested, we made the assumption of similar relationship between stroke counts and FMR for both sexes. In the absence of information relating both information for male elephant seals, we acknowledge that is a strong assumption leading possibly to a miscalculation of the FMR. The second assumption states that the energy expenditure, defined in this way, represents the sum of all components costs (digestion, maintenance and locomotion) except for the energy lost in via faeces, urine and thermoregulation (Maresh *et al.*, 2015).

Given the above, the proportion of the deviance explained by our model to predict the number of flipper strokes was 60 %. Given the high deviance explained, we believe this model captures a sufficient part of the stroke counts variability to use it to predict on the post-moulting SESs. The shape of the residual distribution from this model suggests a tendency to overestimate small number of flipper stroke, resulting in an overestimation of low FMR values. In accordance with several studies, we found that the number of strokes per dive, and so the energy expenditure, was linked to diving parameters (Arnould *et al.*, 1996; Costa & Gales, 2000; Elliott *et al.*, 2013). Using method developed by Gordine *et al.* (2015), the calculated proxy of the animal's body density accounted for 13 % of the deviance explained, which reveals the buoyancy variation as a strong driver of the animal energy expenditure. This is consistent with the findings of Thums *et al.* (2008), which found that drift rate accounted for 77 % of the deviance explained in a model that investigated the relationship between body lipid content and several diving variables. These results are also in accordance with previous studies like Richard *et al.* (2014), which found that one percent variation in buoyancy resulted in a 20 % variation of swimming effort, and Jouma'a *et al.* (2016) demonstrating that the time spend at the bottom increases with the animal buoyancy.

Using this model to predict the number of flipper strokes associated with each post-moulting dive, we found that the variability in the energy expenditure during post-moulting trip could be related to several parameters (Table 5.3). We found that no matter the destination, the sex or the year, the central phase of SES trip at sea costs less energy than the outward phase, and more energy than the return phase. This is consistent with previous

studies focusing on the buoyancy variations of elephant seals (Aoki *et al.*, 2011; Richard *et al.*, 2014; Adachi *et al.*, 2014). Once elephant seals leave the land after the moulting period, they have poor body condition with a negative buoyancy (Thums *et al.*, 2008) due to the high energy requirements over the moulting fast (Slip *et al.*, 1992). As they feed on more and more prey during their trip at sea, they make fat, improving therefore their body condition by increasing the percentage of their body lipid content (Thums *et al.*, 2008). By approaching the neutral buoyancy, they reduce the cost of transport (Sato *et al.*, 2013; Adachi *et al.*, 2014) and so the energy expenditure, which likely explain its decrease from the outward phase to the return phase.

In the same way, regardless of their sex, the year or the trip phase, SESs reaching Antarctica have higher energy expenditure than the others remaining on the Kerguelen shelf or pelagic compartments. While this relationship was expected for the central phase of their trip at sea, because SESs reaching those regions have to deal with sea ice when approaching Antarctica (Bailleul *et al.*, 2007; van den Hoff *et al.*, 2014; Labrousse *et al.*, 2015), it was not the case for the others part of their trip. As suggested by Bailleul *et al.* (2007), we believe that sea ice locality presents particular environmental conditions explaining the presence of richer habitats. This means better prey quality or a wider range of prey sources that could justify higher energy costs during the outward and return phases. In this way, we assume the energy required for transit phases (outward and return phases) would be compensated by higher energy intake once near Antarctica. More than the energy expenditure associated with a foraging zone, it is the difference between energy expenditure and energy intake that should drive animal's decision. One can well imagine that higher energy expenditure would allow SESs to access better prey quality, resulting in a higher net energy gain. Indeed, it would be interesting to see if animals reaching Antarctica have higher reproductive success and survival rate.

The explanatory model also revealed that male SESs have higher energy expenditure than the females, and no matter where they are going, the year or the trip phase. As no sexual difference was found in the swimming speed of northern elephant seals (Hassrick *et al.*, 2007), we believe that differences in the energy expenditure was mainly due to a higher flipper stroke frequency required to move the male SESs' body. Since male SESs are several times heavier than females (McCann *et al.*, 1989), they probably need to increase their flipper stroke frequency to swim as fast as the females. This increase in the number of strokes per unit of time results in an increasing FMR. We should, however, take this result with caution since the model used to predict FMR male SESs, was fitted on female SESs, including then a possible bias in the estimation of energy expenditure of males. With all uncertainties around the measurement of our FMR, we also found that female SESs have

similar energy expenditure than those found in northern elephant seals (80.9 ± 39.2 kJ kg^{-1} d^{-1} vs. 69.4 ± 3.0 kJ kg^{-1} d^{-1}, respectively, Maresh *et al.*, 2014).

These sexual differences in the variation of the energy expenditure enabled to highlight an inter-annual variability (Figure 5.3) that was not detected in our explanatory model (Table 5.3) because of confounding covariates. The lack of individuals for some years prevented from statistically identifying a specific year different from the others in both, male and female time series. This could be due to a small number of SESs equipped in some years, e.g. 2006 was only represented by one male and one female SESs. A greater number of SESs would have provided a better picture of the inter-annual variability at the population level. We however observed a trend toward reduction in energy expenditure in 2007, with a possible increase in 2011 for male SESs energy expenditure (Figure 5.3).

There might be numerous and complex reasons for this inter-annual variability. These variations in the energy expenditure are linked to their ecological niches, since adult male and female SESs are known to forage in different habitats (Bailleul *et al.*, 2010a). Males mainly forage from the Antarctica coasts within the sea-ice pack, while females forage in more pelagically habitats. The accessibility and quality of resources therefore strongly differ among sexes, which could explain the differences observed in the energy expenditure. The accessibility to prey resources may be driven by climatic events through respectively the extent of sea-ice (Wolff *et al.*, 2006) and changes in mixed layer depth (Sallée *et al.*, 2010). Climatic variations such as El Niño Southern Oscillation (ENSO) or the Southern Annular Mode (SAM) are known to influence the productivity of the Southern Ocean and the abundance, quality and distribution of prey, where SESs forage (Wilson *et al.*, 2001; Atkinson *et al.*, 2004), which in fine could influence the variations in energy expenditure.

Since elephant seals are capital breeders, they depend on the energy collected and stored as lipids during their foraging migration for the costs of maintenance and the costs of reproduction. This is particularly true for females in which the survival in the first year of their pups is directly related to their ability to store and acquire resources (McMahon & Burton, 2005). It is also true for males which have to be in a good condition to fight for access to the breeding. In addition, SESs are known to be faithful to their foraging area (Bradshaw *et al.*, 2004), so any changes of the area quality due to large scale oceanographic events could have an important impact on the energy expenditure and potentially on the survival and the breeding success (Authier *et al.*, 2012).

L'éléphant de mer austral, bio-échantillonneur de la distribution des ressources marines

Résumé : Du fait de l'isolement géographique de l'océan austral et des conditions météorologiques qui y règnent, la collecte de données océanographiques par les moyens conventionnels est particulièrement couteuse dans cette région du globe. Pour pallier à ces difficultés, l'utilisation d'enregistreurs électroniques embarqués sur des prédateurs marins, et notamment sur les éléphants de mer australs, s'est révélée être une approche intéressante. Les femelles éléphant de mer s'alimentent en grande partie de petits poissons méso-pélagiques bioluminescents, les myctophidés. Leur forte abondance et leur comportement de migration nycthémérale confèrent à ces organismes un rôle écologique de première importance dans l'océan austral. Cependant, la distribution spatiale des proies de l'éléphant de mer, et les processus physiques et biologiques qui influent sur la dynamique de cette distribution sont encore mal connus. Cette thèse se propose d'enquêter sur ces sujets à partir des données à haute fréquence d'échantillonnage collectées par des femelles éléphants de mer. L'analyse du comportement de plongée des femelles éléphants de mer, en relation avec les variations du taux de rencontre de proie dont les données d'accélération permettent avoir une estimation, est cœur des différents travaux développés dans cette thèse. Les résultats obtenus suggèrent notamment, (1) une diminution de l'abondance des proies avec la profondeur ainsi qu'une homogénéisation de leur distribution, (2) une distribution en couches de cette ressource, (3) l'intervention de contraintes verticales délimitant l'étendu verticale de ces couches et ainsi capable de moduler leur densité, (4) au sein des couches, une dispersion relativement importante des proies en comparaison de la portée des capacités de perception du prédateur, et enfin (5) un rôle significatif des tourbillons méso-échelle et de leur bordure sur la structuration de la distribution des ressources alimentaire de l'éléphant de mer durant l'été austral.

Mots clés : Eléphant de mer austral, bio-logging, myctophidés, océan austral, fine échelle, comportement de plongée, interactions prédateur-proies

Southern elephant seal, samplers of marine resources distribution

Summary : Because of the remoteness and harsh meteorological conditions of the southern ocean, data sampling is more costly in this area. Use of electronic devices attached to marine predators (Bio-logging), such as southern elephant seals, has emerged as an interesting approach to cope with this problem. Female southern elephant seals primarily feed on small bioluminescent meso-pelagic fishes called myctophids. Because of their large abundance and of their diel vertical migration behaviour, these organisms have a major ecological importance in the southern ocean. However, the spatial distribution of the elephant seals prey, as well as the bio-physical processes affecting the dynamics of this distribution, are still poorly known. This thesis intends to investigate this issue using high sampling frequency bio-logging data collected by female southern elephant seals. This work is based on the analysis of elephant seals diving behaviour in relation to changes in the occurrence of prey encounter events detected from acceleration data. Our results suggest that (1) prey abundance decreases with depth and that their distribution tend to standardize, (2) prey are distributed into layers, (3) vertical constraints could modulate the prey density by acting on the vertical spread of these layers, (4) prey items are well dispersed in comparison to the perception range of elephant seals, and finally (5) that meso-scale eddies, notably their edges, play a structuring role in the prey distribution during the austral summer.

Keywords : Southern elephant seals, bio-logging, myctophids, southern ocean, fine scale, diving behaviour, predator-prey interactions

Centre d'Études Biologiques de Chizé
U.M.R. 7372 - CNRS
Université de La Rochelle
79360 Villiers-en-Bois